Understanding The Regional Migration Routes And Field Charging History Of The Oued Mya – Hassi Messaoud Petroleum System, Algeria

By
Djamel Boutoutaou

A thesis submitted to the University of Newcastle upon Tyne
In partial fulfilment of the requirements for the degree of
Doctor of Philosophy
In the Faculty of Science

School of Civil Engineering and Geosciences
University of Newcastle Upon Tyne, U.K.

March 2003

Declaration

I hereby certify that the content of this thesis is the original work of the author, except where otherwise acknowledged, and has not been submitted previously for a degree at this, or any other, university.

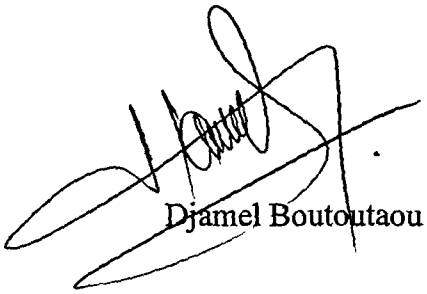

Djamel Boutoutaou

Table of Contents

Chapter 4. Geochemical outline of the Oued Mya basin-Hassi Messaoud ridge petroleum system

Chapter 5. migration and charging directions of the reservoirs of the Oued Mya-Hassi Messaoud ridge petroleum system

Acknowledgments

Firstly, I would like to thank Sonatrach-BP-Amoco association for financial support throughout the duration of this project and Sonatrach for providing samples and data.

I would like to thank my supervisor Professor Steve R. Larter for his guidance of the research, his constructive criticism and correction of my manuscript. I would like to thank Dr. Barry Bennett, Dr. Thomas Oldenburg and Professor Andrew Aplin for their suggestions and useful discussions during my study.

I would like to acknowledge the technical assistance provided by several people at NRG, namely Paul Donohoe, Kim Noke and Berni Bowler. I would like also to thank Yvonne Hall for her help over the three years.

I would like to thank my colleagues Ghalem Zoheir, Boukendakdji Karima, Makhlouf Tahar from SH/CRD, Agonizera Sissani from SH/exploration, Megnouche Nabil and Gribi Aziza from PED, and Belghomari Karim from SH/production Hassi Messaoud for their help and encouragements.

A special thanks to my wife Faïma, for her encouragement, support and patience throughout the last three years, My son Mohamed Wassim, to whom I owe a lot. My parents and family also deserve special thanks for their support and encouragements.

Abstract

This thesis describes a detailed geochemical evaluation of the Oued Mya-Hassi Messaoud ridge petroleum system, located in the central Sahara-Algeria. The study area consists of several fields: (1) the Devonian and the Lower Triassic fields located in the Oued Mya basin which are generally small and in direct contact with the Silurian source rock in the basin, (2) the broad low-relief structural traps developed in the Cambro-Ordovician quartzite reservoirs on the adjoining El-Agreb-Hassi Messaoud ridge, 50 to 60 km east of the Oued Mya basin.

Utilising conventional biomarker facies and maturity parameters and aromatic hydrocarbons, it is shown that all the oils from the Devonian, the Lower Triassic and the Cambrian fields across the whole petroleum system are similar to the Silurian source rock strata which are widely recognised to be the main source in the region. The oils in the study area are discriminated into three main groups; I) oils from the Hassi Messaoud, Hassi Guettar and El-Agreb fields located in the Hassi Messaoud ridge, II) oils from the Devonian and the Lower Triassic fields located in the Oued Mya basin and III) oils from El-Baguel and Mesdar Cambrian fields. The oils from the El-Baguel and Mesdar Cambrian fields are believed to be generated from the Silurian source rocks located in the Berkine basin, east of the Hassi Messaoud ridge.

The biomarker and aromatic hydrocarbon maturity parameters as well as the pyrrolic nitrogen compounds (alkylcarbazoles and benzocarbazoles) data suggest that the oils from Mokh-El-Kebch, N'goussa, Guellala northeast, Guellala and Draa Temra Triassic fields have undergone the least migration distances and were predominantly charged vertically from the underlying Silurian source rocks which are in direct contact with the Devonian and the Lower Triassic reservoirs. The oils from the Haoud Berkaoui and the Benkahla fields appear to have experienced both vertical followed by lateral migration (probably ~20 km). Charging of the Hassi Messaoud reservoirs occurred predominantly from the west-northwest and east sectors. The oil experienced long lateral migration distances (40-60 km) starting from the Silurian source rock strata in the northeast of the Oued Mya basin and the Silurian source rock strata located around the Dzabat area east of the field. Once in the Hassi Messaoud reservoirs, the oil migrated upwards towards the crest located in the centre, then downwards to the north, south and finally west parts of the field.

Charging of the Hassi Guettar and El-Agreb fields occurred from the north (i.e. from the Hassi Messaoud field). It seems that El-Agreb oils have experienced the longest migration distances across the whole petroleum system (120 to 140 km). Finally, the charging of the Mesdar and El-Baguel fields took place laterally from the south-southeast starting from the Silurian source likely located in the Berkine basin east of the Hassi Messaoud ridge. The oil in the El-Baguel field seems to have experienced longer migration distance then the oil from the Mesdar field.

The study of the petroleum fluid inclusions in the Hassi Messaoud field revealed a reasonable model of temperature and charge history of the Hassi Messaoud field. The modelling results suggest that the Hassi Messaoud sandstone member was at a depth of 2.8 to 3.3 km during the time of petroleum migration into the reservoirs and petroleum inclusion formation. The temperature range at this depth was between 106°C to 118°C from Late Cretaceous to Palaeogene.

The distribution of biomarkers and aromatic hydrocarbons in the palaeo-oils extracted from the petroleum inclusions in 6 samples from Hassi Messaoud field and 1 sample from Haoud Berkaoui field revealed that: (1) the palaeo-oils trapped in petroleum inclusions of both fields and the present-day produced oils are similar, likely generated from the Silurian, main source rocks in the region; (2) the palaeo-oils are less mature than the present-day produced oils; and (3) the palaeo-oil trapped in the Haoud Berkaoui Triassic reservoir is even less mature than the palaeo-oils trapped in the Hassi Messaoud reservoirs which may suggest an earlier oil charging of the Haoud Berkaoui field compared to the charging of the Hassi Messaoud field.

Chapter 1
Introduction

1. Introduction

1.1. Background and objectives

The Oued Mya-Hassi Messaoud petroleum system is located approximately 800 km southeast of Algiers in the east-central Sahara desert (Figure 3.1). It is considered to be the largest petroleum province so far discovered in Algeria and one of the largest in the world. Fields assigned to this system are those believed to be sourced from a kitchen in the Oued Mya depocentre. Attar and Hammat (1993) reported oil-in-place estimate of 47 BBO (billion barrels oil) across the whole petroleum system, however accounted recoverable reserves in Hassi Messaoud giant field are only 10.2 BBO, largely because of unfavourable reservoir conditions. There is no doubt that the main effective source rock is the Lower Silurian "hot shales" (Benamrane et al.,1993), since the Devonian is eroded out on the Hercynian unconformity across the Oued Mya basin. The most important fields concerned in this system consist of: 1) Fields reservoired in the Lower Devonian and Lower Triassic and located in the Oued Mya basin (Hammouda, 1980), which are generally small and often relate with sand pinchouts; 2) the Cambro-Ordovician quartzite reservoirs on the adjacent Hassi Messaoud Arch (Balducchi and Pommier, 1970; Odeh, 1975).

The Oued Mya-Hassi Messaoud petroleum system appears to be well explored; however, the origin and migration directions of the oils reservoired in the area, including the giant Hassi Messaoud field, are still very poorly understood. There are ample geochemical data for the whole petroleum system, but these data are disparate and poorly processed.

Determination of the source rock(s) that have generated the petroleum and the assessment of the relative extent of regional petroleum migration and the filling directions of the reservoirs are important, since they can exert a profound influence on current/future exploration activities across the Oued Mya-Hassi Messaoud petroleum system. Elucidation of the oil migration routes can potentially aid in the discovery of further small reserves near the Hassi Messaoud giant petroleum accumulation, where the existing infrastructure would make such reserves economic.

The aims of this study were:

i. To find out if the petroleums hosted in the fields across the Oued Mya-Hassi Messaoud petroleum system have any genetic relationship.

ii. To establish the source rocks responsible for generating and expelling these petroleums.

iii. To suggest the migration pathways and filling directions of the fields across the study area.

iv. To determine the role of faults with respect to petroleum migration within the Hassi Messaoud field.

v. To understand the compartmentalisation and the communication between compartments within the Hassi Messaoud field.

vi. To determine the filling history and timing of charging of the Hassi Messaoud reservoirs.

1.2. An Introduction to the concept of petroleum migration

The distribution of petroleum (oil and gas) in sedimentary basins is controlled by the combination of a number of processes that might have evolved all through geological history of the basins. The processes that direct the petroleum potential of a basin are the generation, primary and secondary migration of petroleum and the accumulation and preservation of petroleum in reservoirs. Petroleum migration system is a vital process in the formation and distribution of petroleum accumulations and nature of petroleum in sedimentary basins.

The occurrence of petroleum accumulations are generally found in relatively coarse-grained porous and permeable reservoir rocks, which contain small or no insoluble solid organic matter. This suggests that the large quantities of petroleum discovered in these reservoir rocks are unlikely to have originated in them from solid organic matter of which now no trace remains. Rather, petroleum is generated in large quantities only through geothermal action on high molecular weight organic kerogen, preserved in fine-grained sedimentary source rocks (Tissot and Welte, 1984). Therefore, the formation of oil and gas accumulations in reservoir rocks requires some kind of

transport from source to trap locations. This transport process is known as petroleum migration (Hobson and Tiratsoo, 1975; Tissot and Welte, 1984; Verweij, 1993).

An understanding of the processes involved in petroleum migration is of fundamental importance in petroleum exploration. Oil explorationists searching for economic petroleum accumulations need information on the dimensions and residual oil saturations of carrier systems which are not achievable using seismic or other remote sensing methods. Tentatively, organic geochemistry can be used to resolve petroleum migration history, to determine the volume of petroleum migrating and the volumes of water they interact with directly and to distinguish between oils which have migrated through the pore system in fine-grained rocks and those which have migrated via fractures and faults (Later and Aplin, 1995). For many years, geochemists have sought indicators of migration distances (Krooss et al., 1991).

In theory, compounds with different molecular weight, polarities and stereochemistries should behave differently during the various adsorptive/desorptive processes which take place during the movement of petroleum in the subsurface. Early efforts to describe regional petroleum migration pathways made use of biomarker alkanes (Seifert and Moldowan, 1978). However, it is well established that parameters derived from biomarker alkanes are strongly affected by other factors such as source input, depositional environment and thermal maturity (Yamamoto et al., 1991). Hence, application of biomarker alkanes to migration of petroleum in the subsurface is restricted (Peters and Moldowan, 1993). Moreover, the composition of hydrocarbon fractions (e.g. biomarker alkanes) has been found to be in general little influenced by petroleum migration in a geological more realistic experimental system (e.g. Greibrokk et al., 1994; Later et al., 2000).

During the last decade, both field studies and laboratory experiments have revealed potential indicators of petroleum migration distance in more polar compounds in petroleum; such as aromatic nitrogen compounds (e.g. carbazoles and benzocarbazoles) and phenols (Yamamoto et al., 1991; Yamamoto, 1992; Li et al., 1992, 1993, 1994, 1995b, 1997; Taylor, 1994; Larter and Aplin, 1995; Larter et al., 1996a, Larter et al., 2000; Terken and Frewin, 2000). Common polar compounds (i.e. organic nitrogen compounds and phenolic compounds) present in petroleum show characteristic partition behaviour between the migrated oil, water, mineral surfaces

and solid organic material (kerogen). Field studies and laboratory experiments have shown polar compounds to be depleted from petroleum during petroleum migration in the subsurface. The compositional changes can be credited to interactions with rock surfaces and water; these compounds are therefore potentially appropriate to assessments of petroleum migration and reservoir filling processes (Yamamoto et al., 1991; Yamamoto, 1992; Taylor, 1994; Chen, 1995; Larter and Aplin, 1995; Li et al., 1995b).

Nitrogen and oxygen compounds correspond to a small fraction of petroleum compared to the distillable hydrocarbons and sulphur compounds which constitute the major component of petroleum (Tissot and Welte, 1984). Nevertheless, these nitrogen and oxygen compounds may play a vital role in understanding the petroleum system; mostly because of their high chemical reactivity compared to hydrocarbons, hence, more sensitive indicators of the physicochemical environment of petroleum.

Although nitrogen and oxygen compounds are present in low concentrations in petroleum, due to their high polarity and interaction with mineral surfaces and other petroleum compounds may affect the viscosity and pressure-volume-temperature (PVT) properties of petroleum (Thomas et al., 1993; Stoddart, 1994; Larter and Aplin, 1995). Moreover, polar compounds can also influence wettability through adsorption onto mineral phases (Li et al., 1992; Thomas et al., 1993; Stoddart, 1994; Larter and Aplin, 1995).

1.3. Subsurface petroleum migration

The petroleum formed in the source rocks is generally expelled from them towards lower pressure zones. Hence, the formation of commercial accumulations of oil and gas in reservoir rocks necessitates the movement of petroleum from the fine-grained, organic-rich source rocks via a carrier bed towards the reservoir rocks location. This transport process is known as petroleum migration (Hobson and Tiratsoo, 1975; Tissot and Welte, 1984; and Verweij, 1993).

Petroleum geochemists are making great interest in understanding migration processes. For example, in a given petroleum system, if it were possible to estimate the petroleum potential from an active source rock and understand the regional petroleum migration extent across the system it may well be possible to assess the

ultimate remaining potential and help explorationists to discover new economic petroleum accumulations (Larter et al., 1996b).

Two successive migrations can be distinguished: primary and secondary migration. Both primary and secondary migration are dominated by separate phase flow, driven by the hydrodynamic potential (overpressure gradients), gravity forces (buoyancy) and capillary pressures (England et al., 1987). Primary migration is defined as the movement of the newly generated petroleum from the low permeability source rocks through and out of the fine-grained source rocks towards more permeable rocks (Tissot and Welte, 1984). Secondary migration is an efficient process involving the movement of petroleum after expulsion from a source rock, through wider pores of more permeable and porous carrier and reservoir rocks, until an oil or gas accumulation is produced (Schowalter, 1979; Tissot and Welte, 1984; and England et al., 1987; and Verweij, 1993) (Figure 1.1).

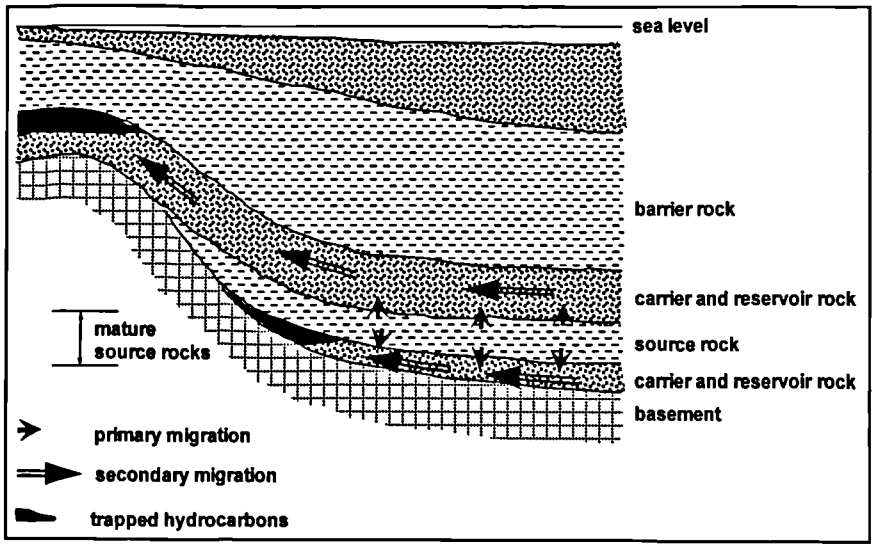

Figure 1.1 Schematic illustration of primary and secondary migration. (After Verweij, 1993).

Within source rocks buried at depths of 2 to 3 Km (with permeability less than 1mD), petroleum movement is mainly controlled by the overpressure potential gradients with vertical movement occurring. Whereas, when the petroleum enters the larger pores of the carrier rock (with permeability greater than 1mD), the main driving force that controls secondary migration is buoyancy, which results from the density difference between the migrating petroleum and the associated water phase. The greater the density difference, the greater will be the buoyant force for a given length of petroleum column (Schowalter, 1979). In this case lateral (and upward) migration of

petroleum in carrier beds is predominant. The main resistive force opposing buoyancy is capillary pressure, which is a function of the pore-throat radii of the carrier bed, the petroleum-water interfacial tension and wettability (Schowalter, 1979). The capillary pressures are mainly encountered by petroleum at lithological boundaries, i.e. cap rocks which function as seals (England et al., 1987).

Ranges of secondary migration distances reveal large variations (Larter et al., 1996a). Very short-range migration distances are recognised within fractured shale source rock/reservoir systems such as the Miocene Monterey Formation in the Santa Maria Basin (USA). The migration distance is possibly less than 1 km, where differentiation between primary and secondary migration processes becomes particularly difficult to distinguish (Larter et al., 1996b). Whereas, lateral migration of petroleum within the Upper Cretaceous Viking Formation in the Western Canada Basin is in the order of several hundred kilometres (Creany and Allen, 1990; Piggot and Lines, 1991).

1.3.1. Secondary migration efficiency

Petroleum migration in the subsurface takes place when a dendtritic network of continuous interconnected oil communicating pathways is established along the initially water-saturated carrier rocks (Schowalter, 1979 and England et al., 1987), with approximately 50% of the available porosity being petroleum saturated. Theoretical and field studies of oil migration point out that, in common, only small portions (1-10%) of the carrier porous volume are in fact concerned in the movement of oil (England et al., 1987) (Figure 1.).

The remaining 90 to 99% of the carrier rock is unstained (England et al., 1987). During secondary migration process, the petroleum string will migrate laterally up dip in a tortuous way (Schowalter, 1979 and England et al., 1987), utilizing only the coarser-grained parts of the accessible carrier system (Verweij, 1993). Consequently, this tortuous movement will leave behind some rocks with residual oil saturation, through which the oil has migrated, whereas the immediate neighbouring rocks will be entirely unstained by oil (Schowalter, 1979 and England et al., 1987). Mackenzie and Quigley (1988), argued that a reliable estimation of migration losses is not possible and that migration reduces drastically the charge of petroleum available for entrapment. England et al. (1987), stated that petroleum will continue to migrate only if the expulsion of hydrocarbons from the source rock is continuous, otherwise, if the

source rock stops charging the carrier rock, then petroleum migration will terminate leaving a petroleum residue along the carrier bed. This residual volume (amount of petroleum remaining in a bed) is approximately equivalent to that necessary to construct the continuous interconnected pathways along the carrier rock, between the source and the reservoir. Evidences to support these assumptions are:

1 – After the supply of petroleum from the source rock has ceased, the water is unlikely to displace the residual oil in carrier rock because the capillary forces dominate viscous forces.

2 - Examples of migration pathways either encountered by drilling, or by observation of uplifted and eroded pathways.

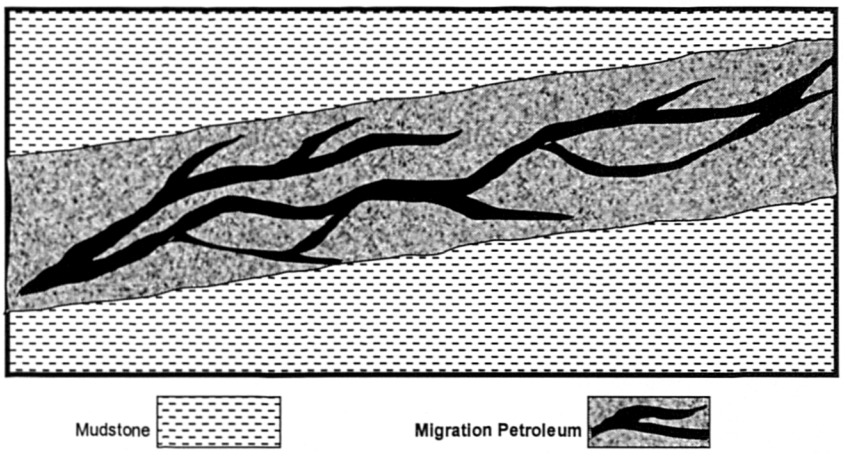

Figure 1.2 Dendtritic migration pathways predicted for secondary migration throughout a water-wet carrier bed. (After England, 1990).

The total volume of petroleum lost during secondary migration from the source rock towards the reservoir rock can be predicted according to the following equation given by Mackenzie and Quigley (1988):

$$V_{pl} = \Phi x f_r x V_D \quad \text{.....(1.1)}$$

Where, V_{pl} is the volume of petroleum lost along secondary migration;

Φ is the porosity of the carrier bed;

f_r is the residual saturation; and

V_D is the volume of rock through which the petroleum flow (drainage volume).

1.4. Compositional variations in petroleum during subsurface migration

It is well established that petroleum composition is predominantly controlled by the type of the organic matter in the source rock. However, during its migration from source to trap, numerous processes may occur, and are capable of changing the chemical composition of petroleum (England et al., 1991). Phase partitioning and geochromatography are considered to be the main processes that are able to change petroleum composition during secondary migration.

Phase partitioning can take place when petroleum is expelled from the highly pressured, high temperature source rock and migrates up-dip towards lower pressure and temperature carrier and reservoir rocks (England, 1994). Lower pressure and temperature causes gas to exsolve from the liquid phase. Therefore, petroleum in the subsurface can be trapped as a gas (C_1-C_5) or condensate/oil (C_6+). Low molecular weight compounds are lost from the migrating condensate/oil into the gaseous phase, becoming denser; and the gaseous phase loses high molecular weight compounds into the condensate/oil phase, resulting in a lower density and thus greater migration potential (England et al., 1991).

Geochromatography defines the separation of two or more compounds showing different affinities for the stationary and mobile phases (Nagy, 1960), and results from dissimilarities in the partition coefficients of individual compounds between stationary and mobile phases. The compounds in petroleum which are prone to interact with water, mineral and organic matrices are those containing active functional groups capable of strong acid/base or hydrogen bond interactions, such as carboxylic acids, carbazoles, quinolines and phenols. Several laboratory simulations have shown the effects of petroleum interactions with the rock matrix (Chen, 1995; Li et al., 1994, 1997; Larter et al., 2000).

1.4.1. Molecular indicators of secondary petroleum migration - the migration tracer concept

Geochemical tracers are chemical components which should initially exist in only one part of a migration system, either in the oil, water or solid phases, and should be distributed in a predictable fashion between the various phases during the course of secondary migration of petroleum (Larter et al., 1996a,b).

Geochemical tracer molecules interact and partition between petroleum, waters and rock phases. The partition is controlled by molecular geometry, alkyl-substitution positions, polarity and petroleum and water bulk composition. Involvement of solid phases, both mineral and solid organic matter in the fractionation of these compounds during secondary migration appears certain, with both polar and hydrophobic interaction mechanisms involved (Larter et al., 1996b). The geochemical tracer would be totally conserved within the system, being neither produced or influenced by maturity nor consumed by chemical or nuclear reaction (Larter et al., 1996b).

1.4.2. Pyrrolic nitrogen compounds as indicators of petroleum migration in the subsurface

The geochemical characterisation of nitrogen and oxygen compounds in petroleum offers the possibility to use geochemical parameters to estimate petroleum migration distances and the relative volumes of interacting petroleum and water in petroleum systems (Larter and Aplin, 1995). The distribution and/or concentration of the polar compounds (nitrogen and oxygen compounds) are continuously changing as petroleum interacts with increasing volumes of water and mineral/organic surfaces during secondary migration. Hence, it is promising to utilise these compounds in the modelling of natural fluid flow since these compounds may well interact with formation water and rock surfaces (e.g. Taylor et al., 1997).

The majority of the total nitrogen compounds are found within the high molecular weight fraction (NSO compounds /asphaltenes) of petroleum (Richter et al., 1952). The nitrogen concentrations of kerogens and coals are believed to be appreciably larger than in petroleum by ca. 10 times. Moreover, Bakel and Philp (1990) reported that petroleums generated from phosphatic shales contain higher concentrations of organic nitrogen compounds compared to those sourced from carbonate source rocks.

Nitrogen compounds in petroleum are present mainly as aromatic heterocycles, with predominance of neutral pyrrolic structures over basic pyridinic forms (Dorban et al., 1984; Wilhelms et al., 1992). The nitrogen content in petroleums varies between 0.1 to 2.0 wt%. The main nitrogen compounds investigated in this study are the pyrrolic nitrogen compounds such as alkylcarbazoles and benzocarbazoles (Figure 1.3)

Nitrogen compounds in petroleum and source rocks are ubiquitous, but their origin and the controls on their abundance are still poorly understood. Li et al. (1993a) suggested that pyrrolic nitrogen compounds are not inherited directly from biological precursors but most likely represent diagenetic artefacts through reworking of nitrogen-containing sedimentary organic matter, or incorporation of inorganic nitrogen species (NH_4^+) into organic carbon skeletons.

During the last decade, petroleum geochemists have focused their research on the possible use of polar compounds such as pyrrolic nitrogen (e.g. carbazoles and benzocarbazoles) and oxygen (e.g. alkylphenols and fluorenones) compounds to better understand and quantify petroleum migration processes (Yamamoto, 1992; Yamamoto et al., 1991; Li et al., 1993a,b, 1995b, and 1997; Stoddart, 1993; Stoddart et al., 1995; Chen, 1995; Brincat, 1996; Larter et al., 1996a,b and 2000; Taylor, 1994; Taylor et al., 1997; Bennett and Larter, 1997; Bennett et al., 2002).

The pyrrolic nitrogen compounds play a vital role in the adsorption/absorption of petroleum on carrier and reservoir rocks and influence processes involved in petroleum migration and production (Larter and Aplin, 1995). Preliminary measurements of the distribution coefficients of pyrrolic nitrogen compounds between various liquid/solid phases suggest that adsorptive interactions between organic nitrogen compounds and solid organic/mineral phases are largely responsible for the migration-related fractionations of pyrrolic nitrogen compounds in petroleum (Li and Larter, 1993). The operating mechanisms appear to be similar to a "normal phase chromatographic process" involving irreversible adsorption (Li et al., 1994; Larter et al., 1996b, 1997, 2000; Frolov, 1997).

Figure 1.3 shows the molecular structures of both alkylcarbazoles and benzocarbazoles present in petroleum. The alkylcarbazoles identified so far within petroleum and source rocks are: carbazole, methyl-, and dimethyl-carbazoles isomers. Trimethyl-carbazoles are also present; however, they have not yet been completely identified because of the absence of appropriate standards (see section 2.1.4.2 in chapter 2). Li et al. (1995b) classified the different alkylcarbazole isomers on the basis of the position of alkyl-substituents relative to the active pyrrole functionality N-H: 1) Pyrrolic N-H shielded isomers, in which both carbon positions 1 and 8 are substituted by an alkyl group: e.g. 1,8-demethylcarbazole, 2) Pyrrolic N-H partially shielded

isomers, in which either position 1 or 8 is substituted by an alkyl group: e.g. 1,4-dimethylcarbazole, and 3) Pyrrolic N-H exposed isomers, in which the alkyl substituent are present at carbon positions other than 1 and 8: e.g. 3,4-demethylcarbazole.

The pyrrolic NH group of the carbazole molecule can interact with OH groups present on mineral surfaces within the carrier system. An alkyl group adjacent to the NH group will cause partial shielding reducing the strength of any sorptive interaction. The presence of two alkyl groups, one either side of the NH group (e.g. 1,8-dimethylcarbazole) reduces sorptive interaction to an even greater extent. Thus, when petroleum migrates through the carrier system, alkylcarbazole isomers with exposed NH group will tend to be sorbed more strongly by mineral surfaces resulting in their depletion from the migrating petroleum. Consequently, the migrating petroleum will become enriched in the NH-shielded isomers. Previous studies have shown that the NH-shielded to NH-exposed isomer ratio increases with increasing migration distance (Li et al., 1995b, 1997).

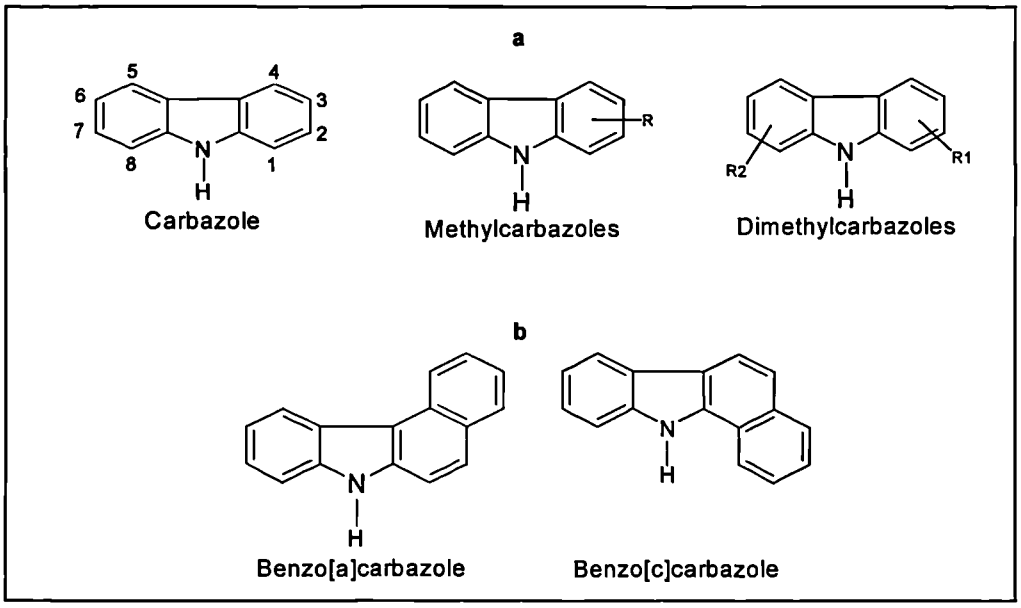

Figure 1.3 Molecular structure (a) of alkylcarbazoles and carbon numbering system for alkyl-substituents and (b) benzo[a]carbazole and benzo[c]carbazole.

The concentrations and distributions of pyrrolic nitrogen compounds are controlled to a large extent by primary and secondary migration (Yamamoto, 1992; Li and Larter, 1993; Li et al, 1995b). Laboratory simulation experiments carried out by Li and Larter (1993) showed that during migration, nitrogen shielded isomers are less strongly retained on mineral surfaces compared to partially-shielded and exposed nitrogen

isomers. This might be explained by the shielding effects of the nitrogen functionality by the methyl groups. Furthermore, Li et al. (1994) emphasised these observations in experimental studies of the fractionation of synthetic model carbazole compounds and a petroleum pyrrolic nitrogen fraction using a range of laboratory chromatographic systems. They revealed that partition of these compounds was principally restricted by steric effects associated to the alkylation position with respect to the active pyrrolic functionality.

Li et al. (1995b) considered the effect of primary and secondary migration on the distribution of alkylcarbazoles and benzocarbazoles in source rocks and crude oils taken from a number of basins. They concluded that primary and secondary oil migration has a strong impact on the distribution of pyrrolic nitrogen compounds in reservoired petroleum. Moreover, these authors showed that source rocks contained higher concentrations of alkylbenzocarbazoles whereas crude oils were relatively enriched in alkylcarbazoles. This observation may be linked to the increased number of aromatic rings in the alkylbenzocarbazoles, restraining their expulsion from the source rocks (Leythaeuser and Schaefer, 1984). On the other hand, migrating oils exhibited enrichment in nitrogen shielded isomers and higher molecular weight homologues compared to nitrogen exposed isomers and lower molecular weight compounds, respectively.

More recently, Larter et al. (2000) illustrated that geochromatography does take place during migration through water wett rock in laboratory experiments. The experiment was carried out on a North Sea oil sample which was flowed through water saturated siltstone under realistic subsurface conditions of temperature and pressure. They found that the hydrocarbon fractions showed minor fractionation compared to the polar fraction. Comparison of the sterane based "Biomarker migration index" proposed by Seifert and Moldowan (1978) in the original and migrated oils revealed no statistically detectable variation. However, the non-hydrocarbon polar fraction exhibited substantial changes in concentration and composition as the experiment proceeded. These variations are expressed by the systematic removal of carbazoles, benzocarbazoles and phenols during oil migration, a systematic increase in the proportion of C_2 alkylcarbazoles compared to lower homologues, and a reduction in the benzocarbazole [a]/[c] ratio were observed in this laboratory simulation(Figure

1.4). These observations appear to be similar to the compositional changes seen in migrated oils in the subsurface (Li et al., 1995b; Li et al., 1998; Larter et al., 1996a; Terken and Frewin, 2000). These findings confirm that distribution and concentrations of pyrrolic nitrogen compounds show significant variations during secondary oil migration.

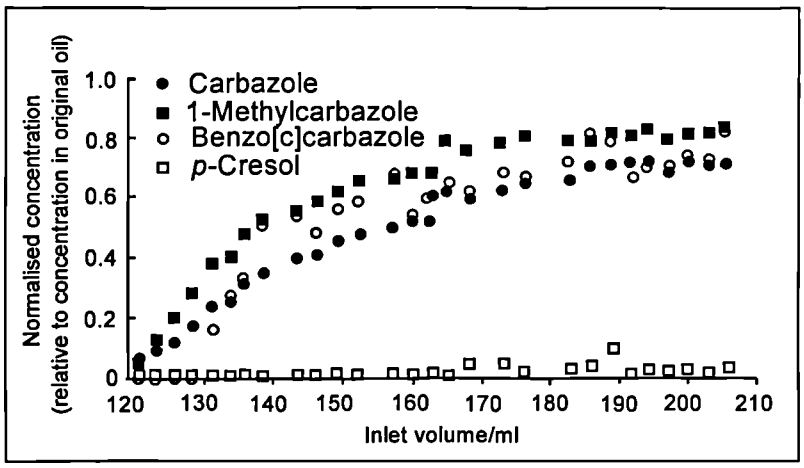

Figure 1.4 Variation in concentrations of selected tracer compounds in oil fractions collected throughout laboratory simulated migration experiment, normalised to concentrations in the original oil sample. (After Larter et al., 2000).

Larter et al. (2000) suggested that fractionation intensity of pyrrolic nitrogen compounds depends on: (1) the volume of the migrated petroleum and (2) the size of the carrier systems involved in the migration (i.e. volume carrier/volume migrated petroleum ratio). For instance, small petroleum reservoirs charged through a comparatively long migration pathway (i.e. volume carrier/volume reservoired oil is large) would be characterised by large fractionation (i.e. reduction) in pyrrolic nitrogen compound concentration: e.g. the 2nd White Speckled Shale (source) – Cardium/Viking Formation (carrier/reservoir) petroleum systems of the Western Canada foreland sedimentary basin (Larter et al., 1996a), the Bakken oils in the Canadian portion of the Williston basin with source rocks in the USA (Li et al., 1998), the Dhahaban sourced oils of Oman which have also migrated well over 200 km from their source basin (Terken and Frewin, 2000), and El-Agreb oils in the Hassi Messaoud Ridge which have migrated over 120 km from their source in the Oued Mya basin (see Chapter 5, this volume). However, in prolific basins (i.e. with high throughput carriers), large volumes of oil will migrate through the same migration pathways, eventually saturating the carrier to equilibrium saturation with the feed oil. Therefore, the final reservoired petroleum will be characterised by little net tracer

fractionation. Such examples include the Kimmeridge Clay Formation (source) – Hugin Formation/Paleocene/Eocene sand (carrier/reservoir) petroleum systems of the Tertiary reservoirs in the Viking Graben, North Sea (Larter et al., 1997), where many oil reservoirs have been charged through a single focussed pathway and the Sonde de Campeche system (Horsfield et al., 1998).

1.4.3. Application of benzocarbazoles as migration tracers

The use of benzocarbazoles as indicators of secondary petroleum migration distance and reservoir charging direction has been proposed by Larter et al. (1996a). They showed that both absolute and relative concentrations of benzocarbazoles decrease with migration distance of petroleum independent of the maturity of the oils (Figure 1.5a). They further demonstrated that the ratio of benzo[a]carbazole to benzo[a]carbazole + benzo[c]carbazole (BC ratio) obtained from the analysis of reservoired oils in five different petroleum systems with relatively well known secondary migration pathways and distances does decrease with migration distance (Figure 1.5b).

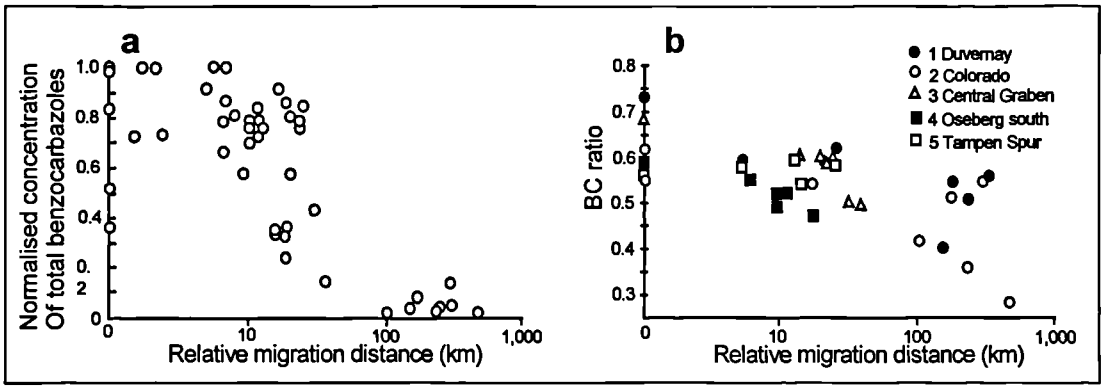

Figure 1.5 Variation in the (a) relative concentration of benzocarbazoles and (b) ratio of benzo[a]carbazole/(benzo[a]carbazole + benzo[c]carbazole) as a function of relative migration distance of oils. (After Larter et al., 1996a).

Earlier work revealed that during secondary migration, the shielded benzo[a]carbazole isomer is preferentially removed from petroleum rather than the exposed benzo[c]carbazole isomer, due to interactions with the carrier bed (Larter et al., 1996a). These authors suggested that preferential removal during migration of the more rod-shaped benzo[a]carbazole relative to the sub-spherical benzo[c]carbazole results from selective sorption of benzo[a]carbazole from the petroleum onto clay minerals and into solid organic matter along the carrier bed. Thus, molecular shape

phenomenon appears to be the important factor controlling these migration related fractionations (Larter et al., 1996a).

Benzocarbazoles have been effectively applied as geochemical tracer molecules in several case stories (e.g. Larter et al., 1996a, 1996b, 1997; Li et al., 1997; Bennett and Larter, 1998; Terken and Frewin, 2000). Terken and Frewin (2000) analysed benzocarbazoles in oils from the Dhahaban petroleum system of Oman. The BC ratio was used in combination with basin modelling to estimate the relative migration distances for the different oil accumulations across the petroleum system. They found that oils have migrated up to 300 km and the origin of the oils was supposed to be from two different source areas.

More recently, Gong et al. (2001) have studied the effects of geochromatography on crude oil compositions. A 50/50 sand/montmorillonite mixture was used to simulate the carrier bed material, and black North Sea oil was used as starting oil. The experiment was conducted under subsurface conditions of pressure and temperature for 45 days. Polar fractions obtained from thirty effluent oils and the original oil were analysed by GCMS. The results show that benzocarbazoles were strongly retained on mineral surfaces in the first eluted samples, followed by a stage of relatively rapid increase in concentration, and finally a stage of more gradual increase to concentrations approximately 50% of those found in the original oil. The reduction of benzocarbazole concentrations may be attributed to sorptive interactions within the carrier bed. Moreover, benzo[a] and benzo[c] carbazoles were differentially adsorbed by the mineral surfaces, validating that the ratio of these two components ([a]/[a]+[c]) could be used as a molecular indicator to assess secondary migration distance.

In some recent works, Brincat and Larter (1997); Clegg et al. (1997, 1998a,b); Horsfield et al. (1998); Li et al. (1997 and 1998); and Bakr and Wilkes (2002) demonstrated that maturity and source facies effects do occasionally exercise a most important role in influencing the pyrrolic nitrogen compound composition of source rocks and crude oils. Li et al. (1997) showed that concentrations of various pyrrolic nitrogen compounds in the rock extracts taken from the Upper Devonian Duvernay Formation in the central Alberta portion of the Western Canada Sedimentary Basin increase significantly with increasing thermal maturity, together with major compositional variations related to alkyl substitution position. Moreover, Li et al.

(1998) concluded that determination of absolute migration distances of a set of Duvernay-sourced oils analysed is not feasible in some areas, due to maturity and source effects on the pyrrolic nitrogen compounds. Clegg et al. (1997, 1998a) also showed that the distribution and concentrations of alkylcarbazoles and benzocarbazoles may be influenced by maturity and source facies. Firstly, in the study of the alkylcarbazole distribution in carbonate clastic source rocks, they showed that samples deposited under restricted, elevated salinity environmental conditions containing organic matter largely composed of filamentous algal mats have carbazole and benzo[c]carbazole as the prevailing carbazole species present. Samples deposited under marine conditions with abundant algal bloom phytoplankton, deposited under photic zone anoxia are dominated by C_4 and C_5 carbazoles. Secondly, they observed an overall increase in the concentration of alkylcarbazoles and benzocarbazoles in source rock bitumen up to a maturity of 0.88% Rc, due to generation, followed by a decrease at 1.45 %Rc, possibly due to dilution and expulsion as hydrocarbon production is increased in the source rock (Figure 1.6).

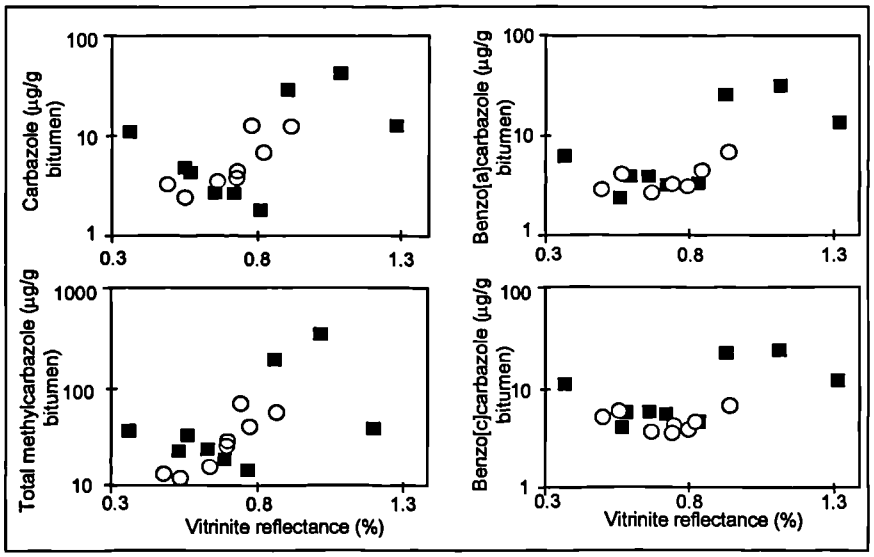

Figure 1.6 Concentration of (a) carbazole and benzo[a]carbazole (µg/g bitumen) for Tithonian source rocks (filled squares) and oils (circles) as a function of maturity. (b) Concentration of total methylcarbazoles and benzo[c]carbazole (µg/g bitumen) for Tithonian source rocks (filled squares) and oils (circles as a function of maturity. (After Clegg et al., 1998).

Furthermore, they confirmed that the [a]/([a]+[c]) benzocarbazole ratio is strongly controlled by maturity of the source rock and crude oils in situations where efficient vertical migration dominates (Figure 1.7).

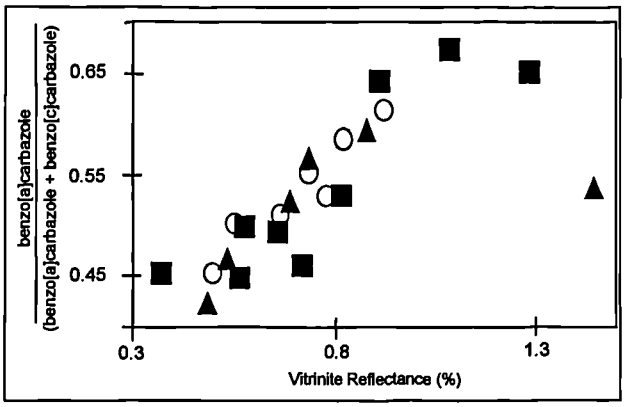

Figure 1.7 The ratio of benzo[a]carbazole/(benzo[a]carbazole+ benzo[c]carbazole) vs. maturity for both source rocks (filled squares and triangles) and crude oils (circles). (After Clegg et al., 1998).

Bakr and Wilkes, (2002) showed that the benzocarbazole [a]/([a]+[c]) ratio displays a consistently positive correlation with API gravity, Pr/Ph and Ts/(Ts+Tm) ratios in a suite of crude oils from the Gulf of Suez (GOS), Egypt with a relatively narrow maturity range (0.86-0.98 %Rc). Bakr and Wilkes (2002) showed that in the central sector of the GOS, where the oils are mostly sourced from carbonates deposited under strongly reducing conditions, [a]/([a]+[c]) values are commonly less than 0.5. However, in the southern and northern sectors of the GOS where source rocks were deposited under less reducing conditions and received significant clastic input, [a]/([a]+[c]) values are generally above 0.5. Based on these observations, the authors concluded that that facies and depositional environment of the relevant source rocks are the main factors controlling the benzocarbazole distributions.

Bennett et al. (2002) summarised the changes in benzocarbazole concentrations and ratios with maturity, source facies and migration in several North Sea source rocks and related crude oils and reviewed literature data. They found a poor correlation between benzocarbazole ratio [a]/([a]+[c]) with maturity in their own studies and those in the literature, suggesting that other factors such as source organic matter and expulsion contribute to changes in benzocarbazole distribution.

It can be concluded that alkylcarbazoles have a limited use as secondary petroleum migration, with the best parameters being the absolute concentrations and relative abundance of the summed C0, C1 and C2 alkylcarbazoles. Migration tracers are most likely to work in the case of foreland basins, where sufficient sorption sites are provided for small oil volumes migrating through a long carrier bed (e.g. Larter et al., 1996a; Li et al., 1998; Terken and Frewin, 2000). The use of benzocarbazoles as

geochemical tracers of absolute migration distance is still viable; however, maturity, source facies and depositional environment effects have to be constrained carefully before benzocarbazoles may be used successfully as indicators of secondary migration distances (Li et al., 1997).

1.5. Fluid inclusions

Fluid inclusions are microscopic vacuoles within minerals, containing liquid and/or gas that were trapped when the mineral cement formed within petroleum reservoir units and carrier beds in sedimentary basins (Roedder, 1984; McLimans and Horsfield, 1987; Narr and Burrus, 1990; Bodnar, 1990; Earnshaw et al., 1993; Karlsen et al., 1993; Swarbrick, 1994; Laresse and Hall, 1996). The fluids trapped within these inclusions are thought to be representative samples of the petroleum and/or aqueous fluids present in the pore space at the time of mineral formation. Fluid inclusions can be thought of as time capsules storing invaluable sources of information about the evolution and migration of petroleum in sedimentary basins. Fluids within inclusions (water, petroleum and gas) may be accessible for geochemical analysis. Thus the first significant information that we can acquire from a fluid inclusion study is the source and maturity of the petroleum present in the carrier bed or reservoir at that time, by extracting and analyzing the fluid hosted within the fluid inclusions. Consequently, models of fluid migration and reservoir filling evolution through geological time can be derived (Karlsen et al., 1993; Jones et al., 1996; Jones and Macleod, 2000; Isaksen et al., 1998 and references therein). Secondly, provided that the inclusions have not undergone any kind of changes in their volume through geological time (i.e. no leakage of fluids into or out of the inclusions since trapping), they can offer an estimate of the temperature and the pressure at which the fluid inclusions formed (Roedder, 1984; Goldstein and Reynolds, 1994). Thirdly, palaeo-pressure can be assessed when the P-T phase diagram of the included petroleum is defined. This will require the determination of the composition of the petroleum within the inclusion (see section 2.2 in chapter 2).

Fluid inclusions can be divided into two main categories based on their fluid contents: petroleum inclusions and aqueous inclusions. Petroleum inclusions contain oil and/or gas that was present in the pore space at the time of trapping. These inclusions usually

contain a vapour bubble. Aqueous inclusions contain predominantly water associated with gaseous components.

1.5.1. Fluid inclusion classification

Fluid inclusions are generally subdivided into four possible types: primary, secondary, pseudosecondary, and unknown inclusions (where a definite classification cannot be determined).

1.5.1.1. Primary fluid inclusions

Primary inclusions are defined by the relationship they play with the original mineral grain or development of the mineral overgrowth (Roedder, 1984; Goldstein and Reynolds, 1994). They generally are formed either in the detrital grain, at the intersection in between the detrital grain and the overgrowth, or within the overgrowth. They are best identified by their relationship to the cement overgrowth zonation. Such inclusions can be trapped on the following cement overgrowths: calcite, dolomite and ankerite, quartz, feldspar, halite, anhydrite, gypsum, and fluorite.

1.5.1.2. Secondary and Pseudosecondary fluid inclusions

Secondary fluid inclusions are those inclusions which are trapped later due to fracturing and cracking of mineral grains, after the mineral overgrowths have been completed. These deformations (fractures and cracks) then heal by mineral precipitation, leading to the formation of fluid inclusions. These type of inclusions cross-cut the detrital grain and the cement overgrowth, as they usually post-date overgrowth development (Roedder, 1984).

Like secondary inclusions, pseudosecondary inclusions form due to the healing of cracks and fractures. These inclusions bear all of the characteristics of secondary fluid inclusions except that the planar arrays of fluid inclusions end abruptly at a growth zone boundary. These inclusions look like secondary inclusions, but they are trapped during mineral growth (Roedder, 1984; Emery and Robinson, 1993). The identification of these inclusions is difficult because some secondary inclusions may not necessarily cross-cut the overgrowth either (Figure 1.8).

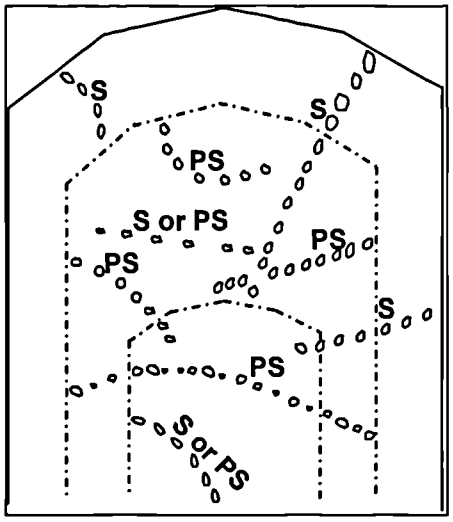

Figure 1.8 Sketch illustrating distinction between secondary (S) and pseudosecondary (PS) fluid inclusions. All inclusions occur in linear arrays because they were trapped along healed fractures. Secondary inclusions are trapped after crystal growth is complete, but pseudosecondary inclusions are trapped before final growth zone have formed. (After Goldstein and Reynolds, 1993).

In general, a single mineral grain may contain all types of the inclusions mentioned above, therefore, it is important to identify and interpret each with great accuracy. These distinctions are extremely important in carrying out a fluid inclusion study. Data obtained from primary inclusions can inform us about the timing of mineral growth (reservoir diagenesis), whereas, data obtained from secondary fluid inclusions can give information about phase of fracture healing that post-dated growth of the host mineral.

Secondary fluid inclusions commonly occur in planar arrays or along curved surfaces that cut across growth zonation. It is important that any fluid inclusion study should start first with a petrographic study; the goal is to describe the setting of the inclusions in the rock fabric and so ascribe them to groups related to features of the history of the sample (Figure 1.9). The fluid inclusions generally encountered in diagenetic minerals are those bearing petroleum oil and/or gas, and water and gas. Oil-bearing fluid inclusions are readily detected by fluorescence microscopy because of their distinctive fluorescence emission colours. Therefore, they can be easily distinguished from water and/or gas bearing inclusions.

Figure 1.9 Relating fluid inclusions to features of a sample history: from a thin section of cemented sandstone. Inclusions A are isolated within the clastic quartz grains and were probably trapped during crystallization of the granitic rock from which they were eroded. Inclusions B lie along a healed fracture but do not pass either through diagenetic cements or two adjacent grains so were probably trapped in the source terrane. Inclusions C are isolated in a quartz overgrowth and will provide information about the conditions of quartz cement precipitation. Inclusion D is secondary, trapped in the sediment after quartz cementation. Inclusion E is related to calcite cement growth and inclusions F are secondary and later than both quartz and calcite cements. (After Emery and Robison, 1993).

1.6. Techniques used in the fluid inclusions study

A number of different analytical techniques are used in fluid inclusions studies (Lasater, 1958; Roedder, 1984 and 1990; Goldstein and Reynolds, 1994). Techniques can be divided into various categories based upon the nature of the analyses and the type of information gained from them. Analyses can be either non-destructive or destructive, and will be qualitative, semi-quantitative or quantitative. To get maximum information from a sample, non-destructive techniques should be applied, such as fluid inclusion petrography, microthermometry and Confocal Laser Scanning Microscopy (CLSM), followed by a destructive technique which commonly involve the breaking open of the inclusions and the release of the contained fluid (for more detail, see section 2.2 in chapter 2).

Microthermometric analysis is unquestionably the most popular and extensively used non-destructive analytical technique (Shepherd et al., 1985). The technique is very useful for discovering the temperature at which minerals form, the thermal history a rock has experienced, and the composition of the fluids that traversed a rock in its history. Microthermometry is based upon a careful observation and recognition of the

phase changes which take place within a fluid inclusion during heating or cooling stages. Moreover, a meaningful interpretation of microthermometric data requires that the time of trapping the inclusions represents a homogenous system (Shepherd et al., 1985).

CLSM is a new technique used to produce three dimensional images of single petroleum inclusions. Because the liquid petroleum strongly fluoresces under the laser, the liquid can be clearly distinguished from the vapour bubble within the petroleum inclusions. This will provide a more accurate measurement of liquid:vapour ratio within individual inclusions at room temperature. The liquid:vapour ratios obtained can be coupled with homogenisation temperatures and the chemical composition of an oil from the same reservoir using PVT software (VTFLINC) to determine the bulk composition, phase envelope, isochore, and physical properties of the included petroleum (for more details see section 2.2 in chapter 2).

Other methods involve the use of a variety of micro-spectroscopic techniques such as UV-epifluorescence (Bodnar, 1990; Guilhaumou et al., 1990), Infra Red Spectroscopy (Guilhaumou et al., 1990) , FT-IR (Pironon and Barrés, 1990 and 1992), and UV-fluorescence excitation emission spectroscopy (Khile, 1996). The problem with these techniques is that they do not provide a sufficiently detailed and accurate liquid:vapour ratios because of the irregular shape of the petroleum inclusions.

Destructive techniques consist of the crushing of the samples allowing the extraction of fluids within the inclusions and analyzing their contents using gas chromatography or gas chromatography-mass spectrometry (Horsfield and McLiman, 1987; Burrus, 1987, 1992; Karlsen et al., 1993; Macleod et al., 1994; Macleod et al., 1995; Bigge et al., 1995; Jones et al., 1996; and Jones et al., 2000).

1.7. Application of fluid inclusions in petroleum migration and reservoir filling studies

The applications of fluid inclusions to the study of petroleum systems have been carried out for many years (Burrus, 1981; Horsfield and McLimans, 1987; Narr and Burrus, 1984; Burrus et al., 1985; McLimans, 1987; Etminah and Hoffmann, 1989; Bodnar, 1990; Karlsen et al, 1993; Nedkvitne et al., 1993; Larter and Aplin, 1995; and Macleod et al., 1995; Parnell and Monson, 1996; George et al., 1997a and 1997b;

George et al., 1998a and 1998b; Bhullar et al., 1998; Munz et al., 1999 and Aplin et al., 1999). A number of methods have been used on petroleum and aqueous inclusions (e.g. microthermometry, CLSM), from which palaeo-conditions of fluid inclusion formation were obtained and used to better determine the petroleum generation and movement in sedimentary basins.

Fluid inclusions are applied to obtain the following information:

1.7.1. Palaeo-temperature and palaeo-pressure

So far, it is well established that in most cases, the temperature obtained by microthermometry of petroleum fluid inclusions corresponds to the minimum trapping temperature of petroleum. True trapping temperature can be determined when a co-existing aqueous inclusions or if the petroleum in the inclusion is known that it was trapped in the critical conditions. The homogenisation temperature of an aqueous inclusion (assuming that water is saturated with methane) is considered to be equivalent to the true trapping temperature of the inclusion (see chapters 2 and 6). Whereas the homogenisation temperature of a petroleum inclusions are strongly related to the chemical composition of the petroleum in the inclusion, which determines the phase behaviour of petroleum.

The determination of the true trapping temperature and pressure requires a known chemical composition of the included petroleum to be known or at least estimated from the chemical composition of the oil from the same reservoir. Thus, a phase envelope can be constructed on a P-T diagram and the isochore (line of equal density) can then be extended from the phase envelope and a vertical isochore from the homogenisation temperature of the correcting aqueous inclusion. The intersection of the two isochores (petroleum and aqueous) correspond to the point of true trapping temperature and pressure of the petroleum inclusion (Roedder and Bodnar, 1980).

1.7.2. Diagenesis, porosity and fluid evolution

Fluid inclusions microthermometry has been used previously to estimate the temperatures and thus times of cementations in clastic reservoirs (Hazeldine et al., 1984; McLimans, 1987; Jourdan et al., 1987; Glasmann et al., 1989; Burely et al., 1989; Walderhaug, 1990; Saigal and Bjolykke, 1992; Earnshaw et al., 1993, Karlsen et al., 1993; Nedkvitne et al., 1993; Worden et al., 1998). Fluid inclusions provide a

unique method of studying subsurface systems and evolution through time of the environmental and chemical conditions at the time of their formation. It is difficult to understand the physical, chemical and geological processes which have taken place in the past. But fluid inclusions can provide a "snapshot" of fluid history rather than using indirect extrapolations from conditions today. They can provide information on temperature of fluid entrapment, pore pressure and fluid chemistry evolution; which are essential for the understanding of the burial history, uplift and compositional evolution of subsurface fluids through time.

1.7.3. Composition of palaeo-fluids

During the last decade, a number of authors have used gas chromatography (GC) and gas chromatography-mass spectrometry (GCMS) for the determination of petroleum inclusion composition (Macleod et al., 1993; Karlsen et al., 1993; Nedkvitne et al., 1993; Bigge et al., 1994 and 1995; George et al., 1997a and 1997b; George et al., 1998a, b; Bhullar et al., 1999b, 2001; Isaksen et al., 1998; Jones and Macleod, 2000). Whereas, microthermometry of aqueous inclusions was used to determine the palaeo-salinity of water: wt% NaCl equivalent palaeo-salinity (Goldstein and Reynolds, 1994).

1.7.4. Petroleum migration and thermal history

Fluid inclusions provide one of the best records of petroleum migration history available, giving information about petroleum composition and the temperature and pressure conditions at which the inclusions were trapped. This information is derived from a combination of both petroleum and aqueous inclusions. Fluid inclusions analysed from reservoir rocks or from migration pathways offer a significant amount of information when their origin and formation is known in the paragenetic framework. In addition to providing an estimate of the temperature and pressure of the trap at the time of filling, compositional information can be obtained when the petroleum is analysed and fingerprinted; leading to a reconstruction of petroleum migration history.

Thermal history of a given sedimentary basin can be improved using fluid inclusions data when evaluating sedimentary sequences due to the paragenetic relationship to

mineral. This information when used is valuable for basin modelling packages leading to determine more realistic basin histories.

1.7.5. Palaeo-petroleum formation fluids

The origin of petroleum (within inclusions) in carrier beds, dry holes or reservoir units can be linked with microthermometry and thus used to model petroleum generation and migration in the subsurface. Using petroleum inclusions it is possible to determine changes in palaeo-GOR (gas to oil ratio) due to several trapping periods during diagenesis and microfracturing (Bigge, 2000). It is also possible to obtain biomarker source and maturity information using GC and GCMS techniques (see chapters 2 and 6). From this information PVT-X (pressure, volume, temperature and composition) information can be obtained as well as information on the trapping conditions (Roedder and Bodnar, 1980).

The integration of petroleum inclusion data can be used to enhance many aspects of our knowledge of petroleum systems. Petroleum inclusions can be used to interpret effective source rock facies in a basin and thus identify the maturity and timing of oil generation and migration distance of trapped oil. Other useful information which can be obtained are the total volume of generated oil, compared with the present reserves in the trap which can give the total volume of oil (petroleum) lost along carrier bed or dis-migration and the direction(s) of reservoir filling.

1.8. Thesis outline

Following this introduction, the analytical techniques used in this project are described in Chapter 2.

Chapter 3 presents an overview of the geological background of the Oued Mya-Hassi Messaoud petroleum system.

A description of the petroleum geochemistry of the Oued Mya-Hassi Messaoud petroleum system is provided in Chapter 4, which comprises a presentation of the geochemical evaluation of the source rocks as well as the crude oils trapped in the various accumulations across the petroleum system.

Chapter 5 describes the distribution of pyrrolic nitrogen compounds in both the Silurian and the Ordovician source rocks, and includes a discussion of the probable geochemical controls on the occurrence of these compounds in the source rock strata. Moreover, a detailed discussion is given of the possible charging directions of the Hassi Messaoud reservoirs and the other oil accumulations throughout the petroleum system, based on the integrated study of concentrations and relative distributions of pyrrolic nitrogen compounds, as well as biomarker and aromatic maturity parameters of the oils.

Chapter 6 presents a detailed discussion of petroleum inclusions in the Hassi Messaoud reservoirs, including microthermometry, PVTX as well as geochemical evaluation of the included palaeo-oil.

And finally, Chapter 7 presents a summary of the overall conclusions and suggestions for future work.

Chapter 2
Experimental and Methods

2. Experimental and Methods

The study covers four types of samples: dead crude oil samples collected from the well head, dead drill stem test oil (DST), reservoir core samples, and source rock core samples collected from Silurian (Tannezuft Formation) and Ordovician (El Gassi shale, El Azzel shale, Microconglomeratic shale, Oued Saret Formations) rocks which were suggested to be the main source for all the reserves discovered so far within the study area (Sonatrach unpublished reports; Daniel and Emme, 1995; Makhous et al., 1997a,b).

The oil samples analysed were:

* 70 oil samples from the Hassi Messaoud field;
* 2 oil samples from the Hassi Guettar satellite field;
* 1 oil sample from the Rhourde Chegga satellite field;
* 3 oil samples from El Gassi, Zotti, El Agreb fields (1 sample from each field);
* 11 oil samples from different fields within Oued Mya basin;
* 4 oil samples from Rhourde El Baguel and Mesdar fields (2 samples from each field), and
* 1 DST oil sample from well OL#2.

A total of 340 reservoir core samples were also taken on a 2 to 3 m scale (depending on the reservoir thickness and reservoir heterogeneity). These samples were collected from eight wells in Hassi Messaoud reservoirs Ra and R2; well OMM#33 (43 samples), well OMJ#41 (50 samples), well OML#712 (22 samples), well MD#213 (27 samples), well MD#141 (37 samples), well MD#319 (7 samples), well MD#177 (38 samples), and well OMO#712 (57 samples); one well in Benkahla -central Oued Mya basin well OKJ#202 (15 samples); one well from Hassi Guettar well HGA#1 (9 samples); and one well from El Gassi field well AR#62 (22 samples). Forty six source rock core samples (26 from the Silurian and 20 from the Ordovician) were also analysed. All of these source rock core samples have undergone all the geochemical analyses available in the laboratory.

2.1. Geochemical analysis methods

2.1.1. Soxhlet extraction of source rock core samples

Superficially cleaned and crushed source rock samples were extracted using a Soxhlet extraction apparatus. All cellulose extraction thimbles and cotton wool were pre-extracted in a Soxhlet for 24 hours using an azeotropic solvent mixture of DCM:MeOH (93:7). A weighed amount of the powdered shale samples (10 to 70 grams) were placed into pre-extracted cellulose thimbles. The cellulose thimbles, plugged with pre-extracted cotton wool, were then placed into the Soxhlet extraction apparatus. An azeotropic solvent mixture of DCM:MeOH (93:7) was used for the organic matter extraction. Activated copper turnings were added to the extraction flasks in order to remove any elemental sulphur from the extracts. The extraction was performed from 24 to 72 hours according to the richness of the samples.

2.1.2. Micro-extraction of reservoir core samples

Micro-extraction is a very fast extraction procedure for extracting a large suite of rock samples. This method was used for the extraction of the 340 reservoir rock samples. Three to four grams of finely crushed cleaned samples were mixed with a known volume of solvent (ca 5 ml of DCM:MeOH 93:7) in 10 ml vials, then sealed and sonicated for 15 minutes. The samples were placed in the fridge for 1-2 days and were shaken three times during that period. The extract was then taken directly out of the vials by syringe, i.e. 3 µl of extract is applied directly onto the Iatroscan chromatographic rods, avoiding the need for a concentration step.

2.1.3. Thin Layer Chromatography-Flame Ionisation Detection (TLC-FID) (Iatroscan)

Iatroscan calibration was achieved using oil sample OKP#88 taken from the Benkahla field located in the Oued Mya basin (Figure 3.1 in chapter 3). Separation of the oil sample OKP#88 into aliphatic hydrocarbons, aromatic hydrocarbons, resins and asphaltenes was performed using column chromatography on silica and alumina. First, the asphaltenes in 100 mg of oil sample were precipitated in an excess of hexane, left overnight in the fridge. The sample with an excess of hexane was centrifuged to allow the whole asphaltenes to be removed and weighed. The maltene fraction was then applied on to 50 cm chromatography column containing pre-cleaned silica and alumina. Aliphatic hydrocarbons were separated using 100 ml of petroleum

ether aromatic hydrocarbons were first eluted with a mixture of 100 ml of solvents petroleum ether:DCM (4:1) and then another 60 ml of toluene. Resins were elutted using 100 ml of DCM:methanol (1:1). The composition of oil OKP#88 obtained is displayed in Table 2.1.

Table 2.1 Composition based on weights of fractions of oil OKP#88 from Benkahla field used as standard for quantification of reservoir core extracts.

Fraction	Percentage
Aliphatic	71.6
Aromatic	23.6
Resin	3.6
Asphaltene	1.6

Combined thin layer chromatography (TLC) and flame ionisation detection (FID) of the Iatroscan TLC-FID instrument were used for geochemical screening of 340 core (selected from 7 wells in Hassi Messaoud) and 70 oil samples from the Hassi Messaoud and some satellite fields. The technique of TLC-FID offers a fast and relatively accurate method for quantifying aliphatic and aromatic hydrocarbons as well as non-hydrocarbons in rock extracts and crude oils (Karlsen and Larter, 1991). The principle of this technique involves the application of a small volume of sample (3 µl of solution of oil or rock extract) to chromatographic rods and development of the rods in a series of solvents to separate the various compound classes. Each separated fraction (aliphatics, aromatics, resins and asphaltenes) is then detected and quantified by moving the rod through a flame ionisation detector. Iatroscan analysis was carried out using an Iatroscan MK-5 analyser equipped with a flame ionisation detector (FID). Chromarod-S III silica rods were used. The results were collected and processed using Atlas software.

Directly before sample application to the rods, the rods were burned through the FID to eradicate any contaminants and achieve constant activity of the silica layer. A 3 µl aliquot of the supernatant extract or of the diluted oil sample (10 mg oil/10 ml DCM) was carefully applied dropwise from a 10 µl syringe onto chromarods. A volume of 3 µl of oil (OKP#88) with known percentages of aliphatic hydrocarbons, aromatic hydrocarbons, and resin and asphaltene fractions was also spotted onto separate chromarods within the same rack containing the rods spotted with the samples. The rods were then subsequently developed by stepwise elution in a series of solvents:

1 - Elution of the rod in *n*-hexane up to 100% of the silica-coated rod length (for approximately 25 minutes) then air-dried for 3 minutes.

2 - Elution in toluene up to 60% of the silica-coated rod length (for approximately 15 minutes) then air-dried for 6 minutes.

3 - Elution in freshly prepared DCM:MeOH (93:7; volume:volume) up to 30% of the silica-coated rod length.

The chromarods were dried in an oven at 60 °C for 90 seconds in order to remove residual solvent and were then analysed using the Iatroscan MK-5 instrument. The resulting four peaks in the chromatogram (e.g. Figure 2.1) correspond to the four separated fr60actions: aliphatic hydrocarbons, aromatic hydrocarbons, resins and asphaltenes.

The response factors were calculated for each fraction (aliphatic hydrocarbons, aromatic hydrocarbons, and resin and asphaltene fractions) in all the samples using the oil sample from Benkahla field (OKP#88) with a known bulk composition i.e. percentages of: aliphatic hydrocarbons, aromatic hydrocarbons, and resin and asphaltene fractions.

$$\text{Response factor (RF)} = \frac{\text{Area of standard}}{\text{Standard conc. x Volume standard solution applied onto rod (3 } \mu\text{l)}} \quad \text{.....(2.1)}$$

Standard conc. = % of individual fractions x concentration of oil OKP#88 x vol. of oil loaded (3 µl).

The concentration of each fraction in the reservoir core extracts and oils was quantified by the following formula:

$$\text{F (mg/g of rock)} = \frac{\text{Area F} \times \text{Vol. of solvent used (5ml)} \times 1000}{\text{RF std} \times \text{Rock (g)} \times \text{volume of sample loaded (3 } \mu\text{l)}} \quad \text{.....(2.2)}$$

Where,

F = Fraction to be quantified;
RF std = Response factor of the appropriate standard fraction; and
Rock (g) = Weight of extracted reservoir rock sample.

All of the samples were analysed in duplicate and the average value of the peak areas obtained was used in the calculation of the concentration of the component fractions in each sample.

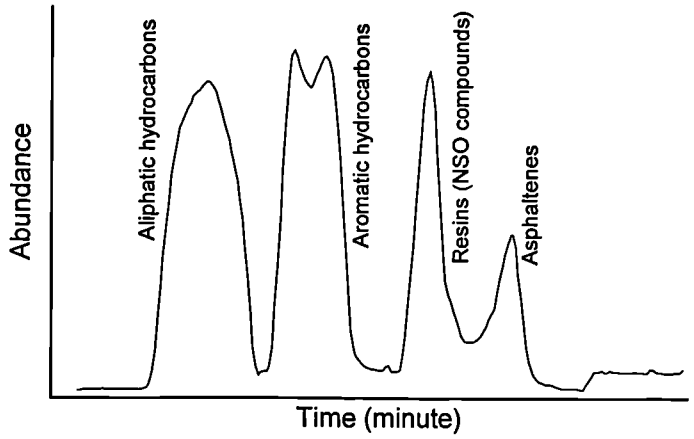

Figure 2.1 Iatroscan TLC-FID chromatogram showing the distribution of saturated hydrocarbons, aromatic hydrocarbons, resin, and asphaltene fractions in core extracted petroleum from Hassi Messaoud Field.

2.1.4. Isolation of polar compounds from petroleum using solid phase extraction (SPE)

Solid phase extraction is a simple preparation technique based on the principle of liquid-solid chromatography using commercially available cartridges packed with different sorbents. This technique offers many advantages compared to the traditional geochemical methods; it allows rapid analysis times (up to 30 samples per day), avoids cross-contamination of samples by minimising sample handling, and highly reduce the solvent consumption by up to 90% (Moors et al., 1994).

Before starting the solid phase extraction, mixtures of internal and external standards were prepared. The quantification of the alkylcarbazoles and benzocarbazoles was achieved by the N-phenylcarbazole internal standard. The N-phenylcarbazole standard was prepared at the concentration of 12.68 mg/100 ml of DCM.

Two different internal standards D6-phenol (2.90 mg/25ml of hexane:toluene 9:1) and 2-Naphthol (22.45 mg/100ml hexane:toluene 9:1), were used for alkylphenol recovery examination and quantification, respectively. Both standards were accurately prepared (in volumetric flasks). In addition, a mixture of alkylphenol standards (C_0 to C_3) was prepared separately in a 100 ml volumetric flask, and used for alkylphenols

identification and determination of individual response factors (Table 2.22). The standard solutions were stored in the fridge away from light (in foil-wrapped flasks).

Table 2.2 Concentration (mg/100 ml) of alkylphenol standards used for alkylphenol quantification in oil and source rock samples.

Compound	Quantity (mg/100 ml of DCM)
Phenol	11.6
O-Cresol	57.8
M-Cresol	21
P-Cresol	9.8
2-Ethyl P	21.9
2,5-DMP	15.5
2,4-DMP	70.8
2,6-DMP	28.3
3,5-DMP	5.9
4-Ethyl P	5.1
2,3-DMP	7.8
3,4-DMP	7.9
2-Propyl P	12.5
4-isopropyl P	27
2,4,6-TMP	22.7
2,3,5-TMP	17.7
2,3,6-TMP	8.7
3,4,5-TMP	2.6
3-isopropyl P	12.3

P= Phenol; O= ortho; M =meta; P= para; DMP= dimethylphenols; TMP= trimethylphenols.

2.1.4.1. Isolation of pyrrolic nitrogen compounds (alkylcarbazoles and benzocarbazoles) from petroleum

2.1.4.1.1. Oils

Figure 2.2 shows the methods developed for a rapid isolation of the alkylcarbazole enriched fraction from crude which was developed at Newcastle Research Group (Bennett et al., 1996; Larter et al., 1996a). Separation of oils was achieved using a C18 non-endcapped solid-phase extraction. The columns were conditioned with 3 ml of hexane and residual solvent removed with a gentle air flush. In general, 50 to 70 mg of samples of oil were cautiously transferred on the top frit of the cartridges using a Pasteur pipette. In cases where the sample has not been readily adsorbed into the sorbent after fixing the cartridges in the clamps, gentle positive (air) pressure was applied until the samples were adsorbed below the level of the top of the frit. Using a clean Pasteur pipette, half a millilitre of hexane was added to the cartridge to wash oil from the wall of the barrel and into the sorbent (thus insuring total sample transfer to the sorbent in a minimal volume charge). After allowing the solvent height to fall to the level of the frit, a second half millilitre aliquot of hexane was added and allowed

to elute throughout the column as above. The remaining volume of hexane (4 ml) was added in 2 x 2ml aliquots. At the end of hexane elution, a gentle air flush was applied to displace residual hexane from the sorbent bed, and the lower tip of the cartridge was washed with half millilitre of hexane using a Pasteur pipette.

The five millilitres of hexane eluate sampled in a 10 ml vial contained the following compounds:

Aliphatic hydrocarbons -including *n*-alkanes and biomarkers, Aromatic hydrocarbons: fluorenes, naphthalenes, phenanthrenes, mono- and tri-aromatic steroids, biphenyls, etc..., and Neutral non-hydrocarbons e.g. alkyldibenzofurans and alkylthiophenes.

The hexane fractions were kept in the fridge for further separations into aliphatic and aromatic hydrocarbons (see section 2.1.5 below).

The pyrrolic nitrogen compounds were eluted from the sorbent phase with 5 ml DCM. Half a millilitre (0.5 ml) of DCM was taken from 5 ml of DCM and cautiously added on to the top frit and lower walls of the cartridge, the solvent was allowed to elute to below the level of the top frit. Another half millilitre of DCM was added and allowed to elute through the column as above. Remaining 2x2 ml added DCM fraction was concentrated by evaporation under a stream of nitrogen prior to GCMS analysis.

2.1.4.1.2. Rock extracts

Reservoir and source rock bitumen samples were first passed through Florisil sorbent columns for removing the asphaltenes from the samples (Figure 2.2 b) prior to the fractionation described above. This additional preparation step was requested because asphaltenes precipitate during the initial hexane eluate step. Asphaltenes form a suspension in hexane and may be deposited onto the frits and sorbent of the cartridge. This may lead to restricted solvent flow, trapping aromatic and aliphatic hydrocarbons on the column and inevitably leading to poor separation and irreproducible results. In addition, asphaltene sorption modifies the properties of the SPE column. Asphaltenes are also soluble in DCM and are therefore eluted with the polar fraction causing problems with GC separation. Afterwards, 20 to 50 mg of deasphalted samples were transferred on the top frit of the SPE cartridges following the same procedure as normal oils.

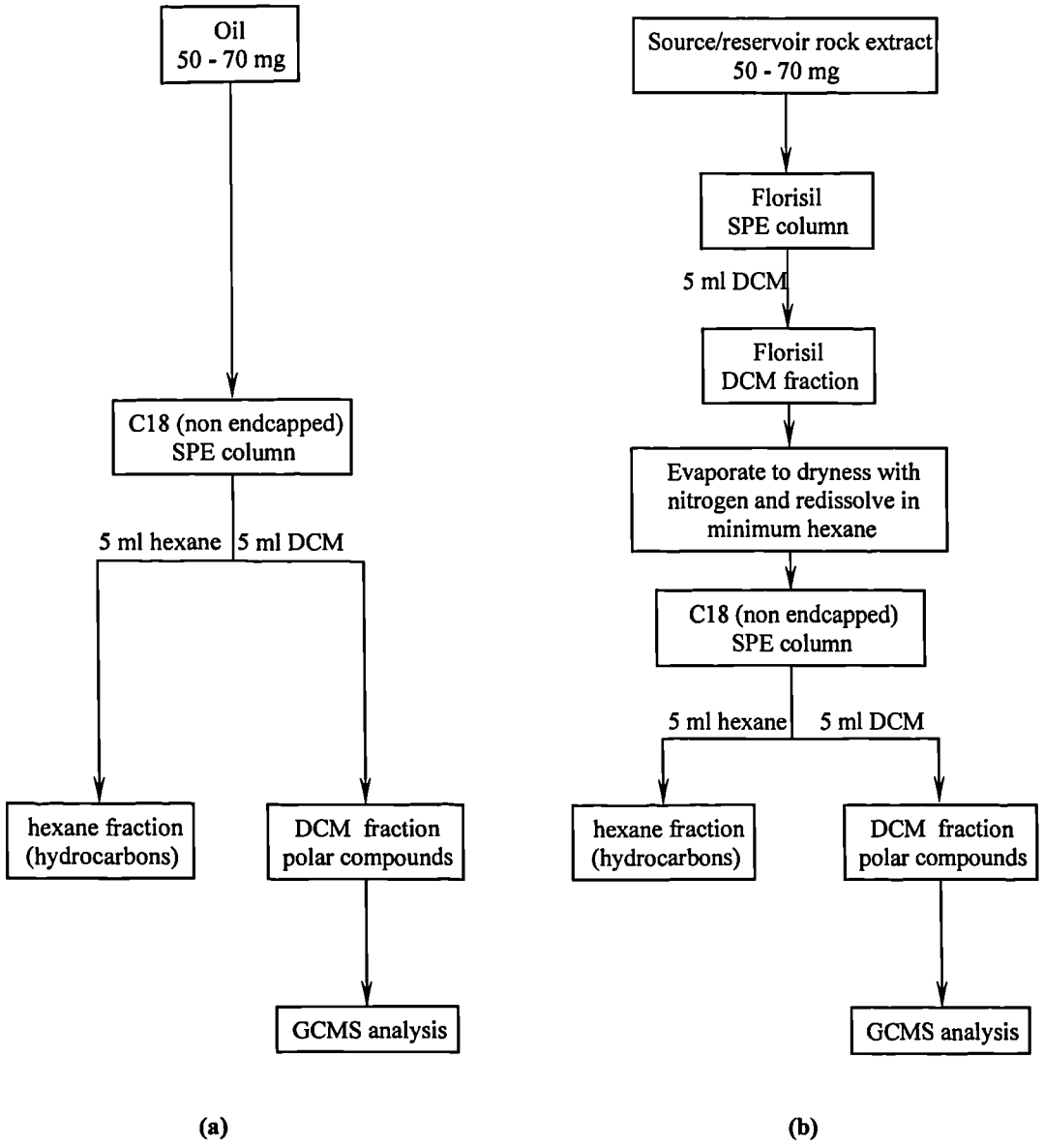

Figure 2.2 Schematic showing the methods for (a) the isolation of a polar rich fraction from crude oils (b) preferred method for high viscosity, high asphaltene oil, source rock and reservoir core extracts. (After Bennett et al., 1996).

2.1.4.2. Analysis of pyrrolic nitrogen compounds by GCMS

After volume reduction of DCM solvent to c. 100 µl, the samples were transferred to 150 µl tapered inserts in auto sampler vials and sealed. At this stage the samples are ready for GC-MS analysis.

Alkylcarbazoles and benzocarbazoles were analysed on a Hewlett Packard 6890 GC (split/splitless injection at 310 °C) coupled with a Hewlett Packard 5973 MSD. The acquisition was controlled by HP Chemstation software in selected ion mode (30 ions, 35 ms dwell time) for greater sensitivity. The sample (1 µl) was injected by a HP

6890 series auto-sampler and the split closed for 1 minute. After the solvent peak has passed the GC temperature program and the acquisition commenced. Separation was performed using (30m x 0.25mm x 0.25mm) HP-5, 5% phenyl methyl silicone stationary phase. The injector inlet temperature was 310 °C, and the gas chromatograph oven was first held at 40 °C for 3 minutes, programmed from 40 °C to 200 °C at 10 °C/min temperature ramp, then from 200 °C to 310 °C at 4 °C/min temperature ramp, and held at 300 °C for 14 minutes. Helium was used as carrier gas at a flow rate of 1ml/min and pressure of 50KPa.

The mass spectrometer was operated in selective ion monitoring (SIM) mode scanning for molecular ions for compounds of interest:

Compound	**Molecular Ion (M^+)**
Carbazole	m/z 167
C_1 alkylcarbazoles	m/z 181
C_2 alkylcarbazoles	m/z 195
C_3 alkylcarbazole	m/z 209
Benzocarbazoles	m/z 217
C_1 alkylbenzocarbazoles	m/z 231
C_2 alkylcarbazoles	m/z 245
N phenylcarbazole	m/z 243

The internal standard N phenylcarbazole (typically 0.653 μg) was added to the DCM fraction prior to GCMS analysis. The N phenylcarbazole was not added at the start of the separation procedure due to its less polar nature; therefore it was found to elute with the hydrocarbons in the hexane eluate.

Isomer distributions for C_0-C_2 alkylcarbazoles and benzocarbazoles were determined by identification based on Bowler et al. (1997) and comparison of retention characteristics with North Sea oil. Figure 2.3 shows molecular ion mass chromatograms of the distributions of C_0-C_2 alkylcarbazoles and benzocarbazoles from a SPE fraction isolated from a typical Silurian source rock sample. **Error! Reference source not found.** displays peak assignments for the m/z 167, 181, 195, 209, and 217 mass chromatograms of the carbazoles and benzocarbazoles.

The peak areas were then derived through integration of the appropriate peaks. The concentrations of individual compounds were calculated using the following formula, assuming a response factor of 1; this analysis is therefore only semi-quantitative:

$$C\ (\mu g/g\ \text{oil/extract}) = \left(\frac{1000}{Wt.S.}\right) x IS(\mu g) x \left(\frac{A_C}{A_{IS}}\right) \quad \text{.....(2.3)}$$

Where:

C = Compound to be quantified;
Wt S = weight in grams of the sample (oil or extract) applied to the SPE;
IS (μg) = weight of N-phenylcarbazole added to the pyrrolic nitrogen fractions;
A_C = peak area of the alkylcarbazole isomer;
A_{IS} = the peak area of the N-phenylcarbazole;

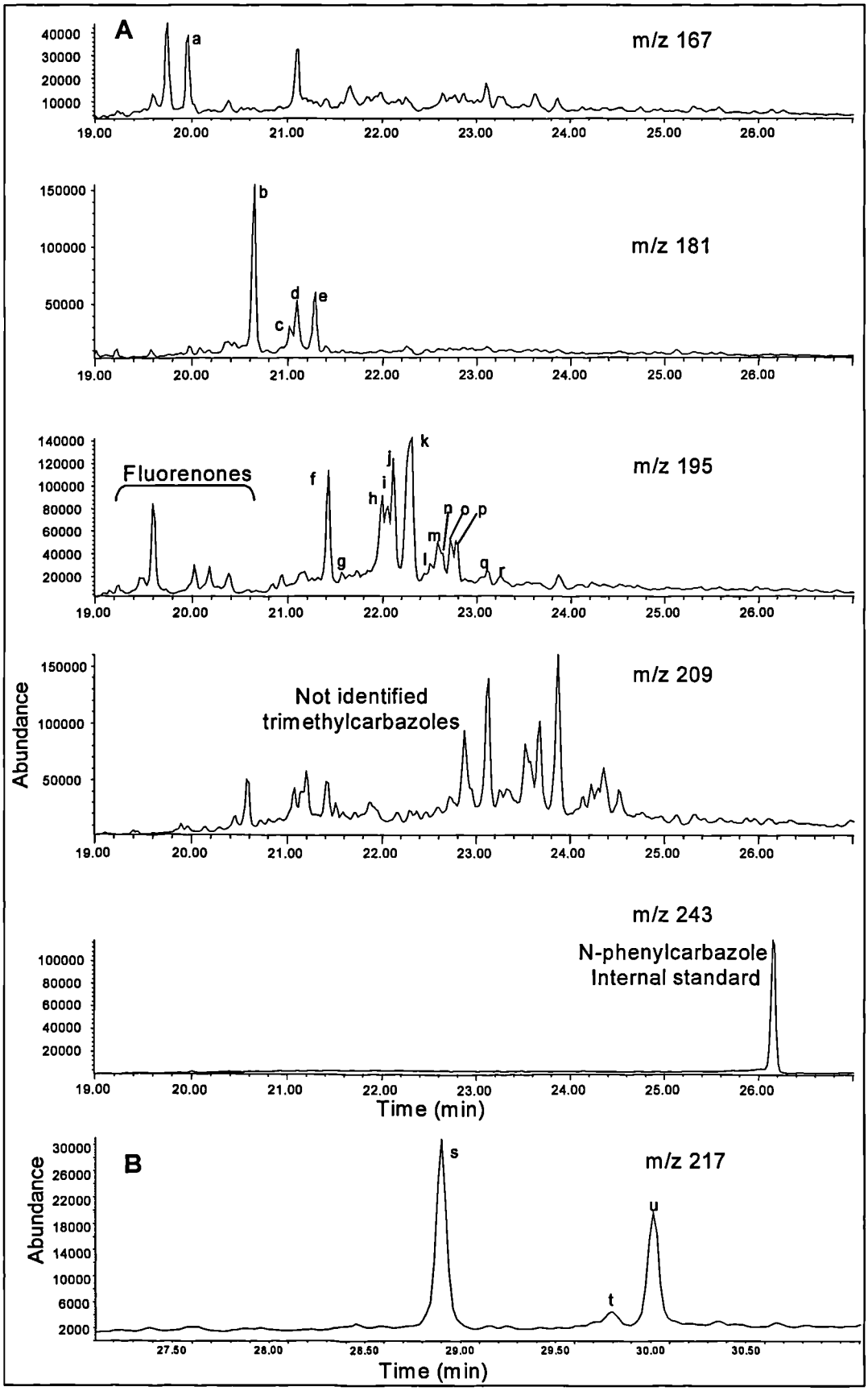

Figure 2.3 Partial m/z 167 + 181 + 195 + 209 + 217 mass chromatograms of (A) carbazoles and (B) benzocarbazoles in a typical Silurian source rock sample from Oued Mya basin. For peak assignments see Table 2.3.

Table 2.3 Peak assignments for the m/z 167, 181, 195, 209, and 217 mass chromatograms of the Carbazoles and benzocarbazoles.

Peak Identification	Compound Name
a	Carbazole
b	1-Methylcarbazole
c	3-Methylcarbazole
d	2-Methylcarbazole
e	4-Methylcarbazole
f	1,8-Dimethylcarbazole
g	1-Ethylcarbazole
h	1,3-Dimethylcarbazole
i	1,6-Dimethylcarbazole
j	1,7-Dimethylcarbazole
k	1,4- + 1,5-Dimethylcarbazoles + + 3- + 4-Ethylcarbazoles
l	2,6-Dimethylcarbazole
m	2,7-Dimethylcarbazole
n	1,2-Dimethylcarbazole
o	2,4-Dimethylcarbazole
p	2,5-Dimethylcarbazole
q	2,3-Dimethylcarbazole
r	3,4-Dimethylcarbazole
s	Benzo[a]carbazole
t	Benzo[b]carbazole
u	Benzo[c]carbazole

2.1.4.3. Isolation of alkylphenols from petroleum using SPE

C18 (non-endcapped) SPE columns were initially washed with 5 ml DCM and allowed to dry overnight on the top of an oven. The columns were then conditioned with 3 ml hexane and 50 to 70 mg of oil samples were cautiously transferred on the top frit of the cartridges using a Pasteur pipette as described for the pyrrolic compounds (section 2.4.1.1). 2 Naphthol (1.123 μg) and D_6 phenol (0.145 μg) were added in a hexane:toluene solution (9:1) to the SPE columns before the first elution with 5 ml hexane. The alkylphenol fraction was eluted with 5 ml DCM as described for the pyrrolic compounds. The DCM fractions collected were concentrated by gentle evaporation under nitrogen prior to GCMS analysis.

Important For alkylphenols analysis, it is essential that the sample (DCM fraction) is not allowed to become dry through complete evaporation of solvent. Phenol is volatile and will be lost if the sample is allowed to go to dryness, this may be indicated by the loss of D_6 phenol added as internal standard.

2.1.4.4. Derivatisation of alkylphenols

Alkylphenols are not amenable to gas chromatography analysis using common liquid phases such as HP-1, HP-5 or their equivalent. The phenolic hydroxyl group sorptively interacts with the gas chromatography column phase, leading to poor chromatography manifested as peak broadening and peak tailing. To get better chromatographic performance, alkylphenols are analysed as trimethylsilyl (TMS) derivatives obtained through derivatisation with N,O-Bis (trimethylsilyl) trifluoroacetamide (BSTFA). After volume reduction of the DCM fraction to c. 100-200 µl by evaporation, the samples were transferred to 3 ml vials. 50 µl of BSTFA were added to the samples and the vials were immediately sealed. Solutions were thoroughly mixed; the vials were then kept in an oven at 60 °C for at least one hour. During the silylation process, active hydrogen is replaced by a TMS group as shown in Figure 2.4.

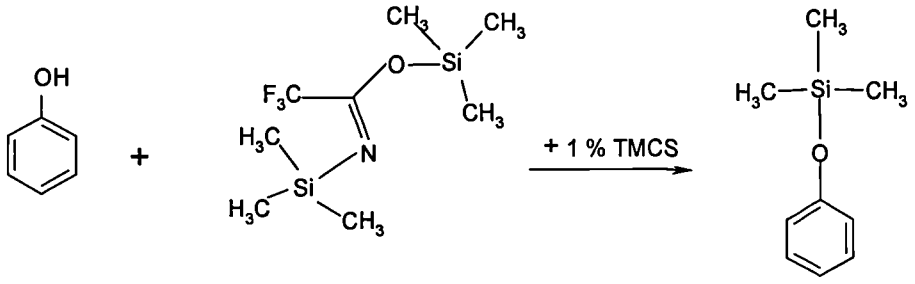

Figure 2.4 Derivatisation of phenol with BSTFA

2.1.4.5. Analysis of alkylphenols by GCMS

The TMS derivatised alkylphenols were analysed on a Hewlet Packard 6890 GC (split/splitless injection at 280 °C) coupled with a Hewlett Packard 5973 MSD. The acquisition was controlled by HP Chemstation software in selected ion mode (30 ions, 35 ms dwell time) for greater sensitivity. The sample (1 µl) was injected by a HP 6890 series auto-sampler. Separation was using a fused silica capillary column (30m x 0.25mm id x 0.25mm film thickness) coated with HP-5 (5% Phenyl Methyl Silicone) stationary phase as for the hydrocarbons. The gas chromatograph oven was first held at 35 °C for 10 minutes, programmed from 35 °C to 120 °C at 2 °C/min temperature ramp, then from 120 °C to 300 °C at 8 °C/min temperature ramp, and held at 300 °C for 5 minutes. Helium was used as carrier gas at a flow rate of 1ml/min and head

pressure of 25 kPa. The mass spectrometer was operated in selective ion monitoring (SIM) mode scanning for molecular ions for compounds of interest:

TMS derivatised Compound	**Molecular Ion (M^+)**	**Fragment ion $(M-15)^+$**
C_0 alkylphenol	m/z 166	m/z 151
C_1 alkylcarbazoles	m/z 180	m/z 165
C_2 alkylcarbazoles	m/z 194	m/z 179
C_3 alkylcarbazole	m/z 208	m/z 193
2 Naphthol	m/z 216	m/z 201
D_6 phenol	m/z 166	m/z 151

2.1.4.6. Identification and quantification of alkylphenols

Isomer distributions for C_0-C_3 alkylphenols were determined by comparison of retention time of authentic standards. Molecular ion mass chromatograms of the identified TMS-alkylphenols of Hassi Messaoud oil are shown in Figure 2.5. The peak areas were then derived through integration of the appropriate phenol/alkylphenol peaks. The concentrations of the compounds in the samples were then calculated using the formula:

$$\text{C p}\,(\mu\text{g/g oil}) = \left(\frac{1000}{Wt.oil.}\right) x IS(\mu g) x \left(\frac{A_p}{A_{IS}}\right) \quad \text{.....(2.4)}$$

Where:

C_P = the calculated concentration of phenol;
A_P = peak area of phenol;
A_{IS} = peak area of 2-naphtol;
IS = weight (μg) of 2-naphtol added in the sample; and
Wt oil = weigh (mg) of oil sample added to the SPE.

This method of calculating concentrations makes the assumption that the fragmentation response of the phenols is the same as that of the internal standard (i.e. RRF = 1). The calculation of the concentration of phenols needs the integration of the relative response factor (RRF) for each compound within the sample. Hence the new formula used was:

$$RRF = \left(\frac{C_{IS}(\mu g)}{A_{IS}.}\right) x \left(\frac{A_p}{C_p}\right) \quad \text{.....(2.5)}$$

Where:

RRF_P = Relative response factor for TMS derivatised alkylphenol isomer;
C_{IS} = weight (μg) of 2-Naphtol added to the standards mixture,
A_{IS} = area of 2-Naphthol added to the standards mixture,
A_P = Peak area of alkylphenol isomer;
C_P = concentration of the alkylphenol (μg) added to the standards mixture.

Equation 2.5 provides a response factor value for each of the 20 TMS-alkylphenols in the standard mixture. These response factors are applied to the values calculated from equation 2.4 to determine the actual concentrations for individual TMS-alkylphenol isomers in oil samples:

$$CactofP(\mu g / goil) = \frac{Cp}{RRF} \quad \text{.....(2.6)}$$

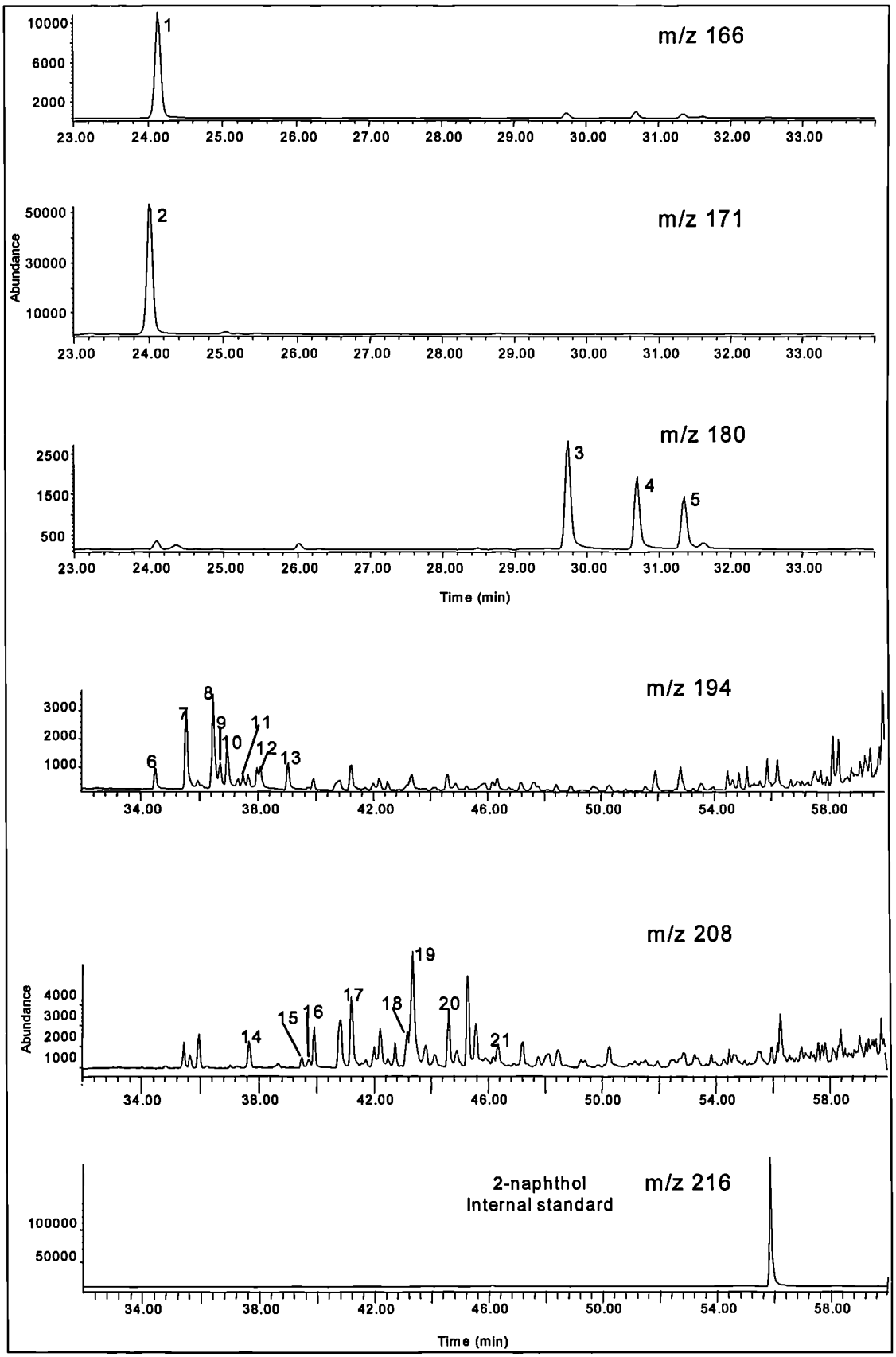

Figure 2.5 Partial m/z 166 + 180 + 194 + 208 mass chromatograms showing the distribution of C_0-C_3 phenols in a typical oil sample from Triassic fields in Oued Mya basin. Peak assignments are given in Table 2.4.

Table 2.4 Peak assignments for the m/z 166, 171, 180, 194, and 208 mass chromatograms of the alkylphenol compounds.

Peak Identification	Compound Name
1	Phenol
2	D6-Phenol
3	Ortho-cresol
4	Meta-cresol
5	Para-cresol
6	2-Ethylphenol
7	2,5-Dimethylphenol
8	2,4-Dimethylphenol
9	3,5-Dimethylphenol
10	2,6-Dimethylphenol
11	4-Ethylphenol
12	2,3-Dimethylphenol
13	3,4-Dimethylphenol
14	2-Isopropylphenol
15	2-Propylphenol
16	3-Isopropylphenol
17	4-Isopropylphenol
18	2,4,6- Trimethylphenol
19	2,3,5-Trimethylphenol
20	2,3,6-Trimethylphenol
21	2,3,6-Trimethylphenol

2.1.5. Separation of aliphatic and aromatic hydrocarbons using silver nitrate impregnated silica solid-phase extraction

2.1.5.1. Column preparation

This method was developed at NRG (Newcastle University) by Bennett and Larter (2000). To make 40 solid phase extraction (SPE) columns, 30 g of Kiesel gel (60G) were weighed into a conical flask containing 60 ml of distilled water and 3 grams of silver nitrate. The mixture was thoroughly shaken, covered with foil, and left in a drying oven until completely dry (up to 1 week). Then, the columns were prepared by taking approximately 550 mg of the silica which was added to the individual empty SPE cartridge barrels, and carefully compacted using a glass rod. The prepared columns were cleaned with 5 ml of hexane, using a positive air pressure to flush the solvent through the columns.

2.1.5.2. Sample addition

The hydrocarbon fractions (hexane fraction) obtained from the C18 (non-endcapped) solid phase extraction in section 2.1.4.1 isolated from the crude oil, source rock and reservoir core samples were evaporated to 1 ml (1000 μl). Ten microlitres (10 μl) of

standards solution containing a mixture of 1,1-binaphthyl (10.1 mg) and squalane (53.7 mg) prepared in 25 ml of hexane used to quantify the aromatic and *n*-alkane hydrocarbons, respectively and 10µl of D_4 cholestane prepared at 1.33 mg/25 ml hexane used to quantify the biomarker alkanes, were added to the solution containing aliphatic and aromatic hydrocarbons. Then 100 µl of the solution (containing aliphatic and aromatic hydrocarbons with the appropriate internal standards) were removed using a syringe and carefully added to the Ag^+ impregnated silica columns. First, the frit and barrel wall of the column were washed by 0.5 ml of hexane taken from 2 ml hexane. Second, the remaining volume of hexane (1.5 ml) was added to the column. At the end a gentle air flush was applied in order to remove the remaining hexane in the column and the bottom tip of the column was cleaned with 0.5 ml of hexane. The fractions collected contain aliphatic hydrocarbons (*n*-alkanes, isoprenoid alkanes and biomarkers). The aromatic fractions were extracted from the columns using 4 ml of DCM and collected in separate vials.

2.1.6. Gas Chromatography (GC) of the crude oils and the aliphatic hydrocarbon fractions of the source rock and reservoir core samples

The whole oil samples and the hydrocarbon fractions obtained from the C18 non endcapped solid phase extraction of the source rock and reservoir core extract samples were analysed on a Fisons (Carlo Erba) Gas Chromatograph 8000 series equipped with automatic injection. Samples were analysed on a fused silica capillary column, HP-5 (5% polar methyl silicone stationary phase), film thickness 0.25 mm, 30 m x 0.25 mm internal diameter. The gas chromatograph oven was first held at 50 °C for 2 minutes, then temperature programmed from 50 °C to 300 °C at 4 °C per minute, and then held at 300 °C for 20 minutes. The carrier gas was hydrogen with a flow rate of 1 ml/min at 50 kPa column head pressure.

Quantification of the *n*-alkanes and isoprenoid alkanes was achieved using squalane as internal standard. The concentration of individual compounds is given by the following formula:

$$X\,(\mu g/g\ \text{oil, extract}) = \left(\frac{1000}{Wt.oil.}\right) x C_{IS}\,(\mu g)\, x \left(\frac{A_x}{A_{IS}}\right) \quad \text{.....(2.7)}$$

Where,

X = concentration of *n*-alkanes (μg/g of oil or extract);
Woil/ext = weight of oil or extract sample in mg;
C_{IS} = concentration (μg) of the internal standard (squalane) added to the sample,
A_X = peak area of the *n*-alkane; and
A_{IS} = peak area of the internal standard (squalane).

2.1.7. Gas Chromatography-Mass Spectrometry (GC-MS)

GC-MS analyses of the aliphatic and aromatic hydrocarbons obtained from all the different sample sets (oils, source rock core extracts, and reservoir core extracts) were carried out using a Hewlett-Packard 6890 gas chromatograph fitted with split/splitless injector (280°C) and interfaced to an HP 5973 Mass Selective Detector (electron voltage 70 eV, source temperature 230 °C, interface temperature 310 °C). Separation was performed on an HP-5 fused silica capillary column (phenyl-methyl silicone stationary phase; 30m long, 0.25mm internal diameter, and 0.25mm film thickness). Helium was used as carrier gas at a flow rate of 1ml/min and column pressure of 51.1 kPa. The mass spectrometer was operated in selective ion monitoring (SIM) mode for both fractions as well as full scan mode for a limited number of aliphatic and aromatic hydrocarbon fractions.

A fast heat temperature program was used to analyse the biomarkers (steranes and tricyclic terpanes and hopanes). The temperature used was 40 °C to 175 °C at 10 °C/min, then 175 °C to 225 °C at 6°C/min, then 225 °C to 300 °C at 4 °C/min, and finally the temperature was held at 300 °C for 20 minutes. However a slow heating rate temperature program was used in the case of aromatic compounds. The oven temperature was first held at 40 °C for 5 minutes and then programmed from 40 °C to 300 °C with a 4 °C/min temperature ramp, the oven then held at 300 °C for 20 minutes.

Concentrations of individual steranes and tricyclic terpanes and hopanes were achieved by comparing the peak area of the appropriate compounds relative to D_4-cholestane internal standard. Aromatic hydrocarbons including aromatic steroid hydrocarbons and heterocyclic sulphur compounds (alkylthiophenes) were quantified using 1,1'-binaphthyl (m/z 253) as surrogate standard.

The concentrations of biomarkers and aromatic compounds were calculated as follows:

$$X_{b(a)}\ (\mu g/g\ \text{oil, extract}) = \left(\frac{1000}{Wt.oil/extract}\right) x C_{IS}\ (\mu g) x \left(\frac{A_{b(a)}}{A_{IS}}\right) \quad \text{.....(2.8)}$$

Where, $X_{b(a)}$ = concentration (μg/g of oil or extract) of the compound to be quantified (biomarker or aromatic hydrocarbon);

Woil/extract = weight in mg of oil or rock extract taken for analysis;

C_{IS} = concentration in μg of surrogate standard added to the sample (D4 cholestane for biomarker alkanes and 1,1-bynaphthyl for aromatic hydrocarbons);

$A_{b(a)}$ = area of biomarker or aromatic hydrocarbon;

A_{IS} = area of D4 cholestane or 1,1-bynaphthyl.

Note that quantitative values were not corrected for differences in mass spectral response between the various compounds and the corresponding standards. The concentrations reported in this study are therefore semi-quantitative.

2.2. Fluid inclusions

Measurements of homogenisation temperatures and inclusion vapour/liquid ratios were made on reservoir sandstone samples using microscopes equipped with a heating stage and Confocal Laser Scanning Microscope (CLSM), respectively. The samples were collected from a number of wells in the Hassi Messaoud and Haoud Berkaoui fields. A list of the wells, sample depths, formations and the numbers and types of analyses is shown in Table 2.5. Reservoir core samples with relatively high petroleum yields (from Ra and R2 units) based on the data obtained from the Iatroscan screening were selected for fluid inclusion analysis.

Thin section wafers made from cleaned sand grains impregnated with non fluorescing epoxy and polished on both sides were used for microthermometry and CLSM. The nature of inclusion fluids was determined by inspection under a combination of transmitted plane polarised light and incident UV light under the microscope. The petroleum inclusions can be distinguished as they fluoresce under UV light whereas aqueous inclusions do not (Murray, 1957; Burrus, 1981). Petroleum inclusion assemblages (FIA) were sought and then highlighted using a marker pen to facilitate their detection later for further analysis (i.e. for microthermometry and CLSM). By definition an FIA is a group of petroleum and aqueous inclusions that is related temporally and spatially.

Table 2.5 List of the samples selected for fluid inclusion analysis.

Well	Number of samples	Depth (m)	Field	Reservoir	Reservoir unit	Microthermometry Petroleum	Microthermometry Aqueous	CLSM	GC	GC-MS
		3291.35		Cambrian	Ra					
MD#177	4	3324.5	Hassi	Cambrian	Ra	260	38	9	2	2
		3339.5	Messaoud	Cambrian	Inter-zones					
		3379.9		Cambrian	R2					
		3324.9		Cambrian	Ra					
OMO#712	4	3345.6	Hassi	Cambrian	Ra	218	27	3	1	1
		3378.5	Messaoud	Cambrian	R2					
		3387.65		Cambrian	R2					
		3451.6	Hassi	Cambrian	Ra					
MD#213	3	3468.15	Messaoud	Cambrian	Ra	131	24	3	1	1
		3499.5		Cambrian	Ra					
OML#712	2	3426.95	Hassi	Cambrian	R2	106	13	-	1	1
		3437.45	Messaoud	Cambrian	R2					
OMJ#41	2	3390.1	Hassi	Cambrian	Ra	15	-	-	-	-
		3463.5	Messaoud	Cambrian	R2					
		3413.75		Cambrian	Ra					
OMM#3	4	3464.5	Hassi	Cambrian	Ra	22	2	-	-	-
		3476.85	Messaoud	Cambrian	Ra					
		3483.75		Cambrian	Ra					
MD#319	1	3453.25	Hassi Messaoud	Cambrian	Ra	23	9	2	-	-
MD#141	2	3438.65	Hassi	Cambrian		49	7	3	1	1
		3450.4	Messaoud	Cambrian	Ra					
OKJ#202	1	3327.5	Haoud Berkaoui	Triassic	Lower Triassic	31	1	-	1	1
Total	23					855	121	20	7	7

The minimum trapping temperature of single included petroleums can be directly determined. This is the temperature at which the fluid inclusion homogenises into a single phase upon heating in the laboratory. In contrast, the minimum trapping pressure cannot be measured directly and can only be estimated if the P-T phase diagram of the included petroleum can be defined. Constructing the P-T phase diagram of petroleum requires that the composition of the included petroleum is known. The composition of petroleum is routinely estimated using a variety of direct methods such as crushing inclusions and analysing their contents using gas chromatography or gas chromatograph-mass spectrometry (Burrus, 1987, 1992; Karlsen et al., 1993; Macleod et al., 1994; Bigge et al., 1995; Jones and Macleod, 2000) or estimated using a variety of micro-spectroscopic techniques e.g. UV-epifluorescence (Bodnar, 1990; Guilhaumou et al., 1990), Infra Red Spectroscopy (Guilhaumou et al., 1990), FT-IR (Pironon and Barrès, 1990, 1992), and UV-fluorescence excitation emission spectroscopy (Kihle, 1996). However these techniques do not provide full boiling-range composition so they do not allow accurate PVT modelling of the included petroleum.

Aplin et al. (1999) have developed a new approach to determine the composition of petroleum in single inclusions and to derive the PVT properties of petroleum inclusions. The approach is basically the same as described by Roedder and Bodnar (1980) which describes that the minimum trapping pressure can be determined if the

pressure-temperature phase diagram and isochores of petroleums in individual inclusions can be constructed. From this phase diagram, the true trapping temperature and pressure is the point where isochores of coexisting petroleum and aqueous inclusions intersect (Figure 2.6).

For this purpose, three pieces of information are needed:

1. the homogenisation temperature of single petroleum inclusions and coexisting aqueous inclusions determined by microthermometry,

2. the volume percentage of the liquid and vapour phases in the petroleum inclusions determined using Confocal Laser Scanning Microscopy (CLSM),

3. the detailed composition from methane (C_1) of the included petroleum.

Accurate composition of the included petroleum is difficult to determine directly since there is no way of extracting and analysing petroleum from a single inclusion. Aplin et al. (1999) proposed an indirect method using iterative series of PVT calculations, using the VTFLINK PVT package trying to match two parameters: 1) the molar volume of the petroleum at room and homogenisation temperature; 2) the liquid:vapour ratio of the inclusion obtained by CLSM at room temperature. To derive an initial fluid for modelling, Aplin et al. (1999) proposed to use detailed composition of an oil preferably from the same reservoir and genetically related to the petroleum trapped in the inclusion or at least a composition which accurately mimics the petroleum's physical properties.

Finally, the three pieces of information are used in association with the commercially available simulator of petroleum phase behaviour (i.e. VTFLINK) to determine P-T phase diagrams, trapping pressure and temperature, saturation pressure, gas:oil ratio (GOR at STP conditions of 15 °C and 1 bar), isochores, viscosity, density and the composition of the petroleum trapped within individual inclusions (see below for more details).

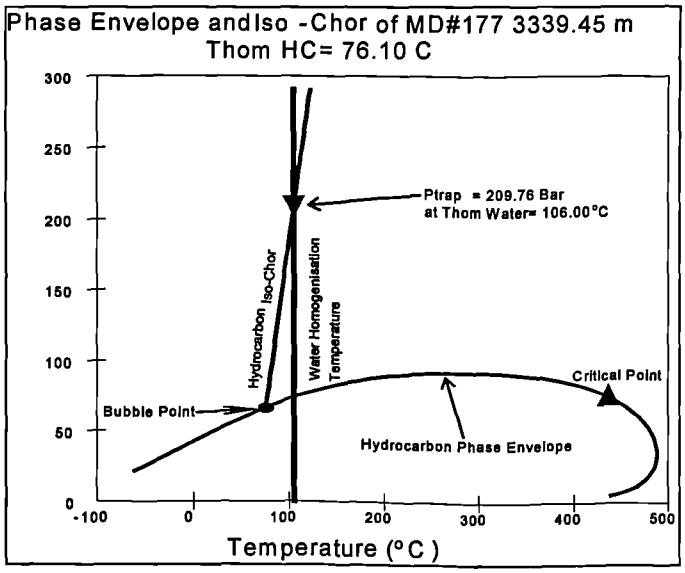

Figure 2.6 Intersecting isochore technique for coexisting petroleum and aqueous inclusions analysed in sample MD#177 (3339.45m). The intersection of petroleum and aqueous isochores provide the true trapping pressure and temperature of the included petroleum. (After Roedder and Bodnar, 1980).

2.2.1. Determination of homogenisation temperatures of petroleum and coexisting aqueous inclusions using microthermometry

Microthermometry analysis of petroleum and aqueous inclusions follows the general procedure outlined by Shepherd et al. (1985). In the subsurface, petroleum and aqueous inclusions in diagenetic cements and detrital grains are most likely to trap as a single phase.

The determination of temperatures of phase changes within fluid inclusions during heating and cooling of samples is termed microthermometry. Microthermometric analysis is unquestionably the most popular and extensively used non-destructive analytical technique (Shepherd et al., 1985). The technique is very useful for discovering the temperature at which minerals form, the thermal history a rock has experienced, and the composition of the fluids that traversed a rock. Microthermometry is based upon a careful observation and recognition of the phase changes which take place within a fluid inclusion during heating or cooling on a heating and cooling stage. Moreover, a meaningful interpretation of microthermometric data requires that the time of trapping the inclusions represent a homogenous system (Shepherd et al., 1985).

2.2.1.1. Principle of microthermometry technique

Consider that a sandstone containing single phase, liquid petroleum fluid inclusions formed in the subsurface at reservoir conditions of temperature and pressure (point A Tt and Pt in Figure 2.7). When the sample is brought to the surface, it cools to room conditions. Assuming that the volume of fluid inclusions remained constant; the density and the molar volume of fluid inclusion content remain constant as the pressure and temperature conditions change. During cooling, the pressure-temperature (P-T) conditions within the inclusion are thus constrained to fall along an isochore, line A-B in Figure 2.7 (line of constant density and molar volume). At the intersection of the isochore line and the phase envelope, point B, the first bubble of gas is exsolved from the fluid. This point is known as the "bubble point". If the cooling continues, more vapour continues to be exsolved from the liquid phase resulting in an increase of vapour:liquid ratio of the inclusion. Finally, at room conditions (point C), the fluid inclusion is a two phase (liquid + vapour) system and its temperature is that of the room but its pressure is higher than atmospheric pressure.

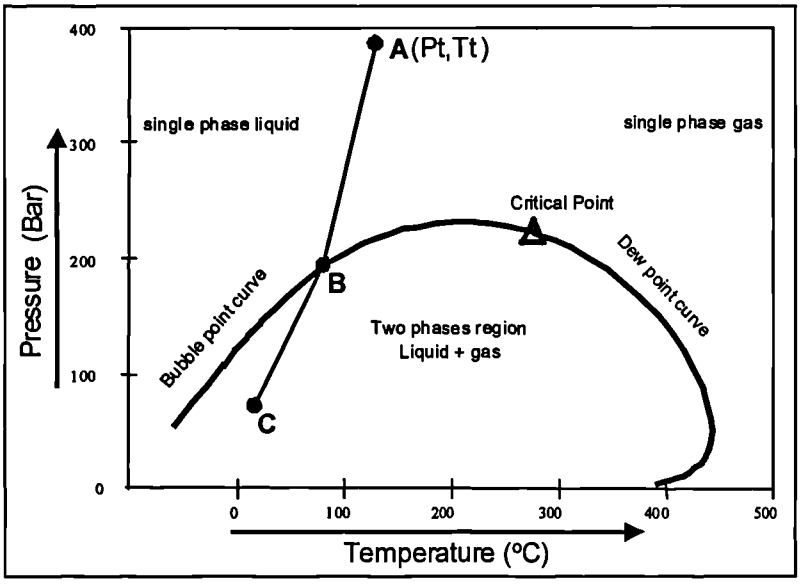

Figure 2.7 Phase diagram of hydrocarbon mixtures

In the laboratory, the natural cooling process undergone by the fluid inclusion (line A-B-C Figure 2.7) can be reversed by heating the sample under observation with a microscope. During this operation (heating of the fluid inclusion in the laboratory), the inclusion will follow the same path C-B-A. As at point C, the inclusion is in two phases, the bubble will gradually shrink (decrease in size) along the line C-B, and at point B (intersection with the bubble point/dew point curve) the bubble will

completely disappear, therefore the inclusion becomes homogeneous. The temperature at point B is known as the homogenisation temperature (Th), which is also known as the saturation temperature and pressure of the petroleum in the fluid inclusion. An oil inclusion will homogenise to a liquid, whereas a gas or gas-condensate inclusion will homogenise to a critical or single phase gaseous phase, and a water filled inclusion will homogenise to a water phase. This phase-change temperature is the most important in the technique of fluid inclusion microthermometry, as it provides an estimate of the trapping temperature of the fluid inclusion.

The double polished wafer was mounted on a conventional stage, with micrometer drive for the 'x' and 'y' axes. An Olympus BX60 tri-nocular microscope was used, fitted with 10x eye pieces, and 10x, 20x, 50x long working distance air objectives, giving 100x, 200x, and 500x magnification. The left eye piece is fitted with a calibrated graticule. Actual dimension calibration for each objective was conducted using a standard calibrated scale slide, which was placed on the stage. Calibration accuracy was $^{+}/_{-}$ 1μm. This calibration allowed reasonably precise measurements to be made of fluid inclusions. The BX60 microscope is fitted with a UV lamp attachment; the excitation filter wavelength band width is 300-385 nm, and the barrier filter used was 420 nm. Polarising filters were fitted below the stage and above the objectives. With both polarisers in place, it was possible to identify grain types, and to help discriminate detrital grains from diagenetic overgrowth, or indeed to discriminate the junction of two grains in solid solution contact.

Fluid inclusions recorded were highly variable in size, ranging from 4 to 60 μm in the longest dimension. In transmitted white light, under the microscope, all fluid inclusions appear transparent and colourless. UV light is used to determine which inclusions contain petroleum. Under UV excitation, petroleum is stimulated to emit light in the visible spectrum. The light emission is from the aromatic ring compounds. The colour was blue in most instances, with very occasional pale blue inclusions.

Measurements of homogenisation temperatures of both petroleum and aqueous inclusions were made with a Linkam THMSG 600 heating/cooling stage, attached to a Linkam TMS 94 control unit. Each FIA was located and observed with a combination of both reflected UV and transmitted white light.

Homogenisation of inclusions was observed with a Nikon 50X long working distance objective. During the measurements, the heating rates of 20 °C/min were used until homogenisation was imminent. At this stage the vapour bubbles usually became mobile, moving randomly inside the inclusion. When the bubbles became highly mobile, the heating rate was reduced to 5 °C/min. To determine the homogenisation temperature, a cycling procedure was used; when it was considered that the bubble had disappeared, or at least was no longer visible, the temperature was reduced until it was visible again (Goldstein and Reynolds, 1994). The cycling procedure was repeated until it was clear that the bubble no longer re-appeared. The principal is that after significant cooling, the bubble "pops" back in to view, and usually fairly large and therefore obvious. In a true FIA, homogenisation temperatures of individual inclusions should be within 10-15 °C, if temperatures are seen to be outside of this range, it could be that the assemblage is not a true FIA, or that necking down has occurred.

Very precise homogenisation temperature measurements of aqueous inclusions were, in many instances, difficult to obtain. This is because the vapour phase (bubble) in the aqueous inclusions frequently attaches to the mineral wall before homogenisation, and false optical effects at the inclusion wall made perfect readings tricky on minute inclusions. This was not a problem for the petroleum inclusions because here the vapour phase always remained in the central part of the inclusion, where the image was generally good.

2.2.2. Determination of the liquid:vapour ratio using Confocal Laser Scanning Microscope

Simple 2D observation of petroleum inclusions cannot usually assess the liquid:vapour ratio due to the different shapes of petroleum inclusions. Confocal Laser Scanning Microscopy was used in this project to precisely determine the liquid:vapour ratio of the petroleum inclusions.

The fundamental principles and application of the Confocal Laser Scanning Microscopy (CLSM) are described in detail by Sheppard and Shotton (1997). The CLSM offers the ability to generate three-dimensional images of thick specimens; therefore, the CLSM is used to determine the exact volumetric liquid:vapour ratio of

petroleum inclusions (Macleod et al., 1996; Aplin et al., 1999). This information is valuable for accurate PVT modelling of the included petroleum.

CLSM is an optical sectioning procedure generating images free from out-of-focus blur. It is a light microscopy technique and universally employs visible wavelength lasers as light sources and confocal apertures or 'pinholes' in the detection path (Figure 2.8). Confocal denotes that together the illumination focal volume and the detection focal volume are coincident. This optical constraint ensures that light from outside the focal region does not reach the detector. In the Confocal imaging system, only light reflected back from that particular and very narrow focal plane is selected. Light from other depths is blocked from view by a pinhole between the sample and the photo detector. Since the Confocal Microscope delivers a point image, a two-dimensional x-y image slice of the specimen is built up by rapidly scanning the specimen using galvanometer-driven mirrors. A pseudo-3D-image is obtained by taking a series of Confocal images at successive layers down through the specimen (a 'z' series, see Figure 2.9). Each image is digitised and stored in a computer and then superimposed to provide a pseudo-3D-images of the sample (e.g. fluid inclusion).

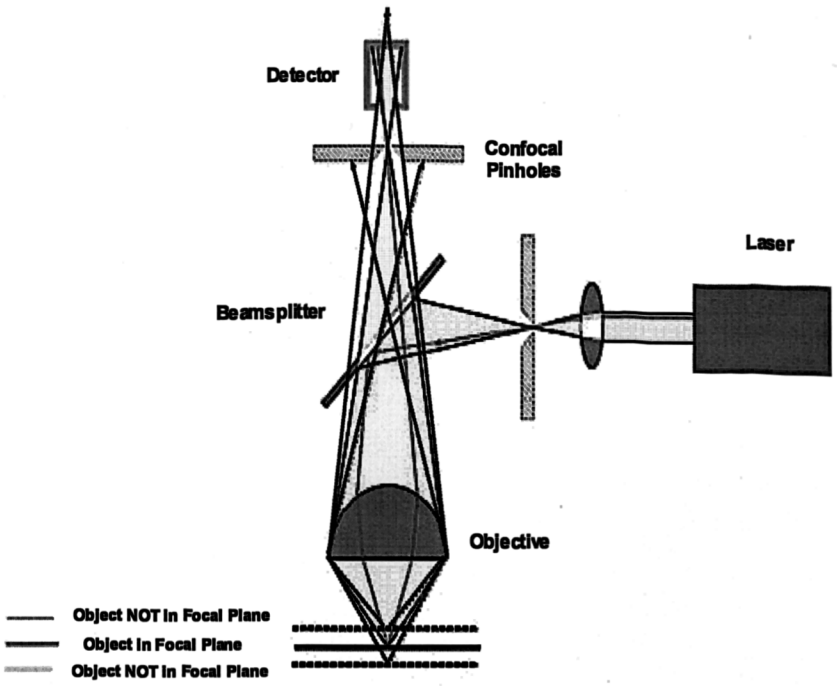

Figure 2.8 The basic principle of a Confocal microscope. (After Leica, http//www.llt.de/conprin.html).

In this project, doubly polished wafers of reservoir rocks previously used for microthermometry, were studied on the CLSM under oil immersion with a x60

magnification lens. For the CLSM analysis, only petroleum inclusions with the largest sizes were selected from fluid inclusion assemblages (FIAs) which show consistent homogenisation temperatures falling within the range of ±15°C as they were considered unalterated since entrapment. Furthermore, it is essential that only inclusions with static vapour bubbles were used, as moving bubbles would result in invalid data due to distortion during scanning.

A Leica TCS SP2 UV Laser Scanning Confocal Microscope (CLSM) attached to a Leica MS2 Confocal laser unit was used. The CLSM is controlled by a microcomputer running the commercial LCS 2.00.770 Confocal software; this software is also used for the analysis of the resulting images. The Argon (Ar) laser produced excitation at 488 nm with K1 and K2 filters. The petroleum within inclusions fluoresces brightly when excited at this wavelength, emitting strongly in regions around 520 nm and allowing the differentiation of liquid and vapour parts of the inclusion. The computer controlled stage is used to locate the top and the bottom of the inclusion by visual observation. Scans are then made at approximately 0.5 μm to 1 μm (depending on the inclusion depth) steps through the inclusion. Once scanned, a composite of all layers and a gallery of the layers can be displayed.

When the CLSM data have been gathered, it was processed to obtain the volumetric data of liquid and vapour bubble volumes. The Leica software has an inbuilt interpretation utility program for calculating selected areas. The operator displays each of the Z-series scan images, one at time for every inclusion scanned. Then, an outline is manually drawn around each inclusion layer; the enclosed area is then calculated by the software. The same procedure is used for each layer that has a vapour bubble visible. All area data are then entered into a spreadsheet for the calculation of volumes and relative liquid:vapour percentages (Table 2.6).

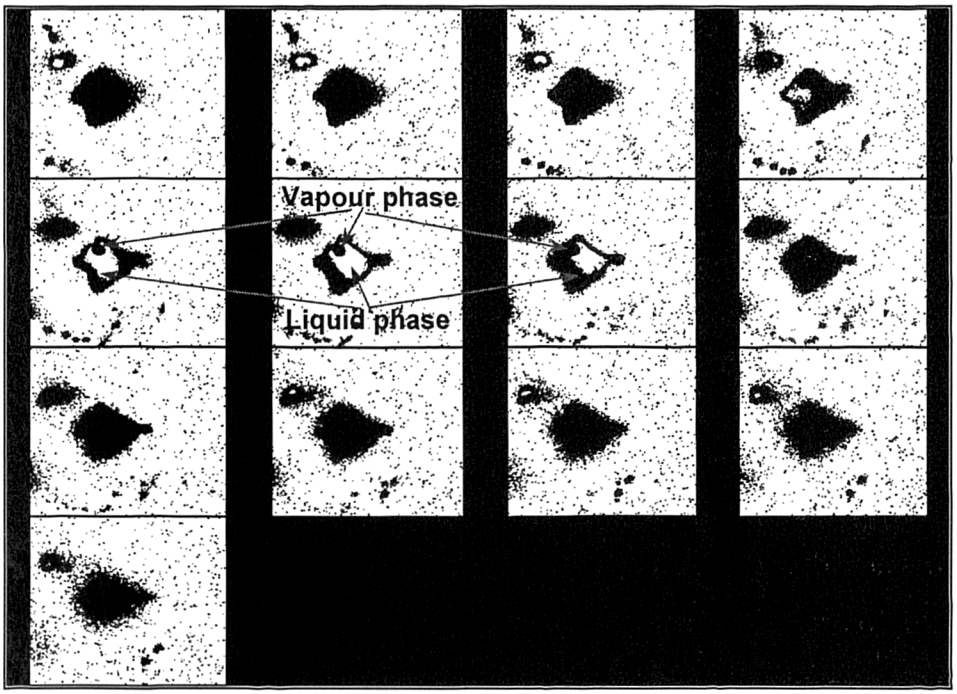

Figure 2.9 A selection of the 13 Confocal Scanning Laser Microscope images taken through secondary petroleum bearing fluid inclusion. The laser image shows the inclusion and its bubble alter shape at various depths of the inclusion.

Table 2.6 Calculated areas and volumes in images obtained with a Confocal Laser Scanning Microscope as z series through a petroleum inclusion in sample MD#213 3499.5 m.

MD#213	3499.5 m	Th = 71.7 °C		
Zi (μm)	Area liquid petroleum (μm^2)	Volume liquid petroleum (μm^3)	Area vapour petroleum (μm^2)	Volume vapour petroleum (μm^3)
0.6920	5.25	3.6330	19.75	13.6670
	9.41	6.5117	23.72	16.4142
	11.38	7.8750	24.78	17.1478
	16.24	11.2381	24.93	17.2516
	20.1	13.9092	25.28	17.4938
	23.29	16.1167	19.97	13.8192
	24.26	16.7879	15.13	10.4700
	19.73	13.6532	9.37	6.4840
	15.52	10.7398	5.68	3.9306
	77.94	53.9345		
	101.86	70.4871		
	131.39	90.9219		
	164.95	114.1454		
	182.59	126.3523		
	194.82	134.8154		
	210.71	145.8113		
	220.47	152.5652		
	219.13	151.6380		
	201.5	139.4380		
	188.66	130.5527		
	156.1	108.0212		
	110.23	76.2792		
	77.19	53.4155		
	46.85	32.4202		
	13.74	9.5081		
total volume of liquid petroleum (μm^3)	total volume of vapour petroleum (μm^3)	total volume of inclusion (μm^3)	volume % of liquid petroleum	volume % of vapour petroleum
1690.77	116.68	1807.45	93.54	6.46

2.2.3. Phase envelopes and isochores: VTFLINK

VTFLINK is a Windows based software package developed by Calsep A/S in co-operation with Newcastle Research Group (NRG, Newcastle University). VTFLINK is developed to process optically derived microthermometric and volumetric data from petroleum inclusions using equation of state procedures to derive compositional and pressure data for the included petroleum (Aplin et al., 1999). In the PVT modelling using the VTFLINK software, several important assumptions are made:

1. The aqueous inclusions are saturated with gas. Thus, the homogenisation temperature of aqueous inclusions is close to the true trapping temperature. Hence, during microthermometry analysis of petroleum inclusions it is essential to record homogenisation temperatures of coexisting aqueous inclusions.

2. The host crystals are considered to be impermeable to chemical changes and that an inclusion represents a chemically closed system from the time of entrapment (Burrus, 1986).

3. The volume of an inclusion remains constant (isochoric) since entrapment. This is because of the rigidity of host crystals, and because fluids have much greater coefficients of thermal expansion than the enclosing host crystals (Burrus, 1986).

In this PVT simulation, I created a data base entry comprising, the homogenisation temperatures of petroleum and coexisting aqueous inclusions obtained by the microthermometry technique, the liquid:vapour ratio obtained by CLSM and detailed composition of present day produced black oil from well OMM#412 located in the west of the Hassi Messaoud field (see Table 6.2 in chapter 6). These pieces of information were used in the VTFLINK PVT simulator to construct the phase envelop of the included petroleum (Figure 2.6) and to calculate the accurate composition of the single inclusion (i.e. optimum fluid see Table 6.4 in chapter 6). The composition of the gas titrated into or out of the initially chosen petroleum composition is essential to the exact calculation of the optimum composition of included petroleum (Aplin et al., 1999). Aplin et al. (1999) have tested four possible strategies using fictitious petroleum inclusions to obtain an estimate of gas composition based on the

composition of the initial petroleum selected for input to the iterative procedures using VTFLINK:

1. This strategy first calculates the saturation pressure at the observed homogenisation temperature of the analysed inclusion and then calculates the composition of the first gas formed at the saturation point (liquid at a dew point for a gas or condensate inclusion or gas at a bubble point for an oil inclusion).

2. In this strategy, the gas composition for the iterative titration is the equilibrium gas composition obtained from a flash of the chosen petroleum composition to standard conditions of 1 atmospheric pressure and 15°C.

3. The gas composition used for the iterative titration in this strategy is taken at the equilibrium gas from a flash of the initially chosen petroleum composition at 1 atmospheric pressure and inclusion homogenisation temperature.

4. The gas composition used for the iterative titration is the equilibrium gas derived from a flash of the initially chosen petroleum at 1 atmosphere pressure and a temperature 50°C higher than the homogenisation temperature of the petroleum inclusion.

Aplin et al. (1999) found that the best agreement between the actual and calculated physical properties of the included petroleum was obtained using strategy 4. They showed that none of the other three methods give such good agreement as strategy 4. This method titrates a more realistically wet gas into or out of the chosen composition of petroleum. It appears to give accurate results even when the initially chosen petroleum is compositionally somewhat different to that in the inclusion. Though, it is preferable that the composition of the initially chosen petroleum is close to that of the included petroleum, which in turn will increase the accuracy of the compositional calculation of the included petroleum.

Hence, in my study I used directly strategy N° 4 to derive the live composition, the trapping temperature and pressure, the saturation pressure, the GOR together with other physical properties such as viscosity, density and surface tension of the included petroleum (see Table 6.3 and 6.4 in chapter 6). The process of calculations of the

physical properties of the included petroleum is summarised below (Aplin et al., 1999):

1. First, the composition of the present day reservoir oil (initial petroleum), relative percentages of liquid and vapour and the homogenisation temperatures of the petroleum and coexistent aqueous inclusions are entered.

2. Then a PVT simulator calculates the saturation pressure of the reservoir oil at the homogenisation temperature of the inclusion.

3. The oil is "flashed", calculating the phase fraction-composition at homogenisation temperature and saturation pressure. The total molar volume of the petroleum is stored.

4. Saturation pressure of the initial petroleum is calculated at room temperature. The saturation pressure in the inclusion is at a maximum, because the included petroleum is two-phases.

5. A series of flash calculations are performed at room temperature and at a series of pressures below the calculated saturation pressure. The volume and composition of liquid and gas phases are computed, as well as the molar volume of the petroleum in each case. When the molar volume obtained by calculations at homogenisation temperature matches the molar volume of the mixture at room temperature, the two points are linked in P-T space, explicitly they lie on the same isochore. Component density can be used to make these calculations, but is less accurate.

6. Calculation of the initial petroleum liquid:vapour chosen at room temperature and the internal pressure of the included petroleum are performed. If the calculations show that the volume % of liquid and vapour that temperature and pressure match the CLSM data, the composition of the chosen petroleum is considered to be a physical illustration of the inclusion petroleum.

7. If the calculated liquid:vapour % in the inclusion do not match the measured values, gas is titrated in or out of the initial petroleum, and the calculations are

repeated. The choice of the gas composition is critical to the success of the iterative procedure.

8. Steps 2-7 are repeated until the calculated volume % matches the CLSM measured values. The composition of the petroleum is now very close to that of the included petroleum, and can be considered to at least be an "effective composition" as it mimics its PVT properties. The final composition is used to construct the phase diagrams and isochore for the included inclusions (see Table 6.4 and Figure 6.14 in chapter 6).

2.2.4. Sample preparation and crushing for geochemical analyses of petroleum inclusions

The amount of rock material needed to liberate the necessary quantity of petroleum for a reproducible biomarker analysis is directly proportional to the abundance of petroleum inclusions present in the samples. Therefore, before selecting samples for crushing and geochemical analysis, it is important to perform first a petrographic study of the samples. In total, seven (7) reservoir core samples containing reasonably high numbers of petroleum inclusions were selected for further analysis by gas chromatography and gas chromatography-mass spectrometry of the included oils (palaeo-oils).

2.2.4.1. Cleaning method

All adsorbents (alumina, silica gel) and cotton wool plugs were pre-extracted before use. All the glassware used was cleaned by immersing in chromic acid and then rinsed in distilled water before use.

The reservoir rock samples (10 to 20 g) were first disintegrated as smoothly as possible using a pestle and mortar so as not to cause any excessive losses of the included fluids in mineral grains (Jones and Macleod, 2000). The disaggregated samples were then ultrasonically extracted five times with successive 30ml of DCM:MeOH (93:7) mixture. The samples were left to dry for 24 hours on the top of an oven, and were then Soxhlet extracted for 24 hours using 250ml of DCM:methanol (97:3) mixture. After a thorough drying (24 hours on the top of an oven), the extracted rocks were transferred to 200 ml beakers to which about 50 ml of chromic acid was

added, and left for 24 hours; the chromic acid removes most of the residual organic matter from the grains (Karlsen et al., 1993). Afterwards, chromic acid was removed by washing with tap and distilled water. This stage was followed by another treatment (24 hours) with the less viscous oxidising agent, hydrogen peroxide (H_2O_2) (George et al., 1997) to remove residual or non-extractable organic matter from fissures and cracks. Samples usually showed the generation of many small bubbles at this stage as oxidation occurred. The beaker was then stirred to assure thorough mixing and coverage by the H_2O_2. After 24 hours the peroxide was decanted off and a fresh quantity of peroxide added. This procedure was repeated twice more giving a total of 4 peroxide treatments over 4 days. The samples generally broke up to individual sand grains during peroxide treatment, possibly due to the oxidation of an organic cement or matrix. At the end of the final peroxide treatment, fines and clays were removed by washing several times by thorough washing with tap water followed by distilled water and then methanol. Finally, the samples were air dried for 24 hours. The dried rock grains were then extracted by ultrasonication in 30 ml of DCM:MeOH mixture for 20 minutes, to remove any possible bitumen from the grain surfaces and fissures opened after the first two treatments.

2.2.4.2. Crushing method

The rock grains were crushed under 30 ml of DCM:methanol (93:7) using a pestle and mortar to break open and powder the grains to liberate the hydrocarbons from the petroleum fluid inclusions in the rock particles. This procedure is known as the crush-leach extraction. The resultant extracts were transferred to round bottom flasks and they were carefully rotary evaporated just to dryness so that the suspended material (clay material) remained attached to the walls of the flasks. The flasks were then carefully rinsed with DCM and the extracts obtained were concentrated to about 200 µl and analysed directly by GC and GC-MS.

2.2.4.3. GC and GC-MS of fluid inclusion

Fluid inclusion extracts obtained after crushing the sandstone grains were analysed by GC. In all the samples, a half microlitre of the extract was injected on-column, onto a 30m x 0.25mm x 0.25mm, HP-5 column (5% Phenyl Methyl Silicone stationary phase). The oven temperature was held for two minutes at 50 °C, then programmed from 50 °C to 300 °C at 4 °C/min, and finally held at 300 °C for 20 minutes. Figure

2.10 shows a comparison between the petroleum in the inclusions and petroleum extracted from the reservoir core extract from the same depth in well MD#177, Hassi Messaoud field.

The samples were analysed by GC-MS, using the same instrument, the same column, and the same conditions as reported above for the oil and source rock samples.

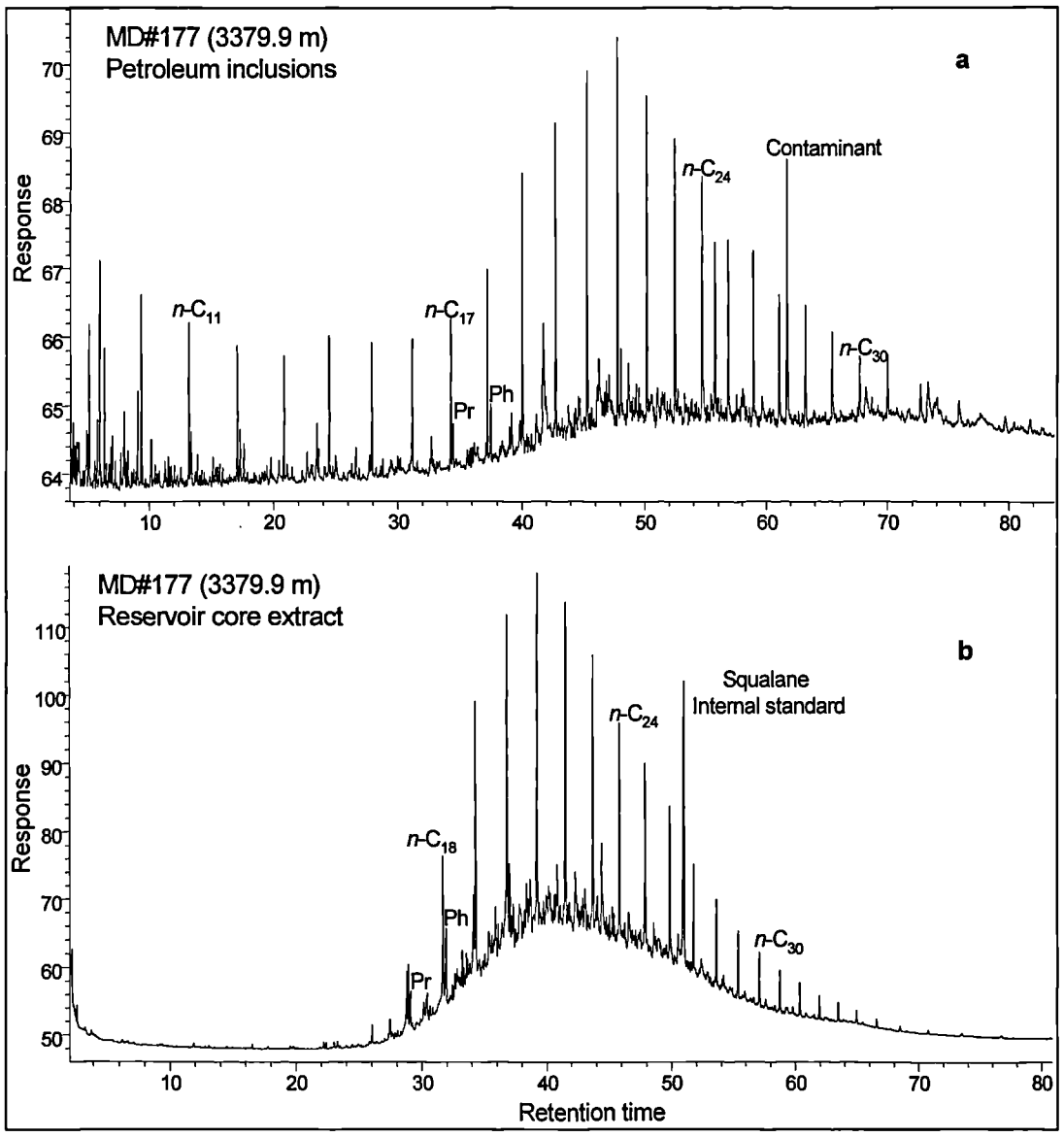

Figure 2.10 Gas chromatograms illustrating the comparison of *n*-alkane and isoprenoid alkane distributions between (a) petroleum inclusions and (b) the reservoir core extract at the same depth from well MD#177, Hassi Messaoud field.

Chapter 3
Geological Framework of the Study Area

3. Geological framework of the study area

3.1. General Introduction

Algeria can be subdivided into two major structural regimes; the Atlas mountain zone to the north and the Saharan platform to the south. Within the Saharan platform four major basin areas exist, one of which, known as the Oued Mya basin, is located within the study area. The Oued Mya basin is located east of one of the largest gas-condensate accumulations in the world (Hassi R'mel field) and west of the largest oil accumulation in North Africa named Hassi Messaoud field.

The north-east-south-west trending Hassi Messaoud arch (El Agreb-Hassi Messaoud arch) belongs to the large Triassic basin situated to the north-east of the Saharan platform. The study area is located approximately 800 km southeast of Algiers in the east-central Sahara desert (Figure 3.1). It is considered to be the largest petroleum province so far discovered in Algeria and one of the largest in the world.

3.1.1. History of the discovery of oil in the study area

Hassi Messaoud field was discovered by the *Société Nationale de la Recherche et de la Production en Algérie (SN.Repal)*. The drilling of the first well named MD#1 was completed by May 1956; the target was the Cambrian quartzitic sandstones (unit Ra) at a depth of 3329 to 3368 m. A few months later another discovery (well OM#1) about 8km to the north of MD#1 confirmed the existence of Hassi Messaoud oil field. Within the same period of time, the laborious effort of prospecting realised by both *SN.Repal* and *la Compagnie Française du Pétrole en Algérie-C.F.P.A* companies had led them to the discovery of the largest accumulations of oil in the Hassi Messaoud Cambro-Ordovician sandstones and gas condensate in the Hassi R'mel Triassic sandstones. Since then, a number of other discoveries have been made around the area including: oil in Cambrian reservoirs in El Gassi field approximately 90 km to the south-southwest of Hassi Messaoud, oil in Cambrian reservoirs in El Baguel and Mesdar about 80 km to the east, oil in the Lower Triassic reservoirs in Haoud Berkaoui and Benkahla 30 km to the west and other accumulations within Lower Triassic and Devonian reservoirs 30 - 40 km to the northwest of Hassi Messaoud field within the Oued Mya basin.

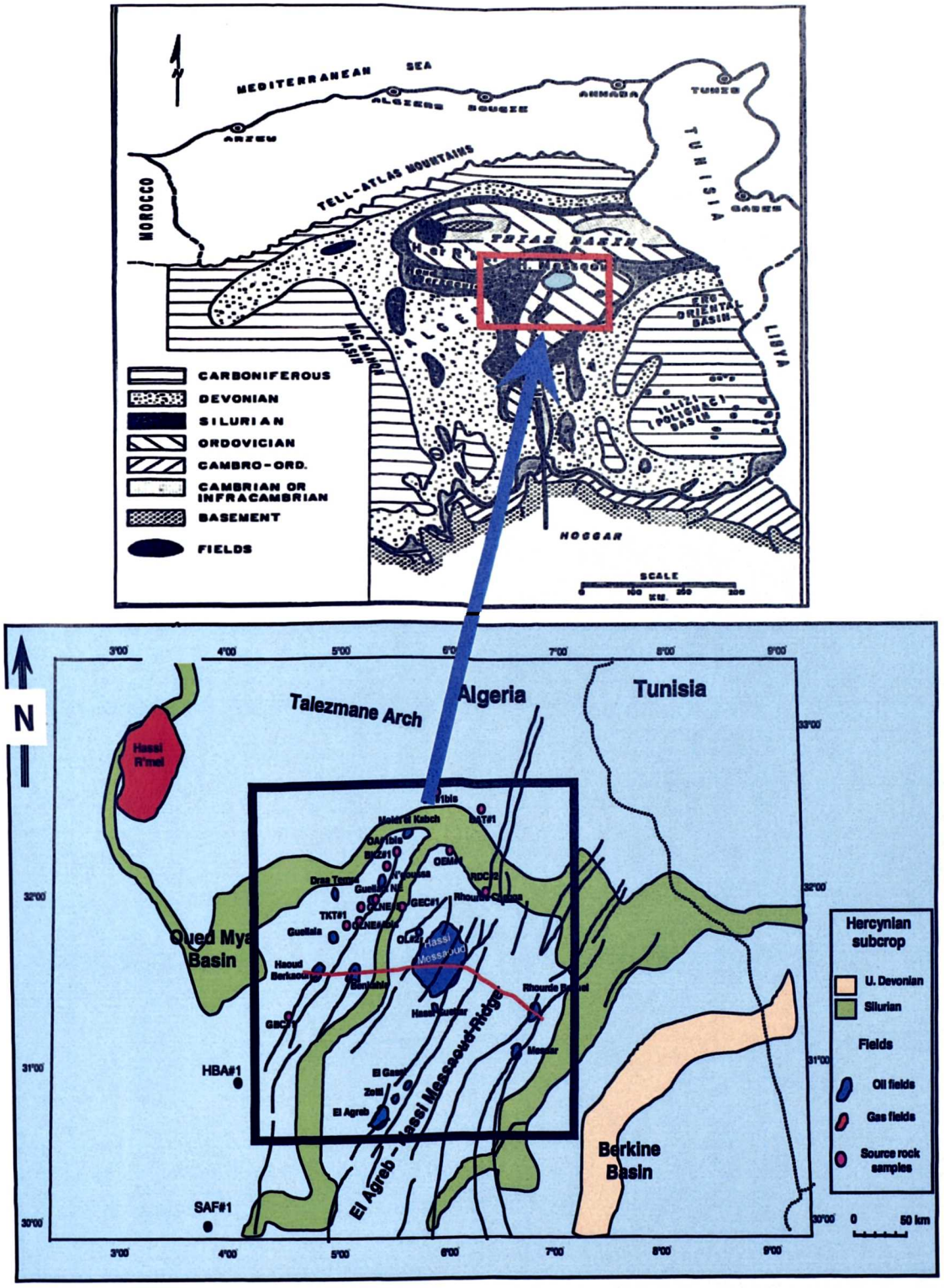

Figure 3.1 Location map of the study area, the area extent of total petroleum systems and Silurian source rocks (Gothlandian), and locations of stratigraphic cross section shown in Figure 3.4. (After ARCO, 1994).

Attar and Hammat (1993) reported an oil-in-place estimate of 47 BBO (billion barrels oil) across the whole area of the Oued Mya basin and the Hassi Messaoud arch (25 BBO in Hassi Messaoud alone), though accounted recoverable reserves in Hassi

Messaoud giant field are only 10.2 BBO, largely because of unfavourable reservoir conditions. Indeed, despite appreciable numbers of wells so far drilled by *SONATRACH* and the number of studies carried out (e.g. *C.F.P.A*, 1969-1970; Massa et al., 1972; Montadert, 1963; Beuf, et al., 1971; I.F.P, 1979), the Hassi Messaoud reservoir is far from being well understood because of its high complexity.

3.2. The tectonic setting

There is evidence for strong deformation of the pre-Late Cambrian metamorphic and granitic basement rocks at selected locations across the Saharan platform. The bulk of the Cambrian sandstones, however, were deposited on a broad, relatively stable subsiding area. The general palaeo-current direction for most of the Cambrian rocks outcropping in the Hoggar Massif (south of the Hassi Messaoud high) was to the north, implying the same to be true for the whole region. The developing Hassi Messaoud structure was briefly active at the end of deposition of the Ra formation where up to 50 m of that unit has been eroded from an area just south of the present-day structural crest.

The effects of the Hercynian orogeny are very perceptible at the Hassi Messaoud high. The Cambrian and the Ordovician rocks are locally characterised by widespread faulting and deep erosion. The subcrop map of the Hercynian unconformity (Figure 3.1) shows the extensive consequence of the continuing tectonic events and erosion that have occurred in the Sahara platform area during the Late Devonian through the end of the Permian period. This activity resulted in the formation of the Hassi Messaoud-El Agreb anticlinorium that extends about 700 km in a northerly direction from the Hoggar Massif (Figure 3.1).

The final phase of the Hercynian orogeny was closed by the local deposition of Triassic clastic sediments in the severely eroded topographic low areas and the local extrusion of Triassic igneous rocks onto the landscape. De Lapparent (1961) considered these to be andesite flows. It is possible that the source of these flows and the source of the intruded igneous rocks found in several wells in the southwest part of the Hassi Messaoud field may be the same.

The Sahara platform gently subsided from pre-Late Triassic to almost the end of the Cretaceous, with the entire area receiving a relatively thick sequence of evaporite and

clastic sediments. Positive orogenic movement along the Hassi Messaoud-El Agreb high during the early Tertiary is postulated from the absence of rocks of this age in the area. The presence of flat-lying continental Miocene-Pliocene rocks suggests the tectonic activity had ceased by that time. The Hassi Messaoud area has remained tectonically inactive since.

3.3. Regional structural style

As shown on the map (Figure 3.1), the Hassi Messaoud-El Agreb anticlinorium is situated in the Trias basin extending between two vast depression zones. This positive element (the Hassi Messaoud-El Agreb high), separates the Oued Mya basin on the west which shows a northeast – southwest trend formed during the Palaeozoic and corresponds to a vast synclinal (Busson, 1970). The Oued Mya basin is essentially comprised by the Ordovician, Silurian and Devonian formations. To the east and southeast, the Berkine and Illizi basins, respectively. The Berkine basin presents more or less complete section of Palaeozoic sequences starting from the Cambro-Ordovician to the Upper Carboniferous. These sediments deeply buried during the Palaeozoic, the Mesozoic and the Cenozoic comprise significant hydrocarbon potential in the Triassic basin.

This "Basin and high" complex is the result of both mild tectonic activity during the deposition of the Early Palaeozoic sediments on the Saharan platform, which covered a large part of the north African continent, and the more intense tectonism of the Hercynian orogeny that began in Late Devonian (Balducchi and Pommier, 1970; Bishop, 1975; Malenfer and Tillous, 1963).

3.4. Stratigraphy of the Hassi Messaoud ridge

A generalised stratigraphic section (Figure 3.2) is modified from Balducchi and Pommier (1970), De Lapparent (1961), and Malenfer and Tillous (1963). This section identifies the various rock units that are normally encountered in the Hassi-Messaoud ridge area.

3.4.1. Pre-Hercynian sedimentary cycle

3.4.1.1. Palaeozoic

3.4.1.1.1. Cambrian

The Cambro-Ordovician sediments have a variable thickness. They constitute the principal reservoir of Hassi Messaoud ridge oilfields. The Cambrian stratigraphic sequence in the Hassi Messaoud field has been subdivided by Malenfer and Tillous, (1963) into five major units. These comprise, from Lower to Upper, the (1) *Zone R3*, (2) *Zone R2*, (3) *Zone Anisometrique* (Ra), (4) *Zone Isometrique* (Ri), and (5) *Zone des altenances*. The Ra is the most important reservoir unit with the Ri and R2 identified by these authors as secondary reservoirs. The discussions that follow are mainly derived from the works published by Balducchi and Pommier (1970); Bacheller and Peterson (1991); and Fennouh (1996).

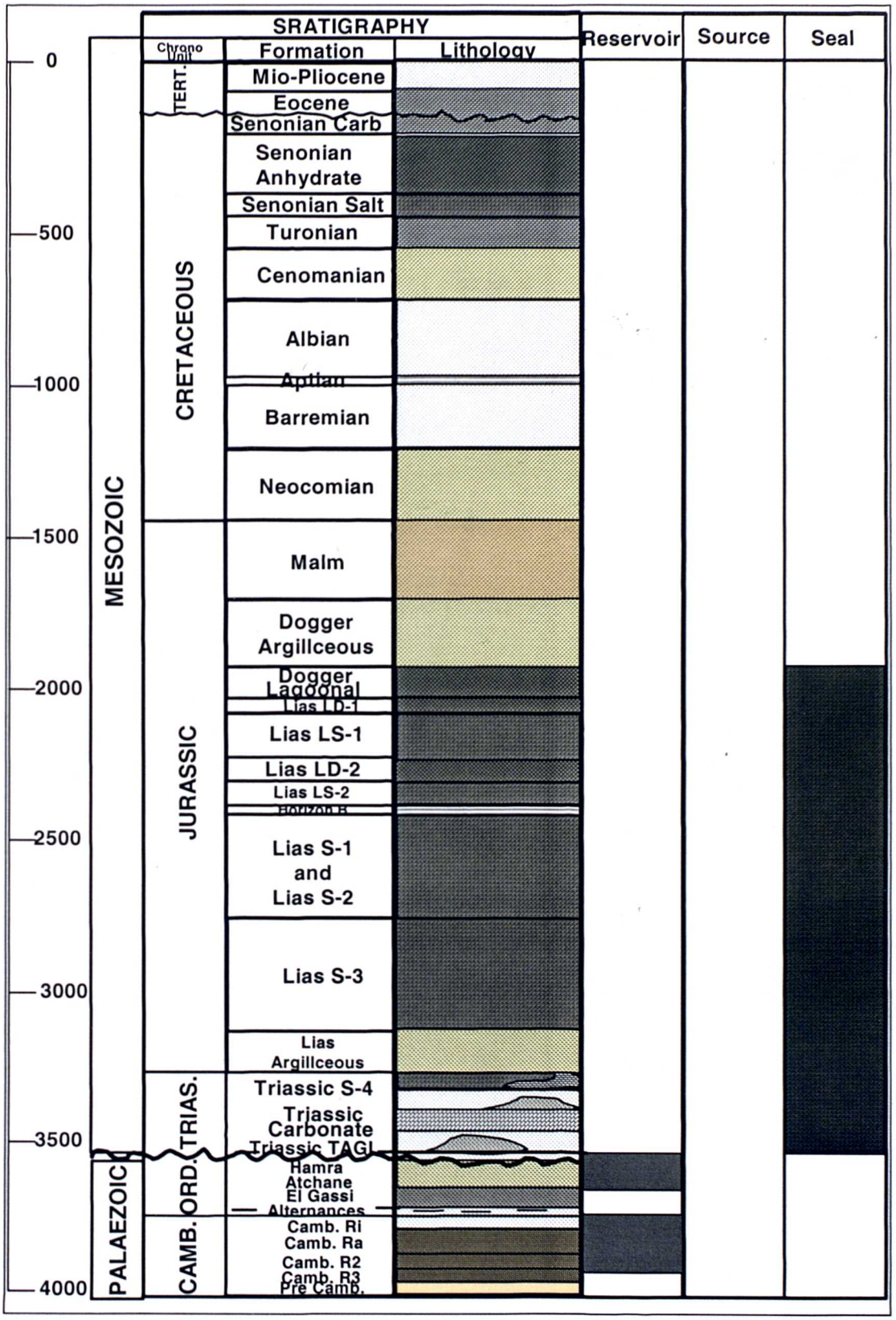

Figure 3.2 Stratigraphic columnar sections, Hassi Messaoud Ridge, Algeria. (After Canadian Petroleum, 1998).

The Cambrian unit R3 (*zone R3*), is highly cross-bedded, arkosic, very argillaceous quartzose sandstone and micro-conglomerate with poorly sorted and angular grains. It

is composed of about 60% quartz and 30% clay, mostly illite. The section also includes a pebble to cobble basal conglomerate. The R3 section thickens from 275 m in the south-central part of the Hassi Messaoud field northward to 368 m north of the field. It rests unconformably on the crystalline Precambrian formations or on the granitic basement. These deposits would come from moraines, tillites deposited at the time of the Eco-Cambrian and redistributed by the alluvial streams.

The Cambrian unit R2 (*zone R2*), is a consistently thick sequence of highly cross-bedded, medium- to coarse-grained quartzose sandstones comparable to the Ra zone sediments except that these (R2) have a much higher clay content, occurring as interstitial clay and irregular thin inter-beds of shale. The clay minerals are predominately illite with minor amounts of kaolinite. Because of the clays, this zone has poor reservoir quality and is generally non-productive. In the north-eastern part of the field, however, the upper 20 m or so is included as part of the producing interval. Where it is not eroded, this zone is 80 m thick.

The Cambrian unit Ra (*Zone Anisometrique*) is the principal reservoir of the Hassi Messaoud field. Where not affected by the Hercynian and the pre-Ri zone erosion cycles, the Ra zone has a maximum total thickness of 150 m in the western portion of the field. The Ra zone has been subdivided into five sub-zones. These sub-zones, from upper to lower, include Drain 4, Drain 3, Drain 2, Inter-drain, and Drain 1. All sub-zones are basically comparable lithologically, with the exception of Drain 3, in that they all consist of highly cross-bedded, very poorly sorted, medium-grained to micro-conglomeratic quartzose sandstones with irregularly interbedded lenses of shaly siltstone. The Ra is composed of about 70% quartz; 14% secondary silica, and 8% clay; in some wells the clay is chiefly kaolinite.

Drain 3 varies in that it is the only sub-zone in the Ra that contains abundant tubular fossils (scolites) and is generally finer grained and is not cross-bedded. Also, the primary clay mineral in Drain 3 is kaolinite. Drain 3 is L'Homer's (1967) "Median Zone". L'Homer's (1967) study of the Ra interval at Hassi Messaoud and the outcrop study by Beuf et al. (1971) of equivalent sediments in the Hoggar Mountains reveal that these sediments were deposited in a series of alluvial fan and associated depositional environments. Taking this into consideration, the thickness and the continuity of the sub-zones are remarkably uniform on a fieldwide basis.

The Cambrian Ri (*Zone Isometrique*) is a 50 m thick quartzitic sandstone unit characterised as homogeneously thick, well-sorted, medium-grained sandstone with interbeds of shale and silstone. It encloses copious tubular fossils (scolites) all through the section, except for the basal meter or so that comprises winnowed debris from the underlying formation. The Ri unconformably overlies the Ra zone, and this contact compares to L'Homer's (1967) "Gamma Zero" marker in his fieldwide correlations. Where present above the oil-water-contact, the Ri encloses hydrocarbons but it is not regarded as an important producing zone because of its poor reservoir characteristics. Although the fact that this unit rarely produces, the top of the Ri is considered the top of the reservoir section.

The Zone des Alternances as its name suggests, this unit includes alternating layers of quartzites, silstones, and black shales, totalling from 25 to 40 m. This unit is considered the base of the Ordovician section by other investigators.

3.4.1.1.2. Ordovician

Although the different Ordovician rock units are eroded over practically the whole broad crestal area of the Hassi Messaoud field, they are present in the area immediately around the field (Figure 3.3). Some of these formations are also found within the field boundary since they were conserved in the narrow grabens seen on the structure map in the southern part of the field and in the northeast sector (Figure 3.4 and Figure 3.5). According to Malenfer and Tillous (1963), the Ordovician section comprises from the Lower to Upper:

* El Azzel Shales Formation.
* Ouargla Sandstones Formation.
* Hamra quartzite Formation, a fine-grained quartzite with low porosity and permeability.
* El Atchane Sandstones Formation, 15 m thick fine-grained quartzitic sandstones having numerous shale partings and poor reservoir quality.
* El Gassi Shales Formation, a black glauconitic, graptolitic marine shale that is as much as 70 m thick at Hassi Messaoud.

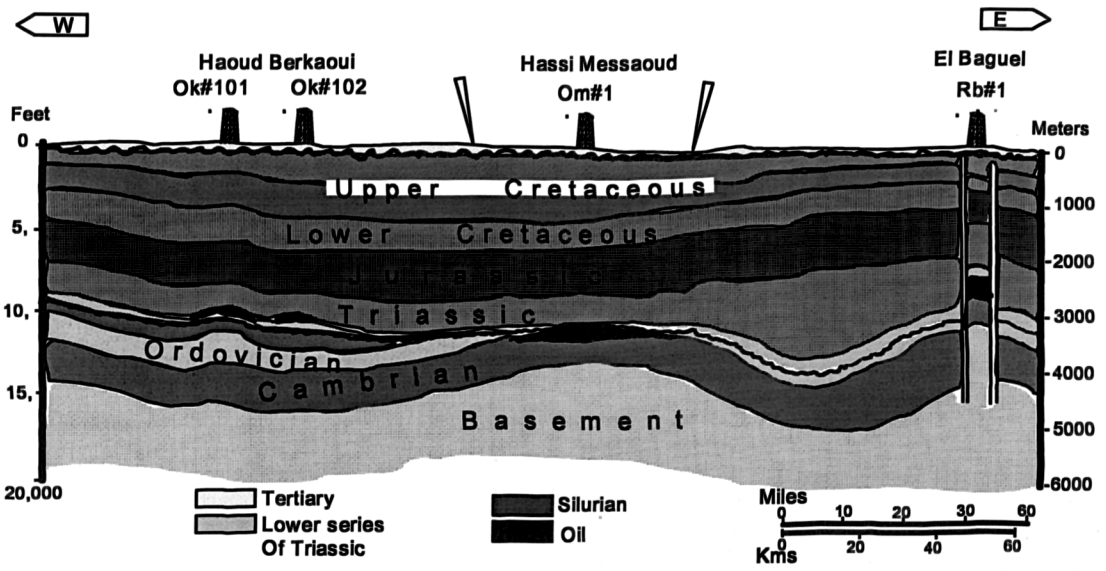

Figure 3.3 West-east cross section of Oued Mya basin, from Haoud Berkaoui to El Baguel. (After Balducchi and Pommier, 1970). Section marked on Figure 3.1.

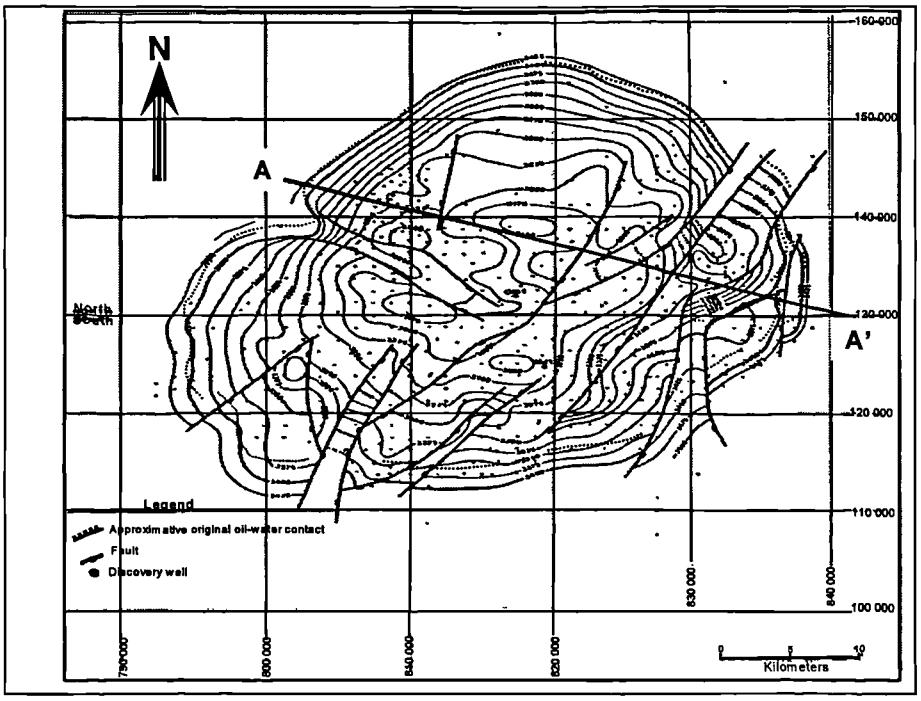

Figure 3.4 Structure map of the Hassi Messaoud field contoured on the top of reservoir R2. (After Bacheller and Peterson, 1991).

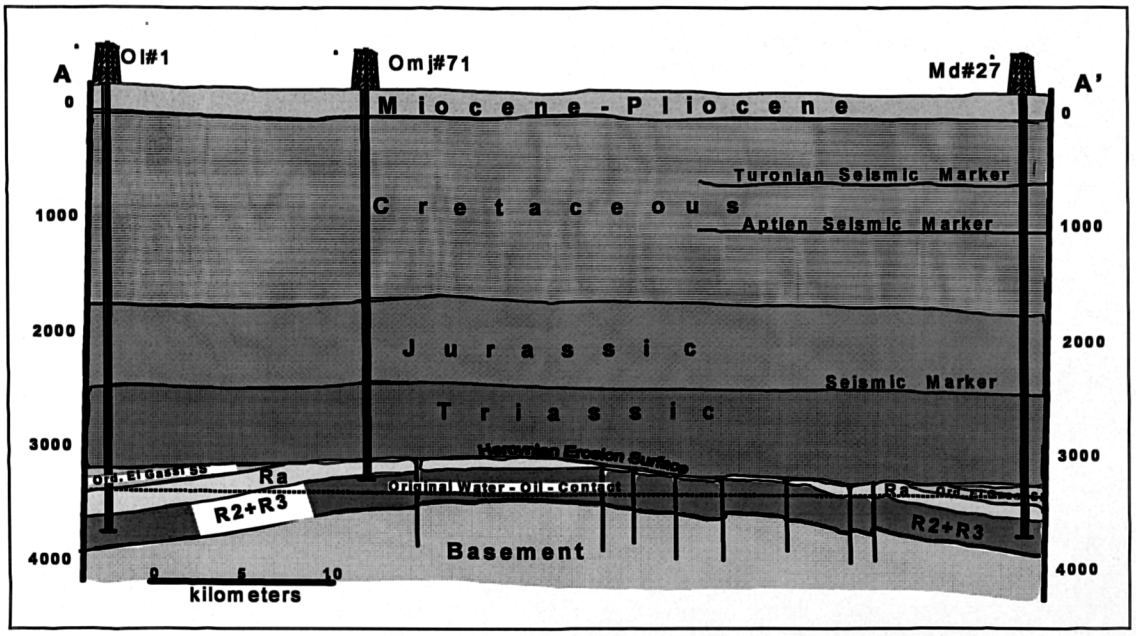

Figure 3.5 Generalised west-northwest to east-southeast structural section, Hassi Messaoud field. See Figure 3.4 for location of cross section. (After Balducchi and Pommier, 1970).

3.4.2. Post Hercynian sedimentary cycle

3.4.2.1. Mesozoic

3.4.2.1.1. Triassic

The Palaeozoic rocks are overlain unconformably by transgressive series of Triassic age, divided into two units. The bulk of this 550 m thick section is composed of massive anhydrite and halite (i.e. Upper Triassic), overlying a basal clastic section (i.e. Lower Triassic). The thickness of this basal unit is highly variable due to the very irregular erosion surface upon which it was deposited (up to 30 m topography).

3.4.2.1.2. Jurassic

The upper third of the 850 m thick Jurassic interval consists of massive dolomite. A thick shale section, identified in Figure 3.2 as the Dogger Lagunar, separates the overlying dolomite from the massive salt and anhydrite unit below.

3.4.2.1.3. Cretaceous

The upper 800 m of the Cretaceous section includes a very large amount of anhydrite, halite, limestone, and dolomite with minor interbedded shale. The lower Cretaceous is a massive clastic unit with siltstone, shale, and fine-grained sandstone throughout its

850 m thickness. A very widespread dolomite bed about 25 m thick occurs in the middle of this lower unit.

3.4.2.1.4. Miocene-Pliocene

About 250 m of sand, sandstone, and sandy shale comprise the sediments of the Miocene-Pliocene.

3.4.3. Source Rocks

The principal source rock in the Oued Mya basin is the Silurian Gothlandian formation (Benamrane et al., 1993; Daniels and Emme, 1995; Makhous et al., 1997a,b). The Hercynian erosion removed virtually all of the Silurian sediments to well beyond the limits of the Hassi Messaoud field. Some exploratory boreholes have encountered Silurian sections at least 25 km or more away, west of Hassi Messaoud field (Figure 3.3). Silurian shales were deposited over the Upper Ordovician (peri-) glacial sandstones during the initial early Silurian transgression that was a result of the melting of the late Ordovician icecap (Lüning et al., 2000). The earliest Silurian sections represented by Rhuddanian stage (*acuminatus, atavus* and probably early *cyphus* graptolite biozones) contain the main organic-rich shale unit. This unit is also known as the "hot" shales due to its gamma ray signature; it was deposited during a short period (1-2 m.y.), where a favourable combination of factors in parts of North Gondwana existed which led to the development of exceptionally strong oxygen-deficiency in the basin (Lüning et al., 2000).

Lower Silurian source rocks consist of grey/dark highly radioactive, algal shales with graptolite fauna. The source rocks are classified as Type II marine; low sulphur; oil-prone source rocks containing up to 17% residual total organic carbon (TOC) (unpublished Sonatrach reports; Makhous et al., 1997a,b). The Silurian source rock samples analysed in this study revealed relatively high organic matter content with TOC values ranging from 0.99 to 14.30 wt% (average 9.21 wt%) and low to extremely high residual petroleum potential ranging from 1.31 to 34.60 mg HC/g of rock (average 20 mg HC/g of rock) (Table 4.1 in chapter 4).

Lowermost Silurian organic-rich "hot" shales are considered to be the origin of 80-90% of the Palaeozoic sourced petroleum in North Africa and in the Arabian Peninsula (Makhous et al., 1997a,b; Boote et al., 1998; Macgregor, 1996 and 1998;

Lüning et al., 2000). The thickness of the "hot'' shale unit, however, varies regionally between only a few metres and 28m. The post- Rhuddanian Silurian shales are, in general, organically lean and have not made a significant contribution to petroleum generation.

The Lower Silurian shales entered the onset of the oil window at the beginning of the Cretaceous (0.65 $\%R_o$); peak of oil generation (0.70 $\%R_o$) occurred as early as the Albian (Makhous et al., 1997a,b). Makhous et al. (1997a,b) concluded that petroleum generation occurred at two different stages. Minor amounts of petroleum may have been generated in the Takhoukht region northeast of the basin during the Palaeozoic. Makhous et al. (1997a,b) showed that the yield during the Carboniferous (from 360 to 260 Ma), prior to the Permian erosion accounts for about 6% of the total generated petroleum, but generation was halted during Hercynian deformation. The first stage of petroleum generation ceased because of the Hercynian uplift followed by massive erosion of sediments (up to 2.2 km). A second and final stage of petroleum generation occurred during the Campanian (120-90Ma) where source rock temperature exceeded 100 °C. Oil generation and migration most likely started no earlier than Late Triassic and peaked in Late Cretaceous to early Tertiary (Figure 3.12) (Makhous et al., 1997a,b).

Today, the Silurian shales in the Takhoukht region are mature (R_o = 0.71 - 0.73 %), whereas in the south they are over-mature (R_o = 1.25 - 1.70%) and peak oil generation occurred in the Palaeozoic (Figure 3.1 and Figure 3.6) (Sonatrach unpublished reports; Makhous et al., 1997a,b; ARCO, 1994). The northern part of the Oued Mya depocentre has never attained maturities corresponding to gas generation; therefore, only oil is available to charge the reservoirs in the region (Makhous et al., 1997a,b). The Hassi Messaoud structure appears to be a positive feature throughout much of the basin evolution. It was in place to receive petroleum from Oued Mya since Austrian (Early Cretaceous) time (Makhous et al., 1997a,b; ARCO, 1994).

The *El Gassi* and *El Azzel* shale Formations in the Ordovician are considered as secondary source rock units in the study area. These formations contain mainly sapropelic, or mixed organic matter (marine and bacterian) and have an average total organic carbon (TOC) of 0.17 to 2.36 wt%. The residual petroleum potential for these

Formations shows low to moderate values ranging from 0.15 to 2.30 mg HC/g rock (Table 4.1 in chapter 4).

The *El Gassi* shales Formation shows a homogenous assembly of thick black, grey green, silty, graptolitic marine shale, often glauconitic, which supplies coastal forms of "burrowers" at the base, then becomes planktonic, after the last traces of sandstones at the base. Unexpectedly, some geologists believe that the *El Gassi* shales Formation is the main source rock that contributed to the generation of the oil reserves trapped in the Hassi Messaoud oilfield and its surrounding fields. Their conclusions are only based on (1) the proximity of these shale units to the Hassi Messaoud field (compared to the Silurian shales) and (2) the great thickness of *El Gassi* shales in the area (*El Gassi* shales thickness vary between 60 to 200 m). In section 4.5 chapter 4, I show that the main source rock for all the oil reserves in the study area are the Silurian source strata with little contributions from the Ordovician source rock Formations.

The *El Azzel* shales Formation contain black shales with graptolites, brachiopods, trilobites and lamellibranches, deposited in more basinal conditions developed in anoxic conditions.

The thermal model carried out by Makhous et al. (1997a,b) for the Takhoukht (TKT#1) region (Figure 3.1) showed that the base of the Ordovician section reached the main stage of oil generation (R_o = 0.70%) at the end of Cretaceous. In the southern part of the basin, the main stage of oil generation could have been reached as early as the end of the Palaeozoic. Today, in the northern part (Takhoukht area) the Ordovician shales are mature with respect to oil generation (R_o=0.73-0.77%), in the southern part of the basin the Ordovician shales are in the gas window (Figure 3.6) (Makhous et al., 1997a,b).

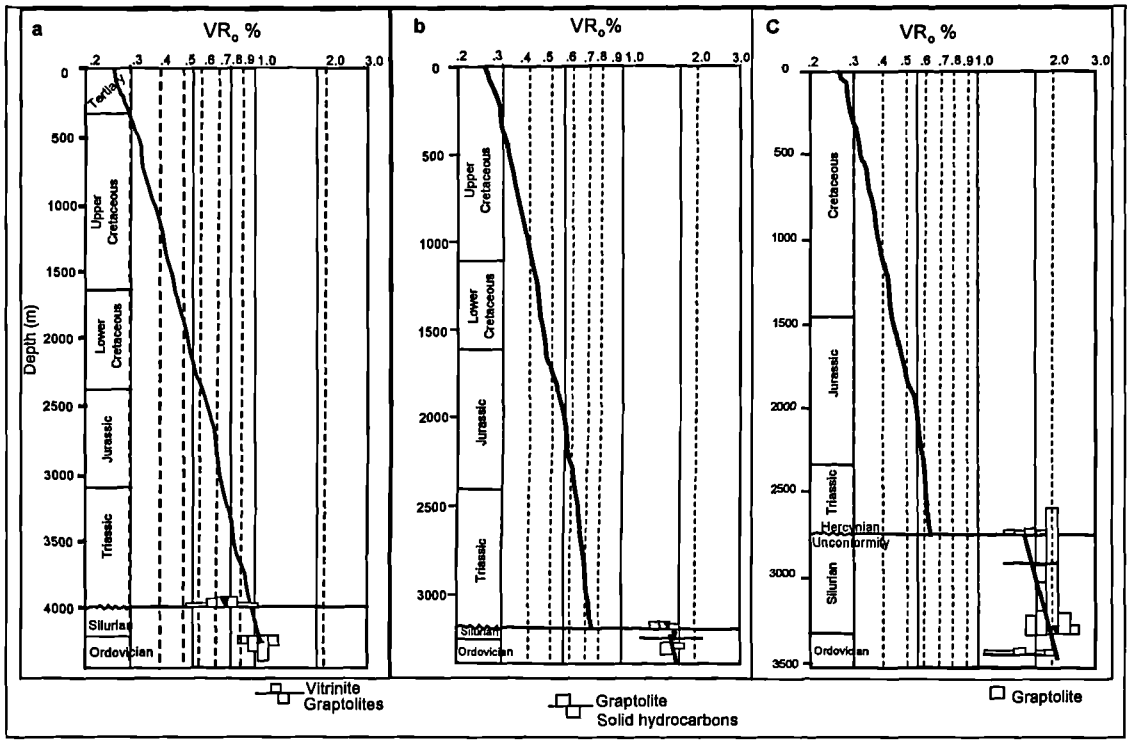

Figure 3.6 Depth versus measured vitrinite and graptolite reflectance showing the difference of maturity variation between (a) well BKZ#1 in the northeast, (b) well GBC#1, and (c) well HBA#1 in the southwest of Oued Mya basin. (After Sonatrach and Pecten Algeria Company).

Middle to Upper Devonian mudstones may provide another source of petroleum but is not present across the Hassi Messaoud Ridge and over most of the Oued Mya basin (Makhous et al., 1997a,b; Boote et al., 1998). The Devonian and Carboniferous source rocks were truncated by erosion during Hercynian deformation. Devonian is present only in the south western part of the total petroleum system.

In this study, I have analysed Silurian and Ordovician source rock samples taken mainly from the north-eastern parts of the Oued Mya basin. Only 6 source rock samples (2 from the Silurian and 4 from the Ordovician source rocks) were analysed in the southern parts, more exactly from well GBC#1 (Figure 3.1).

3.4.4. Reservoir Rocks

In the Hassi Messaoud ridge area, the primary reservoirs are fine to coarse grained sandstones of Cambrian Ri, Ra, R2, R3 Members, the Ordovician Hamra/Atchane, Ouargla, and M'Kratta Members, the Devonian and lower Triassic series (Figure 3.7). However the Ra member is considered to be the best quality reservoir unit in the fields across the Hassi Messaoud ridge (. Reservoir characteristics of each of these units vary depending on their lithology, diagenetic history, fracture characteristics,

and position either beneath or above the Hercynian unconformity surface. The major fields producing from the Cambrian reservoirs include the:

1. Hassi Messaoud field;

2. Hassi Guettar field, located a few kilometres south of the Hassi Messaoud field.

3. El Gassi, Zotti, El Agreb fields, located in separate structural highs on the large, faulted El Agreb-El Gassi anticline about 90 km southwest of the Hassi Messaoud on the Hassi Messaoud anticlinorium.;

4. Rhourde El Baguel and Mesdar fields located about 80 km east of the Hassi Messaoud field.

The fields so far discovered in the Oued Mya basin produce oils mainly from the Lower Triassic units and the Devonian sandstones which in most cases are in direct contact with the Silurian source rocks in the basin. The fields discovered in the Oued Mya basin and the Hassi Messaoud Ridge are reported to contain approximately 28.2 billion barrels of oil in place. Table 3.1 and Figure 3.7 summarise the generalised properties and parameters of the Palaeozoic sandstones in Hassi Messaoud Ridge.

Table 3.1 Generalised petrophysical properties for the Cambrian and Ordovician section. Data in [brackets] from Malenfer and Tillous (1963). All other from Balducchi and Pommier (1970).

Zone	Thickness (m)	Quartz (%)	Secondary Silica (%)	Clay		Mean Grain size (microns)	Mean Porosity (%)	Mean Permeability (md)
				Amount (%)	Type			
El Gassi Shale	91	50	15	20	Illite	300-400	–	–
El Gassi Sandstone	61	70	20	6		300	–	0.0
Ri	–	–	–	–	(Illite)	–	(Mediocre)	–
Ra	122 (400)	70	14 (10)	8 (8/15)	Kaolinite	300	8 (8/15)	0-100.0
U. R2	34 (112)	65	9	15	Illite-Kaolinite	400	11	0-100.0
L. R2 (All)	52 (171)	60	5 (7)	30 (20)	Illite	450	– [12.5]	0.0 [>1.0]
R3	274-366 (899-1201)	55-60	2-5	35-25	Illite	500-800	–	0.0

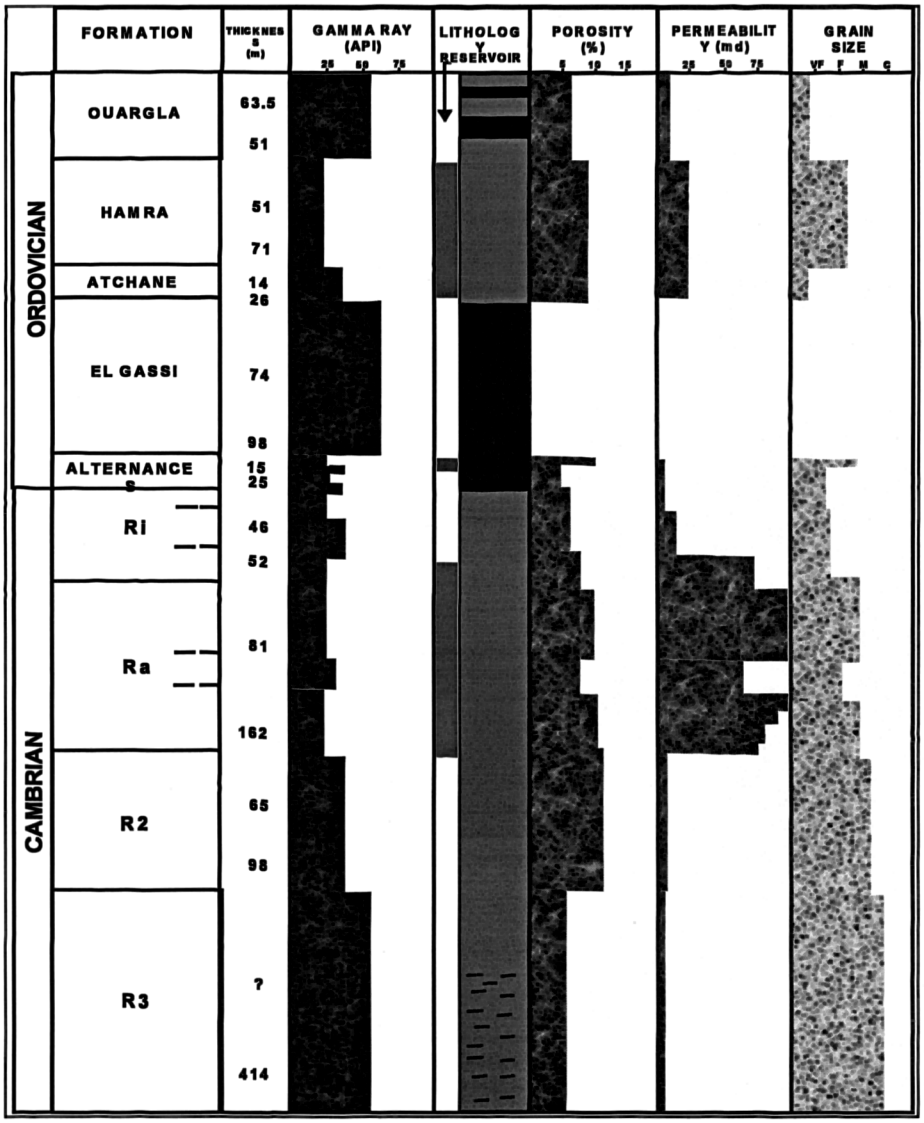

Figure 3.7 Detailed stratigraphy of the Cambro-Ordovician reservoir units in Hassi Messaoud Ridge. (After Canadian Petroleum).

3.4.4.1. Reservoir diagenesis

The Cambrian deposits in the Hassi Messaoud field are characterised by sandy and siliceous-clay facies, and contain the primary petroleum reserves in the region. The reservoir sandstones exhibit a succession of detrital sequences mainly deposited under a fluviatile regime and reflecting an evolution from coarser micro-conglomeratic, anisometric and poorly sorted sandstones in the basement to fine, isometric and well sorted sandstones towards the top of the Cambrian (Fennouh, 1996).

The Hassi Messaoud reservoirs present sandstone facies containing siliceous-clay cements with a variable average composition, containing about 75% of quartz, 1 to 5% of rock (lithic) fragments, and 20 to 25% distributed between total cement (quartzitic and kaolinitic cements) and the rock porosity (Figure 3.8) (Balducchi and

Pommier, 1970; Fennouh, 1996). The neo-formed silica is distributed in a heterogeneous manner around the detrital grains. Several and successive aureoles probably showing several silicification episodes are seen in some horizons. The silicification intensity is variable from one level to another, one well to another and in some extreme cases, can reach a rate of 20% of the total rock volume, and occlude all the available porous space leading to a genuine quartzite. In addition to the secondary silica, basically present as grain overgrowths and lithic fragments, the clays comprise the most important cement of the reservoir sandstones. In the Hassi Messaoud reservoirs, 95% of the clayey cements are represented by kaolinite in various forms.

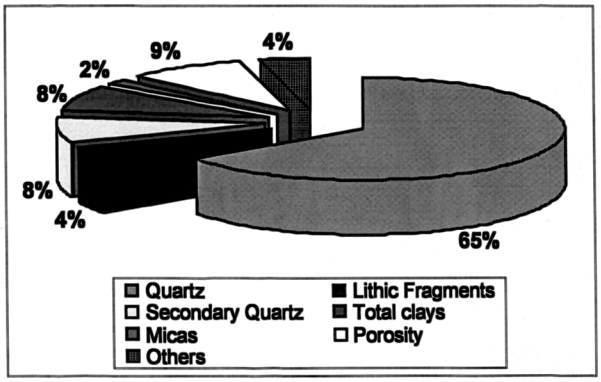

Figure 3.8 Average mineralogical composition of Hassi Messaoud sandstones. (After Fennouh, 1996). Others = by order of importance: Anhydrite, Solid bitumen, carbonate, pyrite, heavy minerals, and exceptionally alkaline feldspars (Fennouh, 1996).

3.4.4.2. Chronology of the diagenetic events

Fennouh (1996) proposed a model for the diagenetic evolution of Hassi Messaoud sediments. His work was inspired from the studies carried out by Vatan (1962). Hassi Messaoud sandstones have experienced an intense and multiphasic diagenesis; and the most significant events during the Palaeozoic and the Mesozoic are listed below:

1. An early and pene-contemporaneous diagenesis occurring at the time of Cambro-Ordovician sedimentation, where alteration of illitic clays and alkaline feldspars into kaolinite took place; this was followed by liberation of silica which resulted in the first quartz cement deposition on the detrital grains. The kaolinitisation and silica deposition are two parallel diagenetic processes. Fennouh (1996) suggested that this phase took place early after deposition of the Cambrian sediments, and probably during Ordovician time which marks the end of an exclusively continental regime and coincides with the beginning of the Ordovician transgression.

2. During the Palaeozoic sediments burial, lithostatic loads exerted by the overlying sediments increase. Deep burial was followed by dissolution of contact points at the top and base of the grains leading to the formation of stylolites. Silica generated provides a source for quartz cement, thus provoking an angular overgrowth of the grains within pore spaces. This silica can also be transported far away and precipitates leading to the formation of a genuine quartzite without any residual porosity. This phase reveals the mechanical and chemical compaction of sediments where the grains undergo intensive overlap. Moreover, Fennouh (1996) suggested that pressure-dissolution phenomena post-dated the early silicification of Hassi Messaoud sandstones.

3. The first registered Hercynian movements at the beginning of the Carboniferous provoked a regional uplift particularly more pronounced within the Hassi Messaoud region. The buried Cambro-Ordovician sediments at about 3000 m maximum burial progressively rose to the surface due to an intense erosion of Silurian and Devonian sediments. Interestingly, Fennouh (1996) noticed the occurrence of petroleum inclusions associated with some cement zones formed during oil emplacement, which indicates progressive arrival of oil in the reservoir before the rocks outcropped beneath the Hercynian unconformity. In fact, Makhous et al. (1997a,b) showed that the local source rocks (Ordovician, Silurian and Devonian) entered the oil window during the Carboniferous and were capable to generate petroleum at this time. Makhous et al. (1997a,b) showed that the Silurian source rock has generated only about 6% of the total generated hydrocarbons during the Carboniferous (from 360 to 286 Ma), prior to the Permian erosion (see section 3.5 above).

4. The uplift to the surface of the Cambro-Ordovician reservoir levels provoked the destruction of the first oil accumulations caused by continuous Hercynian orogenic activity during the period starting from the Carboniferous until the end of the Permian.

5. The presence of a certain palaeo-oil accumulation in the Cambro-Ordovician reservoirs would have played an important role in preventing rapid alteration of the Palaeozoic kaolinite, since the first diagenetic illites started to develop only from the Upper Permian. Through this period of time, the palaeo-accumulations of oil were likely destroyed because of the uplift followed by intense erosion of the Silurian and

Devonian strata. The orogeny then reached its paroxysm, and provoked the development of the illitic cements on the mass of kaolinite generated during the Palaeozoic.

Mesozoic evolution of the Cambro-Ordovician sediments finally involved late diagenesis due to a second burial of the sediments to temperatures above which results in an illitisation of authigenic kaolinite minerals with brines. It seems that this late diagenetic episode took place before the second and final main oil charge that occurred during the Late Cretaceous-early Tertiary (Makhous et al., 1997a,b; Fennouh, 1996). The ages recorded on the authigenic illites vary from 260 to 160 Ma BP; this is equivalent to approximately 100 Ma of diagenesis at relatively high temperatures and high pressures caused by sediment burial below 2.0 km, approximately. The oldest authigenic illites, dated at 260 Ma, are related to the Hercynian orogeny. Therefore, the illitisation process remains continuous throughout the Mesozoic burial. The last (youngest) generation of illites is dated at 160 Ma, which corresponds to the Upper Jurassic. This period probably corresponds to the age of the main arrival of oil and its accumulation in the reservoir during the Mesozoic (Fennouh, 1996). However, results obtained from the study of petroleum inclusions in the Hassi Messaoud sandstones revealed that the oil might have reached the reservoir later than the period suggested by Fennouh (1996). PVT modelling of petroleum inclusions showed that the main filling stages of the Hassi Messaoud reservoirs took place probably between late Cretaceous (about 90 Ma BP) and Palaeogene (about 40 Ma BP) which is in agreement with the results obtained by Makhous et al. (1997a,b) (see section 6.4.3 in chapter 6).

The quartz-cemented, kaolinised, illitised, and doubly compacted sandstones constitute the reservoirs. The Triassic evaporite sediments lying unconformably above make the cap rocks. The arrival of oil in the reservoir during the late Cretaceous produced the oil field. The progressive slow down of diagenesis seen in clay cements of the sandstones, reflects the build up of the oil leg in the late Cretaceous-early Tertiary.

6. Precipitation of sulphate and carbonate cements in the reservoirs driven by the brines percolating into the underlying sedimentary sequence (Cambro-Ordovician series) slowly buried during the Mesozoic period. These Mesozoic age minerals,

generally represented by the anhydrite and other carbonate cements, seem to be mainly associated with the occurrence of fissures and micro-fissures rather than in normal porosity sedimentary deposition character (Fennouh, 1996). Moreover, in some places the anhydrite seems to fill the pores left behind after that the main phase of quartz cementation has ceased. The anhydrite in this Cambro-Ordovician has been introduced through the cracks formed in totally quartz-cemented rocks during the post-Triassic, before arrival of the main oil charge in the reservoirs. The quantities of sulphate and carbonate cements in the sediments generally do not affect the reservoir properties of the moderately quartz-cemented sandstones. On the contrary, in the highly quartz-cemented zones they strongly affect the reservoir properties.

3.5. Hassi Messaoud field

The Hassi Messaoud oil field is separated into twenty five producing oil compartments (Figure 3.9) defined using well tests. Theoretically these compartments are separated by dry zones (non productive zones). Each compartment comprises a number of well connected reservoir segments, and is completely isolated from the adjacent compartments. The limits of one compartment consist for example of permeability barriers inherited from tectonic, sedimentary or diagenetic events which control the petroleum movements during production. However, this compartmentalisation is not absolute since, during operations of gas injection tests, supposed dry wells situated outside productive compartments can be progressively stimulated. This confirms the complexity of the reservoir structure which is still poorly understood. The reservoirs quality vary significantly, even within the same production compartment, because we can often encounter wells with very low or no productivity.

3.5.1. Nature of oil in Hassi Messaoud

Oil in Hassi Messaoud is quite light, characterised by high API gravity (43.5-49°), low viscosity (0.189-0.370 cP), low density (0.604-0.661 g/cm3), low sulphur content (wt% 0.13), and it is under-saturated in gas (the average gas to oil ratio: GOR 221 m^3/m^3). The initial pressure of the reservoir was 483 bars (present day pressure 400 bars) and the present day temperature of the reservoirs ranges between 120 to 132°C. The oil-water contact is approximately situated between 3400 to 3500 m. The total

thickness of the producing reservoir sandstones varies between 175 to 240 m, whilst the oil column thickness can reach up to 310 m.

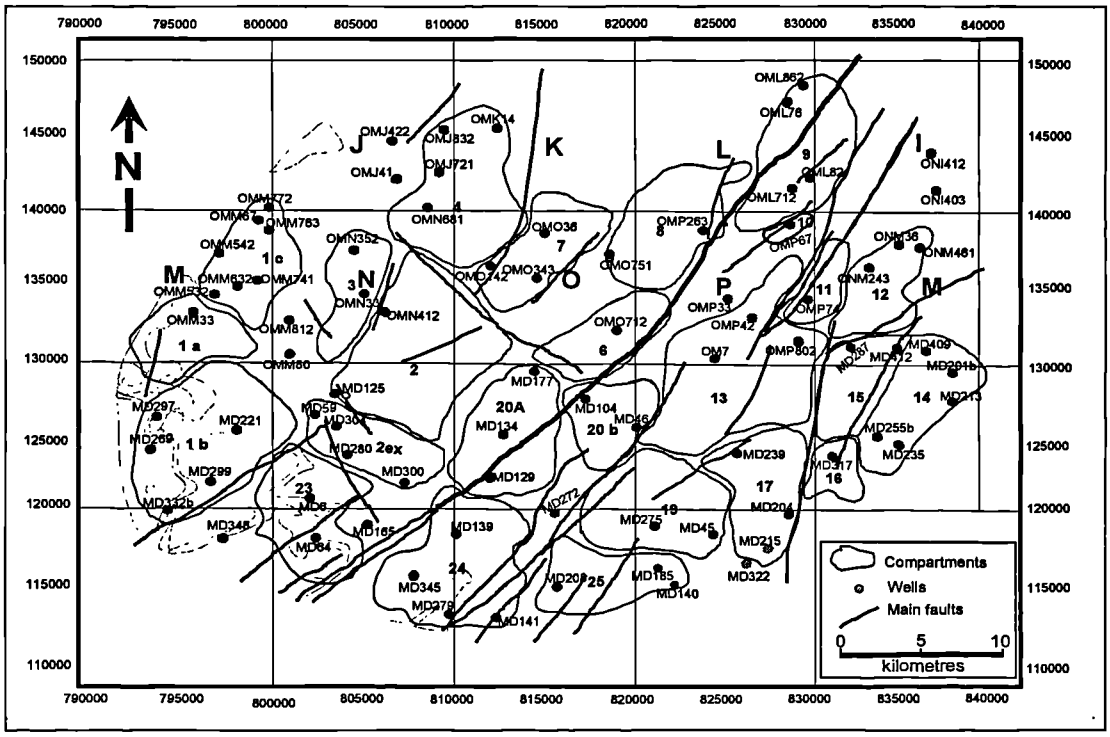

Figure 3.9 Map showing the compartment boundaries within Hassi Messaoud field. (After IFP, 1979, modified by Beicip-Franlab, 1995).

3.6. Review of the burial History and thermal evolution of the study area

So far there is no published work on the burial history of Hassi Messaoud clastic sediments. Nevertheless, it is possible to illustrate the main stages of this evolution by comparison with the Oued Mya clastic sediments, whose stratigraphic and geologic aspects are widely comparable. These discussions are inspired from the work on the Oued Mya basin carried out by Makhous et al. (1997a,b).

The Oued Mya basin shows a stratigraphic section reasonably similar to that of the adjacent Hassi Messaoud ridge (Figure 3.3). Two major structural stages can be distinguished: the Palaeozoic and the Mesozoic separated by the regional Hercynian unconformity (Figure 3.2). In the Hassi Messaoud ridge, the Cambro-Ordovician sediments outcrop along the Hercynian unconformity. The Cambro-Ordovician reservoir layers are unconformably roofed by the impermeable Mesozoic rocks (i.e. Triassic and Jurassic evaporites) (Figure 3.2). Whereas in the Oued Mya region, on the same Hercynian unconformity area generally outcrop the Lower radioactive Silurian shales (Gothlandian Formations). These are capped by the Permo-Triassic

and the Triassic containing quite thick impermeable rocks, which constitute the main seal for the Palaeozoic reservoirs.

Burial and thermal history modelling for the Oued Mya basin was achieved using the 1D GALO model (Makhous et al., 1997a). This model generates numerical simulations of the evolution of a sedimentary basin. The program calculates variations in the sedimentary bed thickness, predicts the thermal regime in the sedimentary cover or in the basement, and estimates the potential hydrocarbon yield of the source rocks. The key parameters for the GALO model comprise the present-day sedimentary cross section, estimates of the amplitude and rate of erosion, the lithological composition and petrophysical characteristics of rocks, the structure of the lithosphere (basement) and its rock parameters, paleotemperature markers (vitrinite reflectance), paleoclimate, sea paleodepths, present-day surface heat flow, depth-temperature profiles, and information on the paleotectonics and the present-day tectonic setting of the basin. Data displayed in Table 3.2 and Table 3.3 have been used by Makhous et al. (1997a) to establish the thermal evolution and burial history in the Takhoukht region, Oued Mya basin. The input data on basin evolution assume that about 2.2 km of Silurian and Devonian sediments were eroded during the Permian Hercynian orogeny. The presence of thick layers of these sediments in neighbouring sedimentary sections supports this assumption.

The geological history of the northern Oued Mya basin shows two major stages of Palaeozoic and Mesozoic subsidence separated by the Hercynian orogeny and uplift (Figure 3.10, Table 3.2) (Makhous et al., 1997b). During the first period of the basin evolution (i.e. from 600 to 480 Ma), minor variations in the amplitude of tectonic subsidence illustrate simply moderate variations in heat flow during this time. During the Cambro-Ordovician, the calculated heat flow stabilises around 50mW/m^2 (Figure 3.11). Basement subsidence which occurred in the Silurian and Devonian (400 to 350 Ma) accompanied the deposition of about 2500 m of clays and sands (Makhous et al., 1997a). This event seems in agreement with an important basement stretching. This rifting would have started during the middle Ordovician, when the water column in the marine basin reached more than 100m.

Sinking of the isotherms at about 490 Ma is related to climate cooling (Figure 3.10), which continued up to Early Carboniferous (Makhous et al., 1997a). The subsequent

increase of the isotherms at 450-350 Ma is related to the transition from low-temperature gradients in the basement (high thermal conductivity) to higher temperature gradients in the sedimentary cover (low thermal conductivity).

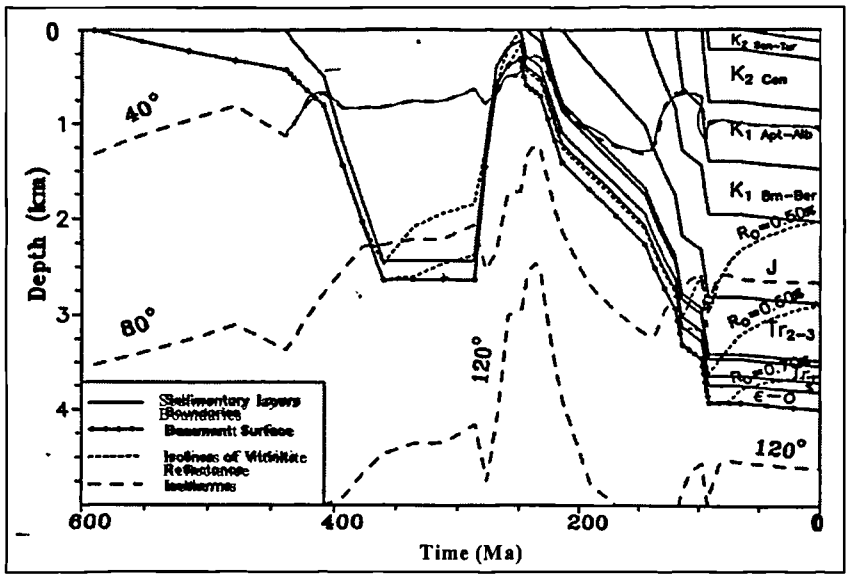

Figure 3.10 Burial, thermal and maturation histories of the sedimentary section in Takhoukht region of the Oued Mya basin resulting from basin modelling. (After Makhous et al., 1997a).

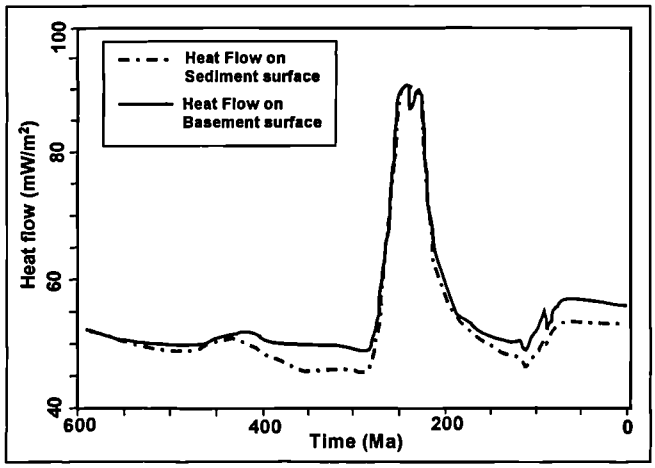

Figure 3.11 Computed variations in the Heat flow during the Oued Mya basin modelling, Takhoukht region. (After Makhous et al., 1997a).

Table 3.2 The main stages of the Oued Mya basin evolution at the Takhoukht region. (After Makhous et al., 1997a).

N	Stage of evolution	Geological time (Ma)	Depth (m)	Rock type	Surface temperature (°C)	Sea level (m)
1	Sedim.	0-65	0-125	sn,lm	15	0
2	Hiatus	65-91	125	-	15-18	0
3	Sedim.	91-93	125-322	lm,dl,lm	12-18	0-30
4	Sedim.	93-97.5	322-870	hl,an	12-13	30-80
5	Sedim.	97.5-113	870-1042	cl,an	13-15	80-170
6	Sedim.	113-119	1042-1489	cl,sn	15	170
7	Sedim.	119-144	1489-2033	cl,sl,dl,ml	15-18	170-130
8	Sedim.	144-213	2033-2886	cl,dl,hl,an,ml	18	130-0
9	Sedim.	213-231	2886-3485	cl,hl,an	18	0
10	Sedim.	231-243	3485-3540	cl,sn,hl	18	0
11	Sedim.	243-248	3540-3711	vl	18	0
12	Eros.	248-286	2200-2200	-	15-18	0
13	Sedim.	286-360	3711-3711	cl,sn	8-15	0
14	Sedim.	360-408	3711-3711	cl,sn	7-8	0-240
15	Sedim.	408-428	3711-3854	cl,sn	5-7	240-350
16	Sedim.	428-438	3854-3924	cl,sn	5	350
17	Sedim.	438-590	3924-4100	cl,sn	5-15	350-0

Depth column shows present-day depths of the bottom (first number) and roof (second number) of the sedimentary layers; that is, the erosion amplitude. Sed. = sedimentation, Eros. = erosion, an = anhydrite, cl = clay and shale, dl = dolomite, hl = halite, lm = limstone, ml = marl, sl = silstone, sn= sandstone, vl = volcanics.

Table 3.3 Petrophysical parameters of sedimentary rocks in the Takhoukht region of the Oued Mya basin. (After Makhous et al., 1997a).

N	*Po*	*B (km)*	*Km* *(W/m°C)*	*Al* *($°C^{-1}$)*	*C υ* *(Mj/m^3K)*	*ρ_m* *(g/cm^3)*	*A* *(mkW/m^3)*
1	0.429	2.77	4.00	0.0027	2.872	2.66	0.816
2	-	-	-	-	-	-	-
3	0.572	1.91	3.49	0.0011	2.696	2.73	0.578
4	0.244	0.86	5.61	0.005	1.943	2.3	0.050
5	0.577	1.39	3.71	0.003	2.332	2.52	0.888
6	0.600	2.06	2.96	0.0017	2.575	2.71	1.465
7	0.635	1.88	2.82	0.0011	2.487	2.7	1.394
8	0.296	1.2	5.17	0.0043	1.993	2.32	0.209
9	0.354	1.24	4.12	0.004	1.955	2.3	0.431
10	0.620	1.94	2.81	0.0015	2.462	2.66	1.549
11	0.500	3.27	2.01	0.0001	2.500	2.7	1.005
12	-	-	-	-	-	-	-
13	-	-	-	-	-	-	-
14	0.610	2.03	2.88	0.0016	2.549	2.68	1.516
15	0.684	1.84	2.24	0.0007	2.324	2.69	1.968
16	0.684	1.84	2.24	0.0007	2.324	2.69	6.699
17	0.684	1.84	2.24	0.0007	2.324	2.69	1.968

N = number of the basin's evolution stage; *Po* = average rock porosity within the near-surface layer at the depth of 0-200m; *B* = scale for porosity change vs depth in the law [$(Pz = Po\ exp(-z/B))$]; *Km* = heat coductivity of the matrix rocks at the temperature T = 0°C; *Al* = temperature coefficient of matrix heat conductivity [$K(t) = Km/(1.0 + Al \times T(°C))$]; *C υ* = volume heat conductivity of matrix rocks; A = heat generation per unit volume . The values in this Table were computed according to relative content of facies and data in Table 3.1.

Devonian sedimentation was followed by a long interruption that lasted during the Carboniferous (Makhous et al., 1997a,b). The subsequent Hercynian orogeny resulted in uplift and erosion of the north-eastern part of the basin, including the Takhoukht region.

During the Permian, the Hercynian orogeny results in the erosion of approximately 2.2 km of Devonian and Silurian (Makhous et al., 1997a,b). At Hassi Messaoud, this erosion would have been more intense, removing all of the Siluro-Devonian strata. However, the erosion of the Siluro-Devonian strata would have slowed down the rates of diagenesis across the Cambro-Ordovician reservoirs. Therefore, this would have probably contributed to the improvement of the Cambro-Ordovician reservoir properties.

In this model, the first Hercynian orogenic activation started at the end of the Carboniferous (280 Ma, Figure 3.10). Throughout this event, the heat flow at the surface reached up to 90 mW/m^2 (Figure 3.11). Furthermore, the presence of the interstratified volcanic formations confirms the occurrence of high heat flow (Fennouh, 1996). This orogeny reaches its paroxysm in the Permian and is then followed by pronounced post Triassic subsidence. This secondary subsidence is characterised by a rapid cooling of the anomalously warm basement (Makhous et al., 1997a,b). Fast sedimentation of salts and the anhydrites characterised by high heat conductivity, also contributed to the significant fall of the isotherms at the Jurassic and the Cretaceous (Figure 3.10). In the Cretaceous, sedimentation was accompanied by stretching of the lithosphere, which lasted to the end of the Cenomanian (Makhous et al., 1997a,b). The last thermal activity of the lithosphere seems to have started much before the second phase of stretching has finished. The rising of isotherms in the Lower Cretaceous is related to this heating event, as well as to the deposition of low-conductivity sediments (Makhous et al., 1997a,b). However, the sedimentation of 800 m of salt during the Albian and Cenomanian resulted in short-term sinking of the isotherms. Slow sedimentation during the Cenozoic resulted in only negligible variation in the depths of isotherm and heat flow (Figure 3.10 and Figure 3.11). The present-day temperatures correlate well with the temperatures measured at 3739, 3785, and 3989 m in boreholes (Makhous et al., 1997a,b).

In summary, we can say that the principal geological information that we can extract from this brief overview on the subsidence history of these sediments are mainly linked to the existence of two long burial periods: the Palaeozoic period (590 to 360 Ma) and the Mesozoic period (286 Ma to present), separated by a major Hercynian

uplift event which is responsible for several very important features of the geology (Figure 3.10).

1. During the Palaeozoic, the central part of Oued Mya basin and the adjacent uplifts including the arch containing Hassi Messaoud field are characterised by a thick series of sediments which reached 3000 m in thickness. Then, at the end of the Carboniferous, the average depth of the burial of the Palaeozoic sediments for the whole central province would have been around 3000 m for the Ordovician, 2800 m for the Silurian shales, 2500 m for the lower Devonian and 2200 to 1500 m for the middle and the upper Devonian section, respectively. The Hercynian orogeny has provoked a significant uplift causing erosion of 2.2 m of the Siluro-Devonian sections, reaching well into the Palaeozoic section.

2. During the first phase of burial, i.e. the Palaeozoic, the organic matter in the Palaeozoic sections including potential source rocks in Silurian and Ordovician Formations undergone its first maturation phase with maximum temperatures of 82-84 °C and 84 to 90 °C, respectively likely estimated to have been reached in the Takhoukht region (Makhous et al., 1997a,b). In fact at the end of the Carboniferous, the organic matter contained in the lower Palaeozoic sediments (Ordovician, Silurian, and probably Devonian sediments) were susceptible to generate liquid hydrocarbons and gas (Figure 3.12). In the case of the Hassi Messaoud area, we can suppose that the eroded Silurian and Devonian sediments had also high organic carbon content with good petroleum potential. These sediments would have generated hydrocarbons which formed the first accumulations in the Cambro-Ordovician sandstones simply by vertical "per ascendum" and lateral migration from the neighbouring source rocks (Makhous et al., 1997a,b).

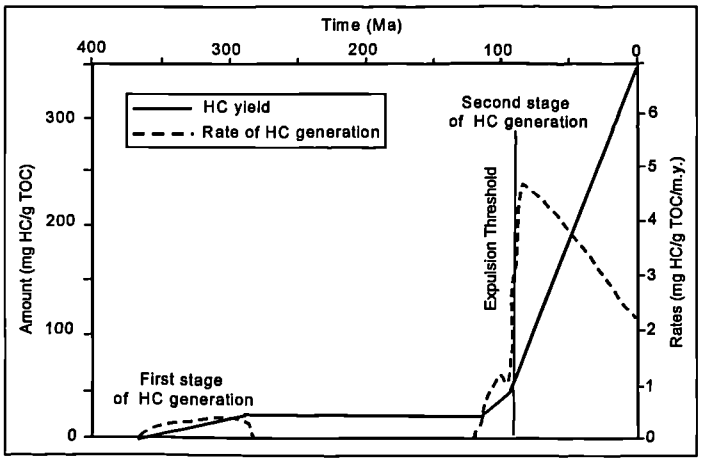

Figure 3.12 Hydrocarbon yields (solid line), rates of hydrocarbon generation (dashed line), and expulsion threshold in the geological history of the Silurian source shales of the Oued Mya basin. Calculations used time-temperature history of the Silurian source rocks and activation energy shown in Makhous et al. (1997a). Two stages of hydrocarbon generation took place in the basin history: in the pre-erosion Carboniferous and during the Cretaceous-Cenozoic. (After Makhous et al., 1997b).

3. The Hercynian orogeny provoked a regional uplift. The main effect of this event on the Hassi Messaoud region was severe erosion of the Palaeozoic formations, and a cessation of the petroleum generation process. Therefore, the pre-existing petroleum in the Hassi Messaoud generated during the first cycle of the Palaeozoic subsidence was likely lost during the uplift followed by the erosion of the Siluro-Devonian sections and the outcrop of the Cambro-Ordovician reservoirs (Makhous et al., 1997a,b). Microscopic observations of the oxidised solid bitumen on the pore surfaces in the Cambro-Ordovician sediments of the Hassi Messaoud reservoirs may be considered as an evidence for the existence of palaeo-petroleum in the Hassi Messaoud reservoir (Fennouh, 1996). Fennouh (1996) reported that in several samples (mainly samples from the top parts of the Hassi Messaoud reservoirs) the organic matter plugging the pore surfaces is severely altered by oxidation, showing a characteristic reddish colouring. This oxidation may represent the direct consequences following the uplift and the outcrop of the Hassi Messaoud Cambro-Ordovician sediments.

4. During the Mesozoic, intense subsidence of the whole region including the Oued Mya basin and the adjacent rocks of the Hassi Messaoud area took place. Deposition of a great thickness of evaporites, shales and carbonate (e.g. thickness of the Triassic and the Jurassic only account for 1500 m) provoked a long and progressive burial, returning the Palaeozoic rocks (i.e. Silurian and Ordovician strata) to high temperatures and pressures (Figure 3.10). In some deep parts of the Oued Mya, the

Ordovician sediments reached about 5500 m depth whereas those of the Silurian reached about 4000 to 4200 m of depth. At the end of the Mesozoic, the Silurian and Ordovician organic matter had been probably heated to high temperatures; between approximately 100 and 200 °C depending on the burial depth (Makhous et al., 1997a,b). Therefore, the regional Mesozoic subsidence is an important factor controlling the formation of petroleum. The newly generated petroleum accumulated into Palaeozoic (Cambro-Ordovician and Devonian) and Mesozoic (Lower Triassic) traps across the Oued Mya-Hassi Messaoud ridge petroleum system.

Finally, Figure 3.13 displays an events chart which summarizes the ages and timing of various elements and events in the petroleum system (sources, reservoirs, seals, trap development, and generation and migration of petroleum).

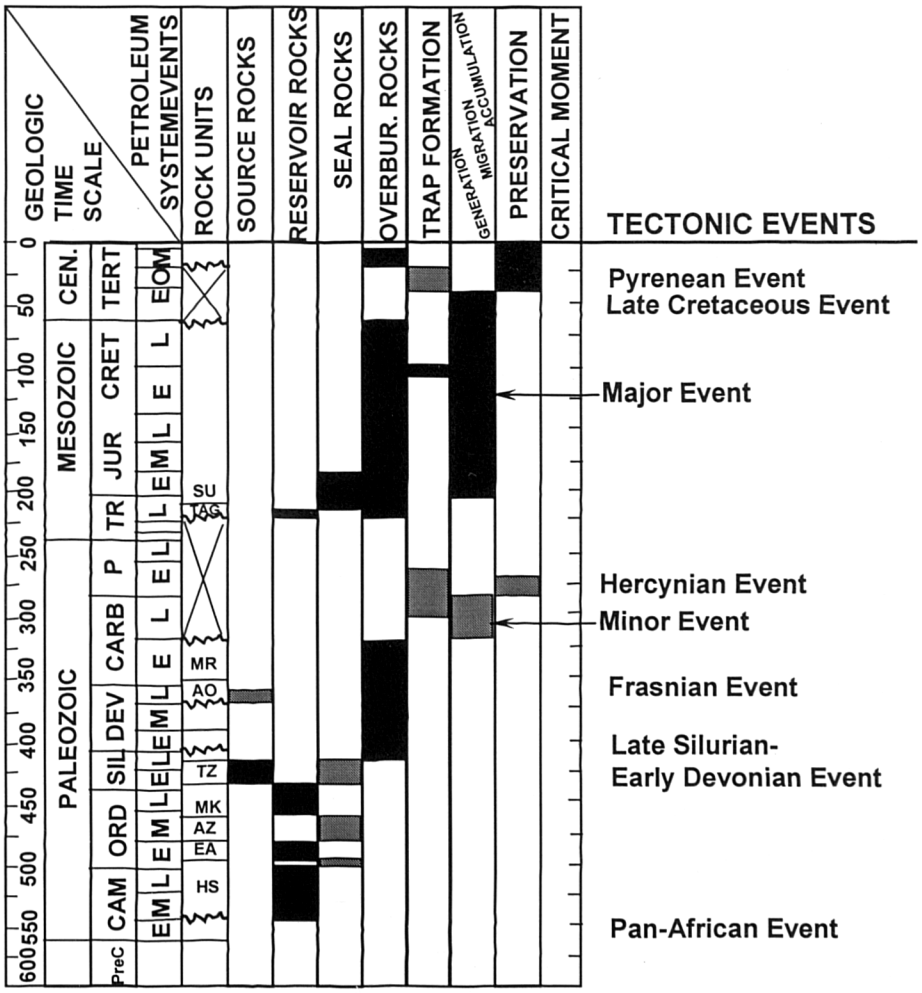

Figure 3.13 Events chart for the Oued Mya petroleum system. Gray boxes indicate secondary or possible occurrences. (After Klett, 2000).

Chapter 4
Geochemical Outline of the Oued Mya Basin-Hassi Messaoud Ridge Petroleum System

4. Geochemical outline of the Oued Mya basin-Hassi Messaoud ridge petroleum system

4.1. Introduction

The aim of this chapter is to present a regional geochemical outline of the study area which includes an assessment of the organic content, source facies and petroleum maturity variations of the potential Ordovician and Silurian source rocks within the Oued Mya basin and reservoired petroleums throughout the Oued Mya depocentre and the Hassi Messaoud Ridge area. This chapter also assesses the main source rock responsible for the generation of all the petroleum so far discovered in the area by performing oil/oil and oil/source rock correlations. The fields concerned in this study fall into two groups; (1) fields reservoired in the Devonian and Lower Triassic, located near the Oued Mya depocentre, which are generally small and often associated with sand pinchouts; (2) the broad low-relief structural traps developed in Cambro-Ordovician quartzite reservoirs on the adjoining Hassi Messaoud Ridge (Balducchi and Pommier, 1970; Odeh, 1975).

The Oued Mya basin is an elongate Palaeozoic cratonic sag west of Hassi Messaoud Ridge, lying unconformably beneath a north-easterly thickening wedge of Mesozoic sediments. The central and southern parts of the Oued Mya basin are unproductive, but the northern arm is prolific, with a number of fields reservoired in basal Triassic sandstones sealed by late Triassic evaporites. Devonian and Lower Triassic sandstones lie unconformably in direct contact over the basal Silurian source rock which is still preserved across Oued Mya basin.

Key controls on petroleum occurrence within the Devonian and Lower Triassic (Oued Mya basin) and Cambro-Ordovician (Hassi Messaoud Ridge) reservoirs are their positioning below the Jurassic evaporites and at the Hercynian unconformity which controls both petroleum migration and entrapment. Liassic salt extends across the area playing a crucial role in preventing any leakage of petroleum. No oil has been encountered in the post salt and no seeps are recorded in the region.

It is generally well documented that the thin basal and highly radioactive Silurian "hot" shales which correspond to the Tannezuft Formation is accountable for the

generation of most of the petroleum (oil and gas) within the entire Sahara platform and particularly in the Oued Mya basin (Sonatrach, unpublished reports; Daniels and Emme, 1995; Makhous et al., 1997a,b; Macgregor, 1996). The Middle to Late Devonian Formations also have excellent source rock quality in the Sahara platform, however, its lateral extent is limited by Hercynian erosion (e.g. the Devonian shales are absent over much of the Oued Mya basin). To a lesser degree, the Ordovician shales (El-Gassi and Azzel Formations) can be considered as potential source rocks within the region largely because of their moderate TOC values (average TOC of 0.9%) and the important thickness (up to 150m) in some areas of the basin (Makhous et al., 1997a,b; Sonatrach, unpublished reports). The present distribution of Ordovician and Silurian source rock shales is a function of their initial depositional distribution and the extent of subsequent Hercynian erosion. Maximum initial thicknesses were recorded in the south, southwest, and west of the basin. Present day thicknesses range from 600 to 700 m in the south to 280 to 660 m in the west and 220 to 460 m in the centre of the basin.

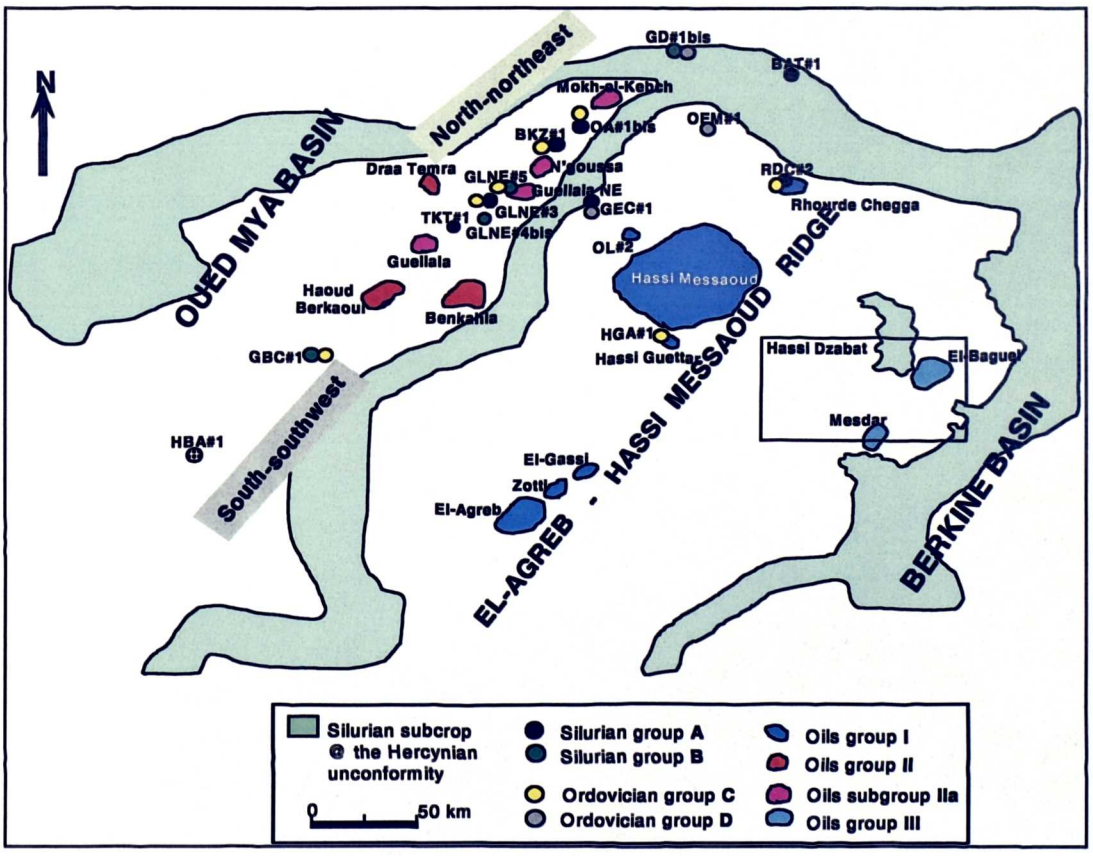

Figure 4.1 Silurian, Ordovician source rock samples and oil fields location map.

4.2. Organic carbon content and petroleum potential variations throughout Oued Mya basin

Geochemical parameters obtained using screening methods for total organic carbon content and Rock-Eval pyrolysis data are displayed in Table 4.1. Fifty six (56) rock samples were selected to represent two different source rocks in the Oued Mya basin, Ordovician (20 samples from El-Gassi, Azzel, and micro-conglomeratic shales and Oued Saret Formations) and Silurian (33 samples) and 3 source rock samples from the El-Gassi shales Formation located in the Hassi Guettar field (Figure 4.1). All of the Silurian samples revealed considerable variations in organic richness; samples show moderate to excellent organic richness indicated by the total organic content (TOC) values ranging from 0.99 to 14.30 wt% (average 9.21 wt%). The lowest TOC values are encountered in the samples GEC#1 (3660.6m), 0.99 wt% and GLNE#3 (3803.45m and 3809.45m) 1.81 and 1.31 wt%, respectively (Table 4.1). The Ordovician samples showed low to moderate organic richness with TOC values ranging from 0.17 to 2.36 wt% (average 0.85 wt%) (Figure 4.2).

The Rock-Eval pyrolysis data agree well with the distribution of the total organic content (TOC) values. The Silurian samples that are extremely rich in organic carbon, revealed low to extremely high residual petroleum potential ranging from 1.31 to 34.60 mg HC/g of rock (average 20 mg HC/g of rock). The lowest residual petroleum potential values are recorded in the samples GEC#1 (3660.6m) and GLNE#3 (3803.45m and 3809.45m) and the highest residual petroleum potential values are recorded in the Silurian samples from wells TKT#1, GLNE#4bis, BAT#1, BKZ#1, OA#1bis, RDC#2, and GLNE#5, respectively. All these wells are located in the northeast of the Oued Mya basin (Figure 4.1). Moreover, two Silurian samples from the well GBC#1 located south of the above wells show low residual petroleum potential despite their high TOC values (5.07 wt% and 9.67 wt%) this is likely because of the high maturity of these two samples. In Figure 3.9b (chapter 3), I have shown that the Silurian source rock in this well is more mature than the Silurian source rocks in the northeast of the basin. The Silurian source rock in the well GBC#1 showed vitrinite reflectance equivalent R_o values between 1% and 2%, however, the Silurian source rocks in the northeast of the basin show vitrinite reflectance R_o values of less than 1%. This is indeed consistent with the Tmax values obtained from the pyrolysis of the source rock samples. The Tmax values range from 440 °C to 452 °C

(average 445.3 °C) in the Silurian source rocks located in the northeast of the basin and range from 454 °C to 458 °C (average 456 °C) in the Silurian source rock from the well GBC#1. Therefore the Silurian source rocks from the northeast of the Oued Mya basin are in the main to late oil window, whereas, further south where well GBC#1 is located the Silurian source rocks are overmature, and probably they have reached the onset of the condensate window. The main phase of oil generation in this region (i.e. nearby GBC#1) likely occurred during the Palaeozoic. The Ordovician samples reveal extremely low to low petroleum potential ranging from 0.32 to 2.62 mg HC/g of rock (average 1.36 mg HC/g of rock). The Ordovician source rock samples show the same range of maturity as the Silurian source rock samples in the northeast of the basin, the Tmax values vary between 439 °C and 459 °C (average 444 °C) (Table 4.1).

The Silurian source rock samples from the wells located in the northeast of the basin show moderate values of the Hydrogen Index (HI) ranging from 132.2 to 309.46 mg HC/g of rock (average 185 mg HC/g of rock); whereas the Silurian source rocks from well GBC#1 reveal much lower Hydrogen Index ranging from 21.1 to 52.84 mg HC/g of rock (average 37 mg HC/g of rock) (Figure 4.2). This is consistent with the very high maturity of the Silurian source rocks in this region, and confirms that the whole petroleum potential of the Silurian in this region was likely generated and expelled during the Palaeozoic. Again, the Hydrogen Index in the Ordovician is generally lower than the Silurian source rocks ranging from 10.26 to 215.85 mg HC/g of rock (average 122.68 mg HC/g of rock). Indeed for relatively mature source rocks, as revealed by Tmax values ranging from 440-458 °C (Table 4.1) and maturity based on the biomarkers and aromatic compounds (section 4.3.1.2.2), such percentages of organic carbon content (TOC) would classify the Silurian as excellent source rocks. These Silurian source rocks have already generated oil and the original TOC values, prior to generation, would have been significantly higher. Moreover, it is well documented that these Silurian source rocks contain Type II marine, low sulphur oil-prone kerogen (Daniels and Emme, 1995; Makhous et al., 1997a,b).

Table 4.1 Bulk geochemical data showing the total organic carbon and pyrolysis data for the Silurian and Ordovician shale source rocks in the Oued Mya basin.

Well	Depth	Age	Formation	CM (wt%)	TOC (wt%)	S1 (mg HC/g rock)	S2 (mg HC/g rock)	HI (mg HC/g TOC)	PP(mg HC/g rock)	Tmax (°C)
RDC#2	3804.7	Silurian	hot shales	1.34	8.11	1.91	10.55	130.09	12.46	445
RDC#2	3805.15	Silurian	hot shales	nm	6.82	2.28	9.21	135.04	11.49	452
RDC#2	3806.4	Silurian	hot shales	1.15	7.91	1.80	13.30	168.14	15.10	440
RDC#2	3808.35	Silurian	hot shales	0.04	14.30	2.92	26.98	188.67	29.90	445
RDC#2	3810.8	Silurian	hot shales	1.32	11.60	2.44	20.20	174.14	22.64	444
BAT#1	3947	Silurian	hot shales	2.23	11.70	5.54	19.49	166.58	25.03	442
BAT#1	3957	Silurian	hot shales	2.03	9.72	4.02	24.43	251.34	28.45	450
BAT#1	3959.55	Silurian	hot shales	1.23	8.06	5.10	17.97	222.95	23.07	447
GD#1bis	3850	Silurian	hot shales	nm	5.88	1.55	16.42	279.25	17.97	451
OA#1bis	4119.3	Silurian	hot shales	1.6	10.70	3.24	24.89	232.62	28.13	446
OA#1bis	4122	Silurian	hot shales	1.05	12.50	3.43	26.77	214.16	30.20	442
OA#1bis	4123.3	Silurian	hot shales	2.2	10.80	2.41	27.78	257.22	30.19	444
OA#1bis	4132.25	Silurian	hot shales	2.02	9.79	2.17	20.54	209.81	22.71	445
OA#1bis	4142.25	Silurian	hot shales	0.32	12.50	3.39	14.34	114.72	17.73	443
OA#1bis	4145.35	Silurian	hot shales	0.53	11.70	2.74	16.03	137.01	18.77	440
OA#1bis	4151.55	Silurian	hot shales	0.36	7.36					
BKZ#1	4180.6	Silurian	hot shales	1.2	7.28	8.58	12.11	166.35	20.69	440
BKZ#1	4183.8	Silurian	hot shales	0.92	9.50	5.30	14.43	151.89	19.73	445
BKZ#1	4187.86	Silurian	hot shales	3.11	12.60	5.07	27.42	217.62	32.49	451
BKZ#1	4189.5	Silurian	hot shales	2.31	12.10	4.02	23.95	197.93	27.97	450
GLNE#5	3983.6	Silurian	hot shales	2.85	8.05	2.59	10.06	124.97	12.65	444
GLNE#5	3987.55	Silurian	hot shales	3.94	8.07	3.05	8.30	102.85	11.35	441
GLNE#5	3994.45	Silurian	hot shales	2.8	9.67	3.82	12.33	127.51	16.15	446
GLNE#5	4001.45	Silurian	hot shales	2.5	12.50	2.49	21.96	175.68	24.45	447
GLNE#4bis	3874.85	Silurian	Hot Shales	3.94	11.00	2.50	24.07	218.82	26.57	444
GLNE#4bis	3876.9	Silurian	Hot Shales	3.11	13.80	3.52	29.31	212.39	32.83	442
GLNE#3	3803.45	Silurian	hot shales	nm	1.81	0.64	3.66	202.21	4.30	446
GLNE#3	3809.45	Silurian	hot shales	nm	1.31	0.51	1.73	132.06	2.24	451
TKT#1	3868.6	Silurian	hot shales	nm	9.79	3.51	19.20	196.12	22.71	449
TKT#1	3872.5	Silurian	hot shales	nm	11.20	5.87	34.66	309.46	40.53	446
GEC#1	3660.6	Silurian	hot shales	nm	0.99	0.93	1.31	132.32	2.24	441
GBC#1	3213	Silurian	hot shales	nm	9.67	1.37	5.11	52.84	6.48	454
GBC#1	3259	Silurian	hot shales	nm	5.07	0.37	1.07	21.10	1.44	458
RDC#2	3911.38	Ordovician	micro-cong. shales	0.4	0.58	0.22	0.80	137.93	1.02	446
OEM#1	3910.45	Ordovician	Oued sarret sand	0.43	1.62	0.22	2.20	135.80	2.42	441
OEM#1	3920.6	Ordovician	Oued sarret sand	0.8	1.64	0.45	2.02	123.17	2.47	436
OEM#1	3924.65	Ordovician	Oued sarret sand	0.84	1.54	0.32	2.30	149.35	2.62	444
OEM#1	3930.65	Ordovician	Oued sarret sand	0.88	0.73	0.45	1.58	215.85	2.03	442
OA#1bis	4367.4	Ordovician	Oued sarret sand	0.75	0.79	0.50	1.11	140.68	1.61	440
OA#1bis	4462.75	Ordovician	Oued sarret sand	1.36	0.67	0.57	0.90	135.14	1.47	444
OA#1bis	4599	Ordovician	El Gassi Shales	nm	0.24	0.18	0.31	129.17	0.49	445
BKZ#1	4198.95	Ordovician	micro cong. shales	0.4	0.75	0.45	1.42	189.84	1.87	450
GLNE#5	4024.05	Ordovician	micro cong. shales	0.67	0.51	0.63	0.98	192.53	1.61	446
GLNE#5	4026.3	Ordovician	micro cong. shales	0.64	0.52	0.36	0.87	166.03	1.23	445
GLNE#3	3936.08	Ordovician	?	nm	0.36	0.24	0.74	205.56	0.98	445
GEC#1	3770.9	Ordovician	?	0.89	0.47	0.17	0.56	118.90	0.73	445
GBC#1	3272.1	Ordovician	Azzel shales	0.73	0.60					
GBC#1	3386.6	Ordovician	Azzel shales	0.41	1.26	1.11	0.83	65.87	1.94	440
GBC#1	3394.4	Ordovician	Azzel shales	0.64	2.36	0.17	0.55	10.26	0.72	445
GBC#1	3398.6	Ordovician	Azzel shales	0.41	0.94	0.91	0.27	28.75	1.18	439
GBC#1	3400.7	Ordovician	Azzel shales	0.52	0.97	0.72	0.15	15.46	0.87	446
HGA#1	3391	Ordovician	El Gassi Shales	nm	0.17	0.08	0.25	147.06	0.33	459
HGA#1	3412	Ordovician	El Gassi Shales	nm	1.15	0.05	0.27	23.48	0.32	446
HGA#1	3439	Ordovician	El Gassi Shales	nm	0.29					

CM = Mineral Carbon, TOC = total organic carbon, HI = hydrogen index, PP =petroleum potential.
nm = not measured

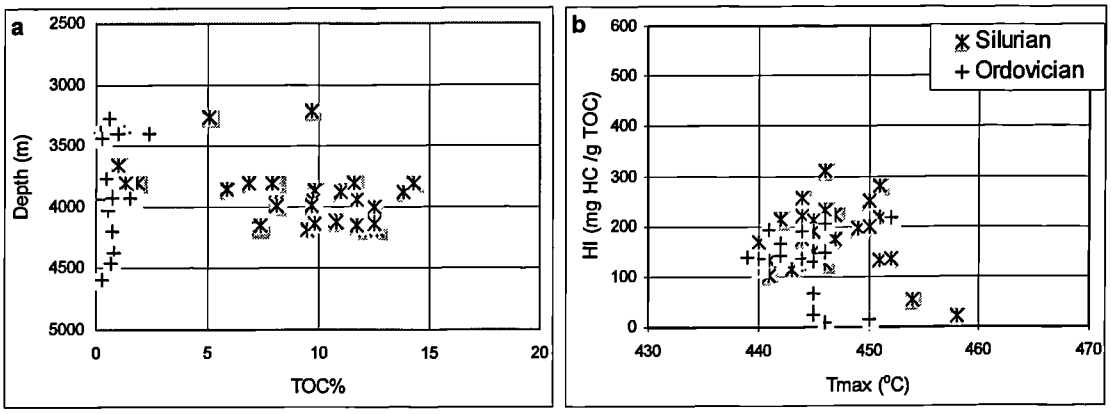

Figure 4.2 Cross plots showing (a) Total organic carbon (TOC) versus depth and (b) Hydrogen index versus Tmax in the Ordovician and Silurian source rocks in the Oued Mya basin.

4.3. Molecular characterisation of source rock and oil samples within the Oued Mya basin and Hassi Messaoud Ridge

This section presents an organic geochemical molecular description of the suite of Ordovician and Silurian source rock samples together with the oil samples collected from the different Triassic reservoirs in the Oued Mya basin and the Cambrian reservoirs in the Hassi Messaoud Ridge area analysed in this project. The source facies and the level of thermal maturity of all these samples will be assessed through the distribution of specific saturated as well as aromatic hydrocarbon compounds.

4.3.1. *Normal*-alkanes and isoprenoid alkanes

A representative gas chromatogram of the saturated hydrocarbon fraction showing the *n*-alkanes and isoprenoid alkane distributions (*n*-C_{10}+) within a typical Silurian source rock samples is displayed in Figure 4.3, and values for geochemical parameters based on *n*-alkanes and isoprenoid alkanes distributions are listed in Table 4.2. In most of the samples collected from the Silurian, the *n*-alkane distribution is generally dominated by short-chain (*n*-C_{10} to *n*-C_{20}) over the long-chain *n*-alkanes (Figure 4.4), and the *n*-C_{17}/*n*-C_{27} ratio ranges from 4 to 11.56; this is characteristic of marine organic matter and may suggest algal input (Debyser et al., 1977 and Dastillung and Corbet, 1978).

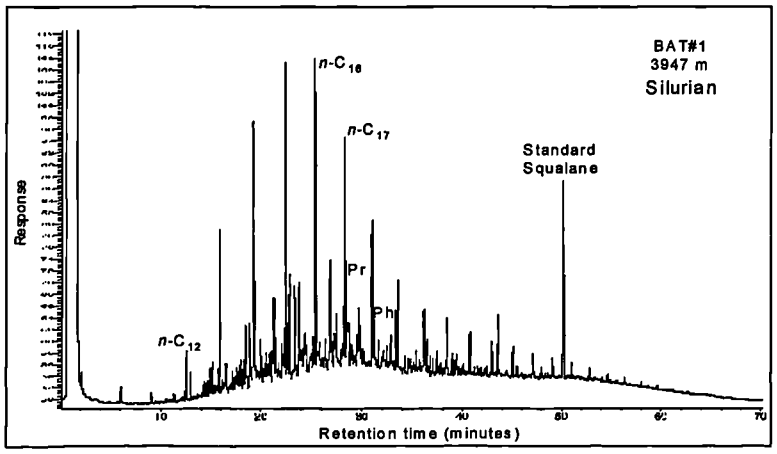

Figure 4.3 Gas chromatogram of the saturated and aromatic hydrocarbon fraction isolated from a typical Silurian source rock (BAT#1 3947m) in the Oued Mya basin. Pr = Pristane and Ph= Phytane.

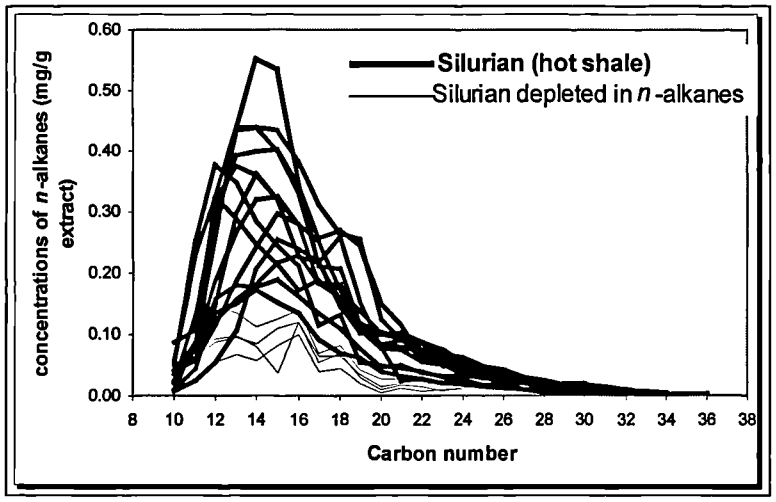

Figure 4.4 *n*-alkane envelopes of Silurian source rock samples in the Oued Mya basin.

Samples collected from wells RDC#2 (3804.70 m, 3806.40 m, 3808.35 m and 3810.80 m), OA#1bis (4142.25 m and 4145.35 m) and to a lesser extent samples from wells GLNE#4bis (3874.85m), BKZ#1 (4187.86m and 4189.95m) and GLNE#5 (4001.45m) exhibit low total *n*-alkane concentrations, ranging from 0.61 to 1.51 mg/g of extract and 1.31 and 2.33 mg/g of extract, respectively (Table 4.2). The gas chromatograms of the samples from wells RDC#2 and OA#1bis are dominated by aromatic hydrocarbons (alkylnaphthalenes and alkylphenanthrenes) over the *n*-alkanes, whereas the gas chromatograms of the samples from wells GLNE#4bis, BKZ#1 and GLNE#5 contain relatively less abundant aromatic hydrocarbons (alkylnaphthalenes and alkylphenanthrenes) than the samples in wells RDC#2 and OA#1bis (Figure 4.6). Moreover, the gas chromatogram of the whole extract sample

RDC#2 (3804.70m) reveals a similar distribution to that shown by the hydrocarbon fraction in the same sample (Figure 4.7).

Interestingly, a number of cases where the composition of organic matter extracts showed a predominance of aromatic hydrocarbons compared to the aliphatic hydrocarbons have been reported in the literature (e.g. Dahl et al., 1988; Lewan and Buchardt, 1989; Horsfield et al., 1992; Schlepp et al., 2001). Dahl et al. (1988) and Lewan and Buchardt (1989) showed that the Cambrian Alum Shales of Sweden contain abundant organic matter (up to 16%) and anomalously high uranium concentrations (up to 420ppm). The Cambrian Alum Shales also showed unusual features such as: a decrease of the kerogen H/C ratios and the amount of the extractable organic matter with increasing uranium concentrations and an increase in the ratio of aromatic to aliphatic hydrocarbons, and the percentage of polars, asphaltene and resins with increasing uranium concentrations. These authors concluded that the extractable organic matter in the Cambrian Alum Shales of Sweden is believed to have been altered by irradiation from the natural decay of uranium. In addition, Dahl et al. (1988) showed that acyclic isoprenoid hydrocarbons are absent in extracts and kerogen pyrolysates of samples with high uranium concentrations. They therefore appear more susceptible to irradiation induced alteration than *normal* alkanes, which are in turn less stable to irradiation than aromatic hydrocarbons. Horsfield et al. (1992) have performed pyrolysis-gas chromatography on a series of seven Alum Shales samples which contain alginitic kerogens at different levels of alteration. They have reported that all the pyrolysates showed abundant presence of lower molecular weight normal, branched and aromatic hydrocarbons. They have suggested that the unusual structure of the Alum Shales alginate might have been caused by uranium related alteration effects and/or might have been directly inherited from biopolymeric or carotenoid-derived precursors in algae and bacteria.

Moreover, Schlepp et al. (2001) investigated the influence of paleoenvironment and radiolytic alteration on the geochemistry of organic matter from Autunian shales of the Lodève uranium deposit, France and observed that (1) parameters such as Hydrogen Index and yield of organic extract are influenced by the uranium content and therefore by radiolytic processes, (2) organic extracts become richer in aromatic hydrocarbons and poorer in aliphatic hydrocarbons with enhanced radiation effects,

and (3) the uranium content in the Autunian Shales does not perturb their molecular characteristics.

The Lower Silurian organic-rich strata (Tannezuft Formation) in North Africa generally and in the Oued Mya particularly are known to be highly radioactive; they are commonly known as Silurian "hot" shales (e.g. Sonatrach, unpublished reports, Lüning et al., 2000). These shales were deposited under anoxic conditions during a short period (1 – 2 Ma) that favoured preservation of organic matter. It is also known that uranium is fixed at the sediment-water interface under reducing conditions and in the presence of a sorbent, which is usually organic matter or phosphate (Wignall and Meyers, 1988). Hence, sediments enriched in uranium tend to be deposited under anoxic conditions that allow both large amounts of organic matter to accumulate and uranium to be fixed (Wignall and Meyers, 1988). The Tannezuft Formation is also characterised by high gamma-ray values (Figure 4.5); increases in gamma-ray values often indicate elevated amounts of TOC where authigenic (non-detrital) uranium is associated with organic matter (Stocks and Lawrence, 1990).

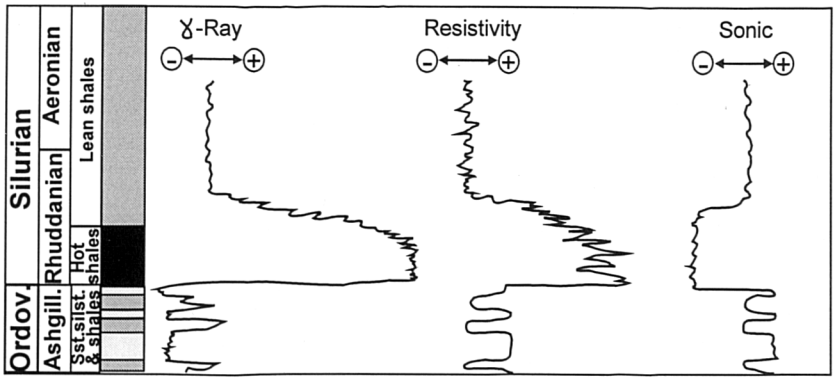

Figure 4.5 Typical response of the Silurian organic-rich shales in wireline logs. Authigenic uranium in the hot shales is responsible for high gamma values, while the essentially non-conductive and low-density organic matter leads to high resistivity and low sonic values. (After Lüning et al., 2000).

The Silurian source rock samples from the wells mentioned above showed lower Hydrogen Index values (Table 4.1), lower *n*-alkane concentrations (Table 4.2), higher aromatic hydrocarbon concentrations (Appendix 4.2), higher alkylcarbazole and benzocarbazole concentrations (Appendix 5.1), and the gas chromatograms of these samples are dominated by aromatic hydrocarbons (alkylnaphthalenes and alkylphenanthrenes) over the *n*-alkanes (Figure 4.6 and Figure 4.7) compared to the rest of the Silurian source rock samples. Consequently, it is possible that the organic

matter analysed in the Silurian source rock samples from RDC#2 (3804.70 m, 3806.40 m, 3808.35 m and 3810.80 m), OA#1bis (4142.25 m and 4145.35 m), GLNE#4bis (3874.85m), BKZ#1 (4187.86m and 4189.95m) and GLNE#5 (4001.45m) has suffered alteration by irradiation from the natural decay of uranium.

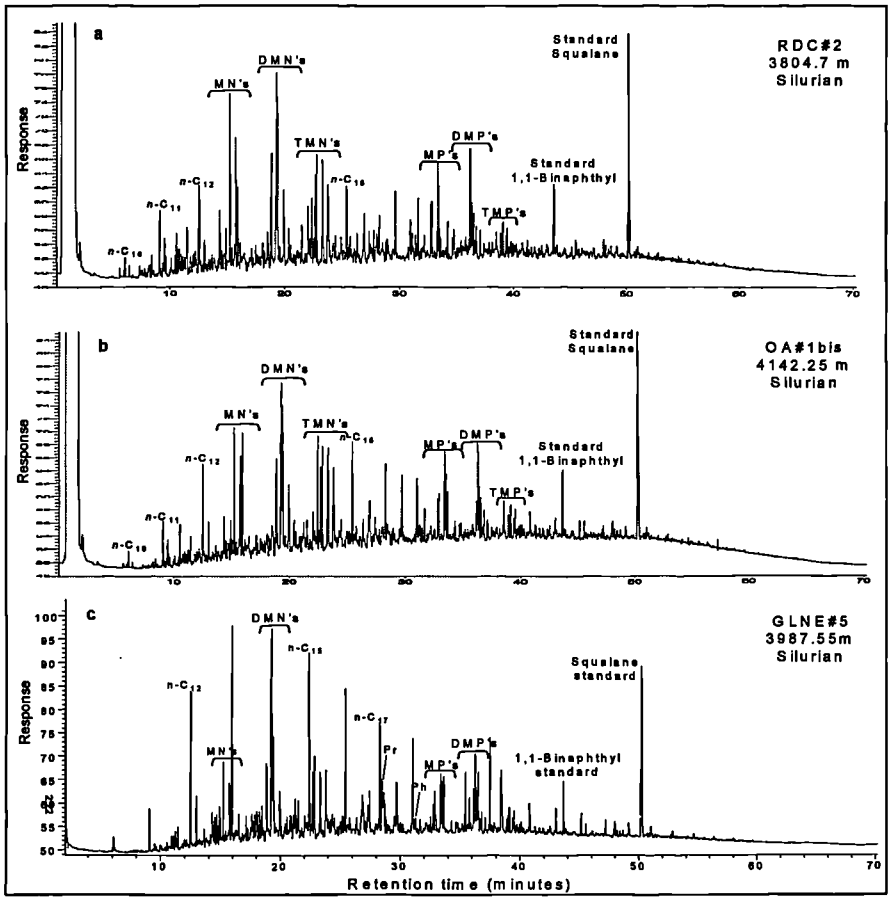

Figure 4.6 Gas Chromatograms of the aliphatic and aromatic hydrocarbons isolated from Silurian source rock samples (a) RDC#2 (3804.7m), (b) OA#1bis (4142.25m), and GLNE#5 (3987.55m) in the Oued Mya basin. MN's = methylnaphthalenes, DMN's = dimethylnphthalenes, TMN = trimethylnaphthalenes, MP's=methylphenanthrenes, DMP's = dimethylphenanthrenes, Pr = pristine, and Ph = phytane.

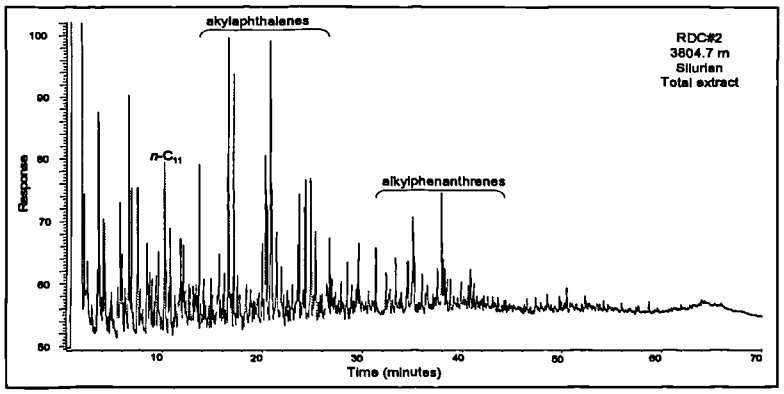

Figure 4.7 Gas Chromatograms of the whole extract from in the Silurian source rock sample RDC#2 (3804.7m).

Table 4.2 Geochemical parameters obtained from the distributions of *n*-alkanes and isoprenoids for the Silurian and Ordovician source rock samples in the Oued Mya basin.

Well	depth (m)	Pr/Ph	Pr/*n*-C_{17}	Ph/*n*-C_{18}	*n*-alkane index *n*-C_{17}/*n*-C_{27}	Sum *n*-alkanes (mg/g extract)
	Silurian					
OA#1 bis	4142.25	1.71	0.28	0.19	8.09	1.51
OA#1 bis	4145.35	1.69	0.25	0.22	7.33	1.50
OA#1 bis	4151.55	1.56	0.42	0.30	10.65	3.31
TKT#1	3868.6	1.62	0.40	0.28	10.22	2.54
TKT#1	3872.5	1.18	0.26	0.32	11.58	3.52
GLNE#4 bis	3878.85	2.05	0.44	0.28	13.36	2.23
GLNE#3	3803.45	1.66	0.31	0.23	5.04	7.26
GLNE#3	3809.45	1.86	0.32	0.21	4.28	8.01
GLNE#5	3987.55	2.20	0.40	0.20	8.62	3.06
GLNE#5	3994.45	2.11	0.42	0.23	6.75	2.82
GLNE#5	4001.45	2.12	0.41	0.24	11.56	2.33
GD#1 bis	3850	2.50	0.23	0.27	11.06	3.11
BKZ#1	4180.6	1.32	0.43	0.42	6.30	2.16
BKZ#1	4183.8	1.81	0.35	0.39	8.39	2.22
BKZ#1	4187.86	1.41	0.40	0.38	6.65	1.61
BKZ#1	4189.5	1.33	0.43	0.42	8.38	1.31
BAT#1	3947	1.81	0.22	0.36	15.02	3.16
BAT#1	3957	1.71	0.25	0.37	9.70	2.36
BAT#1	3959.55	1.82	0.35	0.39	7.98	1.93
GEC#1	3660.6	1.16	0.45	0.43	3.85	1.31
RDC#2	3804.7	1.76	0.24	0.22	4.00	1.23
RDC#2	3806.4	1.62	0.25	0.20	5.00	0.92
RDC#2	3808.35	1.63	0.22	0.35	4.67	0.61
RDC#2	3810.8	1.67	0.48	0.38	4.06	0.80
	Ordovician					
GLNE#5	4024.05	1.64	0.06	0.04	2.95	14.36
GLNE#5	4036.3	1.60	0.06	0.04	2.90	12.06
GLNE#3	3936.08	1.11	0.04	0.04	3.36	27.78
GBC#1	3272.1	1.71	0.30	0.19	1.33	3.85
GBC#1	3386.7	-	0.08	0.03	2.10	7.58
GBC#1	3394.4	1.51	0.43	0.27	0.41	5.15
GBC#1	3398.4	1.54	0.49	0.34	3.87	7.34
OEM#1	3910.45	1.34	0.15	0.13	1.19	5.21
OEM#1	3924.65	1.44	0.21	0.16	4.05	1.69
OEM#1	3930.65	1.65	0.14	0.08	1.24	9.12
BKZ#1	4198.95	1.60	0.05	0.02	2.74	18.34
GEC#1	3770.9	2.00	0.04	0.02	2.27	15.08
RDC#2	3911.38	1.14	0.10	0.09	0.88	10.97
OA#1 bis	4367.4	2.35	0.07	0.03	1.86	12.68
OA#1 bis	4462.75	2.28	0.14	0.05	0.83	8.61

Pr=pristane, Ph=phytane,

Samples representing the Ordovician exhibit different features than the samples analysed in the Silurian source rocks. The Ordovician samples are characterised by significant presence of heavier *n*-alkanes at *n*-C_{22}+ and relatively lower *n*-C_{17}/*n*-C_{27} *n*-alkane ratios ranging from 0.4 to 4.05 (Table 4.2). The GC fingerprints of the

Ordovician samples are indicative of particular organic matter input. For example, bimodal *n*-alkane distributions with a second mode in the *n*-C_{22} to *n*-C_{30} range are usually associated with terrestrial higher plant waxes (Tissot and Welte, 1984). All the Ordovician samples analysed in this study display a bimodal distribution of *n*-alkanes (Figure 4.8 and Figure 4.9). However, in these samples which are taken from strata (i.e. Ordovician) that were deposited prior to the evolution of land plants, the bimodality is not related to higher plant waxes of terrestrial facies. Instead, we observe an odd carbon number predominance in the *n*-C_{15} to *n*-C_{19} range which is uncommon except in Ordovician samples.

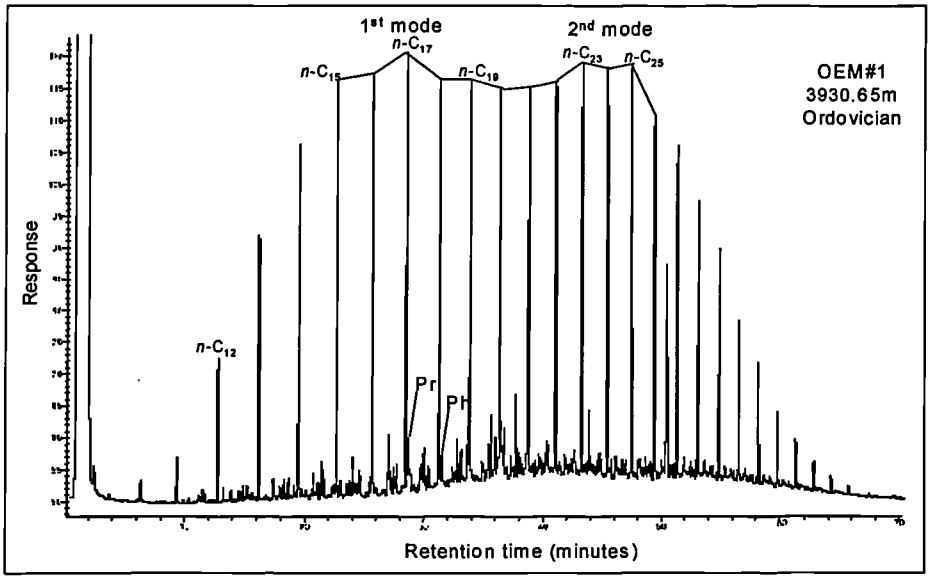

Figure 4.8 Gas Chromatogram of the saturated and aromatic hydrocarbon fraction isolated from a typical Ordovician source rock sample (OEM#1 3930.65 m) in the Oued Mya basin. Pr = Pristane and Ph= Phytane.

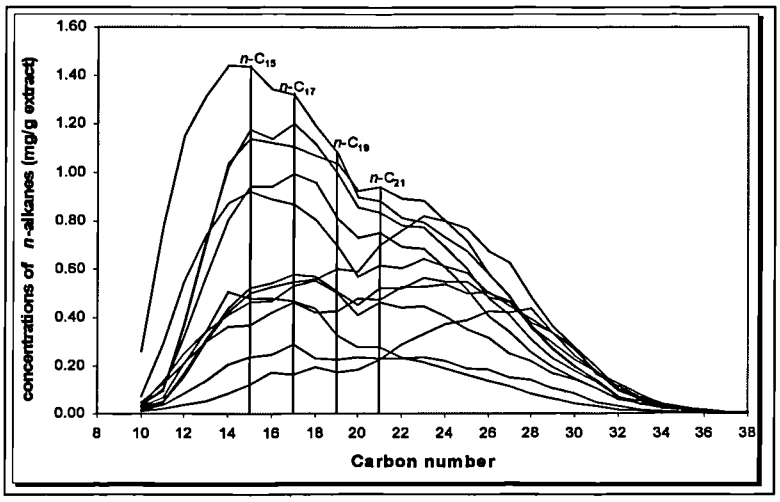

Figure 4.9 *n*-alkane envelopes of the Ordovician source rock samples in the Oued Mya basin

Reed et al. (1986) and Jacobson et al. (1988) documented *Gloeocapsamorpha prisca* bearing Middle Ordovician rocks and oils that generally have dominant C_{15} to C_{19} *n*-alkanes, low amounts of heavier *n*-alkanes, a virtual absence of isoprenoids including pristane and phytane, and an odd carbon number predominance. Moreover, Zhang et al. (2000) showed that Ordovician source rock extracts from the Tarim basin, NW China contain the *Gloeocapsamorpha prisca* influence in C_{15} to C_{19} *n*-alkanes plus a second mode maximising in the *n*-C_{23} to *n*-C_{25} range (Figure 4.10a). The gas chromatogram of oils from Tabei and Tazhong in the Tarim basin exhibit the occurrence of the first mode only, an odd carbon preference and have low levels of isoprenoid alkanes (Figure 4.10b). Zhang et al. (2000) suggested that the absence of the second mode in the oils is because the organic matter that generated the second mode seen in the extracts did not contribute to the oil generation or the second mode has been removed due to the high thermal maturity of the oils.

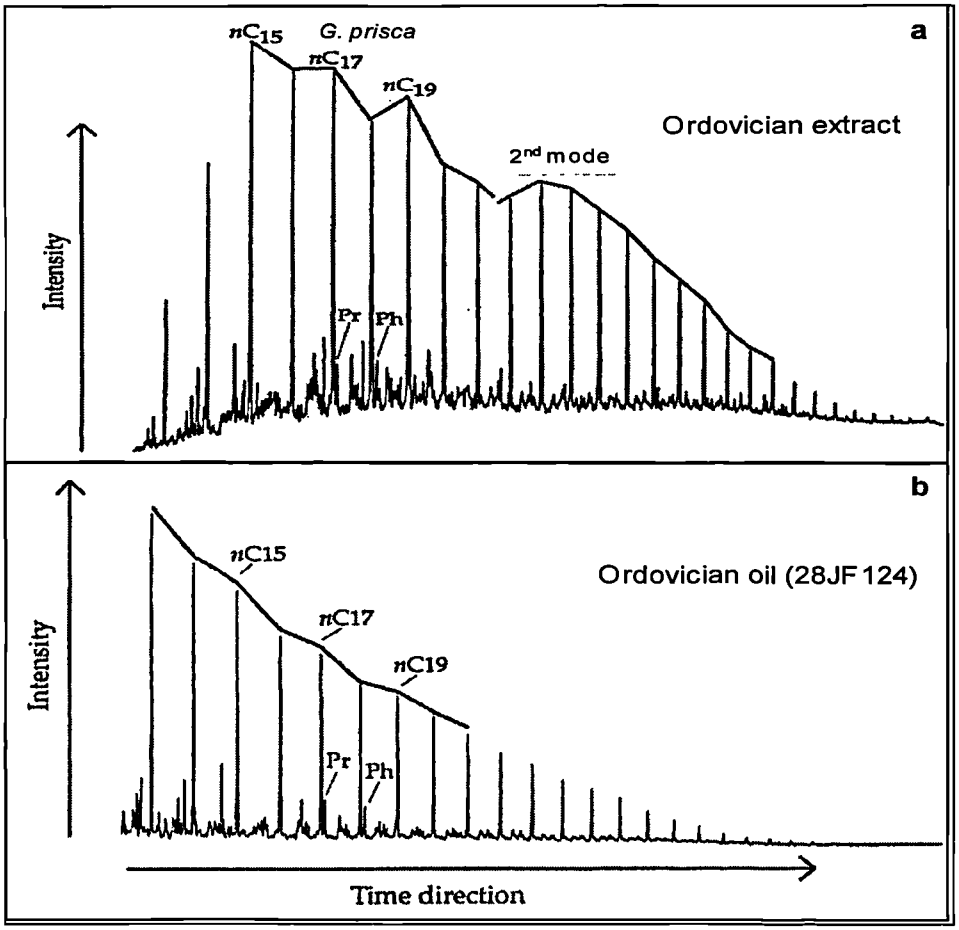

Figure 4.10 Gas chromatogram traces of a Tazhong Ordovician extract (a) showing a bimodal n-alkane distribution and characteristics suggesting derivation from *Gloeocapsamorpha prisca* and (b) gas chromatogram represents oil from the Tabei and Tazhong fields typically displaying slight odd carbon predominance and has low level of isoprenoid alkanes. (After Zhang et al., 2000).

Numerous Ordovician oils and kerogens worldwide are known to contain unusual and distinctive distributions of hydrocarbons (Fowler and Douglas, 1984; Fowler et al., 1986; Reed et al., 1986 and Jacobson et al., 1988). Generally, Ordovician oils and kerogens are characterised by an odd dominance in the C_9-C_{19} range of *n*-alkanes, and an odd dominated homologous series of cyclohexyl substituted *n*-alkanes. Furthermore, they contain an unusually small amount of C_{20}+ components and very low amounts of pristane and phytane. All these features have been suggested to derive from a "unique benthonic mat-forming non-photosynthetic prokaryotic organism" known as *Gloeocapsamorpha prisca* which is a "primitive" prokaryotic organism (Zalessky, 1917; Reed et al., 1986). This organism is believed to be the major contributor of the organic matter during the Ordovician worldwide. Moreover, organic matter-rich sediments from the Canning and Amadeus basins of Australia are known to contain *Gloeocapsamorpha prisca* fossils and to have the same features as outlined above. Hoffmann et al. (1987) showed that pyrolysis of a *Gloeocapsamorpha prisca*-rich kerogen yielded a hydrocarbon mixture with a similar composition to the Ordovician sediment extract. Finally, on the basis of geological, geochemical and palynological data, Hoffmann et al. (1987) suggested that *Gloeocapsamorpha prisca* was probably planktonic, photosynthetic and very possibly eukaryotic and that the unusual feature of Ordovician oils and sediments drive from bacterial and other diagenetic imprints superimposed on the primary signature of this organism.

Most of the Ordovician source rock samples analysed in this project reveal similar *n*-alkane and isoprenoid alkane distributions to that in the Ordovician source rock samples from the Tarim basin shown in Figure 4.10a. Therefore, the Ordovician source rock samples from the Oued Mya basin appear also to have the *Gloeocapsamorpha prisca* influence in the C_{15} to C_{19} *n*-alkanes plus a second mode maximising in the *n*-C_{23} to *n*-C_{25} range. Clearly, this second mode is not the same as that seen in bimodal samples derived from younger strata with higher plant waxes which occur in the *n*-C_{29} to *n*-C_{31} range. The observed bimodality in these samples implies that there was more than one type of organic matter input. Moreover, the Ordovician samples revealed extremely low amounts of the isoprenoid alkanes pristane and phytane compared to the *n*-alkanes, except samples from wells HGA#1 (3391, 3412, 3439m), GBC#1 (3272.1m, 3394.4m and 3398.4m) and OA#1bis (4599m) that show higher amounts of pristane and phytane relative to the *n*-C_{17} and *n*-

C_{18} *n*-alkanes, respectively (Table 4.2). Note also that most of the Ordovician samples exhibit much higher amounts of *n*-alkanes compared to the Silurian source rock samples ranging from 3.85 to 27.78 mg/g of extract (Table 4.2).

Samples GEC#1 (3660.6m) from the Silurian and GBC#1 (3272.1 and 3394.4m) and OEM#1 (3924.65m) from the Ordovician show *n*-alkane distributions that have been severely affected by evaporation of the low molecular weight compounds before *n*-C_{20}. This feature should be taken in account when interpreting the geochemical ratios.

The pristane/phytane (Pr/Ph) ratio for most of the Silurian source rock samples from the wells BKZ#1, TKT#1, BAT#1, RDC#1, OA#1bis GLNE#3 and GEC#1 varies between 1.10-1.86, suggesting minor changes in the Silurian organic facies through the Oued Mya basin. However, slightly higher Pr/Ph values (ca. 2.05-2.50) are recorded in Guellala northeast (GLNE#4bis and GLNE#5) and Gueddicha (GD#1bis) suggesting a different depositional environment (Didyk et al., 1978) in these areas of the basin. Indeed, in section 4.3.2.1 below, the biomarkers (steranes and triterpanes) clearly reveal that the Silurian source rock samples (group B) in the wells GLNE#4bis, GLNE#5, and GD#1bis contain different sterane and triterpane distributions from the Silurian samples (group A) in the wells BKZ#1, TKT#1, BAT#1, RDC#1, OA#1bis GLNE#3 and GEC#1.

The Ordovician source rock samples show Pr/Ph ratios ranging from 1.68 to 2.35, suggesting relatively more oxic depositional environment of the organic matter deposited during the Ordovician compared to the organic matter deposited during the Silurian (Didyk et al., 1978).

4.3.2. Steranes and triterpanes

4.3.2.1. Source facies characterisation

Based on the distributions of steranes and triterpanes, the Silurian source rock samples show heterogeneities in composition. Partial m/z 191 and 217 mass chromatograms showing typical distributions of the triterpanes and steranes in Silurian samples are displayed in Figure 4.11 and geochemical ratios based on steranes and triterpanes used in this work are displayed in Appendix 4.1.

The Silurian source rock samples can be separated into two main groups according to the triterpane and sterane distributions. Group A, comprises the samples from the wells RDC#2 (3804.7, 3806.4, 3808.35, 3840.8m), BAT#1 (3947, 3957, 3959.55m), OA#1bis (4142.25, 4145.35, 4151.55m), BKZ#1 (4180.6, 4183.8, 4187.86, 4189.5m), GLNE#3 (3803.45, 3809.45m), TKT#1 (3868.6, 3872.5m) and GEC#1 (3660.6m). All these samples revealed moderate to extremely high organic carbon content (TOC) and petroleum potential (section 4.2); they are characterised by the occurrence of abundant extended tricyclic terpanes from C_{20} to C_{35}, extremely low abundance of the C_{24} tetracyclic terpane compared with the C_{26} tricyclic terpanes S and R, extremely high Ts versus Tm, C_{29} Ts and C_{30} diahopane relative to the C_{29} 17α(H) hopane, most of the C_{31} to C_{35}17α(H) hopanes S and R homologues coelute with the C_{32}, C_{33}, C_{34}, and C_{35} extended tricyclic terpanes and higher abundance of regular steranes than 17α(H) hopanes. The group B consists of the samples from the wells GD#1bis (3850m), GLNE#5 (3887.55, 3894.45, 4001.45m), GLNE#4bis (3874.85m) and GBC#1 (3213, 3259m) and revealed extremely high organic carbon content (TOC) and petroleum potential as for the group A samples (Table 4.1); however, they show low abundance of the extended tricyclic terpanes, high abundance of the C_{24} tetracyclic compared with the C_{26} tricyclics S and R, similar relative abundance of Ts and Tm, extremely low abundance of the C_{29} Ts and C_{30} diahopane relative to the C_{29} 17α(H) hopane, no occurrence of the extended C_{32}-C_{35} tricyclics, lower abundance of regular steranes than 17α (H) hopanes, and within the steranes, the C_{27} 5α(H), 14α(H),17α(H) 20R isomer is very abundant (Figure 4.11 and Table 4.3). The position of the wells from the groups A and B is highlighted in the location map in Figure 4.1.

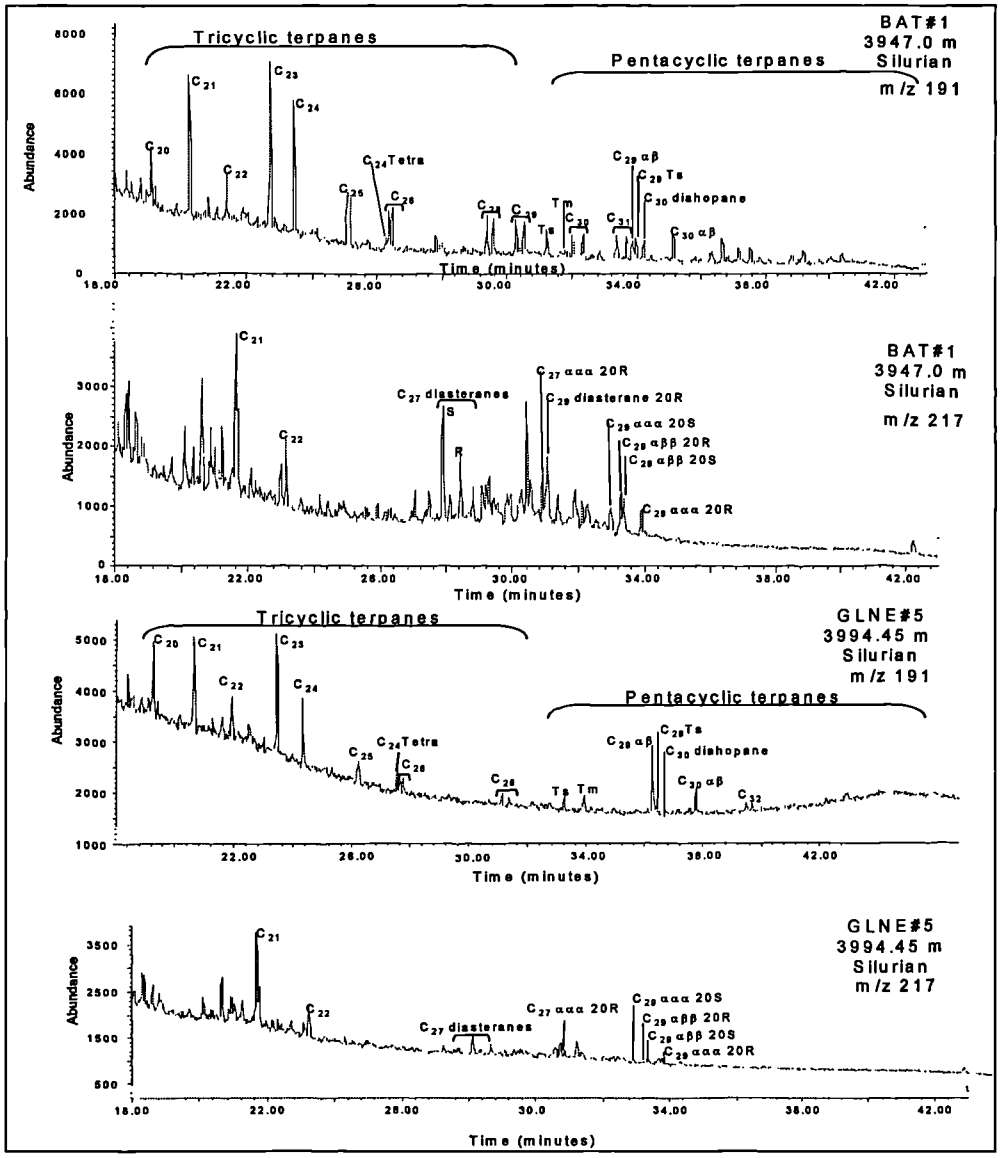

Figure 4.11 Partial m/z 191 and 217 mass chromatograms showing the distributions of triterpanes and steranes in (a) selected Silurian sample (BAT#1 3947m) from group A and (b) selected Silurian sample (GLNE#5 3994.45m) from group B. See location map in Figure 4.1 for the position of these groups.

The partial m/z 191 and m/z 217 mass chromatograms showing the distribution of the triterpanes and steranes of the Ordovician samples (Figure 4.12) suggest that two major groups of samples can be distinguished: Group C containing samples RDC#2 (3911.38m), OA#1bis (4367.4, 4462.75, 4599m), BKZ#1 (4198.95m), GLNE#5 (4024.05 and 4026.3m), GLNE#3 (3936.08), GBC#1 (3272.1, 3386.7, 3394.4, 3398.6m) and HGA#1 (3391, 3412, 3439m), characterised by the presence of abundant extended tricyclic terpanes, low C_{24} tetracyclic terpane relative to the C_{26} tricyclic terpanes S and R, similar abundance of Ts and Tm, extremely low C_{29} Ts and C_{30} diahopane compared to the C_{29} 17α (H) hopane. Group D, containing the samples OEM#1 (3910.45m, 3924.65m, 3930.65m), GD#1bis (3921.5m, 3939m, 4025.9m),

and GEC# (3770.9m) is characterised by lower abundance of the extended tricyclic terpanes, high abundance of the C_{24} tetracyclic relative to the C_{26} tricyclics S and R, and high abundance of the C_{29}Ts and C_{30} diahopane compared to the C_{29} 17α (H) hopane. All of the samples from groups C and D show a predominance of the 17 α(H) hopanes compared to the regular steranes and tricyclic terpanes suggesting relatively higher input from prokaryotic organisms (Tissot and Welte, 1984) and oxic/suboxic depositional environment of the organic matter during the Ordovician. Therefore, intense bacterial reworking took place leading probably to lower preservation of steroidal compounds (Jasper and Gagossian, 1993). This is consistent with the poor organic carbon content (TOC) and the petroleum potential of the Ordovician source rock samples revealed in section 4.2.

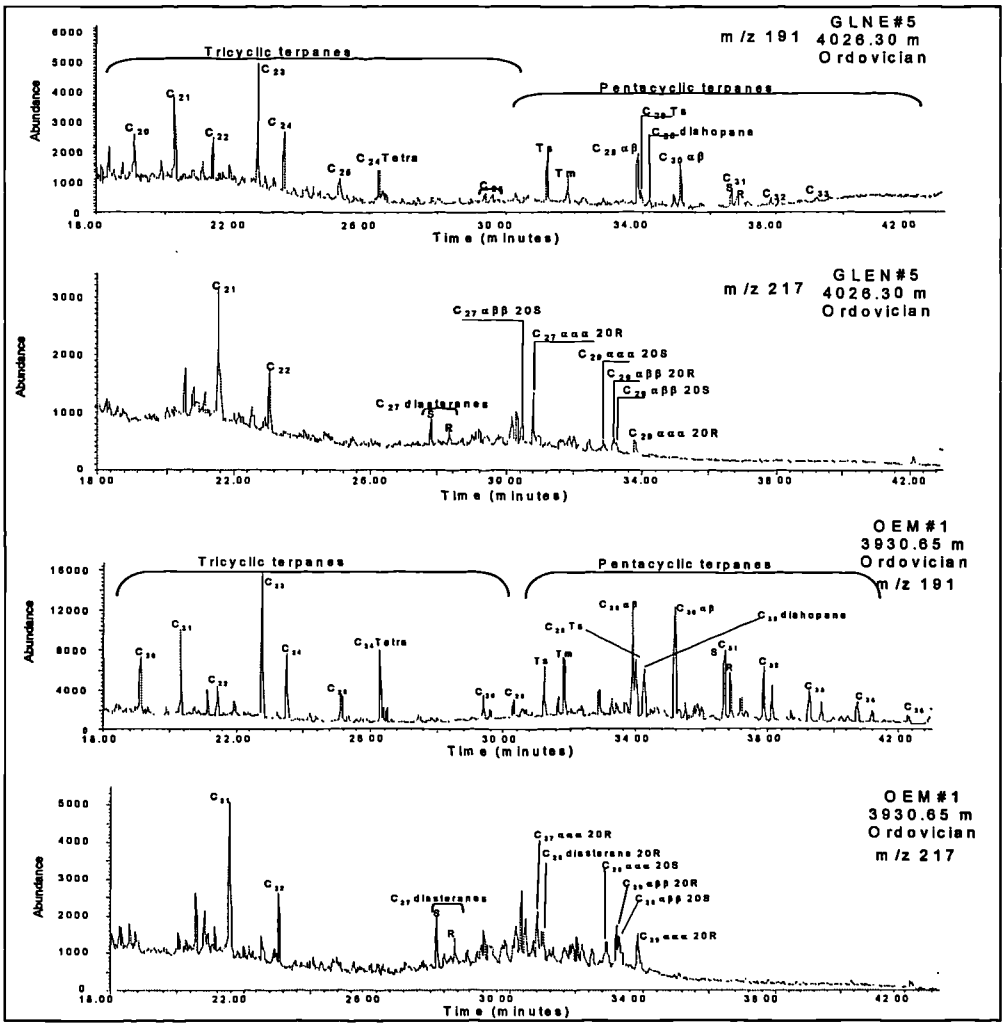

Figure 4.12 Partial m/z 191 and 217 mass chromatograms showing the distributions of triterpanes and steranes in (a) selected Ordovician sample from group C and (b) selected Ordovician sample from group D. See location map in Figure 4.1 for the position of these groups.

Conventional sterane and triterpane facies-derived parameters employed in this work include regular steranes/(regular steranes + 17α(H) hopanes), where the regular steranes consist of C_{29} 5α(H), 14α(H), 17α(H) and C_{29} 5α(H), 14β(H), 17β(H) (20S+20R) compounds and the 17α(H) hopanes consist of C_{29} to C_{30} 17α(H) pseudohomologues (Seifert and Moldowan, 1978; Tissot and Welte, 1984; Moldowan et al., 1985; Connan et al., 1986), extended tricyclic terpanes/[(extended tricyclic terpanes + 17α(H) hopanes)] where the extended tricyclic terpanes consist of C_{28}+C_{29} tricyclic terpanes (S+R) and the 17α(H) hopanes consist of C_{29} to C_{30} 17α(H) pseudohomologues (Peters and Moldowan, 1993), [extended C_{28}+C_{29} (S+R) tricyclics]/Ts and C_{24} tetracyclic/[C_{26} tricyclics (S+R)] (Holba et al., 2001), C_{29} 17α(H)hopane/C_{30} 17α(H) hopane (Subroto et al., 1991), C_{29} βα diasterane R/(C_{29} βα diasterane R + C_{29} 5α(H), 14α(H), 17α(H) 20R sterane) (Curiale, 1992), the C_{27}-C_{28}-C_{29} 5α(H), 14β(H), 17β(H) (20S+20R) regular steranes distribution (Moldowan et al., 1985) and the absolute concentrations of tricyclic terpanes, hopanes and steranes. For the 17α(H) hopanes I have taken in consideration only two compounds C_{29} and C_{30} 17α(H) hopanes because the extended homohopane homologues C_{31} to C_{33} 17α(H) hopanes coelute with the extended C_{32}-C_{35} tricyclic terpanes in most of the Silurian source rock samples rending their quantification difficult. Values of these parameters and concentrations of individual biomarkers are displayed in Appendix 4.1.

Figure 4.13 shows the cross plot of the facies dependant parameters, [extended C_{28}+C_{29} (S+R) tricyclics]/[(extended C_{28}+C_{29} (S+R) tricyclics + 17α(H) hopanes)] versus [C_{29} ααα+αββ (S+R) regular steranes]/[(C_{29} ααα+αββ (S+R) regular steranes + 17α(H) hopanes)]. Both of these ratios are primarily source parameters. The first ratio compares a group of bacterial or algal lipids (tricyclics) with markers that arise from different prokaryotic species (hopanes), the second ratio reflects input of eukaryotic (mainly algae and higher plants) versus prokaryotic (bacteria) organisms to the source rocks (Peters and Moldowan, 1993). These parameters enable us to separate the Silurian samples into two main groups. The group A contains 19 samples: RDC#2 (3804.7, 3806.4, 3808.35 and 3810.8m), BAT#1 (3947, 3957 and 3959.55m), BKZ#1 (4180.6, 4183.8, 4187.86 and 4189.5m), OA#1bis (4142.25, 4145.35 and 4151.55m), TKT#1 (3868.6 and 3872.5m), GEC#1 (3660.6m) and GLNE#3 (3803.45

and 3809.45m) which are characterised by higher regular steranes/(regular steranes + 17α(H) hopanes) and extended tricyclics/(extended tricyclics + 17α(H) hopanes) ratios (Table 4.3). However, the Silurian source rock samples RDC#2 (3804.7, 3806.4, 3808.35 and 3810.8m) and GLNE#3 (3803.45 and 3809.45m) from group A show somewhat lower abundance of the extended C_{28}+C_{29} (S+R) tricyclics relative to the 17α(H) hopanes compared to the other Silurian source rock samples in the same group. Interestingly, all of the Silurian source rock samples from the well RDC#2 are strongly depleted in *n*-alkanes compared to the rest of the samples (section 4.3.1); and the Silurian source rock samples from the well GLNE#3 revealed the lowest total organic carbon content compared to the rest of the Silurian samples.

In the Silurian source rock samples from the group A, higher values of the regular steranes/(regular steranes + 17 α (H) hopanes) ratio suggests higher input from eukaryotic versus prokaryotic organisms, probably due to better preservation of steroidal compounds in a more anoxic depositional environment (Moldowan et al., 1985; Connan et al., 1986). This is consistent with the extremely high organic carbon content (TOC) and high petroleum potential of the Silurian tested within these intervals (see section 4.2). However, group B comprises 7 samples: GD#1bis (3850m), GLNE#5 (3987.55, 3994.45 and 4001.45m), GLNE#4bis (3874.85m) and GBC#1 (3213 and 3259m) exhibit lower regular steranes/(regular steranes + 17 α (H) hopanes) and extended tricyclics/(extended tricyclics + 17α (H) hopanes) (Table 4.3). The Silurian samples from group B also showed high total organic content (TOC) and high petroleum potential (Table 4.1) comparable with the Silurian samples from group A, however their biomarker distributions are different (Figure 4.11 and Figure 4.13). These differences in the biomarker distribution between the Silurian source rock samples in groups A and B are probably caused by differences in the depositional environment. The Silurian source rock samples from group B showed higher Pr/Ph ratios which also support this observation. Moreover, from the same cross plot, the Ordovician samples can also be distinguished into two groups. Group C contains 13 samples: RDC#2 (3911.38m), OA#1bis (4367.45, 4462.75, 4599m), BKZ#1 (4198.95m), GLNE#5 (4024.05 and 4026.3m), GLNE#3 (3936.08), GBC#1 (3272.1, 3386.7, 3394.4, 3398.6m) and HGA#1 (3391, 3412, 3439m), characterised by higher extended C_{28}+C_{29}-(S+R) tricyclics and regular steranes (13 samples); and group D comprises 9 samples: OEM#1 (3910.45m, 3924.65m, 3930.65m), GD#1bis (3921.5m,

3939m, 4025.9m) and GEC# (3770.9m), characterised by lower extended C_{28}+C_{29}-(S+R) tricyclics and regular steranes (see map in Figure 4.1 and Table 4.3)).

The new parameter known as the extended tricyclics ratio; ETR= [C_{28}+C_{29} extended tricyclics (S+R)]/Ts, proposed by Holba et al. (2001) plotted against C_{24} tetracyclics/C_{26} tricyclics (S+R) in Figure 4.14a also separate the Silurian and the Ordovician samples into the same groups mentioned above (i.e. Silurian groups A and B and Ordovician groups C and D). These parameters were carefully concocted by Holba et al. (2001) to minimise the effect of other processes such as maturity and biodegradation. Holba et al. (2001) showed that very high ETR values (ratios of. 4 to 15) are nearly always recorded in samples from upwellings or similar nutrient-rich depositional environments; ETR values ranging from 2 to 4 are relatively high and may also suggest nutrient-rich depositional environment, whereas ETR values below 1.8 are considered to be low, and may be found in samples from nutrient-poor depositional environments (i.e. oxic/suboxic depositional environments).

Most of the Silurian source rock samples from group A fall in the interval of high to very high ETR values (ca. 1.83 to 7.64) indicating that the depositional environment during the Silurian was extremely rich in nutrients favourable for high organic matter input and preservation. This is consistent with the high total organic carbon content (TOC), and high petroleum potential in these Silurian source rock samples (Table 4.1). The Silurian source rock samples from group B show somewhat lower ETR values than the Silurian samples from group A ranging from 1.53 to 3.07, which are also high. The total organic carbon content and the petroleum potential of these samples are as rich as the Silurian source rock samples from group B.

The C_{24} tetracyclic/[C_{26} tricyclics (S+R)] facies-dependant parameter clearly separate the Silurian and Ordovician source rock samples into the same groups: Silurian groups A and B and Ordovician groups C and D. The Silurian source rock samples from group A show lower C_{24} tetracyclic/[C_{26}tricyclics (S+R)] values than Silurian samples from group B; the Ordovician samples show higher values than the Silurian samples. Abundant C_{24} tetracyclic terpane appears to be a marker for carbonate and evaporite depositional environments (Palacas et al., 1984; Connan et al., 1986; Connan and Dessort, 1987; Mann et al., 1987; Clark and Philp, 1989) and is believed to be derived from terrigenous organic matter (Philp and Gilbert, 1986). In the present

study the samples are from strata that were deposited prior to the evolution of land plants, and they do not show any evidence for an evaporite depositional environment. Therefore, the more likely factor that controls the occurrence of the C_{24} tetracyclic terpane is likely to be a carbonate depositional environment. Indeed, the Ordovician source rock samples revealed very high abundance of the mineral carbon content compared to the total organic carbon content (TOC) (Table 4.1). However, the Silurian source rock samples contain much lower abundance of the mineral carbon content relative to the total organic carbon content (TOC). Furthermore, the Silurian source rock samples from group B seem to have higher abundance of the mineral carbon content that the Silurian samples from group A.

Figure 4.14b shows good correlation between the C_{24} tetracyclic/[C_{26} tricyclics (S+R)] and the C_{29} 17α(H) hopane/C_{30} 17α(H) hopane parameters. The highest values for both parameters are recorded in the Ordovician samples which exhibit the highest abundance of the total mineral carbon content relative to the TOC values. Moreover, Subroto et al. (1991) showed that a high abundance of C_{29} 17α(H) hopane relative to C_{30} 17α(H) hopane has been identified in crude oils associated with carbonate source rocks. All these observations do suggest that the differences in the biomarker distributions between the Ordovician and the Silurian source rock samples on the one hand, and between the Silurian samples from group A and group B on the other hand are likely related to the difference in the abundance of the mineral carbon content in the samples.

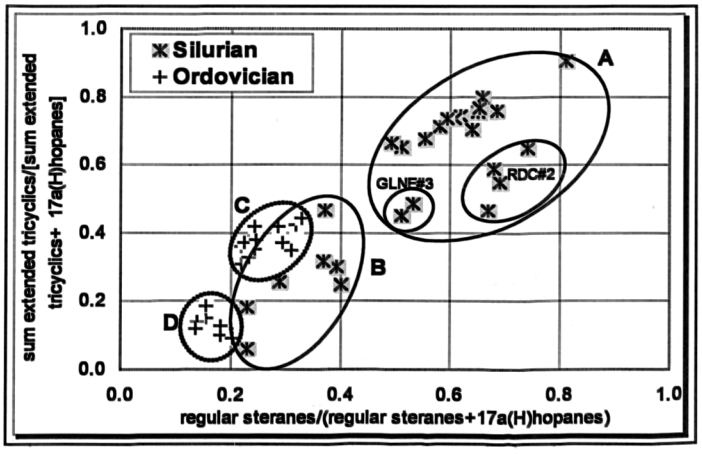

Figure 4.13 Cross plots of the facies parameters (C_{28}+C_{29} extended tricyclics S+R)/[(C_{28}+C_{29} extended tricyclics S+R + C_{29}+C_{30} 17α(H) hopanes) and regular steranes/[regular steranes+ C_{29}+C_{30} 17α(H) hopanes] for the Silurian and Ordovician source rocks in the Oued Mya basin. (See caption 4.1 for the wells location].

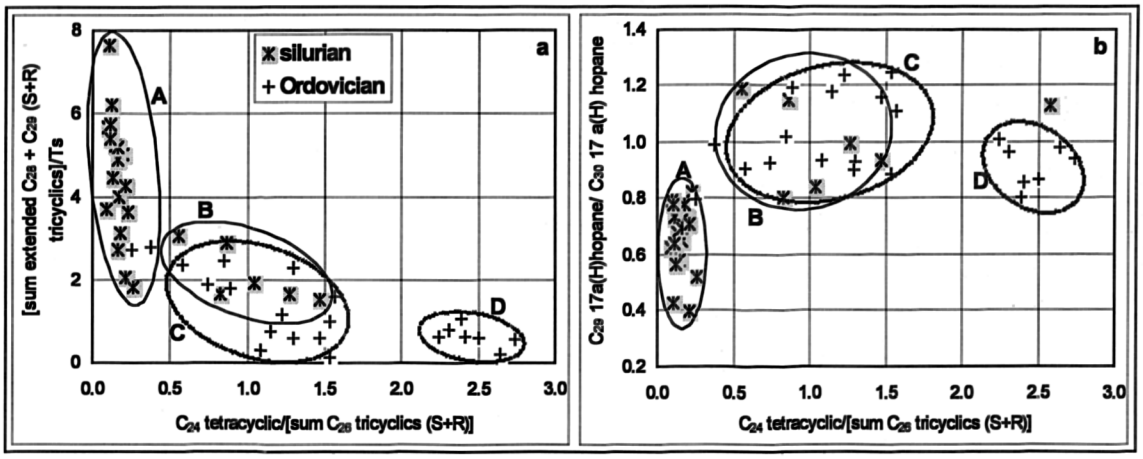

Figure 4.14 Cross plots of the facies parameters (a) [sum C_{28}+C_{29} (S+R) extended tricyclics]/Ts and C_{24} tetracyclic terpane/[sum C_{26} tricyclics (S+R)] and (b) C_{29}17α(H) hopane/C_{30} 17a(H)hopane and C_{24} tetracyclic terpane/[sum C_{26} tricyclics (S+R)] for the Silurian and Ordovician source rocks in the Oued Mya basin.

Table 4.3 Summary of the biomarker parameters showing the distinguished Silurian groups A and B, and Ordovician groups C and D source rock samples in the Oued Mya basin.

Biomarker Parameters	Silurian Group A	Silurian Group B	Ordovician Group C	Ordovician Group D
1	0.49 - 0.74	0.23 - 0.40	0.18 - 0.33	0.14 - 0.20
2	0.55 - 0.91	0.18 - 0.47	0.11 - 0.44	0.08 - 0.16
3	0.09 - 0.26	0.56 - 1.47	0.25 - 1.57	2.24 - 2.74
4	0.24 - 0.61	0.0 - 0.25	0.03 - 0.19	0.17 - 0.41
5	0.36 - 0.64	0.17 - 0.23	0.14 - 0.27	0.22 - 0.37

1 = C_{29} regular steranes/[C_{29} regular steranes + C_{29} + C_{30} 17 α (H)hopanes],
2 = Extended tricyclic terpanes C_{28}+C_{29}(S+R)/[extended tricyclic terpanesC_{28}+C_{29} (S+R)+C_{28}+C_{29}17α(H)hopanes],
3 = C_{24} tetracyclic terpane/C_{26} tricyclic terpanes (S+R),
4 = C_{30} diahopane/(C_{30} diahopane + C_{30} 17 α (H) hopane),
5 = C_{29} Ts/[C_{29} Ts+C_{29} 17 α (H) hopane].

Diasteranes are present in the Silurian and Ordovician source rock samples (Figure 4.11 and Figure 4.12). The backbone rearrangement process involved in the conversion of sterenes to diasteranes during diagenesis of immature sediments is believed to be catalysed by acidic sites on clays (Rubeistein et al., 1975; Sieskind et al., 1979). Diasterenes are ultimately reduced to 13β(H), 17α(H) 20S and 20R diasteranes with minor amounts of 13α(H), 17β(H) 20S and 20R isomers (Ensminger et al., 1978). Consequently, the abundance of diasteranes relative to the regular steranes is often used to discriminate siliciclastic facies, characterised by high diasterane abundances, from carbonate lithologies containing low amounts of diasteranes (e.g. Mello et al., 1988a,b). However, the ratio can also reflect the oxicity

versus anoxicity of the depositional environment. High abundance of diasteranes relative to regular steranes has been observed in bitumens from organic-lean carbonate-rich rocks from the Adriatic basin (Moldowan et al., 1992). These rocks were probably deposited in an acidic (low pH), oxic (high Eh) environment. A correlation between pH, high Eh, and diasteranes/regular steranes ratios has also been reported for the Toarcian shales of south-western Germany (Moldowan et al., 1986). Zumberge (1987) has noted that the same ratio is affected by maturity and tends to increase with increasing maturity.

The abundance of the diasteranes relative to the regular steranes in the Silurian and Ordovician source rock samples has been evaluated for the C_{29} isomers using the ratio C_{29} 13β(H),17α(H)-diasterane20R/[C_{29}13β(H),17α(H)-diasterane 20R+C_{29} 5α(H), 14α(H),17α(H) -sterane20R] (Curiale, 1992). This parameter seems to be higher in the Silurian group A samples than in the Ordovician samples and the Silurian group B samples (Figure 4.15). The Silurian source rock samples from group B and the Ordovician samples show lower abundance of C_{29} 13β(H),17α(H)-diasterane 20R relative to C_{29} 5α(H), 14α(H), 17α(H)-sterane 20R and higher abundance of the C_{24} tetracyclic relative to the sum of C_{26} tricyclics (S+R) compared to the Silurian source rock samples in group A. These observations are consistent with the facies differences revealed by high abundance of total mineral carbon content suggesting a carbonate facies for all the Ordovician samples. Moreover, the Silurian samples in group B seem to contain relatively higher total mineral carbon than the Silurian samples in the group A. Hence, the differences in the abundance of the C_{29} 13β(H),17α(H)-diasterane R in the Silurian group A samples are likely related to higher abundance of clay content and low abundance of carbonate in these Silurian samples compared to the Silurian samples from group B and the Ordovician source rock samples.

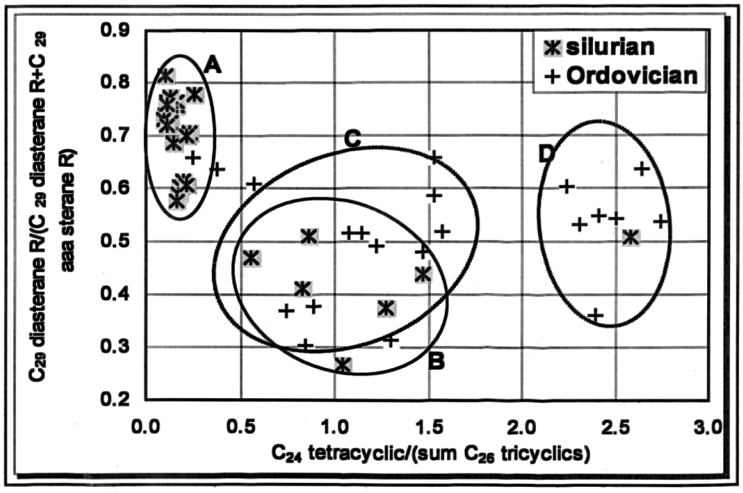

Figure 4.15 Cross plots of the facies parameters $C_{29}13\beta(H),17\alpha(H)$-diasterane20R/ [$C_{29}13\beta(H),17\alpha(H)$-diasterane20R + $C_{29}5\alpha(H),14\alpha(H),17\alpha(H)$-sterane20R] and C_{24} tetracyclic/ [sum C_{26} tricyclics (S+R)] for the Silurian and Ordovician source rocks in the Oued Mya basin. (See caption 4.1 for the wells location].

The relative abundances of C_{27}, C_{28}, C_{29} steranes in source rocks and oils reflect the carbon number distribution of the sterols incorporated into the sediment during deposition, which is, in turn, indicative of the nature of the contributing organisms to the accumulated organic matter in the source rocks for the oils (Mackenzie et al., 1983; Moldowan et al., 1985). For example a relative high abundance of C_{29} steranes in oils may indicate a land-plant origin for the oils, this in agreement with high C_{29} sterol abundances in higher plants compared to the C_{27} sterol predominance in marine plankton (Huang and Meinschein, 1979). However, caution needs to be implemented when interpreting the distribution of the relative abundances of C_{27}, C_{28}, C_{29} steranes, since it has been reported that brown algae and many species of green algae contain predominantly C_{29} sterols (Moldowan et al., 1985). Furthermore, 24-ethylcholest-5en-3β-ol (a C_{29} sterol) has been reported as a significant component in a mixed diatom culture (Volkman et al., 1981).

Nevertheless, sterane ternary diagrams are used extensively to show relationships between oils and/or source rock bitumens (Peters et al., 1989, Peters and Moldowan, 1993). The principal use of the C_{27}, C_{28}, C_{29} sterane ternary diagrams is to distinguish groups of petroleums from different source rocks or different organic facies of the same source rock (Peters and Moldowan, 1993). The distribution of C_{27}, C_{28}, C_{29} 5α(H), 14β(H), 17β(H) (20S+20R) steranes for the Silurian and Ordovician source rock samples is shown in Figure 4.16. The Silurian and Ordovician source rock

samples plot in a narrow region of the ternary diagram showing higher relative abundance of C_{27} and C_{29} 5α(H), 14β(H), 17β(H) (20S+20R) than C_{28} 5α(H), 14β(H), 17β(H) (20S+20R) suggesting a marine shale (more than 350 Ma BP) origin for the organic matter in both of the Silurian and the Ordovician source rock samples (Moldowan et al., 1985). The Silurian source rock samples GLNE#3 (3803.45m and 3809.45m) show lower C_{27} 5α(H), 14β(H), 17β(H) (20S+20R) compared to the rest of the samples.

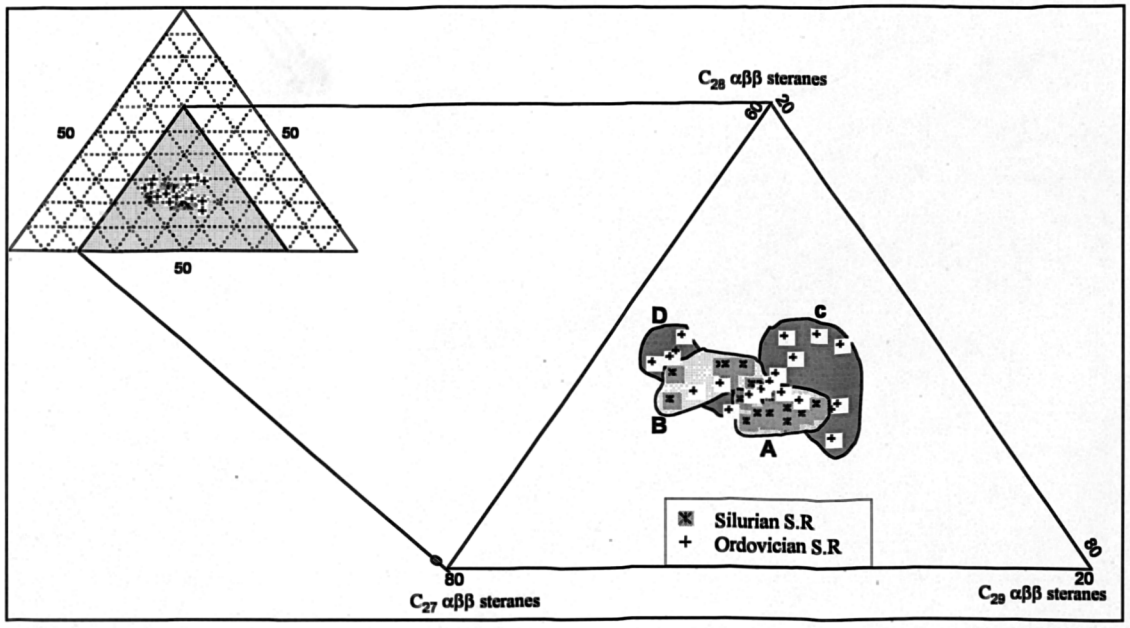

Figure 4.16 Ternary plot of the relative abundance of C_{27}- C_{28}- C_{29} αββ (S+R) steranes for Ordovician and Silurian source rock samples in the Oued Mya basin.

Within most of the Ordovician samples the biomarker alkanes are dominated by the hopanes ranging from 22.56 to 422.3 μg/g extract (average 109.65 μg/g extract). The sterane and tricyclic terpane concentrations in the same samples varies between 14.41 to 186.52 μg/g extract (average 82.72 μg/g extract) and 11.69 to 211.14 μg/g extract (average 105.45 μg/g extract) respectively. In contrast, Silurian source rock samples reveal a predominance of tricyclics and steranes ranging from 14.49 to 185.23 μg/g extract (average 69.13 μg/g extract) and 10.80 to 101.85 μg/g extract (average 50.87 μg/g extract), respectively over hopanes ranging from 3.06 to 37.42 μg/g extract (average 12.45 μg/g extract) (see Appendix 4.1 and Figure 4.17). Interestingly, Silurian source rock samples from the well RDC#2 (3804.70m, 3806.40m, 3808.35m, and 3810.80m) exhibit the lowest concentrations of the tricyclics, steranes and

hopanes. This observation is consistent with the low *n*-alkane concentrations revealed in these samples (section 4.3.1 and Table 4.2).

High concentrations of steranes combined with high regular sterane/17α(H)hopane ratios (Figure 4.13) in most of the Silurian source rock samples in group A indicate marine organic matter with major contributions from planktonic and/or benthic algae (e.g. Moldowan et al., 1985; Peters and Moldowan, 1993). Conversely, low sterane concentrations and low regular sterane/17α(H)hopane ratios in all the Ordovician and the Silurian (group B) source rock samples are more indicative of microbially reworked organic matter (e.g. Tissot and Welte, 1984; Peters and Moldowan, 1993).

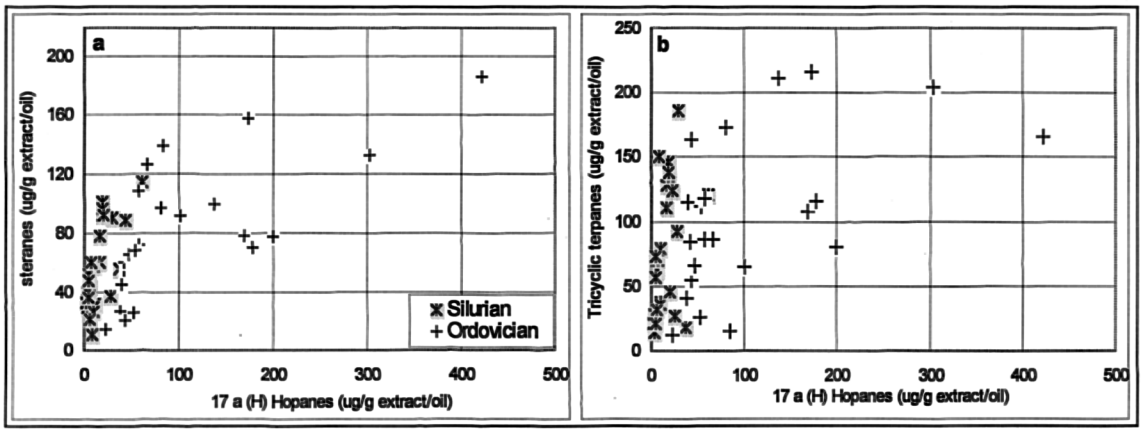

Figure 4.17 Plots of concentrations (μg/g of extract) of (a) total steranes versus total hopanes and (b) total tricyclics versus total hopanes for the Ordovician and Silurian source rock samples in the Oued Mya basin.

4.3.2.2. Principal components analysis (PCA)

Principal components analysis (PCA) is a multivariate statistical approach which recognises relationships between samples and variables in complex data sets, and summarises the main sources of variance as principal components (PCs). The PCA can often illustrate the bulk of data variability in just few principal components, allowing the data to be plotted graphically in two dimensions, whilst still retaining most of the information within the complex data set (Meglen, 1992). The PCs are, by definition, orthogonal to each other, such that no variance explained by one PC will contribute to another.

PCA can be used as an aid when deciding which molecular biomarker maturity, source facies or depositional environment parameters should be plotted since the principal component loadings (PCs) plots extract the biomarker variables related to

maturity, source facies or depositional environment controls. Therefore, PCA can be considered as a data reduction technique capable of handling large volumes of data and able to extract the subtle significant differences between the samples. PCA has been used by a number of authors to analyse geochemical data, e.g. Kvalheim (1987) for oil-source rock correlation studies, Bigge and Farrimond, (1998) and Parfitt and Farrimond, (1998) to find out the extent of biodegradation in a suit of oil seeps along the Dorset coast and Mupe Bay in the Wessex Basin (South of England). The PCA computer programme used in this project is the "SPSS version 10 for Windows"

A data set, comprising 33 variables (TOC, S2, biomarker concentrations, and two maturity parameters) for 26 Silurian and 22 Ordovician source rock samples, was analysed by PCA to establish the major sources of variance within the sterane, tricyclic terpane, and hopane distributions. The variables used in the analysis are listed in Table 4.4. The first three principal components (PCs) obtained, explain 36.42%, 18.11%, and 12.96% of the variance within the scaled data set, respectively. This allows the relationships between the samples to be examined in a simple two-dimensional score plots: PC1 versus PC2 and PC1 versus PC3, which include the effects of all the original variables (i.e. source facies, biomarker concentrations, and maturity), and display the bulk (67.48%) of the scaled data variability (Figure 4.18).

Interestingly, these plots demonstrate that the Silurian and Ordovician source rock samples can be discriminated exactly into the same groups revealed when using conventional biomarker ratios (see Figure 4.13, Figure 4.14, and Figure 4.15). Indeed, the plots of the principal components in Figure 4.18 allow us to separate the Silurian source rock samples into two groups; group A containing samples BAT#1 (3947, 3957 and 3959.55m), BKZ#1 (4180.6, 4183.8, 4187.86 and 4189.5m), OA#1bis (4142.25, 4145.35 and 4151.55m), TKT#1 (3868.6 and 3872.5m), and GEC#1 (3660.6m), and group B comprising samples GD#1bis (3850m), GLNE#5 (3987.55, 3994.45 and 4001.45m), GLNE#4bis (3874.85m) and GBC#1 (3213 and 3259m). The Silurian source rock samples from the wells RDC#2 (3804.7, 3806.4, 3808.35 and 3810.8m), and GLNE#3 (3803.45 and 3809.45m) are discriminated from the main group A. The Ordovician source rock samples are distinguished into group C containing RDC#2 (3911.38m), OA#1bis (4367.4m, 4462.75, 4599m), GLNE#5 (4024.05 and 4026.3m), GLNE#3 (3936.08), BKZ#1 (4198.95m), and GBC#1

(3272.1, 3386.7, 3394.4, 3398.6m), and group D comprising samples OEM#1 (3910.45m, 3924.65m, 3930.65m), GD#1bis (3921.5m, 3939m, 4025.9m) and GEC# (3770.9m). Three samples from the well HGA#1 (3391, 3412, 3439m) representing the El-Gassi shales Formation in the Ordovician plot close to the Silurian source rock samples from group A and away from the rest of the Ordovician source rock samples. These samples show higher abundance of the extended tricyclics and diasteranes and less abundance of the C_{24} tetracyclic terpane and C_{29} 17α(H) hopane compared to the rest of source rock samples from the Ordovician (see also Figure 4.14 and Figure 4.15 and Appendix 4.1).

An explanation of these three PCs is given by the loadings plots in Figure 4.19. These diagrams exhibit the loadings of the different variables within the principal components; large loadings, either positive or negative, indicate a significant influence of the variable on that PC. It is usual to regard loadings as "high" if the values of the loadings are greater than 0.6 (either positive or negative), and "moderately high" if above 0.3 (Kline, 1994). Low loading values (<0.3) may imply that there is no, or almost no, correlation between the variables and the principal component.

The first principal component PC1 explains 36.42% of the total variance of the data set, on which high loadings (>0.6) are obtained for the total organic carbon content (TOC), the residual petroleum potential S2, C_{24} tetracyclic terpane, C_{25}-C_{30} extended tricyclic terpanes, hopanes, and diasteranes (Figure 4.19a). In addition the loadings of C_{24} and C_{31} extended tricyclic terpanes, C_{27} and C_{29} 5α(H), 14β(H), 17β(H) steranes (20S+20R), and calculated vitrinite reflectance (%Rc) are moderately high loadings(>0.3). Consequently, it could be considered that the source facies represented by the quantity of total organic (TOC) and the residual potential (S2) show a major impact on the concentrations and distributions of the biomarkers in the Silurian and Ordovician source rock strata in the Oued Mya basin. Maturity also seems to control the concentrations and distributions of the biomarkers; however maturity effect is less important than source facies.

The second principal component PC2 accounts for 18.11% of the total variance of the data set matrix. High loadings are obtained for C_{21}-C_{25} tricyclic terpanes and C_{21} (ααα+αββ) pregnanes and C_{22} (ααα+αββ) homopregnanes, and moderately high

loadings are obtained for C_{31} extended tricyclic terpanes, C_{29} Ts, C_{30} diahopane, C_{30} 17 α(H) hopane, C_{29} diasteranes, C_{29} 5α(H), 14α(H), 17α(H) steranes (20S and 20R), and C_{29} 5α(H), 14β(H), 17β(H) steranes (20S+20R), the maturity ratio C_{20} TAS/[(C_{20} TAS + C_{28} (S+R) TAS)], and the total organic carbon content (TOC) (Figure 4.19b). Thus, it could be considered that the source facies together with maturity seem also to have an impact on PC2; therefore, on the distribution of the biomarkers in the Silurian and Ordovician source rock strata.

The third principal component is less important than the first two PCs, accounting for only 12.96% of the total variance of the data set. High loadings are obtained for C_{27} 5α(H), 14α(H), 17α(H) steranes 20R, C_{29} 5α(H), 14α(H), 17α(H) steranes 20R, C_{28} 5α(H), 14β(H), 17β(H) steranes (20S+20R) and moderately high loadings are obtained for C_{21} (ααα+αββ) pregnanes and C_{22} (ααα+αββ) homopregnanes, C_{30} diahopane, C_{27} 5α(H), 14β(H), 17β(H) steranes (20S+20R), C_{29} 5α(H), 14α(H), 17α(H) steranes 20S, and calculated vitrinite reflectance. PC3 seems to be mainly controlled by the maturity of the source rock strata in the Oued Mya basin.

Thus, it is interesting to highlight that of three principal components, PC1 and PC2 which account for 54.52% of the total data set display mainly the effect of the source facies and to a less extent maturity, whilst PC3, which accounts for only 12.96% seems to show the effect of maturity on the concentrations and distributions of the biomarkers in the source rocks.

The Silurian source rock samples from group A are dominated by the abundance of C_{24}-C_{31} extended tricyclic terpanes and steranes relative to the C_{24} tetracyclic terpane and hopanes, indicating higher input from eukaryotic versus prokaryotic organisms, possibly due to better preservation of steroidal compounds and tricyclics in a more anoxic depositional environment (Moldowan et al., 1985; Connan et al., 1986). This is consistent with the extremely high organic carbon content (TOC) and high petroleum potential of the Silurian analysed within these intervals (see section 4.2).

PC2 separates the two Silurian source rock samples GLNE#3 (3803.45 and 3809.45m) from the rest of the Silurian source rock samples in group A, because they are relatively depleted in C_{20}-C_{25} tricyclic terpanes, C_{21} (ααα+αββ) pregnanes and C_{22} (ααα+αββ) homopregnanes. PC3 separates the four Silurian source rock samples

in RDC#2 (3804.7, 3806.4, 3808.35 and 3810.8m) from the rest of the Silurian source rock samples in group A, because they are relatively depleted in C_{26}-C_{31} extended tricyclic terpanes, C_{29} Ts, C_{30} diahopane and C_{27}-C_{29} diasteranes. However, the Silurian source rock samples in group B and the Ordovician source rock samples are relatively depleted in C_{24}-C_{31} extended tricyclic terpanes and steranes and relatively enriched in C_{24} tetracyclic terpane and 17 α (H) hopanes.

The Silurian samples from group B also showed comparably high total organic content (TOC) and high petroleum potential (Table 4.1) as the Silurian samples from group A, however their biomarker distributions are different. The differences in the biomarker distributions of the Silurian source rock samples in group A are likely due to differences in the lithology of the Silurian source rock samples in group B which seem to contain higher total mineral carbon content relative to the total organic carbon (Table 4.1). Whereas, the differences in the biomarker distributions in the Ordovician source rock samples are due to the depositional environment of the organic matter which likely was more oxic than the Silurian strata leading to poor organic matter preservation.

Table 4.4 Biomarker compounds used in the principal components analysis.

Source facies	
1	TOC (wt %)
2	S2 (mg HC/g rock)
Tricyclic terpanes and hopanes (*m/z* = 191)	
3	C_{21} Tricyclic terpane
4	C_{22} Tricyclic terpane
5	C_{23} Tricyclic terpane
6	C_{24} Tricyclic terpane
7	C_{25} Tricyclic terpane
8	C_{24}Tetracyclic terpane
9	C_{26} Tricyclic terpanes (22S+22R)
10	C_{28} Tricyclic terpanes (22S+22R)
11	C_{29} Tricyclic terpanes (22S+22R)
12	C_{30} Tricyclic terpanes (22S+22R)
13	C_{31} Tricyclic terpanes (22S+22R)
14	22,29,30-Trisnorneohopane (Ts)
15	22,29,30-Trisnorhopane (Tm)
16	C_{29}17α(H), 21β(H)-30-norhopane
17	18 α (H)-30-norneohopane (C_{29} Ts)
18	C_{30} diahopane
19	C_{30}17α(H), 21β(H) hopane
Steranes (*m/z* = 217)	
20	C_{21}(ααα+αββ) pregnanes
21	C_{22}(ααα+αββ) homopregnanes
22	C_{27} 13β(H), 17α(H) diasterane 20S
23	C_{27} 13β(H), 17α(H) diasterane 20R
24	C_{29} 13β(H), 17α(H) diasterane 20S
25	C_{27} 5α(H), 14α(H), 17α(H) sterane 20R
26	C_{29} 13β(H), 17α(H) diasterane 20R
27	C_{29} 5α(H), 14α(H), 17α(H) sterane 20S
28	C_{29} 5α(H), 14α(H), 17α(H) sterane 20R
αββ **Steranes** (*m/z* = 218)	
29	C_{27} 5α(H), 14β(H), 17β(H) sterane (20S+20R)
30	C_{28} 5α(H), 14β(H), 17β(H) sterane (20S+20R)
31	C_{29} 5α(H), 14β(H), 17β(H) sterane (20S+20R)
Maturity parameters	
32	%Rc = 0.4 + (0.6 * MPI-1)
33	C_{20} TAS/[(C_{20} TAS + C_{28} 5 a(H) (S+R) TAS]

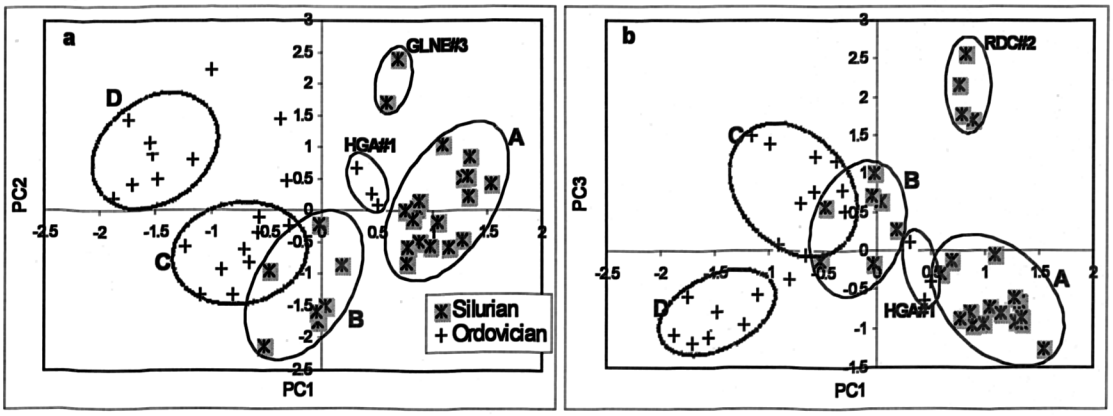

Figure 4.18 Scores cross plots of (a) PC1 versus PC2 and (b) PC1 versus PC3 showing the relationship between the Silurian and Ordovician source rock samples in terms of the first, second and third principal components. PC1 explains 39.54% of the total variance in the scaled data set, PC2 explains a further 18.65%, and PC3 explains a further 13.19%.

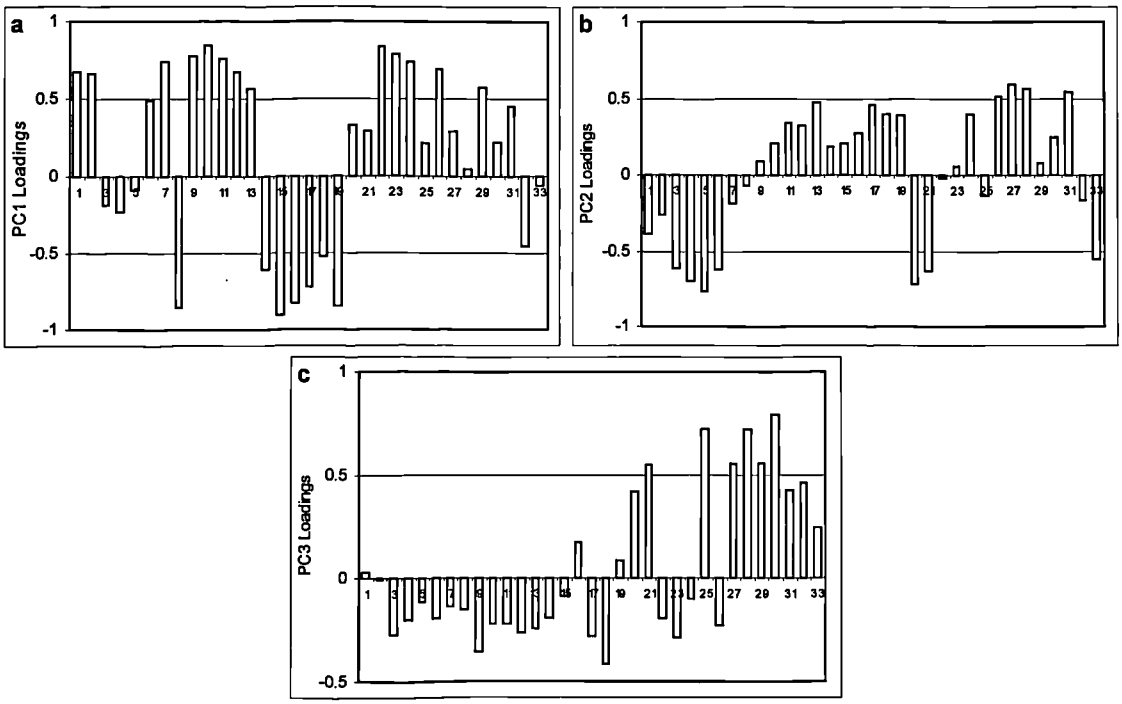

Figure 4.19 Loadings plots showing the composition of the first three principal components, which scored 39.54%, 18.65%, and 13.19% of the total variance in the data set, respectively.

4.3.2.3. Maturity

4.3.2.3.1. Steranes and triterpanes

Biomarkers and aromatic compounds have been used extensively to determine the maturity of source rock samples and oils. However, many ratios calculated from biomarkers and aromatic compounds are sometimes influenced by organic matter facies and depositional environment. In this study, I showed that the Silurian and Ordovician source rock samples are separated into different groups on the basis of

facies-dependant parameters evaluated in the previous section. Therefore, the assessment of the maturity of the Silurian and Ordovician source rock samples using the conventional biomarker parameters becomes difficult when assessing maturity of Silurian and Ordovician source rock samples originating from different facies and environments.

The evaluation of thermal maturity of Ordovician and Silurian source rock samples was achieved using the following biomarker parameters: 20S/(20S+20R)-5α(H),14α(H),17α(H)-C_{29} steranes; 5 α(H), 14β(H), 17β(H)/[5α(H), 14α(H), 17α(H) + 5α(H),14β(H),17β(H)] [αββ]/[αββ+ααα]-C_{29}steranes (20S+20R) (Mackenzie et al., 1980); Ts/(Ts+Tm) (Seifert and Moldowan, 1978); C_{29}Ts/(C_{29}Ts + C_{29}17α (H) hopane) (Hughes et al., 1985; Sofer et al., 1986; Sofer, 1988; Cornford et al., 1988; Riediger et al., 1990) and C_{30}diahopane/(C_{30}diahopane + C_{30} 17α(H) hopane) (Cornford et al., 1991). Values of these parameters are displayed in Appendix 4.1.

The maturation sensitive sterane stereoisomer ratios of most of the Silurian and Ordovician source rock samples based on the percentages of C_{29} 5α(H), 14α(H), 17α(H) 20S steranes and C_{29} 5α(H), 14β(H), 17β(H) (20S+20R) have all reached their end-point values of 0.50 to 0.60 and 0.54 to 0.70, respectively (Seifert and Moldowan, 1986) (Figure 4.20). Therefore, neither of these parameters can distinguish between the maturity of the Silurian and Ordovician source rock samples. Moreover, most of the Ordovician source rock samples exhibit lower percentages for both ratios than the Silurian source rock samples. In fact, this feature is likely due to organic facies differences recorded between the two source rock groups. Factors other than thermal maturity can affect sterane isomerisation ratios. Facies effects on the C_{29} 5α(H), 14α(H), 17α(H) 20S/(20S+20R) ratios have been observed in a sequence of Lower Toarcian rocks from south-western Germany (e.g. Moldowan et al., 1986) and in organic-rich lacustrine rocks from offshore west Africa (Hwang et al., 1989).

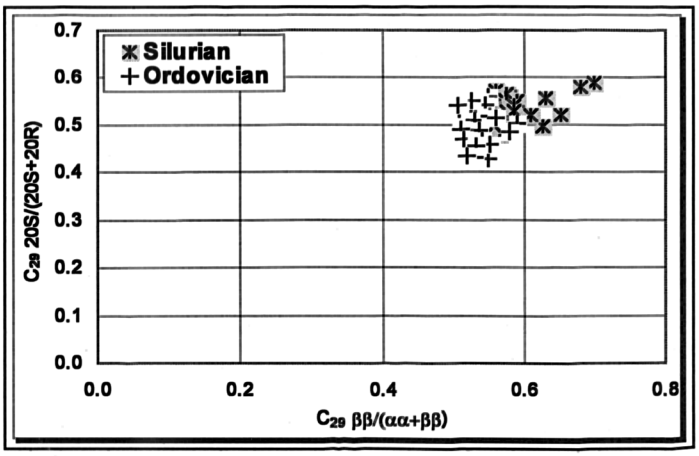

Figure 4.20 Cross plots of the thermal maturity parameters 20S/(20S+20R) and αββ/(ααα+αββ)-C29 steranes for Ordovician and Silurian source rock samples in the Oued Mya basin.

It is well established that maturity ratios such as Ts/(Ts+Tm), C_{29}Ts/(C_{29}Ts + C_{29}17 α (H) hopane) and C_{30} 17 α (H) diahopane/(C_{30} 17α (H) diahopane + C_{30} 17 α (H) hopane) obtained from the m/z 191 mass chromatograms are not only related to maturity, but also to organic facies and depositional environments (e.g. Moldowan et al., 1986). Oils derived from carbonates usually show low Ts/(Ts+Tm), C_{29}Ts/(C_{29}Ts+C_{29}17α(H)hopane) and C_{30}17α(H)diahopane/(C_{30}17α(H)diahopane + C_{30}17 α (H) hopane) values compared to oils generated from shales (McKirdy et al., 1983, 1984). Bitumens of anoxic and acidic hypersaline source rocks generally show high Ts/(Ts+Tm) (Rullkötter and Marzi, 1988).

Interestingly, the cross plots of C_{29}Ts/(C_{29}Ts + C_{29}17α (H)hopane) versus Ts/(Ts+Tm) and C_{30} 17α(H) diahopane/(C_{30}17α(H)diahopane + C_{30}17α(H) hopane) versus C_{29}Ts/(C_{29}Ts + C_{29}17α(H) hopane) in Figure 4.21 separate the Silurian and Ordovician source rock samples into the same groups identified previously using facies-dependant biomarker parameters. This observation indicates that indeed all of these parameters C_{29}Ts/(C_{29}Ts + C_{29}17α(H) hopane), Ts/(Ts+Tm) and C_{30} 17α (H) diahopane/(C_{30}17α(H) diahopane + C_{30}17α(H) hopane) cannot be used to assess the maturity of the Silurian and Ordovician source rock samples because they are strongly affected by facies differences between theses samples. These three parameters show lower values in the Ordovician and Silurian source rock samples from group B compared to the Silurian source rock samples from group A. Zhang et al. (2000) used cross plots of Ts/(Ts+Tm) and C_{27} diasteranes/(C_{27}diasteranes + regular steranes) to differentiate depositional environments of the Cambrian and Carboniferous extracts

from Ordovician extracts in the tarim Basin, China. Hence, it is likely that the explanation for this observation is that all the Ordovician source rock samples and the Silurian source rock samples from group B have higher abundance of total mineral carbon content (carbonate) than the Silurian source rock samples from group A, respectively. This is also in good agreement with the conclusions shown by (McKirdy et al., 1983, 1984).

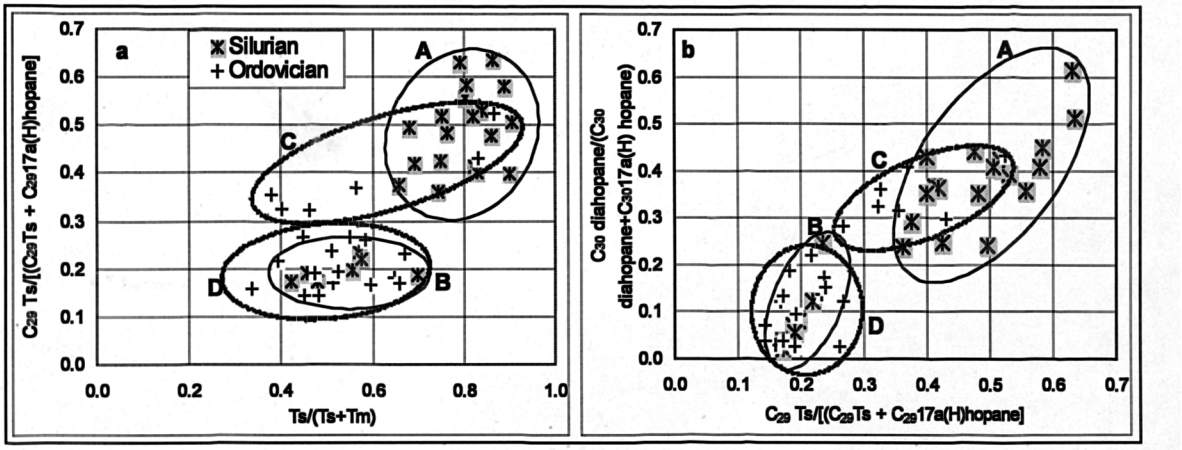

Figure 4.21 Cross plots of the maturity parameters (a) $C_{29}Ts/(C_{29}Ts+C_{29}17\alpha(H)$ hopane) versus Ts/(Ts+Tm) and (b) C_{30} diahopane/(C_{30} diahopane+$C_{30}17\alpha(H)$ hopane) versus $C_{29}Ts/(C_{29}Ts+C_{29}17\alpha(H)$ hopane) for the Silurian and Ordovician source rocks in the Oued Mya basin.

4.3.2.3.2. Aromatic compounds

This section presents the application of a suite of maturity ratios derived from the distribution of aromatised steroid hydrocarbons, alkylnaphthalenes, alkylphenanthrenes and alkylthiophenes isolated from the Silurian and Ordovician source rock samples in an attempt to illustrate further the different levels of thermal maturity which characterise these source rock intervals. Generally, ratios obtained from these compounds rely either on an increase with maturity in the degree of alkylation of a given parent compound or on a shift in the isomer distribution of alkylaromatic homologues towards thermally more stable isomers (Radke, 1987).

4.3.2.3.2.1. Aromatic steroid hydrocarbons

The distribution of C-ring monoaromatic (MA) and ABC-ring triaromatic (TA) steroid hydrocarbons in the Ordovician and Silurian source rock samples were monitored using the m/z 253 and 231 fragment ions, respectively. Typical mass chromatograms showing the distributions of MA- and TA-steroid hydrocarbons in

Silurian and Ordovician source rock samples are shown in Figure 4.22 and Figure 4.23, respectively.

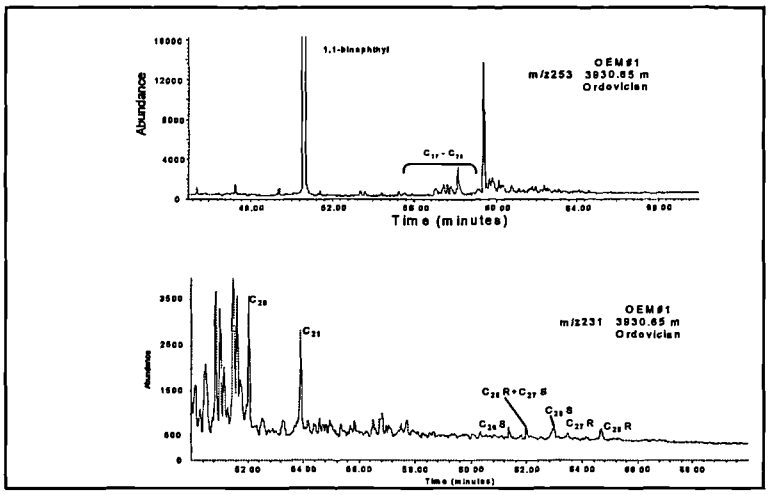

Figure 4.22 Partial m/z 253 and 231 mass chromatograms showing the distributions of C-ring monoaromatic steroids and ABC-ring triaromatic steroid hydrocarbons in a selected Ordovician source rock sample.

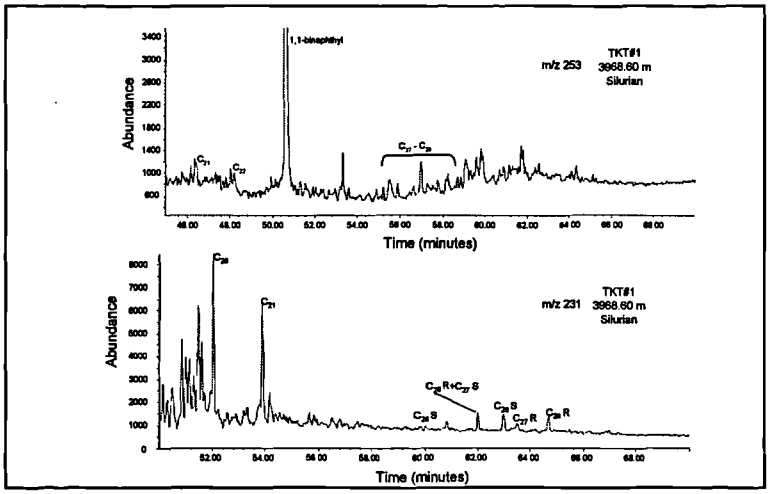

Figure 4.23 Partial m/z 253 and 231 mass chromatograms showing the distributions of C-ring monoaromatic steroids and ABC-ring triaromatic steroid hydrocarbons in a selected Silurian source rock sample.

Visual inspection of the m/z 253 mass chromatograms displayed in Figure 4.22 reveals that monoaromatic-steroid hydrocarbons are completely absent in all Ordovician and Silurian source rocks. Mass chromatograms show only the presence of the surrogate standard 1,1-binaphthyl used for aromatic compounds quantification. This feature suggests that complete aromatisation of C-ring monoaromatic- to ABC-ring triaromatic-steroid hydrocarbons has occurred. The precursor-product aromatisation reaction of the transformation of monoaromatic- to triaromatic-steroid

hydrocarbons (Figure 4.24) has been demonstrated in laboratory heating experiments on a carbonate matrix in the presence of elemental sulphur (Abbott et al., 1984; Abbott and Maxwell, 1988) during hydrous pyrolysis experiments of the Siliceous and Phosphatic members of the Monterey Formation (Peters et al., 1990), in a suite of oils from the Monterey Formation and offshore Louisiana petroleum (Requejo, 1992), as well as in a sequence of shales from the Upper Devonian Duvernay Formation of Western Canada (Requejo, 1994).

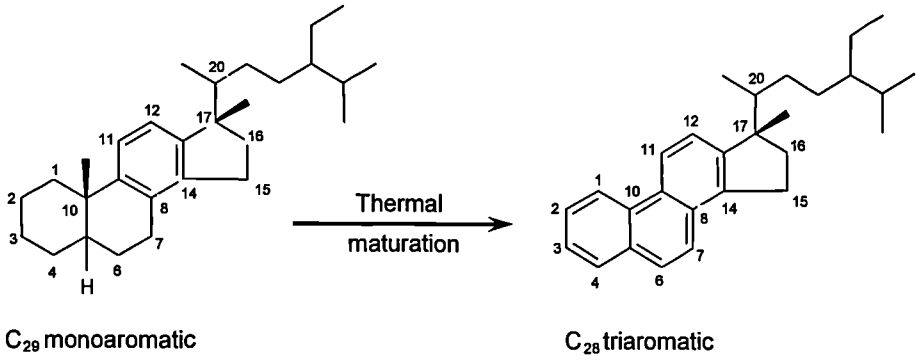

Figure 4.24 Conversion of C_{29}-monoaromatic to C_{28}-triaromatic steroids during thermal maturation. Note the loss of the methyl group attached to C-10 (A/B ring juncture) and loss of the asymmetric centre at C-5 in this reaction

Triaromatic-steroid hydrocarbons in the Silurian and Ordovician source rock samples with m/z 231 mass chromatograms displayed in Figure 4.22 and Figure 4.23 reveal a predominance of the short-chain (C_{20}-C_{21}) compared to long-chain (C_{26}-C_{28}) components. The long-chain C_{26}-C_{28} triaromatic-steroid hydrocarbon homologues are barely present in the majority of Ordovician and Silurian samples, which shows the prevalence of the short-chain components. In this work, the abundance of C_{20} triaromatic-steroid hydrocarbon relative to the C_{28} (S+R) was employed to evaluate the maturity of source rock samples, and the values of this parameter are listed in Appendix 4.2. The values of this ratio range from 61% to 98% for the Silurian source rock samples and 66% to 99% for the Ordovician source rock samples, indicating a high level of maturity for the Silurian and Ordovician source rock samples (Mackenzie et al., 1981). This is consistent with high Tmax values revealed in the Silurian and Ordovician source rock samples (Table 4.1). Moreover, the Silurian source rock samples in the well GBC#1 (3213 and 3259m) located south of the other wells analysed in the Oued Mya basin (Figure 4.1) exhibit the highest (C_{20} TAS)/(C_{20} TAS + C_{28} 5α(H)(S+R) TAS) values (ca. 100%) compared to the other Silurian and

Ordovician source rock samples. This observation confirms that the Silurian source rock strata located towards the south of the Oued Mya basin are overmature (more mature than the Silurian and Ordovician strata located towards the northeast of the Oued Mya basin.). This is again in agreement with the measured vitrinite reflectance equivalent plotted in Figure 3.7 in chapter 3 (Sonatrach, unpublished reports and Sonatrach and Pecten Algeria Company).

The thermal maturity of the Silurian and Ordovician source rocks is assessed by comparison to a sample set identified as marine type II kerogen sourced petroleums from the North Sea. The sample set consists of 9 North Sea oils having a known measured vitrinite reflectance obtained from basin modelling together with biomarker and aromatic hydrocarbon concentrations and maturity parameters. I have selected two aromatic maturity parameters: the C_{20} triaromatic steroids/[(C_{20} triaromatic steroids + C_{28} 5α(H) (S+R) triaromatic steroids)] and MPI-1 which showed good correlation with the measured vitrinite reflectance %Rm (Figure 4.25). The estimated maturity of the Silurian and Ordovician source rock samples analysed in this project show a similar range of maturity for both source rock samples; i.e. 0.92 to 1.12 % Rm, using the plot of measured vitrinite reflectance equivalent %Rm against the ratio of C_{20} triaromatic steroids/[(C_{20} triaromatic steroids + C_{28} 5α(H) (S+R) triaromatic steroids)] and 0.81 to 1.12 %Rm using the plot of the measured vitrinite reflectance equivalent %Rm versus MPI-1. These intervals of the estimated maturity obtained by comparison to a North Sea oil sample set seem to be in agreement with the high Tmax values, 440 to 458 °C for the Silurian source rock samples and 439 to 452 °C for the Ordovician source rock samples (Table 4.1). These findings confirm that the differences between the Silurian and Ordovician source rock samples are mainly due to the different source facies and depositional environments of the organic matter in the two source rock strata. Finally, the range of maturity of the Silurian and Ordovician source rocks estimated by comparison to the North Sea sample set indicate that the Silurian and the Ordovician source rocks in the northeast of the Oued Mya basin have reached a maturity level equivalent to the main and the end of the oil window. This is in agreement with the results found by Sonatrach and Pecten (see Figure 3.7 in chapter 3; Makhous et al. (1997a,b).

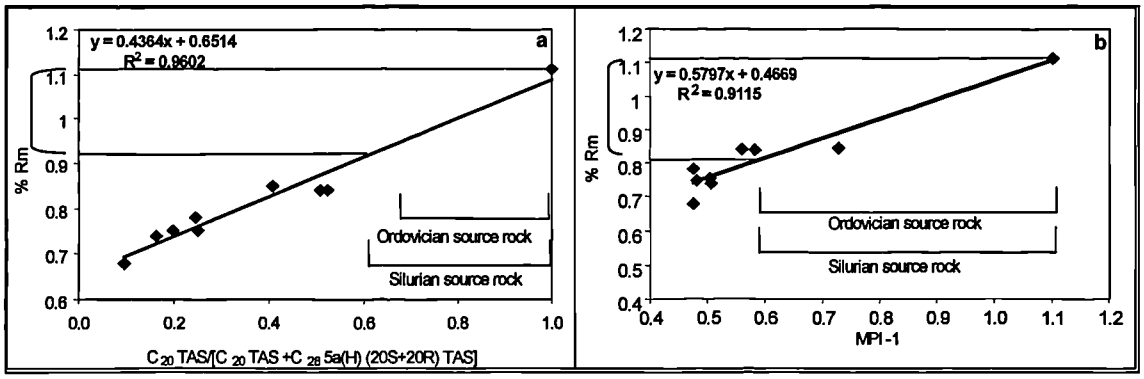

Figure 4.25 Cross plots showing the correlations between (a) the measured vitrinite reflectance (%Rm) and the C_{20} triaromatic steroids/[(C_{20} triaromatic steroids + C_{28} 5α(H)(S+R) triaromatic steroids)] and (b) the measured vitrinite reflectance (%Rm) and MPI-1 for a North Sea oil sample set used for the calibration of the maturity of the Silurian and Ordovician source rock strata in the Oued Mya basin.

Finally, it is important to note that the concentrations of the total triaromatic steroid hydrocarbons are much higher in the Silurian source rock samples compared to those in the Ordovician source rock samples (Appendix 4.2). The Ordovician source rock samples do not show such clear trends as those in the Silurian source rock samples, likely because of facies and depositional environment differences between the two strata. Moldowan et al. (1986) have shown that the triaromatic steroid hydrocarbons are influenced by diagenetic conditions, particularly Eh, in the source sediments.

4.3.2.3.2.2. Alkylnaphthalenes

Methylated naphthalenes are ubiquitous constituents of sedimentary organic matter (Tissot and Welte, 1984). They have been found to occur in crude oils with up to six methyl groups attached to the basic naphthalene carbon skeleton (Bastow et al., 1998). The distributions of alkylnaphthalenes are controlled by the effects of source facies, thermal maturity and biodegradation.

The alkylnaphthalenes are suggested to be derived mainly from sesquiterpenoids and triterpenoids sourced from microbacteria and land-plants (Püttmann and Villar, 1987; Strachan et al., 1988; Forster et al., 1989), though it is likely that methylation of non-specific precursors produce a suite of compounds of this type (Bastow et al., 1999).

Methylated naphthalene isomers which do not present a carbon skeleton reflecting an obvious natural product precursor are believed to be produced through methylation and demethylation reactions which take place by electrophilic aromatic substitution (Bastow et al., 1999). Evidence showed that this process actually does occur in

sedimentary basins. It was shown that increasing maturity in sedimentary basins leads to enrichment of the thermodynamically more stable alkylnaphthalene isomers with β substituted methyl groups. Hence, distributions of methylated naphthalenes can be used to acquire information about the effects that thermal stress (i.e. maturity) have on sedimentary organic matter. According to this concept, a number of maturity ratios involving methylated naphthalenes have been developed over the years and used to assess maturities of source rocks and crude oils (Radke et al., 1982 a & b; 1984; 1986; Radke and Welte, 1983; Radke, 1987 & 1988; Radke et al., 1990 & 1994; Alexander et al., 1984 & 1985; van Aarssen et al., 1999). Most of these parameters are based on the notion that naphthalenes with β-substituted methyl groups (Figure 4.26) are more stable than those with α-substituents (Alexander et al., 1985).

The effects of biodegradation on the distribution of alkylnaphthalenes were first described by Volkman et al. (1984) and were reported recently by Fisher et al. (1996 and 1998). These authors established the order of susceptibility for microbial degradation for DMNs, TMNs and TMNs. They concluded that isomers with 1,6-substitution pattern are more prone to biodegradation than the other isomers. These results enable, in principle, assessment of the biodegradation level of crude oil from the distributions of methylated naphthalenes.

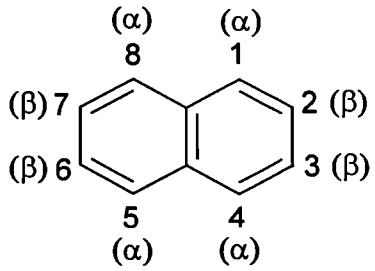

Figure 4.26 Assignments of α/β positions and numbering of the naphthalene carbon skeleton.

Evaluation of the thermal maturity of Ordovician and Silurian source rock samples was achieved using several maturity parameters based on the alkylnaphthalene distributions. Selected parameters are listed in Table 4.5.

Table 4.5 Maturity parameters based on methylated naphthalenes.

Abbreviation	Definition	Substitution pattern	Reference
MNR	2-MN/1-MN	β/α	Radke et al., (1982b)
DNR-1	(2,6-DMN + 2,7-DMN)/1,5-DMN	(ββ + αα)/αα	Radke et al., (1982b)
TNR-1	2,3,6-TMN/(1,4,6-TMN+1,3,5-TMN)	βββ/ααβ+αβα	Alexander et al., (1985)
TNR-2	(1,3,7-TMN + 2,3,6-TMN)/(1,3,5-TMN+1,3,6-TMN+1,4,6-TMN)	(αββ+βββ)/(ααβ+αββ+αα	Radke et al., (1986)
TMNR	1,3,7-TMN/(1,3,7-TMN + 1,2,5-TMN)	αββ/(αββ+αβα)	van Aaessen et al., (1999)
TeNR	2,3,6,7-TeMN/1,2,3,6-TeMN	ββββ/αβββ	van Aaessen et al., (1999)
TeMNR	1,3,6,7-TeMN/(1,2,5,6-TeMN + 1,2,3,5-TeMN)	αβββ/(αβαβ + αββα)	van Aaessen et al., (1999)

MNR = methylnaphthalene ratio
DNR = dimethylnaphthalene ratio
TNR = trimethylnaphthalene ratio
TMNR = trimethylnaphthalen ratio
TeMNR = tetramethylnaphthalene ratio

Partially added mass chromatograms showing the relative distribution of C_0-C_4 naphthalenes in selected Ordovician and Silurian samples are presented in Figure 4.27 and Figure 4.28, respectively.

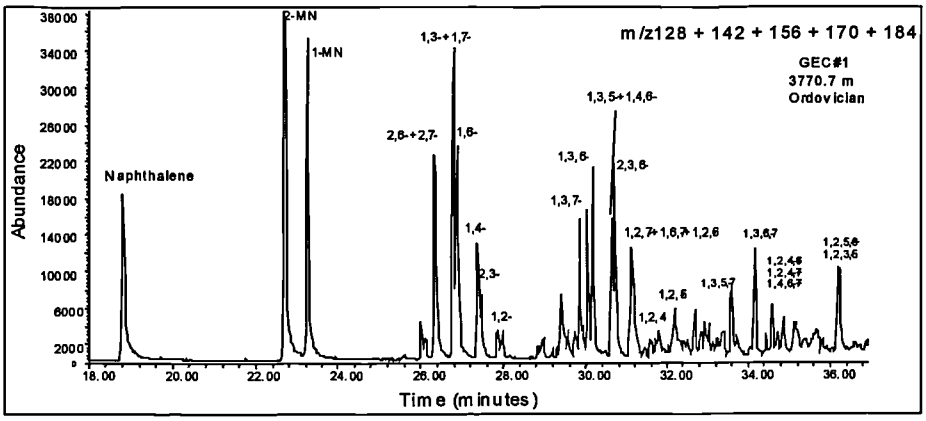

Figure 4.27 Partial m/z 128+142+156+170+184 mass chromatograms showing the distribution of C_0-C_4 naphthalenes in a typical Ordovician source rock sample in the Oued Mya basin.

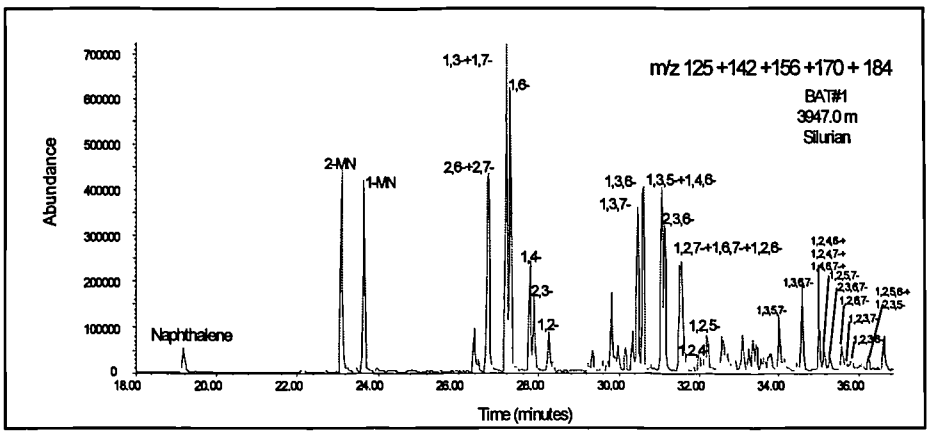

Figure 4.28 Partial m/z 128+142+156+170+184 mass chromatograms showing the distribution of C_0-C_4 naphthalenes in a typical Silurian source rock sample in the Oued Mya basin.

The variations in concentrations (μg/g extract) of C_0-C_4 naphthalenes present in Ordovician and Silurian source rock samples are shown in Figure 4.29. Alkylnaphthalene-based maturity ratios and the concentration of alkylnaphthalenes in all samples analysed in this study are listed in Appendix 4.2. Figure 4.29 reveals that

Silurian samples contain higher concentrations of various alkylnaphthalene components compared to Ordovician samples by one order of magnitude. Moreover, alkylnaphthalene distributions show a regular decrease in the concentration of these components with the increase of the degree of alkylation in both sets of samples.

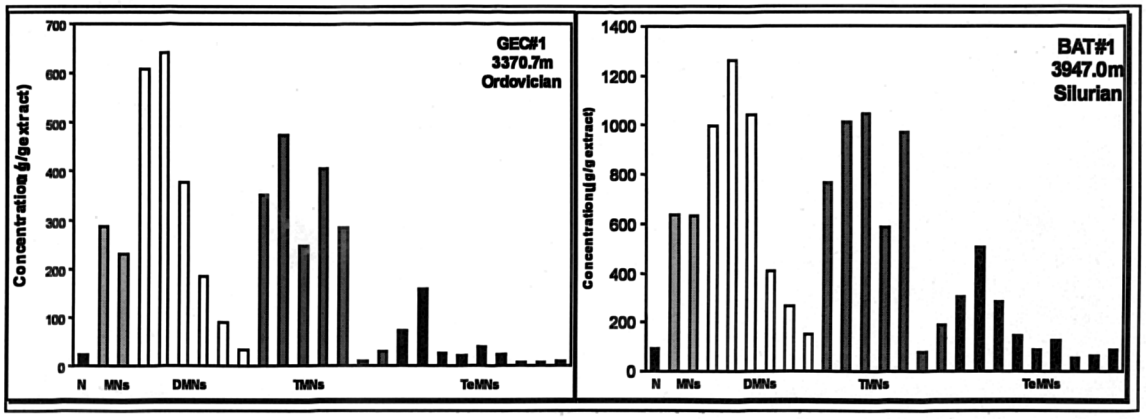

Figure 4.29 C_0-C_4 alkylnaphthalenes distribution in typical Ordovician and Silurian source rock samples in the Oued Mya basin.

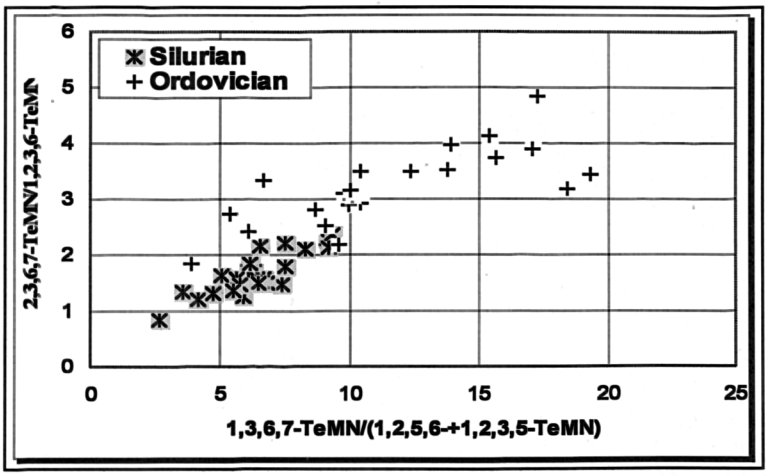

Figure 4.30 Cross plots of the alkylnaphthalene-based maturity parameters 2,3,6,7-TeMN/(1,2,3,6-TeMN) and (1,3,6,7-TeMN)/(1,2,5,6-TeMN + 1,2,3,5-TeMN) for the Silurian and Ordovician source rocks in the Mya basin.

4.3.2.3.2.3. Alkylphenanthrenes

As with the alkylnaphthalenes, the alkylphenanthrene isomers which are substituted at the β-position (Figure 4.31) have been observed to become increasingly dominant at higher maturity levels relative to related isomers with α-substitution (Radke et al., 1982a & b; Radke and Welte, 1983; Garrigues et al., 1984; Hall et al., 1985; Radke, 1987, 1988; Cassani et al., 1988).

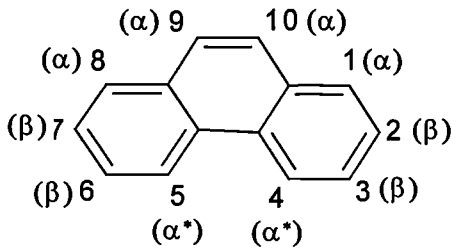

Figure 4.31 Molecular structure and carbon numbering system of phenanthrene. Sterically crowded positions are indicated by asterisk.

Application of alkylphenanthrene maturity parameters is still extensively used in the assessment of oils and sediments maturity. In addition to thermal maturation, it has been shown that the abundance and distribution of polycyclic aromatic hydrocarbons in oils and sediments of different ages are controlled by (1) the type of organic matter (Fan Pu et al., 1990), (2) the presence of mineral catalysts in the source or reservoir rocks (Jovancicevic et al., 1992, 1993), and (3) the mineral composition of the carrier system rocks (Golovko and Ivanov, 1999).

Partial summed mass chromatograms showing the relative distribution of C_0-C_3 phenanthrenes in selected Ordovician and Silurian samples are presented in Figure 4.32 and Figure 4.33, respectively.

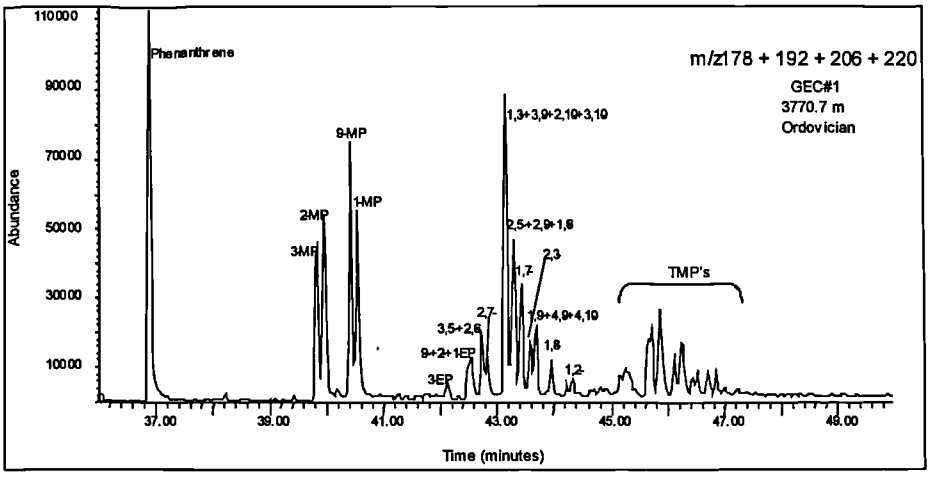

Figure 4.32 Partial m/z 178 + 192 + 206 + 220 mass chromatograms showing the distribution of C_0-C_3 phenanthrenes in a typical Ordovician source rock sample in the Oued Mya basin.

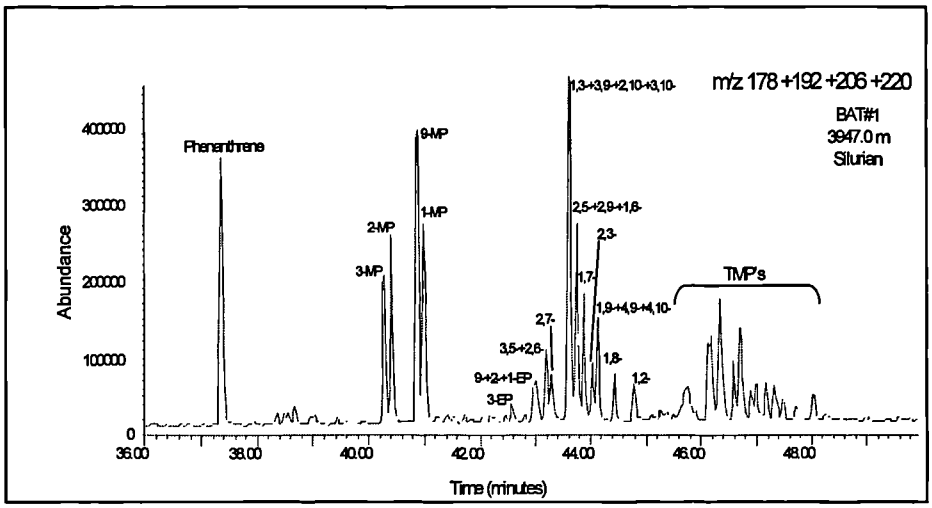

Figure 4.33 Partial m/z 178+192+206+220 mass chromatograms showing the distribution of C_0-C_3 phenanthrenes in a typical Silurian source rock sample in the Oued Mya basin.

The variations in concentrations (μg/g extract) of C_0-C_3 phenanthrenes present in Ordovician and Silurian source rock samples are displayed in Figure 4.34. The phenanthrene-based maturity ratios and the concentrations of the alkylphenanthrenes in all Ordovician and Silurian samples analysed in this study are listed in Appendix 4.2. As can be seen from Figure 4.34, the distribution of alkylphenanthrene isomers is in general similar in both Ordovician and Silurian samples. However, the concentrations of alkylphenanthrene isomers are generally higher (by an order of magnitude) in the Silurian samples versus those from the Ordovician samples (Figure 4.35).

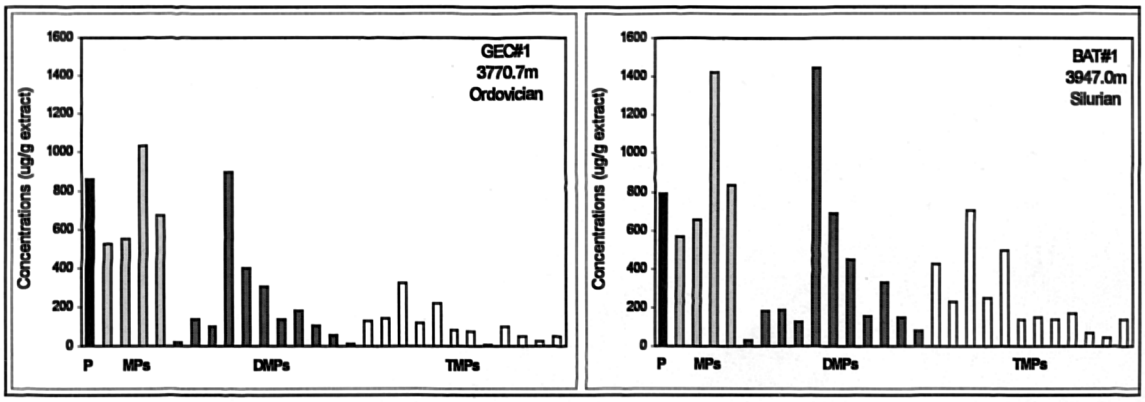

Figure 4.34 C_0-C_3 alkylphenanthrenes distribution in typical Ordovician and Silurian source rock samples in the Oued Mya basin.

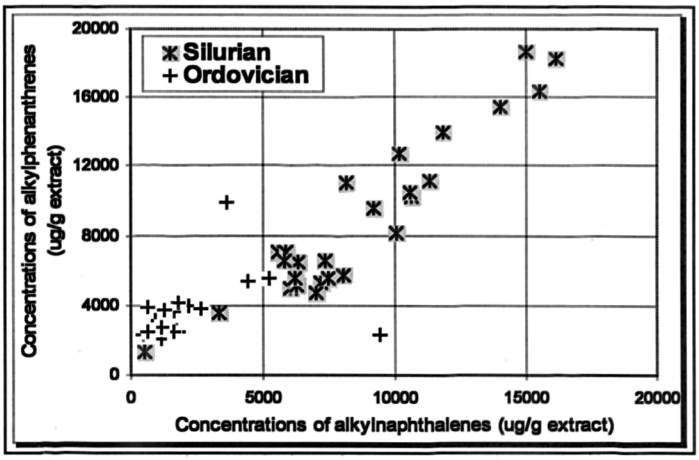

Figure 4.35 Cross plots of concentrations of phenanthrenes versus concentrations of naphthalenes for Ordovician and Silurian source rock samples in the Oued Mya basin.

Maturity parameters based on alkylphenanthrenes used in this study are listed in Table 4.6, and the values for these parameters are listed in Appendix 4.2.

Table 4.6 Maturity parameters based on methylated phenanthrenes

Abbreviation	Definition	Substitution pattern	Reference
MPR	2-MP/1-MP	β/α	Radke et al., (1982b)
MPI-1	1.5*(3-MP+2-MP)/(P+9-MP+1-MP)	ββ/αα	Radke et al., (1982a)
DMPR	(2,6- + 2,7- + 3,5-DMP)/(1,3- + 1,6- + 2,5- +3,9- + 3,10-DMP)	(ββ+ββ+βα)/(αβ+αβ+βα+β	Radke et al., (1986)
%Rc	0.4 + (MPI-1)*0.6	–	Radke et al., (1982b)

MPR = methylphenanthrene ratio
DMPR = dimethylphenanthrene ratio
MPI = methylphenanthrene index

The diagrams plotted in Figure 4.36 again show good correlation ($R^2 = 0.83$) between maturity parameters based on alkylphenanthrenes. However, Ordovician and Silurian samples revealed more similar levels of maturity than estimates based on alkylnaphthalenes plotted above. Moreover, samples GBC#1 (3213 and 3259m) located south of the Oued Mya basin (Figure 4.1) present the highest alkylphenanthrene ratios amongst all Silurian samples, therefore, they are more mature than all the other Silurian samples located in the north-northeast of Oued Mya basin. This is consistent with the higher Tmax, lower HI, and higher $C_{20}/(C_{20}+C_{28}(S+R))$ ratio encountered in these two samples (Table 4.1 and Appendix 4.2). In fact it is well established that the Silurian in the southern part of the Oued Mya basin is overmature and has generated most of its hydrocarbons during the Palaeozoic (Makhous et al., 1997a,b).

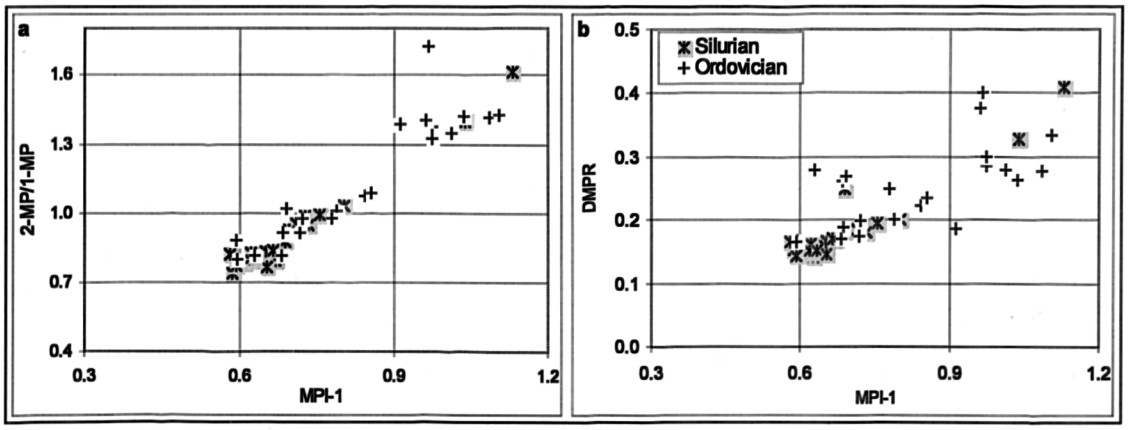

Figure 4.36 Cross plots of the methylphenanthrene-based maturity parameters (a) 2-MP/1-MP and (b) DMPR versus methylphenanthrene index-1 (MPI-1) for the Silurian and Ordovician source rocks in the Mya basin.

Finally, calculated vitrinite reflectance (VRc%) estimates using the formula proposed by Radke et al. (1986) revealed values ranging from 0.76 to 1.06 (average 0.91%) for Ordovician samples and from 0.75 to 0.88% (average 0.80%) for Silurian samples, located in the northeast of the Oued Mya basin. The Silurian source rock samples from the well GBC#1 located further south reveal the highest VRc% values in samples GBC#1 (1.02 and 1.08%). Calculated vitrinite reflectance (VRc%) values indicate that both source rocks have undergone similar thermal stress during basin evolution.

4.3.2.3.2.4. Alkyldibenzothiophenes

Aromatic sulphur compounds such as benzothiophenes and dibenzothiophenes have been extensively used in the assessment of thermal stress because they are common in a variety of both oils and organic-rich sediments (Radke et al., 1986; Radke, 1988; Shou and Myhr, 1988; Radke and Willsh, 1994; Chakhmakhchev and Suzuki, 1995a; Chakhmakhchev et al., 1997; Santamaria-Orozco et al., 1998). However, Huang and Pearson (1999) suggested that aromatic sulphur compounds are affected by both thermal maturation and other factors such as the depositional environment and source rock lithology.

Using distributions of aromatic sulphur compounds, Chakhmakhchev and Suzuki (1995a) distinguished between a set of oil samples derived from source rocks of different lithologies. Furthermore, Hughes (1984) reported that abundant benzothiophenes in crude oils may indicate carbonate-evaporite source environments.

Moreover, Hughes et al. (1995) used dibenzothiophene/phenanthrene versus pristane/phytane cross plot to differentiate depositional environment and lithology of source rocks.

Biodegradation also influences the abundance and distributions of aromatic sulphur compounds, as depletion of alkanes and smaller naphthene molecules leads to residual aromatic sulphur compound enrichment (Bailey et al., 1973). The dibenzothiophene/phenanthrene ratio was used to assess water washing effects on crude oils, because of the higher water solubility of dibenzothiophene compared to phenanthrene (Palmer, 1984; Dahl and Spears, 1986; Williams et al., 1986). Figure 4.37 below shows the molecular structure of dibenzothiophene.

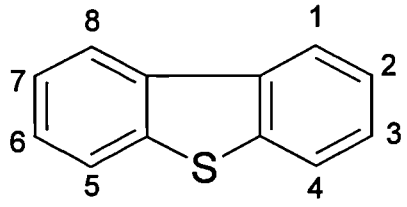

Figure 4.37 Molecular structure and carbon numbering system of dibenzothiophene.

Summed m/z 184, 198, 212, and 226 mass chromatograms showing the typical distribution of C_0-C_3 dibenzothiophenes in Ordovician and Silurian samples are displayed in Figure 4.38 and Figure 4.39, respectively.

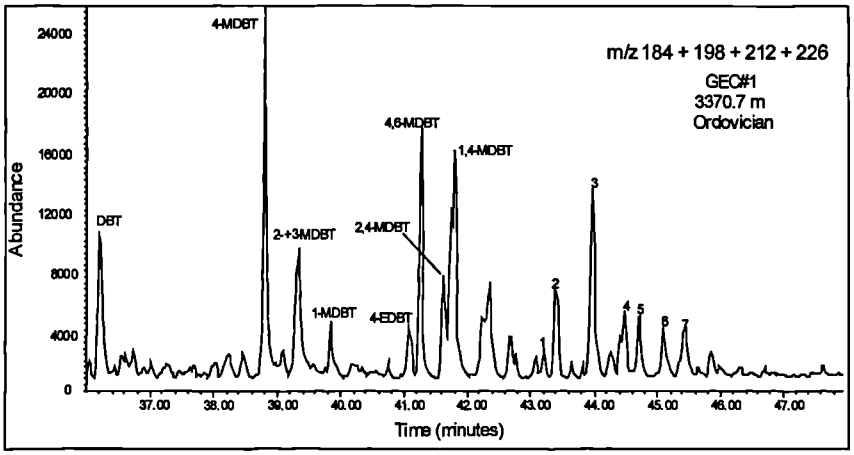

Figure 4.38 Partial m/z 184+198+212+226 mass chromatograms showing the distribution of C_0-C_3 dibenzothiophenes in a typical Ordovician sample in the Oued Mya basin.

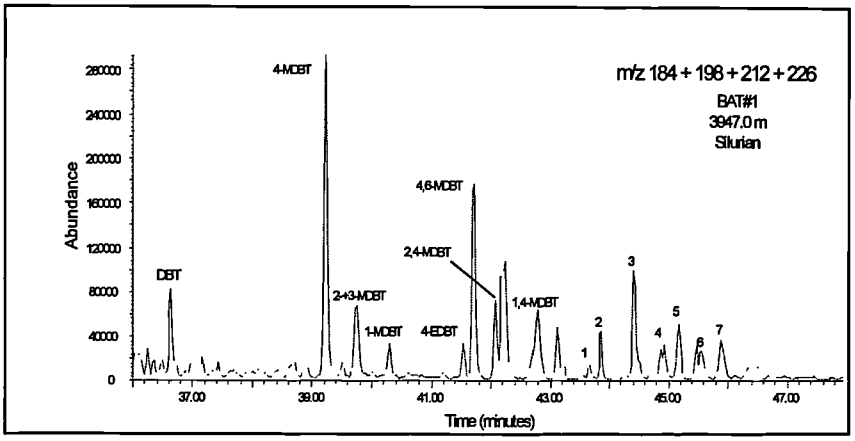

Figure 4.39 Partial m/z 184+198+212+226 mass chromatograms showing the distribution of C_0-C_3 dibenzothiophenes in a typical Silurian sample in the Oued Mya basin.

The dibenzothiophene isomer distributions are different in Ordovician compared to Silurian samples due to different depositional environment and lithology as mentioned earlier (Chakhmakhchev and Suzuki, 1995a; Hughes et al., 1995). Moreover, the quantification of individual dibenzothiophene isomers revealed that Silurian samples contain much greater concentrations (µg/g extracts) than samples from the Ordovician (Figure 4.40).

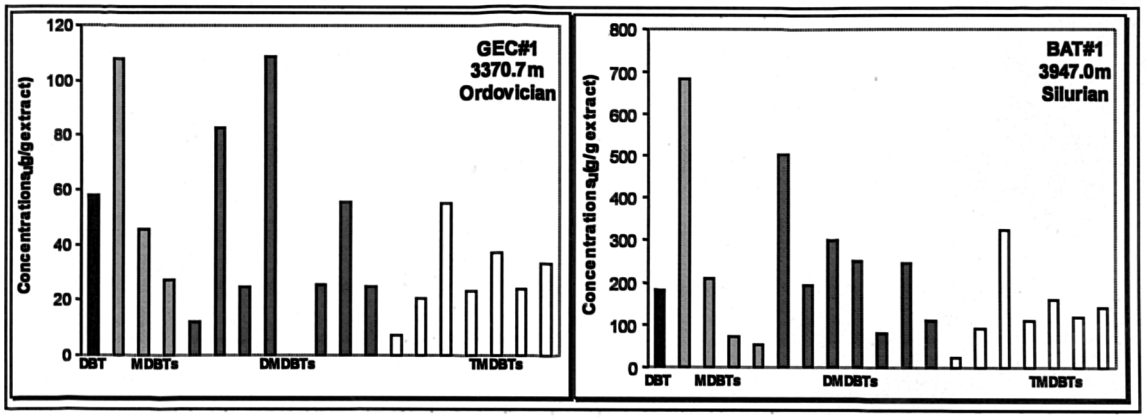

Figure 4.40 C_0-C_3 dibenzothiophenes distribution in typical Ordovician and Silurian source rock samples in the Oued Mya basin.

The maturity parameters employed in this study are listed in Table 4.7 and the values of these parameters and concentrations of individual isomers are listed in Appendix 4.2.

Table 4.7 Maturity parameters based on methylated thiophenes

Abbreviation	Definition	Reference
MDR2,3	(2-MDBT+3-MDBT)/DBT	Radke et al., (1982b)
MDR	4-MDBT/1-MDBT	Radke et al., (1986)
EDR	4,6-DMDBT/4-EDBT	Radke and Willsh, (1994)
	4,6-DMDBT/1,4-DMDBT	Chakhmakhchev et al., 1997
	2,4-DMDBT/1,4-DMDBT	Chakhmakhchev et al., 1998

M=methyl, D=di, E=ethyl, B=benzo, T=thiophene
R=ratio

The cross plots of 4-MDBT/1-MDBT ratio versus 2-+3-MDBT/DBT ratio and 4,6-DMDBT/1,4-DMDBT ratio versus 2,4-DMDBT/1,4-DMDBT ratio (Figure 4.41) show higher values for Silurian source rock samples compared to most of the Ordovician source rock samples in contrast to the maturity parameters based on the alkylnaphthalenes and alkylphenanthrenes. This is most likely due to depositional environment and lithology differences between the two sets of samples. Organic matter in Silurian black shale samples was deposited under anoxic conditions with high sulphur incorporation, whereas organic matter in Ordovician grey shale samples was deposited under more oxic conditions which led to poor organic matter preservation. Moreover, the Ordovician source rock samples revealed higher abundance of the total mineral carbon relative to the total organic carbon content than all the Silurian source rock samples (Table 4.1).

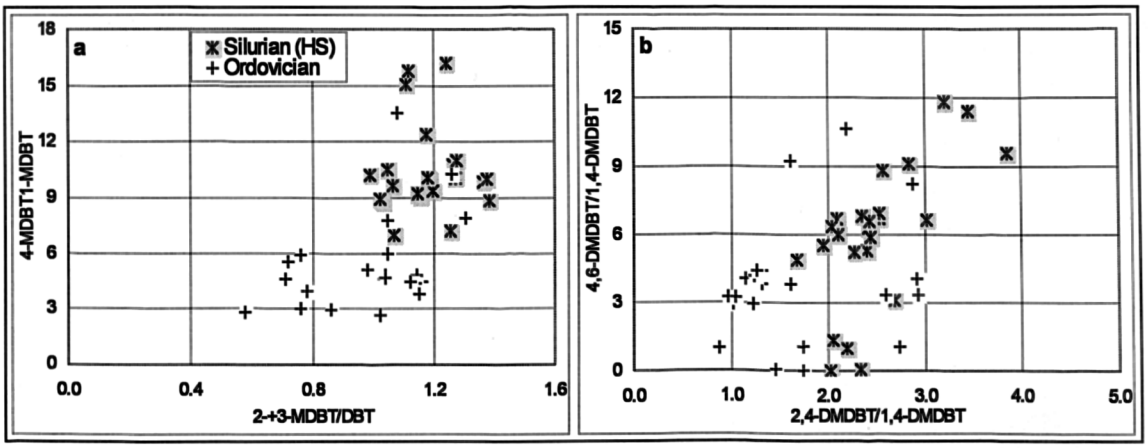

Figure 4.41 Cross plots of the dibenzothiophene-based maturity parameters (a) 4-MDBT/1-MDBT versus 2-+3-MDBT/DBT and (b) 4,6-DMDBT/1,4-DMDBT versus 2,4-DMDBT/1,4-DMDBT for the Silurian and Ordovician source rocks in the Mya basin.

All Ordovician samples and the Silurian samples from group B; GD#1bis (3850m), GLNE#5 (3987.55, 3994.45 and 4001.45m), GLNE#4bis (3874.85m) and GBC#1 (3213 and 3259m), contain some "unknown" peaks which appear in the TIC trace of the aromatic fractions. These peaks are apparent for all the Ordovician samples, but

they are relatively less abundant in the Silurian samples from group B. Moreover, these compounds do not appear in Silurian samples from group A (Figure 4.1) and all the oil samples. Samples containing these compounds were then analysed using the full scan mode and a tentative identification by library revealed that these peaks are probably the 2,6-diisopropylnaphthalenes and benzene, 1,1'-cyclohexylidenebis-. Full scan spectra showed that the major fragment ions and molecular ions of these compounds are m/z 212 and m/z 236 (Figure 4.42). The occurrence of these compounds coincides with the occurrence of *ortho-*, *meta-* and *para-* terphenyls with major fragment ions of m/z 230. Interestingly, all these compounds and terphenyls are completely absent in Silurian samples from group A suggesting a close relationship of the occurrence of these compounds and terphenyls with depositional environment and lithology.

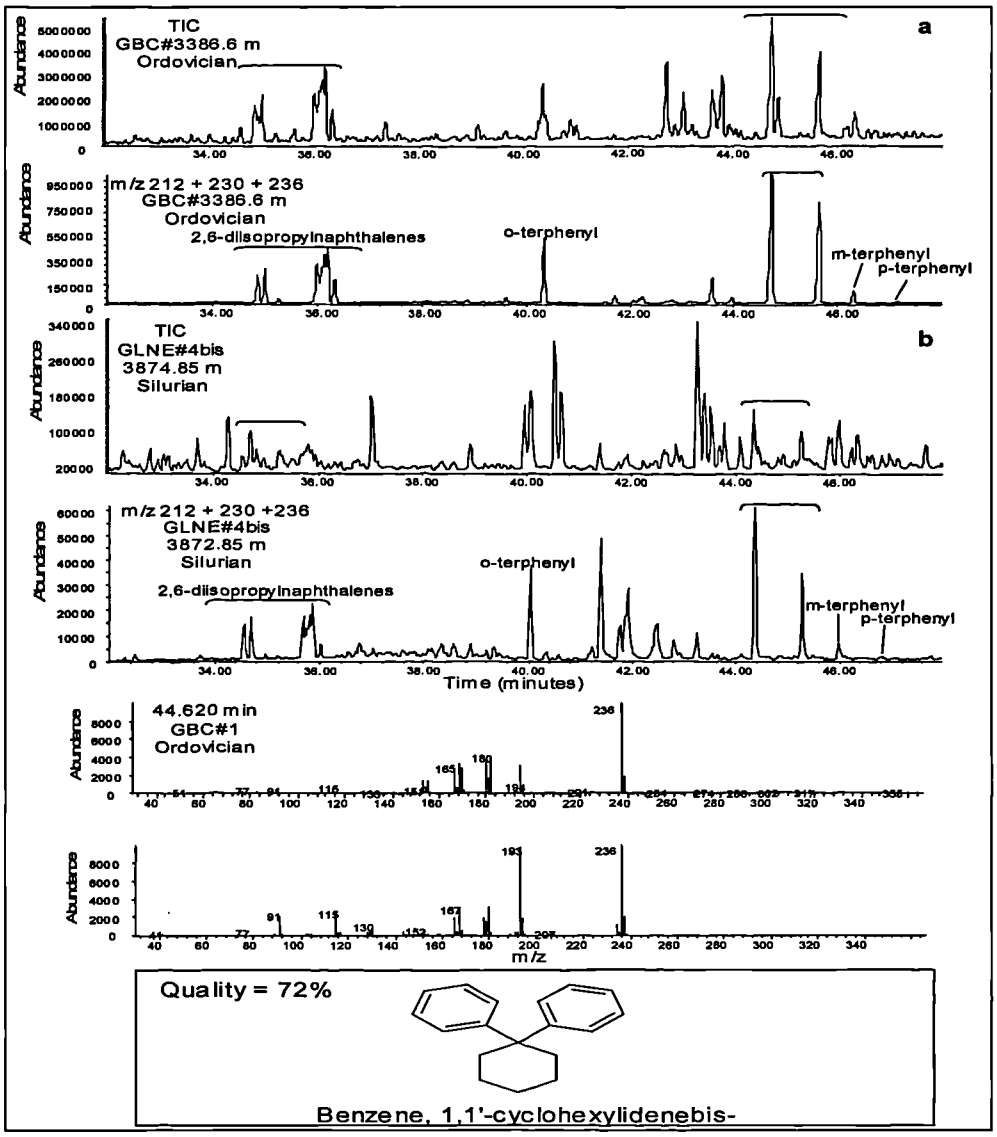

Figure 4.42 TIC and partial m/z 212+230+236 mass chromatograms showing the distribution of terphenyls and the unknown compounds in (a) a typical Ordovician sample and (b) a typical Silurian sample from group B.

The same samples from the Ordovician also show the occurrence of another family of compounds in the aromatic fraction. Tentative identification using mass spectra reveals that these compounds are probably: Bicyclohexyl, 4-phe and para-Dicyclohexylbenzene with major ion fragment m/z 242 (Figure 4.43).

Recently, terphenyls were reported in Palaeozoic source rocks of the Holy Cross Mountains, Poland by Marynowski et al. (2001). Marynowski et al. (2001) found that the so-called ortho-terphenyl isomer is thermally less stable than the two other meta- and para-terphenyl isomers. According to this observation, they have proposed two maturity based ratios: $TrP1 = \frac{p-TrP}{o-TrP}$ and $TrP2 = \frac{(m-TrP + p-TrP)}{o-TrP}$. Furthermore,

they showed positive correlation between TrP1 ratio and MDR ratio within selected sediment samples from the Holy Cross Mountains region.

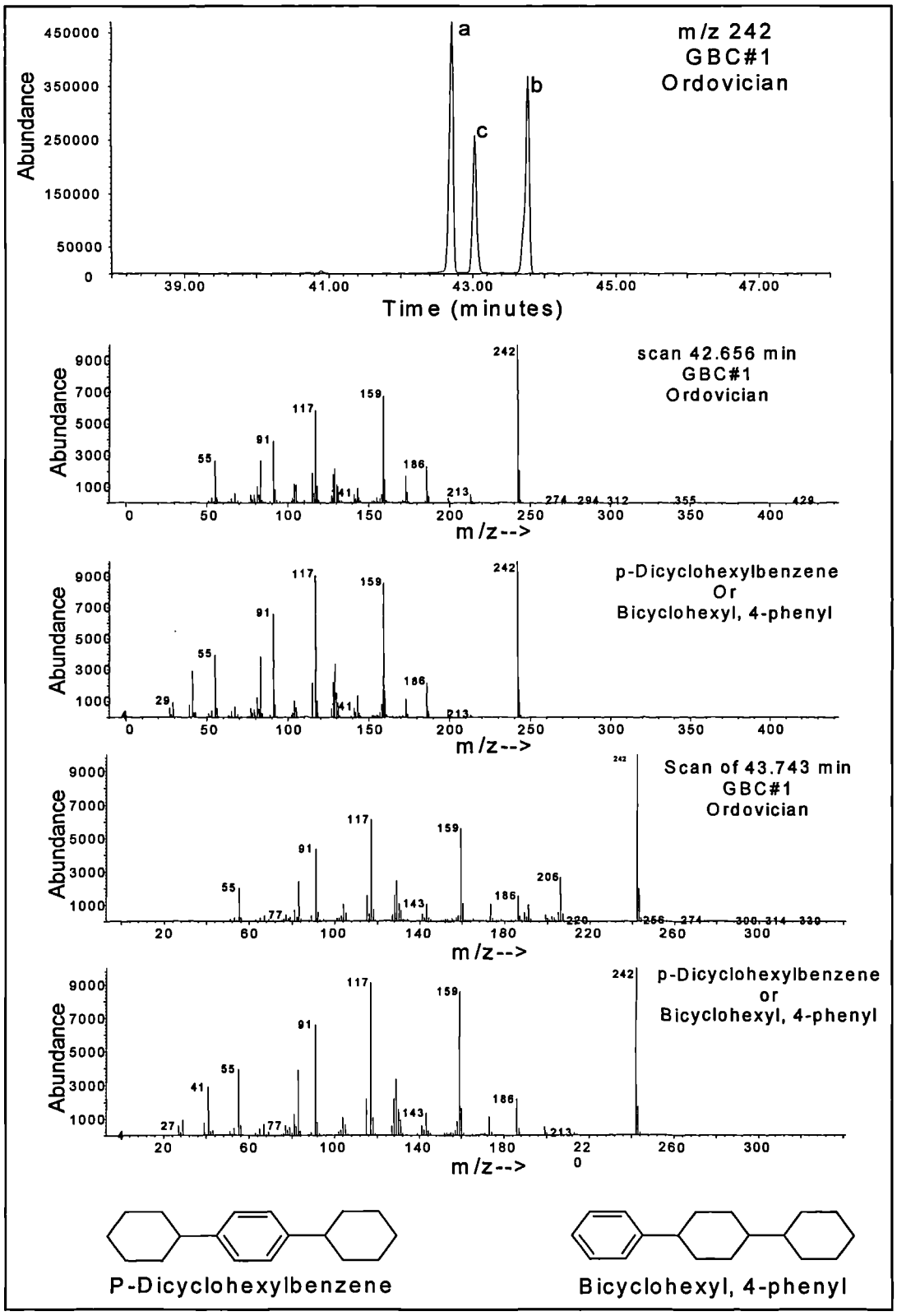

Figure 4.43 Partial m/z 83 mass chromatogram and mass spectrum showing the occurrence of (a) Bicyclohexyl, 4-phe and (b) p-Dicyclohexylbenzene in a typical Ordovician source rock sample.

4.4. Oils

In this section, I will characterise the oils reservoired in the Devonian and Lower Triassic fields in the Oued Mya basin, the Lower Triassic field in the Rhourde Chegga and the Cambro-Ordovician oils reservoired in the Hassi Messaoud, Hassi Guettar, El Gassi, Zotti, El-Agreb, Mesdar and El-Baguel fields, and the DST oil sample from OL#2 (Table 4.8).

Table 4.8 List of the oil fields studied in this project (see map in Figure 4.1 for field locations).

Field	Abbreviation	Reservoir	Location	Legend	Group
Mokh El Kabch	MEK#1	Lower Triassic	Oued Mya basin	O.Mya	IIa
N'Goussa	NGS#2	Devonian	Oued Mya basin	O.Mya	IIa
Guellala Northeast	GLNE#5	Devonian	Oued Mya basin	O.Mya	IIa
Guellala	GLA#16	Lower Triassic	Oued Mya basin	O.Mya	IIa
Draa Temra	DRT#1	Lower Triassic	Oued Mya basin	O.Mya	II
Benkahla	OKP#61	Lower Triassic	Oued Mya basin	O.Mya	II
	OKP#88	Lower Triassic	Oued Mya basin	O.Mya	II
	OKJ#31	Lower Triassic	Oued Mya basin	O.Mya	II
Haoud Berkaoui	OKJ#202	Lower Triassic	Oued Mya basin	O.Mya	II
	OKN#77	Lower Triassic	Oued Mya basin	O.Mya	II
	OKM#88	Lower Triassic	Oued Mya basin	O.Mya	II
Rhourde Chegga	RDC#1bis	Lower Triassic	Hassi Messaoud ridge	R.Chegga	I
DST oil	OL#2	Cambrian	Hassi Messaoud ridge	OL2	I
Hassi Messaoud	HMD	Cambrian	Hassi Messaoud ridge	HMD	I
Hassi Guettar	HGA#2	Ordovician	Hassi Messaoud ridge	H.Guettar	I
	HGA#3	Cambrian	Hassi Messaoud ridge	H.Guettar	I
El-Gassi	GS#1	Cambrian	Hassi Messaoud ridge	El-Agreb	I
Zotti	AR#61	Cambrian	Hassi Messaoud ridge	El-Agreb	I
El-Agreb	AR#22	Cambrian	Hassi Messaoud ridge	El-Agreb	I
Mesdar	MDR#7	Cambrian	Hassi Messaoud ridge	Mesdar	III
	MDR#8	Cambrian	Hassi Messaoud ridge	Mesdar	III
El-Baguel	RB#10	Cambrian	Hassi Messaoud ridge	El-Baguel	III
	RB#18	Cambrian	Hassi Messaoud ridge	El-Baguel	III

4.4.1. Source facies characterisation

4.4.1.1. Alkanes and isoprenoid alkanes

Gas chromatograms of the whole crude oil samples exhibit identical smooth n-alkane distributions, with no evidence of biodegradation being present in any of the oils (Figure 4.44). However, the oil sample collected from OL#2 which is a DST oil shows different *n*-alkane envelope dominated by *n*-C_{11}-*n*-C_{18} and very low amounts of *n*-C_8-*n*-C_{10}. The values of geochemical parameters obtained from the distributions of *n*-alkanes and isoprenoid alkanes together with the concentrations of total *n*-alkanes are listed in Table 4.9.

Table 4.9 Geochemical parameters obtained from *n*-alkane and isoprenoid alkane distributions

Field	reservoir	Well	Pr/Ph	Pr/n-C_{17}	Ph/n-C_{18}	*n*-alkane index n-C_{17}/n-C_{27}	Sum *n*-alkanes (mg/g oil)	Sum isoprenoid alkanes (mg/g oil)
Hassi Messaoud	Cambrian	OMJ#422	1.33	0.37	0.33	5.37	114.45	2.89
		OMK#14	1.35	0.38	0.34	6.24	103.70	2.60
		OML#862	1.33	0.38	0.33	5.39	116.66	3.06
		MD#201bis	1.34	0.34	0.28	6.48	113.67	2.57
		MD#59	1.30	0.34	0.33	6.54	121.17	2.73
		MD#204	1.31	0.34	0.29	6.04	110.32	2.45
		MD#279	1.32	0.34	0.30	6.02	115.26	2.53
		MD#165	1.32	0.34	0.32	6.64	187.76	2.83
		MD#317	1.29	0.33	0.31	6.01	115.67	2.55
		MD#297	1.35	0.34	0.30	5.15	114.34	2.67
		MD#322	1.29	0.33	0.32	6.26	106.97	2.30
		MD#208	1.32	0.34	0.29	6.49	186.58	2.54
		MD#185	1.32	0.33	0.31	6.55	120.80	2.75
		MD#239	1.30	0.33	0.28	6.07	121.45	2.78
		MD#104	1.30	0.34	0.32	6.49	109.00	2.34
		MD#348	1.31	0.35	0.30	6.26	122.86	2.81
		MD#255bis	1.33	0.34	0.31	6.38	120.78	2.82
		MD#332bis	1.34	0.31	0.27	5.38	133.05	3.17
		OMM#33	1.38	0.33	0.29	4.90	110.08	2.51
		OMM#772	1.38	0.35	0.30	4.89	117.98	2.77
		ONI#412	1.33	0.37	0.34	5.89	113.30	2.85
		ONM#36	1.34	0.36	0.30	6.02	116.07	2.70
		OMP#263	1.33	0.37	0.31	6.21	111.28	2.76
		OM#7	1.33	0.35	0.33	6.75	114.45	2.54
		OMO#751	1.30	0.35	0.34	6.38	109.04	2.61
		OMN#352	1.30	0.37	0.35	6.12	108.70	2.63
		OMN#412	1.32	0.36	0.33	6.37	113.80	2.73
		OMO#712	1.30	0.34	0.33	6.79	110.97	2.36
		OMJ#832	1.31	0.37	0.34	5.54	112.76	2.74
		OMO# 36	1.33	0.37	0.35	6.56	118.00	2.75
DST Oil	Cambrian	OL#2	1.40	0.29	0.26	21.01	161.57	5.33
Mokh-El-Kabch	Lower Triassic	MEK#1	1.38	0.37	0.29	5.72	91.40	2.88
N'goussa	Devonian	NGS#2	1.45	0.27	0.22	5.31	89.24	2.27
Guellala northeast	Devonian	GLNE#5	1.49	0.27	0.22	5.00	107.38	1.97
Guellala	Lower Triassic	GLA#16	1.50	0.27	0.21	4.42	110.29	2.07
Draa Temra	Lower Triassic	DRT#1	1.45	0.19	0.15	3.77	107.37	1.92
Haoud Berkaoui	Lower Triassic	OKN#77	1.43	0.26	0.20	3.77	115.58	2.03
		OKJ#31	1.49	0.22	0.17	3.66	118.03	2.18
		OKJ#202	1.43	0.23	0.18	4.07	115.34	2.37
		OKM# 88	1.41	0.25	0.20	3.44	126.91	2.15
Benkahla	Lower Triassic	OKP#61	1.44	0.27	0.22	3.71	109.75	2.10
		OKP#88	1.46	0.25	0.20	3.94	123.06	2.22
Rhourde Chegga	Lower Triassic	RDC#1 bis	1.30	0.32	0.30	6.57	115.71	2.62
Hassi Guettar	Ordovician Cambrian	HGA#2	1.34	0.34	0.30	5.68	106.73	2.39
		HGA#3	1.34	0.34	0.28	6.05	99.37	2.20
El-Gassi Zotti El-Agreb	Cambrian	GS#1	1.33	0.32	0.29	5.89	124.84	2.28
		AR#61	1.35	0.32	0.28	5.55	116.76	2.56
		AR#22	1.35	0.32	0.28	5.43	115.26	2.46
Mesdar	Cambrian	MDR#7	1.44	0.24	0.22	8.09	89.38	1.43
		MDR#8	1.43	0.23	0.22	7.57	90.59	1.38
El-Baguel	Cambrian	RB#10	1.38	0.24	0.23	8.37	87.63	1.31
		RB#18	1.27	0.25	0.25	9.42	69.25	1.33

Pr =pristane, Ph = phytane

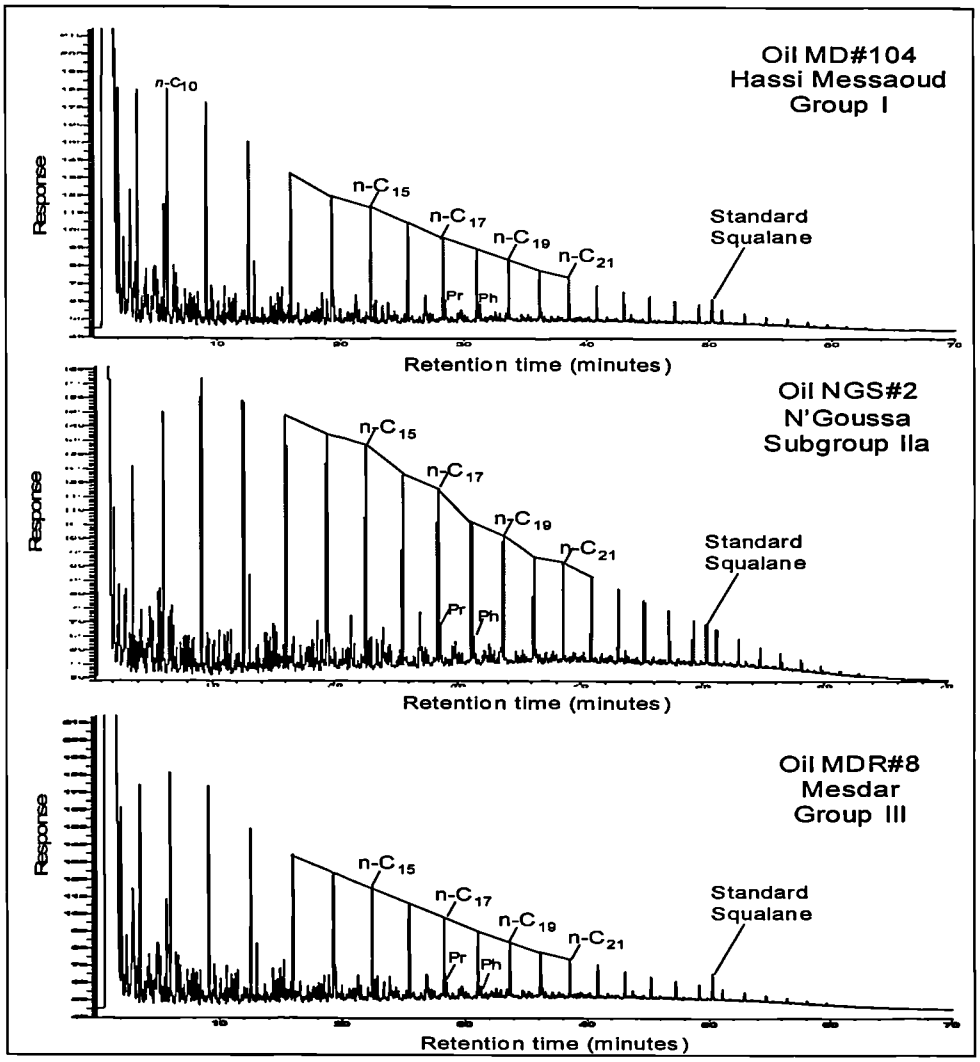

Figure 4.44 Gas chromatograms showing *n*-alkane distributions of selected oil samples representing the Oued Mya basin and Hassi Messaoud Ridge oils.

The *n*-alkane envelopes also show that the Devonian and the Lower Triassic reservoired oils in the Oued Mya basin (O.Mya) contain relatively more abundant heavy *n*-alkanes (*n*-C_{23}+) than in Hassi Messaoud (HMD), Rhourde Chegga (R.Chegga), Hassi Guettar (H.Guettar), and El-Agreb oils, respectively. Mesdar and El-Baguel oils are even lighter than the other oils in the region (Figure 4.45). This feature is expressed by the values of the *n*-alkane index (*n*-C_{17}/*n*-C_{27} alkane ratio) which are relatively higher for the oil samples from Hassi Messaoud, Hassi Guettar, El-Agreb and Rhourde Chegga (ranging from 4.89 to 6.75) compared to those of the oil samples from Devonian and Lower Triassic reservoirs in the Oued Mya basin ranging from 3.44 to 5.72 (Table 4.8). This is probably due to higher maturity of the oil samples from Hassi Messaoud, Hassi Guettar, El-Agreb and Rhourde Chegga relative to the Devonian and Triassic oils from the Oued Mya basin and/or the

Devonian the Lower Triassic reservoirs contain a mixture of oil generated from Silurian and Ordovician source rocks. In fact, the Ordovician source rock samples revealed lower n-alkane index ratios due higher abundances of the heavier *n*-alkanes (C_{23}+) in the Ordovician source rock samples compared to the Silurian source rock samples (see Table 4.2 in section 4.3.1). Moreover, oils from the Devonian and Lower Triassic reservoirs revealed the presence of maxima in the *n*-C_{15}, *n*-C_{17}, and *n*-C_{19} alkanes (Figure 4.44); a feature which was reported earlier in the Ordovician source rock samples (Figure 4.8 in section 4.3.1).

Oil samples from Rhourde Baguel (El-Baguel) and Mesdar (Mesdar) show even higher *n*-C_{17}/*n*-C_{27} values (7.57 to 9.42) suggesting that these oils are more mature than all of the oils in Hassi Messaoud Ridge and probably are generated from the same source rock but with higher maturity. In fact, in the biomarker and aromatic sections below, I show that the oil samples from Mesdar and El-Baguel fields are the most mature oils in the study area. Geographically, these two fields are located east of the Hassi Messaoud ridge and close from the Berkine basin (Figure 4.1), therefore, it is likely that these oils were generated from the Silurian source rock strata located in this basin. Daniels and Emme (1995) and unpublished Sonatrach reports showed that the Silurian source rock strata in Berkine basin are far more mature than the same Silurian strata in the Oued Mya basin .

Figure 4.46 displaying the concentrations of *n*-alkanes versus the *n*-C_{17}/*n*-C_{27} ratio clearly separates oil samples into three groups; group I includes oil samples from Rhourde Chegga Triassic field and Hassi Messaoud, Hassi Guettar and El-Agreb Cambrian fields, group II comprises Devonian and Lower Triassic oils from Oued Mya basin and group III contains Cambrian oils from Mesdar and El-Baguel fields (Figure 4.1). The DST oil sample OL#2 shows the highest *n*-C_{17}/*n*-C_{27} ratio (i.e. 21.01).

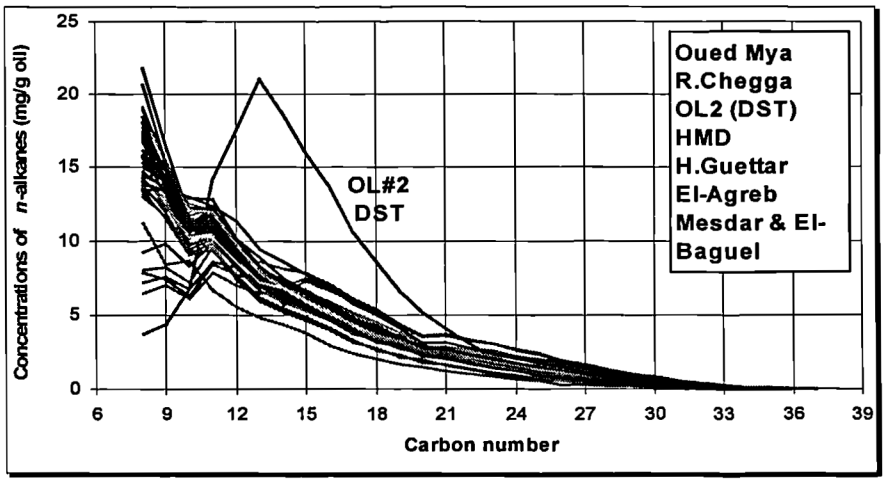

Figure 4.45 *n*-alkane envelopes for the Oued Mya basin and Hassi Messaoud Ridge oils.

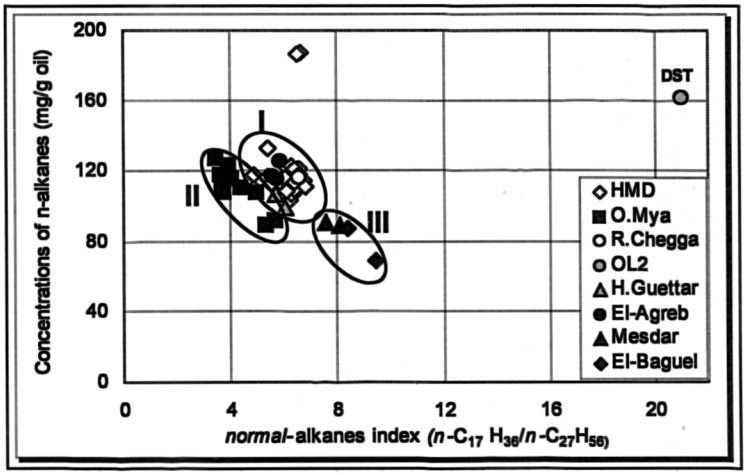

Figure 4.46 Cross plots of the concentrations of *n*-alkanes versus *normal*-alkane index $n\text{-}C_{17}/n\text{-}C_{27}$ ratio for the Oued Mya basin and Hassi Messaoud ridge oils. Chromatograms representing the three groups of oils are displayed in caption 4.44.

The oils in Hassi Messaoud, Hassi Guettar, Rhourde Chegga El-Agreb and Rhourde Baguel fields revealed quite similar and lower Pr/Ph ratio ranging from 1.29 to 1.38. Whereas, oils from the Devonian and Lower Triassic fields in Oued Mya basin, OL#2 and Mesdar fields showed quite similar and slightly higher Pr/Ph ratio ranging from 1.38 to 1.50.

According to the $Pr/n\text{-}C_{17}$ and $Ph/n\text{-}C_{18}$ ratios, the oil samples can be separated into three main groups (Figure 4.47). Group (I) contains the oils from Hassi Messaoud, Hassi Guettar, Rhourde Chegga and El-Agreb fields showing the highest $Pr/n\text{-}C_{17}$ and $Ph/n\text{-}C_{18}$ ratios ranging from 0.31 to 0.38 and 0.27 to 0.35 respectively (Table 4.2). Group (II) includes the Devonian and Lower Triassic oils in Oued Mya basin, and group (III) includes the Cambrian oils from Rhourde Baguel and Mesdar fields

showing the lowest Pr/*n*-C_{17} and Ph/*n*-C_{18} ratios ranging from 0.19 to 0.27 and 0.15 to 0.22, respectively. The DST oil OL#2 plots in between these three separated groups. The relatively low Pr/*n*-C_{17} and Ph/*n*-C_{18} ratios for the Devonian and Lower Triassic oils in the Oued Mya basin is again another evidence for the contribution of both Silurian and Ordovician source rock strata for the generation of these oils with much more contribution from the Silurian source rock.

The Ordovician source rock samples revealed very low Pr/*n*-C_{17} and Ph/*n*-C_{18} ratios ranging from 0.04 to 0.15 and 0.02 to 0.16, respectively compared to the Silurian source rock samples ranging from 0.22 to 0.40 and 0.19 to 0.45, respectively (Table 4.2). Therefore, oil that is generated from a mixture of the Silurian source rock with high Pr/*n*-C_{17} and Ph/*n*-C_{18} ratios and an Ordovician source rock with very low Pr/*n*-C_{17} and Ph/*n*-C_{18} ratios may have Pr/*n*-C_{17} and Ph/*n*-C_{18} values in between the values from the two source rocks. This is probably the case of the Devonian and the Lower Triassic oils in the Oued Mya basin (see Figure 4.81 later). The low abundance of the isoprenoid alkanes relative to the *n*-alkanes in the Devonian and Lower Triassic oils is also consistent with the low *n*-alkane index *n*-C_{17}/*n*-C_{27} values in these oils compared to the rest of the oils in the Hassi Messaoud ridge. The Ordovician source rock samples also showed lower *n*-alkane index *n*-C_{17}/*n*-C_{27} values than the Silurian source rock samples (Table 4.2).

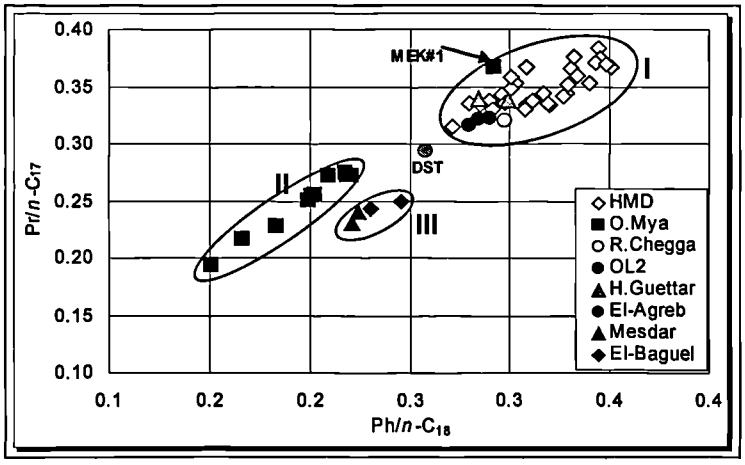

Figure 4.47 Variation in Pr/*n*-C_{17} ratio with Ph/*n*-C_{18} ratio for the Oued Mya basin and Hassi Messaoud Ridge oils.

Oil MEK#1 collected from Mokh-El-Kebch field situated in the far northeast of Oued Mya basin (Figure 4.1) does show different features compared to the other oil samples

from the Oued Mya basin, and it is similar to the oils from the first group (Hassi Messaoud, Hassi Guettar, Rhourde Chegga and El-Agreb oils)

4.4.1.2. Steranes and terpanes

The partial m/z 191 and 217 mass chromatograms of oils selected from the different fields and showing the distributions of triterpanes (tricyclics and hopanes) and steranes are displayed in Figure 4.48. The values of biomarker-based parameters and concentrations of individual biomarkers are listed in Appendix 4.3.

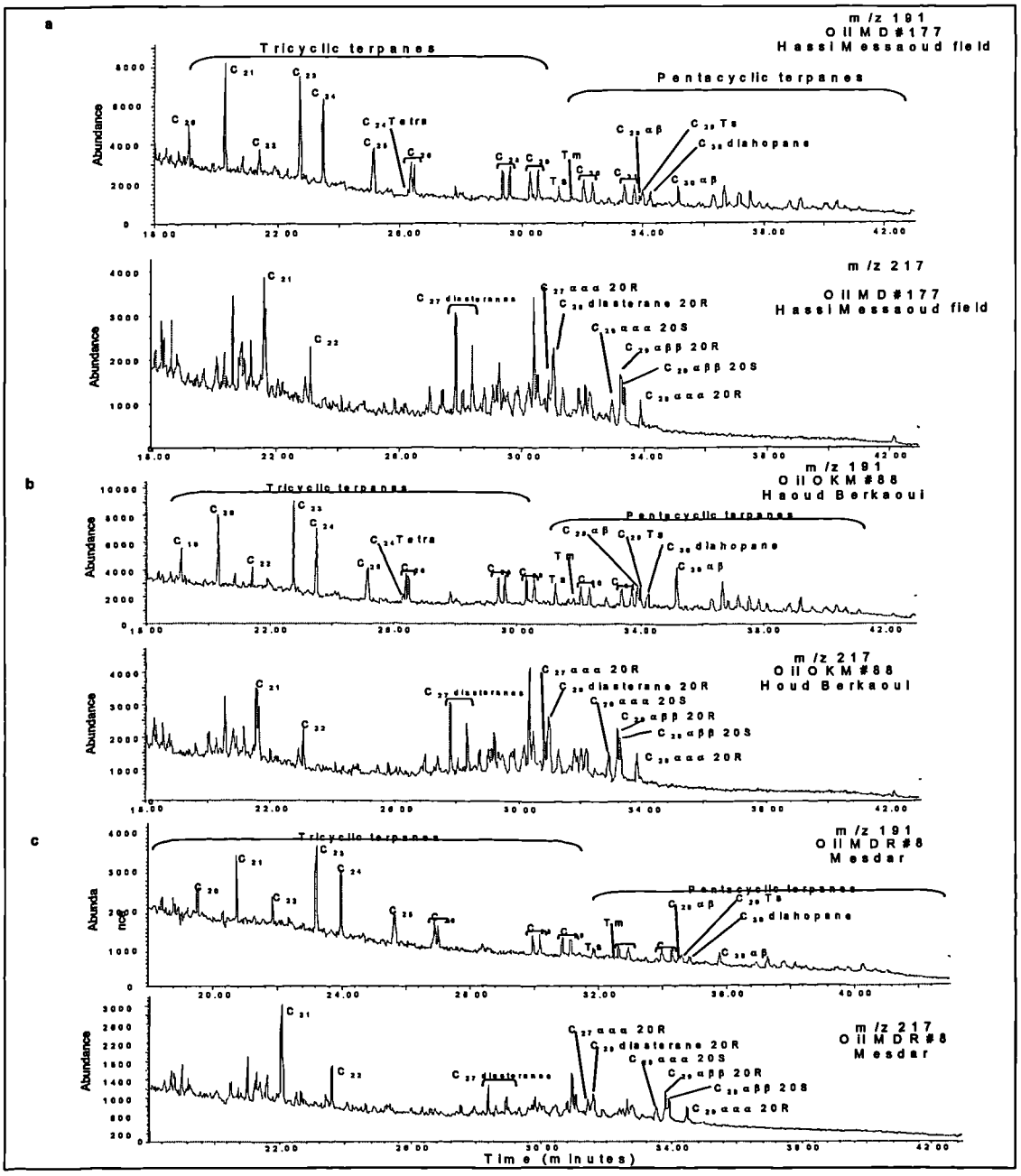

Figure 4.48 Partial m/z 191 and 217 mass chromatograms showing the distributions of triterpanes and steranes representing oil samples in (a) group I (b) group II and (c) group III. (See Figure 4.1 for geographic location of these groups).

The m/z 191 mass chromatograms reveal that the oils analysed in this project contain a higher abundance of the extended tricyclics terpanes than the 17 α (H) hopanes, higher Ts than Tm, and high C_{29} Ts and C_{30} diahopane relative to C_{29} α (H) hopane. The m/z 217 mass chromatograms of the oils are mainly dominated by C_{27} and C_{29} diasteranes relative to the regular steranes, suggesting a shaly nature of the corresponding source rock strata.

In general, the oil samples can be separated into three main groups and the results obtained from the analysis of steranes and triterpanes agree well with those obtained from *n*-alkane and isoprenoid alkane distributions. Group (I) contains oil samples collected from Hassi Messaoud, Rhourde Chegga, Hassi Guettar, El-Agreb fields and oil samples from the Mokh-El-Kebch, N'goussa, Guellala northeast, and Guellala fields in the Oued Mya basin (Figure 4.1). The oils in this group contain high [C_{28}-C_{29}-(S+R) extended tricyclics/[(C_{28}+C_{29}- (S+R) tricyclics + C_{29}-C_{30}17α(H) hopanes)] and [C_{29} (ααα+αββ) S+R regular steranes]/[C_{29} (ααα+αββ) S+R regular steranes +C_{29}-C_{30} 17α (H) hopanes)] ratios. Group (II) contains oil samples from Draa Temra, Benkahla and Haoud Berkaoui Lower Triassic fields in the Oued Mya basin with lower ratios of the parameters mentioned above. The third group (III) contains oil samples collected from both Mesdar and El-Baguel fields with the highest ratios of these parameters (Figure 4.49). Drill stem test oil sample collected from OL#2 plots away from the rest of the oil groups with the lowest [C_{29} (ααα+αββ) S+R regular steranes]/[C_{29} (ααα+αββ) S+R regular steranes +C_{29}-C_{30} 17α (H) hopanes)] ratios.

Oil samples showing higher relative amounts of extended tricyclics terpanes and regular steranes compared to hopanes are believed to be generated from source rocks deposited under anoxic conditions where organic matter from planktonic eukaryotic organisms (mainly marine algae) was well preserved and minor microbial activity took place due to absence of oxygen (Moldowan et al., 1985; Connan et al., 1986).

The oil samples from Mokh-El-Kebch, N'goussa, Guellala northeast, and Guellala fields show different facies-dependent biomarkers, compared to the oil samples from Draa Temra, Benkahla and Haoud Berkaoui fields and are similar to the oil samples from group I (Figure 4.49 and Figure 4.50).

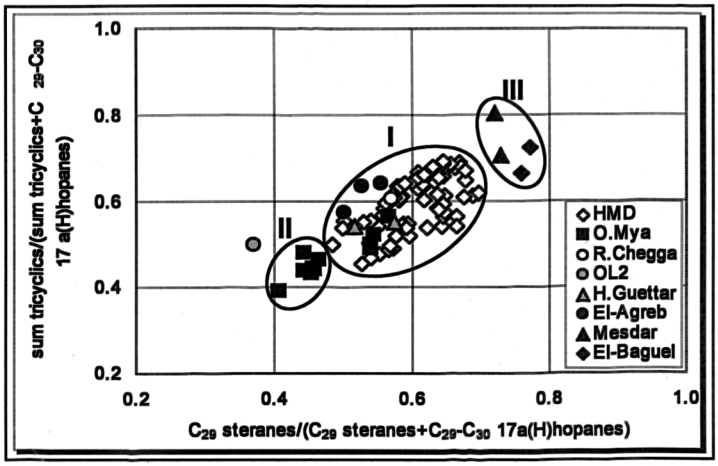

Figure 4.49 Cross plot of the facies parameters [C_{28}+C_{29} (S+R)tricyclics]/[C_{28}+C_{29} (S+R) tricyclics+ C_{29}+C_{30} 17α(H) hopanes] and [C_{29} (ααα+αββ) S+R steranes/[C_{29} (ααα+αββ) S+R steranes+ C_{29}+C_{30} 17α(H) hopanes)] for the Oued Mya basin and Hassi Messaoud Ridge oils.

Conversely, oil samples showing higher amounts of hopanes versus steranes would suggest that the oils were generated from source rocks with organic matter with higher input from prokaryotic organisms versus eukaryotic organisms (Tissot and Welte, 1984).

Seifert and Moldowan (1978) showed that the regular steranes/(regular steranes+ 17α (H)-hopanes) ratio is affected by maturity, but in a study of oils from Oman the regular steranes/(regular steranes + 17 α (H) hopanes) ratio remained relatively constant for a group of related oils of widely different thermal maturity (Peters and Moldowan, 1993). Moreover, Seifert and Moldowan (1978) showed a systematic increase of the tricyclics/17α (H) hopanes ratio with increasing thermal maturity. The ratio increases because proportionally more tricyclics than hopanes are released from kerogen at higher levels of maturity (Aquino Neto et al., 1983). In the laboratory, Peters et al. (1990) showed an increase in the tricyclics/17α (H)-hopanes ratio during hydropyrolysis of Monterey shale. In the present study, both ratios show good correlations with maturity suggesting an increase of regular steranes and tricyclics terpanes compared to the 17 α (H) hopanes (see section 4.3.3.3 below).

Furthermore, the same groups of oils can be distinguished using other facies dependent ratios such as C_{29}diasterane(R)/[C_{29}diasterane(R)+C_{29}ααα sterane(R)] (Curiale, 1992), C_{29}17α(H) hopane/C_{30} 17α(H) hopane (Subroto et al., 1991), [sum extended tricyclics C_{28}+C_{29} (S+R)]/Ts and C_{24} tetracyclic terpane/C_{26} tricyclic terpanes (S+R) (Holba et al., 2001) ratios when plotted in Figure 4.50. Oil samples in

group I including oil samples from Hassi Messaoud, Hassi Guettar, and El-Agreb show higher abundance of diasteranes than regular steranes, lower abundance of C_{29} 17 α (H) hopane than C_{30} 17 α (H) hopane, and lower abundance of the C_{24} tetracyclic terpane compared to the oils from the Triassic reservoirs in the Oued Mya basin. Therefore, the oils in group I were likely generated from shaly source rock containing a high percentage of clay minerals (likely the shaly Silurian source rock in the Oued Mya basin). Clay minerals are believed to play a key role in the occurrence of diasteranes in sedimentary basins (Moldowan et al., 1986). Whereas, group II including oil samples from Draa Temra, Haoud Berkaoui and Benkahla fields show lower abundance of diasteranes and extended tricyclic terpanes than regular steranes and Ts respectively, somewhat higher abundance of C_{29} 17 α (H) hopane relative to C_{30} 17 α (H) hopane and higher abundance of C_{24} tetracyclic terpane; these oils may have been generated from a contribution of both the Silurian and Ordovician source rocks, as the Ordovician source rock samples analysed in this study revealed low abundance of diasteranes and extended tricyclic terpanes and high abundance of C_{29} 17 α (H) hopane and C_{24} tetracyclic terpane compared to the Silurian source rock samples (see section 4.3.2.1).

However, the oil samples in group I show similar features compared to the Silurian source rock samples from group A (see section 4.3.2.1). Subgroup IIa, including oil samples from Mokh-El-Kebch, N'goussa, Guellala northeast, and Guellala, plots in between oils from group II and oils from group I. Group III, containing oil samples from Mesdar and El Baguel fields, plots away from the rest of the oil samples in groups I and II and subgroup IIa; they reveal lower abundance of diasteranes and C_{24} tetracyclic terpane and C_{29} 17 α (H) hopane than regular steranes and C_{26} tricyclic terpanes, and C_{30} 17 α (H) hopane, respectively. All these features are different from those encountered in both groups I and II and subgroup IIa oils. Therefore, it is likely that the Cambrian oils in group III from Mesdar and El-Baguel fields were generated from different source rocks than the oils from groups I and II and subgroup IIa. The oils in group III were likely generated from the Silurian source rock located in the Berkine basin east of the Hassi Messaoud ridge.

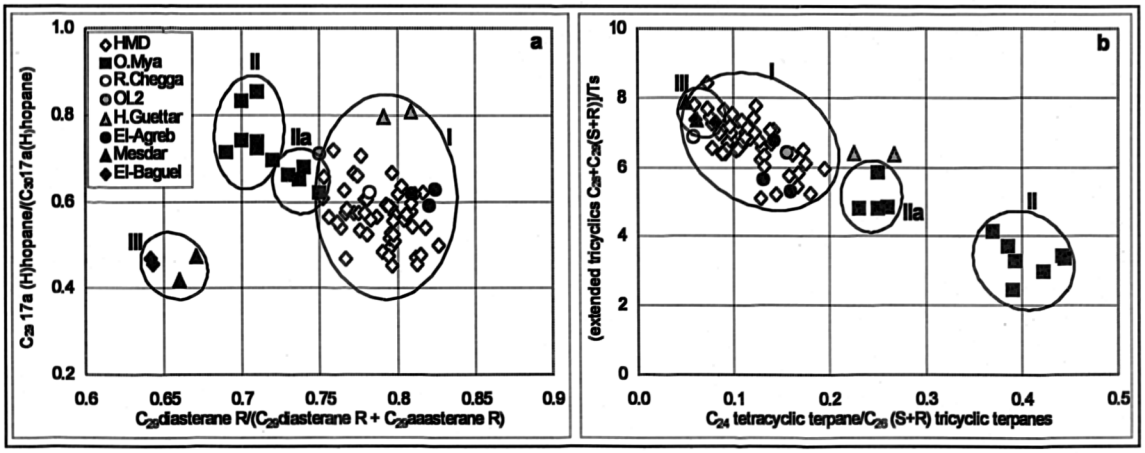

Figure 4.50 Cross plots of the facies dependent parameters (a) C_{29} 17α(H)hopane/C_{30} 17α(H) hopane versus C_{29}diasterane(R)/[C_{29}diasterane(R)+C_{29} ααα sterane(R)] and (b) [sum extended tricyclics C_{28}+C_{29} (S+R)]/Ts versus C_{24} tetracyclic terpane/C_{26} tricyclic terpanes (S+R), for the Oued Mya basin and Hassi Messaoud Ridge oils.

Homohopane isomers in all the oils coelute with the extended tricyclic homologues and their quantification is impossible to be carried out (Figure 4.48).

Sterane ternary diagrams are widely used to illustrate relationships between oils and/or source rock bitumens (e.g. Peters et al., 1989). The distribution of C_{27}- C_{28}- C_{29}-αββ steranes allows the differentiation of groups of petroleums from different source rocks or different organic facies of the same source rock. From the C_{27}- C_{28}- C_{29}-5α(H), 14β(H), 17β(H) (20S + 20R) steranes distribution in Figure 4.51 obtained from the m/z 218 mass chromatograms, it is possible to distinguish Hassi Messaoud, Hassi Guettar, Rhourde Chegga and El-Agreb oil samples (group I) from Devonian and Lower Triassic oils in Oued Mya basin (group II and subgroup IIa), and Mesdar and Rhourde Baguel oil samples (group III). The former group contains similar percentages of C_{27} and C_{29} steranes, whereas the latter is slightly dominated by C_{29} steranes.

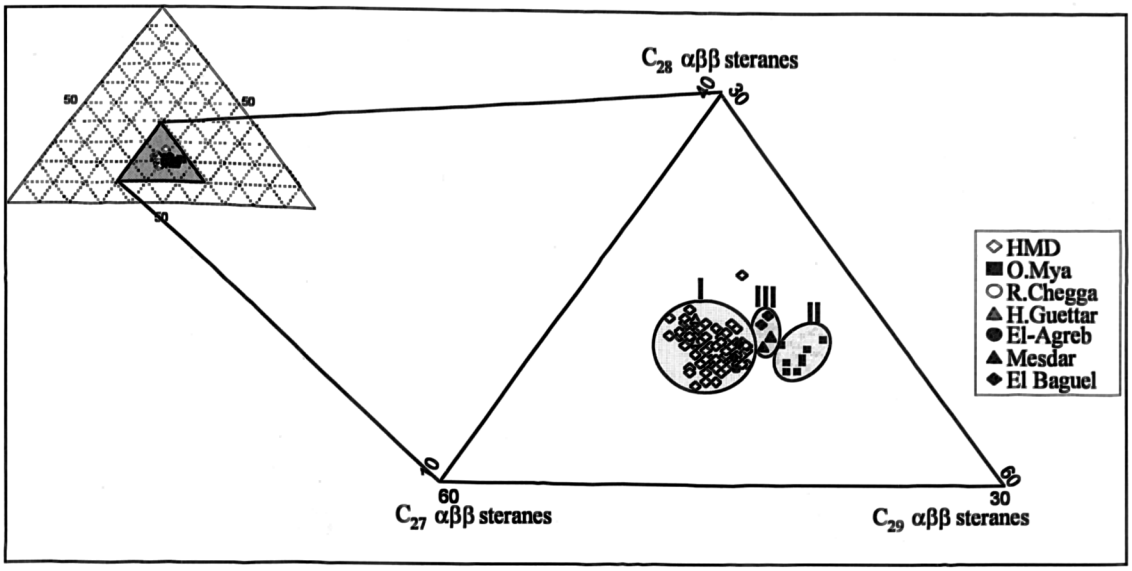

Figure 4.51 Ternary plot of the relative abundance of C_{27}- C_{28}- C_{29} 5α(H), 14β(H), 17β(H) (20S+20R) steranes for the Oued Mya basin and Hassi Messaoud Ridge oils.

The concentrations (μg/g oil) of the biomarkers in the oil samples are displayed in Appendix 4.2. All the oil samples from the three groups contain higher concentrations of steranes than hopanes. Figure 4.52 reveals that oil samples from Draa Temra, Haoud Berkaoui and Benkahla fields (group II) contain the highest concentrations of biomarkers (tricyclics terpanes, hopanes and steranes) compared to the oil samples in groups I and III, and subgroup IIa. Group III which includes oil samples from Mesdar and El Baguel fields exhibit the lowest concentrations of biomarkers.

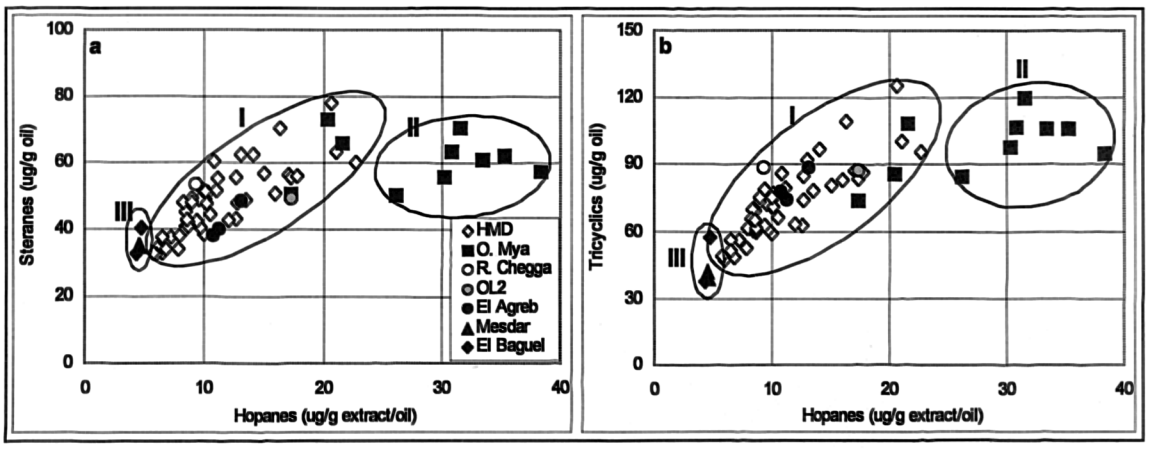

Figure 4.52 Plot of concentrations of steranes, tricyclic terpanes and hopanes for the Oued Mya basin and Hassi Messaoud Ridge oils

In general, high sterane concentration combined with high [C_{29} ααα+αββ (20S+20R) steranes]/[C_{29} ααα+αββ (20S+20R) steranes + C_{29}-C_{30}17α(H) hopanes] ratio (Figure 4.49) seems to typify marine organic matter with major contributions from planktonic

and/or benthic algae of the corresponding source rock(s) (Moldowan et al., 1985). Conversely, low sterane concentration and low [C_{29} ααα+αββ (20S+20R) steranes]/[C_{29} ααα+αββ (20S+20R) steranes + C_{29}-C_{30}17α(H) hopanes] ratio are more indicative of terrigenous and/or microbial reworked organic matter (Tissot and Welte, 1984). The concentration of biomarkers is believed to decrease with increasing thermal maturity because of the release of more thermally stable compounds from kerogen (i.e. *n*-alkanes). Indeed, the present study, the concentration of biomarkers decreases with increasing maturity of the oils from the different fields (for further details see section 4.3.2.3 below).

4.4.1.3. Principal Components Analysis (PCA)

A biomarker data set, comprising 30 variables (29 variables represent biomarker concentrations and 1 variable represents the calculated vitrinite reflectance) for 52 oil samples from the Cambrian reservoirs in Hassi Messaoud, 10 oil samples from the Devonian and Lower Triassic reservoirs in the Oued Mya basin, 3 oil samples from the Cambrian reservoirs in El-Agreb, 2 oils samples from the Cambrian reservoirs in Mesdar and 2 oil samples from the Cambrian reservoirs in El-Baguel, was analysed by PCA to establish the major sources of variance within the sterane, tricyclic terpane, and hopane distributions. The biomarkers used in the analysis are listed in Table 4.10.

The diagram showing the plot of PC1 scores against PC2 scores demonstrates that the oils analysed in this study can be distinguished into the same groups revealed when using conventional biomarker ratios; group I containing the oil samples from the Hassi Messaoud El-Agreb and Rhourde Chegga fields, group II comprising the Haoud Berkaoui and Benkahla oils, and group III containing the oil samples from the Mesdar and El-Baguel fields. Three oil samples from Mokh-El-Kabch (MEK#1) N'goussa (NGS#2) and Guellala northeast (GLNE#5) plot in between oil samples from group I and group II (Figure 4.53). The oil sample GLA#16 from Guellala Lower Triassic reservoir also showed similar biomarker distributions as the oil samples from the subgroup IIa; however, it is not plotted in the score plots because the biomarkers were not quantified in this sample.

Table 4.10 Biomarker compounds and a maturity parameter used in the principal components analysis for the oils.

Tricyclic terpanes and hopanes (*m/z* = 191)	
1	C_{21} Tricyclic terpane
2	C_{22} Tricyclic terpane
3	C_{23} Tricyclic terpane
4	C_{24} Tricyclic terpane
5	C_{25} Tricyclic terpane
6	C_{24}Tetracyclic terpane
7	C_{26} Tricyclic terpanes (22S+22R)
8	C_{28} Tricyclic terpanes (22S+22R)
9	C_{29} Tricyclic terpanes (22S+22R)
10	C_{30} Tricyclic terpanes (22S+22R)
11	C_{31} Tricyclic terpanes (22S+22R)
12	22,29,30-Trisnorneohopane (Ts)
13	22,29,30-Trisnorhopane (Tm)
14	C_{29}17α(H), 21β(H)-30-norhopane
15	18 α (H)-30-norneohopane (C_{29} Ts)
16	C_{30} diahopane
17	C_{30}17α(H), 21β(H) hopane
Steranes (*m/z* = 217)	
18	C_{21}(ααα+αββ) pregnanes
19	C_{22}(ααα+αββ) homopregnanes
20	C_{27} 13β(H), 17α(H) diasterane 20S
21	C_{27} 13β(H), 17α(H) diasterane 20R
22	C_{29} 13β(H), 17α(H) diasterane 20S
23	C_{27} 5α(H), 14α(H), 17α(H) sterane 20R
24	C_{29} 13β(H), 17α(H) diasterane 20R
25	C_{29} 5α(H), 14α(H), 17α(H) sterane 20S
26	C_{29} 5α(H), 14α(H), 17α(H) sterane 20R
αββ **Steranes** (*m/z* = 218)	
27	C_{27} 5α(H), 14β(H), 17β(H) sterane (20S+20R)
28	C_{28} 5α(H), 14β(H), 17β(H) sterane (20S+20R)
29	C_{29} 5α(H), 14β(H), 17β(H) sterane (20S+20R)
Maturity parameters	
30	%Rc = 0.4 + (0.6 * MPI-1)

An explanation of what these two principal components represent is given by the loadings plots in Figure 4.54. These diagrams exhibit the loadings of the different variables within the principal components. The first two principal components (PCs) obtained, explain 34.1% and 30.6% of the variance within the scaled data set, respectively. This allows the relationships between the samples to be examined in a simple two-dimensional scores plot of PC1 versus PC2, which includes the effects of all the original variables (i.e. biomarker concentrations and maturity parameter %Rc), and displays the bulk (64.7%) of the scaled data variability (Figure 4.53).

64.7% of the total variance in the data set is accounted for by the first two principal components (PCs). The first principal component accounts for 34.1% of the total variance of the data set, on which high loadings (>0.6) are obtained for C_{21}, C_{25}, C_{26}, C_{29} and C_{30} tricyclic terpanes, C_{27} and C_{29} 13β(H), 17α(H) diasteranes 20S and 20R, C_{29} 5α(H), 14α(H), 17α(H) sterane 20S and C_{29} 5α(H), 14β(H), 17β(H) sterane 20S and 20R. In addition the loadings of the C_{23}, C_{24}, C_{28} and C_{31} tricyclic terpanes, C_{24} tetracyclic terpane, Ts, Tm, C_{29} 17α(H)hopane, C_{30} 17α(H)hopane, C_{29} 5α(H), 14α(H), 17α(H) sterane 20R, C_{27} 5α(H), 14β(H), 17β(H) sterane 20S and 20R, C_{28} 5α(H).14β(H), 17β(H) sterane 20S and 20R, and the calculated vitrinite reflectance (%Rc) are moderately high (Figure 4.54). The second principal component accounts for 30.6% of the total variance of the data matrix. High loadings (>0.6) are obtained for C_{30} diahopane, C_{29} Ts, C_{29} and C_{30} 17α(H)hopanes, C_{24} tetracyclic terpane, Ts, Tm, C_{21} (ααα+αββ) pregnanes, C_{22} (ααα+αββ) homopregnanes, %Rc, C_{31} tricyclic terpanes, C_{27}, C_{28} C_{29} 5α(H),14β(H), 17β(H) (20S+20R). In addition, the loadings of the C_{22}, C_{23}, C_{29} and C_{30} tricyclic terpanes and C_{27} 5α(H), 14α(H), 17α(H) sterane 20R are moderately high (Figure 4.54).

Consequently, it could be considered that the principal component PC1 in the scores plot mainly displays the different molecular effects related to the source facies; whereas PC2 displays mainly the effect of maturity. Hence, the oil samples from group I (i.e. oil samples from Hassi Messaoud, El-Agreb and Rhourde Chegga fields) which have positive PC1 are mainly dominated by the abundance of C_{21}-C_{31} extended tricyclic terpanes, C_{29} Ts, C_{30} diahopane, C_{21} (ααα+αββ) pregnanes, C_{22} (ααα+αββ) homopregnanes, and diasteranes relative to the C_{24} tetracyclic terpane, hopanes and regular steranes, respectively indicating a shaly nature of the corresponding source rock interval having generated these oils. The Silurian source rock samples from group A did show similar characteristics as the oils from group I (see section 4.3.2.3.1). The oil samples from Draa Temra, Haoud Berkaoui and Benkahla fields (group II) and Mokh-El-Kebch, N'goussa, and Guellala northeast (subgroup IIa) seem to contain more C_{24} tetracyclic terpane, hopanes and regular steranes than extended tricyclics, and diasteranes. These features likely originated from a contribution of two source rocks (1) an Ordovician source rock containing more carbonate and less clay

minerals (see section 4.3.2.3.1), and (2) the shaly Silurian source rock strata in the Oued Mya basin.

The oil samples from the Mesdar and El-Baguel fields (i.e. group III) are dominated by the C_{21} (ααα+αββ) pregnanes, C_{22} (ααα+αββ) homopregnanes and regular steranes over diasteranes, C_{29} Ts, C_{30} diahopane, hopanes and C_{24} tetracyclic terpane. This group of samples seems to be different from the groups I and II and subgroup IIa, therefore it is likely that the oil samples from group III were generated from another source rock (likely the Silurian) located in the Berkine basin (Figure 4.1). The oils from group III are geographically closer to the Berkine basin (10 to 20 km) compared to the Oued Mya basin (>100km). The study of alkylcarbazoles and benzocarbazoles in the following chapter confirmed these observations that the oils in the Mesdar and El-Baguel fields have migrated from Berkine basin (see section 5.7).

Finally, the principal components PC1 and PC2 are plotted against the calculated vitrinite reflectance in order to confirm whether these components are affected by maturity or source facies. Indeed, Figure 4.55a shows no correlation between PC1 and the calculated vitrinite reflectance indicating likely source facies effect on the PC1. However, Figure 4.55b shows a good correlation between PC2 and the calculated vitrinite reflectance indicating more maturity than source facies effect on the principal component PC2. Moreover, I can distinguish two parallel maturity trends, the first trend contains the oil samples from groups I, II and subgroup IIa; the second trend represents the oil samples from Mesdar and El-Baguel (group III). This observation might also indicate different source for the oil samples from group III compared to the oil samples from groups I, II and subgroup IIa.

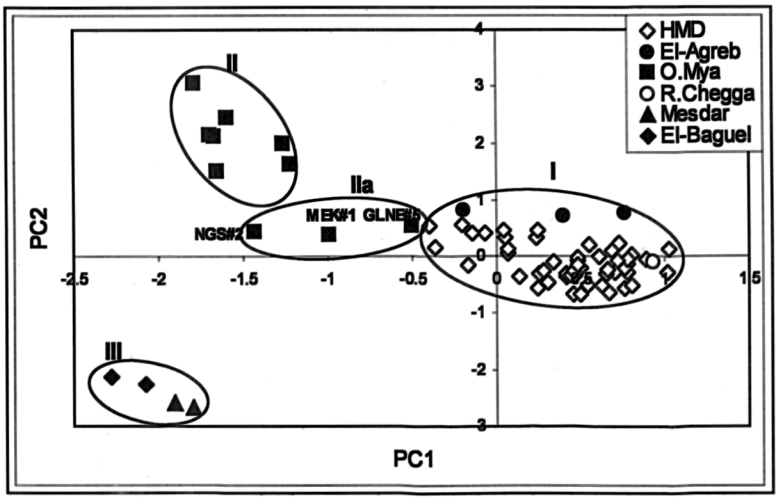

Figure 4.53 A scores plot of PC1 versus PC2 showing the relationship between the oil samples in terms of the first and second principal components. PC1 explains 34.1% of the total variance in the scaled data set and PC2 explains a further 30.6%.

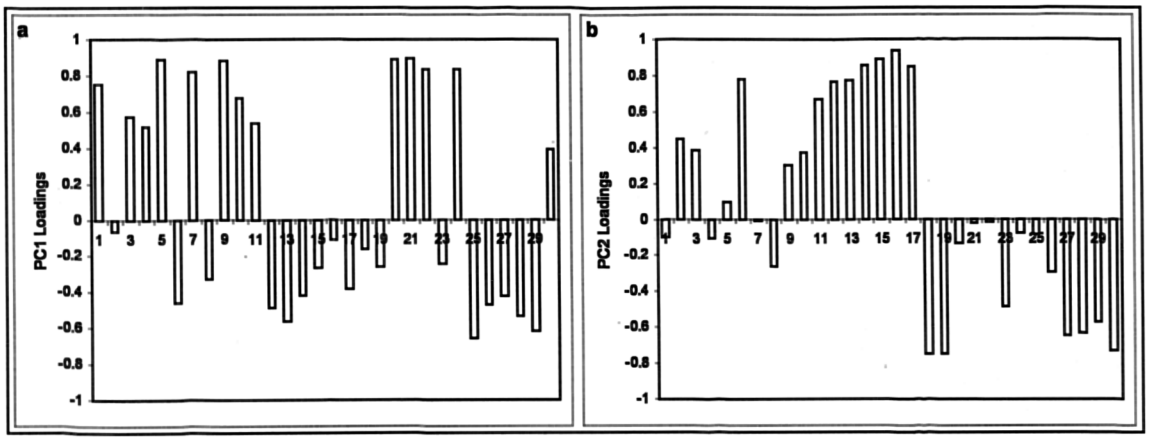

Figure 4.54 Loadings plots showing the composition of the first two principal components, which scored 34.1% and 30.6% of the total variance in the data set, respectively.

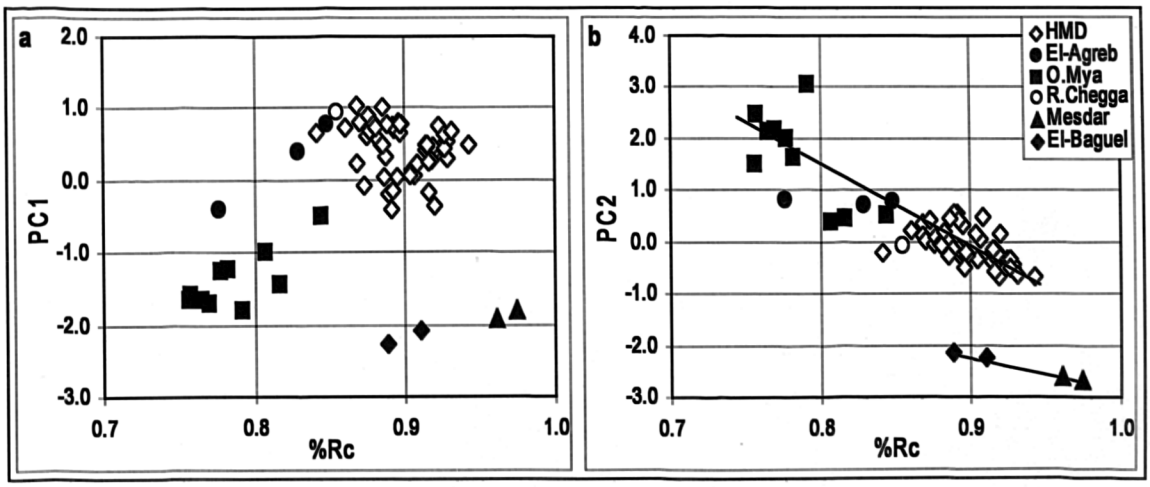

Figure 4.55 Cross plots showing (a) the principal component PC1 and (b) the principal component PC2 versus the calculated vitrinite reflectance (%Rc) for the oils.

4.4.2. Maturity

In this section, I will try to assess the maturity of the oils using the same maturity parameters based on biomarkers and aromatic hydrocarbons used above for the source rock samples. All the values of the maturity parameters used in this section are displayed in Appendix 4.3.

4.4.2.1. Steranes and terpanes

The plot of 20S/(20S+20R)-C_{29} 5α(H),14α(H),17α(H) steranes versus αββ/(αββ+ααα)-C_{29} steranes presented in Figure 4.56 indicates that the 20S/(20S + 20R)-C_{29} 5α(H),14α(H),17α(H) steranes ratio has reached its maximum value (i.e. 0.51 to 0.62 see Appendix 4.3) equivalent to the equilibrium between 20S and 20R isomers (Seifert and Moldowan, 1986). This ratio is also in agreement with the αββ/(αββ+ααα)-C_{29} steranes. Consequently all the oil samples are mature and cannot be differentiated using these ratios. Calibration of the maturity of the oils is displayed below.

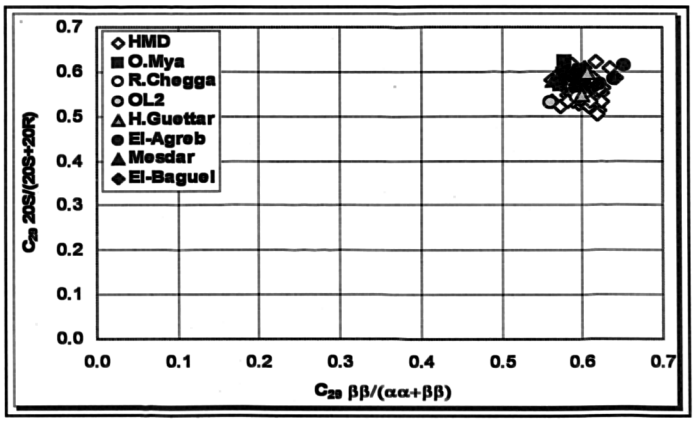

Figure 4.56 Plot of the thermal maturity parameters 20S/(20S+20R) and αββ/(ααα+αββ)-C29 steranes for the Oued Mya basin and Hassi Messaoud Ridge oils.

Maturity parameters such as Ts/(Ts+Tm) (Seifert and Moldowan, 1978), C_{29}Ts/(C_{29}Ts+C_{29}17α(H)hopane) (Cornford et al., 1988; Sofer, 1988; Riediger et al., 1990) C_{30}diahopane/(C_{30}diahopane+C_{30}17α(H)hopane) (Cornford et al., 1986) and C_{23} tricyclic terpane/(C_{23} tricyclic terpane + C_{30}17α(H) hopane) (Curiale, 1992) based on the pentacyclic terpanes in the oil samples, are plotted in Figure 4.57. These cross plots indicate an increase in the maturity of the oil samples from group II (i.e. Haoud Berkaoui, Benkahla, and Draa Temra fields) towards the oils in subgroup IIa (i.e. Guellala, Guellala northeast, N'goussa and Mokh el Kebch fields) and the oils in

group I (i.e. El Agreb, Rhourde Chegga, Hassi Messaoud, and Hassi Guettar fields). The oil samples from subgroup IIa show similar maturity to the oil samples from the western, northern and southern flanks of the Hassi Messaoud field; the highest maturity within oil samples from group I are the oil samples from the central and eastern part of the Hassi Messaoud field. These parameters also show that in group III, the Cambrian reservoired oil samples from Mesdar field are more mature than those from the Cambrian reservoired oil samples from El-Baguel field. Moreover, the oil samples from Mesdar field reveal the highest maturity compared with the rest of the oil samples from groups I and II.

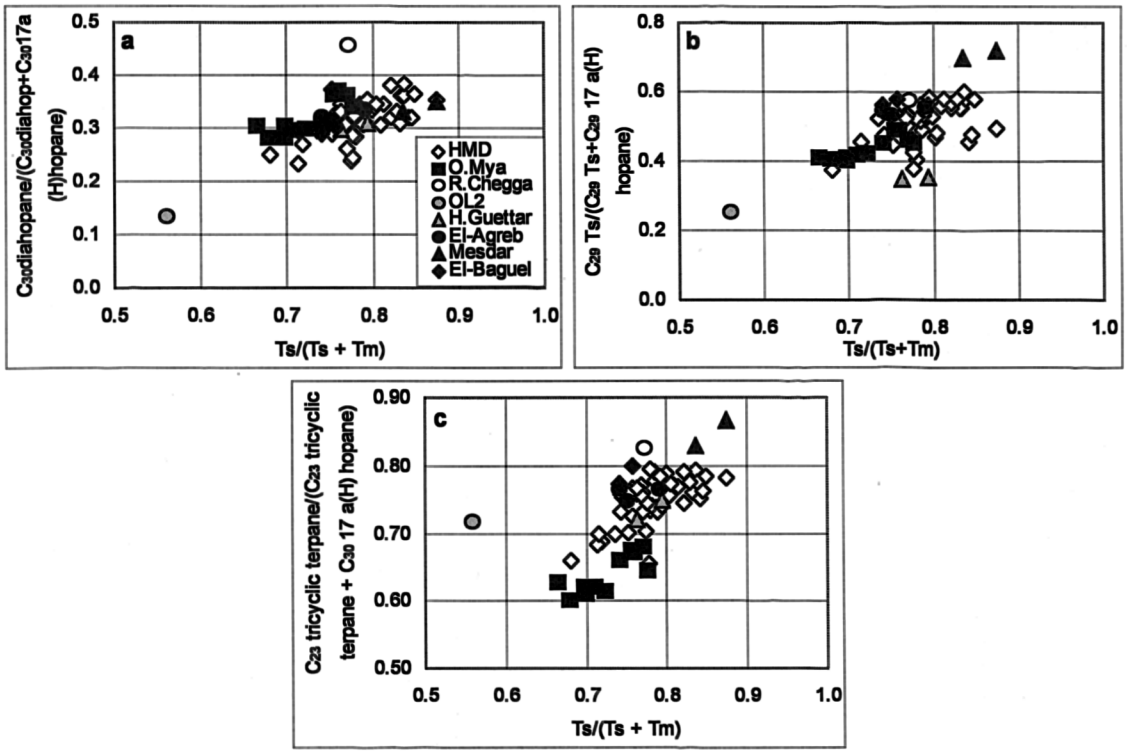

Figure 4.57 Cross plots of the maturity parameters (a) $C_{29}Ts/(C_{29}Ts+C_{29}17\alpha(H)hopane)$, (b) $C_{30}diahopane/(C_{30}diahopane+C_{30}17\alpha(H)$ hopane) and (c) C_{23} tricyclic terpane/(C_{23} tricyclic terpane + $C_{30}17\alpha(H)$ hopane) versus Ts/(Ts+Tm) for the Oued Mya basin and Hassi Messaoud Ridge oils.

The semi-quantitative determination of the maturity-related tricyclic and pentacyclic triterpanes are displayed in Appendix 4.3. The concentration values obtained in this study are only semi-quantitative, as no correction was applied to compensate for differences in the mass spectral responses between the internal standard (D_4-cholestane) and the various tricyclic and pentacyclic triterpane components. In the following section, I investigate the variations in the concentrations of some of the

individual tricyclic and pentacyclic triterpanes as a result of increasing maturity of the oil samples analysed in this study.

The variation in the concentrations of the rearranged hopanes Ts and C_{29} Ts relative to Tm and C_{29} 17 α(H) hopane, respectively are plotted as a function of increasing values of the Ts/(Ts+Tm) and C_{29}Ts/(C_{29}Ts + C_{29}17α(H) hopane) parameters (Figure 4.58 and Figure 4.59).

During catagenesis, Ts (18 α (H)-22,29,30-trisnorneohopane) shows higher relative thermal stability than Tm (17 α (H)-22,29,30-trisnorhopane) (Seifert and Moldowan, 1978). This observation has been confirmed using molecular mechanics calculations for the formation of various hopanes including Ts and Tm (Kolaczkowska et al., 1990). Seifert and Moldowan (1978) have suggested that Ts could be derived from diplopterol, via a mechanism involving the loss of the side chain from diplopterol, followed by an acid-catalysed C-18 to C-17 methyl shift. Whereas, the C_{29}Ts could be derived from diplopterol or diploptene, via a mechanism involving the loss of a methyl group, probably catalysed by active clays (Moldowan et al., 1991).

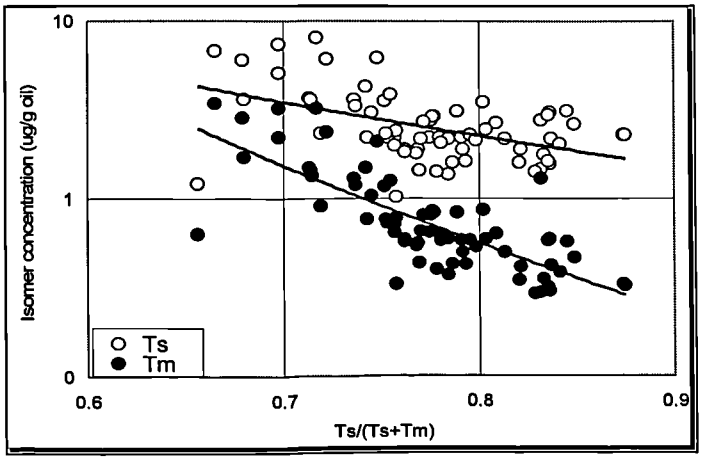

Figure 4.58 Cross plot of the concentrations (μg/g oil) of Ts and Tm versus the maturity parameter Ts/(Ts+Tm) for the oil samples from the Mya basin and Hassi Messaoud ridge. (Note that the Y axis is a logarithmic scale).

Therefore, both of these mechanisms involving the formation of Ts and C_{29} Ts depend on the availability of functionalised precursors, and hence suggest an early diagenetic formation, possibly without incorporation into kerogen matrix (e.g. Noble et al., 1985). Noble et al. (1985) showed that pyrolysis experiments of the solvent-extracted Devonian shale from the Canning basin released only the 17 α(H) hopanes and

moretanes, with no measurable quantities of Ts and C_{29} Ts being present. However, both Ts and C_{29} Ts were present in the bitumen extracted from the same Devonian shale before the experiment. This indicates that neither Ts nor C_{29} Ts are formed from the thermal cracking of the source kerogen under conditions of pyrolysis. Consequently, the decrease in the concentrations of Ts and C_{29} Ts with increasing maturity of the oils (Figure 4.58 and Figure 4.59) may possibly be due to dilution of these compounds by hydrocarbons released from the kerogen through the oil generation process.

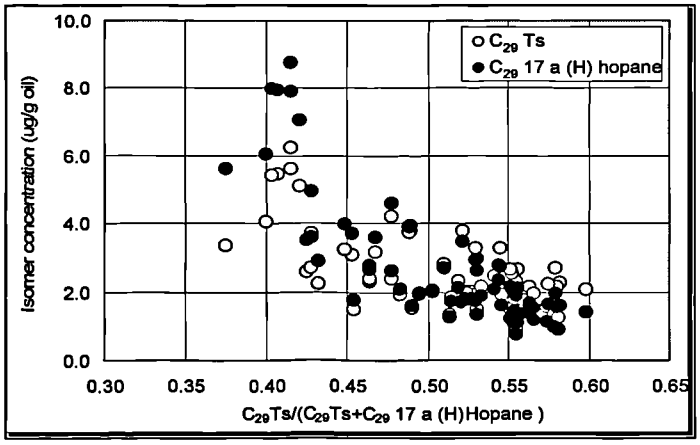

Figure 4.59 Cross plot of the concentrations (µg/g oil) of C_{29}Ts and C_{29} 17 α (H) hopane versus the maturity parameter C_{29}Ts /(C_{29}Ts + C_{29} 17 α (H) hopane) for the oil samples from the Mya basin and Hassi Messaoud ridge.

From the plots in Figure 4.58 and Figure 4.59, it can be observed that both Tm and C_{29} 17 α (H) hopane, which are likely to be released from the kerogen matrix during the early stages of oil generation (e.g. van Graas, 1990), are depleted at a faster rate compared with the Ts and C_{29} Ts, which is evocative of the relative thermal stabilities of the individual components. Therefore, dilution effects cannot fully account for the maturity-related variation in the concentrations of the compounds shown in Figure 4.58 and Figure 4.59. This is consistent with the findings of Kolaczkowska et al. (1990) who showed that Ts should be more stable than Tm by 4.4 kcal/mole and C_{29} Ts more stable than C_{29} 17 α (H) hopane by 3.5 kcal/mole. Finally, the increase of Ts/(Ts+Tm) and C_{29} Ts /(C_{29} Ts + C_{29} 17 α(H) hopane) parameters with increasing maturity is likely to be due to the selective loss of the least stable isomers (i.e. Tm and C_{29} 17 α(H) hopane), probably caused by thermal cracking rather than a result of transformation of the latter to the more stable isomers.

The semi-quantitative variation of tricyclic terpanes relative to the pentacyclic triterpanes (hopanes) with increasing maturity has also been investigated by observing the concentrations of C_{23} tricyclic terpane and C_{30} 17 α(H) hopane components. Figure 4.60 reveals that C_{23} tricyclic terpane has undergone only a minor decrease in concentration compared to C_{30} 17 α (H) hopane with increasing maturity of the oil samples analysed in this study. The concentration of C_{30} 17 α(H) hopane is observed to decrease by approximately an order of magnitude throughout the same range of maturity.

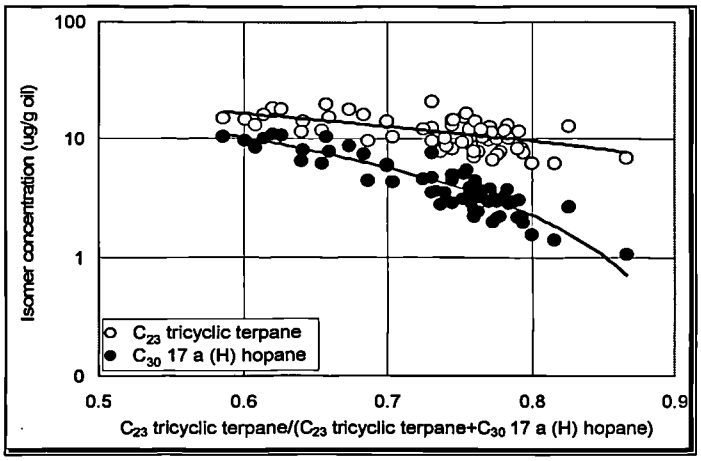

Figure 4.60 Cross plot of the concentrations (μg/g oil) of C_{23} tricyclic terpane and C_{30} 17 α (H) hopane versus the maturity parameter C_{23} tricyclic terpane/(C_{23} tricyclic terpane+ C_{30} 17 α (H) hopane) for the oil samples from the Mya basin and Hassi Messaoud ridge. (Note that the Y axis is a logarithmic scale).

This observation suggests that the increase in the abundance of the tricyclic terpanes relative to pentacyclic triterpanes is likely attributed to the relatively higher thermal stability of the tricyclic terpanes (van Graas, 1990). Furthermore, at higher levels of maturity, the tricyclic terpanes seem to be preferentially released from the kerogen matrix (Peters and Moldowan, 1993) suggesting that any dilution effects of the biomarkers by hydrocarbons released from the kerogen during the oil generation process will likely exercise more impact upon the abundance of the pentacyclic triterpanes than the tricyclic terpanes.

4.4.2.2. Aromatic compounds

4.4.2.2.1. Aromatic steroid hydrocarbons

The distribution of C-ring monoaromatic (MA) and ABC-ring triaromatic (TA) steroid hydrocarbons in the oil samples were monitored using the m/z 253 and 231

fragment ions, respectively. Typical mass chromatograms showing the distributions of MA- and TA-steroid hydrocarbons in oil samples are shown in Figure 4.61. The concentrations of the individual isomers and maturity parameters calculated from the distributions of the triaromatic steroid hydrocarbons are displayed in Appendix 4.4.

Visual inspection of the m/z 253 mass chromatograms reveals that MA-steroid hydrocarbons are completely absent in all oil samples. Mass chromatograms show only the presence of the surrogate standard 1,1-binaphthyl used for aromatic compounds quantification. This feature suggests that the extent of aromatisation of C-ring MA- to ABC-ring TA-steroid hydrocarbons reaction in these samples is complete.

Examination of the m/z 231 mass chromatograms reveals that TA-steroid hydrocarbons are dominated by short-chain (C_{20}-C_{21}) versus long-chain (C_{26}-C_{28}) components within oil samples suggesting high levels of maturity for these samples (Mackenzie et al., 1981). Long-chain C_{26}-C_{28} TA-steroid hydrocarbons are barely present in the majority of oil samples. In this work, the abundance of C_{20} TA-steroid hydrocarbon relative to the C_{28} 5 α (H) (20S+20R) TA-steroid hydrocarbons was employed to evaluate maturity of oil samples.

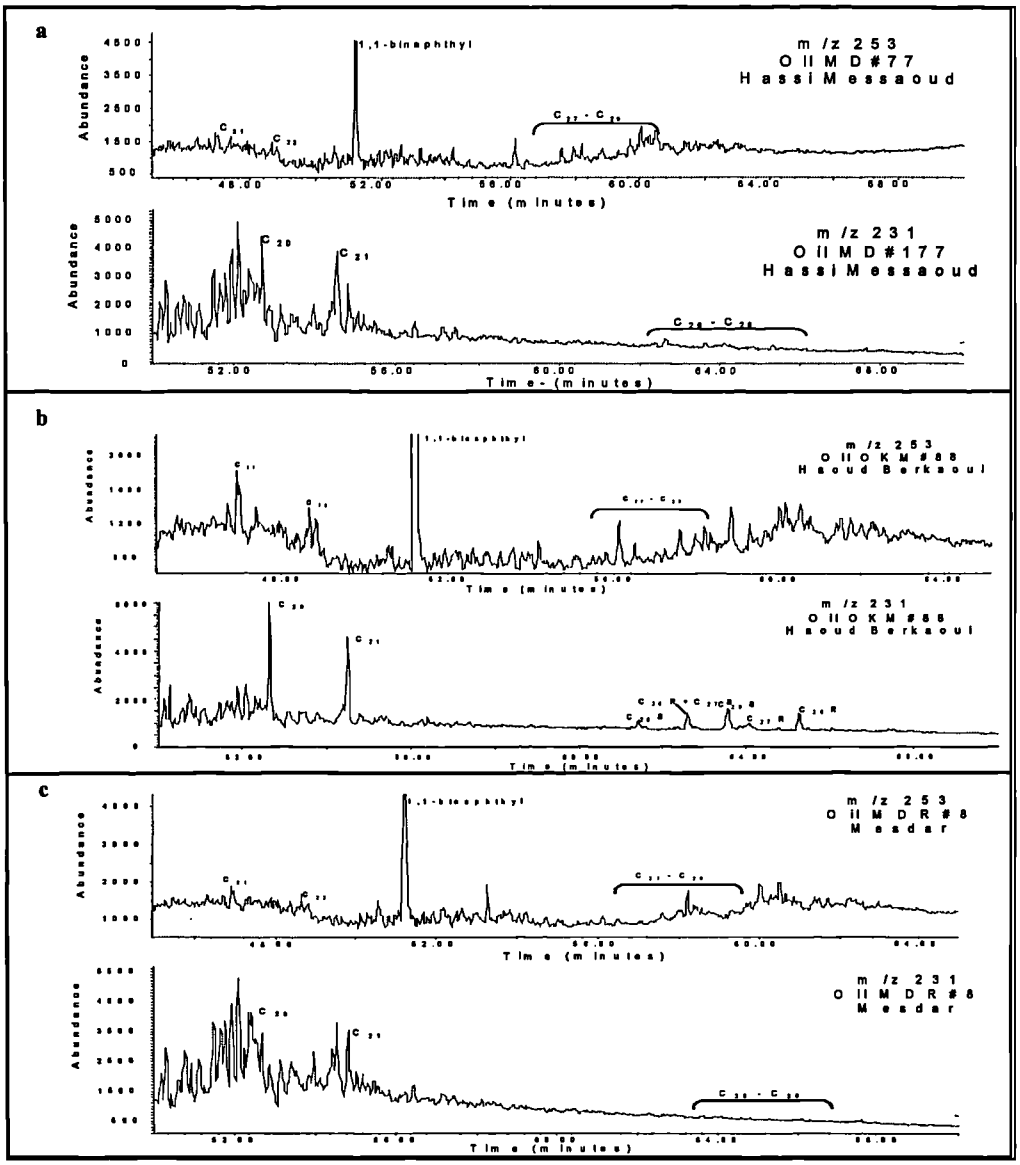

Figure 4.61 Partial m/z 253 and 231 mass chromatograms showing the distributions of C-ring monoaromatic steroids and ABC-ring triaromatic steroid hydrocarbons in (a) Hassi Messaoud oil sample (b) Haoud Berkaoui oil sample and (c) Mesdar oil sample.

The thermal maturity of the oil samples analysed in this work is assessed by comparison to the previously discussed sample set of marine type II kerogen sourced petroleums from the North Sea.. The same sample set was used earlier for assessment of the maturity of the Silurian and Ordovician source rocks. The oil samples analysed in this work are believed to be generated mainly from the Silurian source rock (see section 4.5 below), which is identified as a marine type II kerogen, same as for the sample set from the North Sea. In this section I am going to use the C_{20} triaromatic steroid/[C_{20} triaromatic steroids + C_{28} 5 α (H) (20S+20R) TAS] and the MPI-1 maturity parameters to calibrate the maturity levels of the oil samples analysed in this work. The values of the first maturity parameter range from 0.72 to 0.96 in the oil

samples from group I, 0.62 to 0.67 in the oil samples from group II, and 0.85 to 0.94 in the oil samples from group III; the values of the second parameter range from 0.72 to 0.90 in the oil samples from group I, 0.59 to 0.74 in the oil samples from group II, and 0.81 to 0.96 in the oil samples from group III (see Appendix 4.4). The cross plots in Figure 4.62 show good correlation between both maturity parameters and the measured vitrinite reflectance obtained from the North Sea sample set %Rm (the correlation coefficients are 0.96 and 0.92, respectively).

The estimated maturity of the oil samples analysed in this project using the first parameter reveals that the oil samples from group I (including oils from Hassi Messaoud, Rhourde Chegga, Hassi Guettar and El-Agreb fields see Figure 4.1) exhibit a wide range of maturity, mainly between the oil samples from Hassi Messaoud field itself which contain the highest number of samples (i.e. 81 oil samples). The oil samples from the western, northern and southern flanks are less mature than those from the central and eastern parts of Hassi Messaoud field. The estimated vitrinite reflectance of the oils in group I fall between 0.92 to 1.08 % Rm. However, the oils from group II and group III exhibit narrower ranges of maturity, ranging from 0.93 to 0.94 %Rm in the oils from group II, and 1.05 to 1.07 %Rm in the oils from group III. The second parameter (i.e. MPI-1) reveals more or less similar intervals of maturity for the oils from the 3 main groups. Thus, the estimated vitrinite reflectance ranges between 0.88 to 0.98 %Rm in the oils from group I, 0.82 to 0.89 % Rm in the oils from group II, and 0.94 to 1.03 %Rm in the oils from group III.

These estimated values of the vitrinite reflectance %Rm suggest that the oils from group III (i.e. oil samples from Mesdar and El-Baguel fields) are more mature than the oils from group I. Oil samples from group II (i.e. from the Lower Triassic and Devonian reservoired oils in the Oued Mya basin) and the oil samples from the western and northern flanks of Hassi Messaoud field are the least mature oils analysed in the entire region. In general, the values of the estimated vitrinite reflectance using both maturity parameters fall in the same range as the values of estimated vitrinite reflectance for the Silurian and Ordovician source rock samples.

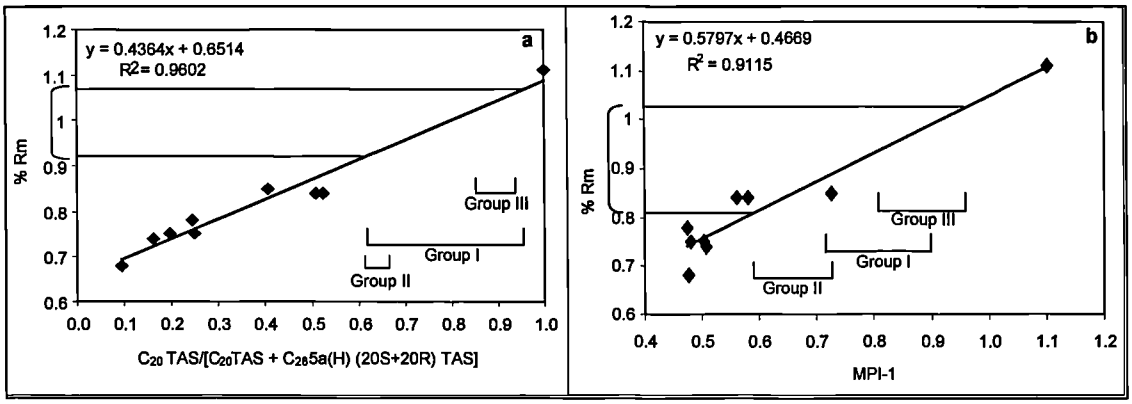

Figure 4.62 Cross plots showing the correlations between (a) the measured vitrinite reflectance (%Rm) and the C_{20} triaromatic steroids/[(C_{20} triaromatic steroids + C_{28} 5α(H)(S+R) triaromatic steroids)] and (b) the measured vitrinite reflectance (%Rm) and MPI-1 for a North Sea oil sample set used for the calibration of the maturity of the oils analysed in this study.

The (C_{20} TAS)/[C_{20} TAS + C_{28} 5α(H)(S+R) TAS)] parameter is believed to increase from 0 to 100% during thermal maturity (Figure 4.63), however, it is not fully understood whether this increase is the result of: 1) conversion of long-chain to short-chain TA-steroids by carbon-carbon cracking, 2) preferential thermal degradation of the long- versus the short-chain series, or 3) both. The concentrations (μg/g oil) of the C_{20} TAS and C_{28} 5α (H) (20S+20R) TAS homologues plotted against the (C_{20} TAS)/[C_{20} TAS + C_{28} 5α (H) (20S+20R)] TAS maturity parameter shown in Figure 4.64 do not offer any evidence for the direct formation of the short-chain components from the higher molecular weight homologues via side chain scission. It appears that the observed increase in the abundance of the short-chain components relative to the long-chain aromatic steroid hydrocarbons, with increasing maturity, is due to the preferential degradation of the higher molecular weight compounds. Figure 4.64 shows that the concentrations of the C_{28} 5α (H) (20S+20R) TA-steroids decrease with thermal maturity, whereas, the concentrations of the C_{20} TA-steroid remain more or less constant. Such findings were observed by Peters et al. (1990) in their hydrous pyrolysis experiments of immature Monterey Phosphatic and Silicious rocks, and Requejo (1994) who performed a quantitative biomarker study in a sequence of shales of varying levels of maturity from the Upper Devonian Duvernay Formation in Western Canada. Furthermore, my results are in agreement with those obtained by Beach et al. (1989) in laboratory heating experiments, who could not monitor any formation of C_{20} TA-steroid hydrocarbon upon heating C_{28} 5α(H) 20R TA-component

on bentonite at 200°C. Instead, these authors noted a faster rate of degradation for the longer-chain TA-steroid hydrocarbon.

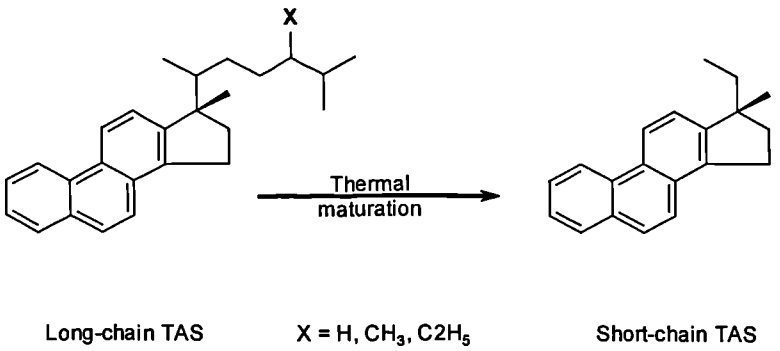

Figure 4.63 Conversion of long-chain triaromatic to short-chain triaromatic steroids by side cleavage during thermal maturation.

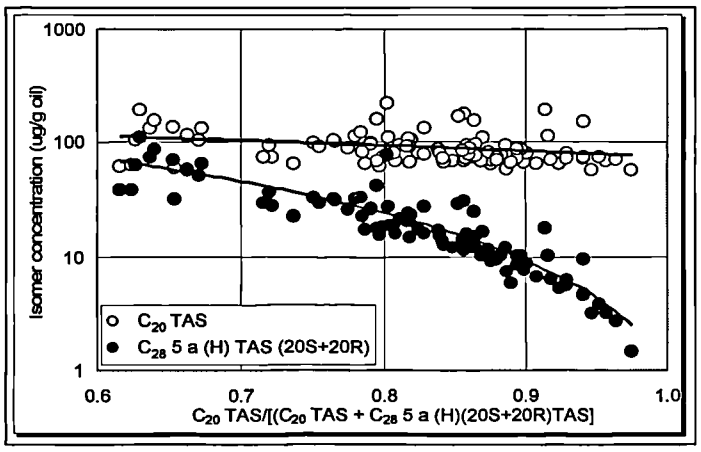

Figure 4.64 Cross plot of the concentrations (µg/g oil) of C_{20} TAS and C_{28} 5α (H) (20S+20R) TAS versus the maturity parameter C_{20}TA-steroid/[C_{20}+C_{28} 5α (H) (20S+20R) TA-steroids] for the oil samples in the Mya basin and Hassi Messaoud ridge. (Note that the Y axis is a logarithmic scale).

4.4.2.2.2. Alkylnaphthalenes

Evaluation of the thermal maturity of the oil samples was achieved using several maturity parameters based on the alkylnaphthalene distributions. Partially added mass chromatograms showing the relative distribution of C_0-C_4 naphthalenes in selected oils from different fields are presented in Figure 4.65. The values of naphthalene ratios and concentrations of individual isomers are listed in Appendix 4.4.

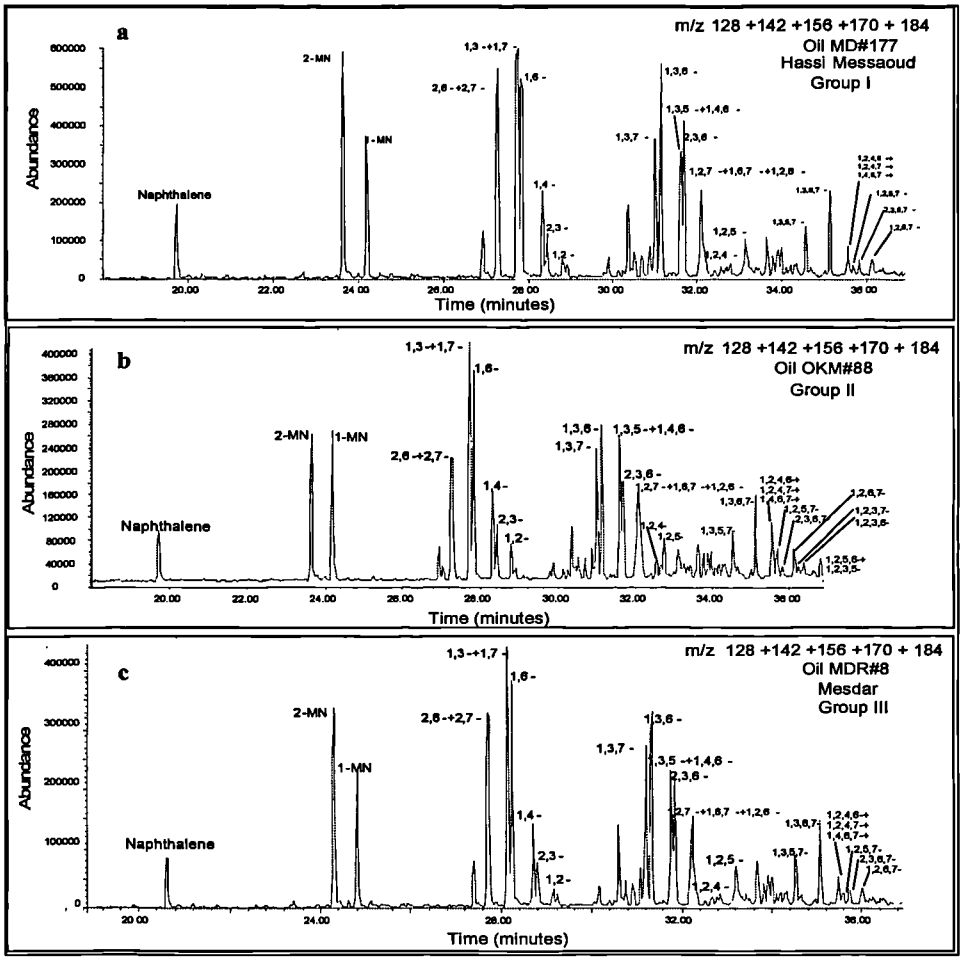

Figure 4.65 Partial m/z 128+142+156+170+184 mass chromatograms showing the distribution of C_0-C_4 naphthalenes in (a) Hassi Messaoud oil (b) Haoud Berkaoui oil and (c) Mesdar oil.

The variations in the concentrations (μg/g extract) of C_0-C_4 naphthalenes present in the oils from different fields are shown in Figure 4.66. Figure 4.66 reveals that oil samples from the Cambrian fields in group III contain higher concentrations of the various alkylnaphthalene component compared to the oil samples from the Cambrian fields in group I, and the fields in the Oued Mya basin, respectively. Moreover, alkylnaphthalene distributions show a regular decrease in the concentration of these components with the increase of the degree of alkylation in all the samples analysed in this work.

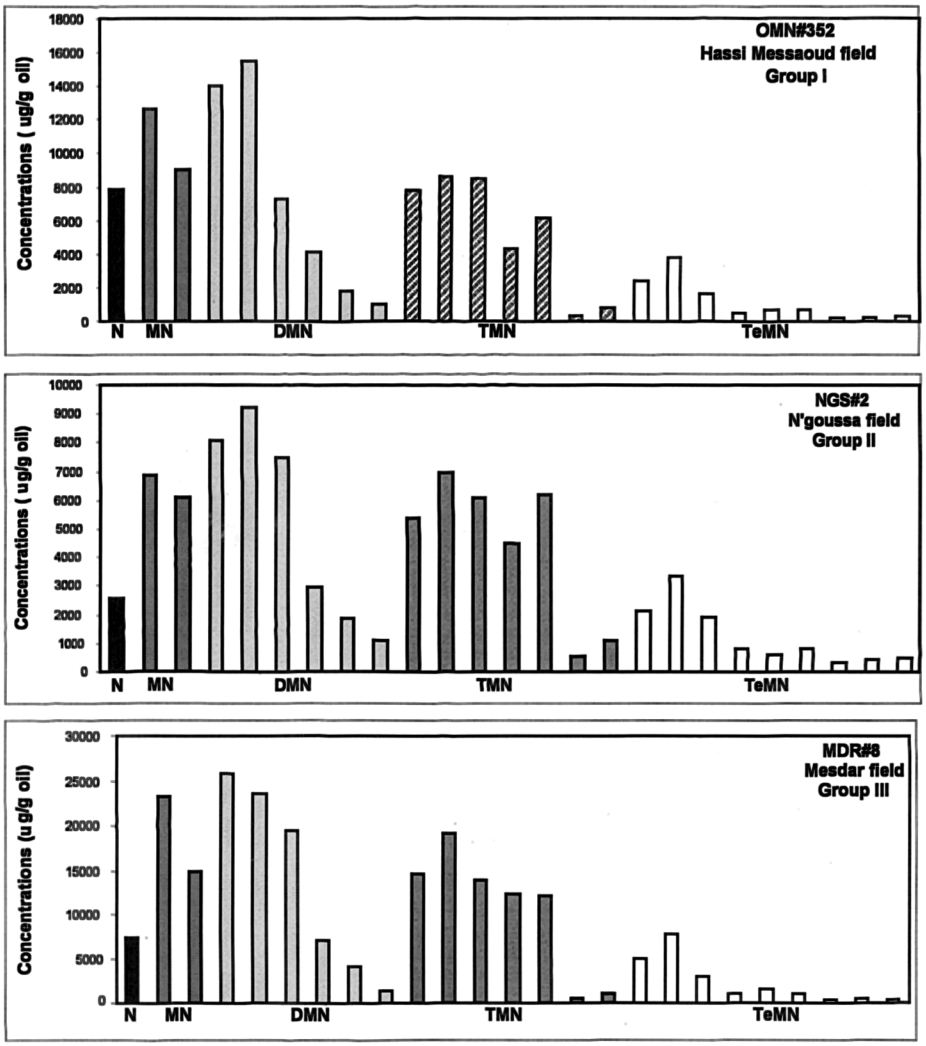

Figure 4.66 C_0-C_4 alkylnaphthalene distributions representing oil samples from Hassi Messaoud field (groupI), N'goussa field (group II), and Mesdar field (group III). (see Figure 4.1 for field positions).

The maturity parameters used for the evaluation of the maturity of the oils are listed in Table 4.4. The concentrations of the individual alkylnaphthalene isomers and the values of the maturity parameters are displayed in Appendix 4.4. The maturity parameters (2,6-DMN+2,7-DMN)/1,5-DMN ($\beta\beta+\beta\beta/\alpha\alpha$) and 1,3,7-TMN/1,2,5-TMN ($\alpha\beta\beta/\alpha\beta\alpha$) plotted against 2-MN/1-MN (β/α) and 1,3,6,7-TeMN/(1,2,5,6-TeMN + 1,2,3,5-TeMN) ($\alpha\beta\beta\beta/(\alpha\beta\alpha\beta+\alpha\beta\beta\alpha)$, respectively used in this work show that oil samples reservoired in the Cambrian fields: Hassi Messaoud, Hassi Guettar, El-Agreb (group I) and Mesdar and El-Baguel (group III) are more mature than those reservoired in the Lower Triassic and Devonian fields in Oued Mya basin (Figure 4.67). The oil samples from El-Agreb fields seem to be the least mature oils within group I. The oil samples from Hassi Messaoud fields exhibit a wide range of differences in maturity, with the oil samples from the central and eastern parts of the field being the most mature compared to the oil samples from the western and

northern flanks. These trends of maturity obtained using alkylnaphthalene maturity parameters agree well with the maturity trends revealed when using biomarker alkane maturity parameters in section 4.4.2.1 above.

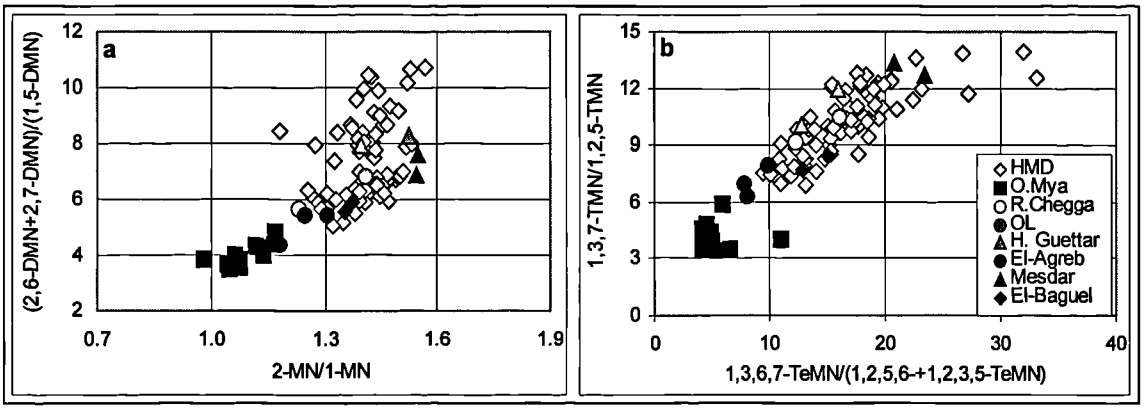

Figure 4.67 Cross plot of the alkylnaphthalenes based maturity parameters (a) (2,6-DMN+2,7-DMN)/1,5-DMN versus 2-MN/1-MN and (b) 1,3,7-TMN/(1,2,5-TMN) versus 1,3,6,7-TeMN/(1,2,5,6-TeMN+1,2,3,5-TeMN) for the Lower Triassic and Devonian oil samples in the Oued Mya basin and the Cambro-Ordovician oil samples in the Hassi Messaoud ridge.

Semi-quantitative determination of alkylnaphthalene isomers used in the evaluation of the maturity parameters of the oil samples reservoired in the Triassic fields in the Oued Mya basin and in the Cambrian fields in the Hassi Messaoud ridge, is used to investigate the quantitative evolution of some specific isomers as a result of increasing maturity. It has been stated that for alkylnaphthalenes β-substituted isomers are thermally more stable than α-substituted isomers (Alexander et al., 1985). Therefore, with increasing maturity, the methyl groups in α positions move to the thermodynamically more stable positions (β positions). The cross plot of the concentrations of 2,6-DMN + 2,7-DMN with methyl groups in 2, 6, and 7 (β) positions (see Figure 4.26) and 1,5-DMN, with methyl groups are in 1 and 5 (α) positions versus the (2,6-DMN+2,7-DMN)/1,5-DMN maturity parameter, displayed in Figure 4.68 does show an increase in the concentrations of the alkylnaphthalene isomers with methyl groups in the β position (i.e. 2,6- and 2,7-DMN) and a small decrease in the concentrations of the isomer with methyl groups in the α position.

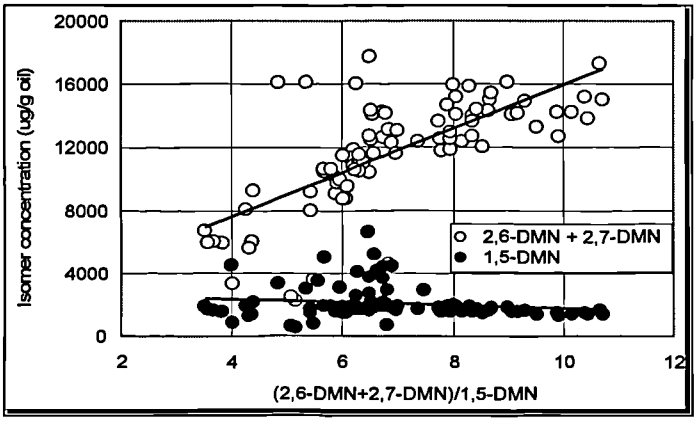

Figure 4.68 Cross plot of the concentrations (µg/g oil) of (2,6-DMN + 2,7-DMN) and 1,5-DMN versus the maturity parameter (2,6-DMN + 2,7-DMN)/1,5-DMN for the oil samples in the Mya basin and Hassi Messaoud ridge.

4.4.2.2.3. Alkylphenanthrenes

Partially summed mass chromatograms showing the relative distribution of C_0-C_3 phenanthrenes in selected oil samples are presented in Figure 4.69.

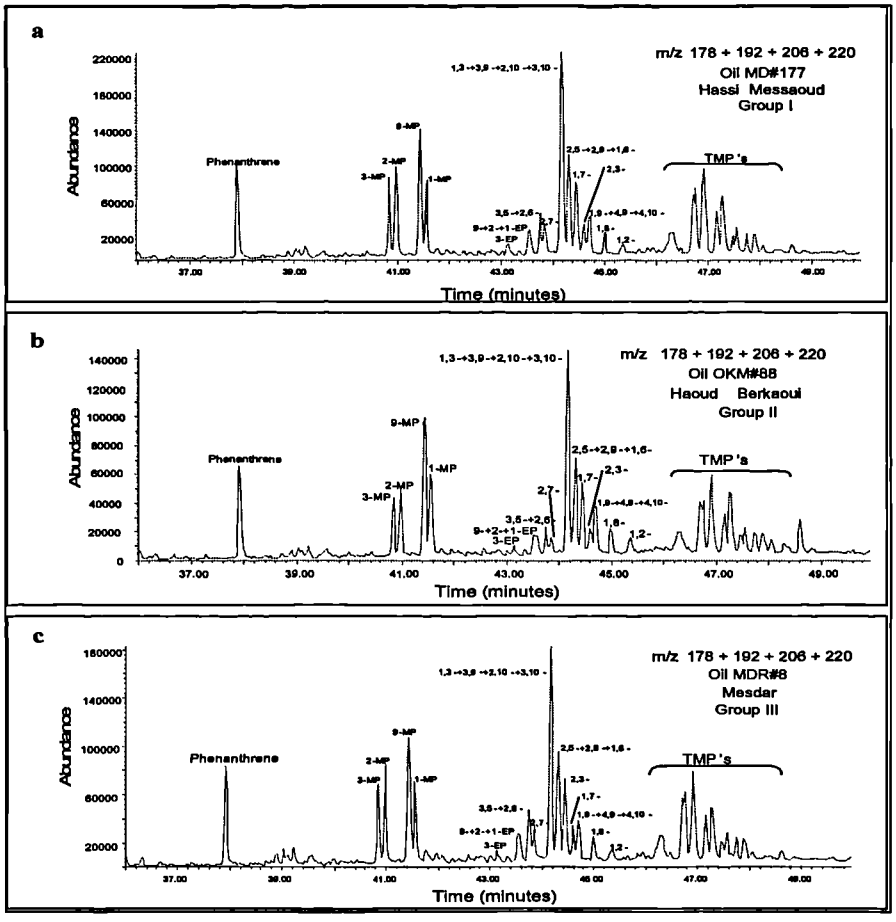

Figure 4.69 Partial m/z 178+192+206+220 mass chromatograms showing the distribution of C_0-C_3 alkylphenanthrenes in (a) Hassi Messaoud oil (group I), (b) N'goussa oil (group II) and (c) Mesdar oil (group III).

The variation in concentrations (μg/g extract) of C_0-C_3 alkylphenanthrenes present in the oil samples are displayed in Figure 4.70 and the alkylphenanthrene maturity parameters used in this section are listed in Table 4.6. The values of the various alkylphenanthrene maturity parameters and the concentrations of the alkylphenanthrenes in all oil samples analysed in this study are listed in Appendix 4.4. As can be seen from Figure 4.70, the distribution of alkylphenanthrene isomers is in general similar in all the oil samples. However, the concentrations of the alkylphenanthrene isomers are higher within Mesdar field compared to Hassi Messaoud, Oued Mya and El-Agreb fields, respectively.

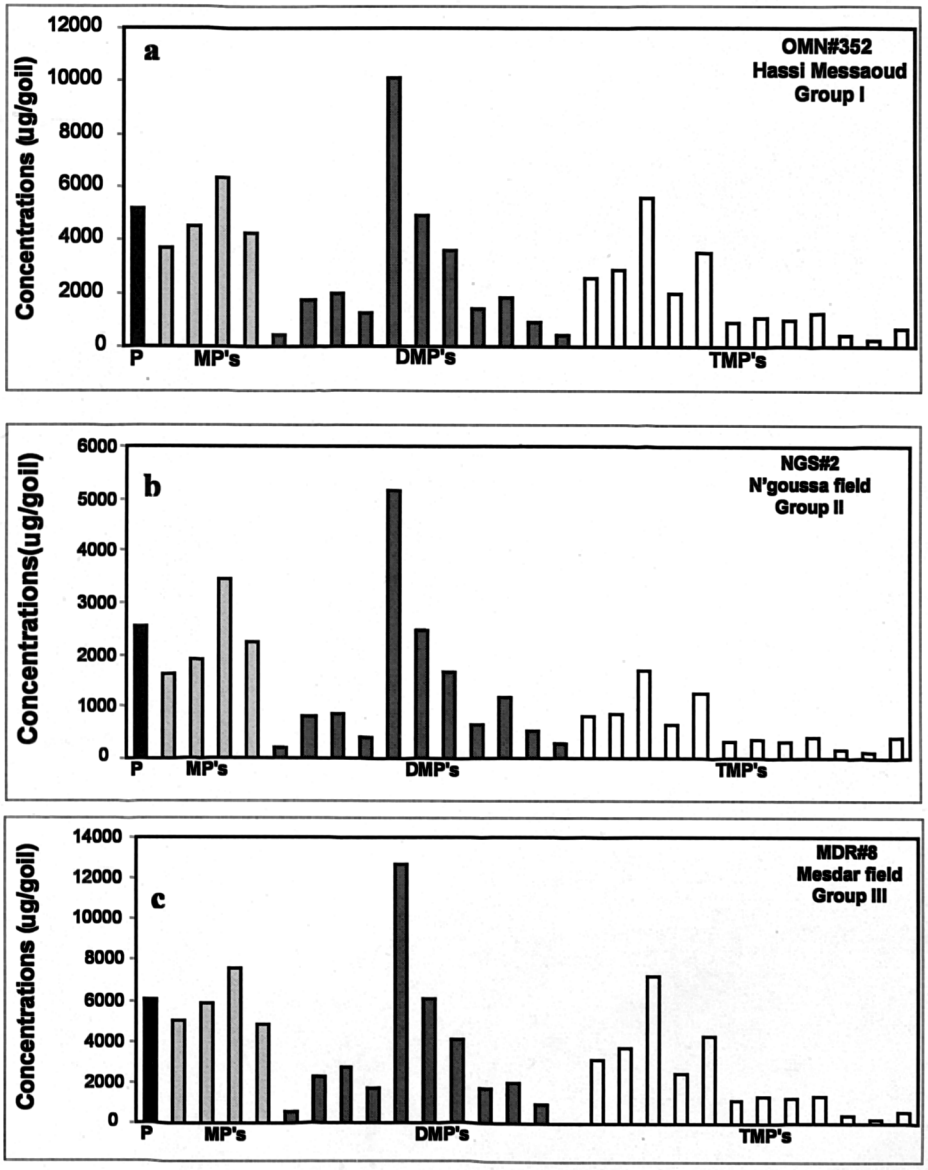

Figure 4.70 C_0-C_3 phenanthrene distributions for the oil samples in (a) Hassi Messaoud oil (group I), (b) N'goussa oil (group II) and (c) Mesdar oil (group III).

Cross plots of the summed alkylnaphthalene isomers versus alkylphenanthrene isomers shown in Figure 4.71, reveal that the Cambrian oil samples in group III contain more aromatic hydrocarbons than the rest of the oil samples from groups I and II, respectively. Moreover, the oil samples from group II (Lower Triassic and Devonian oils in the Oued Mya basin) show more or less similar concentrations of alkylphenanthrene and alkylnaphthalene isomers than the oil samples located in the western, northern and southern flanks of Hassi Messaoud field (group I). In contrast, oil samples from the central and eastern parts of Hassi Messaoud field exhibit higher concentrations than those from the flanks and oil samples from other fields in group I (i.e. El-Agreb, Hassi Guettar, and Rhourde Chegga fields). This is likely due to the differences in maturity between the oil samples from the 3 groups. In a set of source rock samples from the Shahejie Formation of the Liaohe Basin North east China, Li et al. (1994) showed that the aromatic hydrocarbon concentrations in source rock bitumens gradually increase with maturity, whilst concentrations of biomarkers decrease with maturity. In section 4.3.3.3 below I show similar trends of biomarker and aromatic hydrocarbon concentrations with increasing maturity of the oils analysed in this study (see section 4.4.3 for more detail).

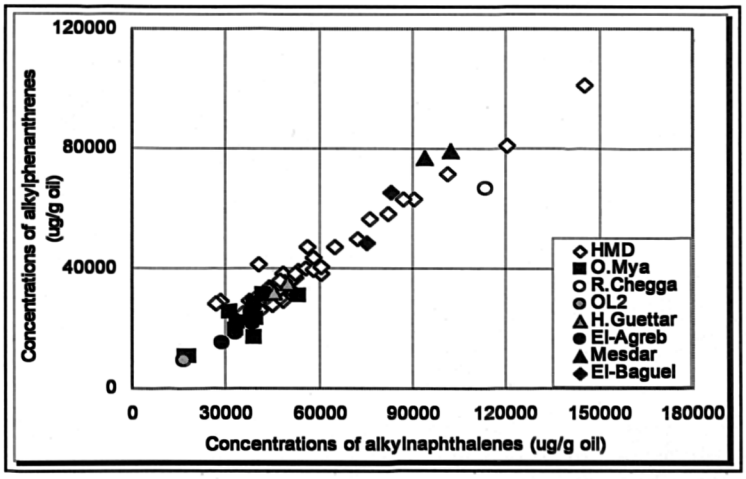

Figure 4.71 Plot of the summed concentrations of alkylphenanthrenes versus the summed concentrations of alkylnaphthalenes for the oil samples in group I, group II and group III.

The alkylphenanthrene isomers which are substituted in the β-position (Figure 4.31) have been observed to become increasingly dominant at higher maturity levels relative to related isomers with α-substitution (Radke et al., 1982a & b; Radke and Welte, 1983; Garrigues et al., 1984; Hall et al., 1985; Radke, 1987, 1988; Cassani et al., 1988).

The diagrams plotted in Figure 4.72 show good correlations (R^2 = 0.77 and 0.88) between maturity parameters based on alkylphenanthrenes. Therefore, the Lower Triassic and Devonian fields in the Oued Mya basin oils (group II and subgroup IIa) appear to be the least mature oils in the region, compared to the Cambro-Ordovician oil samples from group I and group III. Oil samples from Mesdar field (group III) revealed the highest level of maturity. Furthermore, it is also possible to distinguish between maturities within the individual groups of oil samples. Indeed, group I shows trends of maturity among Hassi Messaoud oils, where oils from the centre and to a lesser extent those from the eastern part of Hassi Messaoud reveal higher maturity than samples from the west, north and south flanks of the same field; always in the same group I, satellite field Hassi Guettar shows a north-south trend of maturity with HGA#3 being more mature than HGA#2 oil sample; El-Agreb fields show a north-south trend: El-Gassi-Zotti-El-Agreb show a trend of decreasing maturity with oil from El-Agreb field further south being the least mature and finally, oil sample RDC#1bis from Rhourde Chegga field plots in the area of least mature samples within group I. The oils from Mokh el Kebch, N'goussa, Guellala north east and Guellala fields (subgroup IIa) are in general more mature than the oils from Draa Temra, Benkahla, and Haoud Berkaoui fields (group II; see location map in Figure 4.1). These trends of maturity agree well with those obtained using alkylnaphthalene and biomarker maturity parameters above.

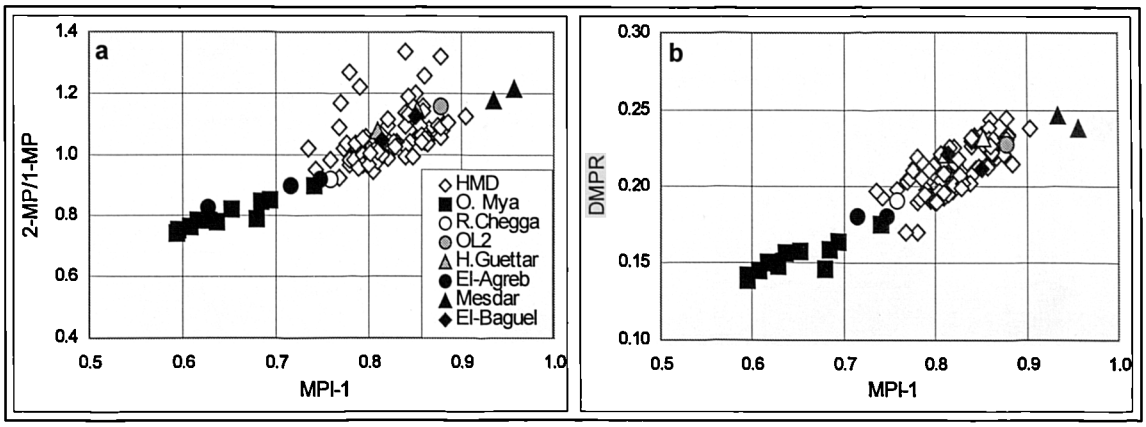

Figure 4.72 Cross plot of the phenanthrenes based maturity parameters (a) 2-MP/1-MP and (b) DMPR versus MPI-1 for the Oued Mya basin and Hassi Messaoud Ridge oils.

4.4.2.2.4. Methylbiphenyls

Changes in the relative abundances of the methylbiphenyls have been shown to be useful for the assessment of thermal maturity of oils and source rock extracts

(Alexander et al., 1986; Cumbers et al., 1987). Cumbers et al. (1986 and 1987) observed that the relative abundance of the three isomeric methylbiphenyls isolated from a suite of Australian oils and rock extracts was in the order: 3-MeBP > 4-MeBP > 2-MeBP (Figure 4.73)

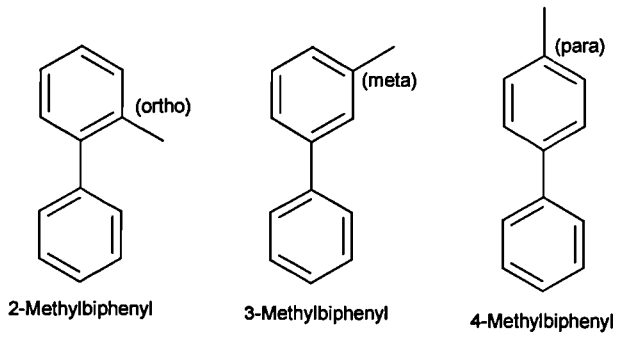

Figure 4.73 Molecular structures of methylbiphenyl isomers.

Cumbers et al. (1986 and 1987) indicated that the relative abundance of the three isomers reflected the thermodynamic stability of the individual compounds, with the *meta*-substituted 3-MeBP isomer being the most stable and the *ortho*-substituted 2-MeBP the least stable.

The partial m/z 168 mass chromatogram showing the distribution of methylbiphenyls present in the oils from the different groups in the current study are displayed in Figure 4.74.

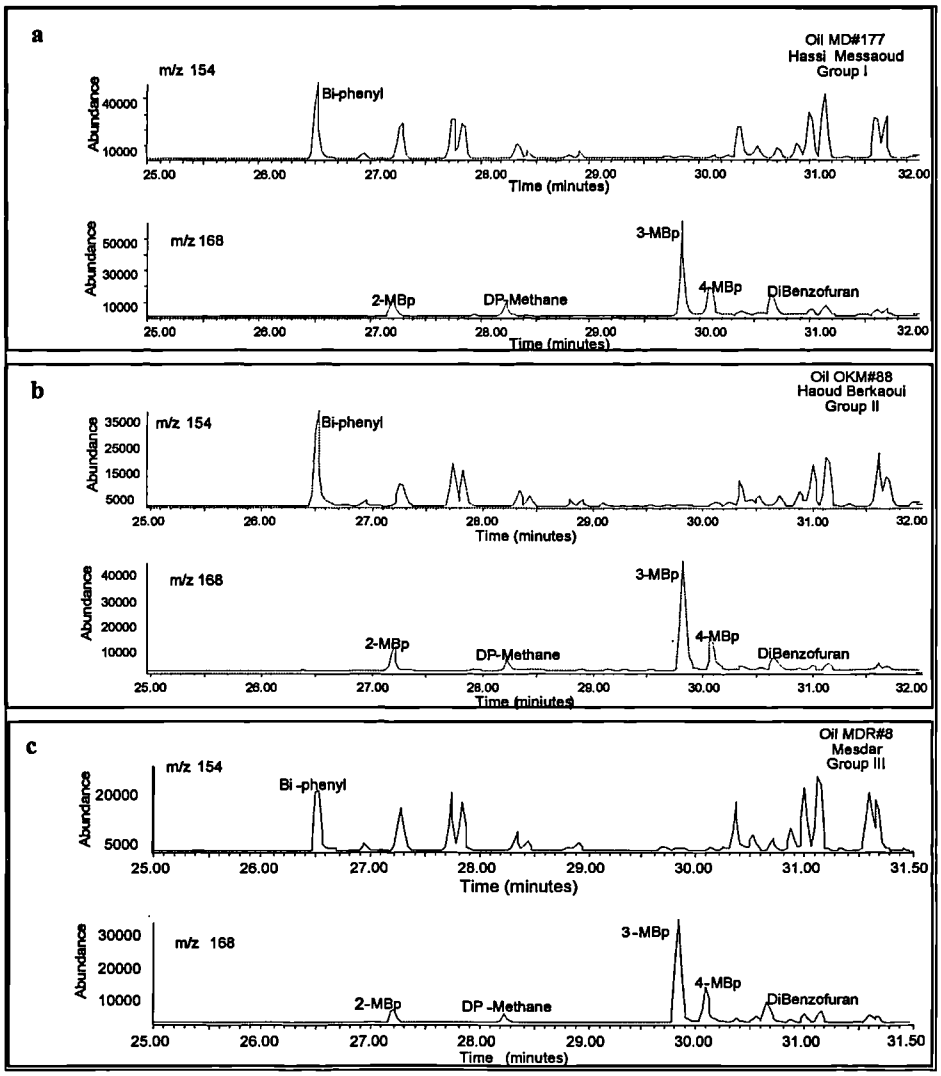

Figure 4.74 Partial m/z 154 and 168 mass chromatograms showing the distributions of C_0-C_1 Biphenyls in (a) Hassi Messaoud oil (group I), (b) Haoud Berkaoui oil (group II) and (c) Mesdar oil (group III).

Two ratios 3-MeBP/2-MeBP and 4-MeBP/2-MeBP (Alexander et al., 1986) were employed to evaluate thermal maturity trend(s) within Oued Mya basin and Hassi Messaoud Ridge. Values for these ratios and concentrations for individual isomers are listed in Appendix 4.4.

The cross plot of 3-MeBP/2-MeBP versus 4-MeBP/2-MeBP ratios showed in Figure 4.75 clearly reveals a systematic increase in both ratios from the Lower Triassic and Devonian oils in group II and subgroup IIa towards the Cambro-Ordovician oil samples from group I and group III. This trend of maturity agrees well with the maturity trends obtained by the other maturity parameters calculated from the aromatic steroid hydrocarbon, alkylnaphthalene and alkylphenanthrene distributions in the sections above.

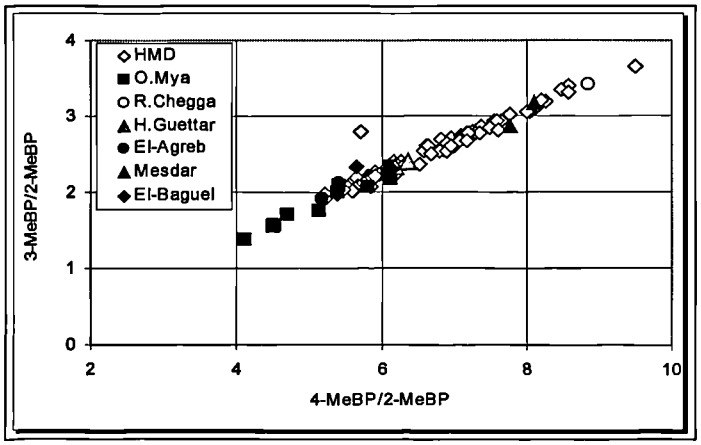

Figure 4.75 Cross plot of the biphenyls based maturity parameters 3-MBp/2-MBp and 4-MBp/2-MBp for the Oued Mya basin and Hassi Messaoud Ridge oils.

The concentrations of methylbiphenyl isomers used in the evaluation of the maturity parameters of the oils analysed in this study are also used to investigate the quantitative evolution of these isomers as a result of increasing maturity. The cross plot of the concentrations of 3-MeBP (*meta-* position) and 2-MeBP (*ortho-* position) versus the 3-MeBP/2-MeBP maturity parameter displayed in Figure 4.76 does show an increase in the concentrations of the 3-MeBP isomer and a decrease in the concentrations of the less stable 2-MeBP isomer. These findings are indeed in agreement with the observations of Cumbers et al. (1986, 1987) who showed that the 3-MeBP isomer is thermally more stable than the 2-MeBP.

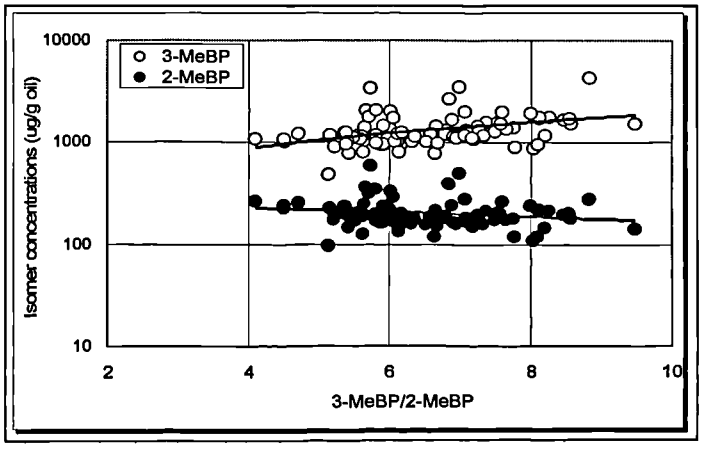

Figure 4.76 Cross plot of the concentrations (µg/g oil) of 3-MBp and 2-MBp versus the maturity parameter 3-MBp/2-MBp for the oil samples in the Mya basin and Hassi Messaoud ridge.

4.4.2.2.5. Alkyldibenzothiophenes

The summed m/z 184, 198, 212 and 226 mass chromatograms showing the distributions of C_0-C_3 dibenzothiophenes in oils from different fields are displayed in

Figure 4.77. The concentrations of C_0-C_3 dibenzothiophenes for all oils analysed in this study and C_0-C_3 dibenzothiophenes based maturity ratios are displayed in Appendix 4.4.

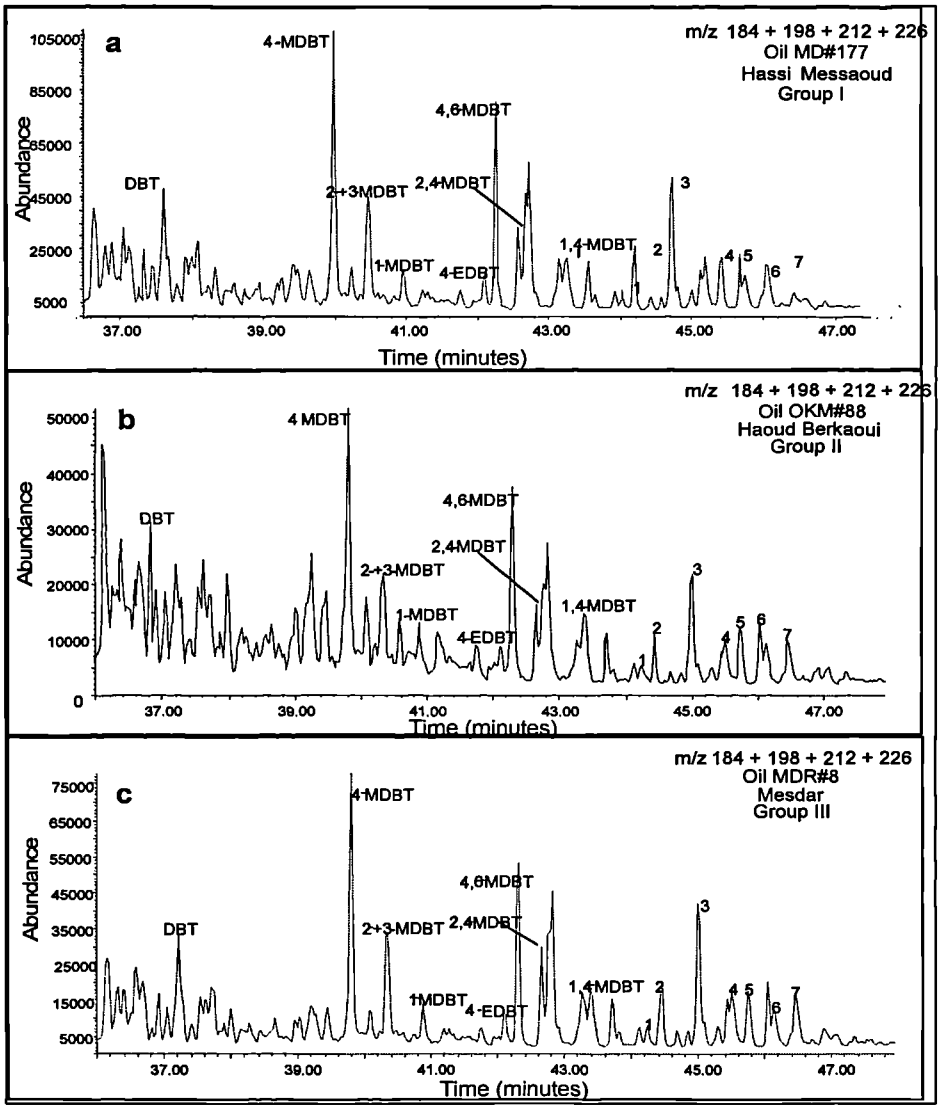

Figure 4.77 Partial m/z 184+198+212+226 mass chromatograms showing the distribution of C_0-C_3 dibenzothiophenes in (a) Hassi Messaoud oil (group I), (b) Haoud Berkaoui oil (group II) and (c) Mesdar oil (group III).

The cross plot of 2-+3-MDBT/DBT ratio versus 4-MDBT/1-MDBT ratio (Figure 4.78) shows that oil samples from group (I) including the Cambro-Ordovician oils in the Hassi Messaoud, Hassi Guettar, El-Agreb and the Lower Triassic oil in the Rhourde Chegga exhibit higher maturity than those from group (II) which includes Lower Triassic and Devonian oils in the fields located in the Oued Mya basin. Moreover, within the individual groups distinguished in this figure, it is possible to observe that:

group (I) shows in general higher maturity of the oils from the central Hassi Messaoud than those from the flanks; in the Hassi Guettar field, oil sample HGA#3 (located north of the field) is more mature than oil sample HGA#2 (south of the field); there is a north-south decreasing trend of maturity between El-Agreb succesive fields with the oil from El-Gassi field being more mature than the oil samples from Zotti and El-Agreb fields, respectively. The Lower Triassic and Devonian oils in the Mokh El Kebch, N'goussa and Guellala northeast are more mature than the oils from the Lower Triassic fields in Draa Temra, Benkahla and Haoud Berkaoui. Finally, within group (III), the oils from Mesdar field are more mature than those from El-Baguel field.

The maturity parameters used for the triaromatic steroid hydrocarbons, alkylnaphthalenes and alkylphenanthrenes showed that the oils from group III are more mature than the rest of the oils analysed in the study area. However, the alkylthiophene maturity ratios used below show that the oils from group III plot along a maturity trend which appears to be parallel to the maturity trend shown for the rest of the oil samples in groups I and II. A possible explanation for this observation is that these ratios seem to be controlled by both maturity and other factors such as depositional environment and lithology (Huang and Pearson, 1999). Therefore, it is possible that the oils from Mesdar and El Baguel (group III) could have been generated from another source rock, which is lithologically different from the source rock having generated the rest of the oils.

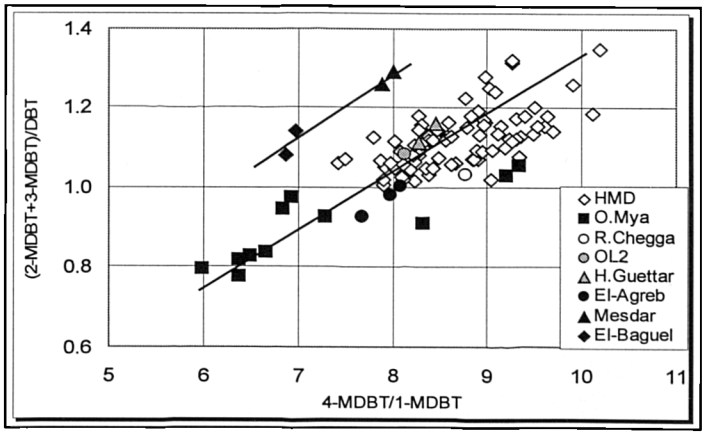

Figure 4.78 Cross plot of the dibenzothiophene-based maturity parameters 2-+3-MDBT/DBT and 4-MDBT/1-MDBT for the Oued Mya basin and Hassi Messaoud Ridge oils.

4.4.3. Effect of maturity on facies-dependent biomarker ratios and concentrations

As I have mentioned earlier in section 4.3.3.1.2, I am going to demonstrate whether differences seen in [C_{29} (ααα+αββ) S+R regular steranes]/[C_{29} (ααα+αββ) S+R regular steranes +C_{29}-C_{30} 17α (H) hopanes)] and [C_{28}-C_{29}-(S+R) extended tricyclics/[(C_{28}+C_{29}-(S+R) tricyclics+C_{29}-C_{30}17α(H)hopanes)] ratios and biomarker and aromatic hydrocarbon concentrations seen in the defined groups I, II and III are partly due to maturity differences between the groups.

Seifert and Moldowan (1978) showed that C_{29} regular steranes/(C_{29} regular steranes + C_{29}-C_{30}17α (H)-hopanes) ratio can be affected by maturity, but in a study of oils from Oman the C_{29} regular steranes/(C_{29} regular steranes + C_{29}-C_{30} 17 α (H)-hopanes) ratio remained relatively constant for a group of related oils of widely different thermal maturity (Peters and Moldowan, 1993). Moreover, Seifert and Moldowan (1978) showed systematic increases in the tricyclic terpanes/17α (H)-hopanes ratio with increasing thermal maturity. The ratio increases because proportionally more tricyclics than hopanes are released from kerogen at higher levels of maturity (Aquino Neto et al., 1983). In the laboratory, Peters et al. (1990) showed an increase in the tricyclic terpanes/17α (H)-hopanes ratio during hydropyrolysis of Monterey shale.

Figure 4.79 shows the [C_{29} (ααα+αββ) S+R regular steranes]/[C_{29} (ααα+αββ) S+R regular steranes + C_{29}-C_{30} 17α (H) hopanes)] and [C_{28}-C_{29}-(S+R) extended tricyclic terpanes/[(C_{28}+C_{29}-(S+R) tricyclic terpanes+C_{29}-C_{30}17α(H)hopanes)] ratios plotted against calculated vitrinite reflectance based on the methyl phenanthrene index MPI maturity parameter (Radke et al., 1986).

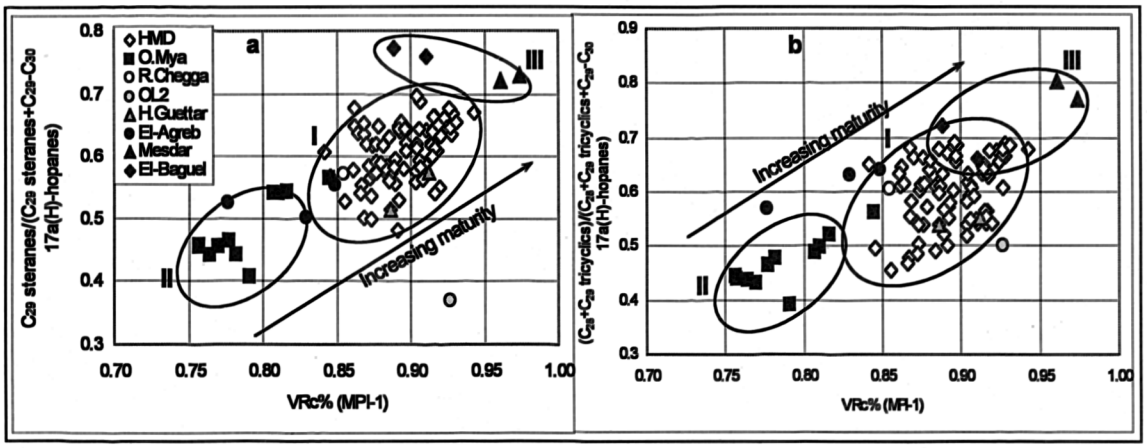

Figure 4.79 Cross plots of (a) C_{29}steranes/(C_{29}steranes +C_{29}-C_{30}17α (H)-hopanes) and (b) (C_{28}+C_{29}tricyclics)/[C_{28}+C_{29}tricyclics+(C_{29}+C_{30})17α□(H)-hopanes] versus the calculated vitrinite reflectance %Rc for the Oued Mya basin and Hassi Messaoud Ridge oils.

Indeed, there is positive correlation between the calculated vitrinite reflectance equivalent (%Rc) and both ratios. Oil samples from Mesdar field in group III with higher maturity exhibit higher ratios; oil samples with the lowest maturity from the fields in the Oued Mya basin exhibit the lowest ratios and oil samples from group I plot in between oils from groups II and III indicating a strong maturity effect on these ratios.

Moreover, the summed concentrations of the biomarkers (i.e. tricyclic terpanes, hopanes and steranes) and the summed concentrations the aromatic hydrocarbons (i.e. alkylnaphthalenes, alkylphenanthrenes, and alkylthiophenes) plotted against the calculated vitrinite reflectance maturity parameter Rc% are displayed in Figure 4.80. Interestingly, biomarker concentrations in the oils gradually decrease with increasing maturity, whilst concentrations of aromatic hydrocarbons increase with increasing maturity (e.g. Li et al., 1995a). It has been suggested that biomarkers are released from the kerogen prior to the main phase of oil generation, as they are bound into the kerogen matrix by relatively weak bonds, such as carbon-oxygen and carbon-sulphur bonds (van Graas, 1990). Thus, the decreasing concentrations of the biomarkers with increasing maturation shown in Figure 4.80a could be due to dilution with non-biomarker material, for instance *n*-alkanes (van Graas, 1990) and aromatic hydrocarbons (e.g. Requejo, 1994) which are generated throughout the oil window. This is consistent with the increase in the concentrations of the aromatic hydrocarbons with increasing maturity in the same oil samples (Figure 4.80b). Furthermore, cracking biomarker molecules (e.g. van Grass, 1990) as well as processes such as

aromatisation reactions of the biomarker components (e.g. Requejo, 1992) may well become significant at increasing levels of maturation, thereby contributing to the observed decrease in the concentration of the biomarkers with increasing maturity. Indeed, the oil samples analysed in this project revealed relatively high maturity levels ranging from 0.82 to 1.08 %Rm (obtained from calibration with a North Sea sample set see section 4.3.3.2.2.1). Hence, the processes of cracking and aromatisation reactions of the biomarker molecules are likely to be important at these levels of maturity.

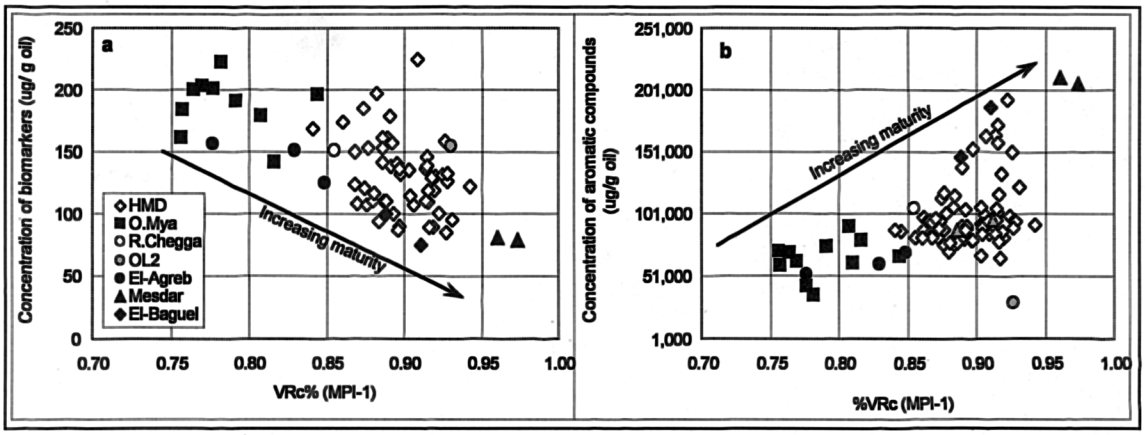

Figure 4.80 Cross plots of the concentrations of (a) biomarkers and (b) aromatic compounds versus the calculated vitrinite reflectance %Rc for the Oued Mya basin and Hassi Messaoud Ridge oils.

4.5. Oil Source rock correlations

The correlation of crude oils with one another and with extracts from source rocks provide valuable tools for helping the exploration geologist answer exploration questions and extend existing exploration trends. Therefore, establishment of oil to oil and oil to source rock correlation is of economic as well as scientific importance and might help in discovering new reserves, by focusing the drilling on prospects within the drainage areas of the defined source rocks as well as the extension of the already discovered reservoirs.

4.5.1. Facies comparison

The Pr/*n*-C_{17} and Ph/*n*-C_{18} ratios are often used in crude oil correlations since they provide information on maturation, biodegradation as well as source (Connan and Cassou, 1980; Shanmugam, 1985; Talukdar et al., 1993). The Pr/*n*-C_{17} and Ph/*n*-C_{18} ratios decrease with maturation due to the increasing prevalence of the *n*-alkanes, and increase with biodegradation due to the preferential loss of the *n*-alkanes (*n*-C_{17} and *n*-

C_{18}). The cross plot of Pr/*n*-C_{17} versus Ph/*n*-C_{18} in Figure 4.81 reveals that the Ordovician source rock samples and the Lower Triassic and Devonian oils in group II contain lower Pr/*n*-C_{17} and Ph/*n*-C_{18} ratios than the Silurian source rock samples and the Cambro-Ordovician oil samples from group I. The Silurian and Ordovician source rock samples revealed more or less the same maturity intervals (see section 4.3.2.3) and the Lower Triassic and Devonian oils in group II revealed lower maturity than the Cambro-Ordovician oils in group I. Therefore these differences are likely caused by the source facies differences between the Silurian and the Ordovician on one hand and the oils in group II relative to the oils in group I on the other hand. Hence, it is likely that the Lower Triassic and Devonian oils were generated from a contribution of both the Ordovician and the Silurian strata in the Oued Mya basin, whereas the Cambro-Ordovician oils were mainly generated by the Silurian source rocks or both, but with much higher contribution from the Silurian source rocks than the Ordovician source rocks. Moreover, the oil samples in the Mesdar and El Baguel fields (group III) exhibit a different trend than the oils from group I and group II, suggesting probably a different source of these oils (likely the Silurian source rocks located in the Berkine basin (Figure 4.1)).

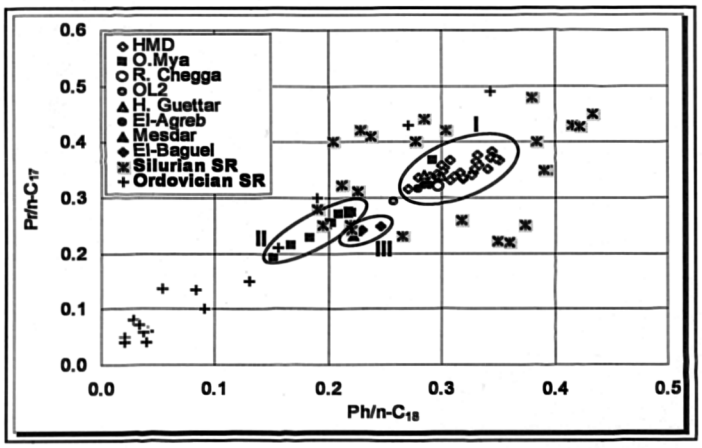

Figure 4.81 Variation in Pr/*n*-C_{17} ratio with Ph/*n*-C_{18} ratio for Silurian and Ordovician source rocks and the oils from the Oued Mya basin and Hassi Messaoud Ridge.

A number of facies-based parameters calculated using sterane and triterpane distributions have been selected in order to perform oil/source rock correlation. The ternary diagram displaying the distribution of C_{27}-C_{28}-C_{29} 5α(H), 14β(H), 17β(H) steranes in Figure 4.82, clearly shows similarities between all the oils and the Silurian source rock samples which belong to group A (defined in section 4.3.2.1 and 4.3.2.2). However, Silurian source rock samples from group B and all of the Ordovician

samples plot well away from the oils. This will suggest that the oils analysed in this project have been mostly generated from the Silurian "hot" shales interval located in the Oued Mya basin.

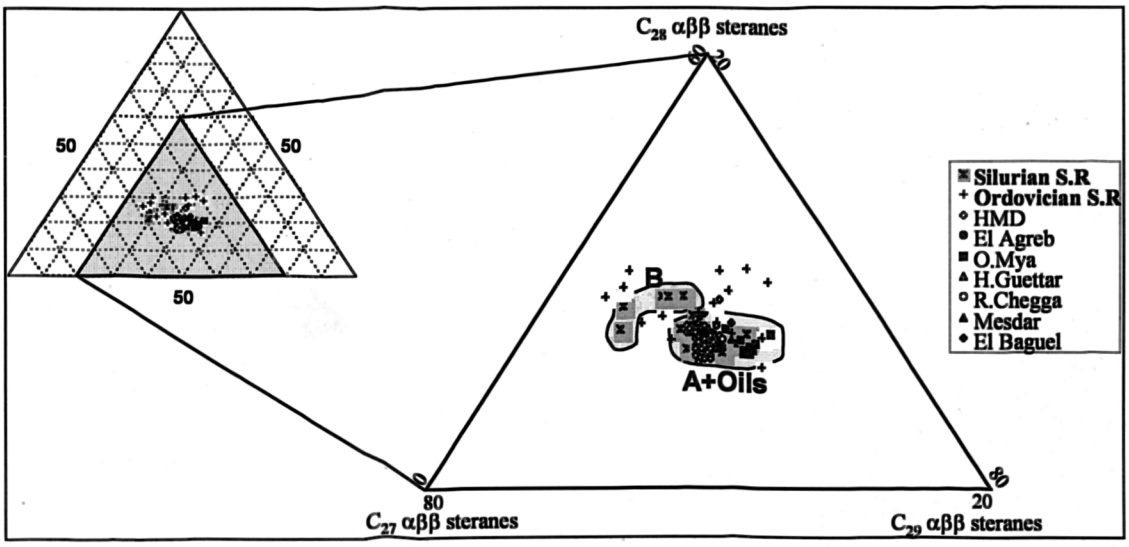

Figure 4.82 Ternary plot of the relative abundance of C_{27}- C_{28}- C_{29} 5α(H), 14β(H), 17β(H) (20S+20R) steranes for the Silurian and Ordovician source rocks and the oils from the study area.

Cross plots of the [C_{28}-C_{29}-(S+R) extended tricyclic terpanes]/[(C_{28}+C_{29}-(S+R) tricyclics+C_{29}-C_{30}17α(H)hopanes)] ratio versus the [C_{29} (ααα+αββ) S+R regular steranes]/[C_{29} (ααα+αββ) S+R regular steranes + C_{29}-C_{30} 17α (H) hopanes)] ratio and the [C_{28}+C_{29}-(S+R)extended tricyclic terpanes]/Ts ratio versus the C_{24} tetracyclic terpane/[C_{26} tricyclic terpanes (S+R)] ratio displayed in Figure 4.83 reveal that all the oils from Hassi Messaoud, Hassi Guettar, El Agreb, and Rhourde Chegga fields (group I) and oils from Mokh El Kebch, N'goussa, Guellala northeast and Guellala (subgroup IIa) plot very close to Silurian source rock samples from group A. There is an obvious difference between all the oils and the Silurian source rock samples from group B and all of the Ordovician source rock samples. The oil samples from Draa Temra, Benkahla and Haoud Berkaoui fields (group II) plot in between the Silurian source rock samples from group A, group B and the Ordovician source rock samples. This observation may also suggest that these oils were generated from contribution of both Silurian and Ordovician source rocks, which is in agreement with the results shown by the Pr/*n*-C_{17} and Ph/*n*-C_{18} ratios above. Oil samples from Mesdar and El Baguel fields (group III) appear to be generated from a source having slightly different features than the Silurian source rocks from group A. Therefore, the source of the oils trapped in these fields is probably the Silurian strata located in the Berkine

basin. The principal components analysis shown in the section below confirmed this suggestion.

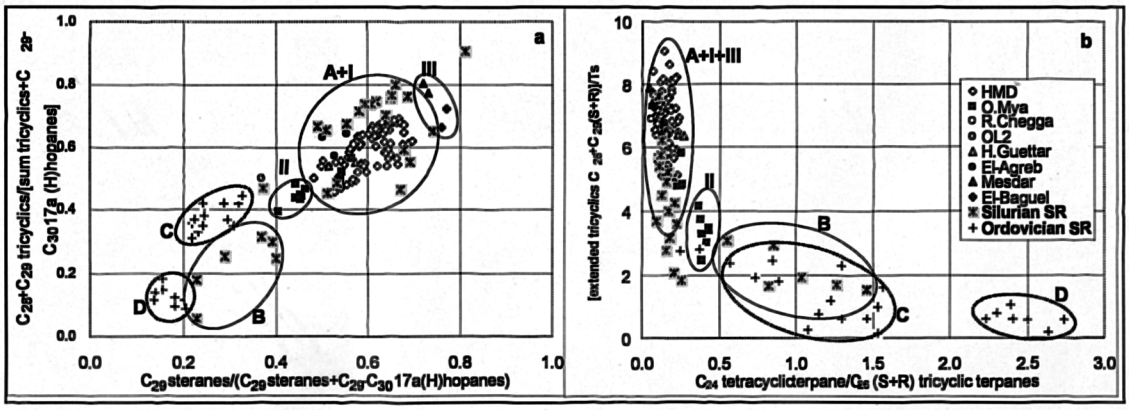

Figure 4.83 Cross plots of (a) the facies parameters [(extended tricyclic terpanes $C_{28}+C_{29}$(S+R)]/[(extended tricyclic terpanes $C_{28}+C_{29}$(S+R)+($C_{29}+C_{30}$ 17α(H) hopanes)] versus C_{29} steranes/[(C_{29} steranes)+($C_{29}+C_{30}$ 17α(H) hopanes)] and (b) [(extended tricyclic terpanes $C_{28}+C_{29}$(S+R)]/Ts versus C_{24} tetracyclic terpane/C_{26} tricyclic terpanes (S+R) for the source rock and oil samples from the study area. (A+I=Silurian source rock samples from group A and oil samples from group I)

4.5.2. Principal components analysis (PCA)

A biomarker data set, comprising 29 variables (biomarker concentrations) for 116 oil and source rock samples (Table 4.11) was analysed by PCA to establish the major sources of variance within the sterane, tricyclic terpane, and hopane distributions. The biomarkers used in the analysis are listed in Table 4.4.

Table 4.11 List of the oil and source rock samples used for the principal components analysis.

Nature of sample	Field	Reservoir	Number of samples
Oil	Hassi Messaoud	Cambrian	51
Oil	Haoud Berkaoui	Lower Triassic	4
Oil	Benkahla	Lower Triassic	2
Oil	Draa Temra	Lower Triassic	1
Oil	Guellala northeast	Devonian	1
Oil	N'Goussa	Devonian	1
Oil	Mokh El Kebch	Lower Triassic	1
Oil	Rhourde Chegga	Lower Triassic	1
Oil	El-Agreb	Cambrian	3
Oil	Mesdar	Cambrian	2
Oil	El-Baguel	Cambrian	2
Source rock	Oued Mya	Silurian	25
Source rock	Oued Mya	Ordovician	22
Total			**116**

The first three principal components (PCs) obtained, explain 45%, 17% and 13% of the variance within the scaled data set, respectively. This allows the relationships between the samples to be examined in simple two-dimensional scores plot: PC1

versus PC2, and PC1 versus PC3 which include the effects of all the original variables (i.e. biomarker concentrations), and display the bulk (75%) of the scaled data variability (Figure 4.84).

The diagrams showing the plot of PC1 versus PC2 and PC1 versus PC3 reveal that the oil samples in group I (i.e. oils from Hassi Messaoud, Rhourde Chegga, and El-Agreb fields) plot closer to the Silurian source rock samples in group A, indicating a genetic relationship between these samples. The oil samples in group II (i.e. oils from Draa Temra, Haoud Berkaoui and Benkahla fields) plot in between the Silurian source rock samples in group A and the Silurian source rock samples in group B and the Ordovician source rock samples indicating that these oils were generated from a contribution of both Silurian and Ordovician source rock strata located in the Oued Mya basin. This is consistent with the results shown by the Pr/*n*-C_{17} and Ph/*n*-C_{18} and biomarker ratios plotted in Figure 4.81 and Figure 4.83 (see the section above). The oil samples in group III (i.e. from Mesdar and El Baguel fields) plot close to the oil samples in group I and the Silurian source rock samples in group A in the first diagram, however, in the second diagram, the oil samples in group III are distinguished from those in group I and the Silurian source rocks (group A). This observation may indicate that the oils in group III were generated from Silurian source rocks which probably have slightly different organic facies and lithology compared to the Silurian strata in the Oued Mya basin. Hence, the source rock that has generated the oils in group III is likely the Silurian located in the Berkine basin east-southeast from the Hassi Messaoud ridge (Figure 4.1). Geographical and structural positions of the oils from Mesdar and El-Baguel fields does support that the source of these oils is located in Berkine basin (Figure 4.1 and Figure 5.70).

The Silurian source rock samples from the wells RDC#2 (3804.7, 3806.4, 3808.35 and 3810.8m), and GLNE#3 (3803.45 and 3809.45m) are also distinguished from the main Silurian source rock samples in group A (for more details see section 4.3.2.2).

An explanation of what these three PCs represent is given by the loadings plots in Figure 4.85. These diagrams exhibit the loadings of the different variables upon the principal components; large loadings, either positive or negative, indicate a significant influence of the variable on that PC. Thus, PC1 essentially distinguishes the oil samples and the Silurian source rock samples in group A, which are relatively

depleted in C_{21}-C_{23} tricyclic terpanes, C_{24} tetracyclic terpane, and hopanes (positive PC1) from the Silurian source rock samples in group B, the Ordovician source rock samples and the Silurian source rock samples from the well RDC#2, which are relatively depleted in C_{21}-C_{31} extended tricyclic terpanes, steranes and diasteranes (negative PC1). PC2 mostly differentiates the Ordovician source rock samples in group D, Silurian source rock samples from the well GLNE#3, oil samples from group II, subgroup IIa and group I which are relatively depleted in C_{21}-C_{25} tricyclic terpanes, C_{21} (ααα+αββ) pregnanes and C_{22} (ααα+αββ) homopregnanes (positive PC2) from the Ordovician source rock samples in group C, Silurian source rock samples in and groups A and B and in the well RDC#2, and oil samples from group III, which are relatively depleted in C_{29} Ts, C_{30} diahopane, Ts, Tm, C_{29}-C_{30} 17 α(H) hopanes, C_{31} tricyclic terpanes, C_{24} tetracyclic terpane, and C_{29} diasteranes (negative PC2). Finally PC3 mainly discriminates the Ordovician source rock samples in group C, the Silurian source rock samples in group B and wells RDC#2 and GLNE#3, oil samples in group III and subgroup IIa, which are depleted in C_{29} Ts, C_{30} diahopane, C_{21}-C_{31} tricyclic terpanes, and C_{27}-C_{29} diasteranes (positive PC3) from the Ordovician source rock samples in group D, the Silurian source rock samples in group A and oil samples in group I and group II, which are relatively depleted in C_{21} (ααα+αββ) pregnanes and C_{22} (ααα+αββ) homopregnanes and C_{27}, C_{28}, C_{29} ααα and αββ regular steranes (negative PC3).

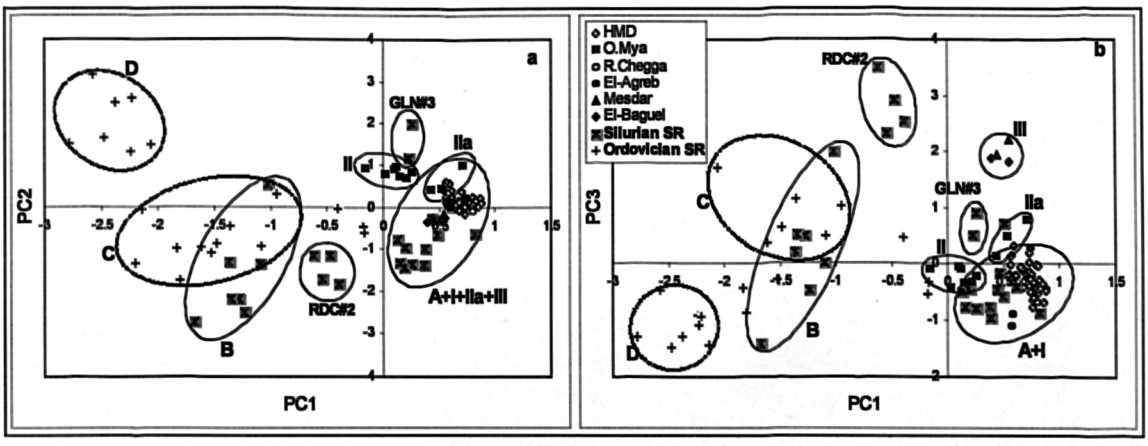

Figure 4.84 Scores plots of (a) PC1 versus PC2 and (b) PC1 versus PC3 showing the relationship between the source rocks (Silurian and Ordovician) and the oils analysed in this project in terms of the first, second and third principal components. PC1 explains 45% of the total variance in the scaled data set, PC2 explains a further 17%, and PC3 explains a further 13%. (A+I+III = Silurian source rock samples in group A with the oil samples in groups I and III and A+I = Silurian source rock samples in group A with the oil samples in group I).

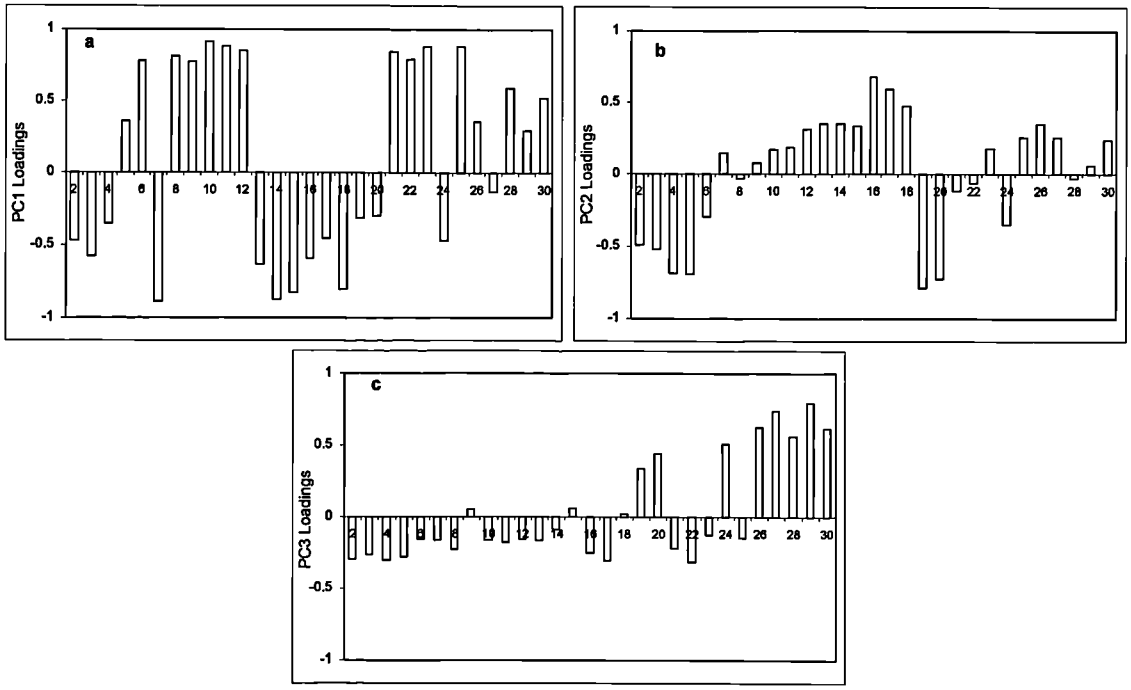

Figure 4.85 Loadings plots showing the composition of the first three principal components, which scored 45%, 17%, and 13% of the total variance in the data set, respectively.

4.5.3. Maturity

Earlier in sections 4.3.2.3.2.1 and 4.3.3.2.2.1, I showed that both of the source rocks (Silurian and Ordovician) and the oils revealed the same range of maturity, when calibrating my sample set with a North Sea sample set (Table 4.12). The North Sea sample set has a known measured vitrinite reflectance together with a number of biomarker and aromatic maturity parameters.

The oils from Haoud Berkaoui, Benkahla, Draa Temra, Guellala, Guellala northeast, N'Goussa and Mokh El Kebch fields in the Oued Mya basin appear to be the least mature oils compared to the rest of the oils from the Hassi Messaoud ridge and the Silurian and Ordovician source rocks. The Hassi Messaoud field exhibits a wider range of maturity, with the least mature oils located in the western, northern, and southern flanks; the central and eastern parts of the Hassi Messaoud field contain oils of higher maturity. The El-Agreb fields show the lowest maturity in the oils from the Hassi Messaoud ridge, similar to the oils from the Hassi Messaoud flanks. Finally, the El-Baguel and Mesdar oils are the most mature oils in the whole of the study area.

Table 4.12 Estimated vitrinite reflectance of the oil and source rock samples obtained using the North Sea sample set.

Nature of sample	Field	Reservoir	%Rm (TAS)	%Rm (MPI-1)
Oil	Hassi Messaoud	Cambrian	0.92 - 1.08	0.89 - 0.99
Oil	Oued Mya	Triassic	0.92 - 0.94	0.82 - 0.89
Oil	Rhourde Chegga	Triassic	1.01	0.91
Oil	Hassi Guettar	Cambrian	1.01 - 1.03	0.93 - 0.96
Oil	El-Agreb	Cambrian	0.99 - 1.02	0.83 - 0.91
Oil	Mesdar	Cambrian	1.05 - 1.07	1.01 - 1.03
Oil	El-Baguel	Cambrian	1.02 - 1.04	0.94 - 0.96
	Basin	Age		
Source rock	Oued Mya	Silurian	0.92 - 1.12	0.81 - 1.12
Source rock	Oued Mya	Ordovician	0.92 - 1.12	0.81 - 1.12

%Rm (TAS) = estimated vitrinite reflectance using the C_{20} TAS/[C_{20} TAS+C_{28} 5a(H) (S+R) TAS]

%Rm (MPI-1) = estimated vitrinite reflectance using the MPI-1

The same maturity ratios obtained from biomarkers and aromatic compounds used for source rocks and oils characterisation will be used in this section to compare maturity of source rock samples and oils.

The maturity-affected biomarker ratios $C_{29}Ts/(C_{29}Ts + C_{29}$ 17α(H) hopane), Ts/(Ts+Tm), and C_{23} tricyclic terpane/(C_{23} tricyclic terpane + C_{30} 17α(H) hopane), displayed in Figure 4.86 show a good correlation between the oils and Silurian source rock samples from group A. This confirms and strengthen the suggestion that these oils were mostly generated from these Silurian source rock strata. Silurian source rock samples from group B and Ordovician source rock samples reveal different features compared to Silurian samples from group A and the oils. The ratios plotted in these diagrams seem to be strongly affected by facies because the maturity parameters based on triaromatic steroid hydrocarbons, alkylnaphthalenes and alkylphenanthrenes and the calibration of the maturity parameters obtained from the aromatic hydrocarbons (see section 4.3.2.3) revealed the same range of maturity for all the Silurian and Ordovician source rock samples in the Oued Mya basin. Moreover, I also showed that these parameters are affected by the source facies differences between the source rock samples (see section 4.3.2.3.1 for more details). Therefore, the close similarities revealed by these ratios between oils and Silurian source rock samples from group A which can be observed in these plots, is additional strong evidence for a genetic relationship between the Silurian source rock samples from group A and the oils analysed in this project (see Figure 4.1 for geographical location of the Silurian source rock samples from group A).

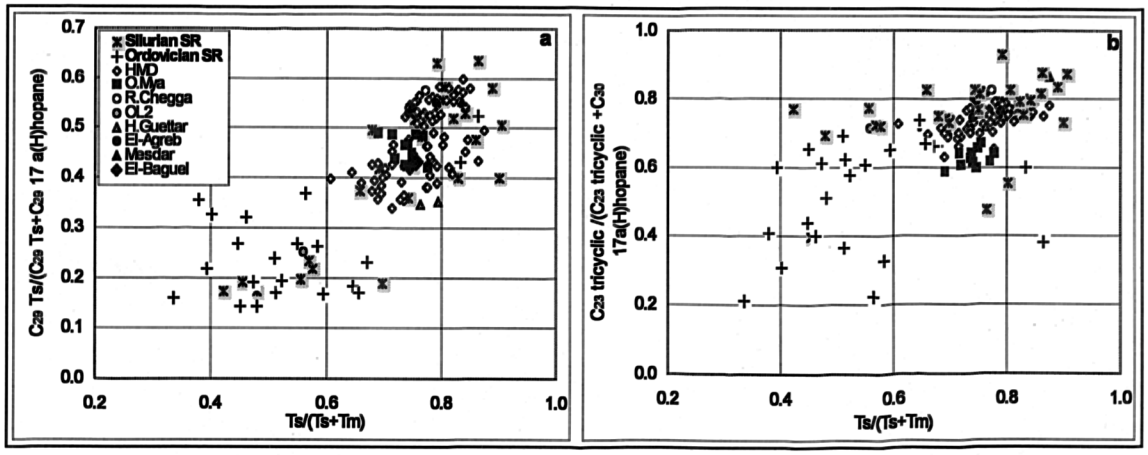

Figure 4.86 Cross plots of the maturity parameters (a) $C_{29}Ts/(C_{29}Ts + C_{29}17\alpha(H)$ hopane) versus Ts/(Ts+Tm) and (b) C_{23} tricyclic terpane/(C_{23} tricyclic terpane + $C_{30}17\alpha(H)$ hopane) for the source rock and oil samples analysed in the study area.

Aromatic maturity parameters based on the distributions of alkylnaphthalenes and alkylphenanthrenes are shown in Figure 4.87 and Figure 4.88. All these maturity parameters show similar levels of maturity between the oils and the Silurian source rock samples. Some Ordovician source rock samples from group C together with the Silurian source rock samples from the well GBC#1 (located southwest of the Oued Mya basin) exhibit higher maturity than the rest of the oil and source rock samples. Moreover, the maturity parameters based on the alkylphenanthrenes reveal that the oils from the fields located in the Oued Mya basin show the lowest maturity compared with the other oils, whereas Mesdar oils show the highest maturity.

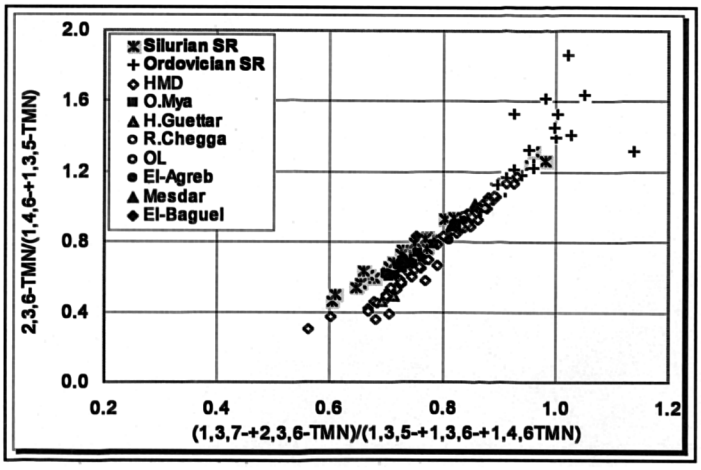

Figure 4.87 Cross plot of the alkylnaphthalene-based maturity parameters 2,3,6-TMN/(1,4,6-TMN+1,3,5-TMN) and (1,3,7-TMN+2,3,6-TMN)/(1,3,5-TMN+1,3,6-TMN+1,4,6-TMN) for the source rock and oil samples from the study area.

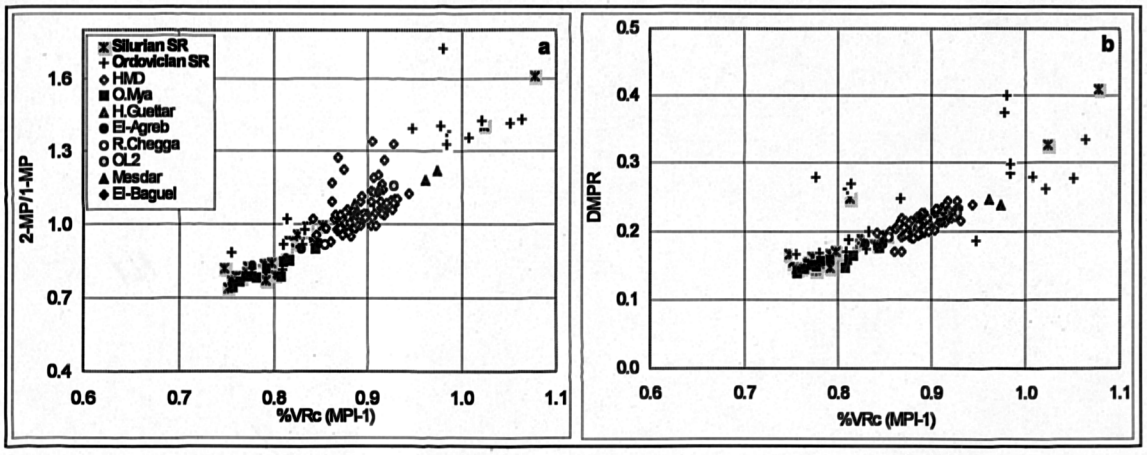

Figure 4.88 Cross plots of the alkylphenanthrene-based maturity parameters (a) 2-MP/1-MP versus %Rc (MPI-1) and (b) DMPR versus %Rc (MPI-1) for the source rock and oil samples from the study area. (%Rc (MPI-1) is the calculated vitrinite reflectance equivalent using MPI-1).

4.6. Summary

Ordovician and Silurian source rock samples revealed large variations in their organic carbon richness and facies. Most of the Silurian source rock samples exhibited extremely rich organic matter intervals represented by total organic content from 0.99 to 14.30 %TOC (average 9.2 %TOC). In contrast, Ordovician samples from different Formations (El Gassi shale, El Azzel shale, Micro-conglomeratic shale and Oued Saret Formations) revealed low to fair organic matter content ranging from 0.17 to 2.36 %TOC (average 0.82 %TOC) (Table 4.1). Therefore, the contribution of Ordovician formations to the generation of the oils in the region of Oued Mya basin and Hassi Messaoud Ridge is likely to be lower compared with the Silurian source rock intervals. This is in agreement with the conclusions established earlier by Daniels and Emme (1995); Makhous et al. (1997a,b); Boote et al. (1998) and Lünning et al. (2000), who stated that the Silurian strata are the main source for all the oils in the study area.

Facies characterisation of the source rock samples using principal components analysis and biomarker ratios enabled me first to distinguish Silurian samples from Ordovician samples, and second to separate Silurian samples into two groups. Group A contains 13 samples from wells: BAT#1 (3 samples); OA#1bis (3 samples); BKZ#1 (4 samples); GEC#1 (1 sample) and TKT#1 (2 samples) and Silurian group B contains 7 samples from wells: GD#1bis (1 sample); GLNE#4bis (1 sample); GLNE#5 (3 samples) and GBC#1 (2 samples) (Figure 4.1). Moreover, 4 samples from well RDC#2, 2 samples from well OA#1bis and to a lesser extent samples from wells

GLNE#4bis (3874.85m), BKZ#1 (4187.86m and 4189.95m) and GLNE#5 (4001.45m) revealed unusual *n*-alkane distributions and a dominance of the aromatic hydrocarbons over the n-alkanes and isoprenoid alkanes. The organic matter in these samples has probably suffered alteration by irradiation from the natural decay of uranium.

Maturity evaluation of source rock samples based on biomarkers and aromatic hydrocarbon distributions revealed a similar range of maturity levels between the Silurian and Ordovician source rock samples. The calibration of the maturity of my source rock samples by comparison to a North Sea sample set with known %Rm values and biomarker and aromatic maturity parameters showed estimated %Rm ranging from 0.81 to 1.12 suggesting that both the Ordovician and Silurian strata in the Oued Mya basin have reached the "main stage of the oil window - end of the oil window". This is consistent with the Tmax values obtained from pyrolysis which showed values ranging from 440°C to 458°C for the Silurian and 439°C to 459°C for the Ordovician source rock samples (Table 4.1). Moreover, the Silurian source rock strata revealed a northeast -southwest trend of increasing maturity in the Oued Mya basin.

Principal components analysis and most of the facies-based parameters employed in this project using *n*-alkane, isoprenoid alkane and biomarker alkane distributions, clearly separate the oil samples into three major groups and one subgroup. Group I includes 1 oil sample from Rhourde Chegga Triassic field, 81 oil samples from Hassi Messaoud, 2 oil samples from Hassi Guettar and 3 oil samples from El-Agreb Cambrian fields; group II comprises 7 oil samples (2 oil samples from Benkahla field, 4 oil samples from Haoud Berkaoui field and 1 oil from Draa Temra); subgroup IIa contains 4 oil samples (1 oil sample from Mokh-El-Kabch field, 1 oil sample from N'goussa field, 1 oil sample from Guellala Northeast field and 1 oil sample from Guellala field); and group III contains 2 samples from Mesdar and 2 samples from El-Baguel fields (Figure 4.1).

The calibration of the maturity of the oil samples analysed in this project by comparison to the North Sea sample set mentioned above revealed an estimated vitrinite reflectance %Rm similar to that obtained for the Silurian and Ordovician source rock strata, ranging from 0.88 to 1.08% for the oils from group I (oils from

Hassi Messaoud, Rhourde Chegga, Hassi Guettar, El-Agreb fields), 0.82 to 0.94 for the oils from group II (oils from the fields in the Oued Mya basin), and 0.94 to 1.07 for the oils from group III (i.e. oils from Mesdar and EL-Baguel fields).

Oil-source rock correlations revealed that all the oils from group I containing the oils from Hassi Messaoud, Hassi Guettar, Rhourde Chegga and El-Agreb fields display similar facies features to the Silurian source rock samples from group A. Therefore, I can suggest that there is a high probability that all these oils were generated from Silurian source rock intervals having similar features as those in group A. The only differences encountered among the oils in group I are shown to be mainly due to maturity differences. In general, the oils in group I show a maturity trend decreasing from Hassi Messaoud field towards El-Agreb fields via Hassi Guettar field (Figure 4.1). Moreover, in the Hassi Messaoud field, there is a trend of decreasing maturity from the centre toward the flanks of the field. The oils from group II and subgroup IIa (located in the Oued Mya basin) revealed similar features to both the Silurian source rock samples and the Ordovician source rock samples. However, it is likely that the Silurian source rock strata have contributed in much higher proportions than the Ordovician source rock strata for the generation of these oils as the biomarker and aromatic hydrocarbon ratios together with the principal components analysis showed that these oils plot relatively closer to the Silurian source rock samples from group A than to the Ordovician source rock samples. These oil samples also revealed the lowest maturity compared to the rest of the oils from groups I and III.

Earlier in section 4.3.1.2.2, I have shown that the Ordovician samples contain ortho-, meta- and para-terphenyl isomers, benzene, 1,1'-cyclohexylidenebis, 2,6-diisopropylnaphthalene, p-dicyclohexylbenzene and bicyclohexyl, 4-phenyl. The Silurian samples from group B also revealed the presence of these compounds, however, in much lower concentrations than in the Ordovician source rock samples. These compounds were not encountered in the oil samples analysed in this project nor in the Silurian samples from group A. This observation strongly supports the suggested genetic relationship between the Silurian source rock samples from group A (and probably group B) and the oil samples analysed in this project. It appears that the contribution of the Ordovician source rock formations to the oils is much lower than the Silurian source rock strata.

The maturity trend exhibited by the source-related oils in group I, group II and subgroup IIa may have important implications in the study of the extent of petroleum migration processes in the Oued Mya-Hassi Messaoud petroleum system (for more details see Chapter 5). In this particular situation, it is predicted that the oils currently reservoired in the Triassic accumulations in the Oued Mya basin (i.e. Benkahla and Haoud Berkaoui fields) represent early expelled oils from the subsiding Silurian source rock strata within the same basin. With increasing source rock subsidence, progressively more mature oil would have been generated, expelled and subsequently migrated updip onto the Hassi Messaoud ridge to charge the Hassi Messaoud trap and continue laterally towards Hassi Guettar field and then El-Agreb fields (Figure 4.1). The most mature oils from the centre and east of the Hassi Messaoud field are likely to represent the entrapment of a relatively late expelled product from the subsiding Silurian source rock strata in the study area.

Oil samples from Mesdar and El-Baguel Cambrian fields were also generated from source rocks having similar features as the Silurian source rock in Oued Mya basin. However, these oils showed the lowest *n*-alkane and isoprenoid alkane concentrations (Tabel 4.8 and Figure 4.46), highest steranes/17α(H)hopanes and tricyclic terpanes/17α(H)hopanes ratios (Figure 4.49), lowest diasteranes/regular steranes ratios (Figure 4.50), lowest biomarker concentrations, highest aromatic hydrocarbon concentrations (Figure 4.80) and highest maturity ratios (Figure 4.62) compared to the rest of the oils analysed in this study. All these criteria would suggest that these oils were generated from another source rock; most likely from the Silurian source rock strata in the Berkine basin.

Daniels and Emme (1995), Makhous et al. (1997a,b) and unpublished reports from Sonatrach showed that the Silurian source rocks in the Berkine basin are more mature (i.e. $\%R_m$ = 1.08 – 1.3) than in the Oued Mya basin (i.e. $\%R_m$ = 0.7 – 0.9). In the Berkine basin depocentre, Silurian sediments are even overmature. Hence, Mesdar and El-Baguel oils were probably generated from the Silurian strata located in the western flanks of Berkine basin.

The evolution of the biomarker-based maturity parameters investigated in this work appears to result from a preferential depletion of the least stable isomers. The decrease in the concentrations of the biomarkers as a function of increasing maturity has been

accredited to the combined effects of thermal cracking of the biomarker molecules themselves, as well as progressive dilution by the hydrocarbons (alkanes and aromatic hydrocarbons) released continuously from the source kerogen throughout the oil generation process.

The evolution of the short-chain relative to the long-chain triaromatic steroid hydrocarbon-maturity parameter observed in this study also appears to result from a preferential thermal degradation of the long- versus the short-chain triaromatic steroid hydrocarbons.

Finally, the evolution of the alkylnaphthalene-based maturity parameters appears to result from the shift of the methyl groups from the less stable "α" position to the thermodynamically more stable "β" position. The same process was also shown for the methylbiphenyl isomers, where the less stable isomer with methyl group in *ortho*-position migrates to the more stable *meta*-position with increasing maturity.

Chapter 5
Oil Migration and Charging Directions of the Reservoirs of the Oued Mya – Hassi Messaoud Ridge Petroleum System

5. Oil migration and charging directions of the reservoirs of the Oued Mya-Hassi Messaoud ridge petroleum system

5.1. Introduction

The aims of this chapter are to establish the migration and filling directions of petroleum from the source rocks located in the Oued Mya basin towards the fields located in the Oued Mya-Hassi Messaoud petroleum system. This is in turn vital to assist geologists for successful exploration of new and economically viable petroleum reserves in the region.

In this chapter, I will assess the occurrence and the effect of source facies and maturity on the concentration and distribution of the alkylcarbazoles and benzocarbazoles in the Silurian and Ordovician source rocks in the Oued Mya basin. The alkylphenols were not investigated for the source rock samples because of the difficulties encountered in their quantification.

The next step will be devoted to the study of the application of the variation in the biomarker and aromatic hydrocarbon distributions, together with the concentrations and distributions of the pyrrolic nitrogen compounds (alkylcarbazoles and benzocarbazoles) in the characterisation of migration-related compositional changes in the oils. The aims of these sections are the understanding of the migration and charging directions of the oils reservoired in the Devonian and the Lower Triassic fields located in the Oued Mya basin, the Cambro-Ordovician Hassi Messaoud field and the other fields: Hassi Guettar (Cambrian and Ordovician), El Agreb (Cambrian), Mesdar and El Baguel (Cambrian) located in the Hassi Messaoud ridge, respectively (Figure 5.1).

The oil fields will be discussed following their geographical location compared to the location of the source rock strata in the Oued Mya basin. Thus, I will start with the Devonian and the Triassic fields located in the Oued Mya basin, then the nearest field from the Oued Mya basin, which is Hassi Messaoud (about 40-60 km east-southeast from the Oued Mya basin), followed by Hassi Guettar satellite field (about 5 km south from Hassi Messaoud), El-Gassi-Zotti-El-Agreb fields (about 70, 80, and 95 km south-southwest from Hassi Messaoud, respectively), and finally Mesdar and El-

Baguel fields located about 80 km east of Hassi Messaoud and 10 to 20 km west-northwest flanks of the Berkine basin. A large part of this chapter will be allocated to the understanding of the migration routes and charging directions of the giant Hassi Messaoud field. It will be shown that lateral and vertical chemical compositional variations are observed throughout the petroleum columns of the Hassi Messaoud field as a result of field charging. At the end of this chapter, I will synthesise all the results and discussions described throughout this chapter.

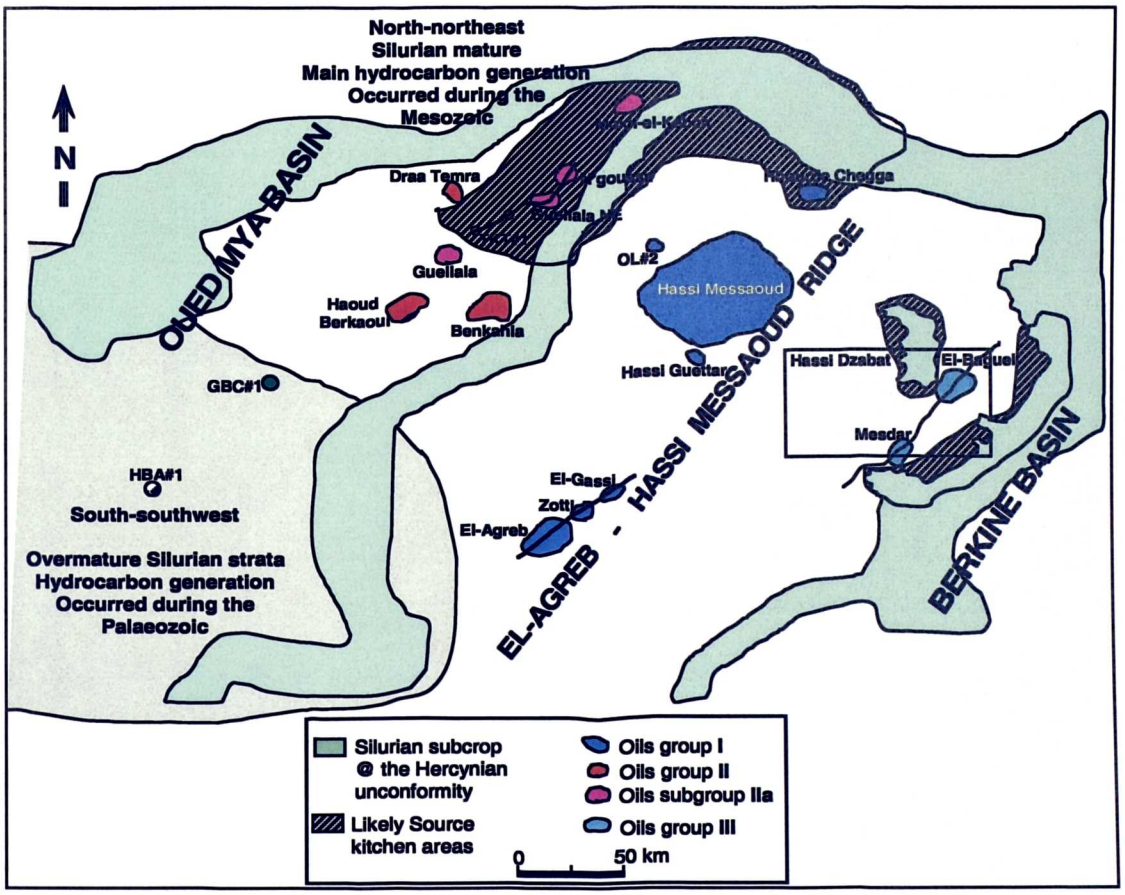

Figure 5.1 Location map showing the geographical position of the fields analysed in this study. The lines crosscutting the fields show the location of the cross sections used in sections 5.5, 5.8, and 5.9.

Statistical evaluation of the geochemical controls on the overall distribution of pyrrolic compounds in the Silurian and Ordovician source rocks from the Oued Mya basin

In this section, I will use principal components analysis to evaluate the effect of source facies and maturity on the distributions, concentrations and ratios calculated from the alkylcarbazoles and benzocarbazoles in a suite of 26 Silurian and 6 Ordovician source rock samples taken from the Oued Mya basin (Figure 4.1). The Silurian source rock samples analysed in the Oued Mya basin revealed a wide range

of total organic carbon content (TOC) ranging from 0.99 to 14.30 %wt (average 8.90%wt). The hydrogen index HI in the same samples ranges from 21.10 to 255.89 mg HC/g TOC (average 174.07 mg HC/g TOC) (see Table 4.1 in chapter 4). The Silurian source rock samples from the northeast of the Oued Mya basin exhibited a narrow maturity interval, and the calculated vitrinite reflectance equivalent ranges from 0.75 to 0.88 %Rc, however two samples from the southwest of the Oued Mya basin (i.e. well GBC#1, see Figure 4.1 in chapter 4) showed higher calculated vitrinite reflectance values (ca 1.02 and 1.08 %Rc). The Ordovician source rock samples showed a narrow range of TOC values varying from 0.47 to 1.62 %wt, and relatively small maturity changes (ca 0.78 to 1.06 %Rc). The concentrations and ratios calculated from the alkylcarbazole and benzocarbazole distributions in the Silurian and Ordovician source rock samples analysed in this study are listed in Appendix 5.1.

Principal components analysis can be used to indicate the existence of possible correlations among the variables. In an attempt to study the inherent relationship between the pyrrolic compounds and other geochemical parameters reflecting facies and maturity of the source rocks, PCA was performed on a geochemical data set derived from the analysis of the Silurian and the Ordovician source rock samples. The data set consists of the total organic carbon content (TOC), the residual petroleum potential (S2), the hydrogen index (HI), two maturity parameters: calculated vitrinite reflectance (%Rc) and C_{20} triaromatic steroid/[C_{20} triaromatic steroid + C_{28} 5α(H) triaromatic steroid (S+R)] ratio, the concentrations and the isomeric ratios of the alkylcarbazoles and benzocarbazoles, using the software "SPSS for Windows". The data matrix is composed of 30 samples and 20 variables (Table 5.1). The first three principal components (PCs) obtained, explain 53.09%, 17.73%, and 7.17% of the variance within the scaled data set, respectively. This allows the relationships between the samples to be examined in simple two-dimensional score plots: PC1 versus PC2 and PC1 versus PC3, which include the effects of all the original variables, and display the bulk (77.99%) of the scaled data variability (Figure 5.2).

The samples highlighted in the left sides of the diagrams in Figure 5.2 (negative PC1) consist of those from the Silurian source rock samples GLNE#3 (3803.45, 3809.45m), GEC#1 (3660.6m), and GBC#1 (3213, 3259m) and all the Ordovician samples. Interestingly, samples from wells GLNE#3 and GEC#1 together with all the

Ordovician samples revealed relatively low TOC and S2 compared to the source rock samples plotted in the right side of these diagrams (positive PC1). However, the samples from well GBC#1 exhibited relatively high TOC values, low S2 values and the highest maturity in the data set (Table 4.1). The remaining Silurian source rock samples plotted in the right side of these diagrams (positive PC1) revealed extremely high TOC values (>7%wt) and higher residual potential (S2>10.3 mg HC/g rock). Moreover, PC3 discriminates the samples RDC#2 (3804.7, 3806.4, 3808.35, 3810.80m) and OA#1bis (4145.35m) which showed the highest alkylcarbazole and benzocarbazole concentrations compared to the rest of the samples. These samples also exhibited GC traces highly depleted in n-alkanes and dominated by alkylnaphthalene and alkylphenanthrene aromatic hydrocarbons (see section 4.3.1 and Figures 4.7 and 4.8 in chapter 4).

The loadings plots from the analysis (Figure 5.3) explain what these three PCs (PC1, PC2, and PC3) represent. These diagrams exhibit the loadings of the different variables within the principal components; large loadings, either positive or negative, indicate a significant influence of the variable on that PC. Hence, it is usual to regard principal loadings as "high" if the values of the loadings are greater than 0.6 (either positive or negative), and "moderately high" if above 0.3 (Kline, 1994). Low loading values (<0.3) may imply that there is no, or almost no, correlation between the variables and the principal component.

The first factor (PC1) explains 53.09% of the total variance of the data set, on which high loadings (>0.6) are obtained for the total organic carbon content (TOC), the residual petroleum potential S2, the concentrations of alkylcarbazoles and benzocarbazoles, the isomeric ratios 1,8-DMC/(1,8-DMC+1-EC), 1,8-DMC/(1,8-DMC+1-MC), 1,8-DMC/(1,8-DMC+4-MC), and the benzocarbazole ratio [a]/([a]+[c]). In addition the loadings of the HI, the calculated vitrinite reflectance (%Rc), and 1,8-DMC/(1,8-DMC+3,4-DMC) are moderately high loadings (>0.3). Accordingly, it could be considered that the source facies represented by the TOC, the residual potential and HI of the source rocks have a strong effect on the concentrations and isomeric ratios of pyrrolic compounds in the Silurian and Ordovician source rock strata in the Oued Mya basin.

The second factor (PC2) accounts for 17.73% of the total variance of the data set; high loadings (>0.6) are obtained for the maturity parameters %Rc and C_{20} TAS/[(C_{20} TAS + C_{28} 5α(H) (S+R) TAS] and the alkylcarbazole ratios 1,8-DMC/(1,8-DMC+1,6-DMC) and 1,8-DMC/(1,8-DMC+3,4-DMC). Moderately high loadings (>0.3) are obtained for the hydrogen index (HI), the ratios 1,8-DMC/(1,8-DMC+1-EC), 1,8-DMC/(1,8-DMC+1-MC), 1,8-DMC/(1,8-DMC+4-MC), 1,8-DMC/(1,8-DMC+2,6-DMC), $C_3/(C_1+C_3)$ and [a]/([a]+[c]). Therefore, PC2 indicates variations in the alkylcarbazole ratios that may be controlled by the maturity and to a lesser extent the organic matter quality (HI) of the Silurian and Ordovician source rocks.

The third factor (PC3) is less important than the two first factors, explaining just 7.17% of the total variance of the data set. PC3 shows only moderately high loadings obtained for the alkylcarbazole ratio 1,8-DMC/(1,8-DMC+1-MC), 1,8-DMC/(1,8-DMC+2,6-DMC) and concentrations of the C_2 exposed isomers and trimethylcarbazoles and the [a]/([a]+[c]) ratio. This factor seems to be controlled by other factors than source facies and maturity of the source rocks.

In summary, the results of the principal components analysis can be taken to tentatively suggest that the concentrations and most of the isomer ratios of the alkylcarbazoles and benzocarbazoles are mainly affected by the quantity and to a lesser extent to the quality of the organic matter in the Silurian and Ordovician source rocks. Indeed, these observations are strongly supported by the plots of the three factors PC1, PC2 and PC3 against the TOC, HI and %Rc (Figure 5.4). PC1 which accounts for 53.09% of the total variance of the data set shows strong correlation (R^2=0.72) with the TOC and poor correlation (R^2=0.29) with maturity parameter %Rc. PC2 which accounts for 17.73%, shows a good correlation (R^2=0.66) with the HI and strong correlation with %Rc (R^2=0.85), finally PC3 which explains 7.17%, reveals no correlation with the source facies and the maturity parameters. In the following section I will focus mostly on the effect of source facies on the concentrations and distributions of alkylcarbazoles and benzocarbazoles, in addition to the effect of maturity on some of the alkylcarbazole ratios.

Table 5.1 List of the parameters used in the principal components analysis for the source rocks.

Source facies	
1	TOC (wt%)
2	S2 (mg HC/g rock)
3	HI (mg HC/g TOC)
Maturity parameters	
4	%Rc
5	C_{20} TAS/[(C_{20} TAS+C_{28} 5α(H) TAS(S+R)]
Alkylcarbazole concentrations (ug/g extract)	
6	Carbazole
7	Sum methylcarbazoles
8	1,8-Dimethylcarbazole
9	Sum partially shielded dimethylcarbazoles
10	Sum exposed dimethylcarbazoles
11	Sum trimethylcarbazole
Alkylcarbazole ratios	
12	1,8-DMC/(1,8-DMC+1-EC)
13	1,8-DMC/(1,8-DMC+1-MC)
14	1,8-DMC/(1,8-DMC+4-MC)
15	1,8-DMC/(1,8-DMC+1,6-DMC)
16	1,8-DMC/(1,8-DMC+2,6-DMC)
17	1,8-DMC/(1,8-DMC+3,4-DMC)
18	C_3/(C_1+C_3)
Benzocarbazoles	
19	Sum benzocarbazoles ([a] + [b] + [c]) (ug/g extract)
20	Benzocarbazole ratio [a]/([a]+[c])

Key: '%Rc = calculated virinite reflectance using the MPI-1 parameter;
MC = methylcarbazole
DMC = dimethylcarbazole
EC = ethylcarbazole
C_1 = Sum methylcarbazoles
C_3 = Sum trimethylcarbazoles

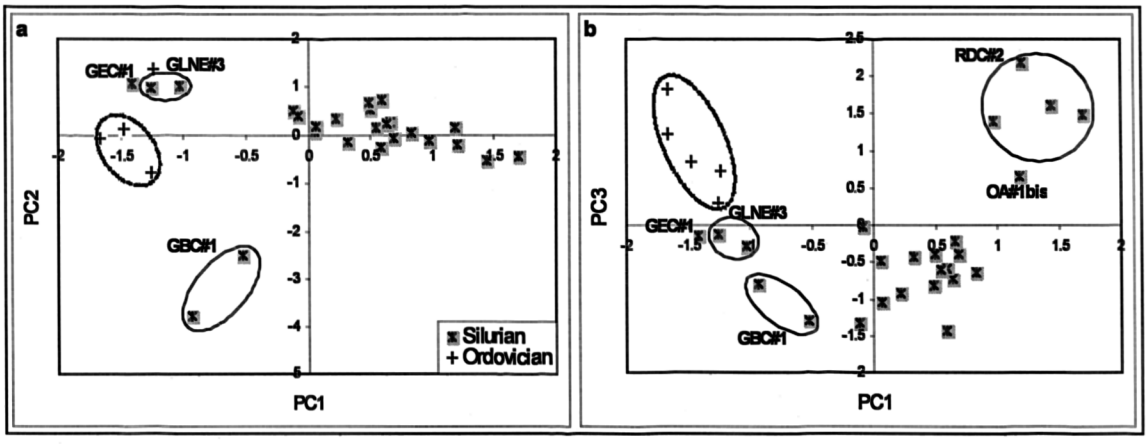

Figure 5.2 Scores plots (a) PC1 versus PC2 and (b) PC1 versus PC3 showing the relationship between the Silurian and Ordovician source rock samples in terms of the first, second and third principal components. PC1 explains 55.74% of the total variance in the scaled data set, PC2 explains a further 12.97%, and PC3 explains a further 11.67%.

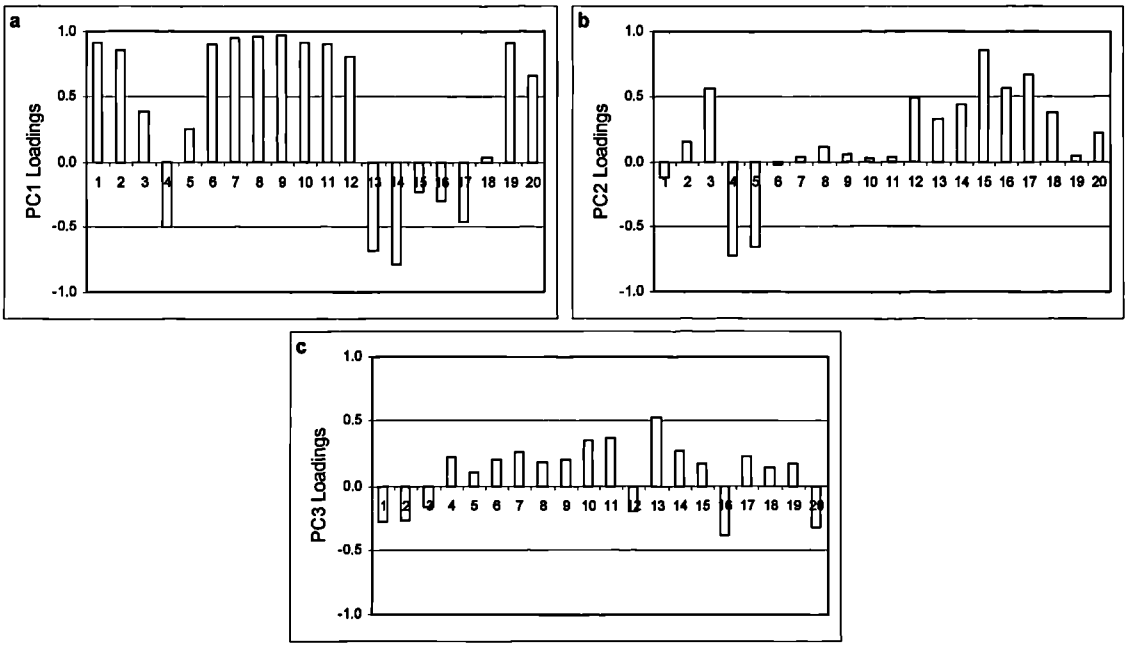

Figure 5.3 Loadings plots showing the composition of the first three principal components, which scored 55.74%, 12.94%, and 11.67% of the total variance in the data set, respectively.

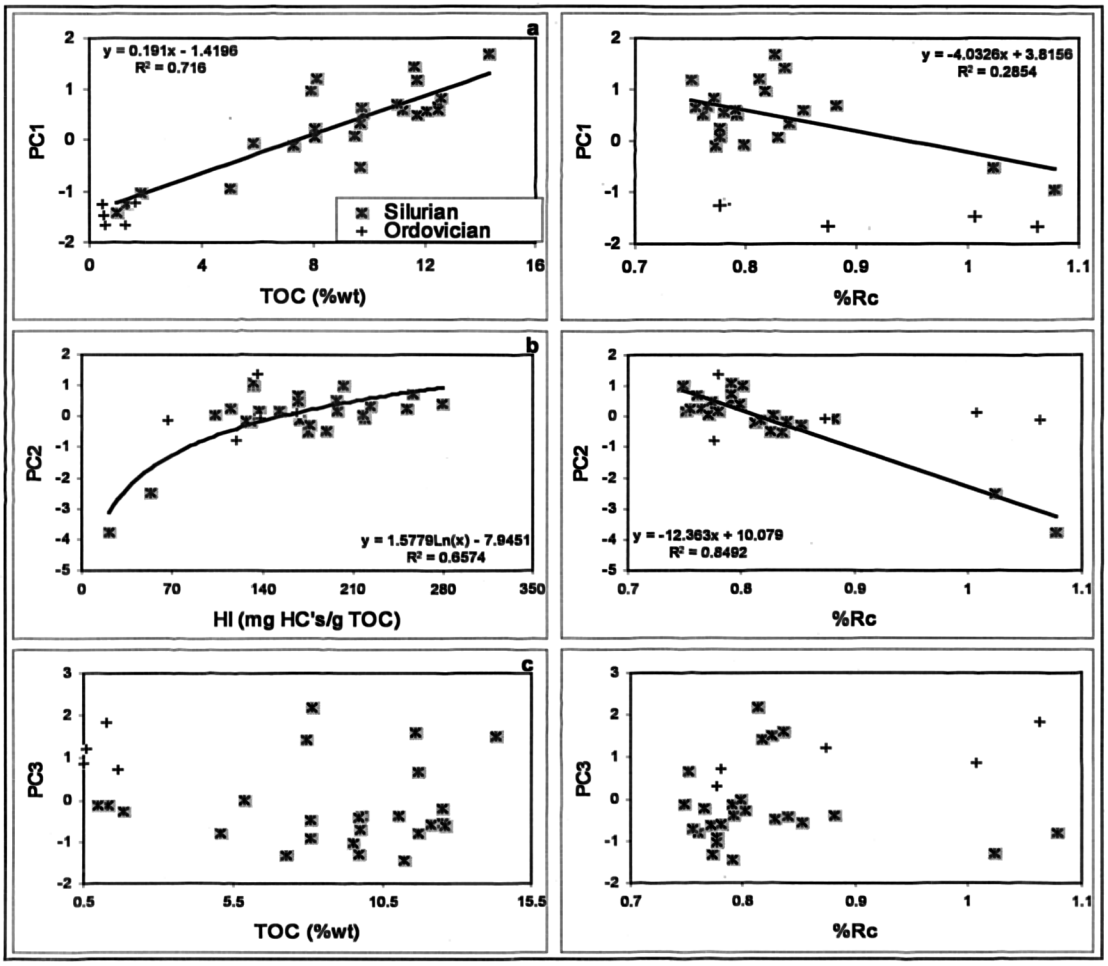

Figure 5.4 Cross plots of the three principal components (a) PC1, (b) PC2, and (c) PC3 versus the source facies and calculated vitrinite reflectance maturity parameters for the Silurian and Ordovician source rock samples.

5.2.1. Geochemical control on pyrrolic compound distributions in the Silurian and Ordovician source rocks

The results obtained from the principal components analysis suggested that the concentrations of alkylcarbazoles and benzocarbazoles, the isomer ratios 1,8-DMC/(1,8-DMC+1-EC), 1,8-DMC/(1,8-DMC+1-MC), 1,8-DMC/(1,8-DMC+4-MC), 1,8-DMC/(1,8-DMC+3,4-DMC) and [a]/([a]+[c]) in the Silurian and Ordovician source rocks might be related to the abundance of the organic matter in the shales. Whereas, it appears that the maturity is affecting only the distribution of alkylcarbazoles (e.g. 1,8-DMC/(1,8-DMC+1,6-DMC); 1,8-DMC/(1,8-DMC+3,4-DMC); 1,8-DMC/(1,8-DMC+1-EC) and 1,8-DMC/(1,8-DMC+1-MC) ratios). Therefore, in this section I will emphasise my investigation on the possible relationship between the alkylcarbazole and benzocarbazole concentrations and distributions with the total organic carbon content and the residual petroleum potential of the Silurian and Ordovician source rock strata. Moreover, I will briefly show the maturity (%Rc) effect on some of the alkylcarbazole ratios.

5.2.1.1. Effect of the organic matter content and the residual potential of the Silurian and Ordovician source rocks on the alkylcarbazole and benzocarbazole concentrations and disfributions

The parameters selected for this investigation are listed in Table 5.2 and the values are listed in Appendix 5.1.

Table 5.2 Parameters selected following the principal components analysis.

Alkylcarbazole concentrations (ug/g extract)	
1	Sum alkylcarbazoles
2	1,8-dimethylcarbazole
3	Sum partially shielded dimethylcarbazoles
4	Sum exposed dimethylcarbazoles
Alkylcarbazole ratios	
1	1,8-DMC/(1,8-DMC+4-MC)
2	1,8-DMC/(1,8-DMC+1-MC)
3	1,8-DMC/(1,8-DMC+1-EC)
3	1,8-DMC/(1,8-DMC+1,6-DMC)
4	1,8-DMC/(1,8-DMC+3,4-DMC)
Benzocarbazoles	
1	Sum benzocarbazoles ([a] + [b] + [c]) (ug/g extract)
2	Benzocarbazole ratio [a]/([a]+[c])

The summed concentrations of alkylcarbazoles in the Silurian and Ordovician source rock samples range from 37.78 to 1600.87 μg/g extract and from 4.09 to 93.84 μg/g extract, respectively and the summed benzocarbazole isomers range from 3.30 to 171.75 μg/g extract and from 0.24 to 7.98 μg/g extract, respectively (Appendix 5.1). The summed concentrations (μg/g extract) of C_0-C_3 alkylcarbazoles and the benzocarbazole isomers [a], [b] and [c] in the Silurian and the Ordovician rock samples are plotted against the total organic carbon content (TOC) and the residual petroleum potential (S2) (Figure 5.5). The summed concentrations of C_0-C_3 alkylcarbazoles and benzocarbazole isomers appear to be positively correlated to TOC and S2 in the samples analysed in the Silurian and Ordovician source rock samples. In addition, the concentrations of the shielded isomer (1,8-dimethylcarbazole), the partially shielded isomers, (PS DMC: 1,3-DMC + 1,6-DMC + 1,7-DMC), and the exposed isomers, (Exp DMC: 2,3-DMC + 2,4-DMC + 2,5-DMC + 2,6-DMC + 3,4-DMC) also reveal positive correlations with the TOC and S2 (Figure 5.6). These findings agree well with the results shown by Chen (1995) and Bennett et al. (2002) in a set of samples from the intra-reservoir shales of the Miller field (North Sea). These authors tentatively suggested that the distribution of pyrrolic nitrogen compounds could be related to the organic matter abundance in the intra-reservoir shales. Therefore, correlations of source rock organic carbon content and residual potential with alkylcarbazole and benzocarbazole concentrations indicate that source organic matter exerts a strong influence on alkylcarbazole and benzocarbazole concentrations, and suggest that the retention of alkylcarbazoles and benzocarbazoles in the Silurian source rocks may well be controlled by sorptive interaction of these class of compounds with organic matter.

Samples showing the highest concentrations of C_0-C_3 alkylcarbazoles and benzocarbazole isomers highlighted (enclosed in a ring) in the diagrams plotted in Figure 5.5 and Figure 5.6 are the Silurian source rock samples from the wells RDC#2 (3804.7, 3806.4, 3808.35, 3810.80m), OA#1bis (4142.25; 4145.35m), GLNE#4bis (3874.85m), and GLNE#5 (4001.45m). Interestingly, all these samples exhibited gas chromatograms dominated by the alkylnaphthalene and alkylphenanthrene aromatic hydrocarbons over the *n*-alkanes and isoprenoid alkanes (see Figures 4.7 and 4.8 in chapter 4). I have suggested that the organic matter analysed in these samples had probably suffered alteration by irradiation from the natural decay of authigenic

uranium (for more details see section 4.3.1 in chapter 4). Dahl et al. (1988) demonstrated that the organic matter in the Cambrian Alum shales of Sweden have been altered by irradiation from the natural decay of uranium. In addition, they showed that bitumen with high uranium concentrations tends to be relatively enriched in aromatic hydrocarbons and contains a larger percentage of polars, asphaltenes and resins. The Silurian samples named above exhibit similar features to the organic matter from the Alum shales such as: higher concentrations of aromatic hydrocarbons (Appendix 4.2), lower HI (Table 4.1), and higher pyrrolic compound concentrations (Appendix 5.1). Hence, the high concentrations of the nitrogen compounds (polar compounds) in the Silurian organic matter represented by these samples are likely due to the loss of the n-alkanes and isoprenoid alkanes (probably caused by irradiation from the natural decay of uranium).

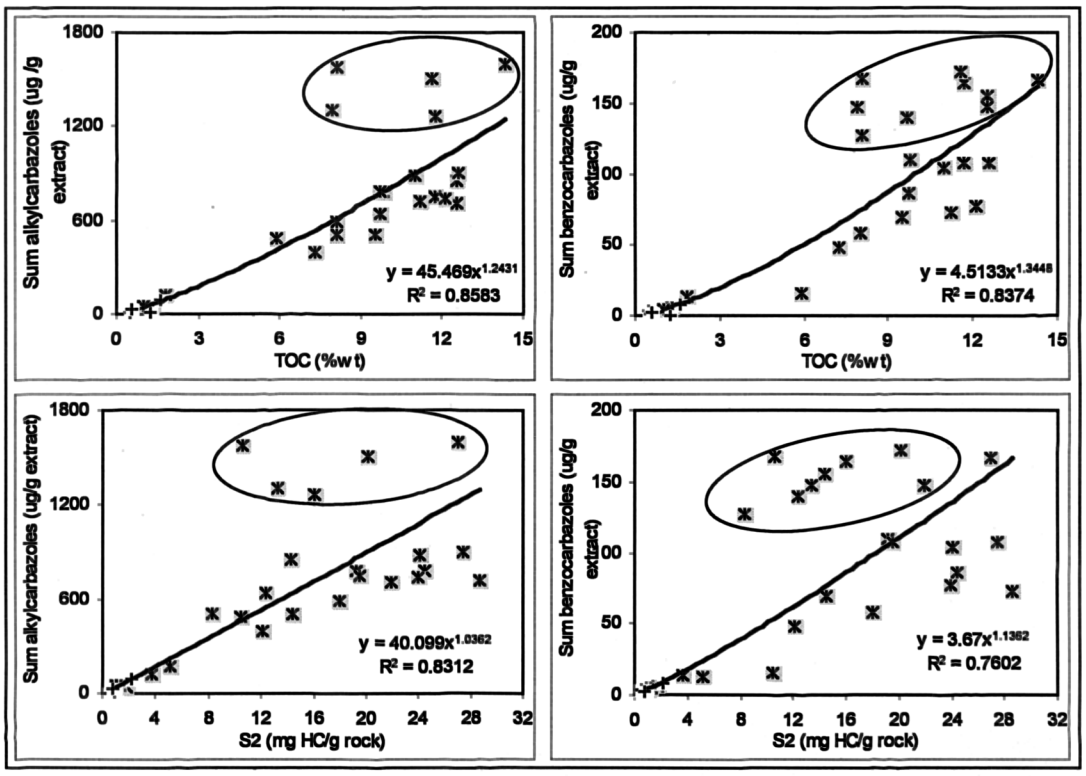

Figure 5.5 Plots of the summed concentrations of C_0-C_3 alkylcarbazoles and the summed concentrations of benzocarbazole isomers (μg/g extract) versus TOC and S2 in the samples from the Silurian and Ordovician source rocks of the Oued Mya basin.

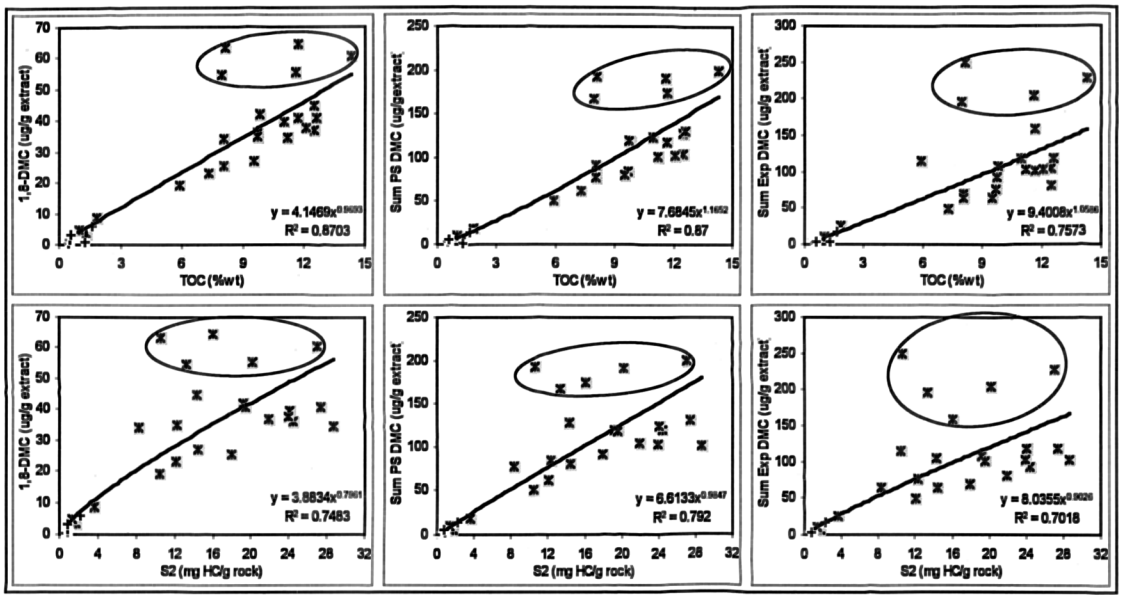

Figure 5.6 Plots of the concentrations of dimethylcarbazoles (μg/g extract) versus TOC and S2 in the samples from the Silurian and Ordovician source rocks of the Oued Mya basin. Key: DMC=dimethylcarbazoles, PS = partially shielded, Exp = exposed.

Furthermore, the ratios which revealed high and moderately high loadings on PC1 (Table 5.2) are plotted as a function of the quantity of organic matter expressed by TOC and S2 (Figure 5.7). All these ratios show fair to good correlation with the TOC and S2. For example, isomeric ratios of 1,8-DMC/(1,8-DMC+1-MC), 1,8-DMC/(1,8-DMC+4-MC), 1,8-DMC/(1,8-DMC+3,4-MC) and 1,8-DMC/(1,8-DMC+1,6-MC) are, to some extent, inversely correlated to TOC and S2, whereas the ratios of 1,8-DMC/(1,8-DMC+1-EC) and [a]/([a]+[c]) appear to be, in general, directly correlated to TOC and S2 (Figure 5.7). Chen (1995) also showed similar trends of these ratios as a function of TOC in the samples from the intra-reservoir shales of the Miller field (North Sea).

These relationships tentatively suggest that the distribution of alkylcarbazole and benzocarbazole compounds could be related to the organic matter abundance in the Silurian and Ordovician shales. The retention of the partially shielded and exposed alkylcarbazole isomers together with the benzo[a]carbazole isomer seem to be directly related to the abundance of organic matter in the shales. This is in agreement with the findings of Bennett et al (2002), when they showed an increase of [a]/([a]+[c]) ratio with the total organic carbon content (TOC) in the Brae Formation (North Sea). Bennett et al. (2002) concluded that the benzo[a]carbazole isomer is more highly retained by the source organic matter than the benzo[c]carbazole. Moreover, the

relatively fair relationship of some ratios as a function of the organic matter abundance may have another explanation. It is possible that other factors such as the petroleum expulsion efficiency, the proportion of reactive and/or inert kerogen may also have a major effect on the concentrations and distributions of the pyrrolic nitrogen compounds (Chen, 1995).

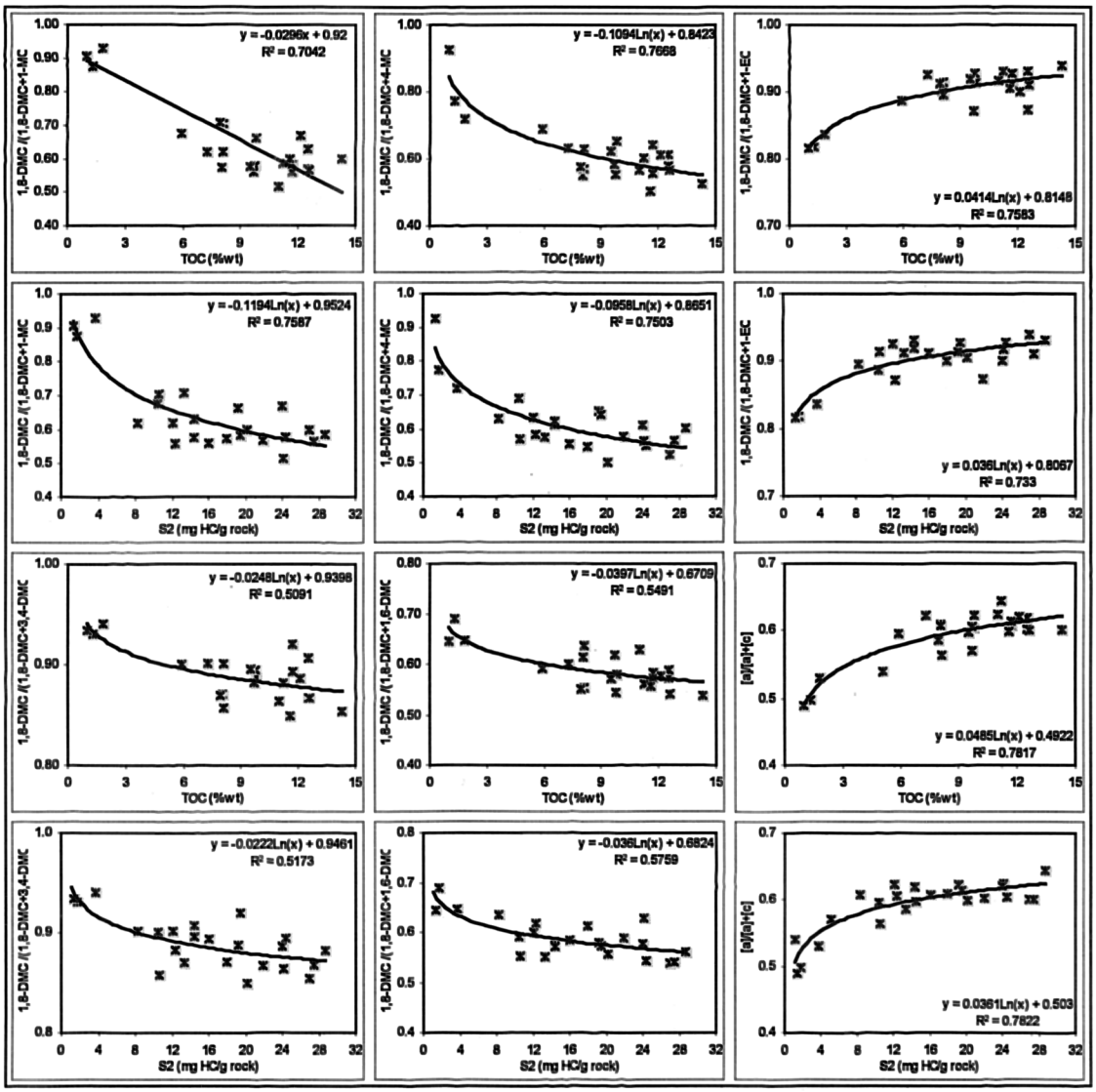

Figure 5.7 Isomeric variations of methyl- and dimethylcarbazoles and benzocarbazoles as a function of TOC and S2 in the samples from the Silurian source rocks in the Oued Mya basin.

5.2.1.2. Effect of the maturity of the Silurian and Ordovician source rocks on the alkylcarbazole and benzocarbazole concentrations and distributions

I mentioned above that the alkylcarbazole and benzocarbazole concentrations are mostly affected by the abundance of organic matter of the source rock samples; however the isomer ratios 1,8-DMC/(1,8-DMC+1,6-DMC), 1,8-DMC/(1,8-DMC+3,4-DMC), 1,8-DMC/(1,8-DMC+1-EC) and 1,8-DMC/(1,8-DMC+1-MC)

which showed high loadings in the second factor PC2 also appear to be affected by maturity (Figure 5.8). All these ratios show a fair to good inverse correlation to the calculated vitrinite reflectance (%Rc). From these plots, it is clear that the effect of maturity is obvious at higher maturity (i.e. Rc>1%). In fact most of my samples cover a narrow maturity range between 0.75 to 0.88 %Rc, only two samples from well GBC#1 located south-southwest of the Oued Mya basin reveal higher maturity. Several authors showed that the distribution of the alkylcarbazoles and benzocarbazoles is affected by maturity (Clegg et al., 1997, 1998a and b; Horsfield et al., 1998; Bennett et al., 2002). These authors showed an overall increase of the alkylcarbazole and benzocarbazole ratios up to 0.88% R_r, followed by a decrease at higher maturity (>1.3% R_r).

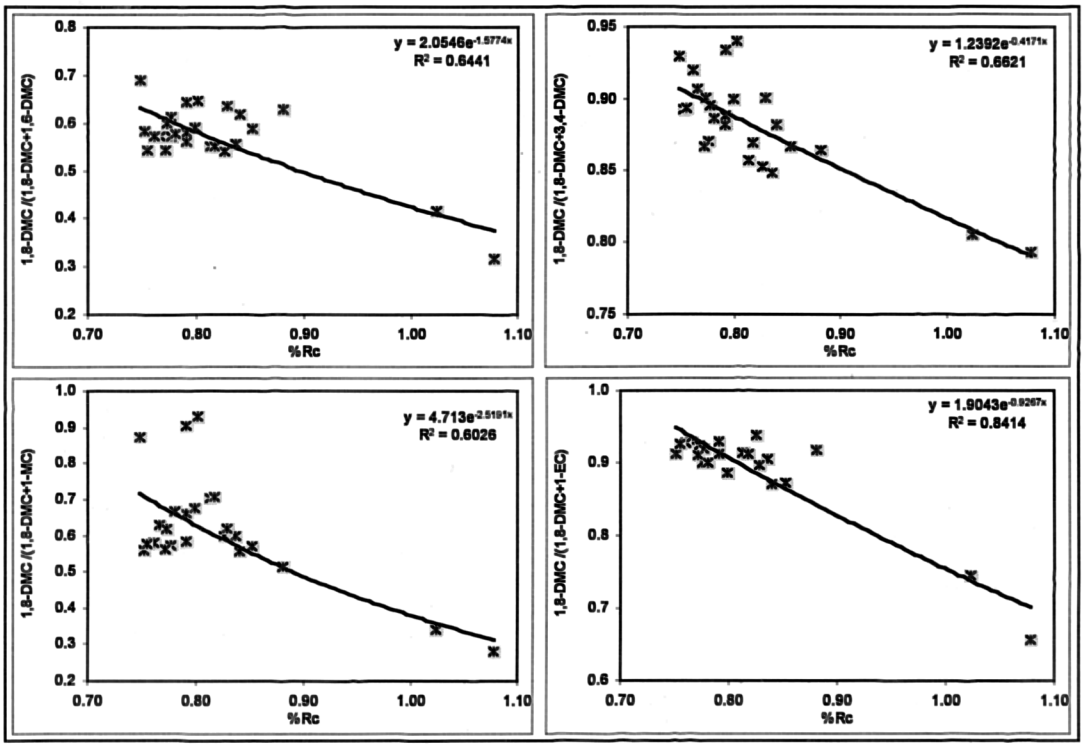

Figure 5.8 Isomeric variations of methyl- and dimethylcarbazoles as a function of the calculated vitrinite reflectance (%Rc) in the samples from the Silurian source rocks in the Oued Mya basin.

In summary, the Silurian and Ordovician source rock samples analysed in the Oued Mya basin revealed that the concentrations and distributions of the alkylcarbazoles and benzocarbazoles are strongly controlled by the organic matter abundance and quality. The maturity effect on the concentrations and distributions of the pyrrolic nitrogen compounds start to prevail at higher maturity (i.e. >1%Rc).

5.3. Evaluation of the migration and charging directions of the oil-fields from the Oued Mya-Hassi Messaoud petroleum system

Determination of the location of field filling points is of significant importance in reservoir geochemistry. It may enable the derivation of more accurate estimates of the petroleum carrier system and identify further exploration potential in local satellite fields (Larter et al., 1990; Horstad et al., 1990). A filling direction for a single reservoir field can be often determined by means of a maturity gradient within the reservoir since the variations would reflect the level of maturity in the source kitchen at the time of expulsion (England et al., 1987; England and Mackenzie, 1989; England, 1990; Larter et al., 1990).

From the geochemical evidence given in chapter 4, it appears that the Tannezuft Formation (Lower Silurian) in the Oued Mya basin is the main source of the Triassic, the Devonian and the Cambro-Ordovician reserves in the entire region. However, the Ordovician shales may have contributed to the generation of these reserves, but its contribution would be in much lower proportion compared to the Tannezuft Formation.

The aims of these sections are the determination of the filling points and migration directions of the fields analysed in this study using conventional biomarker parameters Ts/(Ts+Tm), C_{29}Ts/[C_{29}Ts + C_{29}17α (H) hopane], C_{30} diahopane/[C_{30} diahopane + C_{30}17α (H) hopane] and C_{23} tricyclic terpane/[C_{23} tricyclic terpane + C_{30}17α (H) hopane], aromatic hydrocarbon maturity parameters C_{20} triaromatic steroid/[C_{20} triaromatic steroid + C_{28}5α(H) triaromatic steroid (S+R)], TMNr-1 (1,3,7-TMN/1,2,5-TMN), TeMNr-1 [1,3,6,7-TeMN/(1,2,5,6-TeMN+1,2,3,5-TeMN)] and the calculated vitrinite reflectance %Rc and the concentrations and ratios of the pyrrolic nitrogen compounds. First, I will start this section by a statistical evaluation of the effect of the maturity and/or migration distances on the concentrations and distributions of the alkylcarbazoles and then select the appropriate parameters, which will be commonly used for the following sections.

5.3.1. Statistical approach to identify the geochemical controls on the overall distribution of pyrrolic nitrogen compounds in the oils from the Oued Mya-Hassi Messaoud petroleum system

Principal components analysis is used to evaluate the effect of maturity and relative migration distances on the alkylcarbazole concentrations and ratios calculated from the alkylcarbazoles in a suite of 72 oil samples (11 from the fields in the Oued Mya basin, 51 from Hassi Messaoud field, 1 from Rhourde Chegga, 2 from Hassi Guettar, 3 from El-Agreb, 2 from Mesdar and 2 from El-Baguel) (Figure 5.1).

The data matrix is composed of 72 oil samples and 22 variables (Table 5.3). The first three principal components (PCs) obtained, explain 44.54%, 18.20%, and 8.83% of the variance within the scaled data set, respectively. The concentrations and ratios of the individual alkylcarbazole isomers used in the PCA are listed Appendix 5.2.

The samples plotted in the left sides of the diagrams in Figure 5.9 (i.e. negative PC1) consist of those from the Mokh el Kebch, N'goussa, Guellala northeast, Guellala, Draa Temra, Haoud Berkaoui and Benkahla fields located in the Oued Mya basin, Rhourde Chegga field, Hassi Guettar field, Mesdar field, and oil samples from the western, northern and eastern flanks of the Hassi Messaoud field. Whereas, the samples plotted in the right side of these diagrams (i.e. positive PC1) are those from El-Agreb Cambrian fields, El-Baguel Cambrian field, and those from the centre and the south of the Hassi Messaoud field.

The loadings plots from the analysis (Figure 5.10) explain what these three principal components represent. The first factor (PC1) explains 44.54% of the total variance of the data set, on which high loadings (>0.6) are obtained for the concentrations of alkylcarbazoles, the isomeric ratios 1,8-DMC/(1,8-DMC+4-MC), 1,8-DMC/(1,8-DMC+2,4-DMC), 1,8-DMC/(1,8-DMC+2,5-DMC), $C_3/(C_1+C_3)$, and the relative migration distance. In addition, the loadings of the 1,8-DMC/(1,8-DMC+1-EC), 1,8-DMC/(1,8-DMC+2,6-DMC), concentration of the biomarkers, and the maturity parameters %Rc and C_{20} TAS/[(C_{20} TAS + C_{28} 5α(H) (S+R) TAS] are moderately high (>0.3). Thus, it could be considered that the relative migration distances and to a lesser extent the maturity of the oils have a strong effect on the concentrations and isomeric ratios of pyrrolic compounds and the concentrations of biomarkers of the oils analysed in this study.

The second factor (PC2) accounts for 18.20% of the total variance of the data set; high loadings (>0.6) are obtained for the maturity parameters %Rc, C_{20} TAS/[(C_{20} TAS+C_{28} 5α(H) (S+R) TAS] and Ts/(Ts+Tm) and the alkylcarbazole ratios 1,8-DMC/(1,8-DMC+1,6-DMC) and 1,8-DMC/(1,8-DMC+3,4-DMC). Moderately high loadings (>0.3) are obtained for the ratios 1,8-DMC/(1,8-DMC+1-EC), the concentrations of 1,8-dimethylcarbazole, the sum of the partially shielded dimethylcarbazoles and exposed dimethylcarbazoles, the concentrations of biomarker and aromatic hydrocarbons and the relative migration distances of the oils. Therefore, PC2 suggests that the alkylcarbazole concentrations and some of the alkylcarbazole ratios are controlled by the maturity and to a lesser extent the relative migration distances of the oils. The concentrations of biomarker and aromatic hydrocarbons may be controlled mainly by the maturity of the oils.

The third factor (PC3) is less important than the two first factors, explaining just 8.83% of the total variance of the data set. PC3 shows a high loading for the 1,8-DMC/(1,8-DMC+1,7-DMC) ratio. All the rest of alkylcarbazole ratios, the concentration of the aromatic hydrocarbons and the maturity ratio Ts/(Ts+Tm) show moderately high loadings. Hence, this factor seems to be controlled by other factors than the relative migration distances and maturity of the oils; probably the source facies of the original organic matter having generated these oils.

In summary, the results of the principal components analysis can be taken to tentatively suggest that the alkylcarbazole concentrations and isomer ratios 1,8-DMC/(1,8-DMC+4-MC), 1,8-DMC/(1,8-DMC+2,4-DMC), 1,8-DMC/(1,8-DMC+2,5-DMC), $C_3/(C_1+C_3)$, are mainly affected by the relative migration distances of the oils. However, the alkylcarbazole concentrations and ratios of the 1,8-DMC/(1,8-DMC+1,6-DMC) and 1,8-DMC/(1,8-DMC+3,4-DMC) seem to be controlled to a lesser degree by the maturity of the oils. The biomarker and aromatic concentrations appear to be controlled mainly by the maturity of the oils. Indeed, these observations are strongly supported by the plots of the three factors PC1 and PC2 as a function of the relative migration distances and maturity of the oils (Figure 5.11). PC1, which accounts for 44.54% of the total variance of the data set, shows good correlation with the relative migration distances and poor correlation with maturity parameter %Rc.

PC2 which accounts for 18.20%, shows good correlation with the maturity and fair correlation with the relative migration distances of the oils.

Table 5.3 List of the parameters used in the principal components analysis for the oils.

Alkylcarbazole concentrations (ug/g oil)	
1	Carbazole
2	Sum methylcarbazoles
3	1,8 dimethylcarbazole
4	Sum partially shielded dimethylcarbazoles
5	Sum exposed dimethylcarbazoles
6	Sum trimethylcarbazoles
Alkylcarbazole and benzocarbazole ratios	
7	1,8-DMC/(1,8-DMC+4-MC)
8	1,8-DMC/(1,8-DMC+1-EC)
9	1,8-DMC/(1,8-DMC+1,7-DMC)
10	1,8-DMC/(1,8-DMC+1,3-DMC)
11	1,8-DMC/(1,8-DMC+3,4-DMC)
12	1,8-DMC/(1,8-DMC+2,4-DMC)
13	1,8-DMC/(1,8-DMC+2,5-DMC)
14	1,8-DMC/(1,8-DMC+2,6-DMC)
15	$C_3/(C_1+C_3)$
16	$C_3/(C_2+C_3)$
Biomarker and aromatic concentrations (ug/g oil)	
17	Sum tricyclic terpanes, steranes and hopanes
18	Sum alkyl-naphthalenes, -phenanthrenes and -thiophenes
Maturity parameters	
19	Ts/(Ts+Tm)
20	%Rc
21	C_{20} TAS/[(C_{20} TAS+C_{28} 5α(H)(S+R) TAS]
Relative migration distance	
22	Distance (km)

Key: '%Rc = calculated virinite reflectance using the MPI-1 parameter;
MC = methylcarbazole
DMC = dimethylcarbazole
EC = ethylcarbazole
C_1 = Sum methylcarbazoles
C_2 = Sum dimethylcarbazoles
C_3 = Sum trimethylcarbazoles

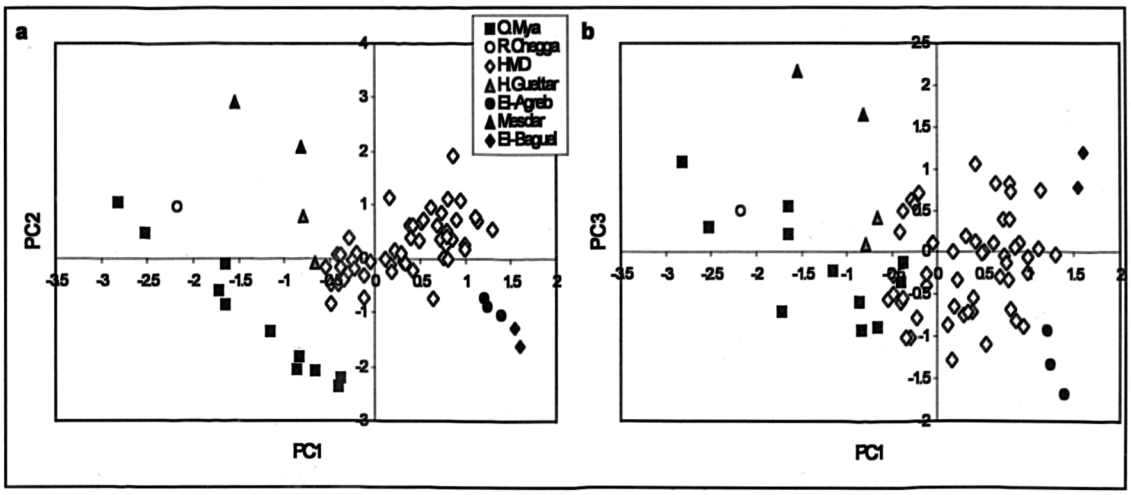

Figure 5.9 Scores plots (a) PC1 versus PC2 and (b) PC1 versus PC3 showing the relationship between the oil samples in terms of the first, second and third principal components. PC1 explains 44.54% of the total variance in the scaled data set, PC2 explains a further 18.20%, and PC3 explains a further 8.83%.

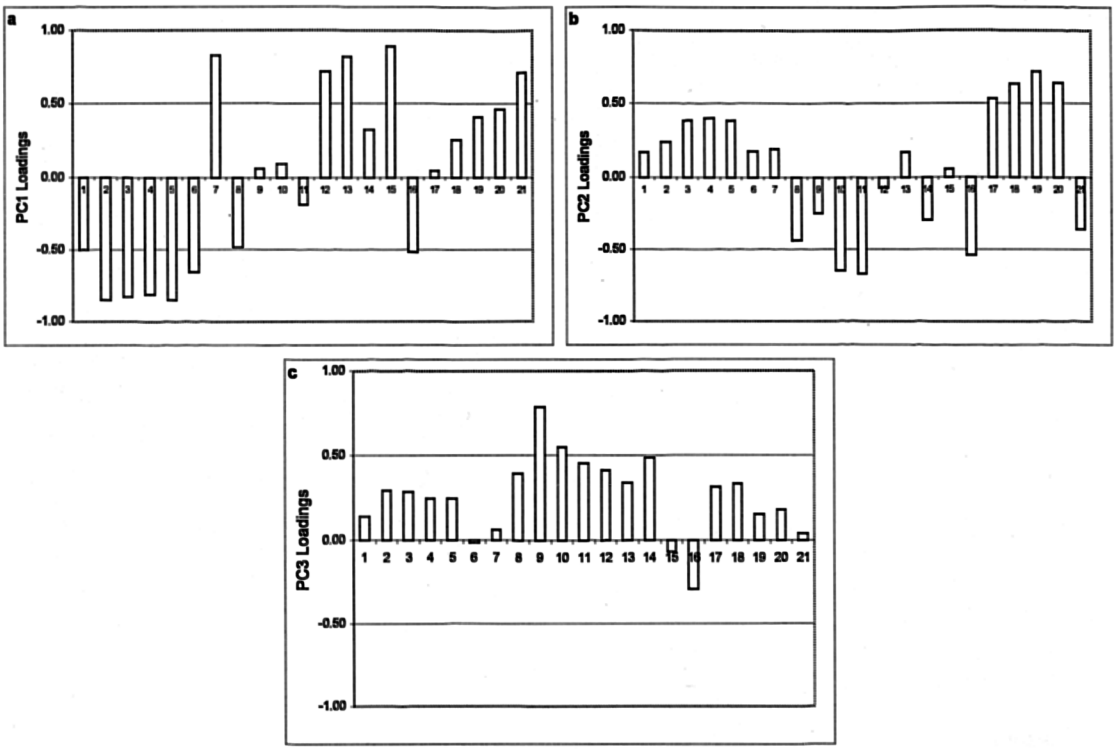

Figure 5.10 Loadings plots showing the composition of the first three principal components, which scored 44.54%, 18.20%, and 8.83% of the total variance in the data set, respectively.

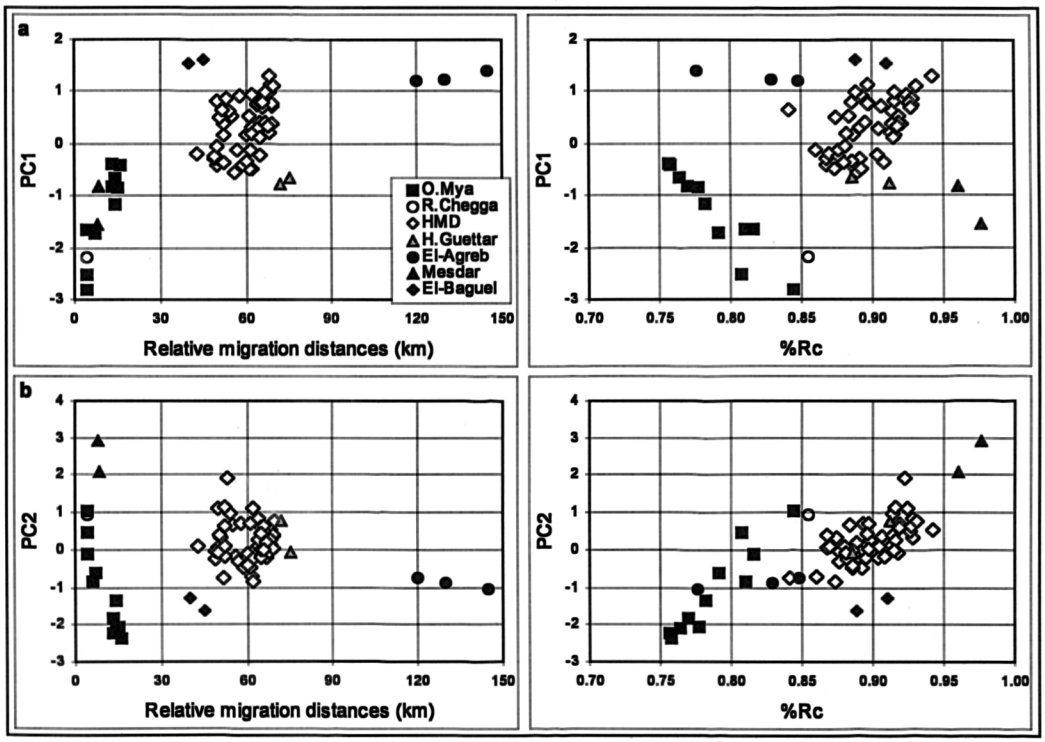

Figure 5.11 Cross plots of the two principal components (a) PC1 and (b) PC2 versus the relative migration distances and calculated vitrinite reflectance maturity parameter for the oils.

The results obtained from the principal components analysis suggest that the concentrations of alkylcarbazoles, the isomer ratios 1,8-DMC/(1,8-DMC+4-MC), 1,8-DMC/(1,8-DMC+2,4-DMC), 1,8-DMC/(1,8-DMC+2,5-DMC) and $C_3/(C_1+C_3)$ in the oils might be mainly related to the relative migration distances. It appears also that the maturity has an effect on the concentrations and distribution of alkylcarbazoles but to a lesser degree than the relative migration distances. Therefore, in the following sections I will emphasise my investigations on the possible relationship between the alkylcarbazole concentrations and distributions with the relative migration distances.

5.4. Triassic and Devonian Fields in the Oued Mya basin

The Triassic and Devonian fields located in the Oued Mya basin (west and northwest of the Hassi Messaoud field) are generally small and the reservoirs are often associated with sand pinchouts (Hammouda, 1980) (Figure 5.1). The reservoirs include fluvial sandstones of the *Triassic Argilo-Gréseux Inférieur* (Lower Triassic) and Devonian sandstones. The largest accumulations recorded in the Oued Mya basin are encountered in Benkahla, Guellala, and Haoud Berkaoui fields west of Hassi Messaoud with 188, 182 and 166 MMBO, respectively, which produce mainly from the Lower Triassic reservoirs. The other fields include Mokh El Kebch (MEK, Lower

Triassic), Guellala northeast (GLNE, Devonian sandstones), Draa El Temra (DRT, Lower Triassic), and N'Goussa (NGS, Devonian sandstones and Lower Triassic) containing 2, 10, 21, and 40 MMBO, respectively. The Devonian reservoirs in the N'goussa and Guellala northeast fields are in direct contact with the main Silurian source rock in the basin along the Hercynian unconformity (Figure 5.12); therefore the oils trapped in these reservoirs might have undergone very short migration distance from the underlying Silurian source rock strata. The lower Triassic reservoirs are unconformably resting on the top of the Devonian strata. The oil water contacts of the Lower Triassic reservoirs are located at -3840 m in the Mokh El Kebch field, -3787 m in the N'Goussa field, -3531 m in the Guellala northeast field, -3480 m in the Draa Temra field, -3470 m in the Guellala field, and -3424 m in the Haoud Berkaoui and Benkahla fields. The overlying Triassic shales and Liassic salt seal the oil accumulations located in the Oued Mya basin.

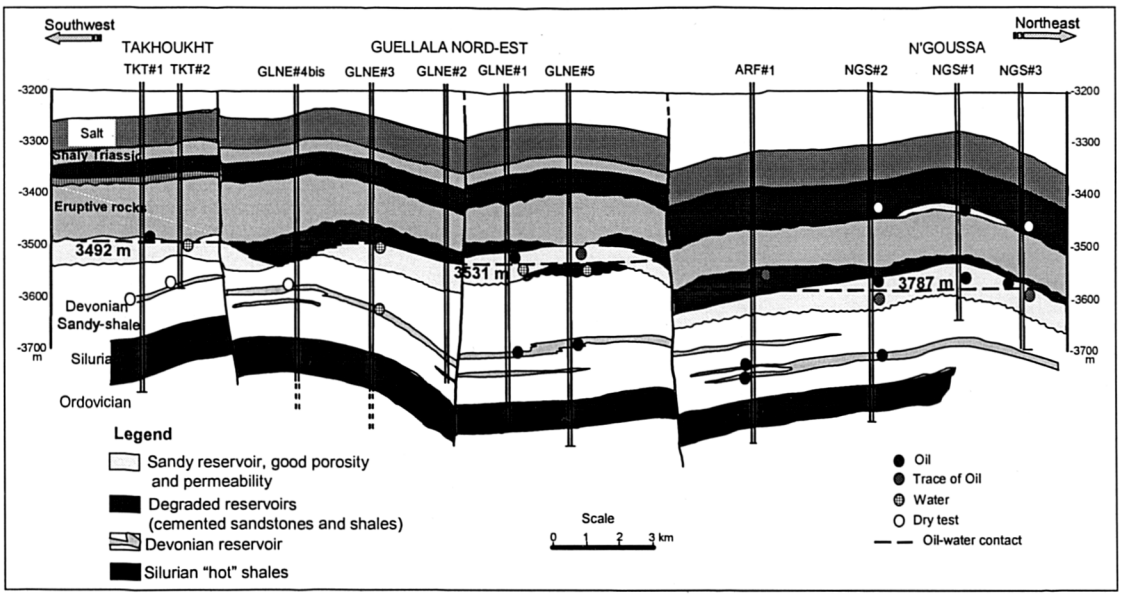

Figure 5.12 Northeast-southwest cross section showing the structures of N'Goussa, Guellala northeast and Takhoukht in the Oued Mya basin.

In the previous chapter, I have shown that the oils analysed in the Lower Triassic and Devonian fields were generated from two source rocks; the Silurian and Ordovician source rocks within the Oued Mya basin, however, with much more contribution from the Silurian compared to the Ordovician source rocks. The oils from Mokh el Kebch, N'Goussa, Guellala northeast and Guellala also appeared to be different compared to the oils from Draa Temra, Haoud Berkaoui and Benkahla fields (see sections 4.4 and 4.5 in chapter 4).

In this section, I will use selected biomarker and aromatic hydrocarbon maturity parameters to explore the maturity differences between the oils trapped in the Devonian and Lower Triassic reservoirs. Moreover, the extent of vertical and lateral migration of the oils trapped in the Devonian and the Lower Triassic in the Oued Mya basin will be investigated using the concentrations and ratios of the alkylcarbazoles and benzocarbazoles.

5.4.1. Geochromatographic compositional fractionation in the migrated Devonian and Triassic oils across the Oued Mya basin

5.4.1.1. *Normal*-alkanes

The distribution of the *n*-alkane concentrations isolated from the oils is also investigated. All the oil samples analysed in the fields from the Oued Mya basin show similar *n*-alkane distributions exhibiting a maximum in *n*-C_{11} and *n*-C_{15} alkanes (Figure 5.13). Oil samples from Mokh el Kebch, N'Goussa, Draa Temra fields and OKJ#31 and #202 from Haoud Berkaoui field show lower concentrations of the lower molecular weight alkanes (*n*-C_8, *n*-C_9 and *n*-C_{10}) compared to the other oil samples, likely due to the loss of the front-end alkanes during sample storage and preparation. The Pr/Ph ratio shows typical values for marine oils with only minor differences between the samples ranging from 1.38 to 1.50 (Table 4.8). The *n*-C_{17}/*n*-C_{27} ratio is slightly higher in oil samples MEK#1, NGS#2, GLNE#5 and GLA#16 from Mokh el Kebch, N'Goussa, Guellala northeast and Guellala fields, respectively relative to the oil samples from Benkahla and Haoud Berkaoui fields (Table 4.8), indicating probably that the former oil samples are more mature than the latter.

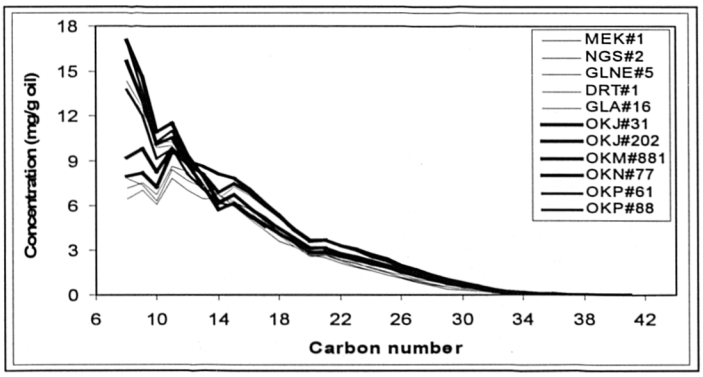

Figure 5.13 *n*-alkane abundance envelopes for the oil samples in the oil fields across the Oued Mya basin.

5.4.1.2. Steranes and triterpanes

The oils revealed a trend of increasing maturity from Haoud Berkaoui and Benkahla fields towards the oils reservoired in Draa Temra (DRT#1), Guellala (GLA#16), Guellala northeast (GLNE#5), N'goussa (NGS#2) and Mokh-El-Kebch (MEK#1) fields located to the north-northeast of the basin (Figure 5.1). Maturity parameters listed in Appendix 4.3, mainly calculated using the tricyclic terpanes and hopanes are plotted in Figure 5.14. It can be seen from these plots that oil samples analysed in DRT#1, GLA#16, GLNE#5, NGS#2, and MEK#1 have higher maturity ratios suggesting that these oils are somehow more mature than oils from Benkahla and Haoud Berkaoui fields. Although the maturity differences between the oils from Haoud Berkaoui and Benkahla fields seem not to be very large compared to those from the fields located to the north-northeast, and most of the parameter values are within the range of the analytical errors these differences appear to be consistent for all the maturity parameters used in this study.

It appears that the more mature oil samples are those trapped in the deeper Devonian reservoirs in Guellala north east and N'goussa fields and the deeper Lower Triassic reservoirs in the Mokh el Kebch, Draa Temra and Guellala fields (i.e. oil-water contacts at -3840 m, -3480 m to 3470 m, respectively) compared to the shallowest Lower Triassic reservoirs in the Haoud Berkaoui and Benkahla fields (i.e. oil-water contact at -3324 m).

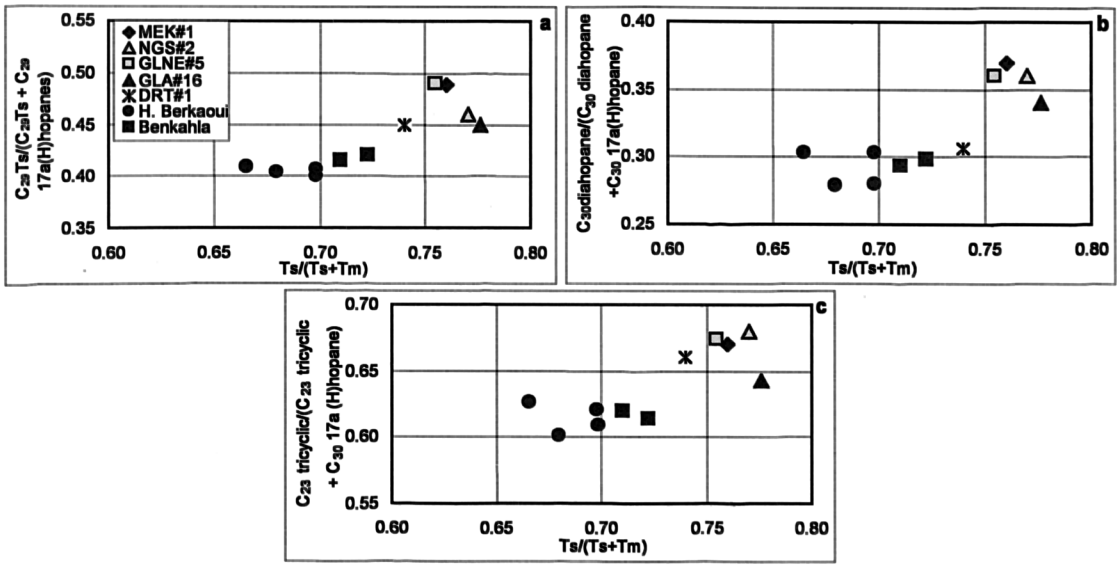

Figure 5.14 Cross plots of (a) (C_{29}Ts)/(C_{29}Ts + C_{29}17α(H)hopane) (b) C_{30}diahopane/(C_{30}diahopane + C_{30}17α(H)hopane) and (c) C_{23} tricyclic terpane/(C_{23}tricyclic terpane + C_{30} 17α(H)hopane) versus Ts/(Ts+Tm) maturity parameters showing the maturity variations within the oil fields across the Oued Mya basin.

5.4.1.3. Aromatic compounds

The maturity trend obtained using the aromatic hydrocarbon based maturity parameters agrees well with the trend obtained by the biomarker maturity parameters (Figure 5.15 and Appendix 4.4). Figure 5.15 displays some selected aromatic hydrocarbon based maturity parameters. It is clearly shown that oil samples analysed in DRT#1, GLA#16, GLNE#5, NGS#2, and MEK#1 exhibit higher maturity than oil samples from Benkahla and Haoud Berkaoui, respectively. The maturity differences between the oils located in the north-northeast (DRT#1, GLA#16, GLNE#5, NGS#2, and MEK#1) and those from Haoud Berkaoui and Benkahla fields are not large but appear to be consistent for all the aromatic hydrocarbon and biomarker alkane parameters investigated in this section.

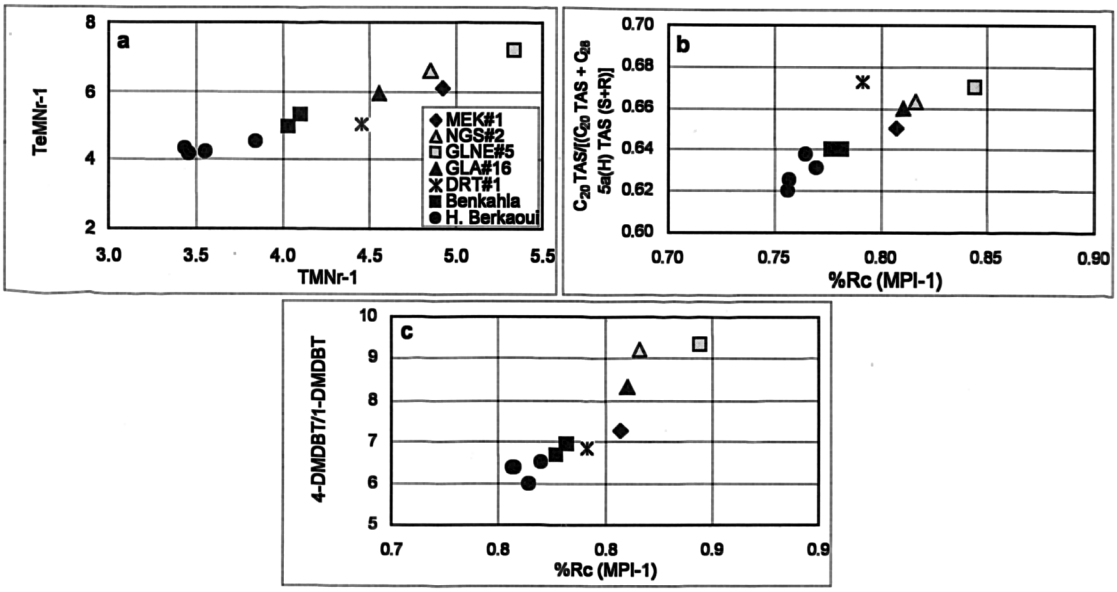

Figure 5.15 (a) 1,3,6,7-TeMN/(1,2,5,6-TeMN+1,2,3,5-TeMN) versus 1,3,7-TMN/1,2,5-TMN, (b) C_{20} TAS/[C_{20}TAS + $C_{28}5\alpha$ (H) (S+R)TAS] and (c) 4-MDBT/1-MDBT versus calculated vitrinite reflectance maturity parameters showing the maturity variations in the oil fields across the Oued Mya basin.

In summary, the maturity trend revealed by these source-related oils may have significant implications in the study of the extent of petroleum migration processes in the Oued Mya basin. In this particular scenario, it is envisaged that the oils currently trapped in the Lower Triassic shallowest reservoirs in Haoud Berkaoui and Benkahla fields may represent relatively early-expelled petroleum from the subsiding Silurian and Ordovician source rock strata within the Oued Mya basin. With increasing source rock subsidence, gradually more mature oils would have been generated, expelled and then migrated up dip to charge the deepest Lower Triassic reservoirs in Guellala (oil-

water contact -3470 m), Draa Temra (oil-water contact at -3480 m), and N'goussa (oil-water contact -3787m), and Mokh el Kebch (oil-water contact -3840 m) and the deepest Devonian reservoirs in Guellala northeast and N'goussa fields, respectively. Accordingly, the relatively low mature oils trapped in the Haoud Berkaoui and Benkahla accumulations may correspond to the most migrated oils in the analysed samples in the Oued Mya basin. The more mature oils trapped in the Lower Triassic in Guellala and Draa Temra reservoirs, could have migrated to a lesser degree from the generating Silurian and Ordovician source rock strata in the basin, relative to the shallower, less mature oils from Haoud Berkaoui and Benkahla fields. The most mature oils trapped in the deepest reservoirs of Guellala northeast, N'goussa and Mokh el Kebch are likely to be characterised by the shortest source rock trap migration distance, compared with the other oils (Figure 5.12). Indeed the alkylcarbazole and benzocarbazole concentrations and ratios investigated in these oil samples in the following section agree well with the scenario described here.

5.4.1.4. Geochemical controls on pyrrolic compound distributions in the Lower Triassic and Devonian oils across the Oued Mya basin

As suggested by the principal component analysis (section 5.4.1 above), the distribution of pyrrolic nitrogen compounds seems to be mainly controlled by the relative migration distance of the oils. This section will focus on how the migration distance of the oils might control the concentrations and distribution of pyrrolic compounds and I will plot these parameters as a function of the principal component PC1 as it represents the migration distances of the oils. Table 5.4 shows the alkylcarbazole parameters selected for this investigation.

Table 5.4 List of the alkylcarbazole parameters commonly used in the following sections.

Alkylcarbazole and benzocarbazole concentrations (ug/g oil)
Sum (C_0 - C_3) alkylcarbazoles
1,8 dimethylcarbazole
Sum exposed dimethylcarbazoles
[a] + [c]
Alkylcarbazole and benzocarbazole ratios
1,8-DMC/(1,8-DMC+4-MC)
1,8-DMC/(1,8-DMC+2,4-DMC)
1,8-DMC/(1,8-DMC+2,5-DMC)
$C_3/(C_1 + C_2 + C_3)$
[a]/([a]+[c])
PC1

For the Triassic and Devonian oils in the Oued Mya basin, in addition to these parameters, I will also use the concentrations and ratio of the benzocarbazole isomers [a] and [c].

Due to their polar nature, pyrrolic nitrogen compounds are highly reactive to their environmental surroundings during primary oil migration (when oil is expelled out of the source rock), and secondary oil migration (involving the movement of oil through carrier beds). Unlike aliphatic hydrocarbons that do not contain active sites in their structures, pyrrolic nitrogen compounds tend to adsorb onto other active sites within the source rocks most likely via hydrogen bonding, thus resulting in compositional fractionations during oil migration. Migration related fractionation effects have been observed both empirically in case studies (e.g. Li et al., 1995b; Chen, 1995; Brincat, 1996; Larter et al., 1996a; Bennett et al., 2002, Silliman et al., 2002; Terken and Frewin, 2000) and experimentally in laboratory simulations (Chen, 1995; Larter et al., 2000). Therefore, pyrrolic nitrogen compounds are potentially useful for assessing migration directions and distances.

Figure 5.16 displays the plots of the alkylcarbazole (C_0-C_3), benzocarbazole [a]+[c] concentrations and ratios as a function of PC1 (migration distances). The concentrations of the C_0-C_3 alkylcarbazoles and benzocarbazoles ([a]+[c]) range from 8.37 to 50.12 μg/g of oil (average 21.17 μg/g of oil) and from 0.03 to 0.46 μg/g of oil (average 0.15 μg/g of oil, Appendix 5.2), respectively. The oils trapped in the deepest reservoirs in the Mokh-El-Kebch, Guellala northeast, and N'goussa exhibit the highest C_0-C_3 alkylcarbazoles and benzocarbazoles ([a]+[c]) concentrations (i.e. 50.12, 43.9, and 29.3 μg of alkylcarbazoles/g of oil and 0.31, 0.46, and 0.24 μg of benzocarbazoles/g of oil, respectively).The oils trapped in the Lower Triassic from Draa Temra and Guellala fields contain lower concentrations (i.e. 24.2 and 21.4 μg of alkylcarbazoles/g of oil and 0.20 and 0.19 μg of benzocarbazoles/g of oil, respectively). The shallower, Lower Triassic reservoirs in the Haoud Berkaoui and Benkahla fields exhibit the lowest C_0-C_3 alkylcarbazoles concentrations ranging from 8.4 to 11.9 μg/g of oil in Haoud Berkaoui and 11.1 to 13.02 μg/g of oil in Benkahla; and the lowest benzocarbazole ([a]+[c]) concentrations ranging from 0.03 to 0.05 μg/g of oil and 0.04 to 0.05 μg/g of oil, in Haoud Berkaoui and Benkahla, respectively (Table 5.5). Therefore, a systematic decrease in the summed concentrations of

alkylcarbazoles and benzocarbazoles ([a]+[c]) can be seen from the oils analysed in deepest reservoirs in the Mokh-El-Kebch, Guellala northeast, N'goussa, Guellala and Draa Temra towards the oils analysed in the shallowest reservoirs in the Benkahla and Haoud Berkaoui fields (Figure 5.16).

The concentration of the alkylcarbazoles in these oils are in agreement with the results obtained by Li et al. (1995b); who showed that crude oils contain much higher proportions of alkylcarbazoles compared to benzocarbazoles while source rocks are enriched in alkylbenzocarbazoles compared to the alkylcarbazoles. Leythaeuser and Schaefer (1984) have shown that increased aromatic ring number retards expulsion in aromatic hydrocarbons and heterocycles from the source rocks. The predominance of alkylcarbazoles over benzocarbazoles in these oils may thus be caused by a similar "geochromatographic" effect during primary migration.

The abundance of N-H-shielded isomer relative to N-H-exposed isomer ratios [1,8-DMC/(1,8-DMC+4-MC) and 1,8-DMC/(1,8-DMC+2,4-DMC)], and the higher molecular weight relative to lower molecular weight alkylcarbazoles ratio [$C_3/(C_1+C_1+C_3)$] show a systematic increase in their values from the oils in the Mokh-El-Kebch, Guellala northeast, N'goussa, Guellala and Draa Temra, respectively towards the oils analysed in Benkahla and Haoud Berkaoui fields (Table 5.5). Whereas, the benzocarbazoles [a]/([a]+[c]) ratio exhibits a systematic decrease from the oils in the Mokh-El-Kebch, Guellala northeast, N'goussa, Guellala and Draa Temra towards the oils analysed in Benkahla and Haoud Berkaoui fields (Figure 5.16 and Table 5.5).

The compositional variations in the concentrations and ratios of the pyrrolic nitrogen compounds as a function of PC1, which represents the alkylcarbazole and benzocarbazole concentrations and ratios and the estimated migration distances of these oils, could be a result of the interaction of the pyrrolic nitrogen compounds with clay minerals and solid organic matter during oil migration through the carrier bed. This is in agreement with the findings of Li et al. (1995b, 1998) who showed that with increasing migration distance, oils from the same source and similar thermal maturity are recognised by observing the decrease in the absolute concentrations of individual nitrogen compounds and some enrichment of: (1) N-H-shielded isomer (i.e. 1,8-DMC) relative to N-H- exposed isomers (i.e. 4-MC, 2,4-DMC) and (2) higher

homologue isomers (i.e. trimethylcarbazoles) relative to the lower homologue species (i.e. carbazole, methylcarbazoles).

Larter et al. (1996) also showed the reduction in the concentration of the benzocarbazoles ([a]+[c]) and the benzocarbazole [a]/([a]+[c]) ratio for data sets derived from the analysis of reservoired oils from five petroleum systems, two in Western Canada and three in the North Sea as a function of migration distance. Terken and Frewin (2000) traced the most likely sources of the Q oil in the Dhahaban petroleum system of Oman by using the benzocarbazole [a]/([a]+[c]) ratio combined with migration modelling. Moreover, in laboratory simulations performed under subsurface conditions with a real rock, Larter et al. (2000) revealed that fractionation of pyrrolic nitrogen compounds does occur during oil migration and that the migration fractionations observed in this experiment are very similar to those seen in field data sets. Therefore, it is likely that the fractionations of the alkylcarbazoles and benzocarbazoles seen in the Lower Triassic and the Devonian oils could be caused by the migration distances experienced by these oils. Consequently, the oils trapped in the shallower reservoirs in Haoud Berkaoui and Benkahla fields may have undergone longer migration distances than the oils reservoired in the deeper reservoirs in Draa Temra and Guellala fields and the deepest reservoirs in N'goussa, Guellala northeast and Mokh-El-Kebch fields, respectively. The alkylcarbazole and benzocarbazole concentrations and ratios calculated for the oil sample from the Lower Triassic reservoir in Rhourde Chegga field are listed in Table 5.5. It also appears that the oil accumulated in this reservoir has undergone short vertical migration distance from the Silurian source rock strata located just bellow the Lower Triassic reservoir.

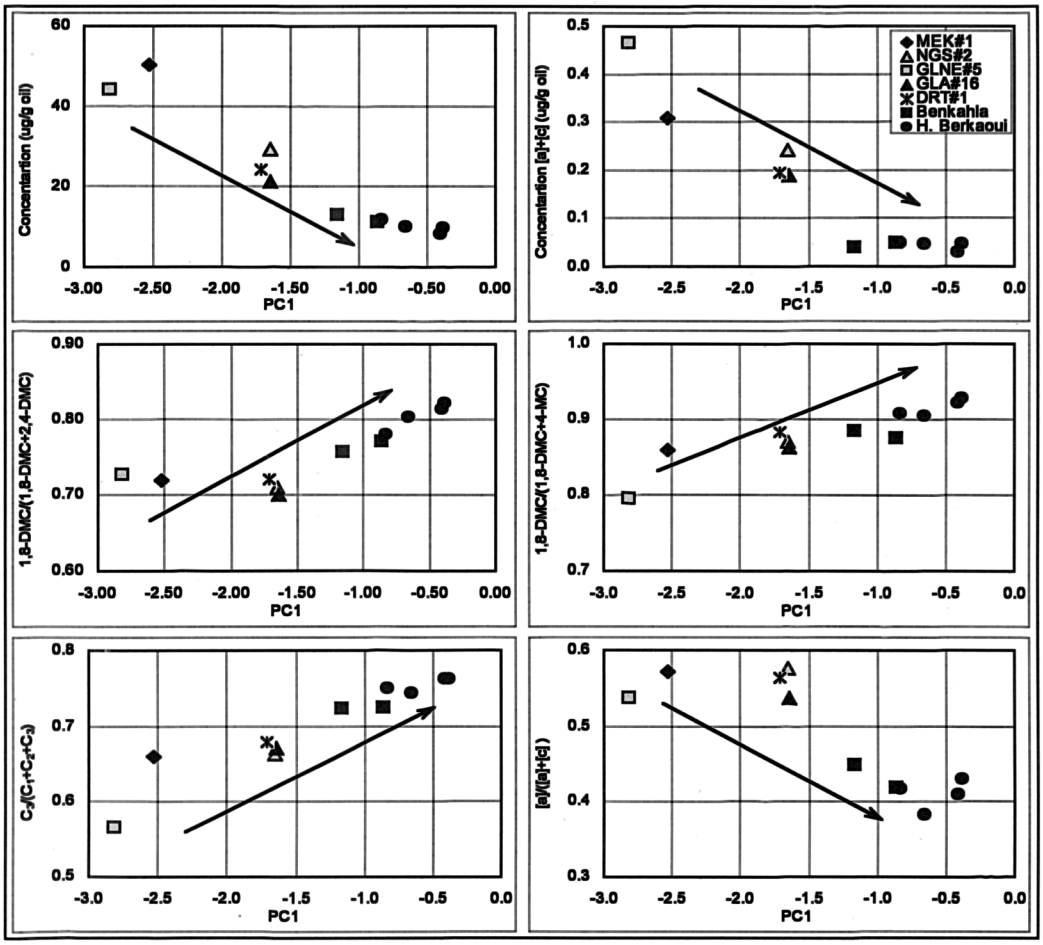

Figure 5.16 Variation in the concentrations and ratios of C_0-C_3 alkylcarbazoles and benzocarbazoles ([a]+[c]) as a function of PC1 for the Triassic oils in the Oued Mya basin, the arrows point out possible migration direction.

Table 5.5 Alkylcarbazole and benzocarbazole concentrations and ratios used in the evaluation of the oils migration across the Oued Mya basin and in the Rhourde Chegga field north of Hassi Messaoud field.

Sample	Reservoir	Sum C_0-C_3 ACAs	Sum BCAs [a]+[c]	1,8-DMC/(1,8-+4-MC)	1,8-DMC/(1,8-+2,5-)	1,8-DMC/(1,8-+2,4-)	C_3/(C_1+C_2+C_3)	[a]/([a]+[c])
MEK#1	Devonian	50.12	0.31	0.86	0.72	0.72	0.66	0.57
GLNE#5	Devonian	43.92	0.46	0.79	0.71	0.73	0.57	0.54
NGS#2	Devonian-Lower Triassic	29.31	0.24	0.87	0.71	0.71	0.66	0.58
DRT#1	Lower Triassic	24.15	0.20	0.88	0.73	0.72	0.68	0.56
GLA#16	Lower Triassic	21.40	0.19	0.86	0.70	0.70	0.67	0.54
OKP#61	Lower Triassic	13.02	0.04	0.88	0.75	0.76	0.72	0.45
OKP#88	Lower Triassic	11.09	0.05	0.88	0.75	0.77	0.72	0.42
OKJ#31	Lower Triassic	11.86	0.05	0.91	0.79	0.78	0.75	0.42
OKJ#202	Lower Triassic	10.05	0.05	0.90	0.75	0.80	0.74	0.38
OKN#77	Lower Triassic	9.63	0.05	0.93	0.77	0.82	0.76	0.43
OKM#88	Lower Triassic	8.37	0.03	0.92	0.76	0.81	0.76	0.41
RDC#1bis	Lower Triassic	27.60	0.20	0.83	0.73	0.69	0.65	0.60

Key: C_0= carbazole, C1= methylcarbazoles, C2= dimethylcarbazoles, C3= trimethylcarbazoles
ACAs= alkylcarbazoles, BCAs= benzocarbazoles, D=di, M=methyl, C=carbazoles.

The comparison of the average concentrations of the summed alkylcarbazoles and benzocarbazole isomers ([a]+[c]) between the reservoired oils in the Triassic and the Devonian fields and their underlying Silurian potential source rock reveals a concentration bias in favour of the Silurian source rocks where the average concentrations of the summed C_0-C_3 alkylcarbazoles and benzocarbazole isomers ([a]+[c]) in the Silurian source rocks account for 25 and 430 times those found in the oils, respectively (Figure 5.17). The average concentrations of the summed alkylcarbazoles and benzocarbazoles in the Silurian source rocks are 518.78 and 64.69 μg/g extract compared to 21.17 and 0.15 μg/g of oil in the oils, respectively (Appendices 5.1 and 5.2). Therefore, we can speculate that the partitioning of the alkylcarbazoles and benzocarbazoles is strongly controlled by primary migration and petroleum expulsion. Indeed, partitioning of petroleum components into solid organic matter has been proposed as important for primary migration (Frolov et al., 1989). Moreover, analysis of the intra-reservoir Brae Formation organic-rich shales in the Miller field (North Sea) showed that the total organic matter abundance, quality and expulsion efficiency of source rocks and variations in the sorptive properties of the kerogen system may exert an impact on both absolute and relative concentrations, and the relative distributions of pyrrolic nitrogen compounds. (Chen, 1995; Bennett et al., 2002, see also section 5.3.1.1).

This is in agreement with the findings of Bennett et al. (2002), who compared the distribution of the average benzocarbazole concentrations ([a]+[c]) obtained from 226 crude oils and 96 related source rock samples collected from different petroleum systems around the world. They reported that the concentrations of benzocarbazoles are clearly much higher in the source rock bitumens compared to the associated oils with concentrations in source rocks ranging from 2 to 80 times the reservoired oil concentrations. Moreover, Li et al. (1994) have reported similar differences in the relative abundances of the alkylcarbazoles, benzocarbazoles and dibenzocarbazoles between source rocks and their related petroleum.

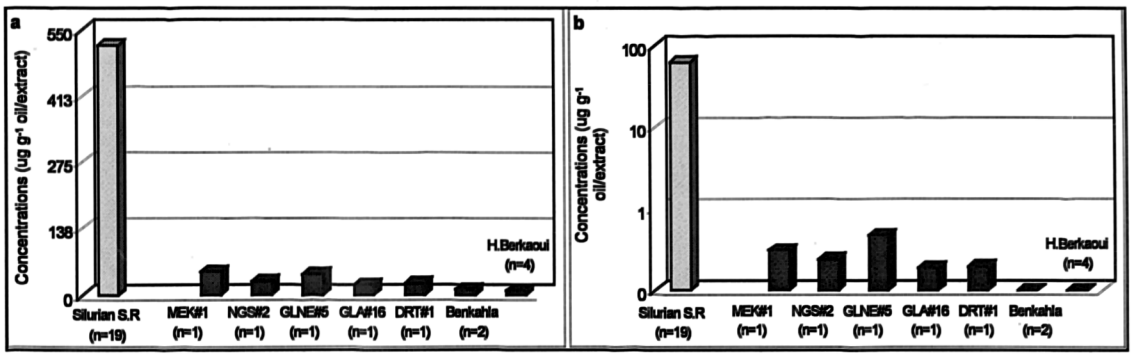

Figure 5.17 Histogram distribution showing comparison of the average (a) of C_0-C_3 alkylcarbazole concentrations and (b) of benzocarbazole isomers ([a]+[c]) in the Silurian source rock (μg g^{-1} extract) and the Triassic oils (μg g^{-1} oil). Note that a logarithmic scale in "Y" axis is used for the benzocarbazole concentrations.

5.4.2. Summary

The conventional biomarker and aromatic hydrocarbon maturity parameters used in this section for oil samples analysed across the Devonian and Lower Triassic oil fields revealed a maturity gradient from the oils trapped in deepest reservoirs towards the oils trapped in the shallowest Lower Triassic reservoirs across the Oued Mya basin. Oil samples analysed in the deepest reservoirs of Mokh el Kebch, N'goussa, Guellala northeast, Guellala, and Draa Temra showed higher maturity compared to the oil samples from the shallowest reservoirs in Benkahla and Haoud Berkaoui fields.

The alkylcarbazole and benzocarbazole concentrations and ratios clearly suggest that the oils trapped in the Haoud Berkaoui and Benkahla reservoirs have probably experienced the longest migration distances compared to the oils trapped in Guellala, Draa Temra, Guellala northeast, N'goussa, and Mokh el Kebch accumulations. The oils trapped in the latter accumulations may have undergone shorter vertical migration (i.e. <<less then 1 km), whereas the oils accumulated in the shallowest reservoirs in Haoud Berkaoui and Benkahla may have undergone both longer vertical and lateral migration distances.

5.5. Hassi Messaoud field

This section is the main part of this chapter; I will investigate the lateral and vertical chemical compositional variations throughout the petroleum columns and use them to determine the charging directions of the Hassi Messaoud field. In addition, the role of faults in dividing the different compartments with respect to migration and communication of petroleum is addressed. The lateral variations throughout the Hassi

Messaoud field will be assessed using the bulk composition of the oils, conventional biomarker parameters Ts/(Ts+Tm), C_{29}Ts/[C_{29}Ts + C_{29}17α(H) hopane], C_{30} diahopane/[C_{30} diahopane + C_{30} 17α(H) hopane] and C_{23} tricyclic terpane/[C_{23} tricyclic terpane + C_{30} 17α(H) hopane], aromatic hydrocarbon maturity parameters C_{20} triaromatic steroid/[C_{20} triaromatic steroid + C_{28} 5α(H) triaromatic steroid (S+R)], TMNR-1: (1,3,7-TMN/1,2,5-TMN), TeMNR-1: [1,3,6,7-TeMN/(1,2,5,6-TeMN + 1,2,3,5-TeMN)], the calculated vitrinite reflectance %Rc, and the results of principal components analysis using biomarker concentrations, and the concentrations and ratios of the pyrrolic nitrogen compounds (Table 5.4) obtained from the oils. The vertical chemical compositional variations of petroleum columns are assessed on a bulk scale using the total concentrations of petroleum, the percentages of the aliphatic, aromatic and polar compounds, and on a molecular scale using the biomarker and aromatic hydrocarbon parameters C_{29} steranes αββ/(ααα+αββ), Ts/(Ts+Tm), C_{30} diahopane/[C_{30} diahopane+C_{30} 17α(H) hopane] and MDR (4-MDBT/1-MDBT) for core extract samples. In chapter 4, I showed that the oil trapped in the Hassi Messaoud reservoirs revealed similar facies and maturity features to the Silurian source rock strata lying across the Oued Mya basin which are believed to be the main source in the study area.

Hassi Messaoud field is located on the El-Agreb-Hassi Messaoud ridge about 40-50 km from the Oued Mya basin. Hassi Messaoud field is separated into twenty five (25) isolated zones, having different petrophysical and pressure characteristics (Figure 3.2 in chapter 3). Theoretically these compartments are separated by dry zones (non-productive zones). Each compartment comprises a number of well-connected reservoir segments, and is completely isolated from the adjacent compartments. The limits of one compartment consist for example of permeability barriers inherited from tectonic, sedimentary or diagenetic events which control the petroleum movements during production.

The Cambro-Ordovician reservoir in Hassi Messaoud is divided into different units based on reservoir quality; these units are R3, R2, Ra, and Ri. The best reservoir qualities are encountered within unit Ra that contains the main oil reserves in Hassi Messaoud field particularly and in all the Hassi Messaoud Ridge generally. The oils analysed in Hassi Messaoud field are produced from the reservoir unit Ra. The

porosity of this unit ranges from 2 to 12 percent, with an average of 8 percent; permeability ranges from 0 to 1000 mD. The original oil-water contact throughout the Hassi Messaoud reservoirs is located at about 3400 m below surface.

Previous studies performed on different parts of the reservoirs within the Hassi Messaoud Ridge showed that the qualities of this reservoir unit (Ra) exhibit large lateral and vertical heterogeneities (e.g. IFP, 1975; Fennouh, 1996). The contour map in Figure 5.18 shows the lateral average horizontal porosity variations of the reservoir unit Ra throughout Hassi Messaoud field. In general the average porosity across the whole reservoir exhibits low to moderate values ranging from 3.50 to 11.50%, compared to North Sea reservoirs where porosity values range from 20 to 25%. Furthermore, the highest porosity values (Φ>8.50 %) are recorded in the centre and the northern parts of which represent the crest of the field, with some localised parts far to the east, southeast and southwest of Hassi Messaoud field. The lowest average porosity values (Φ<8.50 %) are recorded in the west, south, far northeast and northwest of Hassi Messaoud field.

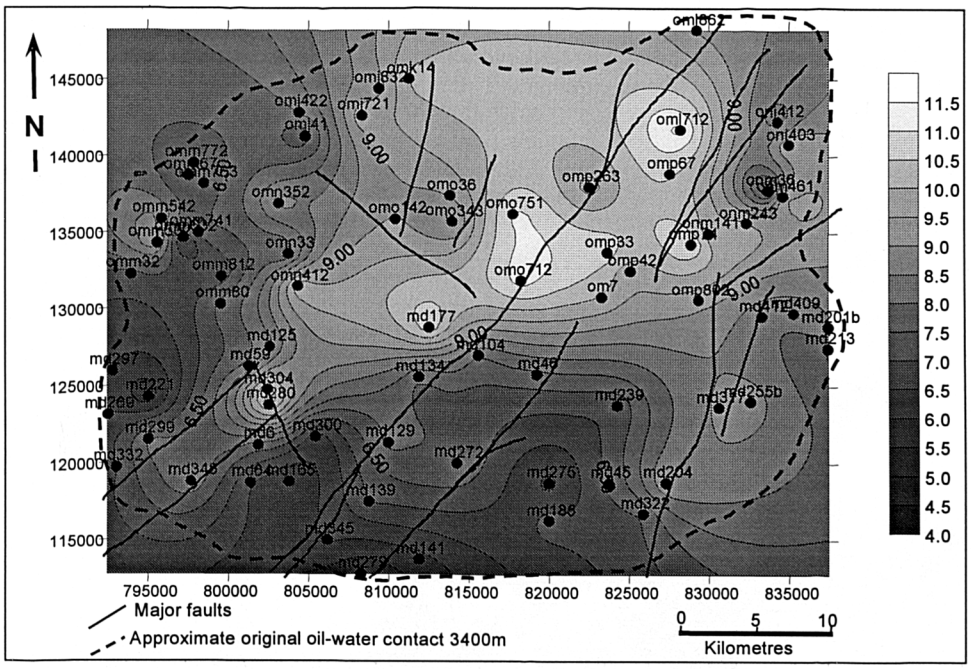

Figure 5.18 Contour map showing the lateral variations of the average porosity of the reservoir Ra throughout Hassi Messaoud field.

5.5.1. Lateral petroleum geochemical variations throughout the Hassi Messaoud field

5.5.1.1. Bulk composition variations of the oils

The results obtained by Iatroscan showing the concentrations and percentages of the C_{15}+ aliphatic and aromatic hydrocarbon fractions and NSO compounds for the Hassi Messaoud oils are listed in Appendix 5.3. The relative distributions of the aliphatic and aromatic hydrocarbon fractions and NSO compounds for Hassi Messaoud oils are displayed in a ternary plot (Figure 5.19). All the oil samples (53) plot in a narrow region of the ternary diagram, dominated by the aliphatic hydrocarbon fraction ranging from 60 to 70% and the aromatic hydrocarbon fraction ranging from 27 to 35%. The oils exhibit quite low percentages of NSO (resins + asphaltenes) compounds ranging from 2.22 to 7.28%. The highest percentages of NSO compounds (5.10% and 7.28% in wells OMM#532 and OMM#33) are found in the northwest of Hassi Messaoud field (zone 1c) where several wells have been closed during the last decade due to asphaltene precipitation problems (Sonatrach internal reports).

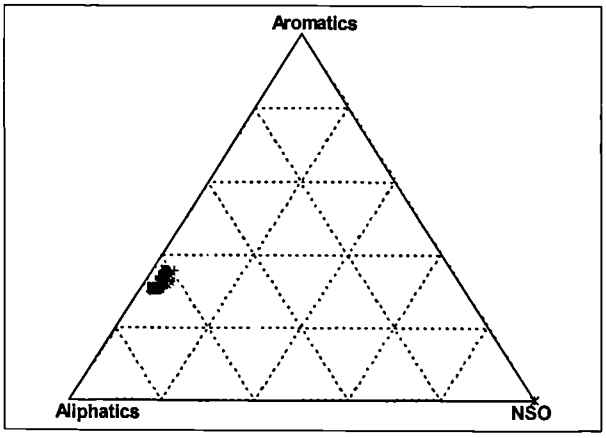

Figure 5.19. Ternary diagram showing the distributions of aliphatic and aromatic fractions and NSO compounds for Hassi Messaoud oils.

The contour map in Figure 5.20 displays the lateral variation of asphaltene content (mg/g oil) throughout Hassi Messaoud field. The highest asphaltene concentrations are encountered in the northwest part of Hassi Messaoud (more accurately within zone 1c of the field), ranging from 8.40 to 12.85 mg of asphaltenes/g of oil (Appendix 5.3). The southern and north eastern parts of the field exhibit moderate amounts of asphaltenes (5.44 to 8.67 mg/g oil) and the central and the eastern parts of the field show the lowest amounts of asphaltenes (3.18 to 6.43 mg/g oil).

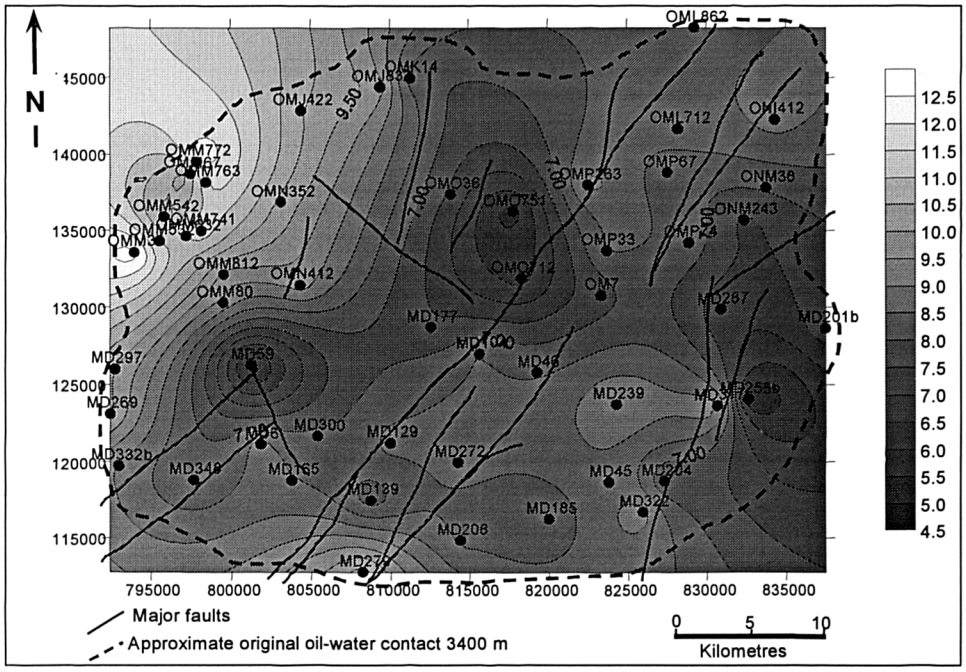

Figure 5.20 Contour map showing the lateral variations of the amount of the asphaltenes in the produced oils (mg/g of oil) throughout Hassi Messaoud field.

5.5.1.2. Molecular composition variations of the oils throughout the Hassi Messaoud field

5.5.1.2.1. Sterane and terpane distributions

The contour maps in Figure 5.21 and Figure 5.22 show the lateral variations in biomarker maturity parameters for Hassi Messaoud oils produced from the same reservoir unit Ra. The biomarker maturity parameters used in this section are: Ts/(Ts+Tm), C_{29}Ts/(C_{29}Ts+C_{29}17α(H)hopane), C_{30}diahopane/(C_{30} diahopane + C_{29}17 α (H) hopane) and C_{23} tricyclic terpane/(C_{23} tricyclic terpane + C_{30}17α(H)hopane). The values of these maturity parameters are displayed in Appendix 4.3.

The results show a general maturity trend with the more mature samples encountered in the centre and east of the Hassi Messaoud reservoir and the less mature oil samples are located towards the western, northern and southern flanks of the reservoir. The obvious trend of maturity that emerges for the distribution of oil maturities within Hassi Messaoud accumulation correlates positively with the distribution of the average porosity shown in Figure 5.18. Over most of the field area, the higher porosity sand intervals (>8.5 %) are filled with a higher maturity oil, whereas the lower porosity zones (<8.50 %) contain a lower maturity oil (Figure 5.21 and Figure 5.22). The values of the Ts/(Ts+Tm), C_{29}Ts/(C_{29}Ts + C_{29}17 α (H) hopane),

C_{30}diahopane/(C_{30} diahopane + C_{29}17 α (H) hopane) and C_{23} tricyclic terpane/(C_{23} tricyclic terpane + C_{30}17 α (H) hopane) parameters range from 0.61 to 0.76, 0.36 to 0.44, 0.25 to 0.31, and 0.63 to 0.70, respectively for the oil samples located towards the western, northern and southern flanks and from 0.76 to 0.84, 0.44 to 0.57, 0.31 to 0.40, and 0.70 to 0.79, respectively for the oil samples in the centre and east parts of the field (Appendix 4.3).

Indeed, in geochemical studies carried out by Leythaeuser and Rückheim (1989) and Hillebrand and Leythaeuser (1992), they have clearly shown pronounced spatial heterogeneities in bulk and molecular composition of unaltered petroleum from a small oil field in Germany named Stockstadt oil field. They found that the oil in high-porosity/high-permeability sand intervals bears a higher maturity signature compared to oils occupying lower-porosity/lower-permeability zones. Leythaeuser and Rückheim (1989) showed that the bulk composition (proportion of aliphatic and aromatic hydrocarbons and NSO's) of the extracted petroleums recovered from high-porosity sandstones ranges from 85.9 to 88.1% of aliphatic and aromatic hydrocarbons and 11.9 to 14.1% of NSO's, which is very similar to that of the DST oil samples from the same field, ranging from 91.4 to 94.5% of aliphatic and aromatic hydrocarbons and 5.5 to 8.6% of NSO's. However, the petroleum extracted from reservoir rocks with less than 13% porosity, revealed regular bulk composition changes with decreasing porosity and permeability; the percentages range from 56.1 to 62.4% of aliphatic and aromatic hydrocarbons and 37.6 to 56.1% of NSO's. Moreover, the oils extracted from the high-porosity/high-permeability sandstones showed higher calculated vitrinite reflectance values, clustering around 0.81%Rc, whereas the extracts from the low-porosity/low-permeability sandstones exhibited lower Rc values, as low as 0.63%. They interpreted these maturity differences as due to: i) successive stages of trap filling due to episodes of increasing burial and maturation of the relevant source rocks, in combination with ii) low rates of in-reservoir mixing of these individual oil charges by convection or diffusion. The accumulation of the more mature oil charges in the reservoir intervals with high porosity and high permeability can be explained as follows: the source rock generally generates and expels oil at different stage of maturity; therefore the first oil charge consists of oil with the low maturity signature.

The observation of pronounced spatial heterogeneities in the oil maturity revealed in the Hassi Messaoud field can be explained by the combination of both successive stages of reservoir filling due to different episodes of increasing burial and maturation of the Silurian source rock intervals in Oued Mya basin responsible for the generation of these oils, and low rates of in-reservoir mixing of the individual oil charges (Leythaeuser and Rückheim, 1989; Hillebrand and Leythaeuser, 1992). Low rates of such in-reservoir mixing processes have been predicted on the basis of model calculations and documented in several case studies (England et al., 1987; England and Mackenzie, 1989; Karlsen and Larter, 1989; Horstad et al., 1990).

The filling of Hassi Messaoud field must not have been accomplished by a single-event of secondary migration. Instead, the accumulation process must have continued over an extended period of time during which the Silurian source rock strata in the Oued Mya basin were subsiding and generating, as well as expelling progressively more mature oil charges. Presumably, the early-expelled oil charge inherited a low-maturity signature as the Silurian source rock strata was probably at moderate burial depths and temperatures. Therefore, the first oil charge migrated up dip towards the structurally highest positions of the trap, likely controlled by buoyancy forces and pore-entry pressures. The first oil charge (low-mature oil) initially accumulated in the high-porosity/high-permeability sand intervals since their displacement pressures are lower than the low-porosity/low-permeability reservoir intervals. Further burial of the Silurian source rock strata in the Oued Mya basin resulted in the arrival of more, and progressively higher maturity oil in the Hassi Messaoud trap. With the increasing height of the oil column, buoyancy eventually exceeded the capillary entry pressure of the lower-porosity reservoir zones. The early-accumulated lower-maturity oil was then displaced by the higher-maturity oil, forcing the former into progressively lower-porosity intervals located towards the west, northwest, southwest flanks of the field. The analysis of petroleum inclusions in the samples selected from the centre, north, west, south and east of the Hassi Messaoud field revealed the occurrence of a higher number of petroleum inclusions in the samples from the centre and east of the field compared to those from the south, west and north flanks (section 6.2 in chapter 6). This observation does suggest that the oil in Hassi Messaoud field has likely spent much more time in contact with the reservoir rocks in the centre and east parts of the field where the reservoir quality seems to be better compared to the western, southern

and northern flanks. Moreover, the differences in the maturity between the petroleum fluid inclusions, the reservoir core extracts and the present day production oil shown in section 6.2.4.2, chapter 6, clearly indicate that charging of the Hassi Messaoud accumulation occurred during a long period of geological time and reflect the increase in the maturity of the Silurian source rock strata responsible for the generation of the oils hosted in this field.

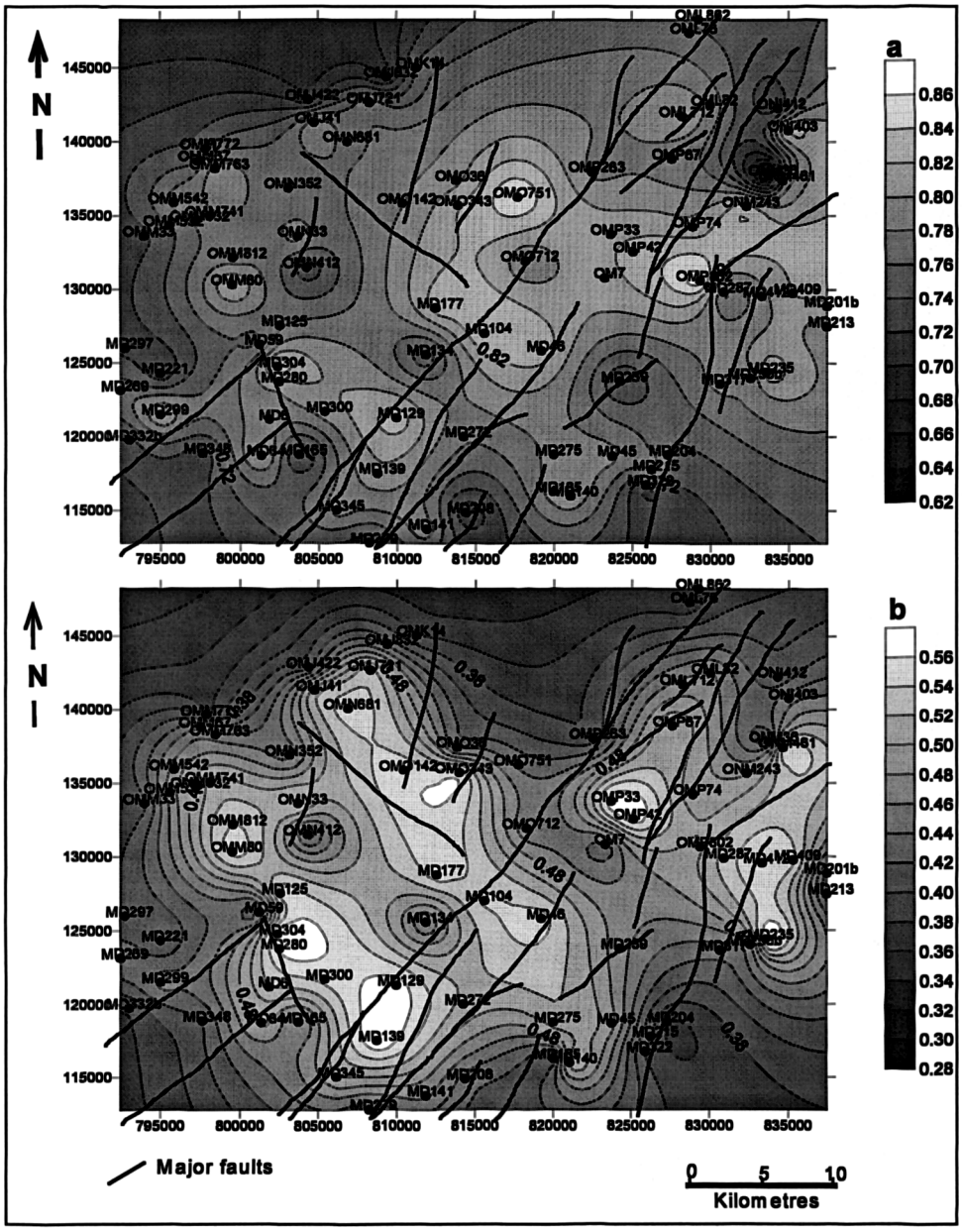

Figure 5.21 Contour maps showing the lateral variations of the (a) Ts/(Ts+Tm) and (b) the $C_{29}Ts/(C_{29}Ts+C_{29}17\ \alpha(H)hopane)$ parameters throughout Hassi Messaoud field.

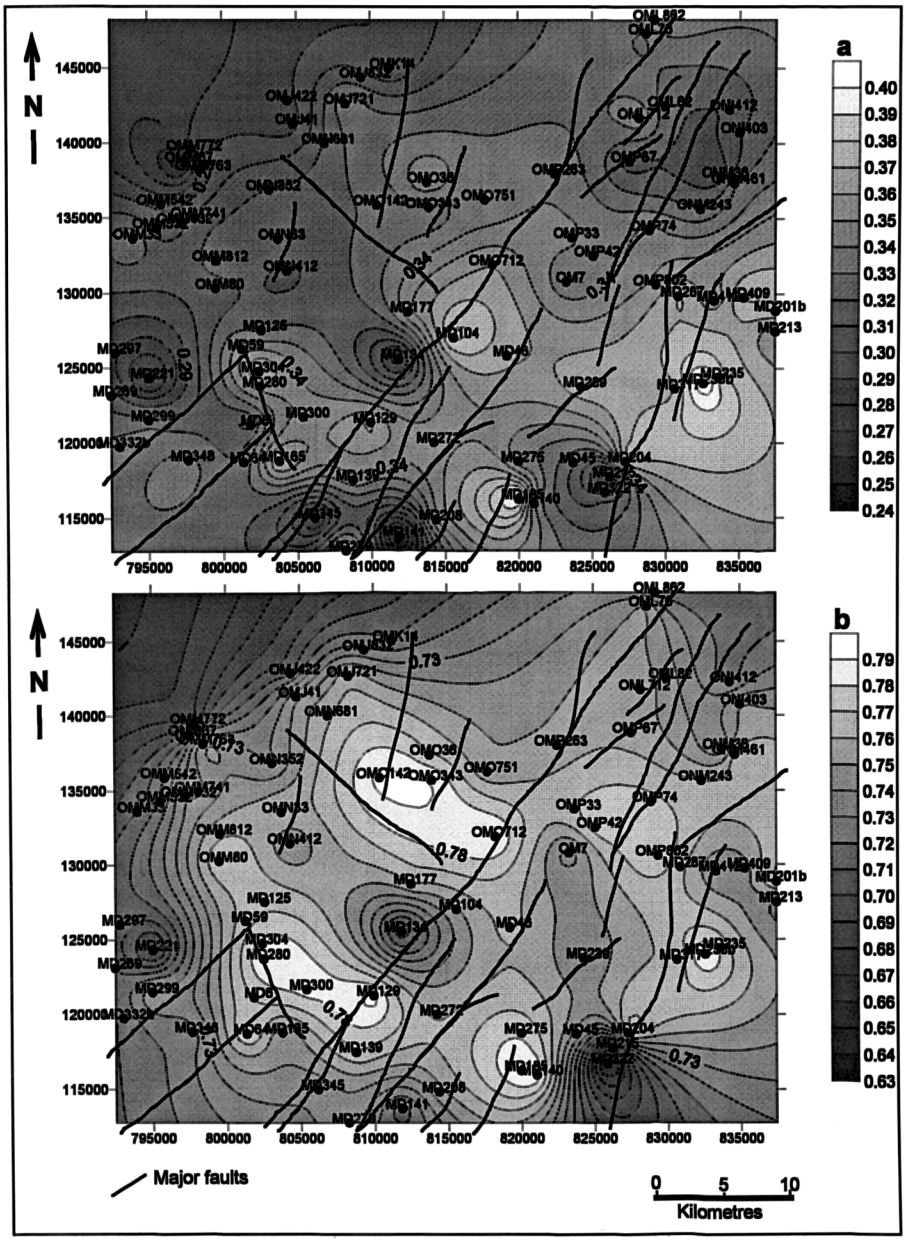

Figure 5.22 Contour maps showing lateral variations of the (a) C_{30}diahopane/(C_{30}diahopane + $C_{30}17\alpha$(H)hopane) and (b) C_{23}tricyclic terpane/(C_{23} tricyclic terpane+$C_{30}17\alpha$(H) hopane) parameters throughout Hassi Messaoud field.

5.5.1.2.2. Aromatic steroids

In this and following subsections, I will use selected maturity parameters obtained from triaromatic-steroid hydrocarbons, alkylnaphthalene, alkylphenanthrene and alkylthiophene aromatic compounds, in order to consolidate the results obtained using the biomarker distributions in the section above. The values of these parameters are listed in Appendix 4.4. The triaromatic steroid hydrocarbon maturity based parameter C_{20}TAS/[C_{20}TAS+C_{28} 5α(H) (S+R)TAS] plotted as a contour map (Figure 5.23) reveals that the oil samples from the centre of Hassi Messaoud field are the most

mature compared to the other parts of the field. Moreover, the oil maturity decreases from the centre towards the flanks of the field and the least mature samples are recorded in the west and northwest of Hassi Messaoud field. This maturity trend agrees well with the maturity distribution revealed earlier using the biomarker distributions.

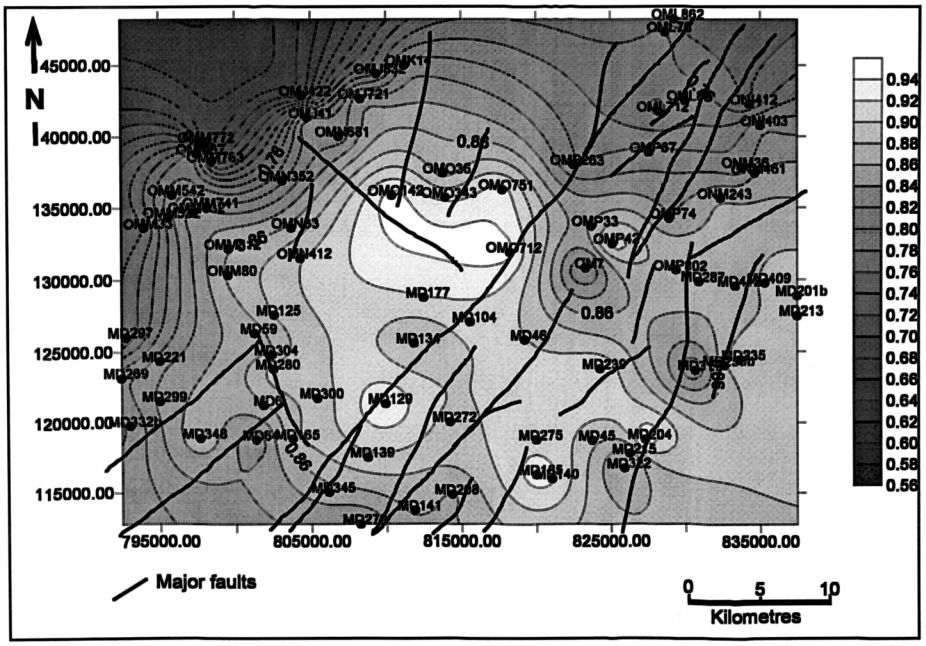

Figure 5.23 Contour map showing lateral variations of the $C_{20}/[C_{20}+C_{28}$ (R+S)] ratio throughout Hassi Messaoud field.

5.5.1.2.3. Alkylnaphthalenes

Most of the molecular maturity parameters based on alkylnaphthalenes listed in Appendix 4.4 in chapter 4 show the same maturity trend as the revealed in the previous sections using biomarkers and aromatic steroids. In this section I have selected two representative parameters, TMNR-1 (1,3,7-TMN/1,2,5-TMN) and TeMNR-1 (1,3,6,7-TeMN/(1,2,5,6-TeMN+1,2,3,5-TeMN). Figure 5.24 shows the contour maps of TMNR-1 and TeMNR-1 parameters throughout Hassi Messaoud field. It is clear that oil samples from the centre and east of the field are the most mature oils within the field; the flanks contain oils of lower maturity except for the southern flank of the field that shows oils with higher maturity. Moreover, an obvious gradient of decreasing oil maturity from the centre towards the west, north and northeast flanks can be seen throughout the Hassi Messaoud field.

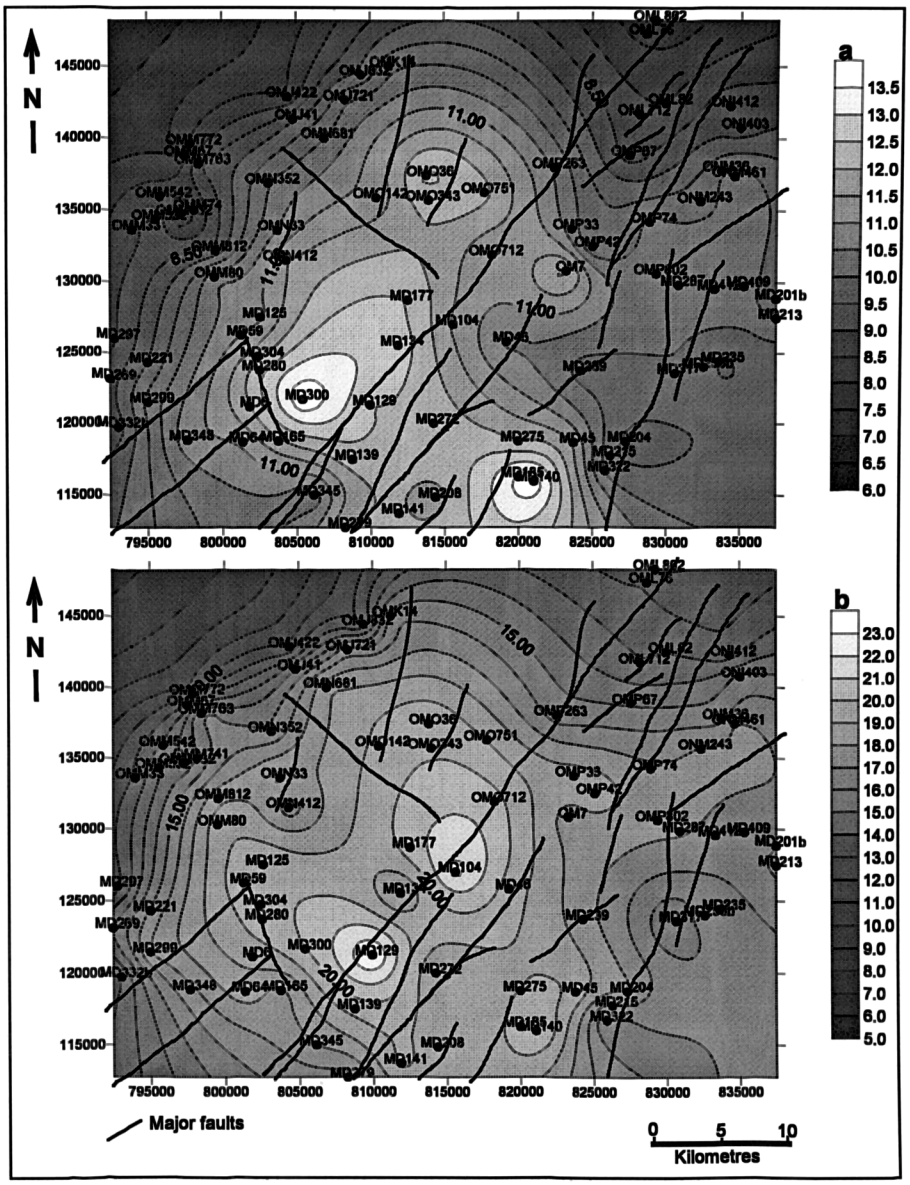

Figure 5.24 Contour map displaying lateral variations of (a) TMNR-1 and (b) TeMNR-1 parameters throughout Hassi Messaoud field.

5.5.1.2.4. Alkylphenanthrenes

The contour map in Figure 5.25 shows the lateral distribution of the calculated vitrinite reflectance equivalent (%Rc) in the oils from Hassi Messaoud field. This parameter agrees well with all the previous parameters based on biomarkers, aromatic steroids and naphthalenes. The %Rc parameter reveals that the oils in the centre, south and east of Hassi Messaoud field are the most mature samples compared to the oils in the flanks. Thus for example oils from the centre of the field show values of the calculated vitrinite reflectance %Rc ranging from 0.88 to 0.94%, whereas oils from the western, northern and the eastern flanks show values ranging from 0.84 to 0.87%

(Appendix 4.4). Moreover a gradient of decreasing maturity from the centre towards the flanks can be clearly seen throughout Hassi Messaoud field.

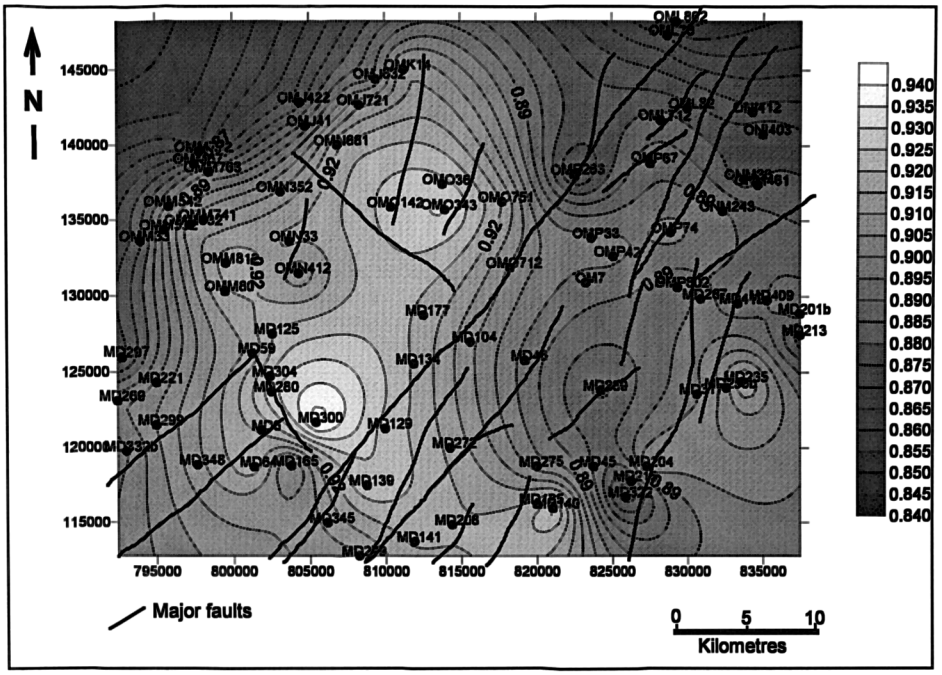

Figure 5.25 Contour map displaying lateral variations of the calculated vitrinite reflectance (%Rc) parameter throughout Hassi Messaoud field.

5.5.1.2.5. Principal components analysis

Principal components analysis was performed on 81 Hassi Messaoud oil samples in order to elucidate the genetic relationship between the oil samples from Hassi Messaoud field previously identified using conventional biomarker and aromatic hydrocarbon maturity parameters. In the following section, I am going to determine the possible filling directions of the Hassi Messaoud reservoirs, explore the role of the major faults separating and/or crosscutting the Hassi Messaoud reservoirs in respect to migration and communication of petroleum between the different compartments, and investigate if the separation of the Hassi Messaoud field into 25 different production zones based on petrophysical properties and pressures of the wells can be confirmed statistically using geochemical parameters (i.e. biomarker concentrations and ratios).

The data matrix consists of 30 variables (28 biomarker concentrations and 2 maturity parameters Table 5.6) and the 81 Hassi Messaoud oil samples. The first 3 principal components accounted for 59.44% of the total variance of the data set, of which PC1 accounted for 36.40%, PC2 for 15.05%, and PC3 for 7.99% of the total variance. It

was thought that the majority of the variance was accounted for by the first 2 PC's, therefore these were the only PC's analysed.

Table 5.6 List of the variables used in the principal components analysis for the Hassi Messaoud oils.

Steranes (*m/z* = 217)	
1	C_{21}(ααα+αββ) pregnanes
2	C_{22}(ααα+αββ) homopregnanes
3	C_{27} 13β(H), 17α(H) diasterane 20S
4	C_{27} 13β(H), 17α(H) diasterane 20R
5	C_{29} 13β(H), 17α(H) diasterane 20S
6	C_{27} 5α(H), 14α(H), 17α(H) sterane 20R
7	C_{29} 13β(H), 17α(H) diasterane 20R
8	C_{29} 5α(H), 14α(H), 17α(H) sterane 20S
9	C_{29} 5α(H), 14α(H), 17α(H) sterane 20R
αββ **Steranes** (*m/z* = 218)	
10	C_{27} 5α(H), 14β(H), 17β(H) sterane (20S+20R)
11	C_{28} 5α(H), 14β(H), 17β(H) sterane (20S+20R)
12	C_{29} 5α(H), 14β(H), 17β(H) sterane (20S+20R)
Tricyclic terpanes and hopanes (*m/z* = 191)	
13	C_{21} Tricyclic terpane
14	C_{22} Tricyclic terpane
15	C_{23} Tricyclic terpane
16	C_{24} Tricyclic terpane
17	C_{25} Tricyclic terpane
18	C_{26} Tricyclic terpanes (22S+22R)
19	C_{28} Tricyclic terpanes (22S+22R)
20	C_{29} Tricyclic terpanes (22S+22R)
21	C_{30} Tricyclic terpanes (22S+22R)
22	C_{31} Tricyclic terpanes (22S+22R)
23	22,29,30-Trisnorneohopane (Ts)
24	22,29,30-Trisnorhopane (Tm)
25	C_{29}17α(H), 21β(H)-30-norhopane
26	18 α (H)-30-norneohopane (C_{29} Ts)
27	C_{30} diahopane
28	C_{30}17α(H), 21β(H) hopane
Maturity parameters	
29	%Rc = 0.4 + (0.6 * MPI-1)
30	C_{20} TAS/[(C_{20} TAS + C_{28} 5 a(H) (S+R) TAS]

The cross plot of PC1 against PC2 scores in (Figure 5.26) reveals that the Hassi Messaoud oils analysed in this study can be distinguished into three main groups. The first group consists of the oil samples located in the west, northwest, south west and south flanks of the Hassi Messaoud field (negative PC1); the second group includes the oil samples from the centre, centre-north and centre-south of the field (positive PC1 and negative PC2), and the third group contains the oil samples from the east, northeast and southeast parts of the Hassi Messaoud field (positive PC1 and positive PC2).

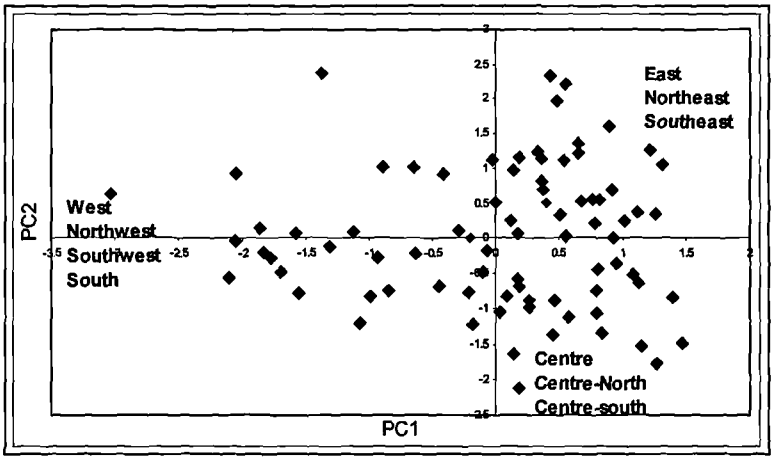

Figure 5.26 A scores plot of PC1 versus PC2 showing the relationship between the Hassi Messaoud oil samples in terms of the first and second principal components. PC1 explains 36.40% of the total variance in the scaled data set; PC2 explains a further 15.05%.

An explanation of these two principal components is given by the loadings plots in Figure 5.27. These diagrams exhibit the loadings of the different variables within the principal components. The first principal component accounts for 36.40% of the total variance of the data set; PC1 mainly discriminates oils from the centre, east northeast and southeast which are relatively enriched in C_{21} (ααα+αββ) pregnanes and C_{22} (ααα+αββ) homopregnanes, C_{27} and C_{29} 13β(H), 17α(H) diasteranes 20S and 20R, C_{21}, C_{24} and C_{25} tricyclic terpanes, and the maturity parameters %Rc and C_{20} TAS/[C_{20}TAS+C_{28} 5α(H) (S+R)TAS] (positive PC1) from oil samples in the west, northwest, southwest and south which are relatively enriched in C_{29} 5α(H),14α(H), 17α(H) sterane 20S and 20R, Ts, Tm, C_{29} 17α(H)hopane, C_{29} Ts and C_{30} 17α(H)hopane (negative PC1). Therefore, it could be considered that the principal component PC1 in the score plots displays mainly the different molecular effects related to the maturity of the oil samples throughout the Hassi Messaoud field. The second principal component PC2 accounts for 15.05% of the total variance of the data set matrix. PC2 distinguishes the oil samples from the east northeast and southeast which are enriched in C_{26}, C_{28}, C_{29}, C_{30}, and C_{31} extended tricyclic terpanes, C_{30} diahopane and C_{27} 13β(H), 17α(H) diasteranes 20S and 20R (positive PC2) from oil samples in the centre, west, southwest and northwest which are enriched in C_{21} (ααα+αββ) pregnanes and C_{22} (ααα+αββ) homopregnanes, C_{29} 5α(H), 14α(H), 17α(H) steranes (20S and 20R), C_{27}, C_{28} and C_{29} 5α(H).14β(H), 17β(H) steranes 20S and 20R, and C_{23} tricyclic terpanes (negative PC2). Consequently, it could be

considered that the principal component PC2 in the score plots is controlled by other factors than maturity; likely facies differences.

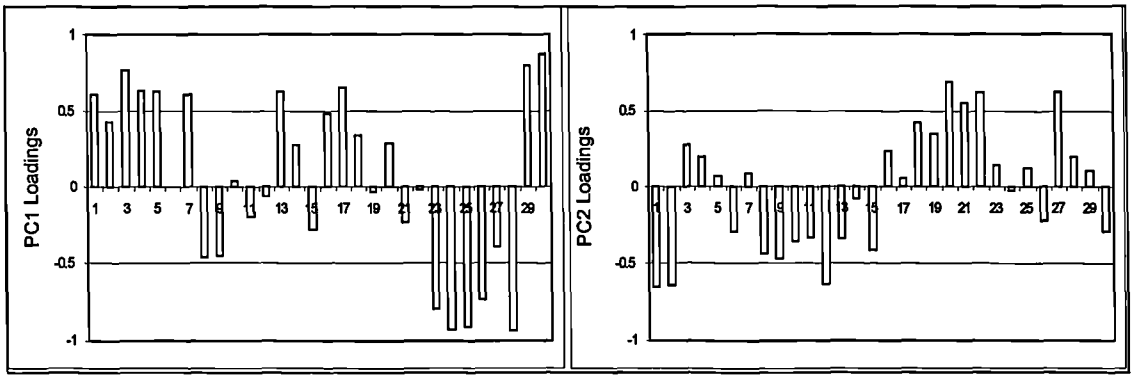

Figure 5.27 Loadings plots showing the composition of the first two principal components, which scored 36.40% and 15.05% of the total variance in the data set, respectively.

In summary, it appears that the principal component PC1 in the score plots displays mainly the different molecular effects related to the maturity of the oils; whereas PC2 likely displays the source facies differences inherited from the source rock strata. The oil samples from the west, northwest, southwest, and south flanks of the Hassi Messaoud field, plotting in the left side of the PC1 are less mature than those from the centre, east, northeast, and southeast parts of the same field, plotting in the right side of PC1. This observation agrees well with the maturity trends shown in the contour maps above using conventional biomarker and aromatic hydrocarbon parameters. Further evidence suggesting that PC1 is predominantly maturity related is shown when PC1 scores are plotted with the inferred biomarker maturity parameters shown in Figure 5.28. Strong correlations are observed between PC1 and Ts/(Ts+Tm), C_{29}Ts/(C_{29}Ts + C_{29}17α (H) hopane), C_{30}diahopane/(C_{30}diahopane + C_{29}17α (H) hopane) and C_{23} tricyclic terpane/(C_{23} tricyclic terpane + C_{30}17 α (H) hopane).

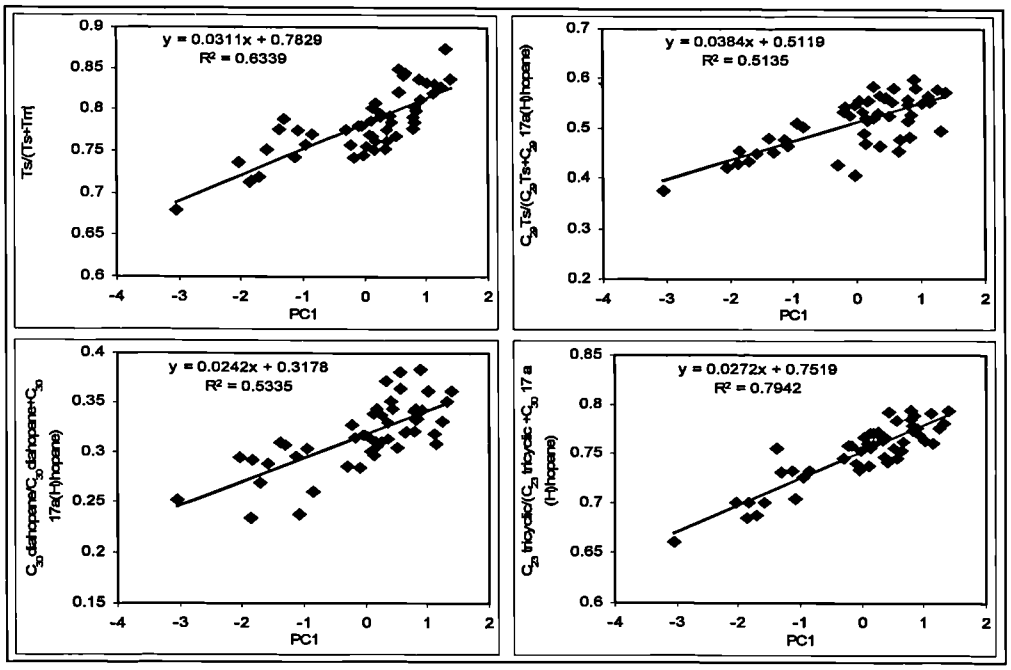

Figure 5.28 PC1 scores plotted with the inferred biomarker maturity parameters, confirming that PC1 in predominantly maturity related.

Figure 5.29 shows the contour maps plotting the score values of the two principal components PC1 and PC2 throughout the Hassi Messaoud field. As it was revealed above, PC1 is predominantly maturity related; therefore in the contour map below (Figure 5.29a), PC1 is differentiating the oil samples showing the highest maturity located mainly in the centre and east of the Hassi Messaoud field, except the oil sample MD#134 located in the centre of the zone 20A in between MD#177 and MD#129, from those with relatively lower maturity located towards the west, northwest, north, southwest, south, and southeast flanks of the Hassi Messaoud field. These maturity trends agree well with those found earlier using the conventional biomarker and aromatic hydrocarbon maturity parameters. Note that the least mature oil samples appear to be trapped in the far western flanks, more accurately within the zones 1A, 1B and 1C; whereas the highest mature oil samples are trapped in the centre, more exactly within the zones 6, 7, 8 and north and south of the zones 20A, 20B, 2ex, and 13 (see Figure 5.30 for the location of these zones). The trends of maturity of the oils across the field do not appear to be disturbed by the major faults cross cutting the different compartments within Hassi Messaoud field.

Figure 5.29b shows the variations in the PC2 scores across the Hassi Messaoud field. It has been shown above that PC2 is maturity independent, and is controlled probably by other factors such as source facies features inherited from the source rocks located

in the study area. It appears that PC2 is distinguishing two major groups of oil samples. The oil samples located towards the east, northeast and southeast of the field, east of the major south-southwest-north-northeast fault which divides the field into two major blocks exhibit the highest PC2 scores. Those located west of this fault exhibit the lowest PC2 scores. Therefore, I believe that the oil samples from the east, northeast and southeast of Hassi Messaoud field were probably generated from Silurian source rock strata (likely located to the east of the field) having slight facies differences from the Silurian source rock strata that have generated the oils located to the west of the major fault (located in the Oued Mya basin, west-northwest of the field). This observation is supported by the following lines of evidence: (1) the oil samples analysed in the eastern parts of the field show higher concentrations of the C_0-C_3 alkylcarbazoles compared to those located towards the west (see section 5.5.1.4 bellow), (2) the bulk composition, obtained by Iatroscan screening of the reservoir core extract samples for well MD#213 located to the far east of the field revealed that the core samples analysed within the interval 3483.45 to 3499.5m with relatively higher permeability and porosity values, show highest total petroleum and polar yields; therefore these reservoir intervals might have been used as migration pathways during the field charging (see section 5.4.3.1 for more details), (3) the core sample at the depth of 3499.5m revealed high abundance of petroleum fluid inclusions (Oxtoby et al., 1995), and (4) an unpublished geotechnical report carried out by the Canadian Petroleum International Resources Ltd (1998) in the Hassi Dzabat permit located about 30-40 km east-southeast of the Hassi Messaoud field, revealed the presence Silurian source rock strata in this region, i.e. about 40 km east of Hassi Messaoud field (Figure 5.1). A remnant of the basinal "hot" Silurian source rocks appears to have been preserved from Hercynian erosion. These observations do suggest that the Hassi Messaoud field was possibly charged from the west-northwest (i.e. from the Silurian source rocks in the Oued Mya basin) and from the east (i.e. from the Silurian source rocks identified in the Hassi Dzabat permit) (Figure 5.30).

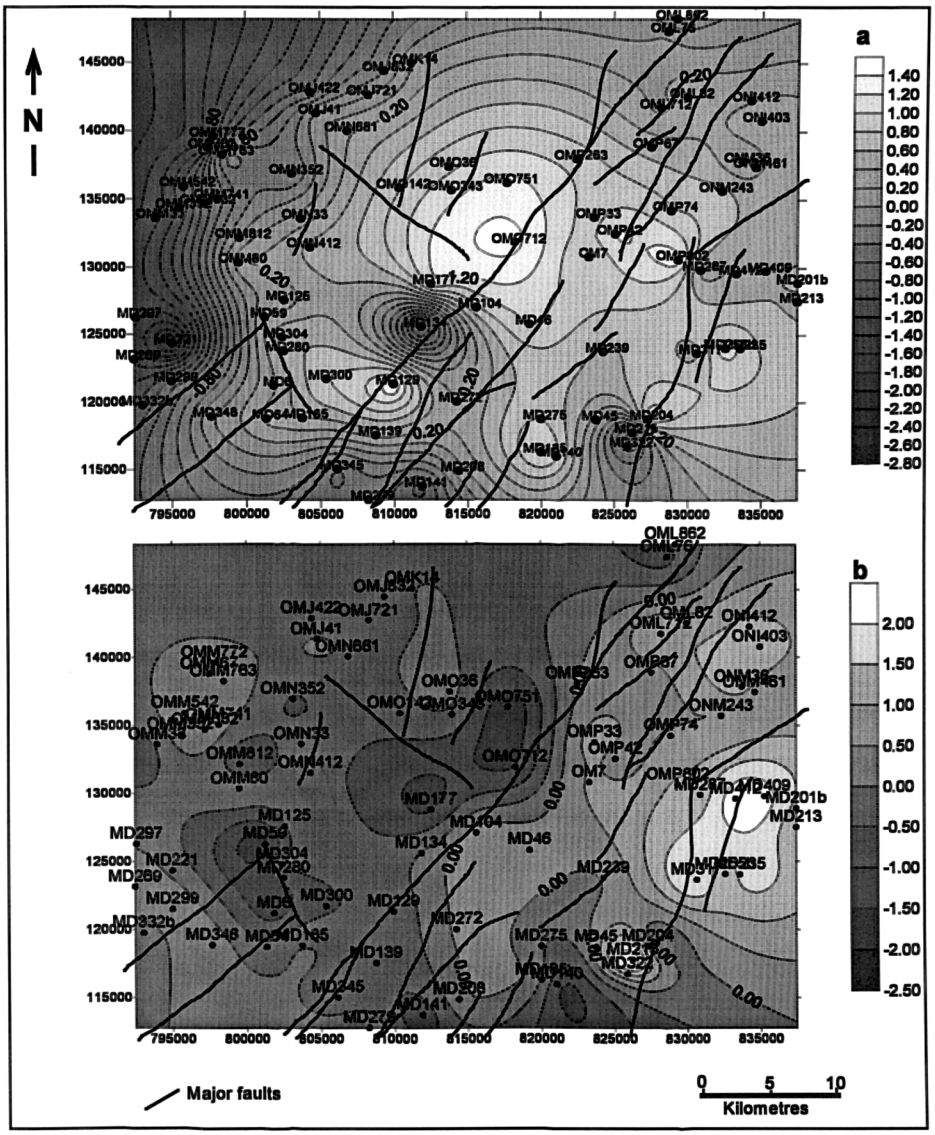

Figure 5.29 Contour map displaying lateral variations of (a) PC1and (b) PC2 scores throughout Hassi Messaoud field.

Figure 5.30 shows the detailed distributions of the Hassi Messaoud oils in terms of the principal components PC1 and PC2. The results show two main groups of oil samples. The oils located west of the main southwest-northeast fault exhibit a general petroleum maturity trend decreasing from the oil trapped in the centre towards the west, northwest, north, southwest and south flanks of the field. The oils located east of the main fault show to some extent similar maturity as those from the centre; however, in addition they seem to contain higher concentrations of diasteranes, diahopane and C_{26}, C_{28}, C_{29}, C_{30}, and C_{31} extended tricyclic terpanes compared to those from the centre and western parts of the field. Therefore, it is likely that the oil trapped in the eastern parts of Hassi Messaoud field were generated from a Silurian source rock strata located to the east (Figure 5.1).

The distinction between the two main groups of oils suggest that the main fault which separates these oils played a role of a barrier preventing mixing of the oils generated from the Silurian source rock strata in the Oued Mya basin west-northwest of Hassi Messaoud field and the oils generated from the Silurian source rock strata located to the east of the field. However, in the southern part of the field (i.e. zones 20A, 23 to the west and zones 24 and 25 to the east), it seems that the same fault is permeable and oils from the western part might have migrated towards the eastern part of the field. The other faults across the field do not show any evidence of preventing communication between the different zones of the Hassi Messaoud field. It seems that these faults were permeable to the oil migration during all the time of field charging.

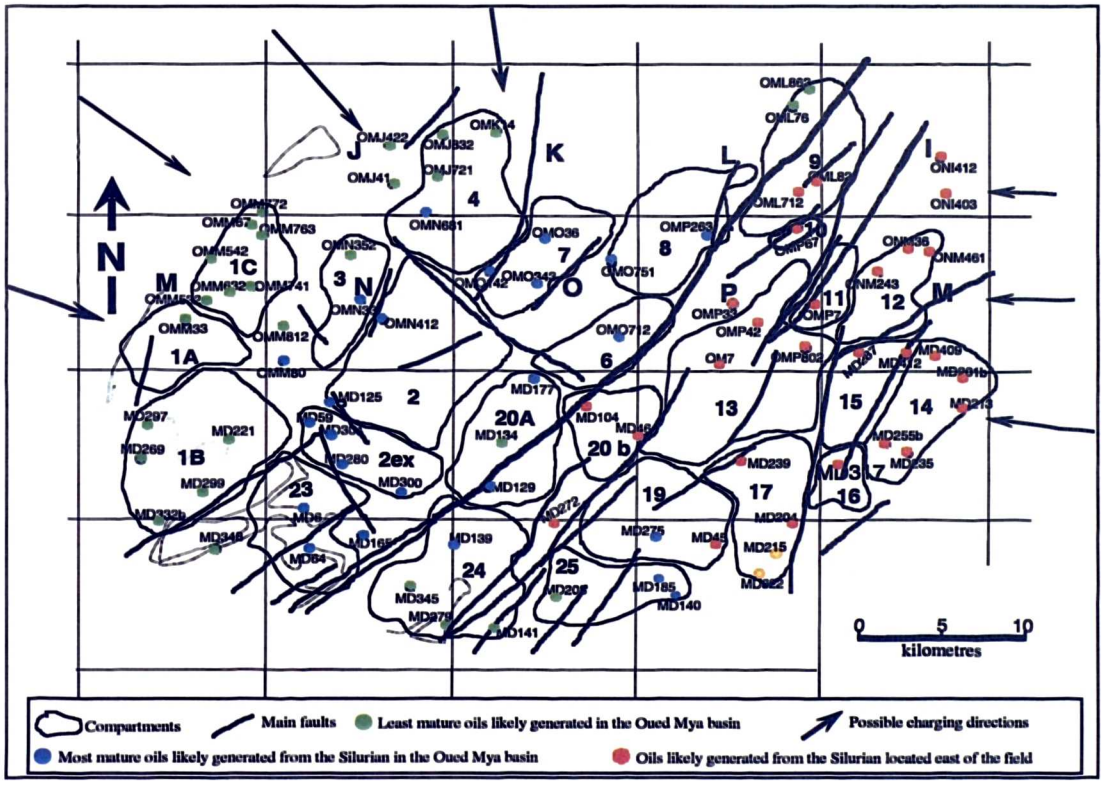

Figure 5.30 Maturity and facies variations across the Hassi Messaoud field obtained from the PC1 and PC2 scores. The arrows show the suggested filling directions.

Figure 5.31 shows that the 25 zones which were distinguished on the basis of the petrophysical properties and the pressures of the wells throughout Hassi Messaoud field appear to be rational. In general, it can be clearly seen from this diagram that the wells analysed in the Hassi Messaoud field can, to a certain extent, be grouped into the same clusters as shown in Figure 5.30, using biomarker concentrations. In total, there are 7 zones (from 25) which show major differences between the wells within them. For instance in zone 17, the oils MD#322 and MD#215 plot separately from the

oils MD#239 and MD#204; zone 24, oil MD#139 plots away from the oils MD#141, #279, and #345; zone 25, oil MD#208 plots away from the oils MD#140 and #185; zone 4, oil OMK#14 plots away from the oils OMJ#832, #721, and OMN#681; zone 3, oil OMN#532 plots away from oil OMN#33; zone 19, oil MD#45 plots away from oil MD#275, and zone 20A, oil MD#134 appears to be different from the oils MD#129 and #177. Moreover, the oil samples in the zones 9, 10, 11, 12, 13, 14, 15, 16, 17, and 20B together with the wells ONI#403 and #412, OMP#33, and MD#272 located outside these zones from the east parts of Hassi Messaoud field plot close to each other showing positive PC1 and PC2; the oil samples in the zones 2, 2ex, 6, 8, 20A, 23, and 25 from the centre, centre–north and centre–south plot close in this diagram with positive PC1 and negative PC2; and the oil samples analysed in the zones 1A, 1B, 1C, 4, and 24 from the western flanks plot in the left side of this diagram with negative PC1.

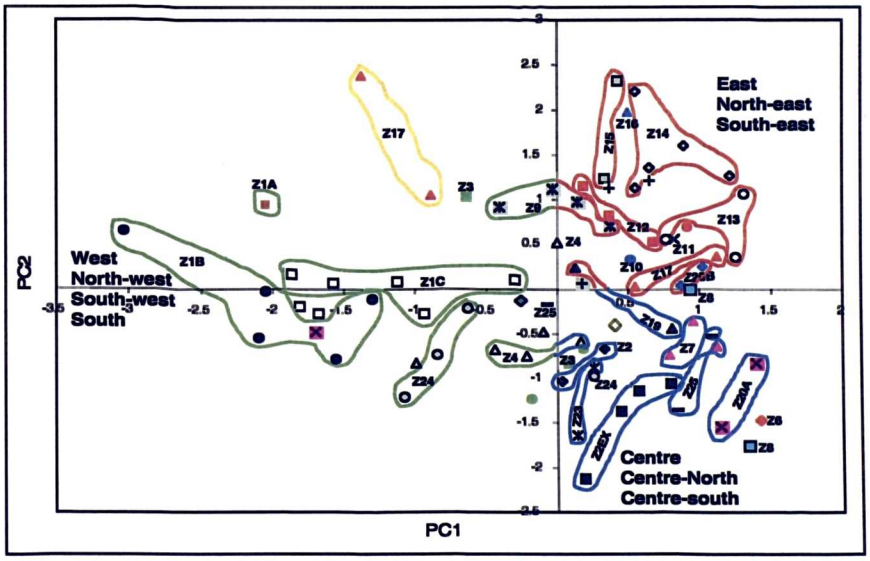

Figure 5.31 Cross plot of the PC1 versus PC2 which confirm the separation of the Hassi Messaoud field into 25 production zones, using the principal components analysis obtained from the biomarker concentrations and maturity parameters.

Distribution of the alkylcarbazoles and benzocarbazoles throughout the Hassi Messaoud field

The principal component analysis (in section 5.4.1) suggested that the concentration and distribution of alkylcarbazoles seem to be mainly influenced by the migration distances of the oils. Therefore, in this section I am going to use the same parameters listed in Table 5.4 and the concentrations of benzocarbazoles across the Hassi

Messaoud field. The concentrations and the ratios of the alkylcarbazoles and benzocarbazoles across the Hassi Messaoud field are listed in Appendix 5.2.

The concentrations of the C_0-C_3 alkylcarbazoles in the Hassi Messaoud field range from 4.59 to 26.84 μg g^{-1} of oil (average 11.58 μg g^{-1} of oil). The highest concentrations are recorded towards the eastern flanks ranging from 9.66 to 26.84 μg g^{-1} of oil (average 16.58 μg g^{-1} of oil) and western flanks ranging from 8.24 to 20.41 μg g^{-1} of oil (average 11.98 μg g^{-1} of oil) of the field. The lowest concentrations are found in the centre, north and south of the Hassi Messaoud field ranging from 4.75 to 14.44 μg g^{-1} of oil (average 8.86 μg g^{-1} of oil) (Figure 5.32a). The concentrations of the benzocarbazole [a] and [c] isomers in the Hassi Messaoud field are very low, ranging from 0.017 to 0.14 μg g^{-1} of oil (average 0.066 μg g^{-1} of oil) (Figure 5.32b). Again, the highest concentrations of the benzocarbazoles are recorded in the eastern and western flanks (average concentrations are 0.084 and 0.076 μg g^{-1} of oil, respectively), whereas the lowest concentrations are found towards the centre of the field (average concentrations 0.054 μg g^{-1} of oil), showing similar trends compared to the distribution of the concentrations of the C_0-C_3 alkylcarbazoles across the field.

Higher concentrations of the C_0-C_3 alkylcarbazoles and benzocarbazole isomers in the oils from eastern and western flanks relative to those from the centre, north and south of the Hassi Messaoud field suggest that the oils trapped in the eastern and western flanks have probably experienced shorter migration distances than the oils trapped in the centre, north and south parts of the field. These findings also suggest two possible filling directions one from the west-northwest of the Hassi Messaoud field (likely originating from the Silurian source rock strata in the Oued Mya basin) and the second from the east of the Hassi Messaoud field (probably from the Silurian located in the Hassi Dzabat area. These observations are in agreement with results obtained by the principal components displayed earlier.

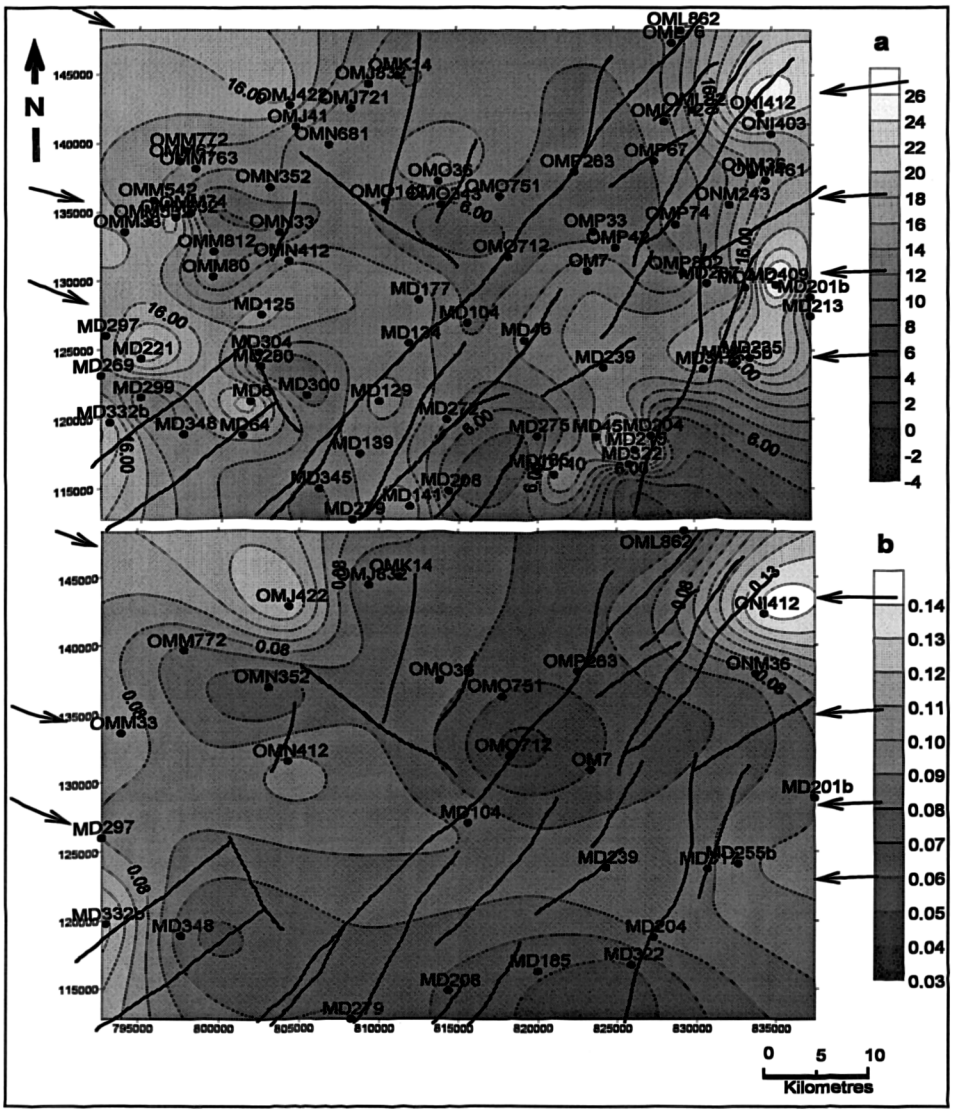

Figure 5.32 Contour map displaying lateral variations of concentrations of the (a) summed C_0-C_3 alkylcarbazoles and (b) benzocarbazole ([a]+[c]) isomers throughout the Hassi Messaoud field. The arrows suggest the possible filling directions.

The Hassi Messaoud oils show similar average concentrations of the C_0-C_3 alkylcarbazoles and benzocarbazoles ([a]+[c]) compared to the oils from Haoud Berkaoui and Benkahla fields, whereas the average of the C_0-C_3 alkylcarbazole concentrations in Hassi Messaoud oils are 3 to 4 times lower than in the oils from Guellala northeast, N'goussa and Mokh-el-Kebch fields and 45 times lower than the concentrations of the same compounds in the Silurian source rock samples analysed in the Oued Mya basin (Figure 5.33a, see also Figure 5.1 for field locations). The average benzocarbazole concentrations ([a]+[c]) are 3 to 7 times lower than in the oils from Guellala northeast, N'goussa and Mokh-el-Kebch fields and over 900 times lower than the average benzocarbazole concentrations in the Silurian source rock samples (Figure 5.33b).

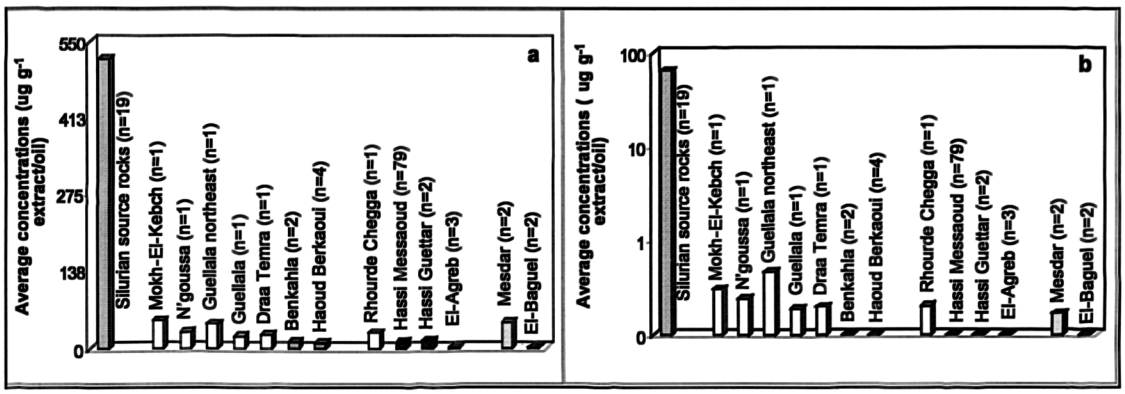

Figure 5.33 Histogram distribution showing comparison of (a) the average concentrations of C_0-C_3 alkylcarbazole and (b) the average concentrations of the benzocarbazoles ([a]+[c]) in the Silurian source rock (μg g^{-1} extract) and the oils (μg g^{-1} oil) analysed in this project. Note that "Y" axis in second diagram is in logarithmic scale.

The strong variation in the alkylcarbazole and benzocarbazole concentrations between the Silurian source rock strata and the related oils analysed in this project is described in section 5.4.2.1.4 above. In addition, the relatively low concentrations of the alkylcarbazole and benzocarbazole in the Hassi Messaoud oils do suggest that these oils have undergone long lateral migration distances (at least 40km) from the Silurian source rock(s) likely located in the Oued Mya basin to the west and in the Hassi Dzabat area to the east of the field.

Figure 5.34 displays the lateral variations of the of N-H-shielded isomer relative to N-H-exposed isomer ratios 1,8-DMC/(1,8-DMC+2,4-DMC) and 1,8-DMC/(1,8-DMC+2,5-DMC) throughout the Hassi Messaoud field. The abundance of N-H-shielded isomer relative to N-H-exposed isomer ratios [1,8-DMC/(1,8-DMC+2,4-MC) and 1,8-DMC/(1,8-DMC+2,4-DMC)] show an increase in their values from the oils in the western and eastern flanks of the Hassi Messaoud field ranging from 0.71 to 0.82 and 0.74 to 0.82, respectively, towards the oils in the centre of the field ranging from 0.84 to 0.96 and 0.84 to 0.96, respectively (Appendix 5.2). Li et al. (1995 and 1998) showed that with increasing migration distance, oils from the same sources and similar thermal maturity display a decrease in the absolute concentrations of the N-H-exposed isomers (e.g. 2,4-DMC and 2,5-DMC) compared to the N-H-shielded isomer (e.g. 1,8-DMC). Therefore, these observations suggest that the oils trapped in centre of the Hassi Messaoud might have migrated further than those from the eastern and western flanks of the fields, which agrees well with the results shown above for the absolute concentrations of the C_0-C_3 alkylcarbazoles and benzocarbazoles ([a]+[c]).

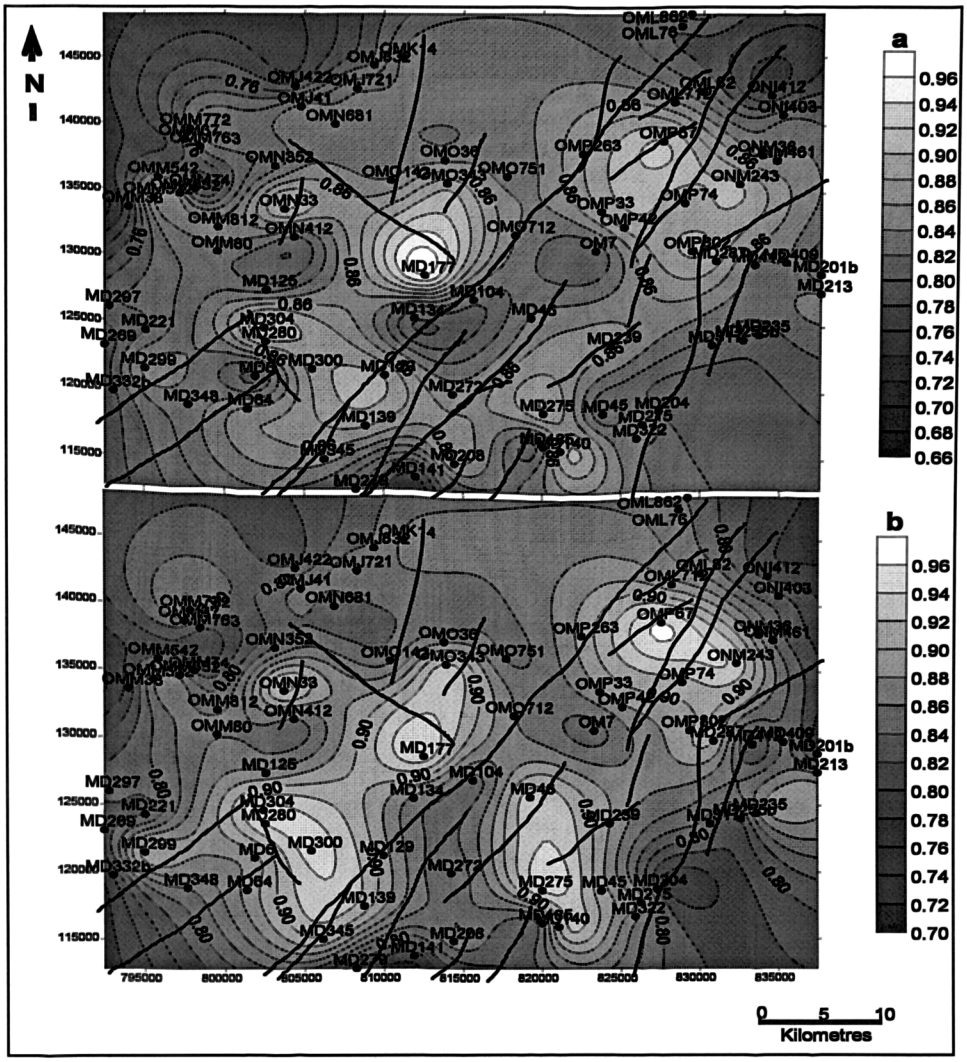

Figure 5.34 Contour map displaying lateral variations of the shielded relative to exposed dimethylcarbazole ratios (a) 1,8-DMC/(1,8-DMC+2,4-DMC) and (b) 1,8-DMC/(1,8-DMC+2,5-DMC) throughout the Hassi Messaoud field.

5.5.2. Lateral geochemical variations of core extract petroleum throughout the Hassi Messaoud reservoir

In this section I will explore the lateral variation across the Hassi Messaoud reservoir units Ra and R2 by performing analysis on the bulk composition, aliphatic and aromatic hydrocarbons in a set of reservoir core samples. In total, twenty nine (29) core reservoir extract petroleum samples extracted from samples from 8 wells in the Hassi Messaoud field have been analysed by gas chromatography and gas chromatography mass spectrometry. These samples were selected from wells located in the centre (MD#177 and OMO#712), east (MD#213), northeast (OML#712), south (MD#141), southwest (MD#319), west (OMM#33), and northwest (OMJ#41) of the Hassi Messaoud field (Figure 5.35). The aim of this section is to check whether the petroleum extracted from the reservoir core samples present any facies and/or

maturity related differences across the Hassi Messaoud reservoir units Ra and R2. Note that some of the reservoir core samples from the same wells and same depths analysed in this section were also selected for fluid inclusions analysis (see chapter 6).

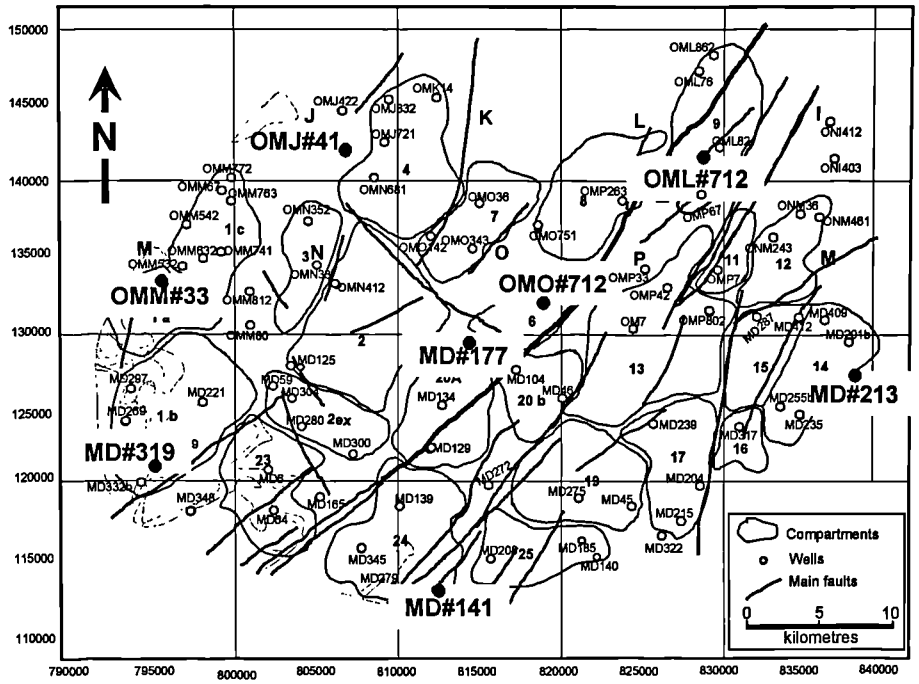

Figure 5.35 Map showing the wells sampled for the Iatroscan screening and geochemical characterisation of the reservoir core extracts in the Hassi Messaoud field.

5.5.2.1. Bulk composition of the core extract samples

The ternary diagram plotted in Figure 5.36 shows significant compositional differences in the C_{15}+ fraction when the compound class distribution (aliphatic hydrocarbons, aromatic hydrocarbons and polar compounds, i.e. resins and asphaltenes) in the produced oils and core extract petroleums for the same wells are compared (Appendix 5.3). This might be normal, since the reservoir core samples have been stored for several years (in the Sahara) and light hydrocarbons would be expected to be preferentially removed. Therefore, during samples storage, aerobic biodegradation may have also played a major role in the removal of the *normal*-alkanes from the oil hosted within the reservoir cores.

Moreover, in an attempt to simulate the evaporation losses during samples storage, Horstad et al. (1990) treated some oil samples by rotary evaporation. They showed that the relative compound class distribution of the evaporated oils had undergone a minor shift towards those of reservoir core extracts, but a significant difference in

composition still persisted. They suggested that the differences in the compound class distributions are real, and mainly affect the relative amounts of aromatic hydrocarbons and polar compounds, whereas the amount of aliphatic hydrocarbons remains practically unchanged.

The core extracts analysed in this study contain lower percentages of aromatic hydrocarbons and higher percentages of polar compounds than the produced oils, suggesting that fractionation may occur during oil production, which is probably caused by adsorbed non-producible polar components (Larter et al., 1990).

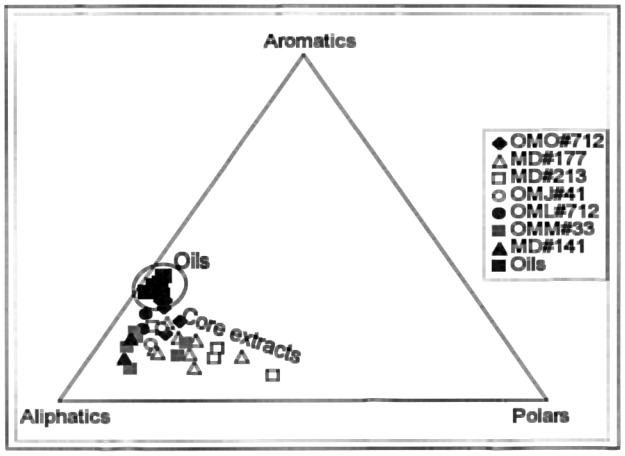

Figure 5.36 Ternary diagram showing bulk composition of produced oils and core extracts from the same wells for Hassi Messaoud field.

5.5.2.2. *Normal*-alkanes distributions

The *normal*-alkanes of the core extract samples analysed by GC reveal similar distributions for all the samples (Figure 5.37). The *n*-alkane distributions show that compounds lighter than C_{20} are depleted from the core extract samples. To a certain extent this may be due to evaporation of the light ends of the samples during storage (i.e. samples were stored for several years in the south of Algeria where the temperatures in the summer can reach up to 45 °C). Some light end loss also occurs during the analytical preparation procedure, but this should be similar for both core extracts and oil samples.

All the samples contain a large unresolved complex mixture (UCM) (Figure 5.37) which may indicate that aerobic biodegradation has occurred during sample storage in unfavourable conditions. In fact, core samples analysed in this study have been stored for several years (ca. 10 to 25 years) at an average temperature of 20 to 35°C.

Therefore during storage, petroleum in the core samples have been biodegraded and oxidized. This phenomenon would cause depletion in some *n*-alkanes, formation of a UCM, and formation of polar compounds (lipids from degrading bacteria). Figure 5.38 shows the presence of oxidized bitumen within two reservoir sandstone samples from the wells OMO#712 and MD#319 in the Hassi Messaoud field, which may also be related to the alteration during storage.

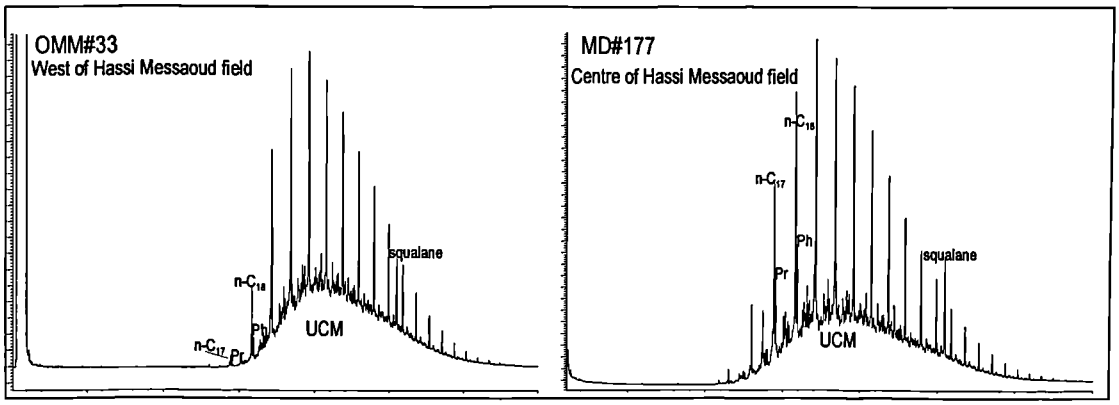

Figure 5.37 Gas chromatograms of the aliphatic fraction showing occurrence of a large UCM in typical core extract samples from the wells OMM#33 and MD#177, Hassi Messaoud field.

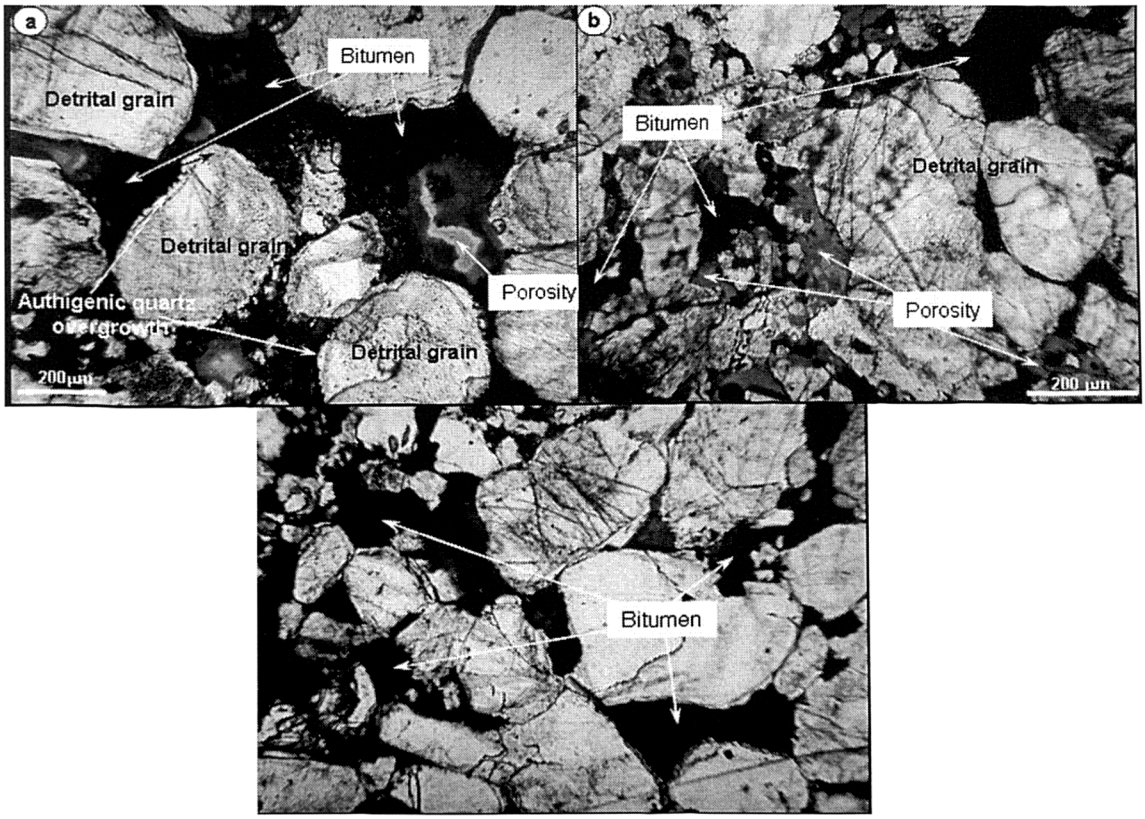

Figure 5.38 Photos illustrating the occurrence of bitumen in (a) OMO#712 (3324.9m) and (b) MD#177 3339.45 m from the centre and (c) MD#319 (3453.25 m) from the southwest of the Hassi Messaoud field.

Typical facies related ratios such as Pr/Ph, Pr/*n*-C_{17}, Ph/*n*-C_{18}, and *n*-C_{17}/*n*-C_{27} (*normal*-alkane index) are not reliable as all of the samples have suffered a substantial evaporation on the lighter compounds up to the C_{20} *normal*-alkane (Figure 5.37).

5.5.2.3. Biomarkers and aromatic compounds

Table 5.7 displays the bulk composition, biomarker and aromatic hydrocarbon parameters calculated from the reservoir core samples throughout the Hassi Messaoud field.

The biomarker alkanes and the aromatic hydrocarbon compound parameters obtained from the core extract petroleum samples are displayed in Table 5.7. The core extracts (except those from well OMO#712 located in the centre of the field) from the reservoir units Ra and R2 analysed by GC/MS show very similar sterane and terpane distributions (Figure 5.39). In general the terpanes are dominated by the tricyclic terpanes over the hopanes, and the steranes are dominated by diasteranes over regular steranes in all the samples.

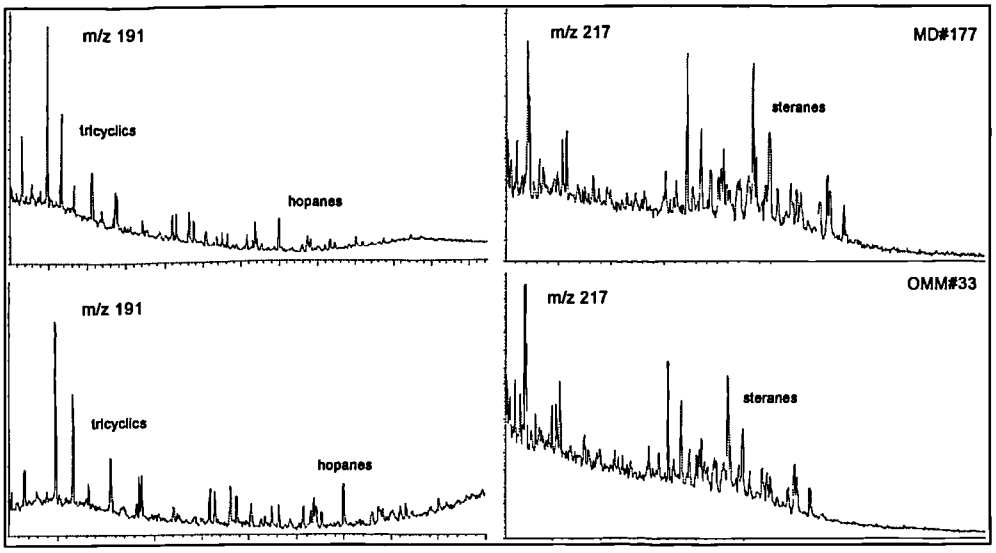

Figure 5.39 Partial m/z 191 and 217 mass chromatograms showing the distribution of terpanes and steranes in two typical core extract samples from the Hassi Messaoud field.

However, four (4) core extract petroleums from well OMO#712 (3336.7, 3345.6, 3354.5 from the reservoir unit Ra and 3387.65 m from the reservoir unit R2) exhibit different features than the samples from the other wells. The terpanes are characterised by similar concentrations of tricyclic terpanes and hopanes, very low abundance of Ts and C_{29} Ts compared to Tm and C_{29} αβ hopane respectively, the

presence of relatively abundant 17β(H) 21α(H) C_{29} and C_{30} hopanes (normoretane and moretane) and finally abundant occurrence of the C_{30} gammacerane (Figure 5.40). The steranes are characterised by a relatively higher abundance of the biological 5α(H) 14α(H) 17α(H) R configurations than the 5α(H) 14α(H) 17α(H) S and the 5α(H) 14β(H) 17β(H) configurations. The extract sample OMO#712 (3406.5 m) shows different steranes and terpanes distributions than the rest of the extract samples from the same well. This extract sample exhibits the same features as the rest of the samples from the other wells, although it still shows the occurrence of gammacerane but in much lower abundance than the other samples.

The occurrence of gammacerane appears to compose a marker for highly saline (stratified) marine and non-marine depositional environments (Peters and Moldowan, 1993). Gammacerane is encountered in many lacustrine oils and bitumens (Hills et al., 1966; Moldowan et al., 1985; Jiang and Fowler, 1986; Fu Jiamo et al., 1986, 1988; Brassell et al., 1988), and in certain marine petroleums from carbonate or evaporite source rocks (Rohrback, 1983; Moldowan et al., 1985; Mello et al., 1988a and b; Moldowan et al., 1992).

So far gammacerane has not been reported either in the Silurian and the Ordovician source rocks nor in any of the produced oils analysed in the Oued Mya basin and the fields on the Hassi Messaoud Ridge. Therefore, the gammacerane in these core extracts must come from another source. Interestingly, Fennouh (1996) reported the occurrence of evaporitic cements in the Cambrian reservoirs in Hassi Messaoud field. He suggested that the presence of these cements in the Cambrian reservoirs is linked with a regime associated with cement deposition from saline fluids coming from the overlying evaporitic Triassic formations. Fennouh (1996) stated that the evaporitic cements observed in the Cambrian sandstones are certainly not contemporaneous to the Cambrian deposit, but occur by infiltration likely after the completion of the Triassic salineferous deposition. Hence, the core extract samples from well OMO#712 showing the occurrence of gammacerane probably contain a mixture of residual oil originated and migrated from the Silurian source rocks in the surrounding area and organic matter transported from the evaporitic Triassic sediments (containing gammacerane) deposited above the Cambrian reservoirs. Fennouh (1996) observed in a few samples that the same anhydrite covers the intergranular rock pores which were

previously plugged by the solid bitumen precipitation. These observations led him to suggest that the solid bitumen originated from migration of the first oil charge into Hassi Messaoud reservoirs which likely took place earlier than the deposition of the salineferous Triassic.

More details about the origin of the petroleum extracted from the samples in well OMO#712 compared to the rest of the samples from the other wells are provided in the following sections.

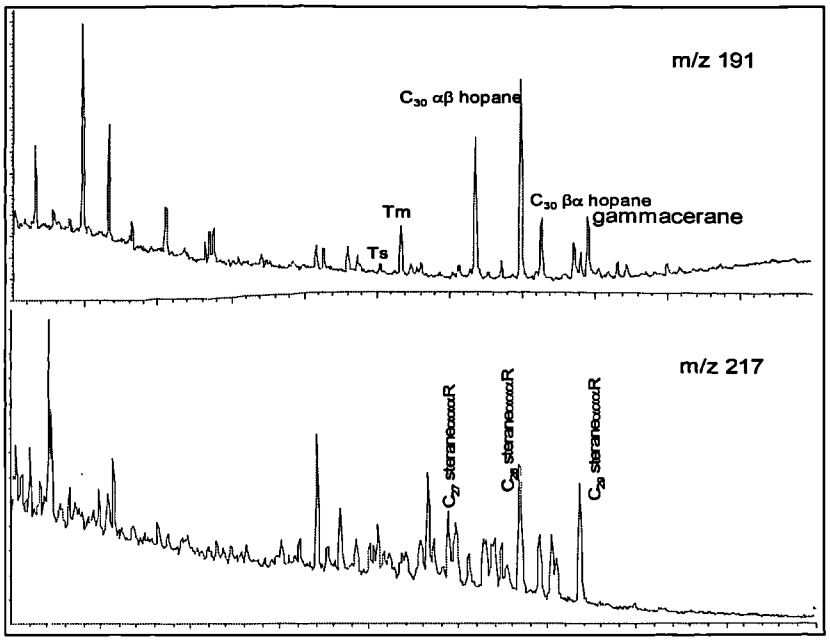

Figure 5.40 Partial m/z 191 and 217 mass chromatograms of an extract sample from the well OMO#712 showing the occurrence gammacerane and immaturity features.

Table 5.7 Bulk composition, biomarker and aromatic hydrocarbon parameters calculated for the reservoir core samples.

Well	Depth (m)	Reserv oir unit	Nature of sample	1	2	3	4	5	6	7	8	9	10	11	12	13	14	15	16	17	18	19	20	21	22	23	24
OMO#712	3336.7	Ra	Sds	3.6	68.6	19.4	12.0	0.40	0.36	0.06	0.03	0.64	0.18	0.40	0.16	7.25	0.28	0.42	0.24	-	-	-	0.89	0.81	0.89	7.15	0.87
OMO#712	3345.6	Ra	Sds	22.2	64.8	28.6	6.6	0.38	0.34	0.06	0.03	0.61	0.18	0.34	0.14	6.63	0.31	0.40	0.21	32.75	27.91	39.34	0.95	0.91	0.94	6.78	0.85
OMO#712	3354.5	Ra	Sds	22.4	65.4	26.5	8.1	0.38	0.33	0.05	0.03	0.65	0.13	0.45	0.15	9.95	0.28	0.40	0.21	-	-	-	-	-	-	-	-
OMO#712	3387.7	R2	Sds	21.8	63.8	28.6	7.6	0.41	0.35	0.06	0.03	0.62	0.21	0.35	0.16	6.48	0.34	0.41	0.22	33.14	28.43	38.43	1.01	0.92	0.95	6.54	0.84
OMO#712	3406.5	R2	Sds	5.1	63.9	22.9	13.2	0.49	0.53	0.23	0.17	0.55	0.49	0.64	0.46	7.75	0.14	0.67	0.40	-	-	-	0.97	0.84	0.91	7.74	0.88
MD#177	3287.5	Ra	Sds	3.2	63.3	17.4	19.3	0.54	0.57	0.28	0.20	0.85	0.56	0.81	0.51	4.86	0.14	0.72	0.38	-	-	-	0.92	0.79	0.88	5.46	0.85
MD#177	3300.4	Ra	Sds	9.9	72.9	15.0	12.0	0.57	0.59	0.30	0.20	0.81	0.61	0.84	0.51	6.13	0.14	0.72	0.40	-	-	-	0.94	0.85	0.91	5.69	0.87
MD#177	3309.5	Ra	Sds	2.3	56.2	12.7	31.1	0.55	0.63	0.36	0.21	0.79	0.64	0.81	0.52	5.21	0.16	0.77	0.41	-	-	-	0.97	0.83	0.90	5.27	0.93
MD#177	3318.6	Ra	Sds	9.2	67.7	9.5	22.8	0.54	0.62	0.28	0.20	0.81	0.60	0.86	0.51	6.71	0.13	0.76	0.37	-	-	-	0.99	0.91	0.95	4.47	0.94
MD#177	3330.5	Ra	Sds	7.5	66.8	13.4	19.8	0.56	0.59	0.26	0.19	0.86	0.60	0.88	0.51	6.91	0.17	0.74	0.36	-	-	-	0.96	0.88	0.93	4.92	0.96
MD#177	3339.5	R2	Sds	15.1	73.2	13.6	13.2	0.54	0.57	0.32	0.16	0.80	0.64	0.79	0.48	6.00	0.22	0.74	0.37	44.47	18.77	36.76	1.01	0.94	0.97	7.27	0.90
MD#177	3351.6	R2	Sds	17.7	68.6	20.9	10.5	0.56	0.57	0.30	0.22	0.84	0.61	0.87	0.56	6.08	0.14	0.73	0.46	-	-	-	0.98	0.92	0.95	6.93	0.93
MD#177	3365.1	R2	Sds	10.3	66.9	17.9	15.3	0.55	0.59	0.29	0.17	0.73	0.68	0.84	0.50	5.44	0.19	0.74	0.39	-	-	-	0.98	0.89	0.93	6.51	0.93
MD#177	3376.9	R2	Sds	7.6	66.7	22.3	11.0	0.53	0.61	0.37	0.27	0.68	0.67	0.75	0.52	5.48	0.21	0.79	0.42	45.13	19.02	35.85	0.96	0.87	0.92	6.72	0.92
OMM#33	3406.5	Ra	Sds	1.7	69.1	13.0	18.0	0.58	0.59	0.45	0.24	0.67	0.73	0.80	0.50	4.96	0.15	0.77	0.39	-	-	-	0.93	0.77	0.86	6.99	0.89
OMM#33	3413.8	Ra	Sds	1.7	65.8	16.6	17.6	0.53	0.60	0.34	0.23	0.67	0.69	0.70	0.51	6.13	0.14	0.77	0.37	-	-	-	0.83	0.75	0.85	5.94	0.87
OMM#33	3446.8	Ra	Sds	2.7	81.0	9.0	10.1	0.58	0.57	0.27	0.13	0.75	0.58	0.80	0.49	6.89	0.10	0.78	0.32	-	-	-	0.80	0.75	0.85	5.66	0.93
OMM#33	3464.5	Ra	Sds	17.9	75.2	18.0	6.7	0.53	0.60	0.26	0.14	0.74	0.56	0.78	0.49	6.13	0.16	0.80	0.32	43.86	20.72	35.42	0.82	0.78	0.87	4.04	0.91
OMM#33	3473.9	Ra	Sds	9.1	78.2	15.3	6.4	0.54	0.58	0.30	0.14	0.66	0.61	0.86	0.50	7.17	0.11	0.81	0.32	-	-	-	0.85	0.80	0.88	4.85	0.92
OMM#33	3483.8	Ra	Sds	10.0	74.4	19.7	5.9	0.53	0.58	0.27	0.13	0.73	0.62	0.75	0.47	5.35	0.21	0.79	0.32	45.45	18.44	36.11	0.69	0.67	0.80	4.32	0.89
MD#213	3458.9	Ra	Sds	-	-	-	-	-	-	-	-	-	-	-	-	-	-	-	-	-	-	-	0.98	0.81	0.89	7.29	0.96
MD#213	3468.2	Ra	Sds	6.6	70.4	21.0	8.6	0.56	0.59	0.29	0.15	0.77	0.70	0.80	0.49	4.29	0.21	0.78	0.37	44.24	23.12	32.64	0.96	0.87	0.92	7.43	0.91
MD#213	3483.5	Ra	Sds	5.6	52.9	6.9	40.2	0.54	0.60	0.35	0.15	0.77	0.72	0.83	0.53	6.38	0.10	0.72	0.37	-	-	-	0.86	0.86	0.91	5.58	0.89
MD#213	3499.5	Ra	Sds	8.5	62.1	12.0	25.8	0.55	0.57	0.30	0.19	0.79	0.70	0.79	0.48	4.37	0.23	0.75	0.34	46.92	18.46	34.63	0.93	0.88	0.93	6.62	0.90
MD#141	3438.7	Ra	Sds	10.1	76.7	17.7	5.6	0.53	0.59	0.34	0.24	0.81	0.70	0.82	0.53	5.53	0.19	0.78	0.39	46.52	18.98	34.51	0.95	0.91	0.94	7.12	0.92
MD#141	3450.4	Ra	Sds	5.6	80.5	12.1	7.4	0.52	0.57	0.31	0.23	0.72	0.67	0.80	0.51	4.96	0.22	0.79	0.38	47.99	19.37	32.64	0.89	0.87	0.92	5.79	0.93
MD#319	3453.3	Ra	Sds	14.3	61.3	15.8	23.0	0.54	0.58	0.19	0.11	0.71	0.64	0.76	0.42	4.87	0.19	0.75	0.27	47.16	19.45	33.39	0.78	0.78	0.87	5.33	0.92
OMJ#41	3390.1	Ra	Sds	14.6	68.6	20.7	10.7	0.52	0.59	0.34	0.19	0.65	0.69	0.84	0.56	6.10	0.17	0.80	0.38	47.77	18.15	34.08	0.94	0.92	0.95	6.12	0.92
OMJ#41	3463.5	R2	Sds	16.2	73.0	16.0	11.0	0.51	0.59	0.34	0.18	0.66	0.65	0.84	0.55	5.92	0.19	0.80	0.39	47.58	19.39	33.04	0.96	0.92	0.95	7.04	0.95
OML#712	3406.2	Ra	Sds	12.5	72.5	20.4	7.0	0.54	0.62	0.41	0.26	0.74	0.71	0.86	0.60	6.33	0.19	0.81	0.44	46.50	18.91	34.59	0.85	0.86	0.91	5.73	0.95
OML#712	3437.5	R2	Sds	23.6	70.0	24.5	5.5	0.55	0.64	0.45	0.24	0.62	0.71	0.87	0.65	6.84	0.17	0.85	0.45	45.65	18.03	36.32	1.03	0.92	0.95	7.17	0.93

Key: 1- total extract yield, 2- % aliphatic hydrocarbons, 3- % aromatic hydrocarbons, 4- % polars, 5- C_{29} steranes aaa 20S/(20S+20R), 6- C_{29} steranes bb/(aa+bb), 7- $C_{29}Ts/(C_{29}Ts + C_{29}$ 17 α (H) hopane), 8- C_{30} diahopane/(C_{30}diahopane + C_{30} 17 α (H) hopane), 9- C_{29} 17 α(H)hopane/C_{30} 17 α (H) hopane, 10- Ts/(Ts+Tm), 11- C_{23} tricyclic terpane/(C_{23} tricyclic terpane + C_{30} 17 α (H) hopane), 12-[(Sum extended tricyclic terpanes C_{28}+C_{29} (S+R))/[sum tricyclic terpanes C_{23}+C_{29} (S+R)+ sum C_{29}+C_{30} 17 α (H) hopanes], 13- Sum tricyclic terpanes C28+C29 (S+R)/Ts, 14- C_{24} tetracyclic terpane/[sum tricyclic terpanes C_{23} (S+R)], 15- C_{29} disterane (20R)/[(C_{29} disterane (20R)+C_{29} aaa sterane (20R)] 16- [C_{29} aaa+abb steranes(S+R)]/(C_{29} aaa+abb steranes(S+R) + C_{27}-C_{30} 17α(H) hopanes), 17- percentage of C_{27} abb steranes, 18- percentage of C_{28} abb steranes, 19- percentage of C_{29} abb steranes 20- 2-methylphenanthrene/1-methylphenanthrene (2-MP/1-MP), 21- Methylphenanthrene index: 1.5*(2-MP+3-MP)/(P+1-MP+9-MP), 22- %Rc(MPI-1) = 0.60 x MPI-1 + 0.40 23- MDR: 4-methyldibenzothiophene/1-methyldibenzothiophene, 24- C_{20} TAS/[(C_{20} Tas+C_{28} 5α(H)TAS (S+R)]

The distribution of C_{27}-, C_{28}-, C_{29}- regular steranes [5α (H), 14β (H), 17β (H) (20S+20R)] for the reservoir core extracts, DST oil OL#2 and the production oil samples in the Hassi Messaoud field is shown in Figure 5.41. The reservoir core extracts analysed in the wells MD#177, MD#213, MD#141, MD#319, OMM#33, OMJ#41, and OML#712, the DST oil sample OL#2, and oil samples plot in a narrow region of the ternary diagram showing higher relative abundance of C_{27} and C_{29} 5α (H), 14β (H), 17β (H) (20S+20R) than C_{28} 5α (H), 14β (H), 17β (H) (20S+20R) suggesting similar source rocks, likely the Silurian shales having generated the production oils and the residual oil extracted from the reservoir cores (Moldowan *et al.*, 1985). However, the reservoir core extract samples in well OMO#712 reveal different distribution with relatively higher percentage of the C_{28} 5α (H), 14β (H), 17β (H) (20S+20R) compared to the rest of the production oils and reservoir core samples. This observation suggests that the residual oil analysed in the samples from well OMO#712 was either generated from a different source, or contains a mixture of residual oil generated from the Silurian source rocks and organic matter originated from another source. Moldowan et al. (1985) and Grantham and Wakefield (1988) showed a relative increase in the relative content of the C_{28} steranes in marine petroleum through geological time, which is related to the increase diversification of

phytoplankton assemblages including diatoms, coccolithophores and dinoflagellates in the Jurassic and Cretaceous. Therefore, the source of the increase in the relative content of the C_{28} steranes in these samples is likely the Triassic evaporitic sediments overlying the Hassi Messaoud Cambrian reservoir. This suggestion is indeed supported by the occurrence of a high abundance of gammacerane marker in all the extract samples of well OMO#712 (see Figure 5.40).

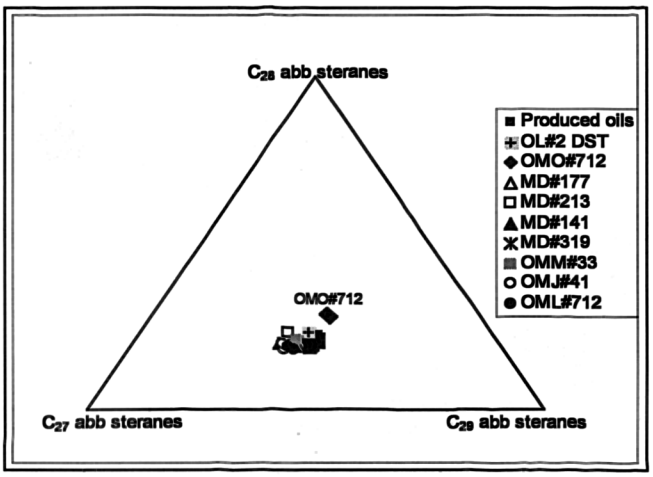

Figure 5.41 Ternary diagram showing the relative abundances of C_{27}-, C_{28}-, and C_{29}- regular steranes [5α (H), 14β (H), 17β (H), 20S + 20R] in the reservoir core extracts and oils from the Hassi Messaoud field.

Figure 5.42 shows the cross plots of source facies parameters [C_{28}+C_{29} extended tricyclics (S+R)]/Ts plotted against C_{24} tetracyclics/C_{26} tricyclics (S+R) (Figure 5.42a) and C_{29} 17α (H) hopane/C_{30} 17α (H) hopane plotted against C_{24} tetracyclics/C_{26} tricyclics (S+R) (Figure 5.42b). A clear difference can be seen between extract samples from the well OMO#712 (3336.7, 3345.6, 3354.5, from reservoir unit Ra and 3387.65 m from R2) and the rest of the samples (production oils and reservoir core extracts from the other wells) which plot very close to each other. This indeed confirms that the extract samples from the well OMO#712 originated from a different source than the rest of the samples and/or contain a mixture of bitumen originating from the Silurian source rock in the Oued Mya basin and the Triassic evaporitic sediments just above the Hassi Messaoud reservoirs.

Maturity parameters and the concentrations of biomarker and aromatic hydrocarbons discussed below confirmed that the petroleum extracted from the samples of well OMO#712 contains a mixture of an "immature" organic matter likely originated from the Triassic evaporitic seal and mature residual oil originated from the Silurian source

rock strata (see sections below for more detail). The extract samples at the depth of 3406.65 m (from reservoir unit R2) in well OMO#712 plots away from the rest of the samples in the same well, and close to the present day produced oils and the core extracts from the other wells. It appears that this sample contains a lower proportion of the evaporitic organic matter, which is confirmed by lower abundance of gammacerane in this sample compared to the other samples from the same well (Figure 5.40). Moreover, plotted in this diagram are the oils produced from the same wells. The oils show higher ratios than the extracts more likely because they are relatively more mature than the extracts.

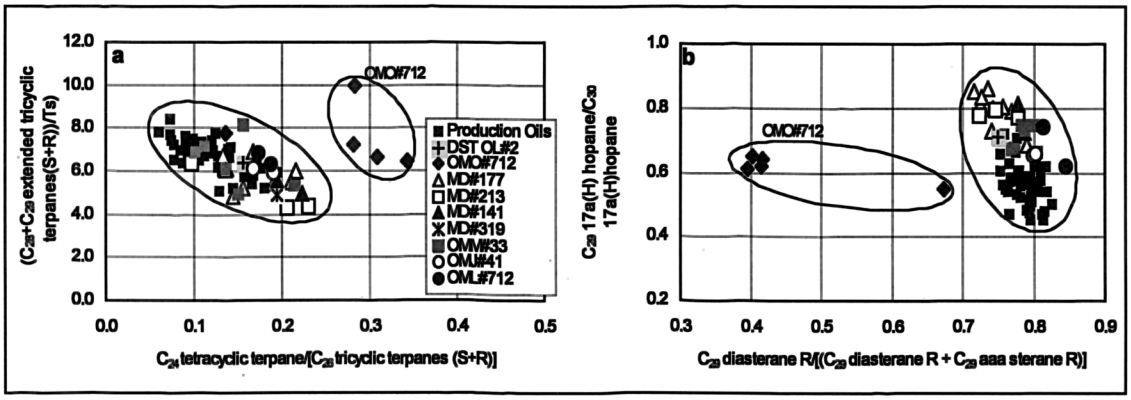

Figure 5.42 Cross plot showing the variation of (C_{28}+C_{29}-tricyclics)/[(C_{28}+C_{29}-tricyclics)+(C_{29}□-C_{30}hopanes)] ratio versus C_{29}steranes/[(C_{29}steranes+C_{29}-C_{30}hopanes)] ratio for the reservoir core extracts and the respective oil samples throughout the Hassi Messaoud field.

Biomarker based maturity parameters plotted in Figure 5.43 clearly show that extract samples from well OMO#712 (except the sample at 3406.65 m) are far less mature than all the extract samples from the other wells and the DST and production oils. The core extract samples from well OMO#712 show that the sterane isomerisation ratios C_{29} ααα steranes 20S/(20S+20R) and C_{29} steranes αββ/(ααα + αββ) values range from 0.38 to 0.49 and 0.33 to 0.53, respectively, whereas the same ratios range from 0.51 to 0.58 and 0.57 to 0.64, respectively (Table 5.7) for the core extract samples from the wells MD#177, MD#213, MD#141, MD#319, OMM#33, OMJ#41, and OML#712, which show similar maturity range compared to the DST and production oils.

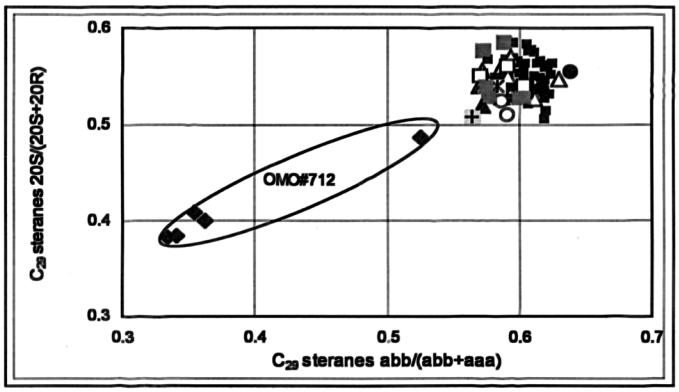

Figure 5.43 Cross plots of the C_{29} steranes 20S/(20S+20R) versus C_{29} steranes αββ/(αββ+ααα) for the reservoir core extracts, DST oil and production oil samples throughout the Hassi Messaoud field.

The maturity parameters C_{29} Ts/(C_{29} Ts + C_{29} 17α (H)hopane), C_{30} diahopane /(C_{30} diahopane + C_{30} 17α (H) hopane) and Ts/(Ts+Tm) plotted in Figure 5.44, also show that the extract samples from well OMO#712 are less mature than the rest of the extract samples, DST oil and present day produced oils. Moreover the values of these three parameters are higher in the production oils compared to the all the extract samples and the DST oil sample (Table 5.7) indicating that the production oils are more mature than all the extract samples and DST oil sample. Interestingly, the DST oil shows similar maturity compared to the reservoir core extracts.

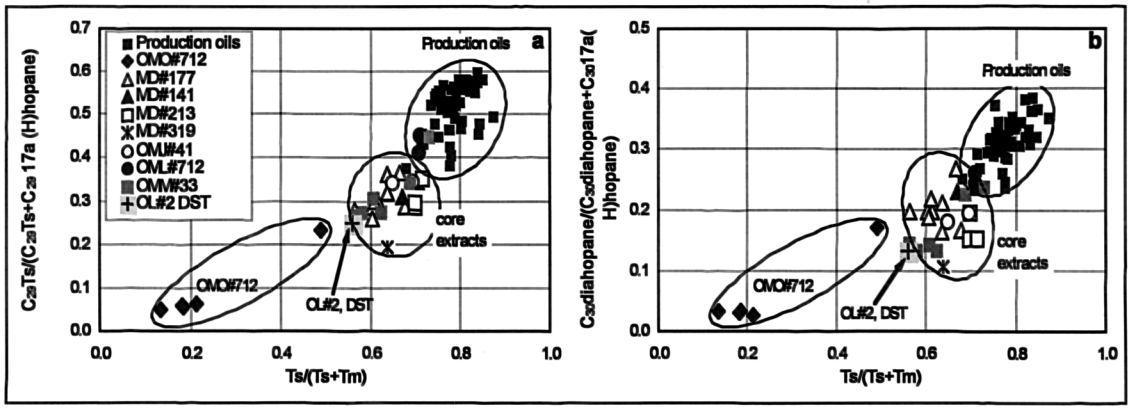

Figure 5.44 Cross plots of (a) the C_{29} Ts/(C_{29} Ts + C_{29} 17 α(H) hopane) and (b) C_{30} diahopane/C_{30} 17α(H) hopane versus Ts/(Ts+Tm) for the reservoir core extracts, DST oil and production oil samples throughout the Hassi Messaoud field.

Calibration of the maturity of the reservoir core extracts, DST oil and production oils was achieved by comparison to a set of North Sea oil samples with known measured vitrinite reflectance values and maturity parameters calculated from biomarker and aromatic hydrocarbons (Figure 5.45). The calibration of the maturity of the core extracts and oils using the Ts/(Ts+Tm) maturity parameter shows that the estimated

vitrinite reflectance values for the extract samples from well OMO#712 are less than 0.5% Rm (<0.5% Rm); for the extract samples from the wells MD#177, MD#213, MD#141, MD#319, OMM#33, OMJ#41, and OML#712 range from 0.75 to 0.9% Rm; for the DST oil 0.8%; and for the production oils range from 0.8 to 1% Rm. However, using the MDR parameter, the core extract samples from well OMO#712 together with the rest of the core extract samples from the other wells reveal similar range of maturity (ca 0.80 – 0.9% Rm).

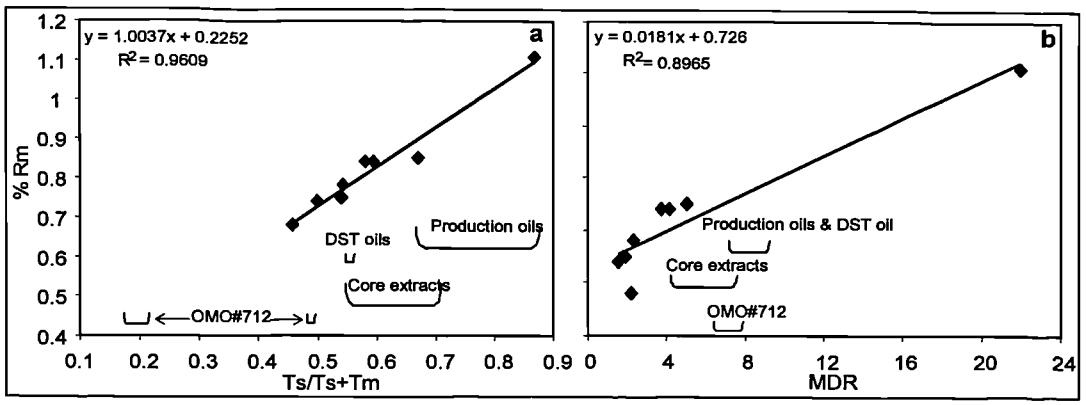

Figure 5.45 Cross plots showing the correlations between the measured vitrinite reflectance (%Rm) with (a) Ts/(Ts + Tm) and (b) MDR for a North Sea oil sample set used for the calibration of the maturity of the reservoir core extracts, DST oil and the production oils analysed in this study.

In fact, the aromatic hydrocarbon based maturity parameters reveal that all the samples from the well OMO#712 are amongst the most mature in this sample set (Figure 5.46a). I have shown above, that the aliphatic biomarker parameters consistently indicate low maturity (vitrinite reflectance <0.5% Rm) of the extract samples from well OMO#712, whereas the aromatic hydrocarbon parameters indicate similar maturity (i.e. vitrinite reflectance ranging from 0.75 to 0.9% Rm) for these extract samples compared to the rest of the reservoir core extracts analysed in this study. This observation is confirmed in the cross plot (Figure 5.46b) which shows positive correlation between the methyldibenzothiophene ratio (MDR) and Ts/(Ts+Tm) parameters for all the core extract and production oil samples except the core extract samples from well OMO#712 which show very low Ts/(Ts+Tm) values suggesting immature petroleum extracts and high MDR values suggesting mature petroleum extracts.

Moreover, the cross plots of the summed biomarker and alkylphenanthrene concentrations (μg g^{-1} extract/oil) in Figure 5.47 a and b against the maturity of the

core extract and the oil samples expressed by the methyldibenzothiophene ratio (MDR) show (1) a decrease in the concentrations of biomarkers and (2) an increase in the concentrations of alkylphenanthrenes with increasing maturity in the core extracts and production oil samples taken together. However, the biomarker concentrations in the two extract samples from the well OMO#712 (3345.6m, Ra and 3387.65m, R2) (Figure 5.47a) are almost two times higher than in the rest of the extract samples analysed in the other wells, despite the fact that the two samples exhibit the same level of maturity as the rest of the samples. This again suggests that the extract samples in the well OMO#712 resulted from the mixing of an immature bitumen containing high biomarker concentrations, with a more mature bitumen containing high aromatic hydrocarbon concentrations. Mixtures of immature bitumens and mature oils were termed "mixed maturity" by Li et al. (1995a), who reported similar features in a case study carried out on a set of crude oils produced from the Shahejie Formation of the Liaohe basin N.E. China.

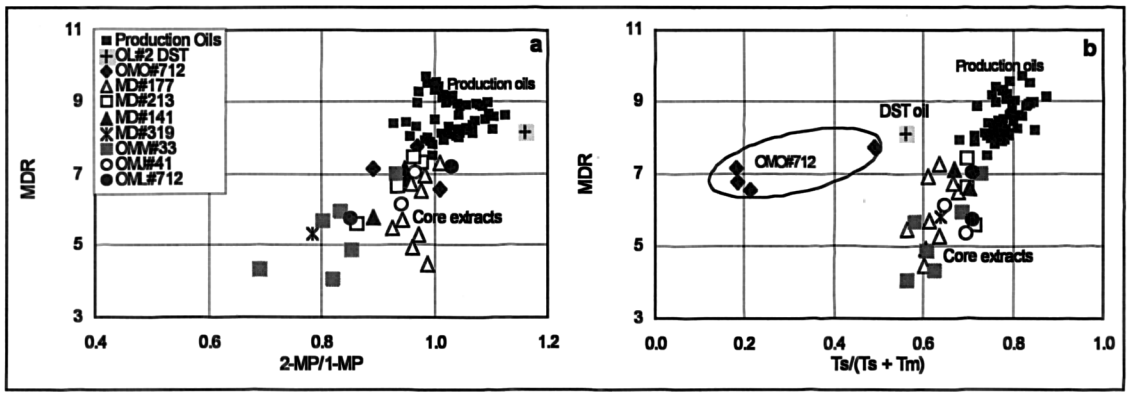

Figure 5.46 Cross plots of 4-MDBT/1-MDBT against (a) 2MP/1-MP and (b) (Ts+Tm) for the reservoir core extracts and the respective oil samples throughout Hassi Messaoud field.

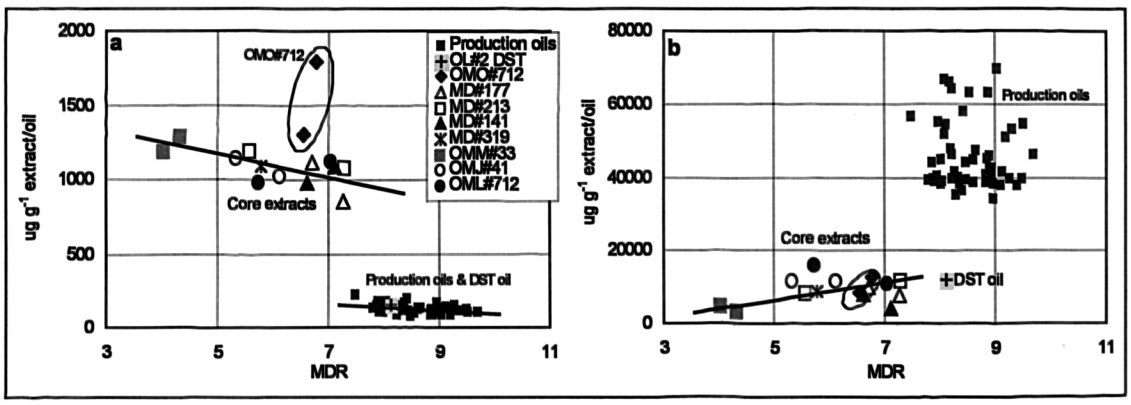

Figure 5.47 Cross plots showing the variation of (a) concentrations of the biomarkers (μg/g of extract/oil) and (b) concentrations of the alkylphenanthrenes (μg/g of extract/oil) for the reservoir core extracts and the respective oil samples throughout Hassi Messaoud field.

5.5.3. Vertical geochemical variations of reservoir core extracts throughout the Hassi Messaoud reservoir

In this section I will show that vertical chemical compositional variations on a bulk and molecular scale are observed throughout petroleum columns of the Hassi Messaoud reservoirs. Bulk geochemical analysis was performed using the Iatroscan TLC FID technique (Karlsen and Larter, 1991). The results obtained from Iatroscan allow a pseudo 3-D characterisation of the bitumen distribution throughout the reservoirs albeit with relatively few samples. Moreover, this technique may also identify samples warranting more detailed examination, locate oil-water contacts (OWCs), and identify residual oil saturation (ROS), locate compartments which never received any pulse of oil and detect tar mats (Bhullar et al., 1999a).

5.5.3.1. Bulk geochemical variations within the Hassi Messaoud reservoirs

A total of 267 core samples from 7 wells were screened using Iatroscan. The results obtained are listed in Appendix 5.3.

Large variations in the absolute yields are seen vertically and laterally in all the wells throughout the Hassi Messaoud reservoirs (Ra and R2) (Figure 5.48). The petroleum yields from the Iatroscan data range from 0.26 mg/g to 27.89 mg/g of reservoir rock. From Figure 5.48 it can be observed that well OML#712 contains the highest petroleum yields ranging from 5.51 to 23.55 mg/g rock (average 13.54 mg/g rock), followed by the wells OMO#712 and MD#177, with an average of 10.57 and 9.28 mg/g rock, respectively. The wells OMJ#41, MD#213, MD#141 and OMM#33 located in the flanks of the Hassi Messaoud field show much lower average petroleum yields of 5.85, 3.96, 2.56, and 2.62 mg/g rock, respectively (see Appendix 5.3).

The variations in the petroleum yields throughout the Hassi Messaoud reservoirs Ra and R2 and individual samples are likely controlled by variations in the rock properties, i.e. porosity. The higher the porosity of the rock, the greater the capacity of the rock to become saturated with petroleum (Figure 5.49 and Figure 5.50). Indeed, the wells with higher petroleum yields (i.e. OMO#712, MD#177 and OML#712), have the highest average porosity throughout the field, 10.4%, 9.25%, and 11.67%, respectively, whereas the wells with lower petroleum yields (i.e. MD#213, OMJ#41, MD#141, and OMM#33) have lower average porosity, 7.41%, 5.4%, 4.82%, and 4.11%, respectively (Leythaeuser and Rückheim, 1989; Hillebrand and Leythaeuser,

1992; Stoddart, 1993). Note that the three wells OMO#712, MD#177, and OML#712 are located in structural crests in the centre and northeast of the Hassi Messaoud field. Therefore, it is likely that the reservoirs in these wells have received the first pulses of oil earlier than most of the wells located towards the flanks of the field (England et al., 1987). The earlier arrival of oil in the reservoirs located in the centre and the northeast of the field may have slowed down cementation of the reservoir. Microscopic analysis carried out on reservoir thin section samples from the wells in the centre and the flanks of Hassi Messaoud field, reveals large differences in the extent of diagenetic cementation between the reservoir rocks from the centre and western and south-western flanks of the field (Figure 5.51). The samples analysed from the wells located towards the flanks show well developed quartz overgrowths and eventually lower reservoir quality compared to the samples investigated in the wells from the centre of the field which show larger pore spaces between the grains, allowing higher volumes of petroleum to be trapped.

Emery et al. (1993) suggested that in cases where oil emplacement predates or is contemporaneous with quartz cementation, early-filled reservoirs or parts of the reservoirs (e.g. structural crests) would have less cement and thus retain superior reservoir quality than the late-filled reservoirs located towards the flanks. Indeed, the trend of decrease in petroleum yields from the wells MD#177, OMO#712, and OML#712 located in the structural crests towards the wells MD#213, OMJ#41, OMM#33 and MD#141 located in the flanks of the Hassi Messaoud field agrees well with the findings of Emery et al. (1993) and the filling model established by England et al. (1987). Moreover, the core samples from the wells MD#177, OMO#712, OML#712 and MD213 located in the centre, northeast and east parts of the Hassi Messaoud field exhibited higher abundance of petroleum inclusions compared to the core samples analysed in the wells MD#141, MD#319, OMM#33 and OMJ#41 located in the south, southwest, west and northwest of the Hassi Messaoud field (see sections 6.2.1 and 6.2.2 in chapter 6). On this basis and from the distribution of the petroleum yields in all the wells analysed here (Figure 5.48), it appears that the filling directions were from the crests towards the north-northwest, the east, and the south and towards the west of the Hassi Messaoud field.

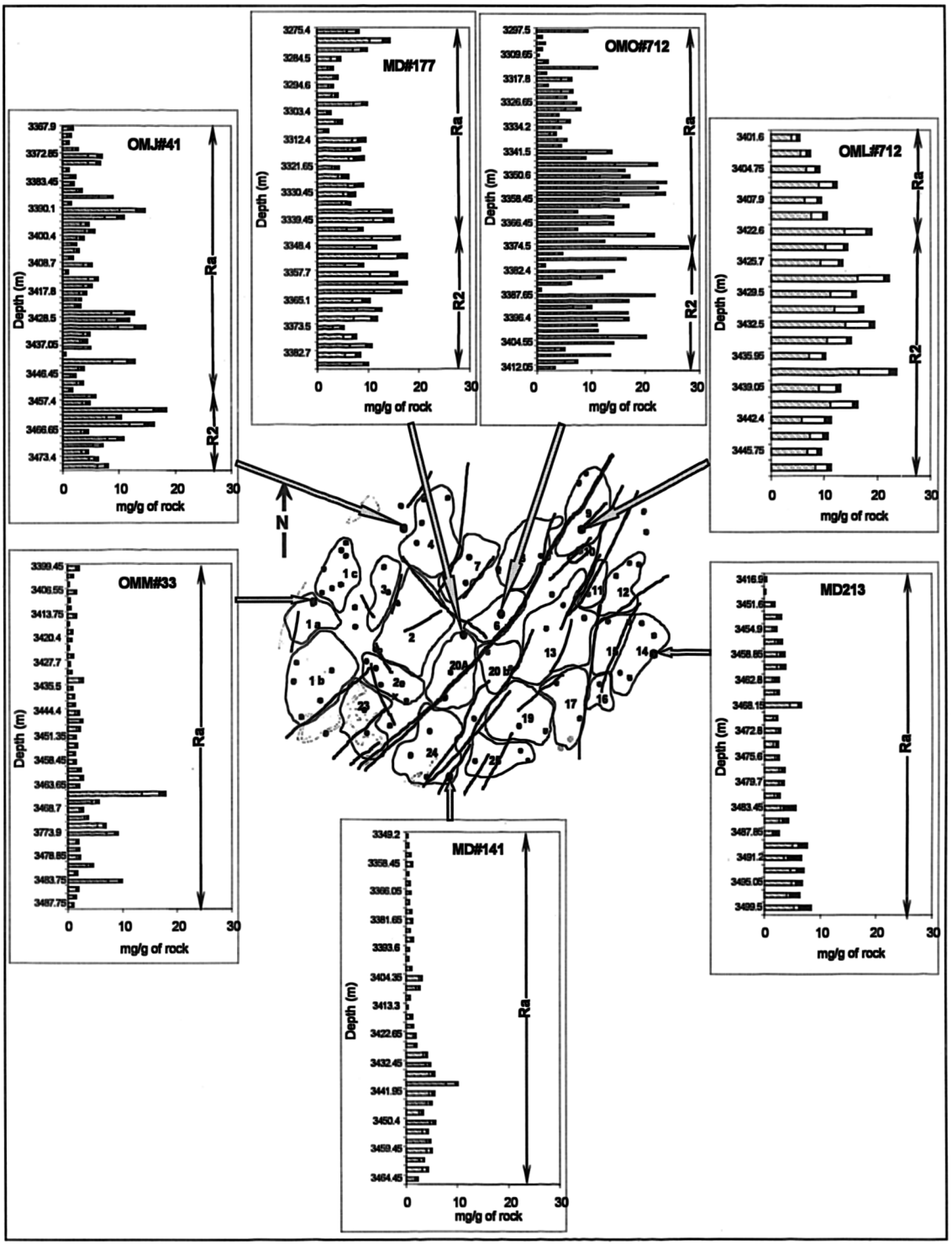

Figure 5.48 Total petroleum yield data plotted for wells from different parts of the Hassi Messaoud field.

England et al.(1987) stated that because the pore sizes of the various layers of a reservoir rock are not uniform, migrating petroleum will enter first the layers with the largest pores (i.e. lowest capillary entry pressures) and the newly arriving petroleum will be forced successively into smaller pores which have higher capillary entry pressures. This situation results in a heterogeneous distribution of the petroleum

yields vertically within individual samples (Figure 5.49). Figure 5.49 shows the variations of petroleum yields with the variations in the porosity and the permeability of the individual samples within wells MD#177 and OMO#712. The variations of the petroleum yields within the reservoir units Ra and R2 in wells MD#177 and OMO#712 do show positive correlation with the porosity throughout the reservoir units Ra and R2; higher petroleum yields are mostly encountered in core samples with higher average porosity. However, in the reservoir unit R2, the average porosity and petroleum yields are as high as in the reservoir unit Ra despite the fact that the permeability in this the reservoir unit R2 is extremely low compared to the reservoir unit Ra (Figure 5.49). This suggests that the variations of the petroleum yields within the reservoir units Ra and R2 of wells MD#177 and OMO#712 are probably mostly influenced by the porosity.

Figure 5.50 shows cross plots of the reservoir porosity and permeability versus the Iatroscan petroleum yield obtained from well OMO#712 analysed in the Hassi Messaoud reservoirs. There is an obvious correlation between porosity and petroleum yields with a high correlation coefficient (R^2= 0.70), however, a poor correlations can be seen from the plot of permeability versus petroleum yields (R^2=0.06). This most likely reflects a poor correlation between porosity and permeability in the reservoirs. Furthermore, the relationship between porosity and permeability has always been quite general and is probably more so in this case since the Hassi Messaoud reservoirs have a fracture related permeability component (Sonatrach-IFP, 1975).

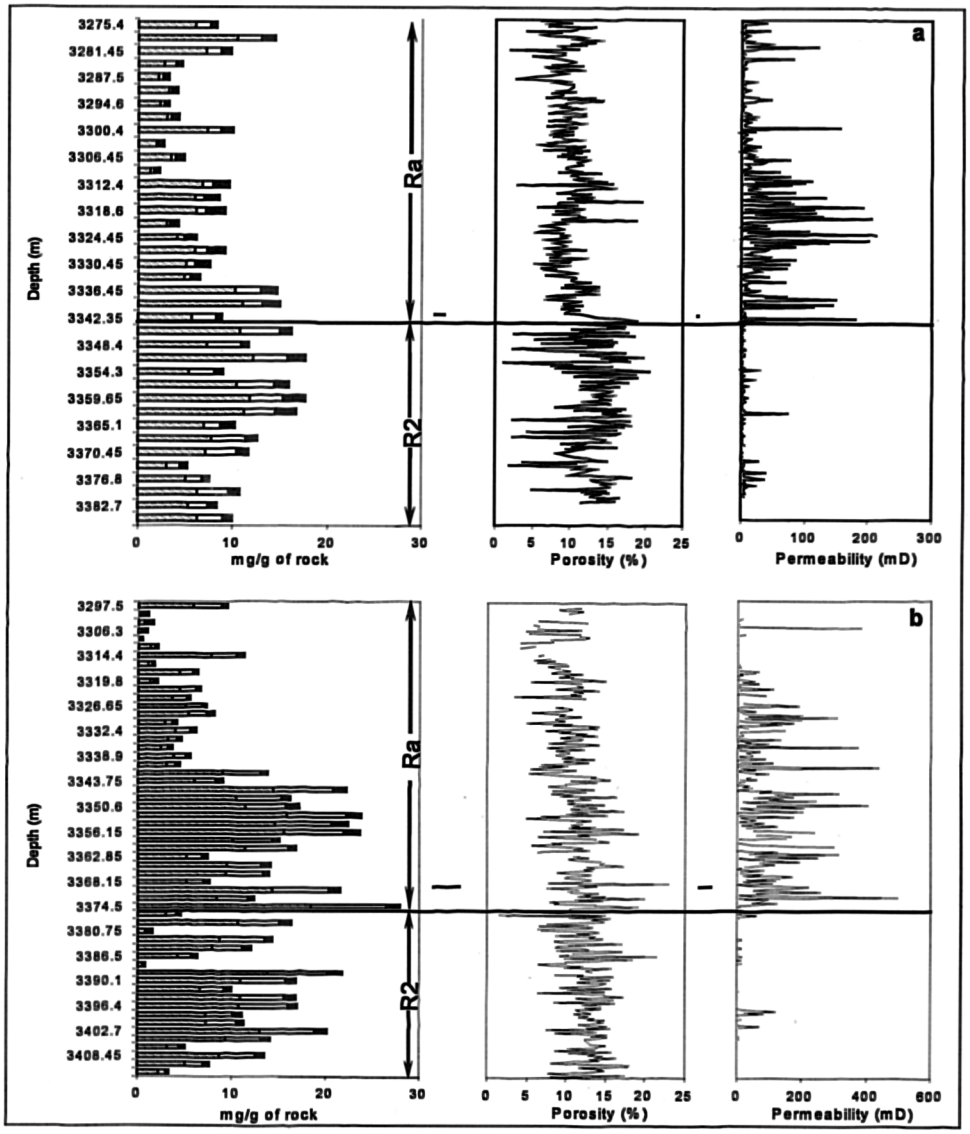

Figure 5.49 Comparison of the total petroleum yields with the porosity and permeability of individual core samples in (a) well MD#177 and (b) well OMO#712 in the Hassi Messaoud field.

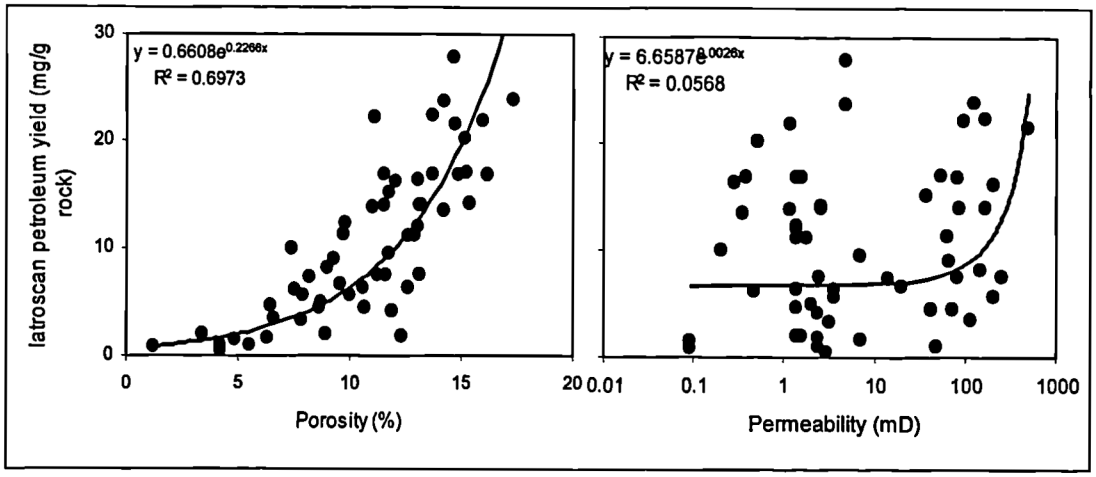

Figure 5.50 Comparison of the Iatroscan petroleum yields with the porosity and permeability values for well OMO#712 analysed in the Hassi Messaoud reservoirs.

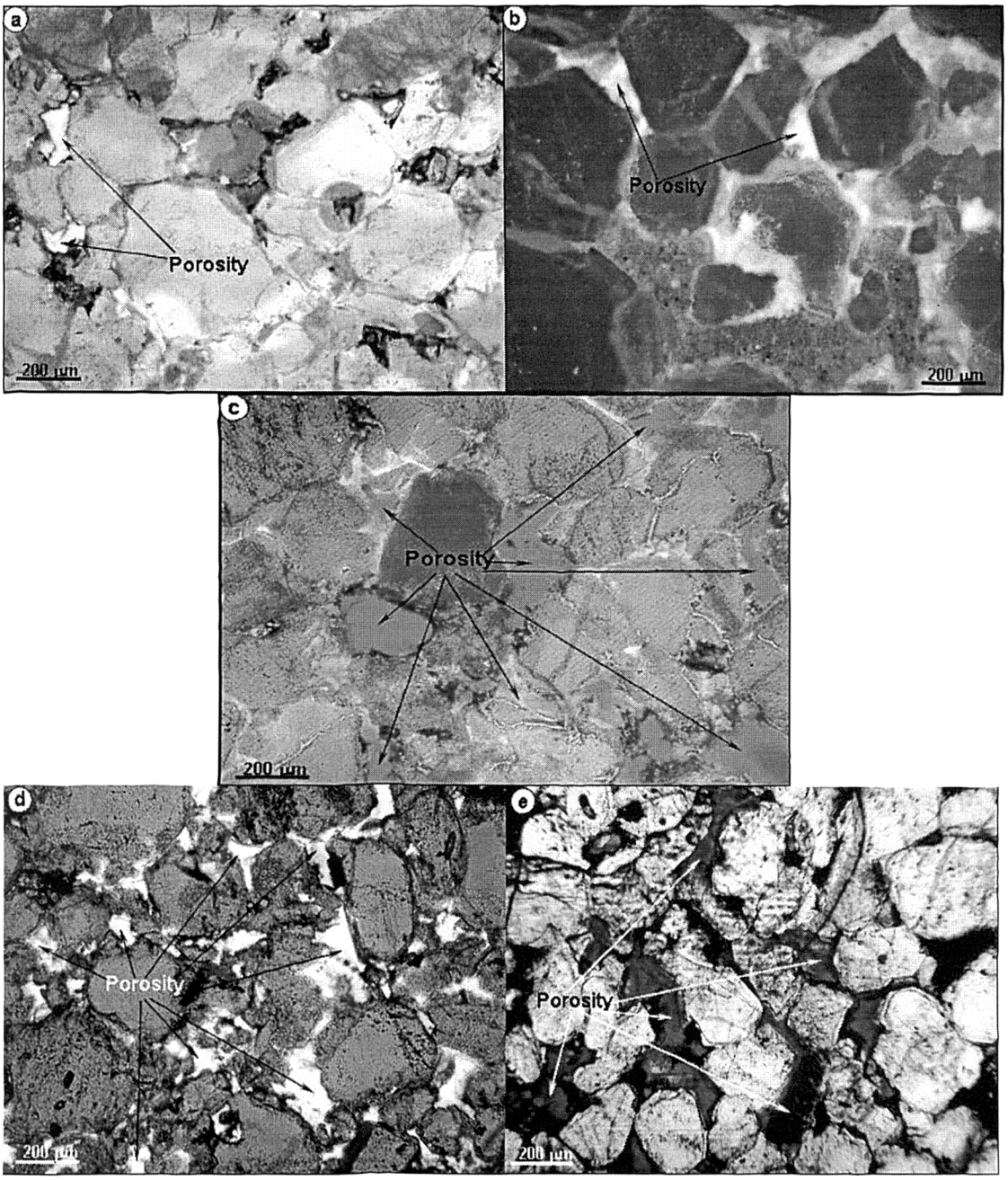

Figure 5.51 Photos showing (a) and (b)) low porosity and permeability caused by high cementation of reservoir unit Ra in well OMM#33, (c), (d) and (e) high porosity/high permeability of the reservoir unit Ra and R2 in wells MD#177, MD#213 and OML#712, respectively, Hassi Messaoud field.

Figure 5.52 shows the vertical variations of total petroleum yield together with the percentages of the aliphatic hydrocarbons, aromatic hydrocarbons and polar fractions in the core extract petroleum from the wells analysed in the Hassi Messaoud field. In general, all the samples are dominated by aliphatic hydrocarbon fractions except for a very few samples which contain high relative amounts of polar compounds found mainly in the petroleum-lean zones of the reservoirs (i.e. samples with <1.0 mg/g rock); these samples contain the lowest petroleum yields (e.g. the top of wells

OMO#712, OMM#33 and MD#141). The aliphatic hydrocarbon fractions are quite similar in all the wells, with the highest percentages found in well MD#141 (average 70.50 wt%) and the lowest percentages recorded in well MD#213 (average 61.86 wt%). The aromatic hydrocarbon fractions also show little vertical variations down the petroleum column within the individual wells, except in the well MD#177, where the percentage of the aromatic hydrocarbon fractions is higher in reservoir unit R2 (ranging from 17.87 to 30.71%; average 25.52%) than in the reservoir unit Ra (ranging from 8.61 to 26.52%; average 13.93%) (Appendix 5.3). This observation is likely caused by maturity differences between the core extract petroleums from unit Ra and those from reservoir unit R2. The core extract petroleum samples from reservoir unit R2 exhibited higher values for biomarker and aromatic hydrocarbon maturity parameters compared to the core extract petroleum samples from the reservoir unit Ra indicating higher maturity of the samples from the reservoir unit R2 compared to those from the reservoir unit Ra (see section 5.4.3.2 below). The polar fractions do not show major variations except within petroleum-lean intervals where they are generally dominant in all the wells.

There is no sign of the occurrence of tar mats in wells OMO#712, MD#177, OML#712, OMJ#41, OMM#33, and MD#141. However, because the sampling intervals vary between 1m to 4m, it is likely that we could miss some small tar mats such as the 10cm-1m thick (i.e. minimats) which are common features in some marine light-oil reservoirs such as Hassi Messaoud (Wilhelms and Larter, 1994a,b). Tar mats are sharply defined zones of asphaltene-rich petroleum, less than one to a few meters thick, usually occurring in light paraffinic oil reservoirs (Jones and Speers, 1976; Dahl and Speers, 1986; Wilhelms and Larter, 1994a,b). Tar mats often occur close to geological discontinuities (Wilhelms and Larter, 1994a,b) including, but not limited to, oil-water contacts (OWCs) and above permeability contrasts. Moreover, the occurrence of tar mats has important implications for both crude oil reservoir exploration and exploitation: (1) tar mats have generally negative effects on the production of oil reservoirs because they contain immovable reserves, (2) tar mats may constitute permeability barriers, (3) tar mats may cause problems during field unitisation because of the difficulties in their areal assessment, and because fields with tar mats often show asphaltene deposition problems when the oils are produced (Wilhelms and Larter, 1994a,b). The study of tar mats may potentially give

indications of the filling history of a given reservoir (Larter et al., 1990; Wilhelms and Larter, 1994b). Reservoir intervals with high poroperm qualities, high total petroleum yields and high proportions of tar mats are believed to have had a major role in the oil migration into a given reservoir (Wilhelms and Larter, 1994b).

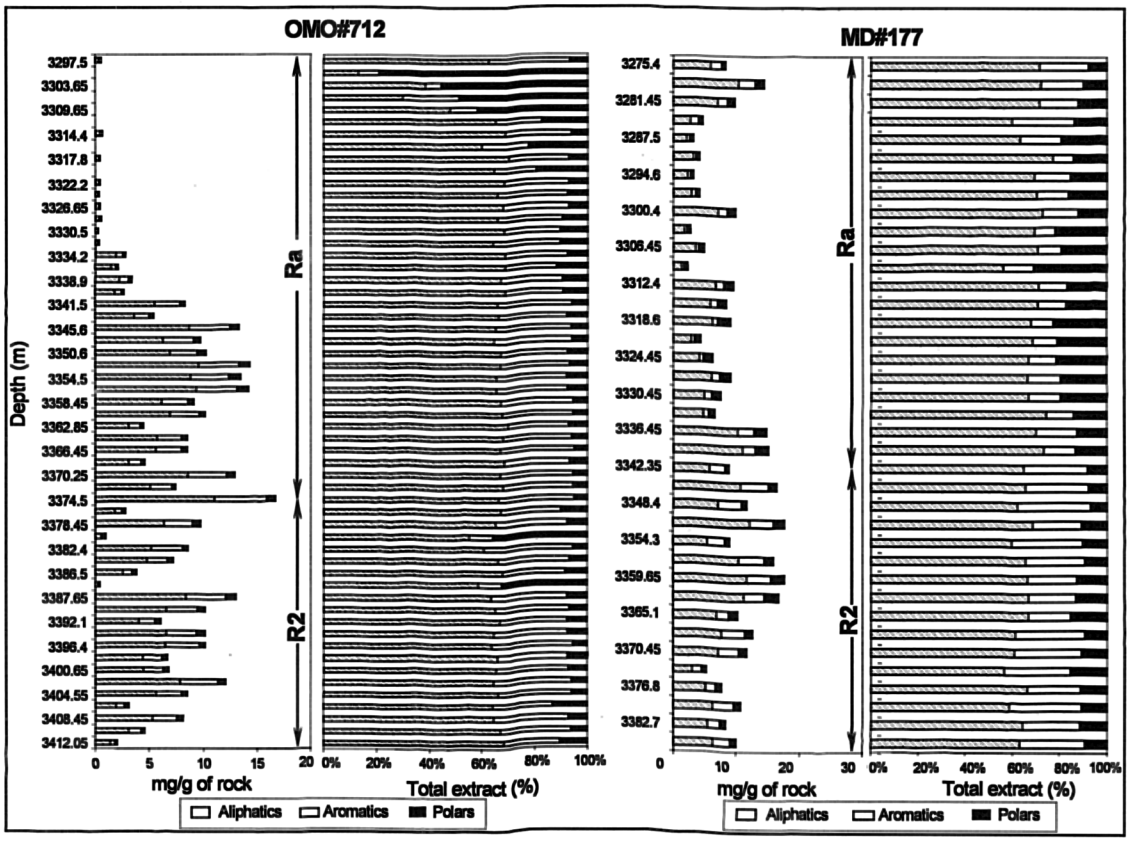

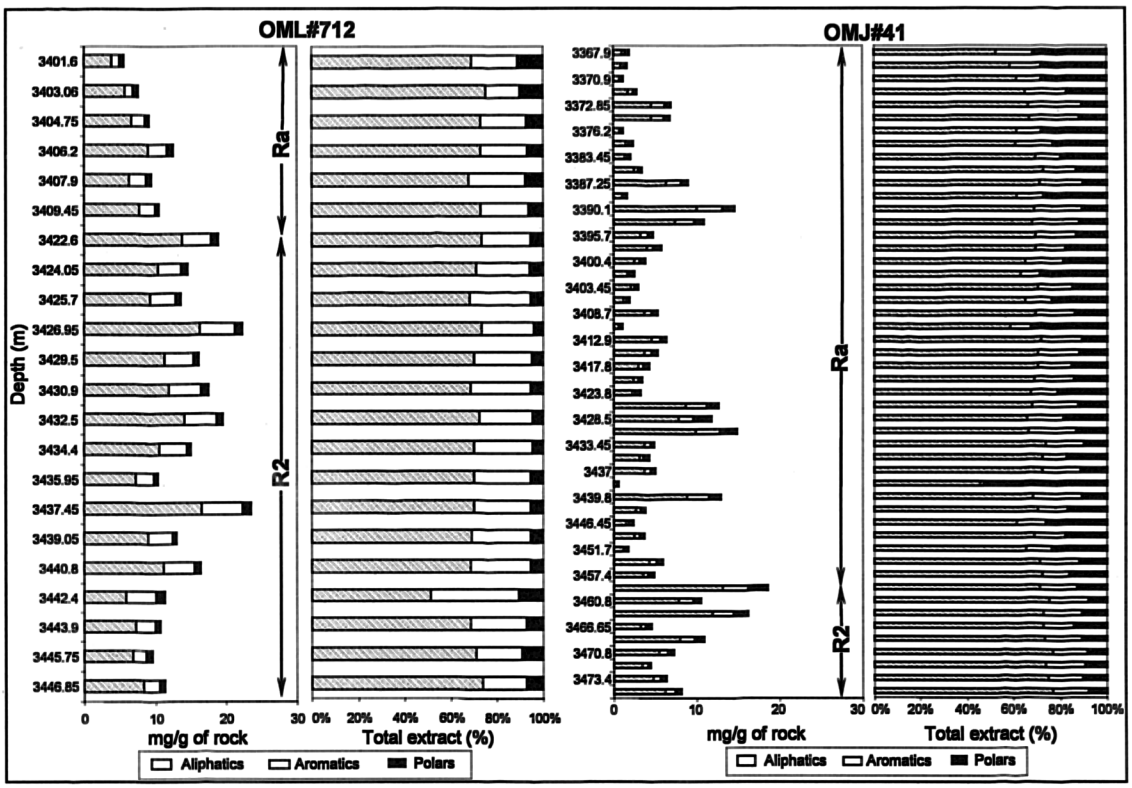
OML#712
OMJ#41
Depth (m)
Ra
R2
mg/g of rock
Total extract (%)
Aliphatics
Aromatics
Polars

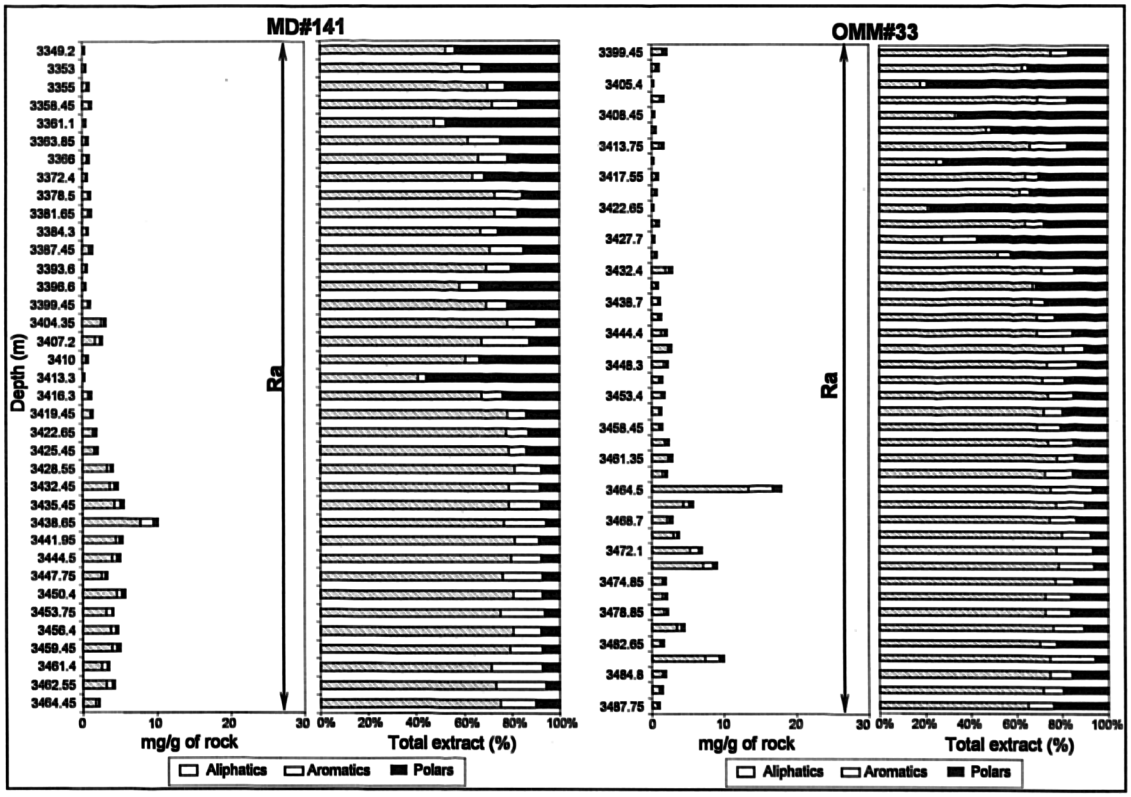
MD#141
OMM#33
Depth (m)
Ra
mg/g of rock
Total extract (%)
Aliphatics
Aromatics
Polars

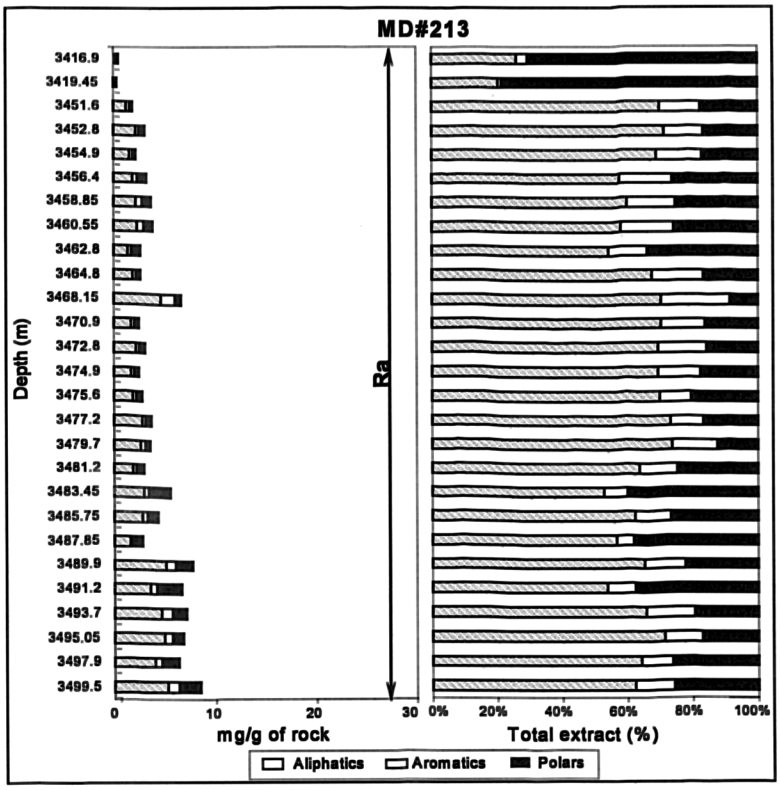

Figure 5.52 Absolute yields and relative concentrations of petroleum fractions (aliphatics, aromatics and polars) obtained from Iatroscan analysis technique from the wells in the Hassi Messaoud field.

Interestingly, well MD#213 shows some vertical variations in the proportions of the three fractions (aliphatics, aromatics and polars). In the interval between 3483.45m to 3499.5m, relatively higher total petroleum yields are associated with higher permeability and porosity values and relatively higher amounts (mg/g of rock) and percentages of polar compounds (Figure 5.53). The samples at 3483.45m, 3491.2m, 3497.9m, and 3499.5m contain the highest percentages of polar compounds but have too low extract yield (ca 5.49, 6.63, 6.31, and 8.47 mg/g rock, respectively) to be considered as small tar mats (Wilhelms and Larter 1994a,b). However, we might argue that these intervals may have been used as migration pathways, because during petroleum migration pressure and temperature reduction occurs in the petroleum systems, leading to reduced polars solubility in petroleum and causing their precipitation along the carrier pathways (Miles, 1990; Larter and Wilhelms, 1994b). This observation is in fact supported by the high abundance of petroleum inclusions found in the sample at 3499.5m compared to the samples analysed at depths of 3468.15 m and 2451.6 m (see section 6.2.2.2 in chapter 6).

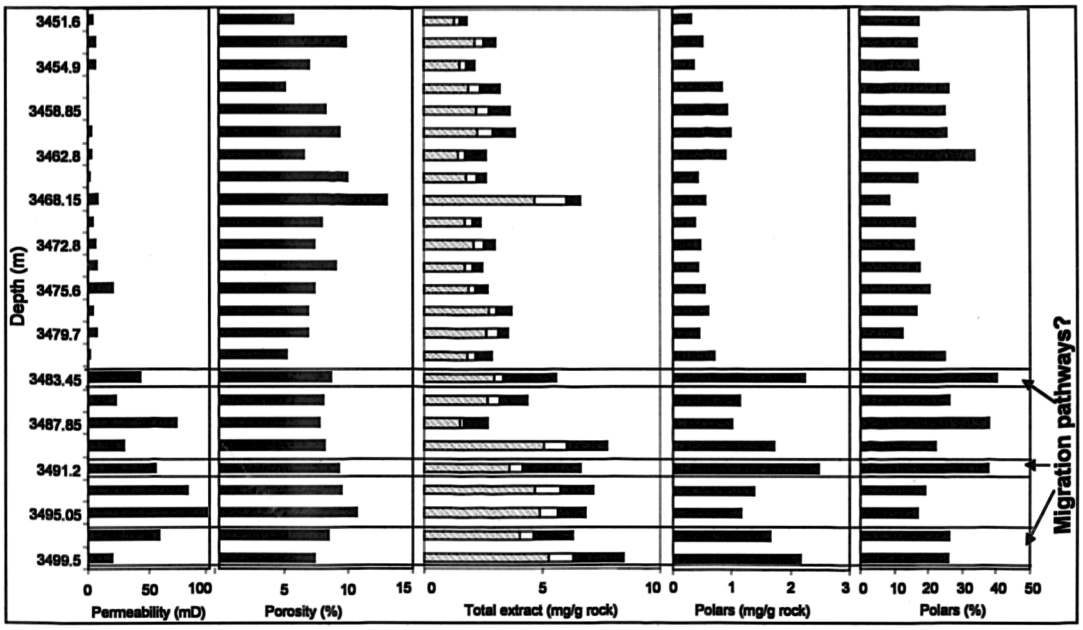

Figure 5.53 Occurrence of polar-enriched intervals identified using total extract, amount and percentages of polar compounds, porosity and permeability values for the well MD#213 in the Hassi Messaoud field.

5.5.3.2. Molecular geochemical variations in the Hassi Messaoud reservoir petroleum columns

Based on the results obtained from the Iatroscan data, further samples were selected for more detailed molecular analysis by GC and GC-MS. In total, 20 samples were selected from 3 wells, 9 samples from MD#177, 5 samples from OMO#712 (both of these wells are located in the centre of the field), and 6 samples from OMM#33 (western flank). The selection of these samples was based on the following criteria, (1) achieving a good coverage throughout the petroleum column, (2) selecting samples with high absolute yields of petroleum, (3) selecting any "unusual" samples (i.e. samples showing for example higher polar compound yields).

The biomarkers and aromatic hydrocarbon parameters used for vertical variation investigations are: C_{29} steranes $\alpha\beta\beta/(\alpha\alpha\alpha+\alpha\beta\beta)$, Ts/(Ts+Tm), C_{30} diahopane/(C_{30} diahopane + C_{29} 17α(H) hopane), and MDR (4-MDBT/1-MDBT) (Table 5.7). These parameters were selected to identify changes in the petroleum composition throughout the Hassi Messaoud reservoir units Ra and R2 since it has been shown by many authors that maturity variations can and do exist laterally and vertically across petroleum reservoirs (England et al., 1987; Leythaeuser and Rückheim, 1989; Horstad et al., 1990; Larter and Horstad, 1992; Hillebrand and Leythaeuser, 1992; Larter and Aplin, 1995; Stoddart et al., 1995; Mason et al, 1995; Holba et al., 1996; Horstad and

Larter, 1997; Leythaeuser et al., 2000). Only two wells were vertically investigated in this section; well MD#177 located in the centre and well OMM#33 located in the western flank of the Hassi Messaoud field (see location in Figure 5.35).

5.5.3.2.1. Well MD#177

All the reservoir core extract samples in the reservoir units Ra and R2 show similar *n*-alkane distributions (Appendix 5.4); the samples also contain a large unresolved complex mixture (UCM) which may indicate the presence of mixed biodegraded and fresh oils or biodegradation during storage (see section 5.5.2.2 for more details).

The values of biomarker and aromatic hydrocarbon maturity parameters are listed in Table 5.7. Visual examination of data using the conventional biomarker and aromatic hydrocarbon parameters listed above suggest that two distinct petroleum populations are present in the reservoir units Ra and R2 (Figure 5.54). The C_{29} steranes αββ/(ααα+αββ)□ biomarker maturity parameter values in the reservoir units Ra and R2 display fairly similar range between 57 and 63% and 57 to 61%, respectively. However, the Ts/(Ts+Tm), C_{30} diahopane/(C_{30} diahopane + C_{29} 17α(H) hopane), and MDR maturity parameters show quite significant variations between the maturity of the core samples in the reservoir unit Ra compared to those from the reservoir unit R2. Hence, the reservoir unit Ra would appear to contain lower maturity petroleum compared to the reservoir unit R2. The major differences between these reservoir units is permeability; Figure 5.49 shows that the permeability values are much higher in the reservoir unit Ra ranging from 1 to 214.1 mD (average 24.4 mD), whereas, in the reservoir unit R2 the permeability values range from 0.1 to 74.4 mD (average 4.2 mD). Therefore, it appears that permeability differences between the two reservoir units might have played a crucial role in preventing petroleum mixing between the Ra and R2 reservoir units. The produced oil in well MD#177 seems to be more mature than the petroleum extracted from the reservoir cores from the same well. The values of C_{29} steranes αββ/(ααα+αββ)□, Ts/(Ts+Tm), C_{30} diahopane/(C_{30} diahopane + C_{29} 17α(H) hopane), and MDR maturity parameters for the oil MD#177 are 61%, 83%, 31%, and 8.89, respectively (see also Figure 5.44 and Figure 5.46, and Appendix 4.3).

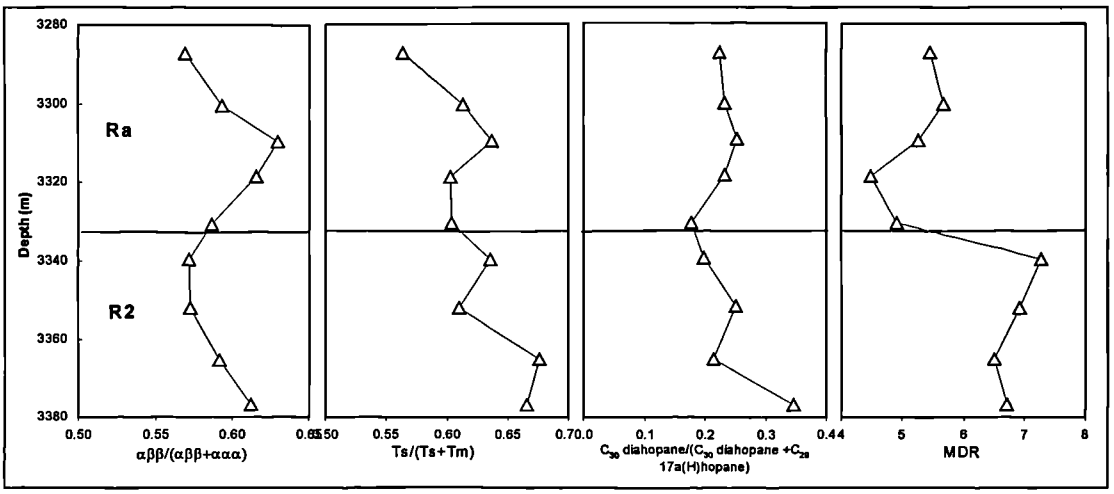

Figure 5.54 Molecular biomarker and aromatic maturity variations within the petroleum column of the well MD#177, Hassi Messaoud field.

5.5.3.2.2. Well OMM#33

The samples from this well are all collected from the reservoir unit Ra. The C_{29} steranes αββ/(αββ+ααα) parameter reveals very similar maturity between these samples with values ranging from 57% to 60%. The changes in this parameter with depth are less pronounced than the hopane and the methyldibenzothiophene maturity parameters (Figure 5.55). All of the Ts/(Ts+Tm), C_{30} diahopane/(C_{30} diahopane + C_{29} 17α(H)hopane), and 4-MDBT/1-MDBT maturity parameters show a general trend of decreasing petroleum maturity from the top towards the bottom of the petroleum column of the well OMM#33. The Ts/(Ts+Tm) values decrease from 73% in the top towards 56% in the bottom, C_{30} diahopane/(C_{30} diahopane + C_{29} 17α(H)hopane) values from 32% to 18% and the MDR from 6.99 to 4.04. The downward decrease in the maturity probably results from the filling process in this western flank of Hassi Messaoud field; the fresh and more mature petroleum with lower density is pushing the existing (less mature, denser) oil towards the bottom of the reservoir. The vertical variations on a molecular scale revealed in well OMM#33, may have been caused by the low reservoir quality; most of the wells drilled in the western flank particularly in zones 1A, 1B, and 1C (1) show low average reservoir porosity ranging from 4 to 8% and average permeability ranging from 0.3 to 5.9 mD and suggest that charging of the Hassi Messaoud reservoirs is likely still active.

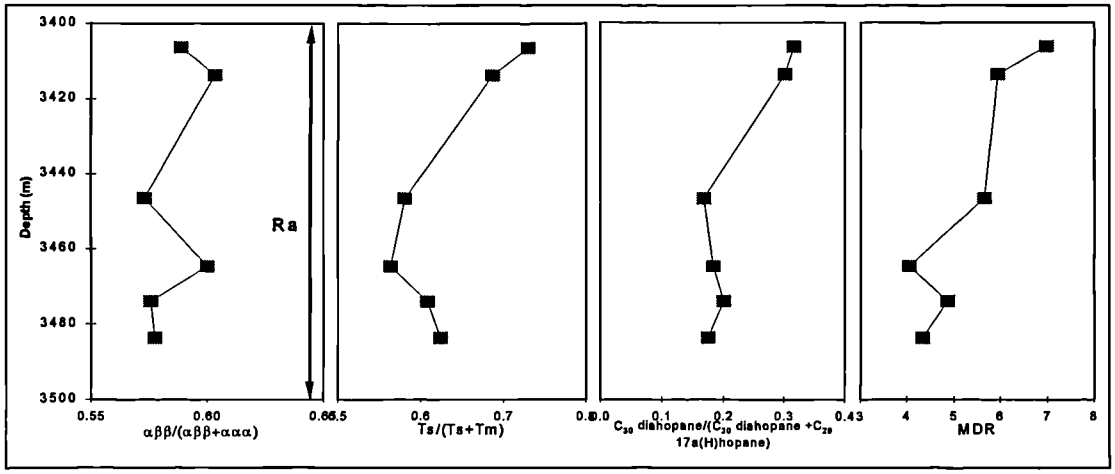

Figure 5.55 Molecular biomarker and aromatic maturity variations within the petroleum column of the well OMM#33, Hassi Messaoud field.

5.5.4. Summary

1. The conventional biomarker and aromatic hydrocarbon maturity parameters used in this section for oil samples analysed across Hassi Messaoud field revealed lateral maturity gradients throughout the field. Oil samples analysed in the centre and east of the field appear to be more mature than the rest of the oil samples from the west, north and south flanks of the field.

2. Statistically, I can distinguish 2 major groups of oil samples, separated by the main northeast southwest fault crosscutting the Hassi Messaoud field. The first group consists of the oil samples located east of the main fault which appear to be generated from the Silurian source rock strata located east of the Hassi Messaoud field, whereas the second group of oil samples are located west of the main fault, likely generated from the Silurian source rock strata lying along the Oued Mya basin (Figure 5.1). Hence, the Hassi Messaoud reservoirs appear to be mainly charged from the east and the west.

3. The principal components analysis using biomarker concentrations allowed me to statistically confirm that the separation of the Hassi Messaoud field into 25 zones is geochemically consistent.

3. The alkylcarbazole and benzocarbazole concentrations and distributions revealed that the Hassi Messaoud oils have experienced long lateral migration distances compared to the oils reservoired in the Triassic fields northeast of the Oued Mya basin (i.e. oils in Mokh-el-Kebch, N'goussa, Guellala northeast, Guellala and Draa Temra

fields). Hence, two major filling directions emerge, one from the east and the other from the west-northwest of the Hassi Messaoud field.

4. The biomarker and aromatic hydrocarbon parameters in the core extract from both reservoir units Ra and R2 (except those from well OMO#712) showed similar source facies features compared to the production oils and the DST oil analysed in the Hassi Messaoud field; however the core extract samples are less mature than the production oils and showed similar maturity to the DST oil. Moreover, the core extract from well OMO#712 appear to contain a mixture of "immature" bitumen originating from the overlying Triassic sediments (cap rock) and mature residual oil having similar characteristics compared to the rest of the core extracts analysed in this study.

5. The Hassi Messaoud reservoirs showed that compositional variations occur vertically through the oil columns on bulk and molecular scale.

5.6. Hassi Guettar field

Hassi Guettar is a satellite field located a few kilometres south of the Hassi Messaoud giant field (Figure 5.1). The field contains four producing wells known as HGA#1, HGA#2, HGA#3 and HGA#4. The first well HGA#1 was drilled in September 1992, followed by the well HGA#2 in April 1995, then one year later (April 1996) the well HGA#3, and finally the well HGA#4 was drilled in January 1998. I have collected two oil samples from two wells: well HGA#3 located towards the north of the field and close to the Hassi Messaoud field (this well produces from the Cambrian reservoir units Ra with average porosity ranging between 5 to 9% and average permeability of 46 mD), and well HGA#2 producing from the Ordovician reservoir Formations Hamra Quartzite and El-Atchane sandstones (Figure 3.9 in chapter 3), located to the south of the field. The oil-water contact in the Hassi Guettar field is located at about 3380m below the surface.

The distribution of the *normal-* and isoprenoid alkanes, the biomarker and aromatic hydrocarbons show similar source and maturity features of the Hassi Guettar oil samples HAG#2 and HGA#3 compared to the oil samples analysed in the Hassi Messaoud field; therefore, it appears that the oil trapped in Hassi Guettar field was likely generated from the Silurian source rock strata that had generated most of the oil reserves in the region (for more details, see 4.4.1, 4.4.2 and 4.5 in chapter 4).

In this section, I will use biomarker and aromatic hydrocarbon maturity parameters together with the concentrations of the alkylcarbazoles and benzocarbazoles to determine the filling direction of the Hassi Guettar satellite field by comparison to the Hassi Messaoud field.

5.6.1. Aliphatic hydrocarbons

5.6.1.1. *Normal*-alkanes

The two oil samples HGA #2 and HGA #3 show similar *n*-alkane distributions and both samples exhibit an elevation of the *n*-C_{11} alkane (Figure 5.56). Moreover the Pr/Ph ratio shows the same value for both samples; however, oil sample HGA#3 seems to be slightly lighter than oil sample HGA#2. This is expressed by *n*-C_{17}/*n*-C_{27} ratio which is higher in HGA#3 oil compared to HGA#2 oil.

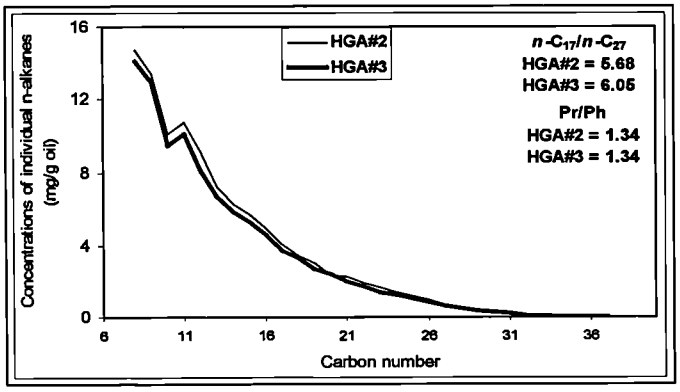

Figure 5.56 *n*-alkane envelopes of the oil samples in the Hassi Guettar field.

5.6.1.2. Steranes and terpanes

Figure 5.57 displays the partial m/z 191 and m/z 217 mass chromatograms for oil samples HGA#2 and HGA#3. The two oil samples show similar sterane and triterpane distributions suggesting the same organic matter facies has generated these oils (see section 4.4.1 in chapter 4). Therefore, in the following discussion, I am going to focus only on the differences related to the maturity of these oils. The sterane and terpane parameters are displayed in Appendix 4.3.

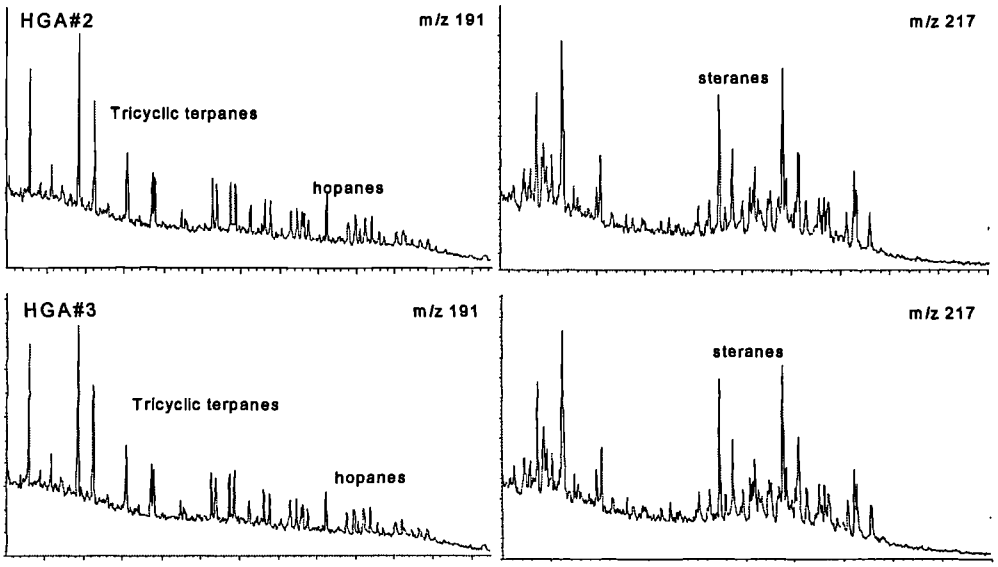

Figure 5.57 Partial m/z 191 and 217 mass chromatograms showing the similarities between the two oil samples HGA#2 and HGA#3, in the Hassi Guettar field.

The same maturity parameters used for the evaluation of the maturity of the Triassic oils in the Oued Mya basin and the Cambrian oils from Hassi Messaoud field are used for the oil sample from Hassi Guettar satellite field. All of the biomarker-based maturity parameters used in this section and those displayed in Appendix 4.3 show minor variations between the two oil samples HGA#2 and HGA#3 (Figure 5.58); however all these parameters reveal that oil sample HGA#3, located towards the north of Hassi Guettar satellite field and close to Hassi Messaoud field might be very slightly more mature than the oil sample HGA#2 located towards the south further away from Hassi Messaoud field. This tentative trend of decreasing maturity from oil sample HGA#3 towards oil sample HGA#2 appears to be consistent for all the biomarker maturity parameters used in this section and the aromatic hydrocarbon maturity parameters used in the section below.

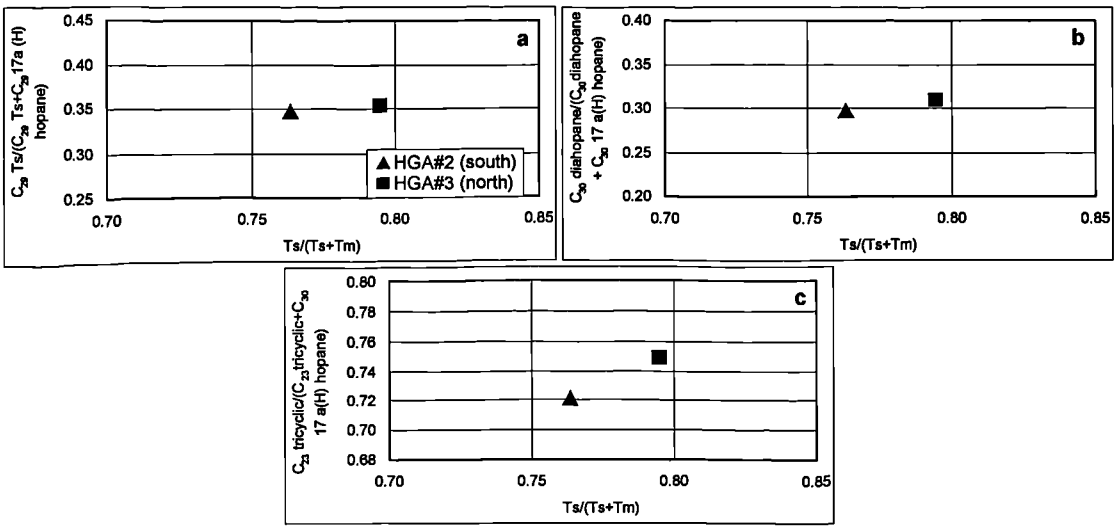

Figure 5.58 Cross plots of (a) $C_{29}Ts/(C_{29}Ts + C_{29}\ 17\alpha$ (H) hopane), (b) C_{30} diahopane/(C_{30} diahopane + $C_{30}\ 17\alpha$ (H) hopane) and (c) C_{23} tricyclic terpane/(C_{23} tricyclic terpane + $C_{30}\ 17\alpha$ (H) hopane) versus Ts/(Ts+Tm) maturity parameters showing the maturity variations within the Hassi Guettar field.

5.6.2. Aromatic compounds

All of the alkylnaphthalenes, alkylphenanthrenes, alkyldibenzothiophenes and aromatic steroid based maturity parameters confirm the tentative and small maturity trend revealed in the biomarkers; with oil HGA#3 being slightly more mature than oil HGA#2 (Appendix 4.3). Some of these parameters are plotted in Figure 5.59. The aromatic maturity parameters seem to show more obvious differences between the two oil samples compared to the biomarker parameters, but the maturity differences are still small. Moreover, the oil sample HGA#3 shows higher concentrations of the aromatic hydrocarbons compared to the oil sample HGA#2, which may also suggest that oil sample HGA#3 is more mature than oil sample HGA#2 (e.g. Li et al., 1995). The concentrations of alkylnaphthalenes, alkylphenanthrenes, and alkylthiophenes in oil sample HGA#3 are 49730.63 µg, 45610.63 µg, and 11614.95 µg/g oil, respectively, whereas in the oil sample HGA#2 the concentrations of the same class of compounds are 45730 µg, 41479 µg, and 10279 µg/g oil, respectively (see also Appendix 4.4).

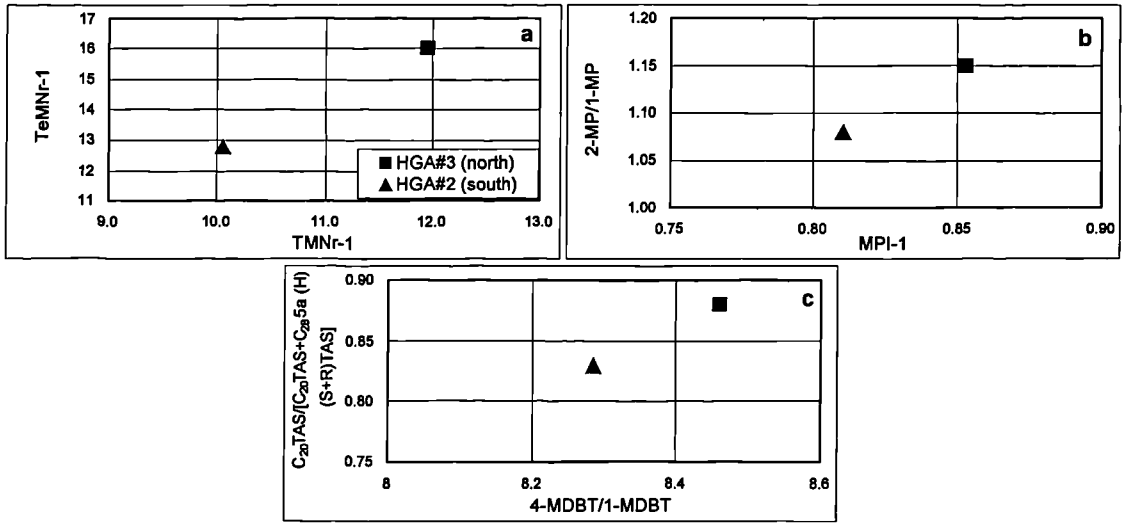

Figure 5.59 Cross plots of (a) 1,3,6,7-TeMN/(1,2,5,6-TeMN+1,2,3,5-TeMN) versus 1,3,7-TMN/1,2,5-TMN, (b) 2-MP/1-MP versus MPI-1, and C_{20} TAS/[C_{20}TAS + C_{28} 5α (H) S+R) TAS]] versus 4-MDBT/1-MDBT maturity parameters showing the maturity variations within the Hassi Guettar field.

5.6.3. Alkylcarbazoles and benzocarbazoles

The concentrations of the pyrrolic nitrogen compounds in the oils analysed in this study are listed in Appendix 5.4. The principal components analysis performed in section 5.4.1 revealed that the alkylcarbazole and benzocarbazole concentrations and ratios are mainly controlled by the relative migration distances in all oils analysed in this study.

The oil samples HGA#2 and HGA#3 exhibit similar source, maturity, and alkylcarbazole and benzocarbazole concentrations compared to the oil samples trapped in the Hassi Messaoud reservoirs (see sections 4.4.1 and 4.4.2 and Appendices 4.3, 4.4, and 5.2). Therefore, I presume that the oil trapped in the Hassi Guettar reservoirs has experienced a similar range of migration distance as the oil trapped in the Hassi Messaoud reservoirs.

Moreover, the oil sample HGA#2 located south of the field seems to have experienced longer migration distance compared to the oil sample HGA#3 located north of the field and close to the Hassi Messaoud field because from Figure 5.60, it is clear that oil HGA#2 contains much lower summed C_0-C_3 alkylcarbazoles and benzocarbazoles ([a]+[c]) than oil HGA#3. The concentrations of the C_0-C_3 alkylcarbazoles and benzocarbazoles in oil sample HGA#3 are 19.50 μg/g oil and 0.11 μg/g oil, respectively; and in oil sample HGA#2 11.90 μg/g oil and 0.05 μg/g, respectively.

The difference in the pyrrolic nitrogen compound concentrations between the two oil samples is more important compared to the biomarker and aromatic hydrocarbons.

5.6.4. Summary

The Hassi Guettar oil samples showed minor but constant decreasing maturity from well HGA#3, north of the field to well HGA#2, to the south obtained from all the biomarker and aromatic hydrocarbon parameters and aromatic hydrocarbon concentrations. The C_0-C_3 alkylcarbazole concentrations are 1.6 times higher in oil HGA#3 than in the oil HGA#2, and the benzocarbazole ([a]+[c]) concentrations are 2.3 times higher in the oil HGA#3 than in the oil HGA#2. In addition, geological evidence shows that well HGA#3 is producing from the Cambrian Ra reservoir unit which is deeper than the reservoir Formations El-Atchane sandstones and Hamra quartzite from where well HGA#2 is producing oil. Hence, these observations would suggest tentative north-south oil charging of the Hassi Guettar field, assuming that the petroleum entering the reservoir last is more mature than the previous pulse of petroleum and displaces the existing less mature petroleum (England et al., 1987).

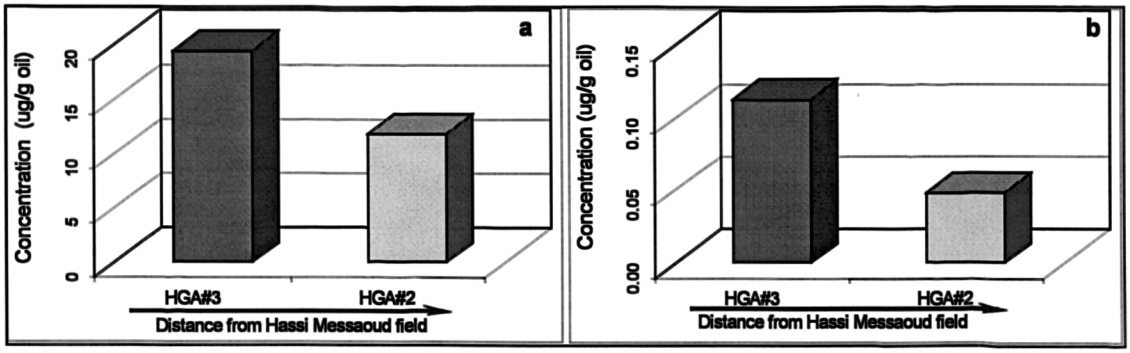

Figure 5.60 Distribution of (a) summed alkylcarbazoles and (b) benzocarbazoles ([a]+[c]) across the Hassi Guettar oils.

5.7. El-Agreb fields (El-Gassi- Zotti-El-Agreb fields)

El-Gassi, Zotti, and El-Agreb constitute a succession of three oil fields located about 80km south-southwest of Hassi Messaoud field (Figure 5.1 and Figure 5.61). El-Agreb field is the farthest field from Hassi Messaoud field, El-Gassi field is the closest from Hassi Messaoud and Zotti field is located in between El-Agreb and El-Gassi fields. The fields produce oil mainly from the Cambrian Ra reservoir, which shows more or less similar reservoir characteristics as the Cambrian Ra in the Hassi Messaoud field. One oil sample from each field was collected; GS#1 from El-Gassi

field, AR#61 from Zotti field and AR#22 from El-Agreb field. The average porosity and permeability are about 8.99% and 21.33 mD, respectively in the well AR#61 from Zotti field and 9.14% and 28.87 mD, respectively in the well AR#22 from El-Agreb field. The depth of the oil-water contacts are: 3090 m for El-Gassi field, 3038 m for Zotti field, and 2975m for El-Agreb field (Figure 5.61); whereas at Hassi Messaoud and Hassi Guettar fields the oil-water contacts are approximately at 3400 m and 3380 m, respectively.

Previously in sections 4.4.1, 4.4.2 and 4.5 in chapter 4, I showed that the oil samples analysed in El-Agreb fields have similar source facies and maturity features compared to the Hassi Messaoud and Hassi Guettar oils, and were likely generated from the Silurian source rock samples analysed in the Oued Mya basin. In this section, I will use biomarker and aromatic hydrocarbon maturity parameters together with the concentrations of the C_0-C_3 alkylcarbazoles and benzocarbazoles to determine the filling directions of the three successive fields and relate them to the Hassi Messaoud and Hassi Guettar fields.

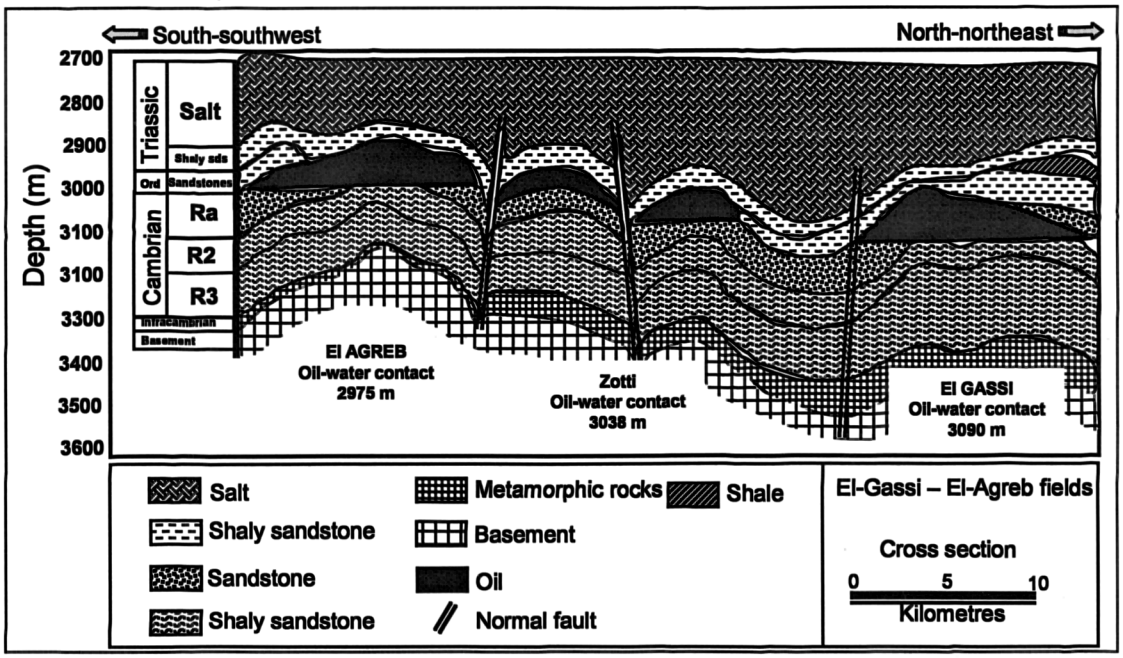

Figure 5.61 Northeast-southwest cross section showing El Gassi-Zotti-El Agreb structures.

5.7.1. Lateral petroleum geochemical variations throughout the El-Agreb fields

5.7.1.1. Aliphatic hydrocarbons

5.7.1.1.1. *Normal* alkanes

The three oil samples GS#1, AR#61, and AR#22 show similar *n*-alkane distributions and all the samples exhibit an elevation at *n*-C_{11} alkane (Figure 5.62). Moreover Pr/Ph ratio shows very similar values for all these oil samples. Oil sample GS#1 seems to be slightly lighter than oil samples AR#61 and AR#22, respectively; with the *n*-C_{17}/*n*-C_{27} ratio being slightly higher in GS#1 oil compared to AR#61 and AR#22 oils respectively (Table 4.8 in chapter 4).

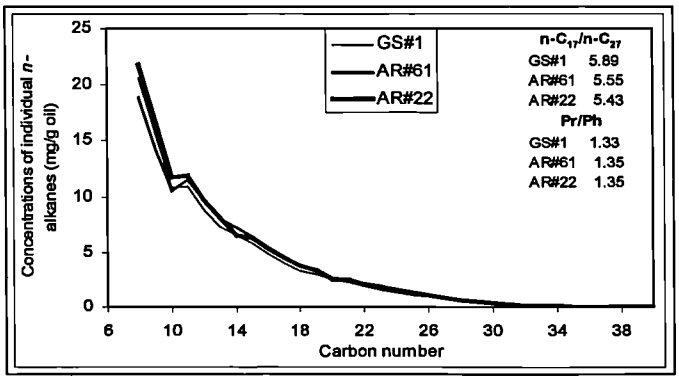

Figure 5.62 *n*-alkane envelopes of the oil samples in the El-Agreb fields.

5.7.1.1.2. Steranes and terpanes

The sterane and triterpane parameters calculated for the El-Agreb oils are displayed in Appendix 4.3. Figure 5.63 displays the partial m/z 191 and m/z 217 mass chromatograms for the oil samples GS#1, AR#61 and AR#22. The triterpane and sterane distributions are similar suggesting the same origin for these oils.

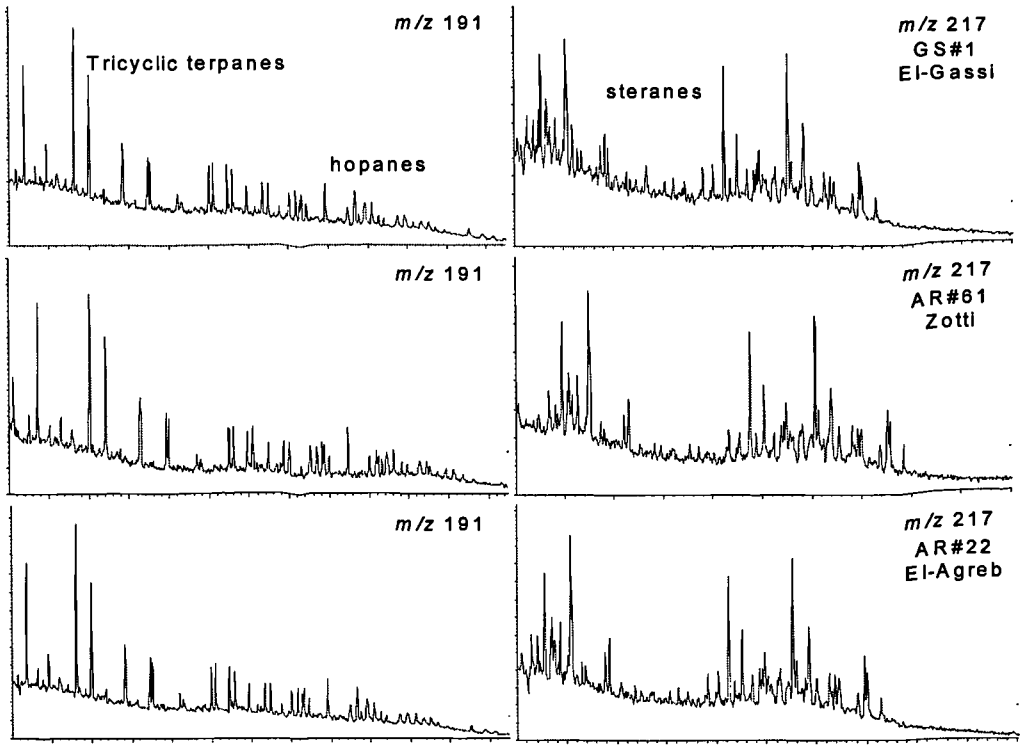

Figure 5.63 m/z 191 and m/z 217 mass chromatograms showing the similarities between the three oil samples GS#1 and AR#61 and AR#22 in the El-Agreb fields.

Maturity parameters plotted in Figure 5.64 suggest a very small north-northeast-south-southwest decrease in the maturity of the oils with GS#1 being the more mature oil compared to AR#61 and AR#22 oils, respectively; however, although the variations in these parameters are consistent, the differences between the parameter values are very close to the analytical errors for these parameters.

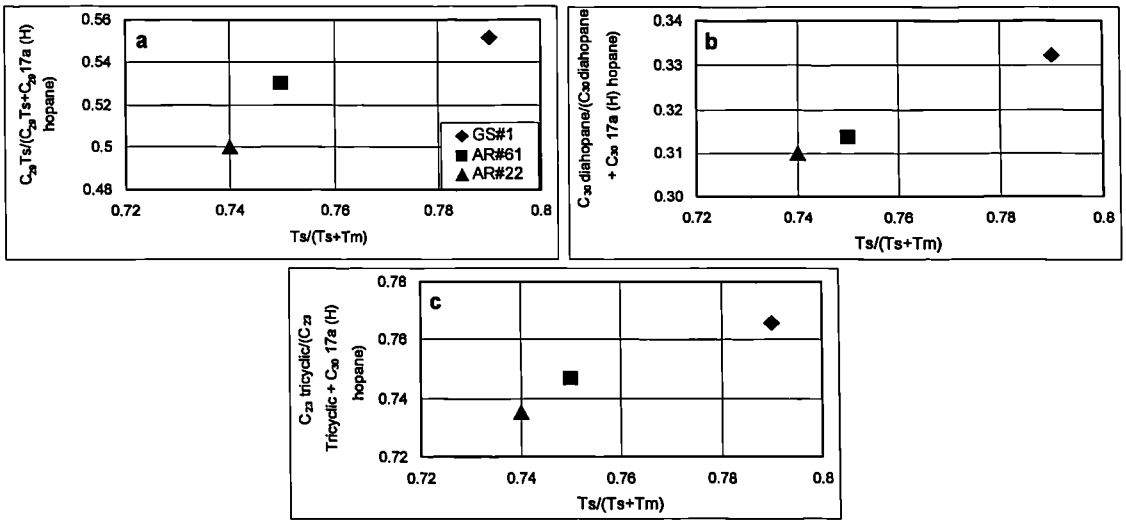

Figure 5.64 Cross plots of (a) $C_{29}Ts/(C_{29}Ts + C_{29}$ 17α (H) hopane), (b) C_{30}diahopane/ (C_{30}diahopane + C_{30} 17α (H) hopane), and (c) C_{30} tricyclic terpane/(C_{30} tricyclic terpane + C_{30} 17α (H) hopane) versus Ts/(Ts+Tm) showing the maturity variations within El-Agreb fields.

5.7.1.1.3. Aromatic hydrocarbon compounds

The aromatic hydrocarbon based maturity parameters confirm the tentative maturity trend shown above using biomarker alkanes (Appendix 4.4.). Figure 5.65 displays some selected aromatic hydrocarbon based maturity parameters. It is clearly shown that oil sample GS#1from El Gassi field located north-northeast of the these three fields is more mature than oil sample AR#61 from Zotti field and oil sample AR#22 from El Agreb field, respectively. The tentative trend of decreasing maturity from the oil trapped in El-Gassi field towards the oil trapped in El-Agreb field is consistent; however, the values of the aromatic hydrocarbon parameters are also close to the analytical error of these parameters.

Moreover, the concentration of the aromatic hydrocarbons in petroleum is believed to increase with increasing maturity, whereas the concentration of the biomarker alkanes decreases with increasing maturity (e.g. Li et al., 1995a, see also section 5.5.2.3 above). The summed aromatic hydrocarbon concentrations decrease from the oil sample GS#1 (78355.96 µg/g oil) towards the oil samples AR#61 (65431.09 µg/g oil) and AR#22 (57824.89 µg/g oil), respectively; and the summed biomarker alkane concentrations increase in the same direction from 107.04 µg/g oil in oil sample GS#1 to 115.09 µg/g oil in oil sample AR#61 and 126.67 µg/g oil in oil sample AR#22 (see also Appendix 4.3 and 4.4). This observation would suggest a trend of decreasing maturity from the oil trapped in El-Gassi field towards Zotti and El-Agreb fields, respectively. Therefore, the tentative north-northeast – south-southeast maturity trend revealed by the biomarker alkane and aromatic hydrocarbon maturity parameters could be considered real.

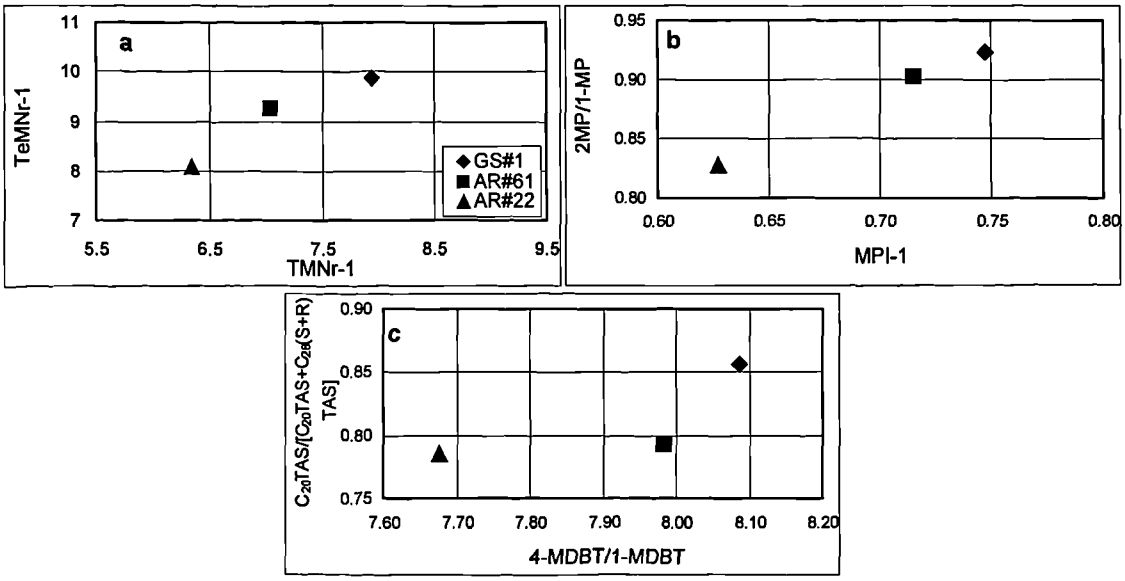

Figure 5.65 Cross plots of (a) 1,3,6,7-TeMN/(1,2,5,6-TeMN+1,2,3,5-TeMN) versus 1,3,7-TMN/1,2,5-TMN, (b) 2-MP/1-MP versus MPI-1, and C_{20} TAS/[C_{20}TAS + C_{28} 5α (H) S+R) TAS] versus 4-MDBT/1-MDBT maturity parameters showing the maturity variations within the El-Agreb fields.

5.7.1.1.4. Alkylcarbazoles and benzocarbazoles in the oils from the El Agreb fields

The concentrations of the individual and summed C_0-C_3 alkylcarbazoles are displayed in Appendix 5.2. The summed C_0-C_3 alkylcarbazole concentrations decrease from El-Gassi oil (GS#1, 2.19 µg/g oil) then Zotti oil (AR#61, 1.27 µg/g oil) towards El-Agreb oil (AR#22, 0.25 µg/g oil) (Figure 5.66). The summed C_0-C_3 alkylcarbazole concentrations in GS#1, AR#61, and AR#22 oils are about 5, 9, and 46 times less, respectively, compared to the Hassi Messaoud oils. Hence, El Agreb oils seem to have experienced much longer lateral migration distance compared to the oils trapped in the Hassi Messaoud and Hassi Guettar fields. The absence of the benzocarbazole isomers ([a] and [c]) (Figure 5.67) confirms that the oils trapped in the three successive fields have undergone longest migration distances compared to the oils trapped in the Hassi Guettar and Hassi Messaoud fields. In addition, the concentration of the summed alkylcarbazoles in oil AR#22 is 5 and 9 times less than the concentrations of the summed alkylcarbazoles in oils AR#61 and GS#1, respectively. This suggests that the oil trapped in El-Agreb field has undergone the longest migration distance compared to the oils trapped in Zotti and El-Gassi fields, respectively.

This North-northeast – south-southwest trend in decreasing alkylcarbazole concentrations may be explained with the following scenario: the oil trapped in El-

Agreb field is likely the first oil that has migrated all the way from Hassi Messaoud towards the present El Agreb accumulations. Therefore, the polar compounds such as alkylcarbazoles in El Agreb oil were subjected to much higher fractionation between oil and "fresh" carrier bed phases, especially solid organic phases and minerals (most probably dispersed organic matter and clay minerals) throughout the migration pathways. With the arrival of more oils containing probably more alkylcarbazoles, the migration pathways along the carrier bed were probably already saturated with alkylcarbazoles lost during the migration of the first charge(s) of oil. Therefore, there was probably less fractionation between the freshly arriving oil and the solid phase along carrier bed (Larter et al., 2000). Hence, the concentrations of alkylcarbazoles in the freshly arriving oil will be higher compared to the previous oil charge, due to reduced migration fractionation.

Figure 5.67 shows the m/z 217, 231, 245, and 259 mass chromatograms representing the alkylbenzocarbazole distributions in the El Agreb fields. The benzocarbazoles are absent in these oils because they were completely removed along the migration pathway(s) of these oils. This is further strong evidence for long distance lateral migration experienced by the El Agreb oils (Terken and Lewin, 2000).

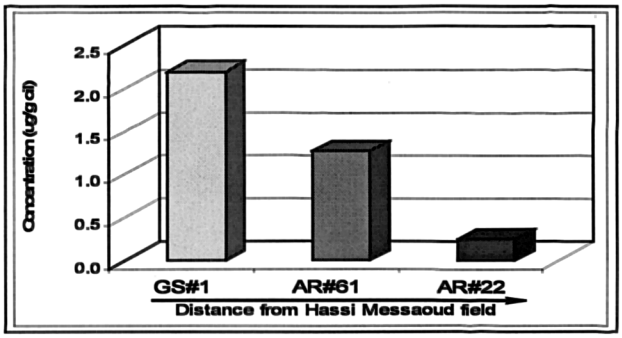

Figure 5.66 Variation in the concentrations of the summed alkylcarbazoles in the El Agreb oils.

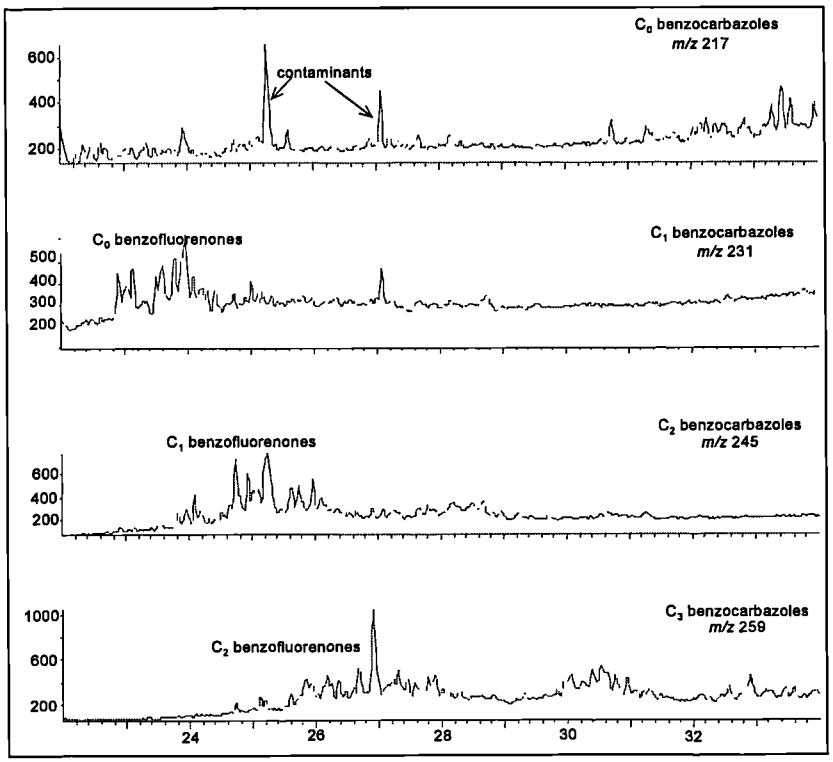

Figure 5.67 Partial m/z 217, 231, 245, and 259 mass chromatograms showing the distribution of the alkylbenzocarbazoles in an El Agreb oil.

5.7.2. Summary

The El-Agreb oil samples showed minor but consistent decreasing maturity, decrease in the concentrations of aromatic hydrocarbons and increase in the concentrations of biomarker alkanes from well GS#1 in El-Gassi field towards the wells analysed in Zotti and El-Agreb fields, respectively (Figure 5.1). In addition, the summed C_0-C_3 alkylcarbazole and alkylphenol concentrations show systematic decrease in the same direction, whereas the benzocarbazole isomers ([a]+[c]) are completely removed from all of the three oil samples analysed in this study.

All these findings together with the geological evidence showing that El-Gassi oil is trapped in the deepest reservoir (i.e. oil-water contact 3090 m) compared to the oils trapped in Zotti and El-Agreb accumulations, with oil –water contacts at depths of 3038 m and 2975 m, respectively (Figure 5.61) would suggest potential oil charging from the north side of the El-Gassi field towards the south side filling both Zotti and El-Agreb fields. Nevertheless more oil and reservoir core samples need to be analysed in these fields in order to confirm these results.

5.8. Mesdar and Rhourde El Baguel fields

Mesdar and Rhourde El Baguel are located about 80 km east-southeast of the Hassi Messaoud field, and about 5 to 30 km from the Berkine basin (Figure 5.1). Both of these fields produce from the Cambrian Ri and Ra reservoirs which present more or less similar reservoir characteristics as the Cambrian in the Hassi Messaoud field. Two oil samples from each field were selected; RB#10 and RB#18 from El-Baguel field and MDR#7 and MDR#8 from Mesdar field. The average porosity and permeability are about 10% and 16.5 mD, respectively in the Mesdar field and 9% and 17.2 mD, respectively in El-Baguel field. The oil-water contact is deeper in Mesdar field (3370 m) and shallower in El-Baguel field (3060 m) (Figure 5.68).

Previously in sections 4.4 and 4.5 in chapter 4, I showed that the oil samples analysed in Mesdar and El-Baguel fields have similar source facies; however, they appear to be different from all the rest of the oils analysed in the Hassi Messaoud ridge and the Oued Mya basins. I have suggested that the oils trapped in Mesdar and El-Baguel fields were likely generated from the Silurian source rock strata in the Berkine basin which probably have slight organic facies differences compared to the Silurian source rock strata analysed in the Oued Mya basin.

In this section, I will use biomarker and aromatic hydrocarbon maturity parameters together with the concentrations of the C_0-C_3 alkylcarbazoles and benzocarbazoles to determine the possible filling directions of both of Mesdar and El-Baguel fields.

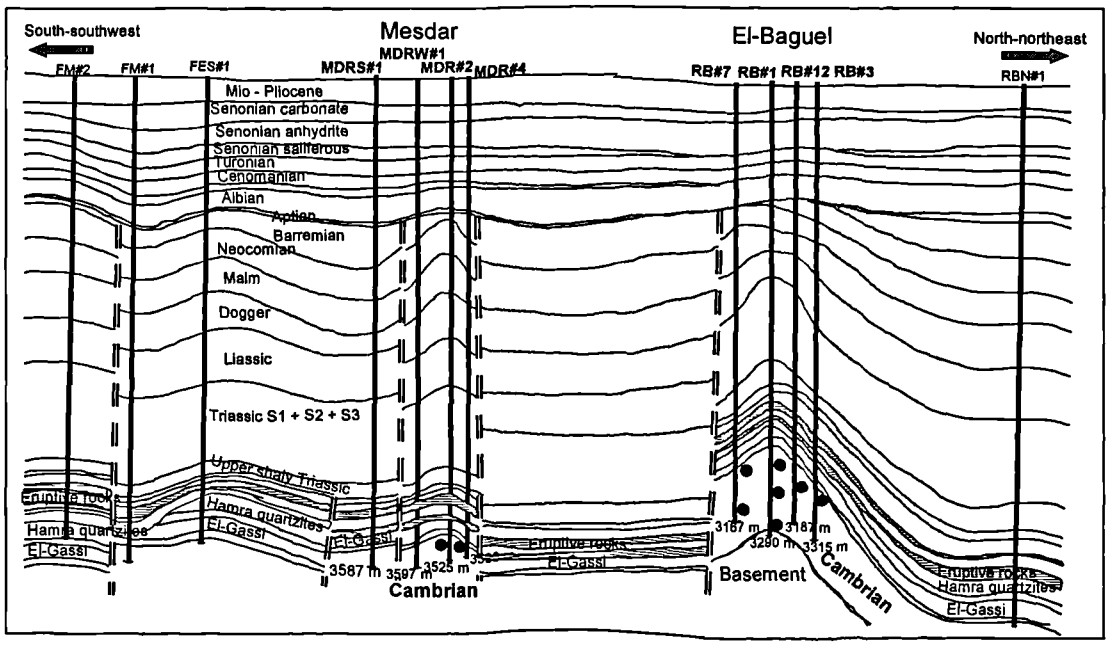

Figure 5.68 South-southwest – north-northeast cross section showing Mesdar and El Baguel structures.

5.8.1. Lateral petroleum geochemical variations throughout the Mesdar and El Baguel fields

5.8.1.1. Saturated hydrocarbons

5.8.1.1.1. *Normal*-alkanes

The oil samples MDR#7, MDR#8, RB#10, and RB#18 analysed in Mesdar and El Baguel fields show similar *n*-alkane distributions dominated by the front end *n*-alkane members (Figure 5.69). This is typical for a marine/algal type of the main source rocks of these oils. Moreover Pr/Ph ratio shows more or less the same values, it is slightly higher in oil samples from the Mesdar field (1.43 and 1.44) than the El Baguel field (1.27 and 1.38).

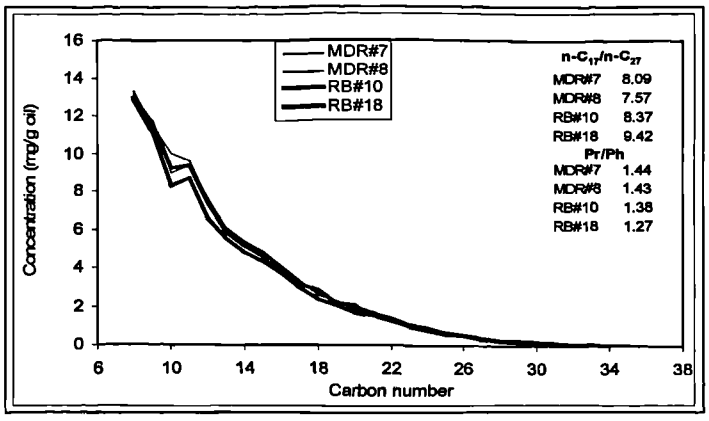

Figure 5.69 *normal* -alkane envelopes of the Cambrian oils in the Mesdar and El Baguel fields.

5.8.1.1.2. Steranes and terpanes

Figure 5.70 displays the partial m/z 191 and m/z 217 mass chromatograms for the oil samples MDR#7 and RB#18. The sterane and terpane parameters are displayed in Appendix 4.3.

The terpane and sterane distributions are similar suggesting the same origin for these oils. The terpanes are strongly dominated by the tricyclics over the pentacyclics (hopanes), and the sterane distributions are dominated by the lower molecular weight homologues (C_{21} and C_{22} steranes) over the C_{27}, C_{28} and C_{29} steranes.

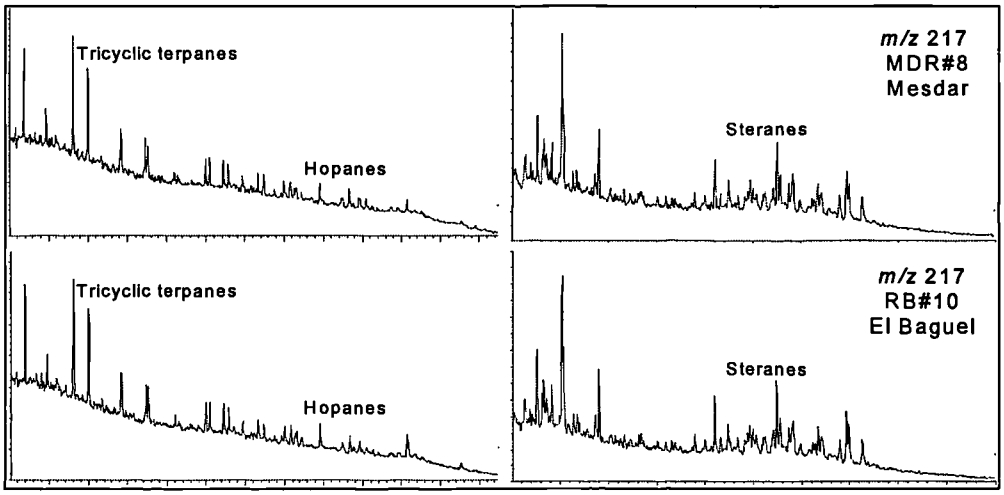

Figure 5.70 m/z 191 and m/z 217 mass chromatograms showing the distributions of terpanes and steranes in the Mesdar and El Baguel fields.

Biomarker maturity parameters plotted in Figure 5.71 with all the other biomarker maturity parameters listed in Appendix 4.3 suggest that oil samples from Mesdar field are slightly more mature than oil samples from El Baguel field. The differences between the values of the biomarker maturity parameters appear to be close to the analytical errors. However, the concentrations of the summed biomarker alkanes (tricyclic terpanes, 17 α (H) hopanes and steranes) are slightly lower in the oil samples from Mesdar field ranging between 81.29 to 78.65 µg/g oil (average 79.97 µg/g oil) compared to the oil samples from El Baguel field ranging between 83.62 to 102.23 µg/g oil (average 92.93 µg/g oil) (see Appendix 4.3). This difference in the biomarker concentrations could be the result of the maturity differences between the oil trapped in Mesdar field compared to the oil trapped in El Baguel field (e.g. Li et al., 1995a). The variations in the aromatic hydrocarbon maturity parameters and

concentrations agree well with the variations in the biomarker maturity parameters and concentrations (see section below for more detail).

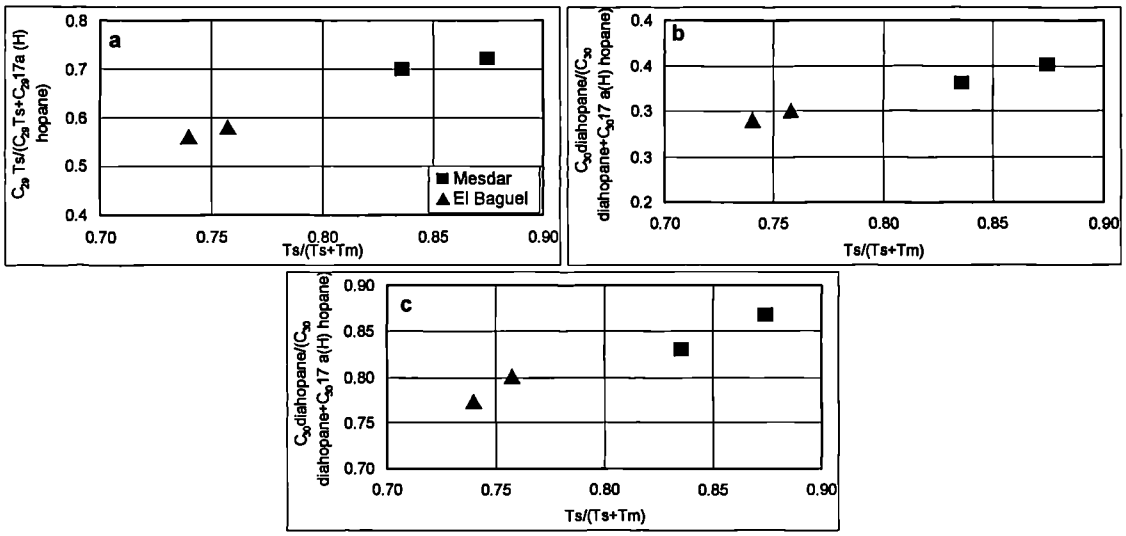

Figure 5.71 Cross plots of (a) $C_{29}Ts/(C_{29}Ts + C_{29}\ 17\alpha$ (H) hopane), (b) C_{30}diahopane/ (C_{30}diahopane + $C_{30}\ 17\alpha$ (H) hopane), and (c) C_{30} tricyclic terpane/(C_{30} tricyclic terpane + $C_{30}\ 17\alpha$ (H) hopane) versus Ts/(Ts+Tm) showing the maturity variations within the Mesdar and El Baguel fields.

5.8.1.1.3. Aromatic compounds

The aromatic-based maturity parameters and concentrations are displayed in (Appendix 4.4). Figure 5.72 displays some selected aromatic hydrocarbon based maturity parameters. It is clearly shown that oil samples MDR#7 and MDR#8 from Mesdar field are more mature than RB#10 and RB#18 from El Baguel field. The difference between the values of aromatic hydrocarbon parameters is higher than the analytical errors. The summed aromatic hydrocarbons (Appendix 4.4) exhibit higher concentrations in the oil samples from Mesdar field ranging between 211374 to 232541 μg/g oil (average 221957 μg/g oil) compared to the oil samples from El Baguel field ranging from 146827 to 209332 μg/g oil (average 178080 μg/g oil). It is well established that the aromatic hydrocarbon concentrations in source-related petroleums increase with increasing maturity, whilst the biomarker alkane concentrations decrease with increasing maturity (e.g. Li et al., 1995a).

In addition, the maturity trend exhibited by these source-related oils may have important implications in the study of the extent of oil migration processes in this area. In this particular situation, it is predicted that the oil currently reservoired in the El Baguel shallowest accumulation (i.e. oil-water contact located at 3060 m)

represents relatively early expelled products from the subsiding Silurian source rock within the Berkine basin. With increasing source rock subsidence, progressively more mature oil would have been generated, expelled and subsequently migrated updip to charge the deepest accumulation in Mesdar field (oil-water contact located at 3370 m) (Figure 5.68). Hence, the relatively less mature oil reservoired in El Baguel accumulation may represent the most migrated oil. The more mature oil trapped in Mesdar accumulation could have migrated to a lesser degree from the generating Silurian source rock within the Berkine basin, relative to the shallower, less mature oil from El Baguel accumulation. The variation in the alkylcarbazole and benzocarbazole concentrations between the oils trapped in Mesdar and El Baguel fields described in the next section agree well with these assumptions.

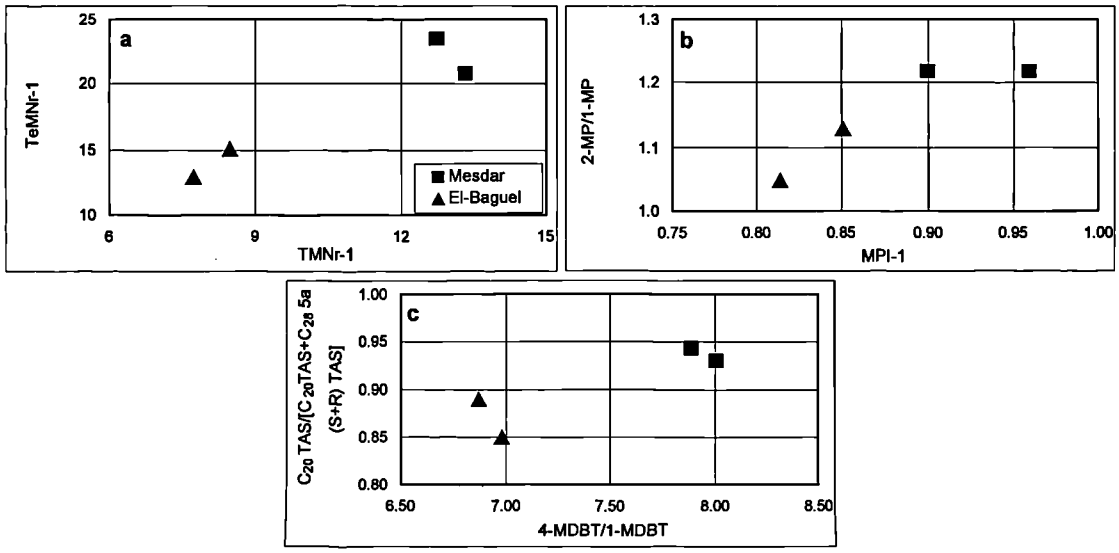

Figure 5.72 Cross plots of (a) 1,3,6,7-TeMN/(1,2,5,6-TeMN+1,2,3,5-TeMN) versus 1,3,7-TMN/1,2,5-TMN, (b) 2-MP/1-MP versus MPI-1, and (c) C_{20} TAS/[C_{20}TAS + C_{28} 5α (H) S+R) TAS] versus 4-MDBT/1-MDBT maturity parameters showing the maturity variations within the Mesdar and El Baguel fields.

5.8.1.1.4. Alkylcarbazoles and benzocarbazoles in the Mesdar and El Baguel fields

The concentrations and ratios of individual and summed C_0-C_3 alkylcarbazoles and benzocarbazoles obtained from the oils analysed in this study are displayed in Appendix 5.2.

The concentration of the summed C_0-C_3 alkylcarbazoles is much higher in the samples from Mesdar field compared to the oil samples from El Baguel field. The average value of the concentrations of the summed C_0-C_3 alkylcarbazoles in the Mesdar oil samples is 46.25 μg/g oil, whereas in the El Baguel oil samples the

average value of the concentrations is 1.56 µg/g oil (Figure 5.73a). The concentration of the summed C_0-C_3 alkylcarbazoles in the Mesdar oils is about 29 times more than the oil samples from the El Baguel field, suggesting probably that oil from the Mesdar field has experienced shorter migration distance than oil from the El Baguel field. Moreover, the oil samples from El Baguel revealed that the benzocarbazole isomers ([a] and [c]) are absent, whereas the average concentration of these compounds in Mesdar oils is 0.16 µg/g oil (Figure 5.73b).

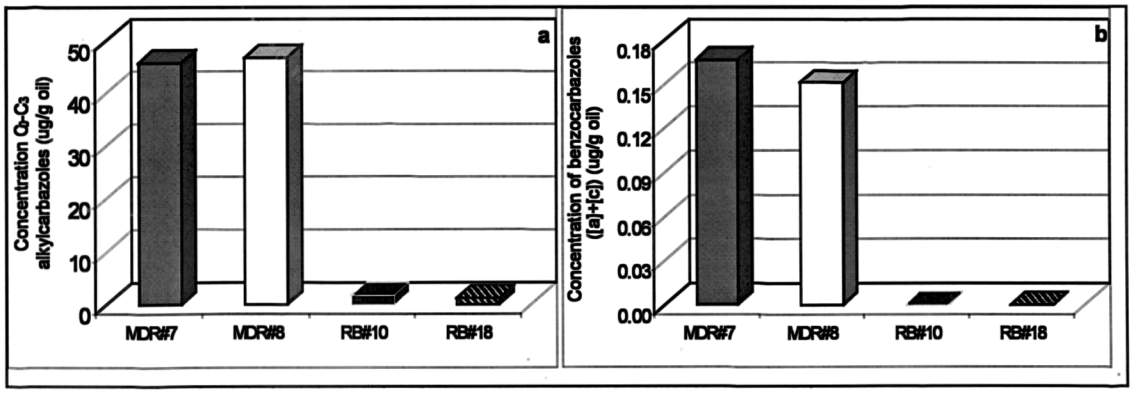

Figure 5.73 Variation in summed alkylcarbazole and benzocarbazole ([a]+[c]) concentrations for the Mesdar and El Baguel oils.

The large difference in the concentrations of C_0-C_3 alkylcarbazoles between the oil samples from the Mesdar and El Baguel fields and the absence of benzocarbazoles in El Baguel oil samples are probably due to the fact that oils from the El Baguel field have experienced much longer migration distance than oils from the Mesdar field. These oils were likely generated from Silurian source rocks located in the Berkine basin, and have migrated north-west towards the Mesdar and El Baguel fields. Moreover, being less mature than oil from the Mesdar field, oil from the El Baguel field was probably the first oil charge that had migrated along the carrier bed between the source rock and the actual reservoir. Therefore, the first oil charge had migrated along an "activated" carrier, where extensive fractionation took place between the mobile phase (oil) and the solid phase (clay minerals and solid organic matter) within the carrier bed. Hence, significant fraction of the polar compounds such as alkylcarbazoles and benzocarbazoles were adsorbed by the solid phase leaving oil with a low alkylcarbazoles and no benzocarbazoles content. The next oil charge that had probably filled the Mesdar field with slightly more mature oil, probably contained more alkylcarbazoles and had migrated along "deactivated" (saturated with regard to

the polar compounds) carrier bed. Therefore, little fractionation between the second oil charge and the solid phase took place leading to relatively higher amount of alkylcarbazoles in the Mesdar oils.

5.9. Summary

The Lower Silurian source rock intervals in the Oued Mya basin are mature. The values of the estimated vitrinite reflectance equivalent (%R_o) obtained in this study range from 0.81 to 1.0 %, whereas Makhous et al. (1997a,b) estimated the maturity of the Silurian to range from 0.7 to 0.9 % R_o. These maturity intervals suggest that the Silurian strata in the Oued Mya basin have reached the main stage of maturity equivalent to the "oil window - end of the oil window". This is consistent with the Tmax values obtained from pyrolysis which showed values ranging from 440°C to 458°C for the Silurian source rock samples (Table 4.1). The Silurian source rock strata analysed in the Oued Mya basin also showed extremely high petroleum potentials capable of generating large volumes of oils. Figure 5.74 shows the variations in maturity of all the oils analysed throughout the Devonian and Lower Triassic fields in the Oued Mya basin and the Cambro-Ordovician oils throughout the Hassi Messaoud Ridge. The maturity of all the oils analysed in this study are plotted against the estimated migration distance from the Silurian source rock intervals located in the Oued Mya basin, north and east of the Hassi Messaoud field. The migration distances of the oils trapped in all the fields analysed in this study were estimated in respect to their geographical location relative to the location of the main source rock strata (i.e. Silurian) identified in this study. In addition, the results obtained from the concentrations and distributions of the pyrrolic nitrogen compounds and maturity in the oils from the different fields were used to derive which of the oils have likely undergone the shortest and the longest migration distances (Figure 5.77). For the Mesdar and El Baguel accumulations, the migration distances were estimated relative to the mature Silurian source rock strata located in the western flanks of the Berkine basin. In sections 4.4 and 4.5 (chapter 4), I showed that the oils analysed in the Mesdar and El Baguel fields are different from the rest of the oils analysed in this study. The maturity of the Silurian strata in the Berkine basin ranges from 1.01 to 1.2 % R_o (Makhous et al., 1997a,b; Daniels and Emme, 1995).

The oils reservoired in the Lower Triassic of Haoud Berkaoui and Benkahla fields reveal the least mature oils in the entire study area (i.e. $\%R_c$= 0.76-0.78). The oils trapped in the deepest accumulations of Mokh El Kebch, N'goussa, Guellala northeast, Guellala, and Draa Temra in the Oued Mya basin, the oils trapped in the western, northern and southern flanks of the Hassi Messaoud field and oils trapped in the El-Agreb fields show higher maturity than those from Haoud Berkaoui and Benkahla fields (i.e. $\%R_c$ = 0.79-0.89). Whereas, the oils trapped in the centre and east of the Hassi Messaoud field, in Hassi Guettar, Rhourde Chegga, Mesdar and El Baguel fields show the highest maturity in the region (i.e. $\%R_c$ = 0.90 – 0.98) (Figure 5.74). These observations would suggest that:

1. The Lower Triassic oils trapped in the Haoud Berkaoui and Benkahla fields in the Oued Mya basin are likely the first charge of oil generated from the Silurian and Ordovician source rock strata.

2. The oils reservoired in the Mokh El Kebch, N'goussa, Guellala northeast, Guellala, and Draa Temra fields in the Oued Mya basin probably account for the second oil charge originated from the underlying Silurian and Ordovician source rock strata.

3. the Hassi Messaoud field contains different oil charges, with the most mature oil charge (i.e. the last oil charge; with $\%R_c$ = 0.90 – 0.94) being trapped in the centre crest and the east of the field and the less mature oil charge (i.e. earlier oil charge; $\%R_c$ = 0.84 – 0.88) being trapped (pushed) towards the western, northern and southern parts of the field.

4. the oils in the Hassi Guettar satellite field show similar maturity compared to the oils in the Hassi Messaoud (i.e. $\%R_c$ = 0.89 – 0.91), with the oil sample located towards the north (close to the Hassi Messaoud field) slightly more mature than the oil sample located towards the south, further from the Hassi Messaoud field. Therefore, a tentative north-south trend of decreasing maturity may be depicted within the Hassi Guettar satellite field.

5. The oil trapped in the El-Gassi, Zotti and El-Agreb fields reveal lower maturity (%R_c = 0.78 – 0.85) compared to the oils trapped in the centre crest and east of the Hassi Messaoud field and the oils from the Hassi Guettar field. Moreover, the oil trapped in El-Gassi field is more mature than the oils trapped in the Zotti and El-Agreb fields respectively, revealing a north-south trend of decreasing maturity.

6. The oil trapped in the Mesdar field appears to be the most mature oil in the region (i.e. %R_c = 0.94 – 0.98) and this is more mature than the oil trapped in the El-Baguel field (i.e. %R_c = 0.89 – 0.91), revealing a south-north trend of decreasing maturity.

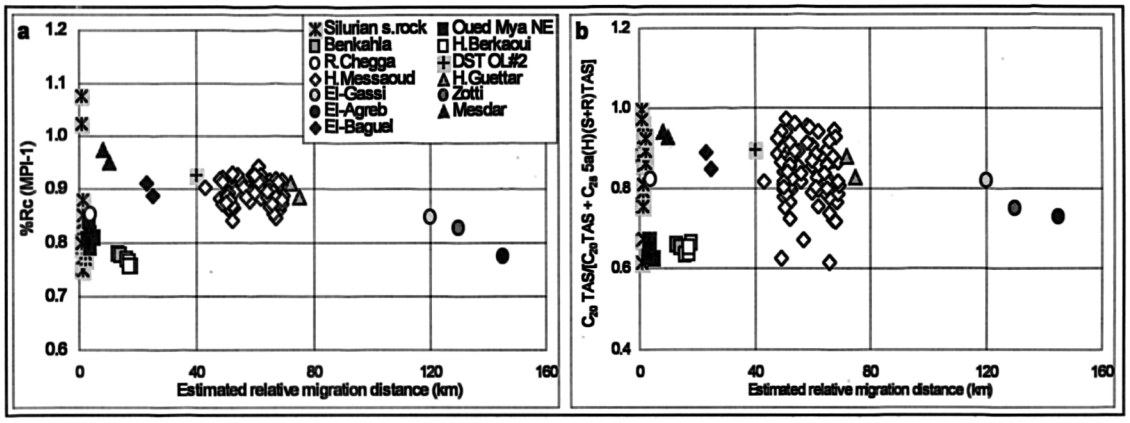

Figure 5.74 Cross plots showing variations in the maturity characterised by (a) calculated vitrinite reflectance equivalent and (b) the ratio of $C_{20}/[C_{20} + C_{28}$ 5 α (H) (S+R)] triaromatic steroids versus the estimated migration distances of the oilfields from the Silurian source rock.

The cross plots in Figure 5.75 show good agreements between the concentrations of biomarkers and aromatic hydrocarbons and the maturity trends revealed above. The least mature oils from the fields in the Oued Mya basin contain the highest concentrations of biomarker alkanes (i.e. tricyclic terpanes, hopanes and steranes) and the lowest concentrations of aromatic hydrocarbons (i.e. alkylnaphthalenes, alkylphenanthrenes and alkylthiophenes) (see Appendices 4.3 and 4.4). The relatively lower maturity oils from the western, northern and southern flanks of the Hassi Messaoud field contain the highest concentrations of biomarker alkanes and the lowest concentrations of aromatic hydrocarbons compared to the more mature oils in the centre and east of the Hassi Messaoud field. The successive El-Agreb fields show an increase in the concentrations of the summed biomarker alkanes and a decrease in the concentrations of the summed aromatic hydrocarbons from the more mature El-

Gassi oil towards the less mature El-Agreb oil. Finally, the oils from the Mesdar and El-Baguel fields show the lowest concentrations of the summed biomarkers and the highest concentrations of the summed aromatic hydrocarbons in the whole region. The concentrations of biomarker alkanes and aromatic hydrocarbons revealed good correlations with the maturity of the oils analysed in this study (see section 4.4.3 in chapter 4).

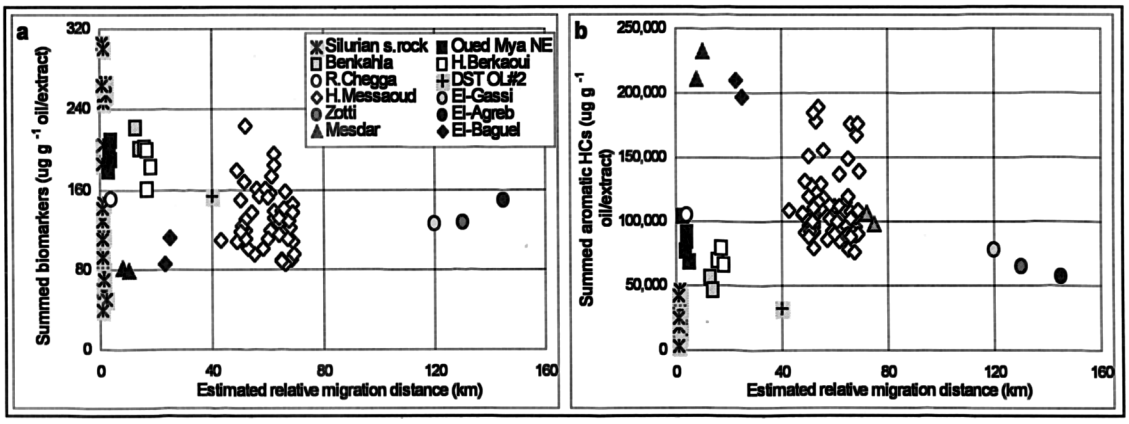

Figure 5.75 Cross plots showing variations in the concentrations of (a) the summed biomarkers and (b) the summed aromatic hydrocarbons versus the estimated migration distances of the oilfields from the Silurian source rock.

The variations in the concentrations of the summed C_0-C_3 alkylcarbazoles and benzocarbazoles ([a]+[c]) in the Silurian source rock strata and the oils plotted against the estimated migration distances show excellent trend between the concentrations of these compounds and the estimated migration distances of the oils (Figure 5.76).

The Silurian source rock samples exhibit extremely high concentrations of the summed C_0-C_3 alkylcarbazoles and benzocarbazoles ([a]+[c]) ranging from 37.78 to 900 μg/g extract (average 578.32 μg/g extract) and 4.94 to 155.45 μg/g extract (average 80.42 μg/g extract), respectively (Appendix 5.1). In contrast, in the oils the concentrations of the summed C_0-C_3 alkylcarbazoles and benzocarbazoles ([a]+[c]) range from 1.24 to 50.12 μg/g oil (average 23.88 μg/g oil) and 0 to 0.46 μg/g oil (average 0.17 μg/g oil), respectively. The concentrations of the summed C_0-C_3 alkylcarbazoles and benzocarbazoles ([a]+[c]) in the Silurian source rocks are 24 and 500 times higher than in the related oils. These observations suggest that the pyrrolic compounds are strongly retained within the Silurian source rocks compared to the related oils. Moreover, the benzocarbazoles appear to show even higher fractionation compared to the alkylcarbazoles (Li et al., 1995).

The concentrations of the summed C_0-C_3 alkylcarbazoles and benzocarbazoles ([a]+[c]) systematically decrease from the Devonian and Lower Triassic fields in the Oued Mya basin and Rhourde Chegga fields located just above the Silurian source rock strata (Figure 5.12), towards Benkahla, Haoud Berkaoui fields in the Oued Mya basin, and Hassi Messaoud, Hassi Guettar, and El-Agreb fields in the Hassi Messaoud ridge, respectively (Figure 5.76 and Figure 5.77). These observations would strongly suggest that oil migration started in the Oued Mya basin towards the Hassi Messaoud field, located east-southeast of the Oued Mya basin, and then oil continued to migrate from the Hassi Messaoud field to the Hassi Guettar satellite field and El-Agreb fields located south-southwest from the Hassi Messaoud field. Moreover, the trend of decreasing concentrations of the pyrrolic compounds from the Mesdar field towards the El-Baguel field suggest other migration directions likely starting from the Silurian source rocks located in the Berkine basin east-southeast of the Mesdar field towards the El-Baguel field north-northeast from the Mesdar field (Figure 5.77).

In section 5.6, I have also shown that the Hassi Messaoud field was also charged from the Silurian located towards the east of the field, in the Hassi Dzabat area (Figure 5.77).

In the Oued Mya basin, the shallowest reservoirs in the Benkahla and Haoud Berkaoui fields revealed lower concentrations of summed alkylcarbazoles and benzocarbazoles relative to the deepest reservoirs in the Mokh el-Kebch, N'Goussa, Guellala north-east, Guellala, and Draa Temra fields and somewhat similar range of concentrations as in the Hassi Messaoud oils. Therefore, it is likely that the oils from Benkahla and Haoud Berkaoui fields have also experienced relatively long lateral migration from the north-northeast of the Oued Mya basin southwards to the actual locations of these fields (Figure 5.77).

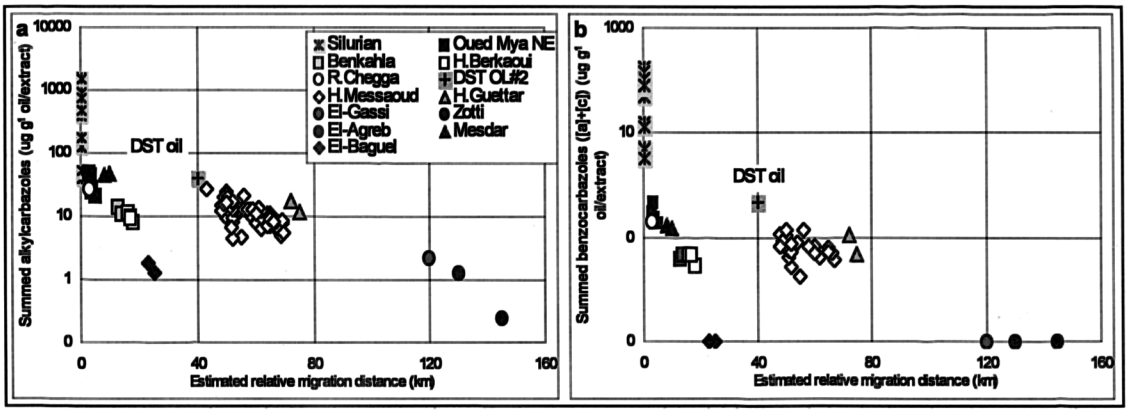

Figure 5.76 Cross plots showing variations in the concentrations of (a) the C_0-C_3 summed alkylcarbazoles and (b) the summed benzocarbazoles ([a] + [c]) versus the estimated migration distances of the oilfields from the Silurian source rock strata. Note that in both plots, the "Y" axis is on a logarithmic scale.

Finally, the following observations can be inferred from the results obtained in this chapter:

1. The organic matter abundance in the Silurian source rocks strongly controls the concentrations and distributions of the alkylcarbazoles and benzocarbazoles.

2. The nitrogen compounds such as alkylcarbazoles and alkylbenzocarbazoles are strongly retained within the Silurian source rock.

3. The oils trapped in the deepest reservoirs in the Mokh-el-Kebch, N'Goussa, Guellala northeast, Guellala, and Draa Temra fields, have probably undergone the shortest migration distances (probably only vertical migration) compared to the oils trapped in the shallowest reservoirs in the Benkahla and Haoud Berkaoui fields. The oils trapped in these fields may have experienced vertical migration from the Silurian and Ordovician source strata probably located in the area of Boukhzana, N'goussa and Guellala northeast towards the overlying Lower Triassic reservoirs and then followed by long lateral migration (~ 30 km) towards the shallowest Lower Triassic reservoirs in the Benkahla and Haoud Berkaoui fields (Figure 5.77). The Lower Triassic reservoirs in the Benkahla and Haoud Berkaoui are located at shallower depths (i.e. oil-water contact depth is -3324 m), whereas the same Triassic reservoir units are located at higher depths in the Guellala (-3470 m), Draa Temra (-3480 m), Guellala north east (-3531 m) and N'goussa (-3787 m) fields (Figure 5.12).

4. The oils trapped in the Hassi Messaoud field have experienced long lateral migration distances probably from the Silurian source rocks located in the Oued Mya basin 40 to 60 km west-northwest of the Hassi Messaoud field and the Silurian source rocks located 40 to 50 km east of the Hassi Messaoud field (Figure 5.77).

5. The Hassi Messaoud reservoirs were filled from the west and the east, upwards towards the crest (centre of the field) and then towards the north, south and west flanks of the field. The western flank of the field has probably received oil much later compared to all the other parts of the field. This observation is supported by low abundance of petroleum inclusions (section 6.2 in chapter 6), low reservoir porosity and permeability (Figure 5.51) and low petroleum yields (section 5.6.3.1 above) in the samples analysed in this part of the field.

6. The Hassi Messaoud reservoirs revealed lateral and vertical heterogeneities inherited from the charging of the field.

7. The oil has continued to migrate south-southwest towards the El-Agreb fields via the Hassi Messaoud and the Hassi Guettar fields. Therefore, the oils actually trapped in the El-Agreb may have experienced the longest migration distances (ca from 120 to 150 km) (Figure 5.77).

8. The oils trapped in the Mesdar and El-Baguel reservoirs were likely originated from the Silurian source rock in the Berkine basin and then migrated following the north-northwest trend. The oil trapped in the Mesdar field appears to have experienced shorter migration distance compared to the oil trapped in the El Baguel field (Figure 5.68 and Figure 5.77).

9. The principal components analysis showed that the main south-southeast – north-northeast fault across the Hassi Messaoud reservoirs (Figure 5.30) may have been impermeable during the main stages of oil charging. This main fault may have played a key role in preventing mixing between the oil generated in the Oued Mya basin (west-northwest of the Hassi Messaoud field) and the oil generated from the east of the field.

1. The principal component analysis allowed me to statistically confirm that the separation of the Hassi Messaoud field into 25 zones is geochemically consistent.

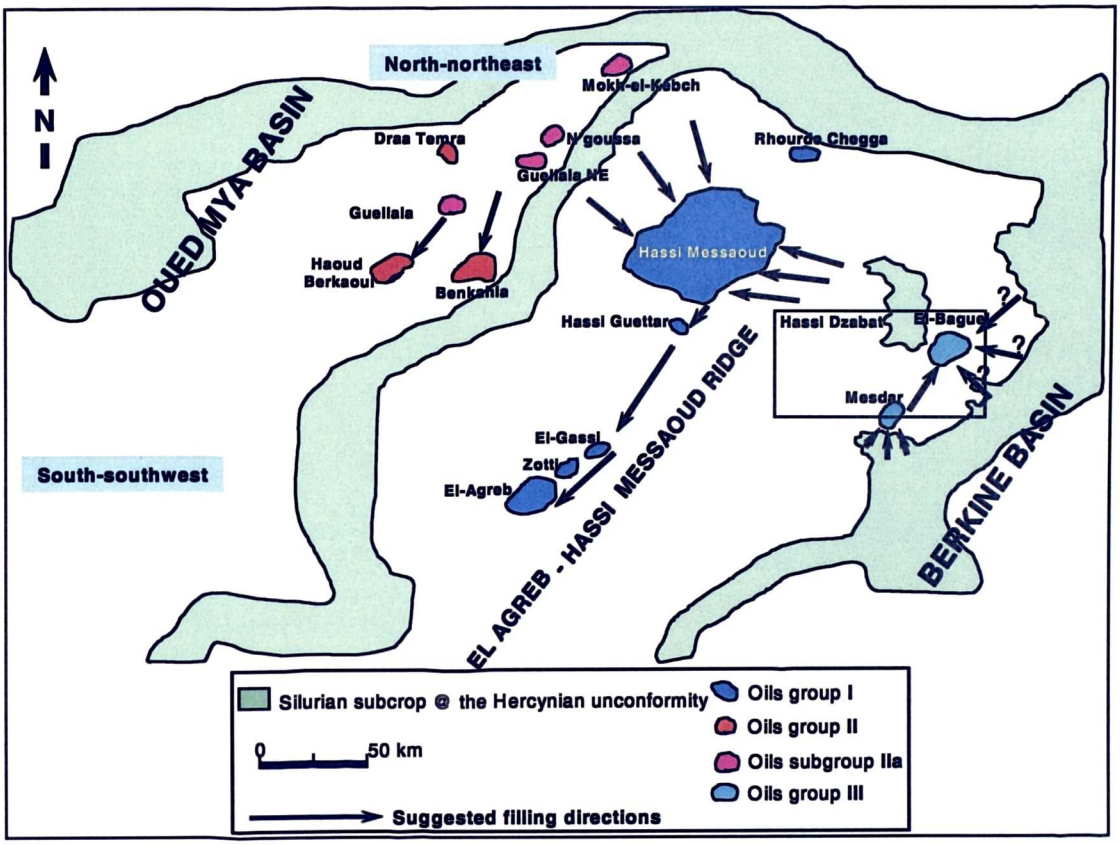

Figure 5.77 Suggested filling directions for the oil fields analysed in the Oued Mya basin and Hassi Messaoud ridge.

Chapter 6
Determination of the Timing of the Hassi Messaoud Reservoir Filling Using Fluid Inclusions, PVT Data and Petroleum Geochemistry of the Palaeo-Oils

6. Determination of the timing of the Hassi Messaoud reservoir filling using fluid inclusions, PVT data and petroleum geochemistry of the palaeo-oils

6.1. Introduction

The integration of petroleum geochemical data with palaeo-petroleum distributions in the reservoir is a useful approach for understanding the filling history of a field (Karlsen et al., 1993; Nedkvitne et al., 1993; Bhullar et al., 1999b, 2001). During the last decade, great efforts have been made to get better understanding of filling history for petroleum reservoirs. In these studies, the key task has been to understand the palaeo-petroleum distributions in the reservoir and the timing of different episodes of filling (Karlsen et al., 1993; Nedkvitne et al., 1993, George et al., 1997; Bhullar et al., 1999b, 2001; Munz et al., 1999). To better understand these factors, microthermometry combined with geochemistry of petroleum in the fluid inclusions from present day and palaeo-petroleum reservoirs has provided an effective method (Karlsen et al., 1993; Nedkvitne et al., 1993, George et al., 1997; Bhullar et al., 1999b, 2001, Munz et al., 1999). Recently, Aplin et al. (1999) have proposed a new approach to determine the palaeo-petroleum composition in single petroleum inclusions and to derive the palaeo-pressure and temperature, GOR and other physical properties such as, density, viscosity, and molar volume of petroleum inclusions. This method uses microthermometry combined with Confocal Scanning Laser Microscopy (CLSM) and PVT simulation of individual fluid inclusions.

Petroleum inclusions in diagenetic minerals may in some cases characterise pristine petroleum present in the trap at earlier times, i.e. the time of authigenic mineral growth (Karlsen et al., 1993; Aplin et al., 1997; George et al., 1997). The known temperature control on the relevant diagenetic mineral reactions (Bjørlikke et al., 1989) and the burial history of a given field may in some cases be used to derive tentative preliminary estimates of the timing of petroleum inclusion formation (i.e. timing of field filling).

The aims of this chapter are to: 1) determine the distribution and abundances of petroleum inclusions in the Hassi Messaoud reservoirs; 2) perform PVT simulations

on selected coexistent petroleum and aqueous inclusions, and 3) perform geochemical analysis on the palaeo-oil trapped in the fluid inclusions and compare them to the present day produced oil. The information gained from the combination of these three investigations will be used in order to understand the filling history and timing of oil-charging of the Hassi Messaoud Cambrian reservoirs and Haoud Berkaoui Lower Triassic reservoir.

In this study, I have selected 23 samples from 9 wells (Table 6.1); 22 samples were collected from 8 wells in the Hassi Messaoud field (MD#177, OMO#712, MD#213, OML#712, OMJ#41, OMM#33, MD#319, and MD#141) and 1 sample from well OKJ#202 in the Haoud Berkaoui field. The position of the wells selected from the Hassi Messaoud field is displayed in Figure 6.1, and the position of the Haoud Berkaoui field is displayed in Figure 5.1, in chapter 5.

Table 6.1 List of samples selected for the fluid inclusions study.

Well	Number of samples	Depth (m)	Field	Reservoir	Reservoir unit
		3291.35		Cambrian	Ra
MD#177	4	3324.5	Hassi	Cambrian	Ra
		3339.5	Messaoud	Cambrian	Ra
		3379.9		Cambrian	R2
		3324.9		Cambrian	Ra
OMO#712	4	3345.6	Hassi	Cambrian	Ra
		3378.5	Messaoud	Cambrian	R2
		3387.65		Cambrian	R2
		3451.6	Hassi	Cambrian	Ra
MD#213	3	3468.15	Messaoud	Cambrian	Ra
		3499.5		Cambrian	Ra
OML#712	2	3426.95	Hassi	Cambrian	R2
		3437.45	Messaoud	Cambrian	R2
OMJ#41	2	3390.1	Hassi	Cambrian	Ra
		3463.5	Messaoud	Cambrian	R2
		3413.75		Cambrian	Ra
OMM#3	4	3464.5	Hassi	Cambrian	Ra
		3476.85	Messaoud	Cambrian	Ra
		3483.75		Cambrian	Ra
MD#319	1	3453.25	Hassi Messaoud	Cambrian	-
MD#141	2	3438.65	Hassi	Cambrian	
		3450.4	Messaoud	Cambrian	Ra
OKJ#202	1	3327.5	Haoud Berkaoui	Triassic	Lower Triassic
Total	23				

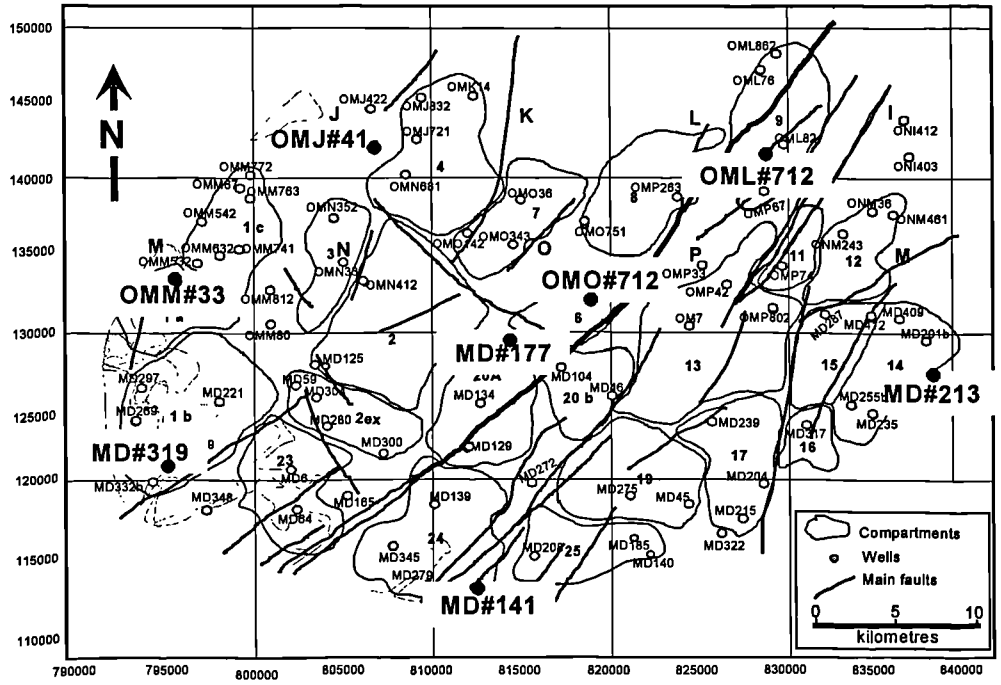

Figure 6.1 Map showing the wells sampled for fluid inclusions study in the Hassi Messaoud field.

6.2. Fluid inclusions petrography

6.2.1. Abundance of petroleum inclusions

Petroleum inclusions in sandstones from the Cambrian reservoir units Ra and R2 in the Hassi Messaoud field have been found in most of the samples from all the wells MD#177, OMO#712, MD#213, OML#712, OMJ#41, OMM#33, MD#319 and MD#141, except for a few samples selected from the wells MD#213 (3468.15 m), MD#141 (3438.65 m), OMM#33 (3464.5 m and 3483.75 m), and OMJ#41 (3463.5 m) that did not show the occurrence of petroleum inclusions. The abundance of petroleum inclusions is generally extremely high in the samples from the wells located in the centre of the field (MD#177 and OMO#712) and from the well MD#213 located in the eastern flank, moderate in the samples from the wells MD#141 and OML#712, and low in the samples from the wells MD#319, OMM#33 and OMJ#41.

6.2.2. Textural occurrence of petroleum inclusions

In general, most of petroleum inclusions are present as secondaries on the detrital quartz grains with rare primaries found trapped in the dust rims and quartz overgrowths. The majority of petroleum inclusions are two phase inclusions at room temperature. There are only three samples which contain a minority of inclusions with

three phases, consisting of two petroleum phases (oil and gas) and one aqueous fluid phase. The majority of petroleum inclusions showed a pale blue to blue fluorescence, whereas a minority of petroleum inclusions showed yellowish fluorescence and their homogenization temperatures are lower than the other group of petroleum inclusions (see microthermometric results bellow). These petroleum inclusions were probably trapped during the arrival of the first oil charge, therefore they may contain a relatively less mature oil charge. Moreover, all petroleum inclusions showed similar phase behaviour as they homogenised to a single liquid phase.

The quartz grains (detrital grains) commonly have well-developed authigenic quartz overgrowths (Figure 6.2). Petroleum inclusions are predominantly present as clusters and isolated inclusions most commonly in the detrital quartz grains. They are highly variable in shape and look like secondary inclusions, probably formed along the original fractures of the detrital grains. Sample MD#141 (3450.4 m), shows common secondary petroleum inclusions which cut through the quartz overgrowth indicating that trapping of these petroleum inclusions post-date formation of the overgrowths; the other samples show quite rare occurrence of fractures containing secondary petroleum inclusions and cross-cutting the quartz overgrowth. The size of petroleum inclusions varies between 4 μm to 50 μm in long dimensions, whereas the aqueous inclusions are much smaller with maximum size up to 15 μm. Although quartz overgrowths are very common in all the samples analysed in this study, petroleum inclusions in the dust rim or primary petroleum inclusions within the overgrowth are quite rare compared to secondary petroleum inclusions. Moreover, the measurement of petroleum inclusions found along the dust rims was often very difficult to perform due to their very small sizes and very thin shapes.

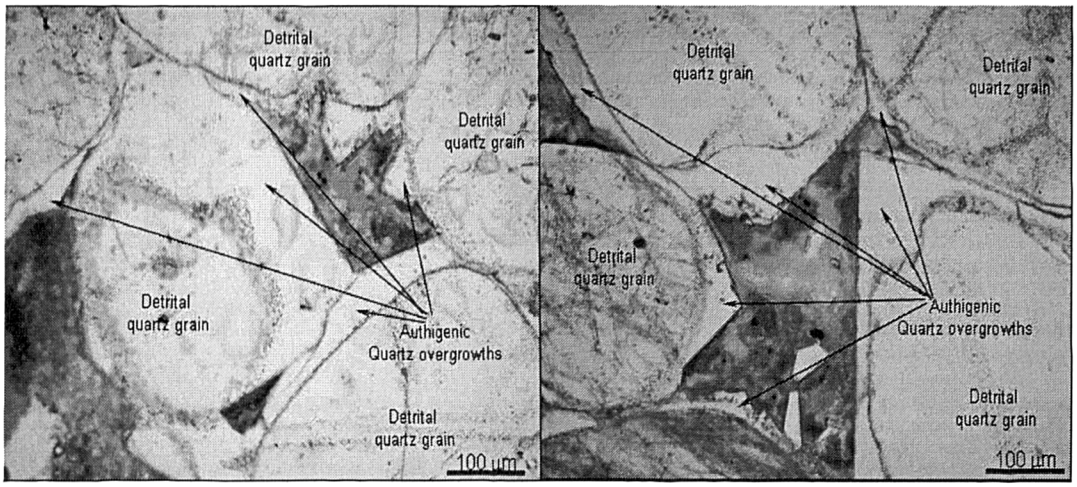

Figure 6.2 Photography illustrating occurrence of well developed authigenic quartz overgrowths in samples from wells MD#141 and MD#319, Hassi Messaoud field.

6.2.3. Aqueous inclusions

Aqueous inclusions were found along the same clusters as petroleum inclusions. A few inclusions in these samples consist of mixtures of petroleum and aqueous fluids (three phases). However, most commonly, petroleum and aqueous fluids occur in separate two phase inclusions along the same clusters (Figure 6.3). Therefore, from this textural association, I assume it is very possible that both aqueous and petroleum inclusions were trapped at similar times; an ideal situation for determining pressure and temperature of trapping (Roedder, 1984). Hence, the measurement of homogenisation temperatures of petroleum inclusions along with those of the coexistent aqueous inclusions gives vital information on the trapping conditions for the petroleum inclusions, and therefore on the arrival of the petroleum into the reservoir.

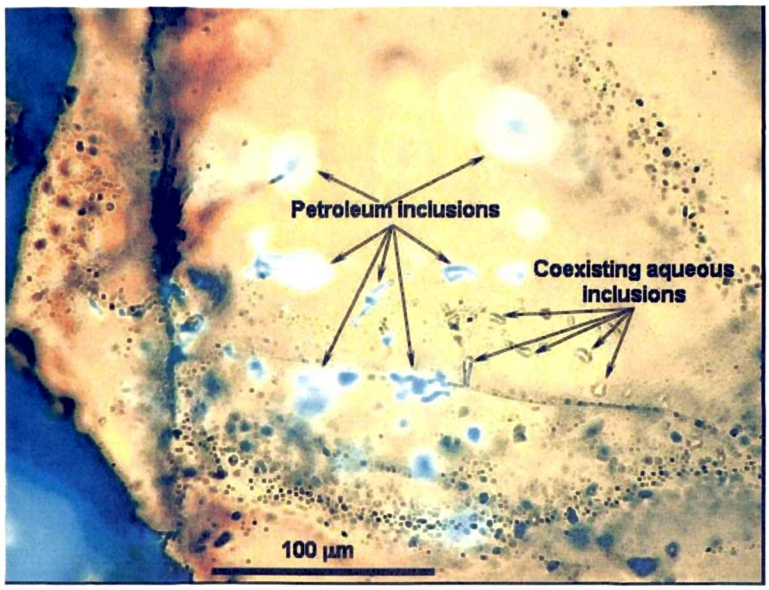

Figure 6.3 Petroleum and water inclusions in a detrital grain, showing occurrence of petroleum inclusions with coexisting water inclusions. Picture photographed under UV light for identification of petroleum inclusions. Sample is a sandstone from the reservoir unit Ra in MD#213 (3499.5 m).

It is well documented that the homogenisation temperatures of the petroleum inclusions measured in the laboratory are equivalent to the minimum temperatures of trapping (Shepherd et al., 1985). Under some circumstances, the homogenisation temperatures can approach the true trapping temperatures when the petroleum is saturated in gas (Roedder, 1984; Bureley et al., 1989). The difference between the minimum and true temperature known as the "pressure correction" depends on the saturation of the included petroleum in respect of gas. The determination of the true trapping temperature (and pressure) therefore entails the measurement of the homogenisation temperature of coexisting aqueous inclusions. This allows the construction a diagram comprising the phase envelopes and isochors of the petroleum and aqueous fluids (Roedder and Bodnar, 1980). The true trapping conditions (temperature and pressure) lie on the intersection of the two isochors (Figure 6.4).

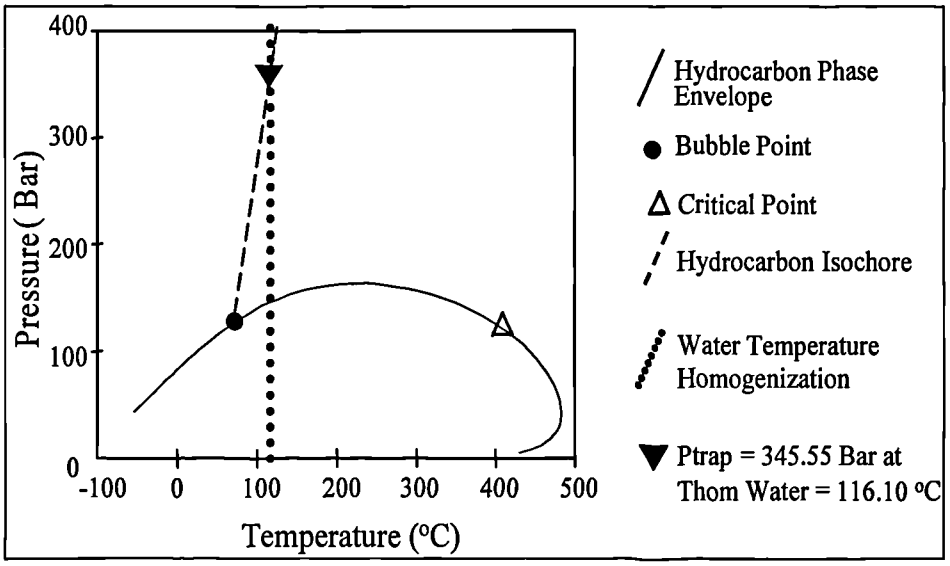

Figure 6.4 P-T diagram showing the intersection Isochors allowing determination of the true trapping pressure and temperature of a petroleum inclusion from well MD#177 (3339.45 m), Thom petroleum = 70.80 °C.

6.3. Microthermometry on fluid inclusions

Microthermometry on fluid inclusions provides information on the pressure and temperature (PT) conditions at the time at which the inclusions were trapped in their host minerals (Roedder, 1984; Goldstein and Reynolds, 1994). Measurements are based on phase transitions induced by temperature changes on a heating-cooling stage observed under the microscope. Phase transitions are reproducible with an accuracy < 1°C (cf. section 2.5, in chapter 2). Fluid inclusion assemblages (FIA) with petroleum and aqueous inclusions were sought. An FIA was categorised by it being apparent that a group was related by being in the same plane, and having coexisting aqueous inclusions. The samples studied were in quartz-rich sandstones; therefore only inclusions within detrital quartz grains and authigenic quartz overgrowths were analysed. Quartz is a robust mineral (Turgarinov and Vernadsky, 1970), so that it is rational to assume that fluid inclusions have remained isoplethic (constant composition), and isochoric (constant volume) since entrapment. Systematic microthermometrical measurements were performed on primary and secondary petroleum and aqueous inclusions (FIA's) identified during petrographic screening. The results of initial petrographical survey indicated that 18 samples contain petroleum inclusions suitable for microthermometry measurements from which 8 samples were found suitable for Confocal Scanning Microscopy study.

I have divided the discussion of the microthermometric results into 4 parts; first I will discuss the results obtained from the wells MD#177 and OMO#712 located in the centre, then the wells MD#213, MD#141 and OML#712 located in the east, south and northeast flanks and the wells OMM#33, MD#319 and OMJ#41 located in the west, southwest and northwest flanks of the Hassi Messaoud field (Figure 6.1), and finally well OKJ#202 located in the Haoud Berkaoui field (Figure 3.1).

6.3.1. Wells MD#177 and OMO#712

Thin section wafers from eight (8) core samples (4 samples from each well) were selected from the two Cambrian reservoir units Ra and R2. The samples from both reservoir units revealed moderate to high abundances of petroleum inclusions suitable for microthermometry, except one sample (MD#177, 3291.35 m from the top reservoir unit Ra) that showed extremely low abundance of petroleum inclusions (i.e. only 6 petroleum inclusions were recorded in this sample). In general, samples from the wells MD#177 and OMO#712 contain the highest abundances of petroleum inclusions compared to the samples selected from the wells located towards the flanks of the Hassi Messaoud field. All observable petroleum inclusions were fluorescing pale-blue to blue with small gas bubbles. Their shapes are highly variable and the sizes of petroleum inclusions are from 4 μm to 60 μm. These inclusions are present as both primary (occurring in authigenic quartz overgrowths and dust rims) and secondary (occurring mainly as clusters and rarely along fractures crosscutting both detrital quartz grains and quartz overgrowths; Figure 6.5). Secondary petroleum inclusions are far more abundant than primary petroleum inclusions in all the samples analysed in this study. The primary and secondary petroleum inclusions in these samples homogenise to a liquid phase; the homogenisation temperatures (Th's) of the primary and the secondary petroleum inclusions range from 64 to 100.9 °C, however most of the petroleum inclusions homogenise between 70 and 85 °C (Figure 6.6).

Coexistent aqueous inclusions are also present, but in much lower number than primary and secondary petroleum inclusions. The sizes of aqueous inclusions are generally smaller than the sizes of petroleum inclusions ranging from 4 to 15 μm, which make it difficult to measure their homogenisation temperatures. The homogenisation temperatures of aqueous inclusions in samples from the wells MD#177 and OMO#712 are generally higher than the homogenisation temperatures

measured for the petroleum inclusions, ranging from 97.8 °C to 148.6 °C (Figure 6.6a).

The core sample from well MD#177 at 3324.5 m contains few inclusions showing the yellow fluorescence colour, whereas the majority of petroleum inclusions in this sample show pale-blue to blue fluorescing colour. The difference in the colours in these inclusions probably represents different oil charges with different maturities (McLimans, 1987; Bodnar, 1990). This observation is in concordance with the homogenisation temperatures as the petroleum inclusions with yellow fluorescence have lower homogenisation temperatures ranging from 58 °C to 68.6 °C, whereas the petroleum inclusions with pale-blue to blue fluorescence have higher homogenisation temperatures ranging from 70.4 °C to 87.3 °C, suggesting a more mature, more gassy or later charge. However, care should be taken when interpreting the charge history of samples containing petroleum inclusions with mixed fluorescence colour populations. Recently, George et al. (2001) have assessed the maturity of oil trapped in fluid inclusions by using visually-determined fluorescence colours and molecular geochemistry data. They showed that samples containing white-fluorescing oil inclusions exhibit similar maturity compared to samples containing mainly blue-fluorescing oil inclusions using molecular maturity parameters. George et al. (2001) concluded that the use of the fluorescence colours of oil inclusions as a qualitative thermal maturity guide is not rational because the fluorescence colours primarily depends on the chemical composition, which is controlled not only by maturity but by several other processes including light petroleum injection, water washing etc.

The majority of petroleum inclusions are two phase inclusions at room temperature. A minority of the inclusions in sample (MD#177 3324.5m) are three phase inclusions, which consist of two petroleum phases (oil and gas) and one water phase. Their homogenisation temperatures lie in between 77 to 115.6 °C (Figure 6.6b). The occurrence of coexisting petroleum and water inclusions together with the three phase inclusions (oil, gas, water) suggest that some of the petroleum and water were coeval. Therefore the water can be assumed to be saturated in respect of petroleum (saturated with the most soluble components dominated by methane). Hence, the homogenisation temperatures derived from the aqueous inclusions can be very close to the true trapping temperatures (Munz et al., 2001).

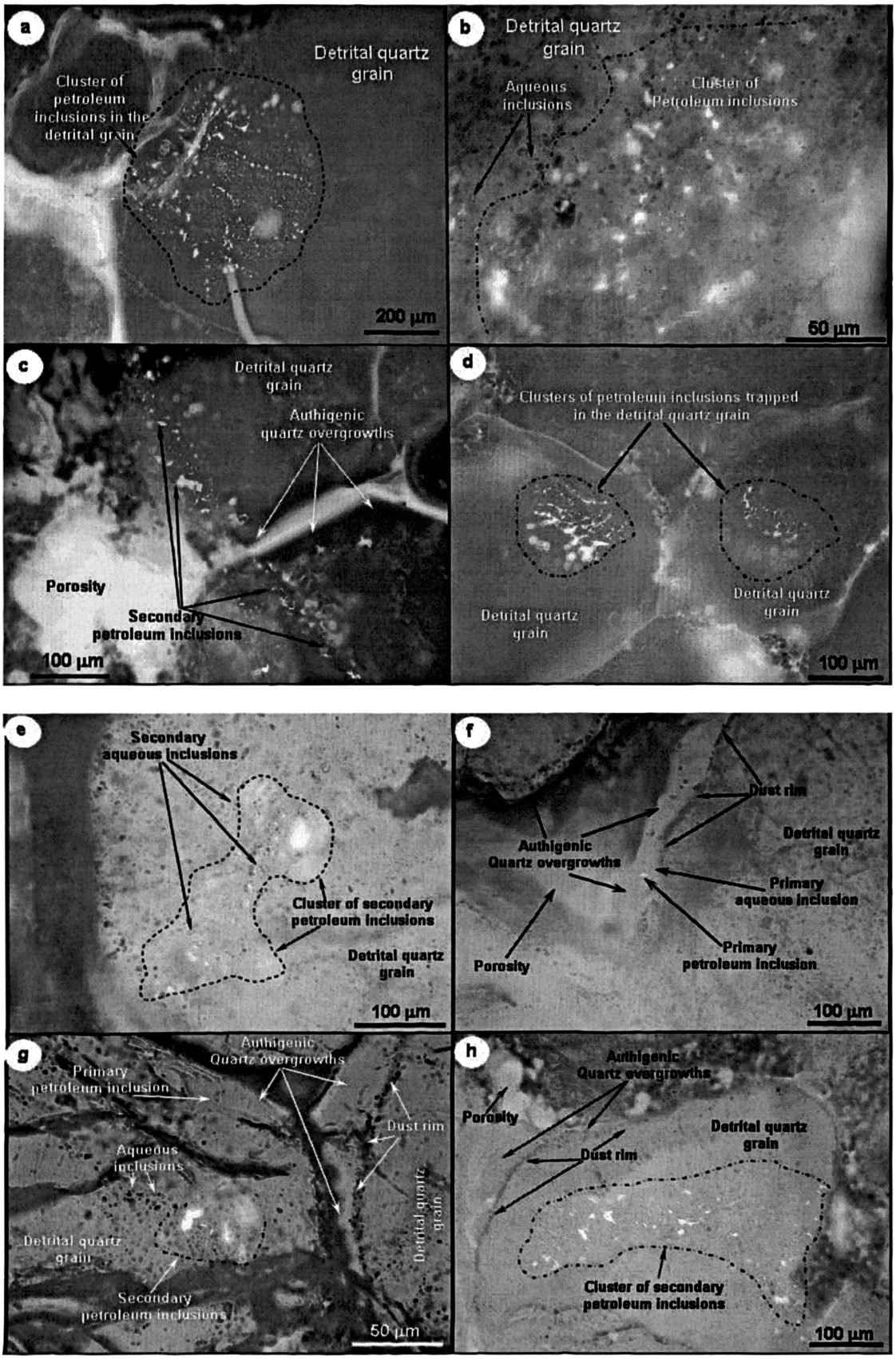

Figure 6.5 Photos showing the occurrence of petroleum inclusions and coexisting aqueous inclusions in (a) sample 3339.45 m from Ra reservoir unit, (b) and (c) sample 3379.9 m from R2 reservoir unit in well MD#177 and (d) to (h) from Ra and R2 reservoir units in well OMO#712 from the Hassi Messaoud field.

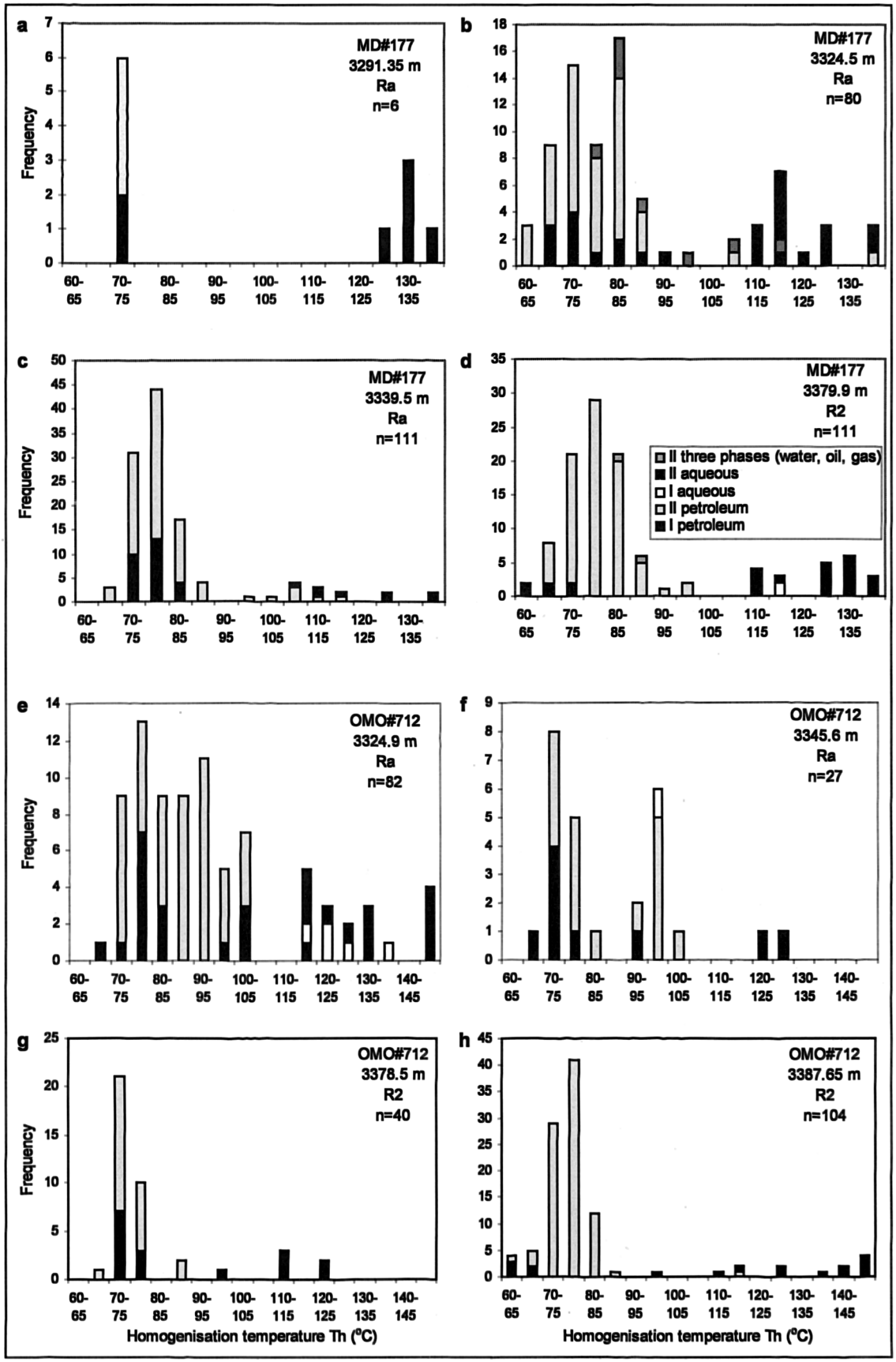

Figure 6.6 Histograms showing the distribution of the homogenisation temperatures obtained from petroleum and coexistent aqueous inclusions in samples from the wells MD#177 and OMO#712. Key: I = primary inclusions, II = secondary inclusions.

6.3.2. Wells MD#213, MD#141 and OML#712

Wells MD#213, MD#141 and OML#712 are located in the east, south and northeast flanks of the Hassi Messaoud field, respectively (Figure 6.1). Thin section wafers from seven (7) core samples (3 samples from well MD#213, 2 samples from well MD#141 and 2 samples from well OML#712) were selected from the two Cambrian reservoir units Ra in the first two wells MD#213 and MD#141, and R2 in well OML#712. Petroleum inclusions occur in five (5) samples; however two samples, one from MD#213 at a depth of 3468.15 m and one from MD#141 at a depth of 3438.65 m did not show the presence of petroleum inclusions.

The samples from the wells MD#213 (3451.6 m), MD#141 (3450.4 m) and OML#712 (3426.95 and 3437.45 m) revealed moderate abundances of petroleum inclusions suitable for microthermometry, whereas the sample from well MD#213 at a depth of 3499.5 m showed relatively higher abundances of petroleum inclusions. Most of the petroleum inclusions recorded in these samples are trapped in the detrital clastic grains of quartz either as clusters or isolated inclusions, and very few are trapped in the authigenic quartz as primary petroleum inclusions (Figure 6.7). However, sample MD#141 at depth of 3450.4 m showed the occurrence of secondary petroleum inclusions along parallel fractures which cut through detrital quartz grains and quartz overgrowths (Figure 6.7d). All petroleum inclusions contain two phases consisting of liquid and gas, except sample MD#141 at depth of 3450.4 m which showed the presence of a few inclusions containing three phases; two liquid phases (aqueous and oil) and one gas phase. Petroleum inclusions in all these samples showed mainly blue fluorescence under UV light, and contain small gas bubbles (Figure 6.7). Most of these petroleum inclusions have diameters of about 4 – 20 μm, but some are as large as 40 – 50 μm.

Homogenisation temperatures (Th's) of petroleum inclusions in the samples from the wells MD#213, MD#141 and OML#712 range from 60 to 100 °C; however most of thr petroleum inclusions showed Th's values ranging from 70 to 85 °C (Figure 6.8). Coexisting aqueous inclusions were also encountered, but in much lower number than petroleum inclusions (Figure 6.7 a,b,c). Their shapes are quite variable and the sizes range from 4 – 10 μm. They showed the presence of two phases, liquid (water) and small gas bubbles, and homogenise to a liquid phase. Homogenisation temperatures of

the aqueous inclusions are higher than in the petroleum inclusions ranging from 92.4 °C to 142.1 °C (Figure 6.8).

High abundances of petroleum inclusions in the sample MD#213 at a depth of 3499.5 m appear to be in agreement with the results obtained by biomarker and aromatic hydrocarbon maturity parameters together with the principal components analysis in sections 5.6.1.2.1, 5.6.1.2.2 and 5.6.1.2.5, respectively and the bulk composition results shown in section 5.6.3.1 in chapter 5. The results obtained from biomarker and aromatic hydrocarbon maturity parameters together with the principal components analysis suggest that the Hassi Messaoud reservoirs were likely charged from the west and the east indicating that oil had migrated from the Oued My basin (west of the Hassi Messaoud field) and from the Silurian located about the Hassi Dzabat area (east of the Hassi Messaoud field where well MD#213 is located).

Moreover, samples analysed in the interval 3483.5 m to 3499.5 m from well MD#213 (including the sample at 3499.5 m) present relatively higher porosity and permeability, together with higher total petroleum yields and yields and percentages of polar compounds. These observations may also suggest the occurrence of migration pathways along this interval of the reservoir. Therefore, oil probably spent a long time in contact with the reservoir rocks in this interval. This is also in agreement with the occurrence of high abundances of petroleum inclusions in the core sample at the depth 3499.5 m. Indeed, Oxtoby et al. (1995) found that the distribution and abundance of petroleum inclusions reflect the manner in which petroleum invades rocks of different permeability, including migration routes below the present oil leg. According to these authors, the relationship between petroleum inclusion abundances and porosity/ permeability results from a higher density of migrating petroleum stringers in rocks of good reservoir quality during filling of the reservoir.

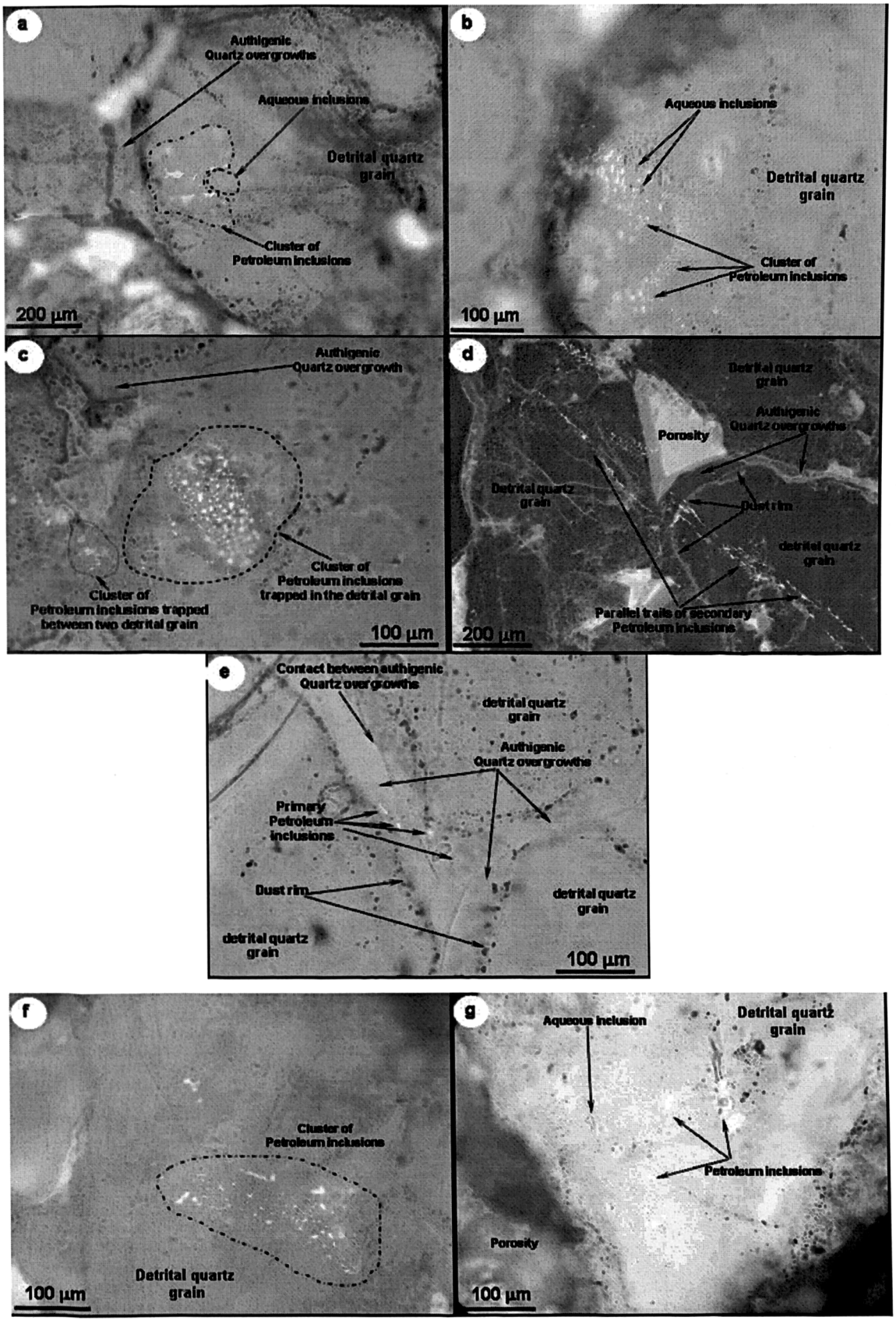

Figure 6.7 Photos showing the occurrence of petroleum inclusions and coexisting aqueous inclusions in (a, b) MD#213, (c,d,e) MD#141, and (f,g) OML#712.

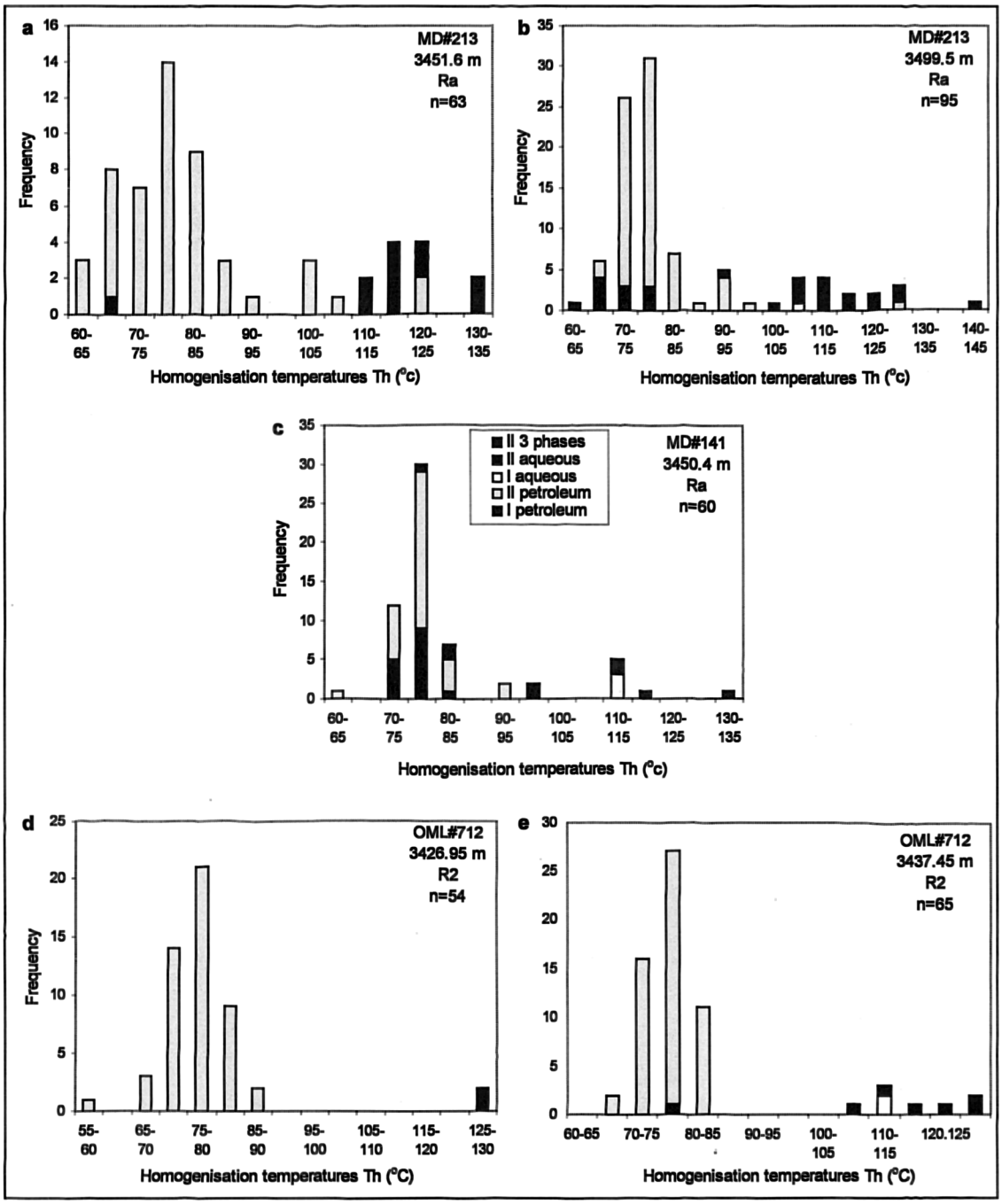

Figure 6.8 Histograms showing the distribution of the homogenisation temperatures obtained from petroleum and coexistent aqueous inclusions in (a, b) samples from well MD#213 (3451.6 m and 3499.5 m), (c) sample from well MD#141(3450.4m), and (d, e) samples from well OML#712 (3426.95m and 3437.45 m). Key: I = primary inclusions, II = secondary inclusions.

6.3.3. Wells OMM#33, MD#319 and OMJ#41

These wells are located in the west, southwest and northwest flanks of the Hassi Messaoud field, respectively. Four (4) samples in the Cambrian reservoir unit Ra from well OMM#33, one (1) sample in the Cambrian reservoir unit Ra from well MD#319 and two (2) samples (1 from Ra and 1 from R2 reservoir units) from well OMJ#41

were examined under UV light to allow petroleum-bearing fluid inclusions to be identified. The survey of the 7 samples under UV light revealed that only 4 samples (OMM#33 3413.75 m and 3476.85 m, MD#319 3453.3 m and OMJ#41 3990.6 m) show occurrence of petroleum inclusions (Figure 6.9). However, these samples contain much lower abundances of petroleum inclusions compared to the samples described above in the wells MD#177, OMO#712, MD#213, OML#712, and MD#141, respectively.

Interestingly the samples studied in the wells OMM#33, MD#319 and OMJ#41 showed compact grains with very well-developed quartz overgrowths compared to the samples in the wells OMO#712 and MD#177 (Figure 5.53 in chapter 5). The core samples analysed in the wells OMM#33, MD#319 and OMJ#41 also exhibited lower petroleum yields than the core samples analysed in the samples from the wells OMO#712 and MD#177 (see section 5.6.3.1 in chapter 5). All these observations may suggest late arrival of oil in the western flanks compared to the centre, east, northeast and south of the Hassi Messaoud field. Therefore, the oil may have spent longer time in contact with the reservoir rocks in the centre and east compared to the western flanks of the Hassi Messaoud field. This in good agreement with the conclusions made by Emery et al. (1993) who stated that in cases where oil emplacement predates or is contemporaneous with quartz cementation, early-filled reservoirs or parts of the reservoirs (e.g. structural crests) would have less cement and thus retain superior reservoir quality than the late-filled reservoirs located towards the flanks.

Petroleum inclusions in samples analysed in these three wells showed pale-blue to blue fluorescence colour (Figure 6.9). All petroleum inclusions occur as secondaries in the detrital quartz grains in the samples from wells OMM#33 and OMJ#41, whereas, the sample from well MD#319 contains both primary petroleum inclusions trapped in the dust rims and quartz overgrowths and secondary petroleum inclusions occurring in the detrital quartz grains. Most of the petroleum inclusions contain two phases; liquid hydrocarbons associated with small gas bubbles. However, the sample from well MD#319 showed a few inclusions containing three phases (oil, water, and gas). The majority of the petroleum inclusions in the samples from the three wells homogenised between 70 °C and 85 °C, except petroleum inclusions in sample OMM#33 at the depth of 3476.85 m which showed lower homogenisation

temperatures ranging from 63.3 to 68.8 °C (Figure 6.10). Coexistent aqueous inclusions with petroleum inclusions are quite rare; the highest number was encountered in sample from well MD#319. Homogenisation temperatures of aqueous inclusions range from 110.6 to 133.6 °C in sample MD#319 (Figure 6.10c) and 89 °C to 99.8 °C in samples OMM#33 at depths of 3413.75 m and 3476.85 m, respectively (Figure 6.10 a and b).

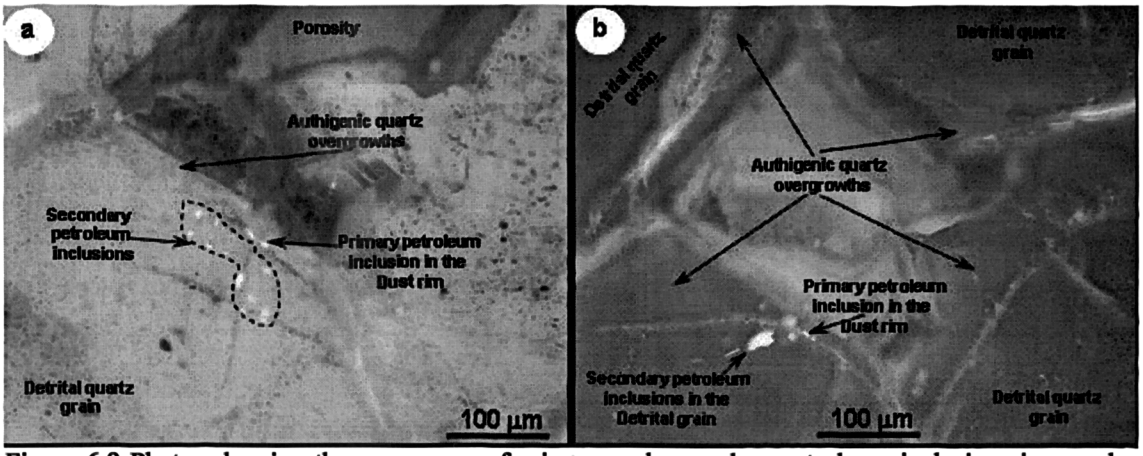

Figure 6.9 Photos showing the occurrence of primary and secondary petroleum inclusions in sample MD#319-3453.3 m.

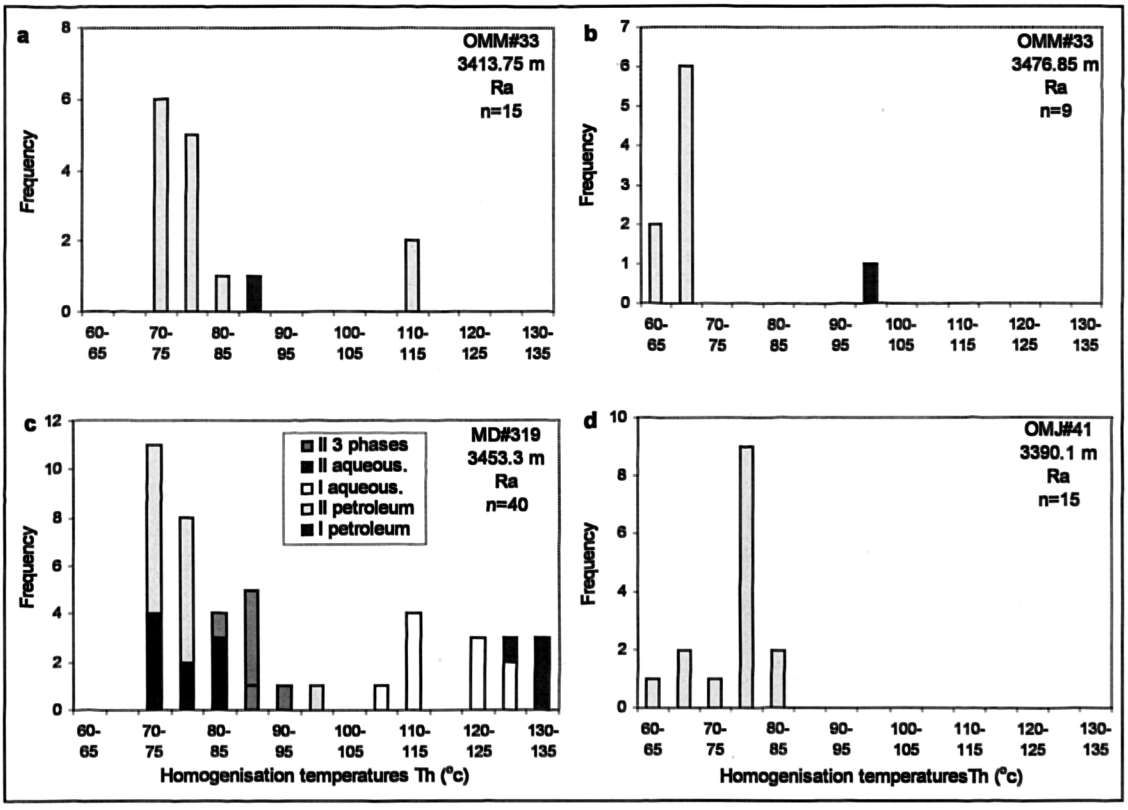

Figure 6.10 Histograms showing the distribution of the homogenisation temperatures obtained from the samples OMM#33 (3413.75 and 3476.85m), MD#319 (3453.3m) and OMJ#41 (3390.1m). Key: I = primary inclusions, II = secondary inclusions.

6.3.4. Well OKJ#202

The well OKJ#202 located in the Haoud Berkaoui field in the Oued Mya basin, produces oil from the Lower Triassic reservoir (Figure 3.1 in chapter 3). Only one sample from 3327.5 m was selected from this well for fluid inclusions study. The scanning of this sample under UV light revealed the presence of moderate abundances of yellowish petroleum inclusions. These petroleum inclusions occur mainly as clusters or as isolated inclusions in the detrital quartz grains (Figure 6.11). The petroleum inclusions show variable shapes and their sizes range from 4 μm to 30 μm. Interestingly, all these petroleum inclusions show low homogenisation temperatures (Th's) compared to the Th's measured for petroleum inclusions analysed in the samples from the Hassi Messaoud field. The Th's values measured in this sample range from 48.5 °C to 63.5 °C, with most temperature values (71 %) only between 50 °C to 57.9 °C (Figure 6.12). Unfortunately, only one coexistent aqueous inclusion was found; this homogenised at 102 °C.

It seems that the relatively low homogenisation temperatures are in good agreement with the yellowish fluorescence colour exhibited by the petroleum inclusions (Burrus et al., 1985; McLimans, 1987; Bodnar, 1990). These observations may suggest an early arrival of low maturity oil in the Triassic reservoir located in the Haoud Berkaoui field.

In fact this suggestion is likely to be correct because geochemical maturity parameters obtained from biomarker alkanes and aromatic hydrocarbons showed that the oil produced in the Haoud Berkaoui field is the least mature oil throughout the entire Oued Mya-Hassi Messaoud petroleum system (see sections 4.4 in chapter 4 and 5.5 in chapter 5). Moreover, the geochemical analysis of the included oils in the samples selected from Haoud Berkaoui and Hassi Messaoud fields revealed that the included oil in the sample OKJ#202 from the Haoud Berkaoui field is the least mature oil compared to the included oils analysed in the Hassi Messaoud samples (see section 6.2.4 bellow). Therefore, I believe that the oil trapped in the inclusions in this reservoir may represent the first ever charge of oil expelled from the source rocks lying in the Oued Mya basin.

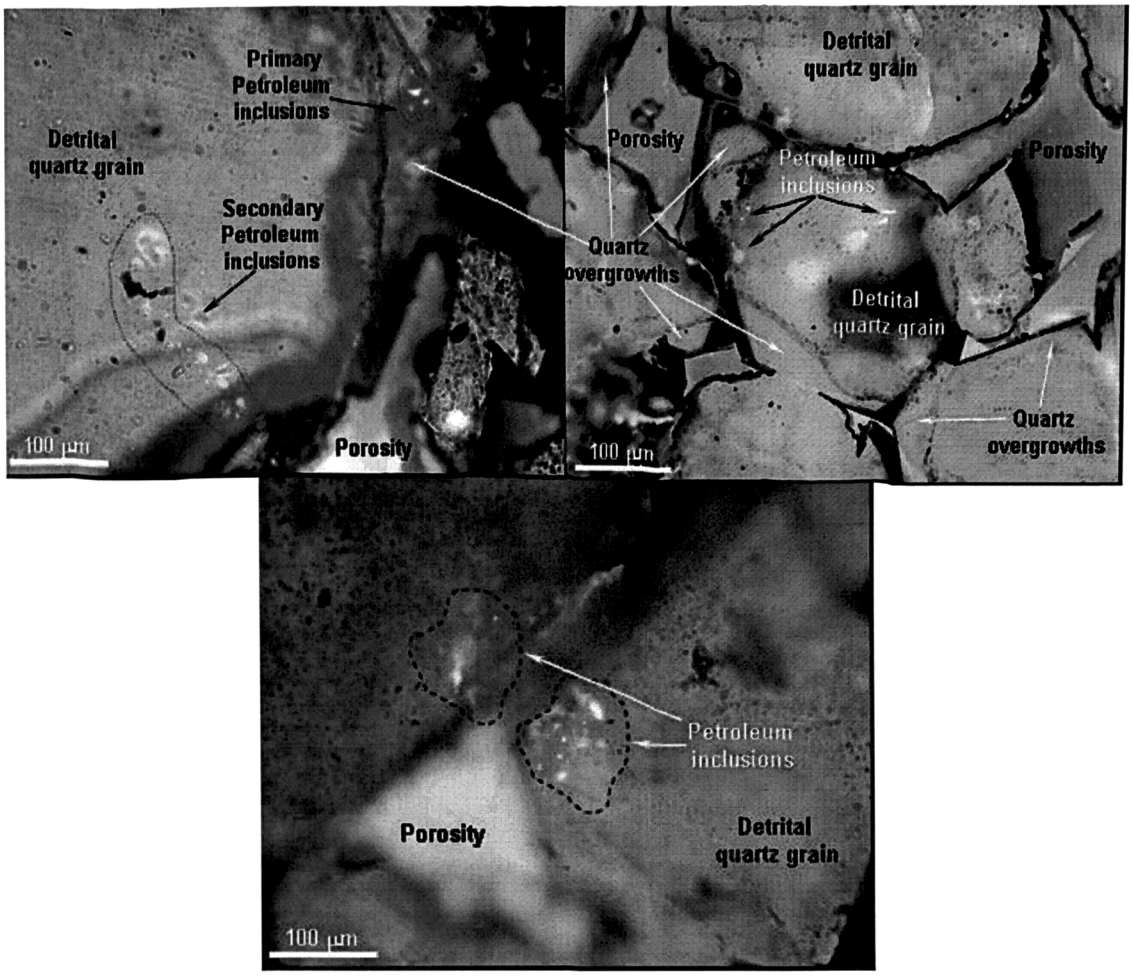

Figure 6.11 Photos showing the occurrence of petroleum inclusions in the sample OKJ#202-3327.5 m from the Haoud Berkaoui field.

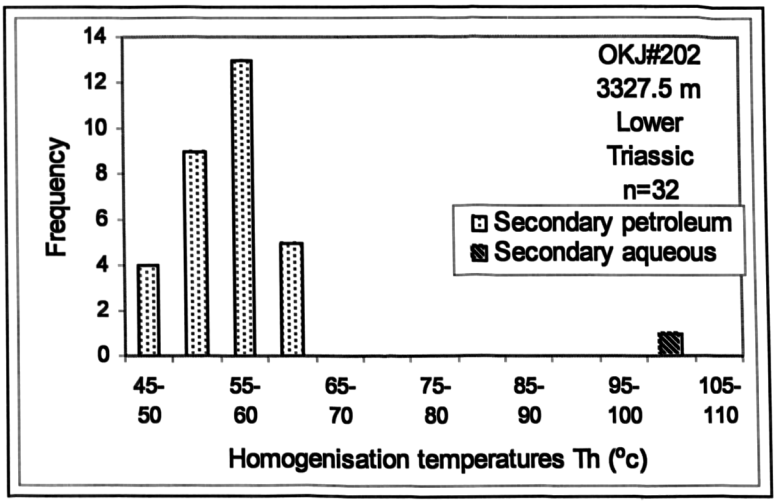

Figure 6.12 Histogram showing the distribution of the homogenisation temperatures obtained from petroleum and aqueous inclusions in the sample OKJ#202-3327.5 m.

6.3.5. Summary

Figure 6.13 shows all petroleum and aqueous fluid inclusion frequencies, for inclusion sets obtained from all the samples analysed in this study. The distribution of the petroleum inclusion Th's is clearly biased to temperature values around 70 to 80 °C, whilst for the aqueous inclusions, the distribution of the Th's is clearly biased to temperature values around 110 to 115 °C. The distribution of petroleum and aqueous inclusion Th's indicate that the Fluid Inclusion Assemblages (FIA's) identified in this study are quite robust. A total of 855 petroleum inclusions and 121 aqueous inclusions were identified and measured for homogenisation temperatures (Th's), of which only 5 petroleum inclusions and 47 aqueous inclusions showed Th's higher than the present day reservoir temperature. Therefore, this observation would suggest that re-equilibration, necking down or two-phase entrapment of the majority (i.e. 99.4%) of petroleum inclusions analysed in this study might not have occurred. In addition, for the aqueous inclusions with the anomalously high Th's; it is possible that some of the inclusions are not actually primary in the reservoir context. It may be that some of these inclusions are in fact primary, in the context of the original detrital grain formation. In other words, they were entrapped during original grain crystallisation.

From the histograms in Figure 6.13 a, b, there is clearly a tendency for the homogenisation temperature to differ by around 30 to 45 °C. Therefore, the averages of the petroleum and aqueous homogenisation temperatures are reasonably obvious suggestions that the inclusion entrapment temperature is greater than petroleum Th's, the difference being about 30 to 45 °C. Thus, it is probable that both systems cannot be saturated with respect to gas. It is likely that the petroleum inclusions are more undersaturated with respect to gas than are the water inclusions, due to higher methane solubilities in oil compared to the methane solubilities in water at any given temperature.

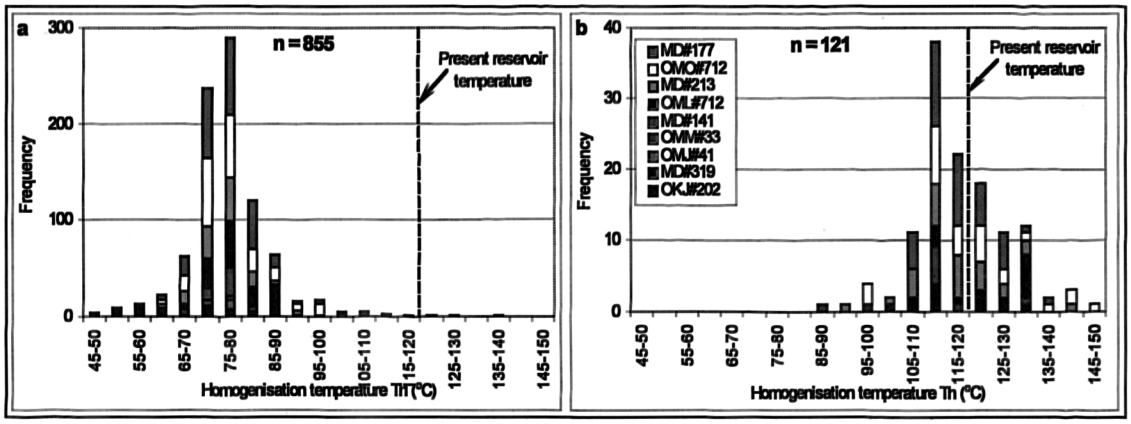

Figure 6.13 Histograms showing stacked frequency data for (a) all petroleum fluid inclusions and (b) all aqueous fluid inclusions from all samples analysed in the Hassi Messaoud and Haoud Berkaoui fields.

The Sample analysed in well OKJ#202 from the Haoud Berkaoui field showed the lowest Th's compared to all the samples analysed in the Hassi Messaoud field.

6.4. Pressure and temperature history using Confocal Laser Scanning Microscopy and PVT modelling on fluid inclusions from the Hassi Messaoud field

In this section, I will describe how the combined technique of microthermometry, CLSM and PVT modelling can be practical to estimate the temperature, pressure and charge history of the Hassi Messaoud field.

6.4.1. Confocal Laser Scanning Microscopy (CLSM)

The wafers previously used for microthermometry were studied under CLSM to determine the true volume fraction of vapour and liquid of a petroleum inclusion at room temperature. Only petroleum inclusions with static vapour bubbles were used, as moving bubbles would result in invalid data due to distortion during scanning. 20 secondary petroleum inclusions selected from 7 samples were examined by CLSM; these inclusions were coexisting with aqueous inclusions. For more details about the CLSM method see section 2.2.2 in chapter 2. Samples examined for CLSM were selected from the Cambrian reservoir units Ra and R2 in the wells MD#177 and OMO#712 located in the centre, MD#213 east, MD#141 south and MD#319 southwest flanks of the Hassi Messaoud field. Petroleum inclusions from samples from the wells OML#712, OMM#33 were not examined by CLSM because the bubbles in the selected petroleum inclusions were mobile making them unusable for CLSM scanning. The vapour:liquid volume percentage for petroleum inclusions

measured by CLSM range from 3.90:96.10 vol% to 7.98:92.02 vol%. The volume fraction of vapour and liquid of petroleum inclusions analysed in this study are displayed in Table 6.3.

6.4.2. PVT modelling using VTFLINC software

Detailed explanation of the VTFLINC data processing is displayed in chapter 2 (Aplin et al., 1999). VTFLINC is a Window based software package that has been developed to process optically-derived microthermometric and volumetric data from petroleum-bearing fluid inclusions using equation of state procedures to derive compositional and pressure data for the included petroleum. VTFLINC software allows properties such as trapping pressure and temperature, saturation pressure together with gas oil ratio (GOR), viscosity and density of individual petroleum inclusions to be determined.

To run VTFLINC program, a database entry is created. The database for individual petroleum inclusions consists of the following: (1) the homogenisation temperatures of petroleum and coexisting aqueous inclusions obtained by microthermometry, (2) the true volume fraction of vapour and liquid of individual petroleum inclusions at room temperature obtained by CLSM, and (3) detailed composition, comprising the mole percentage of N_2, CO_2, and *normal*-alkanes (C_1 to $C_{12}+$) and *iso*-alkanes (i-C_4 and i-C_5) of the present day produced oil from the Hassi Messaoud field (Table 6.2). The detailed composition of the present day produced oil from well OMM#412 located in the western flank of the Hassi Messaoud field was provided by the PVT laboratory of *SONATRACH* Company. Figure 6.14 shows the P-T phase diagram of the present day reservoir fluid from well OMM#412, used as the initial model oil for PVTX simulation of the coeval petroleum inclusions from the Hassi Messaoud field.

Strategy 4 is selected, which uses the homogenisation temperature of petroleum inclusions plus 50 °C, and has been found to give the best results (Aplin et al., 1999). VTFLINC program will then run the iterative analysis, as outlined in section 2.2.3 in chapter 2 (Aplin et al., 1999). It is assumed that aqueous inclusions are saturated with gas in VTFLINC software and thus the homogenisation temperature of aqueous inclusions is close to the true trapping temperature (Burrus, 1992). Secondly, the host crystals are assumed impermeable to chemical changes and that an inclusion

represents a chemically closed (isolepthic) system from the time of entrapment. Finally, the volume of an inclusion is assumed to remain constant (isochoric) since entrapment.

In section 6.1.4 below, the biomarker distribution showed that the palaeo-oil trapped in the inclusions is genetically related to the present day produced oil in the Hassi Messaoud reservoir. Thus, the petroleum produced at present day can be used as an initial estimate of the composition for PVT simulation.

Table 6.2 Composition of the initial model oil (OMM#412) used for PVTX simulation of the coeval petroleum inclusions from the Hassi Messaoud field.

Component name	Molar amount	Molecular weight g/mol)	Density (g/cm^3)
N_2	1.81	28.02	
CO_2	1.71	44.01	
C_1	26.13	16.04	
C_2	12.47	30.07	
C_3	10.59	44.09	
iC_4	2.90	58.12	
nC_4	4.39	58.12	
iC_5	3.34	72.15	
nC_5	1.67	72.15	
C_6	4.34	86.17	
C_7	4.41	92.90	
C_8	2.97	106.20	
C_9	3.02	118.40	
C_{10}	2.84	131.70	
C_{11}	2.20	145.00	
$C_{12}+$	15.21	276.00	0.872
total	100		

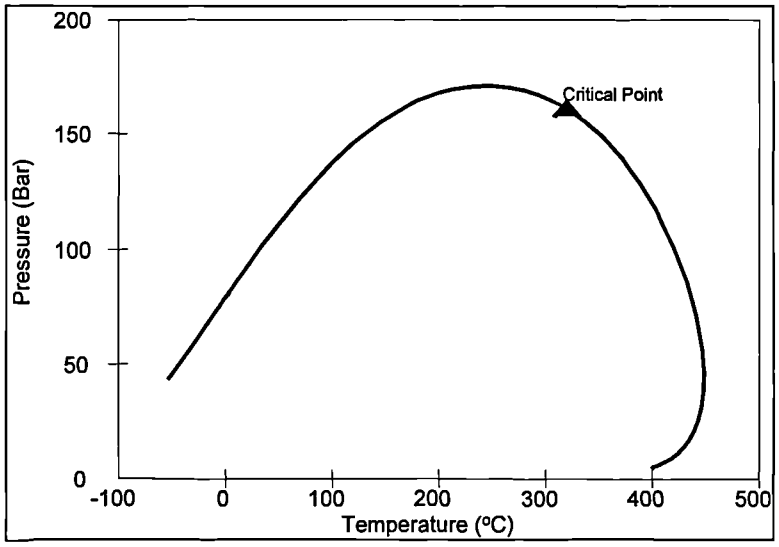

Figure 6.14 P-T phase diagram of the present day reservoir fluid from well OMM#412, used as the initial model oil for PVTX simulation of the coeval petroleum inclusions from the Hassi Messaoud field.

6.4.3. Fluid inclusion dating concept

In Hassi Messaoud samples, both secondary and primary fluid inclusions were observed, however the secondary inclusions were far much more abundant than primary inclusions. In this section, I use petroleum and coexistent aqueous inclusions found in the detrital quartz grains; most of petroleum inclusions found in the authigenic overgrowths showed mobile bubbles, making them unusable for CLSM scanning. Thus, they are not considered in this study.

Homogenisation temperatures of the petroleum and coexisting aqueous inclusions simulated by VTFLINC PVT Software range from 71 to 80.6 °C and 106 to 117.2 °C, respectively (Table 6.3). This table presents the pressures and temperatures of Hassi Messaoud reservoir units Ra and R2 at the time of petroleum entrapment and the GOR, viscosity, average density, molar volume and surface tension of petroleum trapped in petroleum inclusions.

Table 6.3 Calculated physical properties of petroleum trapped secondary inclusions in quartz from the Hassi Messaoud reservoirs. The detailed composition of the individual inclusions obtained by VTFLINC PVT Simulation is given in Appendix 6.3.

Well	Depth	Reservoir	Th (Petr.)	Th (Aqu.)	Vol % (Gas)	Vol% (Liq.)	Ptrap. (Bar)	Psat. (Bar)	GOR (Sm^3/Sm^3)	Viscosity (cP)	Average Density (g/cm^3)	Molar volume(cm^3/mol.)	Surface tension(mN/m)
MD#177	3339.45		76.1	106	4.61	95.39	210	66	41	0.860	0.775	201.74	19.54
MD#177	3339.45		79.7	106	6.17	93.83	215	94	74	0.600	0.735	172.15	17.43
MD#177	3339.45		70.8	106	3.85	96.15	227	53	31	1.021	0.789	212.94	20.50
MD#177	3339.45		71	106	3.9	96.1	227	54	32	1.003	0.788	211.53	20.42
MD#177	3339.45	Ra	76.1	114.4	4.61	95.39	249	66	41	0.860	0.775	201.74	19.54
MD#177	3339.45		79.7	114.4	6.17	93.83	253	94	74	0.600	0.735	172.15	17.43
MD#177	3339.45		70.8	114.4	3.85	96.15	268	53	31	1.021	0.789	212.94	20.50
MD#177	3339.45		71	114.4	3.9	96.1	268	54	32	1.003	0.788	211.53	20.42
MD#177	3339.45		78	116.9	4.05	95.95	233	46	23	1.133	0.798	229.72	20.62
MD#177	3339.45		73	116.9	3.69	96.31	259	43	22	1.182	0.801	228.5	20.97
MD#177	3379.90		77.4	112.9	5.13	94.87	245	77	52	0.748	0.761	189.96	18.79
MD#177	3379.90		74.2	112.9	5.07	94.93	264	80	58	0.711	0.755	183	18.64
MD#177	3379.90		71.6	112.9	4.78	95.22	276	77	57	0.731	0.758	183.59	18.90
MD#177	3379.90		77.4	114.1	5.13	94.87	250	77	52	0.748	0.761	189.96	18.79
MD#177	3379.90	R2	74.2	114.1	5.07	94.93	270	80	58	0.711	0.755	183	18.64
MD#177	3379.90		71.6	114.1	4.78	95.22	282	77	57	0.731	0.758	183.59	18.90
MD#177	3379.90		77.4	117.2	5.13	94.87	264	77	52	0.748	0.761	189.96	18.79
MD#177	3379.90		74.2	117.2	5.07	94.93	284	80	58	0.711	0.755	183	18.64
MD#177	3379.90		71.6	117.2	4.78	95.22	296	77	57	0.731	0.758	183.59	18.90
OMO#712	3387.65		80.6	110.7	6.4	93.6	234	97	78	0.579	0.731	169.89	17.19
OMO#712	3387.65		72.6	110.7	4.04	95.96	242	55	32	0.985	0.787	211.32	20.28
OMO#712	3387.65	R2	74.9	110.7	4.61	95.39	240	68	44	0.836	0.772	198.15	19.45
OMO#712	3387.65		80.6	115	6.4	93.6	253	97	78	0.579	0.731	169.89	17.19
OMO#712	3387.65		72.6	115	4.04	95.96	263	55	32	0.985	0.787	211.32	20.28
OMO#712	3387.65		74.9	115	4.61	95.39	260	68	44	0.836	0.772	198.15	19.45
MD#213	3499.50		71.7	108.9	5.27	94.73	265	88	71	0.636	0.742	171.81	18.11
MD#213	3499.50		72.5	108.9	6.46	93.54	273	106	106	0.472	0.708	152.37	16.42
MD#213	3499.50	Ra	76	108.9	7.98	92.02	263	118	139	0.355	0.678	140.65	14.82
MD#213	3499.50		71.7	112.3	5.27	94.73	281	88	71	0.636	0.742	171.81	18.11
MD#213	3499.50		72.5	112.3	6.46	93.54	288	106	106	0.472	0.708	152.37	16.42
MD#213	3499.50		76	112.3	7.98	92.02	277	118	139	0.355	0.678	140.65	14.82
MD#141	3450.40		78.1	110.5	7.26	92.74	255	110	109	0.440	0.702	152.15	15.88
MD#141	3450.40		74.2	110.5	7.58	92.42	277	116	132	0.371	0.683	141.75	15.13
MD#141	3450.40		76.1	110.5	6.86	93.14	263	107	105	0.465	0.707	153.72	16.21
MD#141	3450.40		78.1	113.4	7.26	92.74	267	110	109	0.440	0.702	152.15	15.88
MD#141	3450.40	Ra	74.2	113.4	7.58	92.42	290	116	132	0.371	0.683	141.75	15.13
MD#141	3450.40		76.1	113.4	6.86	93.14	276	107	105	0.465	0.707	153.72	16.21
MD#141	3450.40		78.1	117.9	7.26	92.74	287	110	109	0.440	0.702	152.15	15.88
MD#141	3450.40		74.2	117.9	7.58	92.42	309	116	132	0.371	0.683	141.75	15.13
MD#141	3450.40		76.1	117.9	6.86	93.14	296	107	105	0.465	0.707	153.72	16.21
MD#319	3453.30		79.5	106.7	4.65	95.35	191	62	36	0.916	0.781	210.67	19.70
MD#319	3453.30		75	106.7	4.66	95.34	222	69	45	0.823	0.771	196.86	19.37
MD#319	3453.30	Ra	79.5	110.6	4.65	95.35	210	62	36	0.916	0.781	210.67	19.70
MD#319	3453.30		75	110.6	4.66	95.34	240	69	45	0.823	0.771	196.86	19.37
MD#319	3453.30		79.5	114.5	4.65	95.35	228	62	36	0.916	0.781	210.67	19.70
MD#319	3453.30		75	114.5	4.66	95.34	258	69	45	0.823	0.771	196.86	19.37

Present day conditions

	GOR and pressure saturation		Average pressure and temperature across Hassi Messaoud field	
	GOR (Sm^3/Sm^3)	Pressure saturation (bar)	Pressure (bar)	Temperature (°C)
			480	120-132
MD#177	204	156		
OMO#712	211	170		
MD#213	205	161		
MD#141	134	146		
MD#319	144	150		

Palaeo-pressures, GOR's and the detailed composition of the individual petroleum inclusions have been determined with combined use of CLSM and VTFLINC PVT Simulation, as reported by Aplin et al. (1999). Phase envelopes with the hydrocarbon isochore were constructed for each individual petroleum inclusion (Figure 6.15),

along which the true trapping temperature and pressure occur at the intersection with aqueous inclusion data.

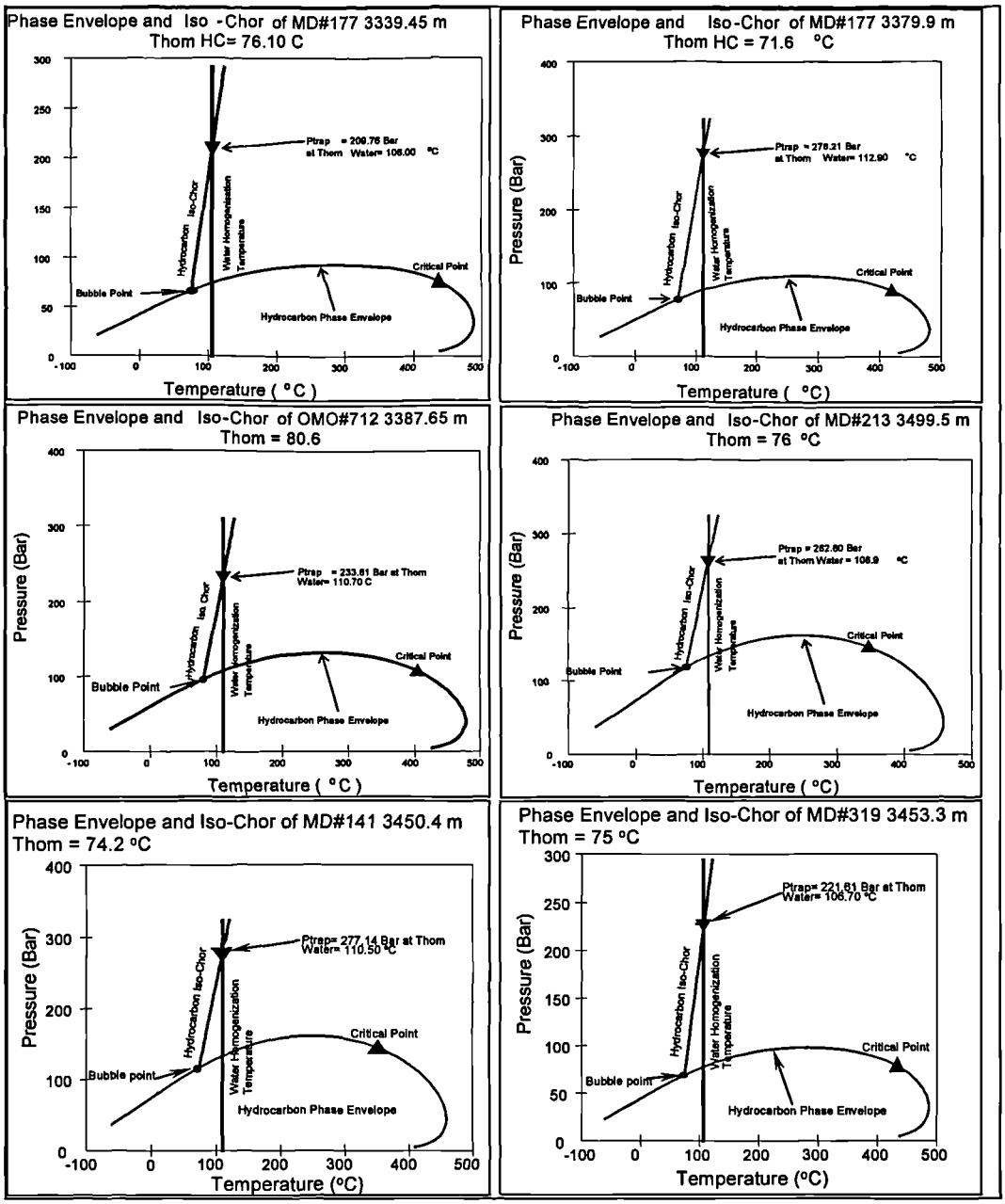

Figure 6.15 Phase envelopes showing calculation of the true trapping temperature and pressure of coexisting fluid inclusions in the wells analysed in the Hassi Messaoud field, using the intersecting isochors technique.

Figure 6.16 shows the reconstructed burial with isotherms modelled from a "pseudo well" representing the sedimentary section in the Hassi Messaoud field obtained by 1D Basin Modelling; Troll V1.0 Single Maturation Modelling System developed by Larter (1988). This "pseudo well" was created on the basis of actual well data. Basin modelling was performed using stratigraphic and lithologic information from the well

logs. The calibration of modelled results of the thermal history was based on constant geothermal gradient taken as 31 °C per km (Bacheller and Peterson, 1991). The input data assume that about 2.2 km of Silurian and Devonian strata were eroded during the Permian-Hercynian orogeny (Makhous et al., 1997a). The burial history diagram shows that there was a slow rate of burial from 600 to 450 Ma followed by a very high rate of burial (ca. 2.5 km) from the Ordovician-Silurian to late Devonian-early Carboniferous. Devonian sedimentation was followed by an interruption that lasted for about 75 Ma throughout the entire Carboniferous. The subsequent Hercynian orogeny resulted in uplift and erosion of about 2.2 km of the Silurian and Devonian strata (Makhous et al., 1997a). Note the considerable rise of isotherms in the post-erosion period probably related to the Permian-Triassic thermal activation in the lithosphere (Makhous et al., 1997a). The Mesozoic was characterised by rapid subsidence, where thick strata of salts and anhydrides were deposited from late Triassic towards the Jurassic time. However from the mid to late Cretaceous the burial rate slowed down, and only ca. 400 m of sediments were deposited during the last 80 Ma. In total about 3 km of sediments were buried throughout the entire Mesozoic period. At present, the Cambrian reservoirs in the Hassi Messaoud field are at temperatures between 120 to 132 °C at depths of 3300 to 3500 m.

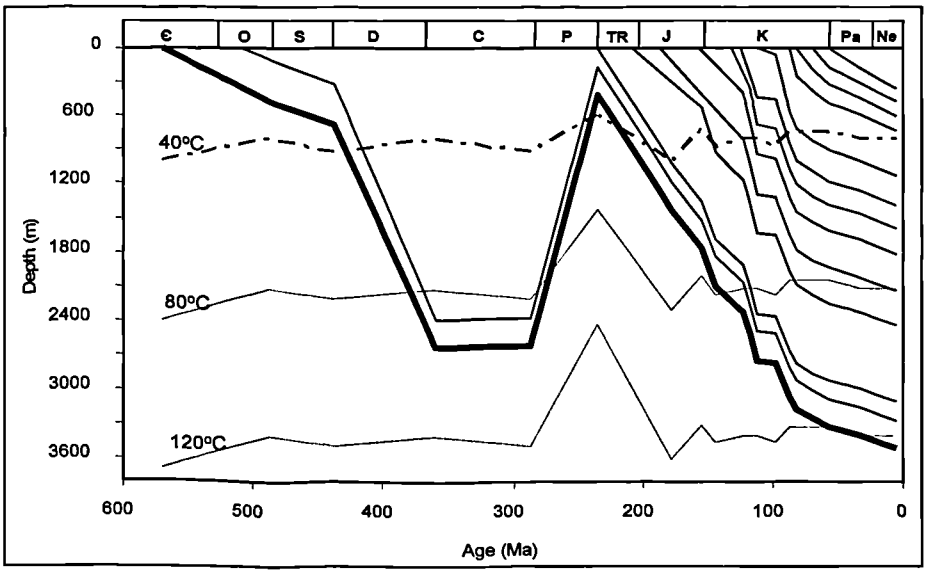

Figure 6.16 Burial and thermal histories of the sedimentary section, Hassi Messaoud modelled using Troll V1.0 "Single Well Maturation Modelling System" (developed by Larter, 1988).

The fluid inclusion trapping temperatures (Table 6.3), when applied with the burial history diagram of the Hassi Messaoud Cambrian reservoir shows that the reservoir

was at depth of 2.8 to 3.3 km during 90 – 40 Ma BP, which is the main period of intensive petroleum inclusion formation. The temperature range at this depth was 106°C to 118°C (Figure 6.17). This finding suggests that the main filling stages of the Hassi Messaoud reservoirs took place probably between late Cretaceous (about 90 Ma BP) and Palaeogene (about 40 Ma BP). This is in good agreement with the finding of Makhous et al. (1997a,b) who showed that the main stage of petroleum generation of the Silurian source rock strata in the Oued Mya basin occurred during the Mid to Late Cretaceous (ca. 120 to 90 Ma BP). These authors assumed that 20% saturation of the free pore space necessary for the most organic-rich Silurian shales having TOC = 11.8% to expel petroleum was achieved at the beginning of the Coniacian (about 88 Ma BP). Whereas, the expulsion threshold for Silurian shales having TOC = 14.4% was reached 3 Ma earlier (i.e. 91 Ma BP). Moreover, in an unpublished report carried out by ARCO in 1994, they suggested that petroleum generation also took place as early as the Late Cretaceous in the centre of the Oued Mya basin and delayed until Tertiary time throughout the rest of the basin. Both results obtained by Makhous et al. (1997a,b) and ARCO in 1994 revealed the same period of petroleum generation from the Silurian source rocks in the Oued Mya basin. If I assume an oil migration rate from the source rocks located in the Oued Mya basin, 40 km from the Hassi Messaoud field, of about 1 cm/year, then the petroleum may have reached the Hassi Messaoud reservoirs about 4 Ma after its expulsion from the source (e.g. Creaney and Allan, 1990). This hypothesis suggests that the timing of generation and expulsion of petroleum proposed by Makhous et al. (1997a,b) and ARCO (1994) is consistent with the timing obtained from the fluid inclusions analysis.

Moreover, in their geochemical modelling, Makhous et al. (1997a,b) also showed that the Silurian source rocks within the study area could have generated petroleum during the end of the Palaeozoic, more accurately during the Carboniferous (360 to 287 Ma), prior to the Permian erosion. The amount of generated petroleum was estimated to account for about 6% of the total generated petroleum. Low petroleum yield rates during the Carboniferous compared to the main petroleum generation which occurred during the Mesozoic are associated with moderate temperatures (82°C-85°C) experienced by the Silurian strata (Makhous et al., 1997a,b). Fennouh, (1996) has also reported quite ubiquitous presence of oxidised bitumen in the Hassi Messaoud reservoirs resulting from degradation of petroleum generated during Carboniferous.

Degradation of the pre-Hercynian petroleum accumulation was likely caused by extensive erosion of Silurian, Devonian and Ordovician strata in the Hassi Messaoud ridge (Figure 6.16). For more details about the occurrence of solid bitumen, see also section 5.6.2.2 in chapter 5.

I did not observe petroleum inclusions which may represent the pre-Hercynian first oil charge in the samples analysed in this study. This observation may suggest that no petroleum inclusions representing the first oil charge were formed; likely because a relatively low volume of oil was generated during the pre-Hercynian compared to the large volume of Cambrian reservoirs available. Nedkvitne et al. (1993) suggested that petroleum inclusions are generally formed in reservoir sandstones with high degree of petroleum saturation (>50%). Nedkvitne et al. (1993) pointed out that a several metre-high column (e.g. 5 m) of oil is required to force oil into small apertures, such as micro-fractures or vacuole entrances of 5 μm width, in water-wet reservoirs. They showed that abundance of petroleum inclusions tends to increase towards the top of every well analysed in the Ula field, North Sea. They also showed that the top of well 7/12-6 (in the field crest) contained the highest number density of petroleum inclusions. Therefore Nedkvitne et al. (1993) concluded that the increase in abundance of petroleum inclusions towards the reservoir crest may be explained as resulting from a high oil column which was in place for longer time than elsewhere in the reservoir.

Thus, during the early stage (i.e. pre-Hercynian) arrival of oil, the Hassi Messaoud reservoirs probably contained variable oil saturation (England et al., 1987). The partially filled Hassi Messaoud reservoirs probably consisted of discontinuous oil–water–oil slugs, perhaps produced by mechanical disruption of the petroleum rivers during earthquake activity which must have been common in the Hassi Messaoud trap during the beginning of the first signs of uplift during late Carboniferous-early Permian.

Another possibility is that because of the relatively small number of samples analysed in this study compared to the area of the Hassi Messaoud giant field (i.e. 43 km x 32 km), it is very likely that I could have missed the intervals which may contain petroleum inclusions representing the early (pre-Hercynian) oil charge.

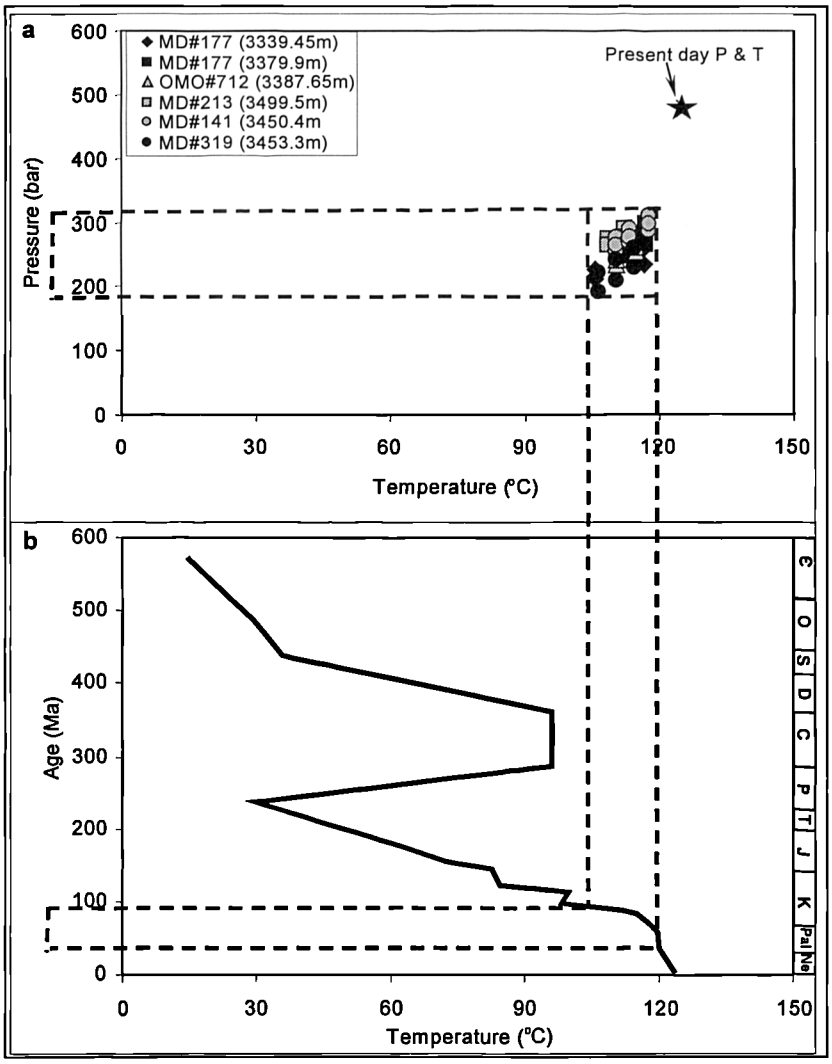

Figure 6.17 (a) The palaeo-pressures and temperatures obtained from petroleum inclusions and (b) the Hassi Messaoud field burial history showing that petroleum was probably present in the Hassi Messaoud reservoirs from 90 to 40 Ma BP.

PVT modeling of petroleum inclusions shows that oil entrapped in inclusions has GOR values ranging from very low values i.e. 22 Sm^3/Sm^3 to higher values i.e. 139 Sm^3/Sm^3. Present day GOR in well MD#177 is 204 Sm^3/Sm^3, in well OMO#712 is 211 Sm^3/Sm^3, in well MD#213 is 205 Sm^3/Sm^3, in well MD#141 is 134 Sm^3/Sm^3, and in well MD#319 is 144 Sm^3/Sm^3 (Table 6.3 and Figure 6.18). The trapping temperatures of the petroleum inclusions show a range of 106 to 118 °C during the period of 40 to 90 Ma BP (Figure 6.17). This may indicate that petroleum migration in the Hassi Messaoud reservoirs may have started about 90 Ma BP. Thus, the first generated oil charge from the Silurian source rock located around the Hassi Messaoud field might have very low GOR composition likely due to low maturity of source rocks. With increasing time and maturity, the source rocks might have expelled oil

with higher GOR as shown in some petroleum inclusions (Figure 6.18). The highest GOR is recorded in samples analysed in the wells MD#213 and MD#141 located in the eastern and southern flanks, respectively. In contrast, lower GOR values are found in samples from the wells MD#177, OMO#712 and MD#319 located in the centre and the south west of the field, respectively. Higher values of GOR and saturation pressure can reflect the higher maturity of petroleum (di Primio et al., 1998). However, biomarker and aromatic hydrocarbon maturity parameters did not show significant variation between maturities of the palaeo-oil analysed in all these samples. Therefore, it is possible that the petroleum inclusions from the wells MD#213 and MD#141 selected for PVT simulation were trapped relatively recently than those selected from the wells MD#177, OMO#712 and MD#319. In fact, the sample analysed in well MD#213 at a depth of 3499.5 m was taken from an interval of reservoir unit Ra which might have been (and/or is being) used as migration pathways (see section 5.6.3.2 in chapter 5). Hence we can argue that some "freshly trapped" petroleum inclusion with higher GOR might have occurred recently compared to the reservoir intervals from the wells in the centre of the field.

The reservoir palaeo-pressure, estimated from this technique ranges from 191 to 309 bar (Table 6.3). The palaeo-pressure in the reservoir unit Ra from the centre of the Hassi Messaoud field ranges between 210 to 268 bar; whereas in the southern and eastern flanks of the field the palaeo-pressure in the same reservoir unit Ra seems to be higher than in the centre ranging from 255 to 309 bar in the south and 265 to 288 bar in the east. The reservoir unit R2 tested only in the centre reveals higher palaeo-pressure than the reservoir unit Ra in the same area of the field (i.e. centre), ranging from 234 to 296 bar. The palaeo-pressure intervals seem to be lower than the hydrostatic conditions during petroleum migration. This may either indicate that petroleum inclusions analysed in both reservoir units Ra and R2 were formed at low pressure or the palaeo-pressure estimated using this technique is not robust.

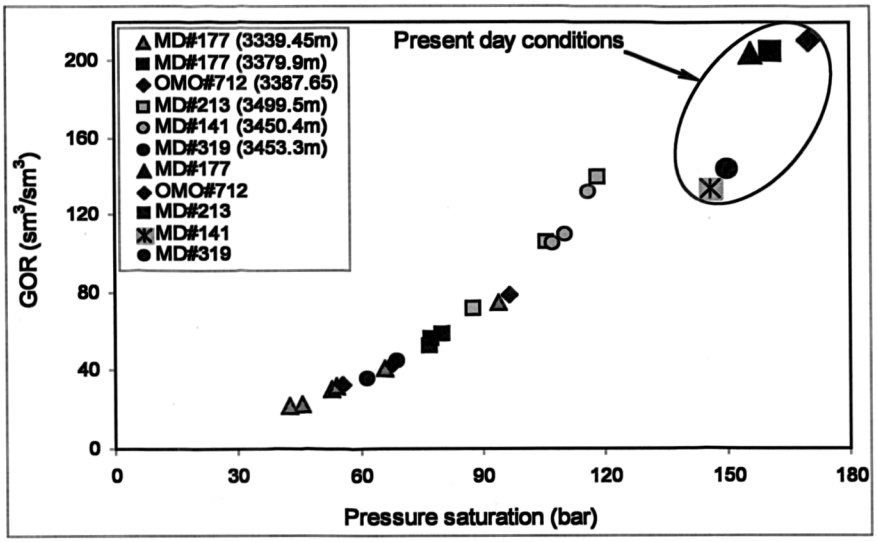

Figure 6.18 Cross plot showing palaeo-GOR and pressure saturation obtained from individual petroleum inclusions and GOR and pressure saturation for the present day produced oils in the Hassi Messaoud field.

6.5. Petroleum geochemistry of the fluids in the inclusions

For long period of time, geochemical evaluation of petroleum reservoirs was limited only to the analysis of present-day fluids to perform correlations and determine the spatial distributions of petroleum populations throughout reservoirs. Recent developments of analytical methods for analysis of petroleum in fluid inclusions allow the analysis of palaeo-fluids in inclusions. The geochemical analyses of oil-bearing inclusions offer an opportunity to gain information on the composition of petroleum during an earlier stage of the fill history. Therefore, comparison between data from present-day fluids and fluid inclusions may establish compositional differences in both space and time. The geochemical analysis of petroleum inclusions has led to the identification of early charges in petroleum reservoirs with both lower maturity and different sources defined (Horsfield and McLimans, 1984; Karlsen et al., 1993; Nedkvitne et al., 1993; Lisk et al., 1996; George et al., 1996, 1997a,b,c, 1998, 2001; Isaksen et al., 1998; Bhullar et al., 1999b and 2001).

In total, seven (7) reservoir core samples were selected for geochemical characterisation of the petroleum trapped in the fluid inclusions. The selection of these samples was obviously based on the abundance of petroleum inclusions obtained from the visual screening of the samples under the UV light, therefore, only samples which revealed high abundance of petroleum inclusions were selected for off-line crushing and analyses by GC and GC/MS. Three samples were selected from the Cambrian

reservoir unit Ra i.e. MD#177 (3339.5 m), MD#213 (3499.5 m) and MD#141 (3450.4 m) and three other samples were selected from the Cambrian reservoir unit R2 i.e. MD#177 (3379.9m), OMO#712 (3387.65m) and OML#712 (3437.5m) from the Hassi Messaoud field. Sample OKJ#202 (3327.5m) was selected from the Lower Triassic reservoir in the Haoud Berkaoui field.

6.5.1. *Normal*-alkanes and isoprenoid alkanes

Distributions of the whole *n*-alkanes and isoprenoid alkanes obtained from the analysis of the petroleum inclusion samples are displayed in Appendix 6.1. Most petroleum inclusions in the samples from both Cambrian reservoir units Ra and R2 in the Hassi Messaoud field are secondaries trapped in the detrital quartz grains; they revealed pale-blue to blue fluorescence under UV light, and their Th's are biased towards values ranging from 70 to 85 °C (Figure 6.6 and Figure 6.8). However, petroleum inclusions found in the Lower Triassic sample from the Haoud Berkaoui field showed lower Th's values compared to the samples analysed in the Hassi Messaoud field, ranging from 48.5 to 63.5 °C. These inclusions were mainly found trapped on the detrital quartz grains showing yellowish fluorescence. Preparation and analysis of the fluid from the petroleum inclusions in these samples are detailed in section 2.2.4 in chapter 2.

Figure 6.19 shows the *n*-alkane envelopes of the fluids from the petroleum inclusions and produced oil samples analysed in the same wells. The *n*-alkanes in the petroleum inclusion and produced oils are normalised to *n*-C_{22} H_{46} *normal* alkane (i.e. relative abundance of *n*-C_{22} H_{46} = 1). The *n*-alkanes distribution is severely modified by evaporative depletion in the *n*-C_1–*n*-C_{17} part. This feature is probably caused by selective removal of low molecular-weight hydrocarbons during crushing and solvent evaporation. The presence of the *n*-alkanes and isoprenoid alkanes in the C_{15}+ fraction confirms that the fluorescing inclusion samples contain oil. Despite relatively severe depletion in the front end *n*-alkanes, the samples show predominance of the lower molecular weight *n*-alkanes (*n*-C_{15}-*n*-C_{22}) over the higher molecular weight *n*-alkanes (*n*-C_{23}+). In contrast the respective production oils have a complete *n*-alkane envelope extending from *n*-C_9 to *n*-C_{39}. The *n*-alkanes distribution from *n*-C_{23}+ in the petroleum inclusions is very similar to the n-alkanes distribution obtained from the present day produced oils (Figure 6.19) with $CPI_{23\text{-}34}$ values similar in both palaeo-

and present day produced oils. These observations may suggest similar origin (likely marine) for the palaeo-oils trapped in the inclusions and the present day produced oils.

Moreover, the lower values of the Pr/Ph, Pr/*n*-C_{17}, and Ph/*n*-C_{18} ratios (Table 6.4) in the petroleum inclusions compared to the produced oils could be partly due to the maturity differences and to a degree to the loss of the front end compounds caused by evaporation during sample handling. Therefore, caution should be taken into account in interpreting these ratios. Maturity parameters based on biomarker alkanes and aromatic hydrocarbons show that present day produced oils are far more mature than the palaeo oils trapped in the inclusions (see sections below).

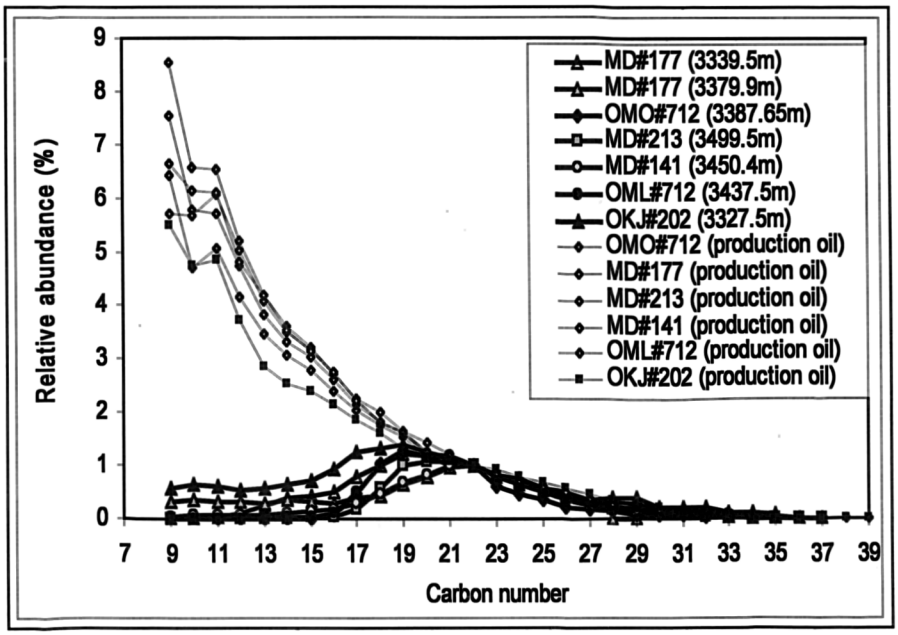

Figure 6.19 *n*-alkane envelopes representing the petroleum inclusion oils and their respective production oils. *n*-alkanes in the petroleum inclusion and produced oils are normalised to *n*-C_{22} H_{46} *normal* alkane.

Table 6.4 Geochemical ratios calculated from the n-alkane and isoprenoid distributions in the petroleum inclusion oils and the respective produced oils.

Sample	Depth (m)	Pr/Ph	Pr/n-C_{17}	Ph/n-C_{18}	CPI_{23-34}
Fluid inclusion oils					
MD#177	3339.5	0.92	0.42	0.37	1.05
MD#177	3379.9	0.81	0.38	0.40	1.04
OMO#712	3387.65	0.46	0.32	0.31	1.03
MD#213	3499.5	0.34	0.32	0.31	0.99
MD#141	3450.4	0.51	0.28	0.34	1.01
OML#712	3437.5	0.54	0.30	0.27	1.08
OKJ#202	3327.5	0.98	0.30	0.28	1.1
Production oils					
OMO#712		1.30	0.34	0.33	0.99
MD#177		1.29	0.33	0.31	1
MD#213		1.34	0.34	0.28	1.02
MD#141		1.32	0.33	0.31	1.03
OML#712		1.33	0.38	0.33	1.05
OKJ#202		1.43	0.23	0.18	1.04

Key: Pr = Pristane, Ph = Phytane
CPI = Carbon Preference Index

6.5.2. Biomarker alkanes and aromatic hydrocarbons

Figure 6.20, Figure 6.21 and Table 6.5 summarise the biomarker alkane distributions and selected biomarker parameters of the fluid inclusion oils and present day produced oils. Partial mass chromatograms showing the distribution of aromatic hydrocarbons in the fluid inclusion oils and production oils are given in Figure 6.22 and the aromatic hydrocarbon maturity parameters are displayed in Table 6.6.

Tricyclic terpane and hopane distributions in the fluid inclusion oils from the samples MD#177 (3339.45m and 3379.9m), MD#213 (3499.5m), MD141 (3450.4m), OML#712 (3437.5m) and OKJ#202 (3327.5m) are very similar to those in the respective present day produced oils. However, fluid inclusion oils show the occurrence of two strong peaks which are contaminants identified by the full scan mode as squalene, the peak eluting just before Ts and cholesterol eluting just before the C_{30} αβ hopane. These contaminants were likely introduced during sample preparation. Section 2.2.4 in chapter 2 describes in detail the steps taken to minimise contamination and the difficulties of analysing included oils.

The C_{23} to C_{31} tricyclic terpanes are predominant over the hopanes in the m/z 191 mass chromatograms for both fluid inclusion oils and present day produced oils. Moreover, the fluid inclusion oils are characterised by relatively low abundance of the

rearranged hopanes C_{29} Ts and C_{30} diahopane and high abundance of Tm than in the present day produced oils.

Sterane and diasterane distributions in the fluid inclusion oils are also for the most part very similar to those in the respective present day produced oils (Figure 6.20), with abundant C_{27} and C_{29} βα diasteranes compared to the respective regular steranes. Similarities in the biomarker distributions strongly suggest that the paleo-oils trapped in the fluid inclusions and the present day produced oils were generated from the same source rock.

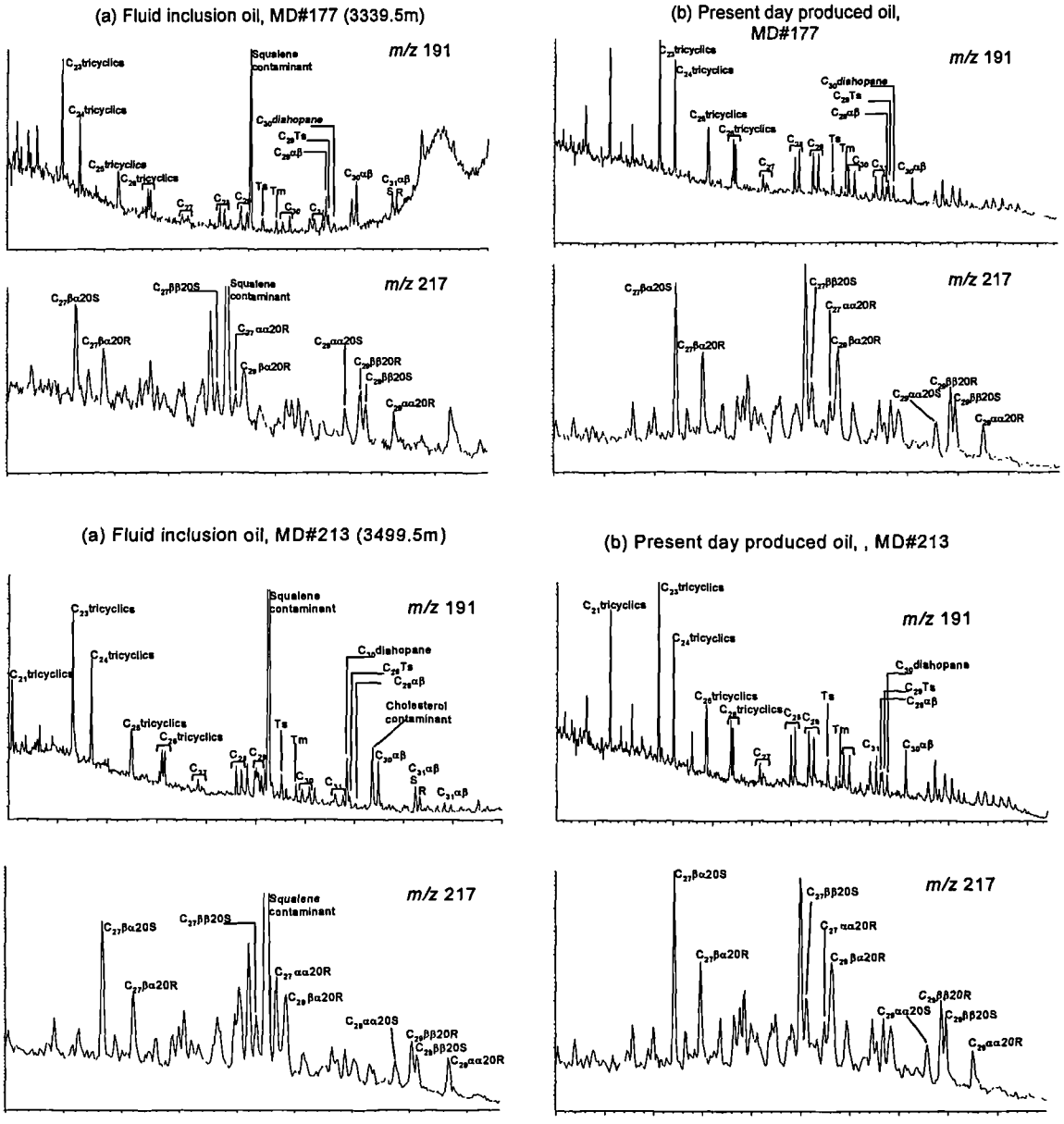

Figure 6.20 Partial *m/z* 191 and *m/z* 217 mass chromatograms for (a) the fluid inclusion oils and (b) the respective present day produced oils in the wells MD#177 and MD#213, in the Hassi Messaoud field.

The fluid inclusion oil sample OMO#712 reveals quite different biomarker distributions compared to the respective present day produced oil from well OMO#712 (Figure 6.21). The fluid inclusion oil shows the occurrence of gammacerane which is sometimes associated with saline depositional environments (Peters and Moldowan, 1993) and is found in certain marine petroleums from carbonate or evaporite source rocks (Rohrback, 1983; Moldowan et al., 1985; Mello et al., 1988a and b; Moldowan et al., 1982). Interestingly, the reservoir core extract from the same sample OMO#712 (3387.65m) also shows the presence of gammacerane (see section 5.4.2.3, in chapter 5 for more details). It has been shown in the previous chapters that neither the Silurian and the Ordovician source rocks, nor any of the oils analysed have shown the occurrence of gammacerane. Gammacerane was found only in the reservoir core extracts analysed in well OMO#712 and is interpreted to be related to the overlying evaporitic Triassic formations (for more details, see section 5.6.2.3 in chapter 5).

The fluid inclusion petroleum also reveals a relatively lower abundance of the tricyclic terpanes than the hopanes, a low abundance of Ts, C_{29} Ts and C_{30} diahopane relative to Tm, C_{29} 17α (H) hopane, and C_{30} 17α (H) hopane, respectively, and finally a relatively high abundance of C_{29} and C_{30} 17β (H) hopanes. All these features are completely different from the present day produced oil in well OMO#712.

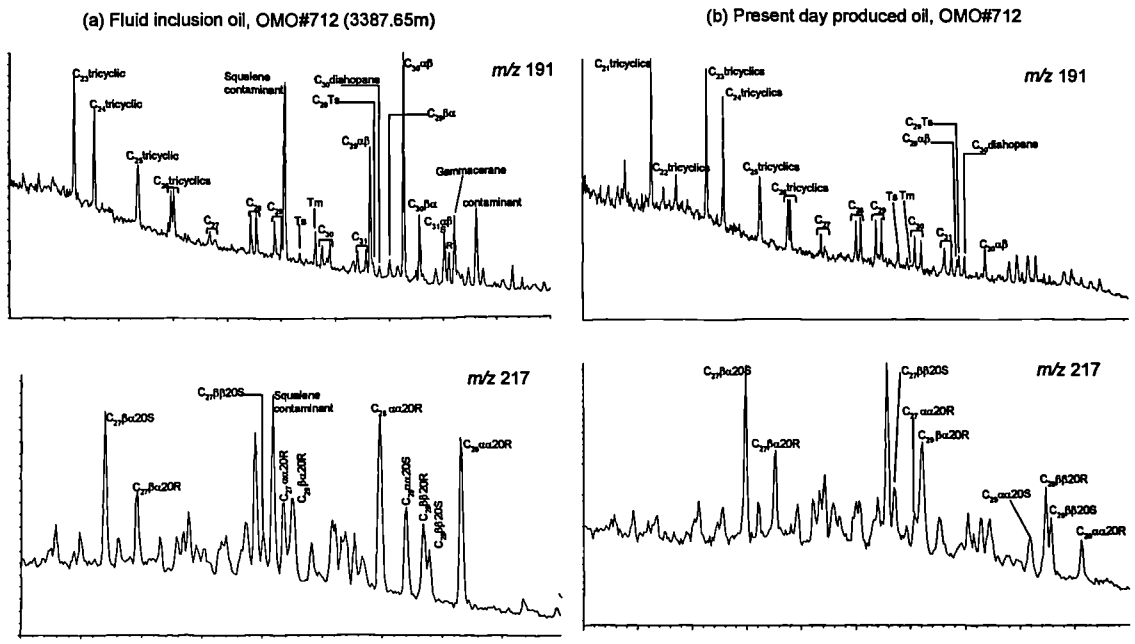

Figure 6.21 Partial m/z 191 and m/z 217 mass chromatograms for (a) the fluid inclusion oil OMO#712 (3387.65m) and (b) the respective present day produced oil OMO#712, Hassi Messaoud field.

Table 6.5 Biomarker hydrocarbon parameters for fluid inclusion oils and produced oils, in the Hassi Messaoud and the Haoud Berkaoui fields.

Sample	Depth (m)	Reservoir	1	2	3	4	5	6	7	8	9	10	11	12	13
Oil inlusions															
OMO#712	3387.65	Cambrian R2	0.36	0.33	-	0.08	0.06	0.24	5.09	0.42	0.36	0.11	29.85	28.31	41.84
MD#177	3339.45	Cambrian Ra	0.49	0.61	-	0.29	0.16	0.52	5.37	0.72	0.31	0.13	36.25	22.43	41.31
MD#177	3379.9	Cambrian R2	0.46	0.60	-	0.30	0.17	0.47	6.37	0.72	0.33	0.13	40.30	22.17	37.53
MD#141	3450.4	Cambrian Ra	0.42	0.60	-	0.28	0.16	0.61	6.37	0.71	0.35	0.12	41.71	21.67	36.62
MD#213	3499.5	Cambrian Ra	0.46	0.54	-	0.25	0.15	0.60	3.80	0.71	0.25	0.17	40.47	23.53	36.01
OML#712	3437.5	Cambrian R2	0.47	0.57	-	0.29	0.19	0.64	4.12	0.74	0.36	0.15	44.07	19.28	36.66
OKJ#202	3327.5	Lower Triassic	0.49	0.52	-	0.18	0.15	0.46	2.58	0.69	0.24	0.28	36.05	25.26	38.69
Production oils															
OMO#712		Cambrian Ra	0.55	0.61	0.55	0.44	0.36	0.78	8.10	0.80	0.57	0.20	40.78	21.62	37.59
MD177		Cambrian Ra	0.57	0.61	0.53	0.55	0.31	0.83	6.73	0.80	0.57	0.11	39.95	19.39	40.66
MD 141		Cambrian Ra	0.53	0.60	0.58	0.46	0.24	0.77	6.20	0.75	0.43	0.13	38.16	22.05	39.79
MD 213		Cambrian Ra	0.55	0.62	0.54	0.40	0.32	0.78	6.41	0.80	0.47	0.09	41.17	19.91	38.91
OML 712		Cambrian Ra	0.55	0.60	0.60	0.47	0.34	0.80	6.88	0.80	0.47	0.11	41.41	19.07	39.52
OKJ 202		Lower Triassic	0.59	0.58	0.62	0.47	0.30	0.74	3.26	0.73	0.34	0.39	36.48	20.52	43.00

1- C_{29} steranes ααα 20S/(20S+20R), 2- C_{29} steranes ββ/(αα+ββ), 3- C_{32} ab hopanes 22S/(22S+22R), 4- C_{29}Ts/(C_{29}Ts + C_{29} 17 α (H) hopane), 5- C_{30} diahopane/(C_{30}diahopane + C_{30} 17 α (H) hopane), 6- Ts/(Ts+Tm), 7- ETR =Extended tricyclic terpanes C_{28}+C_{29} (S+R)/Ts, 8- C_{29}diasteraneR/(C_{29} diasteraneR + C_{29} sterane R), 9- C_{29} ααα + αββ steranes/(C_{29} ααα + αββ steranes + C_{29}-C_{30} 17 a(H) hopanes), 10 = C_{24} tetracyclic terpane/sum C_{26} tricyclic terpanes (S+R), '11- %C_{27} αββ steranes, 12- %C_{28} αββ steranes, 13- %C_{29} αββ steranes.

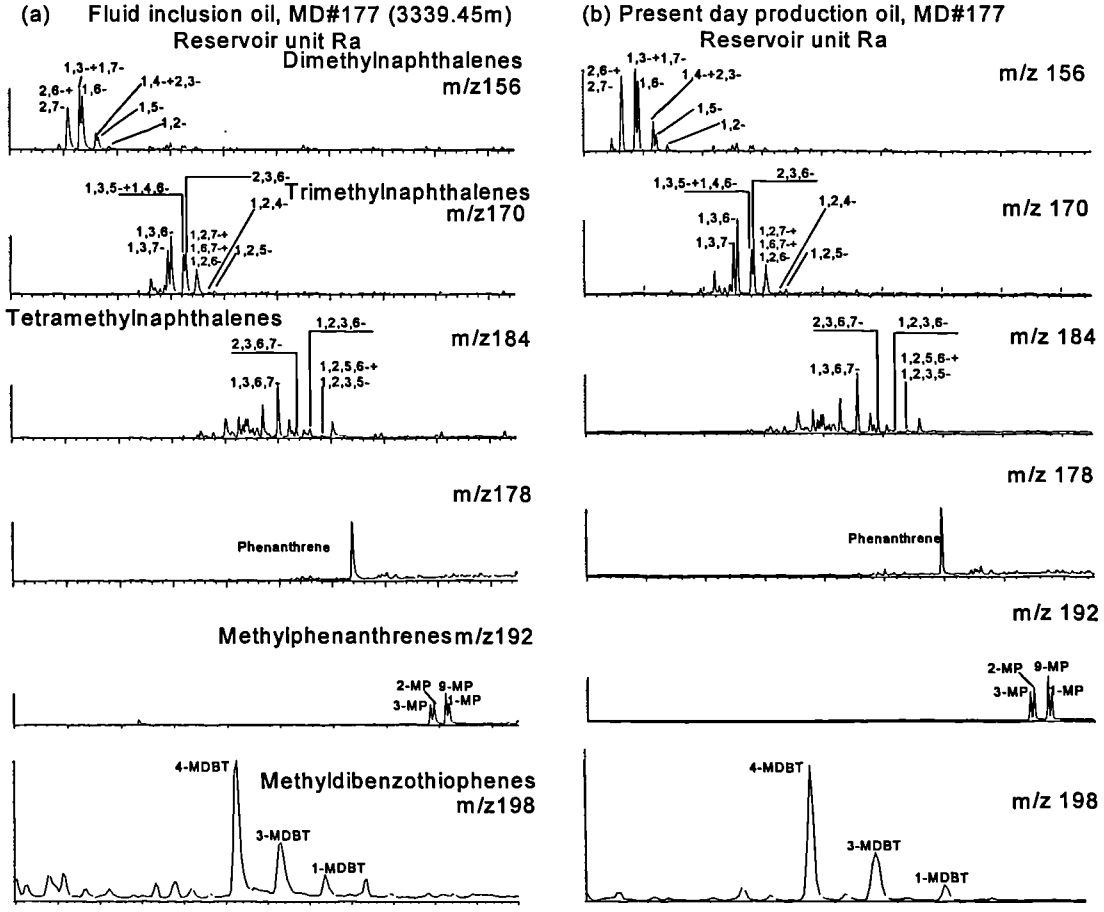

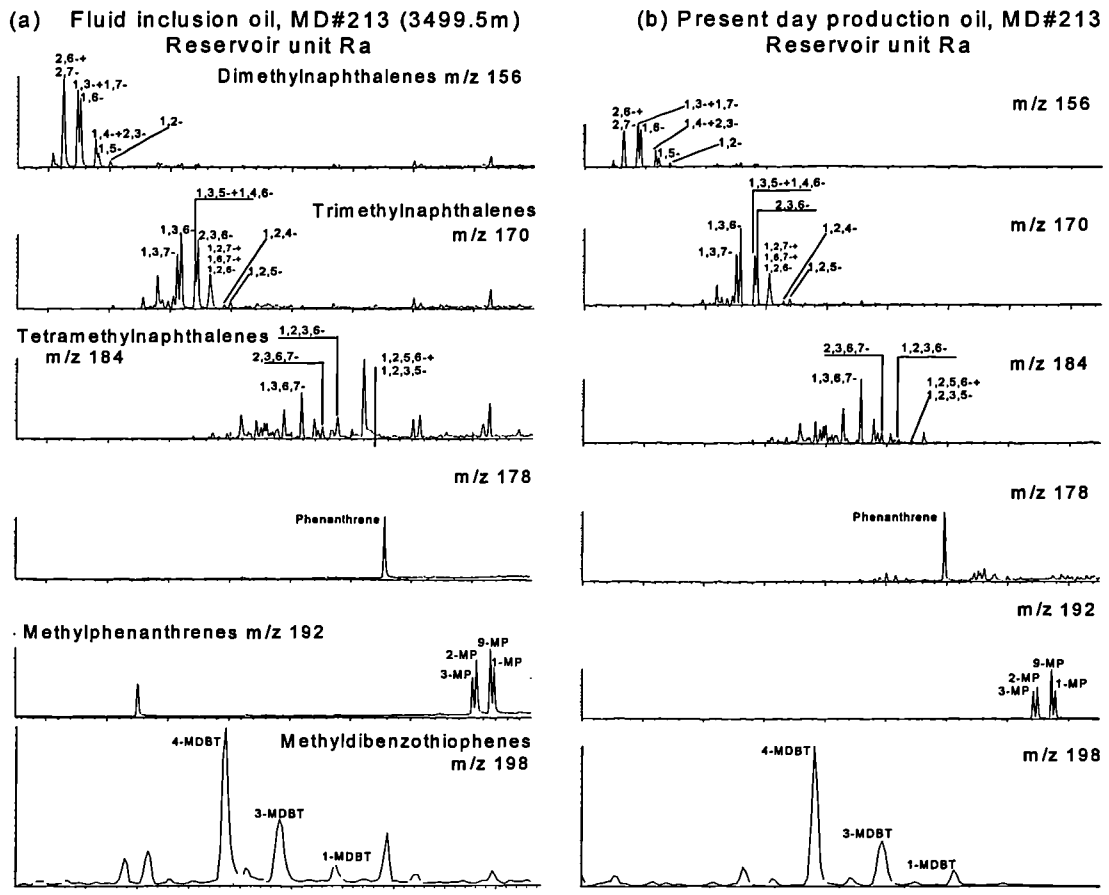

Figure 6.22 Partial m/z 156, 170, 184, 178, 192, and 198 mass chromatograms, showing representative aromatic hydrocarbon distributions in the fluid inclusion oils and present day produced oils from the wells MD#177 and MD#213, Hassi Messaoud field.

Table 6.6 Aromatic hydrocarbon maturity parameters for fluid inclusion oils and present day produced oils, in the Hassi Messaoud and the Haoud Berkaoui fields.

Sample	Depth (m)	Reservoir	1	2	3	4	5	6	7	8
Oil inlusions										
OMO#712	3387.65	Cambrian R2	1.43	4.92	4.09	6.53	0.70	0.49	6.75	0.69
MD#177	3339.45	Cambrian Ra	1.12	4.64	14.43	12.67	1.09	0.73	7.43	0.80
MD#177	3379.9	Cambrian R2	1.36	4.56	13.26	8.72	1.31	0.60	7.03	0.76
MD#141	3450.4	Cambrian Ra	1.38	4.94	11.04	10.54	1.13	0.63	7.67	0.78
MD#213	3499.5	Cambrian Ra	-	4.85	6.86	4.41	0.78	0.60	7.59	0.76
OML#712	3437.5	Cambrian R2	1.23	4.28	9.89	8.03	0.76	0.50	7.69	0.70
OKJ#202	3327.5	Lower Triassic	1.03	2.77	2.71	3.34	0.70	0.31	5.82	0.59
Production oils										
OMO#712		Cambrian Ra	1.42	10.46	11.01	16.93	3.33	0.77	9.61	0.86
MD177		Cambrian Ra	1.50	6.82	12.48	20.50	3.39	0.80	8.89	0.88
MD 141		Cambrian Ra	1.47	6.74	12.04	19.28	3.15	0.79	8.43	0.88
MD 213		Cambrian Ra	1.39	6.26	10.28	17.29	2.72	0.73	9.30	0.84
OML 712		Cambrian Ra	1.41	5.91	8.16	13.07	2.50	0.75	8.42	0.85
OKJ 202		Lower Triassic	1.04	3.68	3.46	4.18	1.18	0.57	5.99	0.74

1 - 2-methylnaphthalene/1-methylnaphthalene, 2 - (2,6-dimethylnaphthalene+2,7-dimethylnaphthalene)/1,5-dimethylnaphthalene

3 - TMNR-1: 1,3,7-trimethylnaphthalene/1,2,5-trimethylnaphthalene

4 - 1,3,6,7-tetramethylnaphthalene/(1,2,5,6- tetramethylnaphthalene+ 1,2,3,5-tetramethylnaphthalene)

5 - 2,3,6,7-tetramethylnaphthalene/1,2,3,6-tetramethylnaphthalene, 6 -Methylphenanthrene index:1.5*(2-MP+3-MP)/(P+1-MP+9-MP)

7 - MDR: 4-methyldibenzothiophene/1-methyldibenzothiophene, 8 - %Rc(MPI-1) = 0.60 x MPI-1 + 0.40.

The triangular diagram in Figure 6.23 reveals that the fluid inclusion oils and present day produced oils plot in the same region of the diagram, very close to each other, showing similar distributions of the C_{27}, C_{28}, and C_{29} αββ regular steranes. Moreover, all the samples show the predominance of C_{27} and C_{29} αββ regular steranes compared to C_{28} αββ regular steranes indicating a marine source of the fluid inclusion oils and the present day produced oils. All these observations indicate a strong genetic relationship between the fluid inclusion oils and the present day produced oils. However, the fluid inclusion oil from sample OMO#712 (3387.65m) shows a somewhat higher percentage of the C_{28} αββ regular steranes than the rest of the samples suggesting contributions from another source with a different type of organic matter. This is in fact in agreement with the occurrence of gammacerane in this sample which also indicates a contribution from another source, probably the evaporitic Triassic sediments overlying the Cambrian reservoir in the Hassi Messaoud field (see section 5.6.2.3).

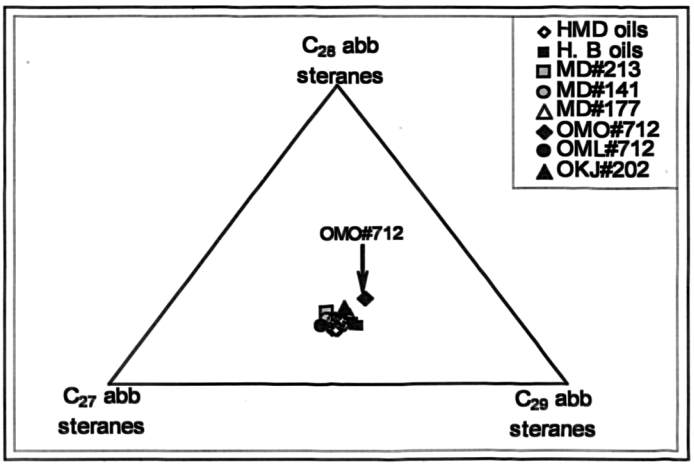

Figure 6.23 Ternary diagram showing the distribution of C_{27}, C_{28}, C_{29} αββ regular steranes for the fluid inclusion oils and production oils. Key: HMD = Hassi Messaoud field, H.B = Haoud Berkaoui field.

The parameters [sum C_{28}+C_{29} extended tricyclic terpanes (S+R)]/Ts (ETR) versus C_{24} tetracyclic terpane/C_{26} tricyclic terpanes (S+R), recently proposed by Holba et al. (2001) are plotted in Figure 6.24. Petroleum inclusion samples analysed in the Hassi Messaoud field show similar values of both parameters for the respective present day produced oils in the Hassi Messaoud field, whereas the petroleum inclusion sample analysed in the Haoud Berkaoui field plots close to the present day oils from the same field. These findings suggest a similar source for the present day produced oils and the palaeo-oils analysed in the Hassi Messaoud field; the source rocks of these oils are

likely the Silurian strata buried in the surrounding basin. In chapter 4, sections 4.4 and 4.5, I showed that the Haoud Berkaoui present day oils were likely generated from both Silurian and Ordovician source rock strata located in the Oued Mya basin, with probably much more contribution from the Silurian source rocks. Hence, the palaeo-oil analysed in the sample from Haoud Berkaoui field appears to be also generated from both Silurian and Ordovician source rock strata in the same basin.

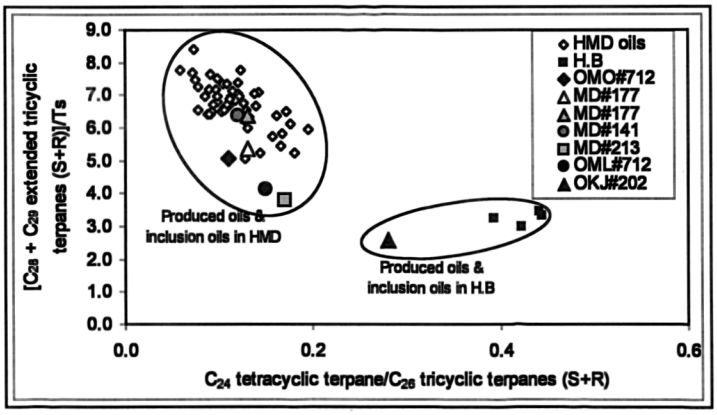

Figure 6.24 Cross plot of facies-dependant parameters [sum C_{28} + C_{29} tricyclic terpanes (S+R)]/Ts versus C_{24} tetracyclic terpane/C_{26} tricyclic terpanes (S+R) in the oil inclusions and present day produced oils from the Hassi Messaoud and Haoud Berkaoui fields.

Biomarker maturity based parameters C_{29} ααα regular steranes 20S/(20S+20R), C_{29} αββ/(αββ+ααα) regular steranes, Ts/(Ts+Tm), C_{29}Ts/ [C_{29}Ts+C_{29} 17α (H) hopane] and C_{30} diahopane/[C_{30} diahopane+C_{30} 17α (H) hopane] are plotted in Figure 6.25. Aromatic hydrocarbon maturity parameters DMNr, TeMNr-1 and TeMNr-2, MDR and %Rc are plotted in Figure 6.26.

The ratio of C_{29} ααα regular sterane 20S/(20S+20R) plotted against the ratio of C_{29} αββ regular steranes/(C_{29} ααα + αββ regular steranes) (Mackenzie et al., 1985) reveal little variation between most of the fluid inclusion oils and present day produced oils. These ratios are at equilibrium indicating that fluid inclusion oils and production oils are mature (Figure 6.25a).

However, all of the other biomarker alkane and aromatic hydrocarbon parameters plotted in Figure 6.25 and Figure 6.26 clearly distinguish between fluid inclusion oils and present day produced oils. In general fluid inclusion oils reveal lower maturities than the present day produced oils. The values of the calculated vitrinite reflectance equivalent range from 0.7 to 0.8 %Rc in the fluid inclusion oils and from 0.86 to 0.95

%Rc for the present day produced oils. These findings indicate that the filling of the Hassi Messaoud field did not involve a single homogenous charge. The first oil charge comprised the least mature oils represented by the palaeo-oils trapped in the inclusion, whilst the second oil charge containing more mature oils is represented by the present day produced oils from the Hassi Messaoud field.

Oil inclusion samples (except oil inclusion sample OMO#712 3387.65 m) from the Hassi Messaoud reservoirs (samples MD#177 (3339.5 m and 3379.9 m, MD213 (3499.5 m), MD#141 (3450.4 m) and OML#712 (3437.5 m)) show minor differences in maturity (i.e. ranging from 0.7 to 0.8 %Rc). This is in good agreement with the observations made earlier using the UV light where most of the oil inclusions showed a similar blue fluorescing colour.

Fluid inclusion oil from the sample OMO#712 (3387.65m) plots away from the rest of the samples showing lower biomarker alkane maturity parameter values (Figure 6.25 a,b,c and Table 6.5). However, the aromatic hydrocarbon parameters show comparatively similar values between the fluid inclusion oil from sample OMO#712 (3387.65m) and the rest of the fluid inclusion samples. This observation may suggest that the palaeo-oil trapped in the inclusions analysed in this sample contains a mixture of "immature" oil characterised by higher biomarker concentrations and low maturity signatures and mature oil characterised by low biomarker concentrations, high aromatic hydrocarbon concentrations and high maturity signatures, probably originated from the Silurian source rocks located in the study area (e.g. Requejo et al., 1992; Li et al., 1995a).

In fact, earlier in section 5.6.2.3 chapter 5, I have suggested that reservoir core extracts analysed from well OMO#712 including the core extract at the depth of 3387.65m contain a mixture of immature bitumen being contributed from the overlying evaporitic Triassic sediments and mature residual oil migrated from the Silurian source rocks in the region. Moreover, the oil trapped in the fluid inclusions from the sample OMO#712 (3387.65m) also shows similar features as the reservoir core extract analysed at the same depth (see Section 5.6.2.3). Therefore, it is likely that the oil trapped in these inclusions contains a mixture of immature Triassic bitumen and mature residual oil generated and migrated from the Silurian source rocks located in the study area. This observation may strongly suggest that trapping of

petroleum inclusions in this sample (or at least in the centre of the Hassi Messaoud field, where well OMO#712 is located), occurred during the post-Triassic time (i.e. post-Hercynian time).

Petroleum inclusion oil in the sample OKJ#202 from the Haoud Berkaoui Lower Triassic reservoir located in the Oued Mya basin is less mature (i.e. 0.59 %Rc) compared to the rest of the fluid inclusion oils from the Hassi Messaoud Cambrian reservoirs (i.e. 0.70 – 0.80 %Rc), and present day produced oils from the Haoud Berkaoui field are also less mature (i.e. 0.76 %Rc) than the present day produced oils from the Hassi Messaoud field (i.e. 0.86 – 0.95 %Rc) (Figure 6.25 and Figure 6.26).

This observation may suggest that the fluid inclusion oil in the sample OKJ#202 from the Haoud Berkaoui field was probably trapped earlier than the fluid inclusion oils from the Hassi Messaoud field, probably indicating that the Haoud Berkaoui Lower Triassic reservoir has received oil earlier than the Hassi Messaoud Cambrian reservoirs.

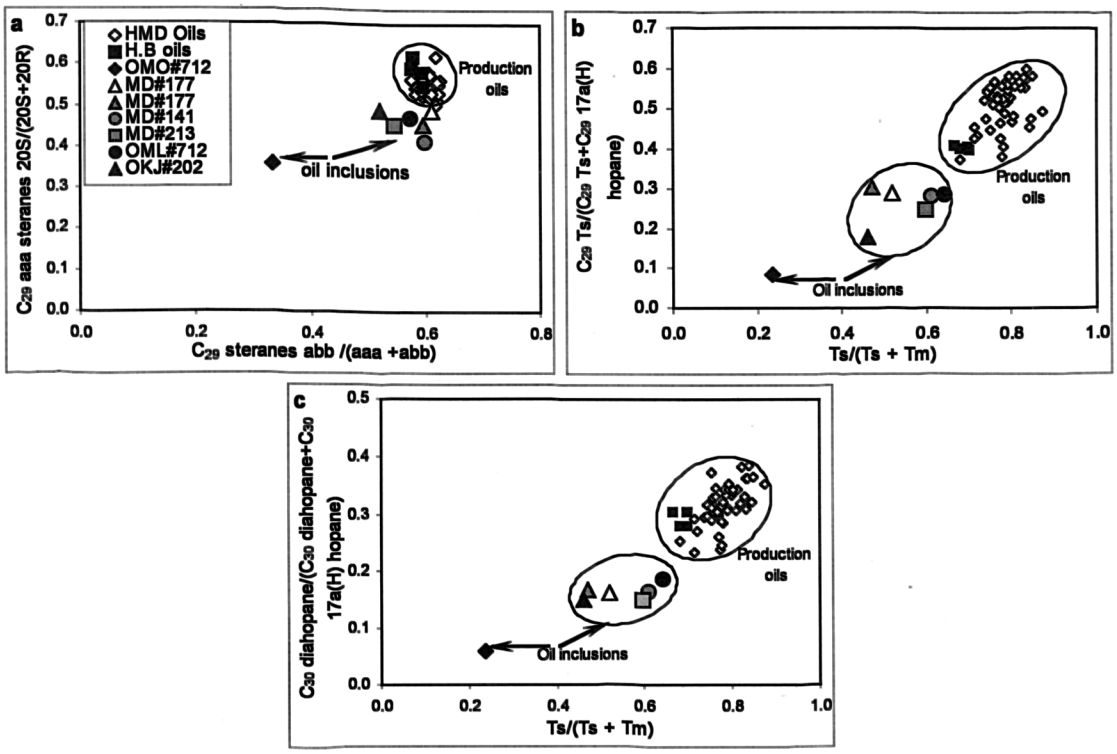

Figure 6.25 Cross plots of (a) C_{29} ααα regular steranes 20S/(20S+20R) versus C_{29} αββ/(αββ+ααα) regular steranes, (b) C_{29}Ts/[C_{29}Ts + C_{29} 17α (H) hopane] and (c) C_{30} diahopane/(C_{30} diahopane + C_{30} 17α (H) hopane) versus Ts/(Ts+Tm) showing comparison between the maturity of the fluid inclusion oils and present day produced oils in the Hassi Messaoud and Haoud Berkaoui fields.

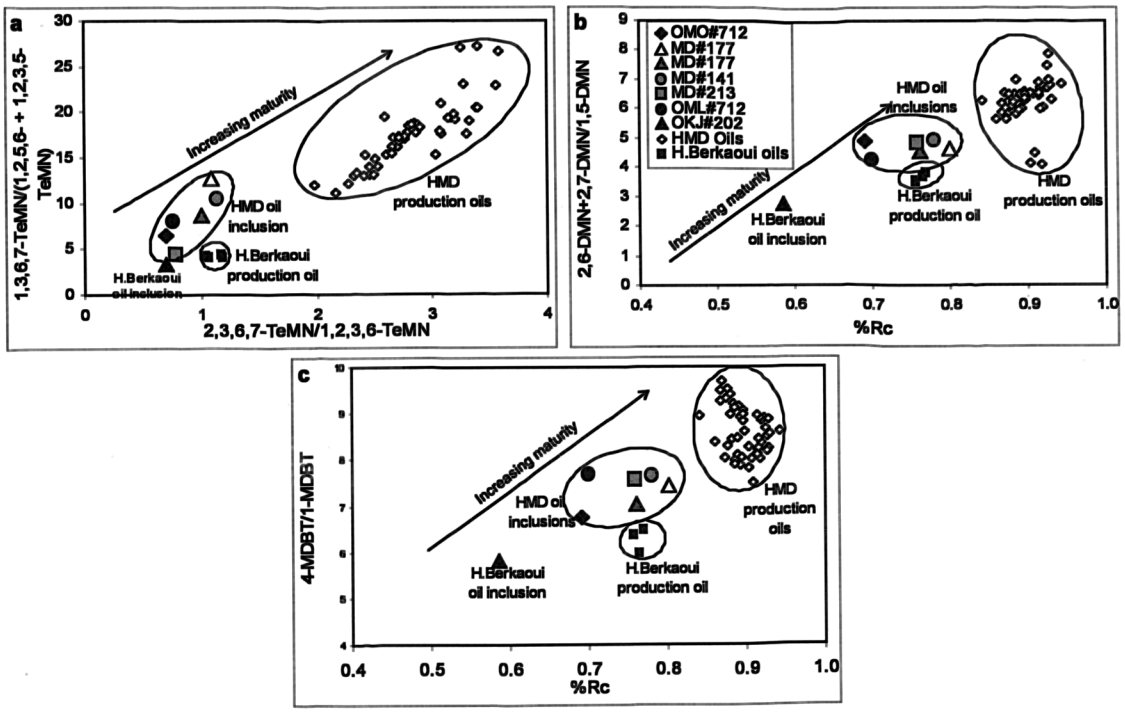

Figure 6.26 Cross plots of (a) 1,3,6,7-TeMN/(1,2,5,6- + 1,2,3,5-TeMN) versus 2,3,6,7-TeMN/1,2,3,6-TeMN (b) 2,6- + 2,7-DMN and (c) 4-MDBT/1-MDBT versus the calculated vitrinite reflectance equivalent (%Rc) showing the maturity of the fluid inclusion oils and the present day produced oils in the Hassi Messaoud and Haoud Berkaoui fields.

6.6. Summary

Petroleum inclusions were found in most of the samples analysed in this study; in total 18 samples showed occurrence of petroleum inclusions while only 5 samples did not show occurrence of petroleum inclusions. These latter samples are mainly from the western and southern flanks of the Hassi Messaoud field. The distribution of petroleum inclusion abundances show that in general samples from the wells located in the centre of the field (MD#177 and OMO#712) and from well MD#213 located in the eastern flank contain the highest number of petroleum inclusions. The samples from the wells MD#141 and OML#712 located in the south and northeast flanks show fewer of petroleum inclusions than those from the centre and east, and the samples from the wells MD#319, OMJ#41 and OMM#33 exhibit the least abundance of petroleum inclusions compared to the samples from the centre, east, south and north east parts of the Hassi Messaoud field. Both Cambrian reservoir units Ra and R2 revealed similar abundances of petroleum and aqueous inclusions.

The distribution of petroleum inclusion abundance agrees well with the distribution of the total petroleum yields and reservoir quality across the Hassi Messaoud field. The

reservoir core samples from the wells MD#177 and OMO#712 (centre of the field) showed the highest total petroleum yield (see section 5.6.3.1 in chapter 5), and the occurrence of the highest abundance of petroleum inclusions. This part of the field (centre) contains reservoir core samples with the highest porosity and permeability values (see section 5.6). Therefore, this can be explained as resulting from the presence of a high oil column which probably was in place for much longer time than elsewhere in the Hassi Messaoud reservoirs. This is in agreement with the findings of Karlsen et al. (1993), Nedkvitne et al. (1993), Oxtoby et al. (1995), Bhullar et al. (1999b) and Munz et al. (1999a).

Although quartz overgrowths are very common in all the samples analysed in this study, petroleum inclusions in the dust rim or within the overgrowths are quite rare. By far the majority of petroleum inclusions encountered in this study were trapped in the detrital quartz grains which are likely secondary in nature. Moreover, a sample analysed in well MD#141 located south of the Hassi Messaoud field exhibited common petroleum inclusions trapped along healed micro-fractures crosscutting both detrital grains and quartz overgrowths (Figure 6.7 d). These observations may suggest that generally speaking, oil charging has post-dated the quartz diagenesis processes; mainly towards the western and southern flanks of the field. This also may be an explanation for the relatively low to moderate reservoir quality in the Hassi Messaoud field; typical porosity and permeability values measured across the main Cambrian reservoir unit Ra range from 4 to 11.5% and 0 to 100 mD, respectively (Mallenfer and Tillous, 1963; Balducchi and Pommier, 1970; Djarnia and Fekirine, 1998).

The technique of combining Confocal Laser Scanning Microscopy with microthermometry and PVT modelling on fluid inclusions revealed a reasonable model of temperature and charge history of the Hassi Messaoud field. The Hassi Messaoud sandstone member was at a depth of 2.8 to 3.3 km during the time of petroleum migration into the reservoir and petroleum inclusion formation. The temperature range at this depth was between 106°C to 118°C from Late Cretaceous to Palaeogene, which in agreement with the timing of generation and expulsion of hydrocarbons from the main Silurian source rocks in the region (Makhous et al., 1997a,b; ARCO, 1994). However, palaeo-pressure estimated from the same technique indicates that the Hassi Messaoud reservoirs were at low pressure during petroleum

migration or that the results obtained from this simulation are not consistent. Palaeo-oil in these reservoirs was of low GOR as compared to the present day petroleum. This is in agreement with the lower maturity of palaeo-oil compared to the present petroleum shown by biomarker and aromatic hydrocarbon maturity parameters.

The geochemistry of petroleum inclusions is evidence for the existence of palaeo-oil in the Cambrian reservoir units Ra and R2 from the Hassi Messaoud field and Lower Triassic reservoir in the Haoud Berkaoui field. The palaeo-oil analysed from both fields showed similar source facies to the present day produced oils suggesting that the same source (mainly Silurian source rocks) had generated the palaeo- and the present day oil in the Hassi Messaoud field, and probably both Silurian and Ordovician source rocks contributed to the generation of the palaeo-oil and present day oil in the Haoud Berkaoui field. Moreover, palaeo-oil also showed lower maturity compared to the present day petroleum. The calculated vitrinite reflectance values range from 0.70 – 0.80 %Rc for the palaeo-oil and 0.86 – 0.95 %Rc for the present day petroleum produced from the Hassi Messaoud field.

The palaeo-oil sample analysed from the Haoud Berkaoui field also revealed lower maturity (i.e. 0.56 %Rc) as compared to the present day produced oil from the same field (i.e. 0.76 %Rc), and compared to the palaeo-oil trapped in the Hassi Messaoud Cambrian reservoirs. This observation may suggest that oil trapped in the Haoud Berkaoui field represents the first oil charge expelled by the Silurian and Ordovician source rock strata in the Oued Mya basin.

So, are there some of you still interested in becoming inclusionists? Just think of all those billions and billions of tiny fluid-filled entities just waiting:

A Fluid Inclusion Speaks Its Mind

Do you like me?
Why do you look
At this tiny thing
That I am?

I see your eyes
And you want to sing to me
To discover my soul.

Don't tell me
That you want to know me
Just to learn my secrets.
Caught you there
With your soul bare.

You want to know my past.
Was I homogeneous?
Was I heterogeneous?
These are the questions
I see in your eyes.

Can you hear me?
I am trying to say something.
I know you can love me.
And when you do,
I will tell it to you all.

Jayanty Guha Chincoutimi, March 6, 1992.

Chapter 7
General Conclusions and Suggestions for Future Work

7. General conclusions and suggestions for future work

This project involves a geochemical study of the Oued Mya basin-Hassi Messaoud ridge petroleum system, east- central Saharan Algeria, in an attempt to establish the source rocks responsible for generating and expelling the oils and elucidate the charging of the Hassi Messaoud field and all the accumulations located across this petroleum system (i.e. the Lower Triassic and Devonian fields along the Oued Mya basin and the Cambro-Ordovician fields: the Hassi Guettar, El Agreb, Mesdar and El Baguel throughout the Hassi Messaoud ridge). An assessment of the extent of petroleum migration on the Oued Mya basin-Hassi Messaoud petroleum system has also been addressed. More detailed reservoir geochemical investigation has been carried out on the giant Hassi Messaoud field in an effort to determine the role of the faults with respect to petroleum migration, understand the compartmentalisation and the communication between compartments, and determine the filling history and timing of charging of the Hassi Messaoud reservoirs. This chapter presents the main conclusions drawn from this work, together with the implications of the results achieved as well as suggestions for future research work.

7.1. General conclusions

7.1.1. Geochemical evaluation of the Oued Mya basin-Hassi Messaoud ridge petroleum system

The thin basal and highly radioactive Silurian (hot shales) which corresponds to the Tannezuft Formation is believed to be the main source rock across the study area. The Silurian source rock samples analysed in this project exhibited extremely rich organic matter intervals; the total organic carbon content ranges from 0.99 to 14.30 wt% (average 9.20 wt%). However, the Ordovician Formations (El Gassi shales, El Azzel shales and Micro-conglomeratic shales) revealed much lower petroleum potential compared to the Silurian strata (i.e. TOC values range from 0.17 to 2.36 wt%, average 0.82 wt%).

The Silurian and Ordovician source rock strata are mature and calibrated measured vitrinite reflectance ranges from 0.81 to 1.12 %Rm. This maturity interval suggests that both of the Silurian and Ordovician source rock strata have currently reached the

main stage of the oil window – end of the oil window. The Silurian and Ordovician strata have reached the gas window toward the south-south west of the Oued Mya basin (not analysed in this project) (Makhous et al., 1997; Sonatrach, unpublished reports).

The Silurian source rock intervals analysed across the northeast of the Oued Mya basin exhibited two main groups of organic facies: group A including samples BAT#1 (3 samples), OA#1bis (3 samples), BKZ#1 (4 samples), GEC#1 (1 sample) and TKT#1 (2 samples) characterised by higher concentrations of the tricyclic terpanes and steranes over the hopanes; Group B comprising 7 samples from wells GD#1bis (1 sample), GLNE#4bis (1 sample), GLNE#5 (3 samples) and GBC#1 (2 samples) (Figure 4.1) characterised by lower concentrations of the tricyclic terpanes and steranes compared to the hopanes. The Ordovician source rock intervals also revealed different facies features compared to the Silurian source rock intervals.

The Silurian source rock samples from well RDC#2 (4 samples), well OA#1bis (2 samples), and to a lesser extent samples from wells GLNE#4bis (3874.85m), BKZ#1 (4187.86m and 4189.95m) and GLNE#5 (4001.45m) revealed unusual *hydrocarbon* distributions mainly dominated by the aromatic hydrocarbons over the *n*-alkanes and isoprenoid alkanes. The organic matter in these samples has probably suffered alteration by irradiation from the natural decay of uranium in the "hot" shales.

Principal components analysis and most of the facies-based parameters employed in this project clearly separate the oils into three major groups and one subgroup. Group I includes 1 oil sample from Rhourde Chegga Triassic field, 81 oil samples from Hassi Messaoud, 2 oil samples from Hassi Guettar and 3 oil samples from El-Agreb Cambrian fields; group II comprises 7 oil samples (2 oil samples from Benkahla field, 4 oil samples from Haoud Berkaoui field and 1 oil from Draa Temra field); subgroup IIa contains 4 oil samples (1 oil sample from Mokh-El-Kabch field, 1 oil sample from N'goussa field, 1 oil sample from Guellala Northeast field and 1 oil sample from Guellala field); and group III contains 2 samples from Mesdar field and 2 samples from El-Baguel field (Figure 4.1).

The oils revealed a similar level of maturity as the Silurian and Ordovician source rock strata. The oil analysed in the Mesdar field appear to be the most mature oil

across the entire study area, whereas, the oils analysed in the Haoud Berkaoui, Benkahla and Draa Temra fields appear to be the least mature oils in the region. The oil samples analysed in the Hassi Messaoud field showed higher maturity in the samples from the centre and east sectors of the field; the oil samples located in the west sector exhibited the lowest maturity within the Hassi Messaoud field. Moreover, a trend of decreasing maturity can be also observed from the Hassi Messaoud towards the El Agreb fields.

Oil-source rock correlations revealed that all the oils from group I (Hassi Messaoud, Hassi Guettar, Rhourde Chegga and El-Agreb fields) display similar facies features to the Silurian source rock samples from group A. Therefore, I can suggest that there is a high probability that all the oils trapped in these fields were generated from Silurian source rock intervals having similar features as those in group A.

The oils from group II and subgroup IIa (located in the Oued Mya basin) revealed similar features to both of the Silurian source rock groups and the Ordovician source rock samples. However, it is likely that the Silurian source rock strata have contributed in much higher proportions than the Ordovician source rock strata for the generation of these oils since the biomarker and aromatic hydrocarbon ratios together with the principal components analysis showed that these oils plot relatively closer to the Silurian source rock samples from group A than to the Ordovician source rock samples.

Oil samples from Mesdar and El-Baguel Cambrian fields were also generated from source rocks having similar features to the Silurian source rock in Oued Mya basin. However, these oils showed some facies features which are different from those shown in the Silurian source rock strata and the rest of the oils analysed in this project. The oils analysed in the Mesdar and El Baguel fields are characterised by the highest steranes/17α(H)hopanes and tricyclic terpanes/17α(H)hopanes ratios, lowest diasteranes/regular steranes ratios, lowest biomarker concentrations, highest aromatic hydrocarbon concentrations and highest maturity ratios compared to the rest of oils analysed in this study. All these criteria would suggest that these oils were generated from another source rock, most likely from the Silurian source rock strata in the Berkine basin.

Daniels and Emme (1995), Makhous et al. (1997) and unpublished reports from Sonatrach showed that the Silurian source rocks in the Berkine basin are more mature (i.e. $\%R_m$ = 1.08 – 1.3) than in the Oued Mya basin (i.e. $\%R_m$ = 0.7 – 0.9). In the Berkine basin depocentre, Silurian sediments are even overmature. Hence, Mesdar and El-Baguel oils were probably generated from the Silurian strata located in the western flanks of Berkine basin.

7.1.2. Oil migration and charging directions of the reservoirs of the Oued Mya-Hassi Messaoud ridge petroleum system

The results obtained from the biomarker and aromatic maturity and facies-based parameters combined with the distributions and concentrations of the alkylcarbazoles and benzocarbazoles of the oils analysed in this project enable me to draw the following conclusions:

The oils trapped in the deepest reservoirs in the Mokh-el-Kebch, N'Goussa, Guellala northeast, Guellala, and Draa Temra fields, have probably undergone the least migration distances (probably only vertical migration) compared to the oils trapped in the shallowest reservoirs in the Benkahla and Haoud Berkaoui fields. The oils trapped in these fields may have experienced vertical migration from the Silurian and Ordovician source strata probably located in the area of Boukhzana, N'goussa and Guellala northeast into the overlying Lower Triassic reservoirs and then followed by long lateral migration (~ 30 km) towards the shallowest Lower Triassic reservoirs in the Benkahla and Haoud Berkaoui fields (Figure 7.1). The Lower Triassic reservoirs in the Benkahla and Haoud Berkaoui are located at shallower depths (i.e. oil-water contact depth is -3324 m), whereas the same Triassic reservoir units are more shallow in the Guellala (-3470 m), Draa Temra (-3480 m), Guellala north east (-3531 m) and N'goussa (-3787 m) fields (Figure 5.12).

The oils trapped in the Hassi Messaoud field have experienced long lateral migration distances probably from the Silurian source rocks located in the Oued Mya basin 40 to 60 km west-northwest of the Hassi Messaoud field and the Silurian source rocks located 40 to 50 km east of the Hassi Messaoud field, probably in the Hassi Dzabat area (Figure 7.1).

The Hassi Messaoud reservoirs were charged from the west and the east sides, upwards towards the crest (centre of the field) and then towards the north, south and west flanks of the field. The western flanks of the field have probably received oil much later compared to all the other sectors of the field. This observation is supported by low abundance of petroleum inclusions (section 6.2 in chapter 6), lower reservoir porosity and permeability (Figure 5.51) and lower petroleum yields (section 5.6.3.1 above) recorded in the samples analysed in the western sectors of the Hassi Messaoud field. The Hassi Messaoud reservoirs revealed lateral and vertical maturity and facies heterogeneities likely inherited from the charging history of the field.

When the Hassi Messaoud reservoirs were filled, the oil continued to migrate south-southwest towards the El-Agreb fields via the Hassi Messaoud and the Hassi Guettar fields. Therefore, the oils actually trapped in the El-Agreb may have experienced the longest migration distances (ca. 120 to 150 km) (Figure 7.1).

The oils trapped in the Mesdar and El-Baguel reservoirs were likely originated from the Silurian source rock in the Berkine basin and then migrated following the north-northwest trend. The oil trapped in the Mesdar field appears to have experienced shorter migration distance compared to the oil trapped in the El Baguel field (Figure 7.1).

The principal components analysis of biomarker concentration data showed that the main south-southeast – north-northeast fault crosscutting the Hassi Messaoud reservoirs (Figure 5.30) may have been impermeable during the main stages of oil charging. This main fault may have played a key role in preventing mixing between the oil generated in the Oued Mya basin (west-northwest of the Hassi Messaoud field) and the oil generated from the east of the field. The principal component analysis also allowed me to statistically confirm that the separation of the Hassi Messaoud field into 25 zones is geochemically consistent.

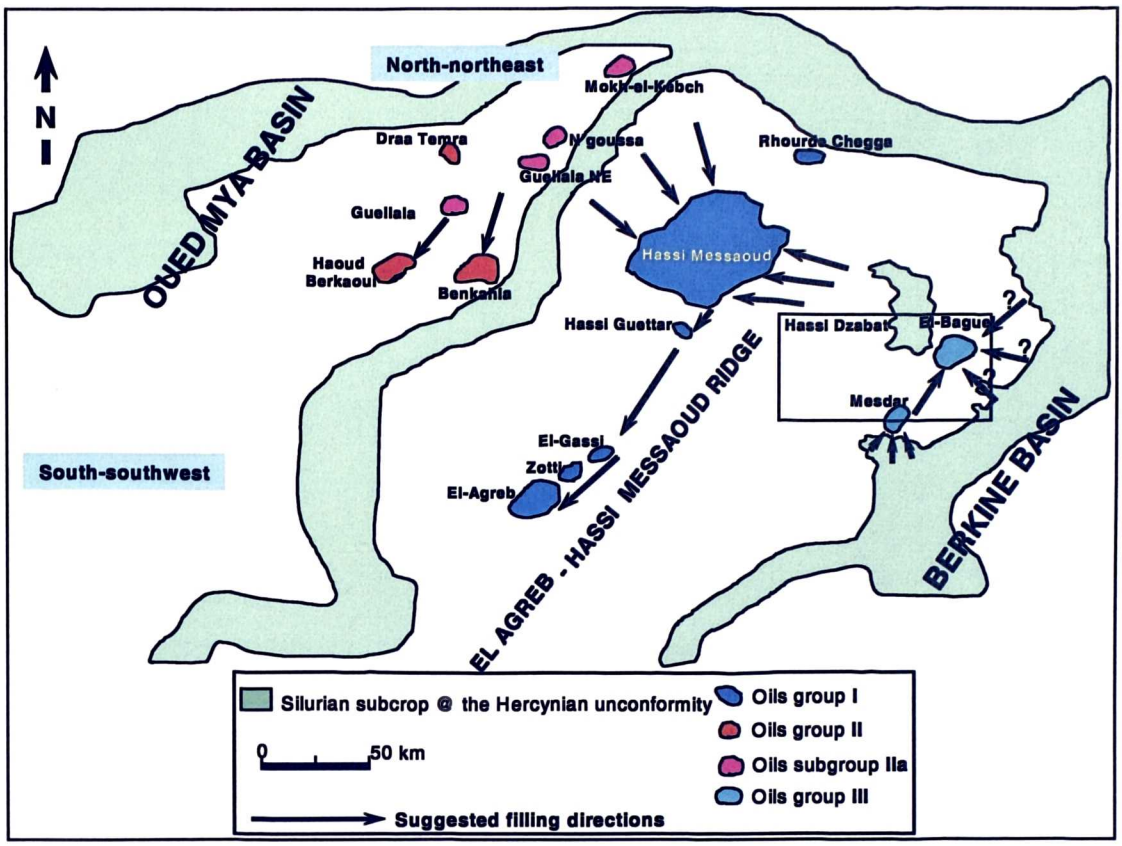

Figure 7.1 Suggested filling directions for the oil fields analysed in the Oued Mya basin and Hassi Messaoud ridge.

7.1.3. Determination of the timing of the Hassi Messaoud reservoir filling using fluid inclusions, PVT data and petroleum geochemistry of the palaeo-oils

Petroleum inclusions were found in most of the samples analysed in this study. The samples from the wells located in the centre of the field (i.e. MD#177 and OMO#712) and from well MD#213 located in the eastern flank contain the highest abundance of petroleum inclusions. The samples from the wells MD#141 and OML#712 located in the south and northeast flanks show lower abundance of petroleum inclusion than those from the centre and east, and the samples from the wells MD#319, OMJ#41 and OMM#33 exhibit the least abundance of petroleum inclusions compared to the samples from the centre, east, south and north east parts of the Hassi Messaoud field.

The occurrence of the highest abundance of petroleum inclusions in the crest of Hassi Messaoud structure (i.e. wells MD#177 and OMO#712) suggest that oil was present here for a longer time than in the flanks, where lower abundance of petroleum inclusions was observed. This supports a model of filling from the crest and downwards (Nedkvitne et al., 1993; Oxtoby et al., 1995; Bhullar et al., 1999; Munz et al., 1999a).

High abundance of petroleum inclusions found below the oil leg of the eastern flank (i.e. in well MD#213), may represent migration pathways updip from the Silurian source rocks located in the Hassi Dzabat, east of the Hassi Messaoud field.

Secondary petroleum inclusions trapped in the detrital quartz grains in most of the samples and along healed micro-fractures crosscutting both detrital grains and quartz overgrowths (e.g. sample MD#141, southern flank) are much more abundant than primary petroleum inclusions, despite common occurrence of well-developed quartz overgrowths. This observation may suggest that generally speaking, oil charging post-dated the quartz diagenesis processes, especially towards the western and southern flanks of the field. This may also be an explanation for the relatively low to moderate reservoir quality in the Hassi Messaoud field; typical porosity and permeability values measured across the main Cambrian reservoir unit Ra range from 4 to 11.5% and 0 to 100 mD, respectively (Mallenfer and Tillous, 1963; Balducchi and Pommier, 1970; Djarnia and Fekirine, 1998).

The petroleum inclusion distributions suggest that in higher permeability rocks, migrating petroleum occupies a large proportion of pore space as a dense network, while in lower permeability rocks it is present as dispersed stringers. In the initial stage of reservoir filling, oil preferentially migrates along higher permeability units, but is concentrated in structurally higher positions because of buoyancy. The high concentration of petroleum stringers will ensure that little cementation can take place, but will result in large numbers of petroleum inclusions being trapped in whatever sites are accessible. As cementation continues in other parts of the structure, permeability is reduced so that oil invasion is more dispersed. Fewer petroleum inclusions are trapped despite similar numbers of potential sites for trapping. This process leads to a correlative decline in numbers of petroleum inclusions with permeability (e.g. western flanks of the Hassi Messaoud field).

The new technique combining Confocal Laser Scanning Microscopy with microthermometry and PVT modelling on fluid inclusions shows a reasonable model of temperature and charge history of the Hassi Messaoud reservoirs. The Hassi Messaoud Cambrian sandstone member was at depth of 2.8 to 3.3 km during the time of petroleum migration into the reservoir and petroleum inclusion formation. The temperature range at this depth was between 106°C to 118°C from Late Cretaceous to

Palaeogene. This is in agreement with the timing of generation and expulsion of hydrocarbons from the Silurian main source rocks in the region (Makhous et al., 1997; ARCO, 1994).

Palaeo-pressures estimated from the same technique range from 210 to 309 bar indicating that the Hassi Messaoud reservoirs were probably at low pressure during petroleum migration or that the results obtained from this simulation are not consistent.

The geochemistry of petroleum inclusions is evidence of the existence of palaeo-oil in the Cambrian reservoir units Ra and R2 in the Hassi Messaoud field and the Lower Triassic reservoir in the Haoud Berkaoui field.

The palaeo-oil analysed from both fields showed similar source facies to the present day produced oils suggesting that the same source (mainly Silurian source rocks) has generated the palaeo- and the present day oil in the Hassi Messaoud field. In the Haoud Berkaoui, probably both of Silurian and Ordovician source rocks have contributed to the generation of the palaeo-oil and present day oil, with much more contribution from the Silurian source rock strata.

The palaeo-oil revealed lower maturity compared to the present day produced petroleum in the Hassi Messaoud field. The calculated vitrinite reflectance values range from 0.70 – 0.80 %Rc for the palaeo-oil and 0.86 – 0.95 %Rc for the present day petroleum.

Palaeo-oil sample analysed from the Haoud Berkaoui field also revealed lower maturity (i.e. 0.56 %Rc) as compared to the present day produced oil from the same field (i.e. 0.76 %Rc). Moreover, the palaeo-oil trapped in the Haoud Berkaoui Lower Triassic reservoir showed lower maturity as compared to the palaeo-oil trapped in the Hassi Messaoud Cambrian reservoirs. This observation may suggest that oil trapped in the Haoud Berkaoui field represent the first oil charge expelled by the Silurian and Ordovician source rock strata in the Oued Mya basin.

7.1.4. Potential implications of the results obtained in these investigations

The results shown in this project can exert a weighty influence on the current/future exploration activities in the Hassi Messaoud ridge area. Any attempts at defining the

actual migration routes and charging directions can potentially assist in the discovery of further small reserves near the Hassi Messaoud giant petroleum accumulation, where existing infrastructures would make such reserves economic. New reserves could be discovered either along the migration pathways to the already discovered large accumulations, or on spill routes from one large accumulation to another.

7.1.5. Suggestions for future work

According to the results obtained in my investigations, some suggestions for any future research work which may be considered as an extension to this study include:

1. Source facies and thermal maturity assessment of the Silurian source rocks located in the Hassi Dzabat area and north-northeast of the Hassi Messaoud field. This will be important since it will confirm the possible charging of the Hassi Messaoud reservoirs from the eastern sides.

2. Establishment of the mass balance between the petroleum generated and expelled in mature Silurian and Ordovician source rocks and the current discovered reserves in the Oued Mya-Hassi Messaoud ridge petroleum system. This will allow assessment the remaining reserves to be discovered across the region.

3. Analysis of additional oil samples from the Devonian and Lower Triassic fields in the Oued Mya basin and the Cambrian fields in the El Agreb, Mesdar and El Baguel fields to further investigate migration pathways and charging directions of these accumulations.

4. Analysis of additional reservoir core samples from the Hassi Messaoud reservoirs to understand the degree to which observed trends in the distribution of petroleum extracts are due to reservoir filling processes.

5. Additional reservoir core samples are needed from the Hassi Messaoud for more fluid inclusion investigations.

References

References

van Aarssen, B.G.K., Bastow, T.P., Alexander, R., and Kagi, R.I.,1999. Distribution of methylated naphthalenes in crude oils: indicators of maturity, biodegradation and mixing, *Organic Geochemistry*, **30**, 1213-1227.

Abbott, G.D. and Maxwell, J.R., 1988. Kinetics of the aromatisation of rearranged ring-C monoaromatic steroid hydrocarbons. *In*: Mattavelli, I. and Novelli, L. (Eds) *Advances in Organic Geochemistry*, 1987, *Organic Geochemistry*, **13**, 881-885.

Abbott, G.D. Lewis, C.A. and Maxwell, J.R., 1984. Laboratory simulation studies of steroidal aromatisation and alkane isomerisation. *Organic Geochemistry*, **6**, 31-38.

Alexander, R., Cumbers, K.M., and Kagi, R.I., 1986. Alkylbiphenyls in ancient sediments and petroleums. *In*: Leythaeuser, D. and Rullkötter, J. (Eds), *Advances in Organic Geochemistry*, 1985, *Organic Geochemistry*, **10**, 841-845.

Alexander, R., Kagi, R.I., Rowland, S.J., Sheppard, P.N., Chirila, T.V., 1985. The effects of thermal maturity on distribution of dimethylnaphthalenes in some ancient sediments and petroleums. *Geochimica et Cosmochimica Acta* **49**, 385-395.

Alexander, R., Kagi, R.I., Sheppard, P.N., 1984. 1,8-Dimethylnaphthalene as an indicator of petroleum maturity. *Nature* **308**, 442-443.

Alexander, R., Larcher, A.V., Kagi, R.I., 1992. An oil-source correlation study using age specific plant-derived aromatic biomarkers. *In*: Moldowan, J.M.P., Albrecht, P., Philips, R.P. (eds.), *Biological Markers in Sediments and Petroleum*. Prentice Hall, Englewood Cliffs, 201-221.

Aplin, A.C., Larter, S.R, Bigge, M.A, Macleod, G. Swarbrick, R.E., Grunberger, D., 2000. Confocal microscopy of fluid inclusions reveals fluid-pressure histories of sediments and an unexpected origin of gas condensate. *Geology* **28**, 1047-1050.

Aplin, A.C., Macleod, G., Larter, S.R., Jones, D.M., Chen, M., Bigge, A.M., Pedersen, K.S., Sorensen, H., & Booth, T. 1997. Petroleum fluid inclusions: improved analytical methods enhance their use as a tool. *Petroleum Geoscience*. GEOFLUIDS II, Belfast, Extended Abstracts.

Aplin, A.C., Macleod, G., Larter, S.R., Pedersen, K.S., Sorensen, H., Booth, T., 1999. Combined use of Confocal Laser Scanning Microscopy and PVT simulation for estimating the composition and physical properties of petroleum in fluid inclusions. *Marine and Petroleum Geology* **16**, 97-110.

Aquino Neto, F.R., Trendel, J.M., Restle, A., Connan, J., and Albrecht, P.A., 1983. Occurrence and formation of tricyclic and tetracyclic terpanes in sediments and petroleum. *In*: Bjorøy, M. et al. (Eds) *Advances in Organic Geochemistry 1981*, John Wiley and sons, Chichester, 659-667.

ARCO Exploration and Production Technology, 1994. Algeria petroleum systems study. Technical Service Report TSR 94-0060.

Attar, M. and Hammat, M., 1993. Hydrocarbon potential of Algeria. *In*: *Proceedings of the Mediterranean Oil and Gas conference (MOEX)*, Valletta, Malta.

Bacheller, W.D. and Peterson, R.M., 1991. Hassi Messaoud field – Algeria Trias Basin, Eastern Sahara Desert. *American Association of Petroleum Geologists, Memoir*, 211-224.

Bailey, N.J.L., Krouse, H.R., Rogers, M.A., 1973. Alteration of crude oils by waters and bacteria-evidence from geochemical studies. *American Association of Petroleum Geologists Bulletin* **57**, 1276-1290.

Bakel, A.J., and Philp, R.P., 1990. The distribution and quantification of organonitrogen compounds in crude oils and rock pyrolysates. *Organic Geochemistry* **16**, 353-367.

Bakr, M.M.Y. and Wilkes, H., 2002. The influence of facies and depositional environment on the occurrence and distribution of carbazoles and benzocarbazoles in crude oils: a case study from the Gulf of Suez, Egypt. *Organic Geochemistry* **33**, 561-580.

Balducchi, A., and Pommier, G. 1970. Cambrian oil field of Hassi Messaoud, Algeria. *American Association of Petroleum Geologists, Memoir* **14**, 477-488.

Bastow, T.P., 1999. Sedimentary processes involving aromatic hydrocarbons. PhD. Thesis, Curtin University pf Technology, Perth.

Bastow, T.P., Alexander, R., Sosrowidjojo, I.B., Kagi, R.I., 1998. Pentamethyl-naphthalenes and related compounds in sedimentary organic matter. *Organic Geochemistry* **28**, 585-596.

Baylis S.A, 1998. Geochemical comparison of core extracts and oil samples in reservoir. *Organic Geochemistry* **29**, 463-484.

Beach, F., Peakman, T.M., Abbott, G.D., Sleeman, R. and Maxwell, J.R., 1989. Laboratory thermal alteration of triaromatic steroid hydrocarbons. *Organic Geochemistry* **14**, 109-111.

Benamrane, O., Messaoudi, M., Messelles, H., 1993. Geology and hydrocarbon potential of the Oued May Basin, Algeria. *American Association of Petroleum Geologists Bulletin*, **77**, 1607 (abstract).

Bennett, B., Bowler, B.F.J. and Larter, S.R., 1996. Determination of C_0-C_3 alkylphenols in crude oils and waters. *Analytical Chemistry*, **68**, 3697-3702.

Bennett, B. and Larter S.R., 1997. Partition behaviour of alkylphenols in crude oil/ brine systems under subsurface conditions. *Geochimica et Cosmochimica Acta*, **61**, 4393-4402.

Bennett, B., and Larter, S.R., 1998. Polar compounds in petroleum reservoirs: compositional differences between produced and in-situ oils. *5th International symposium on evaluation of reservoir wettability and its effects on oil recovery*, Trondheim, Norway, 1998.

Bennett, B., and Larter, S.R., 2000. Quantitative Separation of Aliphatic and Aromatic Hydrocarbons Using Silver Ion-Silica Solid-phase Extraction. *Analytical Chemistry*, **72**, 1039-1044.

Bennett, B., Chen, M., Brincat, D., Gelin, F.J.P., and Larter, S.R., 2002. Fractionation of benzocarbazoles between source rocks and petroleums. *Organic Geochemistry*, **33**, 545-559.

Beuf, S., Biju-Duval, B., Carpal, O.de., Rognon, P., Gariel, O. and Bennacef, A., 1971. Les grès du Paléozoïque inférieur au Sahara. *Publ. IFP, Sc. Et Tech. du Petr.*, **18**, Editions Technip Paris.

Bhullar, A. G., Karlsen, D. A., Lacharpagne, J. C., & Holm, K., 1999a. Reservoir screening using Iatroscan TLC-FID and identification of palaeo-oil zones, oil water contacts, tar-mats and residual oil saturations in the Frøy and Rind petroleum accumulations. *Journal of Petroleum Science and Engineering*, **23**, 41-63.

Bhullar, A. G., Karlsen, D. A., Backer-Owe, K., Seland, R.T. and Le Tran, K., 1999b. Dating reservoir filling – A case history from the North Sea. *Marine and Petroleum geology*, **16**, 581-603.

Bhullar, A.G., di Primio, R., Karlsen, D. A. and Gustin, D., 2001. Application of petroleum geochemical, fluid inclusion and PVT data. AAPG Hedberg Conference (May 9-13, 1999, Colorado Springs, Colorado). American Association of Petroleum Geologists, Memoir on Basin Modelling.

Bigge, M. A., Petch, G. S., Macleod, G., Larter, S. R., & Aplin, A. C., 1995. Quantitative geochemical analysis of petroleum fluid inclusions: problems and developments. *Abstracts of Organic Geochemistry, EAOG, San Sebastian*, September 1995.

Bigge, M.A. and Farrimond, P., 1998. Biodegradation of oils in the Wessex Basin: a complication of correlation. *In*: Underhill, J.R. (Eds) Development, Evolution and Petroleum Geology of the Wessex Basin. *Geological Society of London, Special Publication*, **133**, 373-386.

Bigge, M.A., 2000. Investigation of petroleum-bearing fluid inclusions. PhD. Thesis. University of Newcastle Upon Tyne, UK.

Bigge, M.A., Petch, G.S., Macleod, G., Larter, S.R. and Aplin, A.C., 1994. A new method for on-line crush gas chromatography and gas chromatography-mass spectrometry of petroleum containing fluid inclusions. *EAPG*, Aberdeen.

Bjørlykke, K., Ramm, M. and Saigal, G.C., 1989. Sandstone diagenesis and porosity modification during basin evolution. *Geologische Rundschau* 78, 243-268.

Bodnar, R.J., 1990. Petroleum migration in the Miocene Monterey Formation, California, USA: constraints from fluid inclusion studies. *Mineralogical Magazine*, **54**, 295-304.

Boote, D.R.D., Clark-Lowes, D.D., and Traut, M.W., 1998. Palaeozoic petroleum systems of North Africa, in Macgregor, D.S., Moody, R.T.J., and Clark-Lowes, D.D., (Eds). Petroleum Geology of North Africa: *Geological Society, London, Special Publication*, **132**, 7-68.

Bowler, B. F. J., Larter, S.R., Clegg., H., Wilkes, H. Horsfield, B. and Li, M., 1997. Dimethylcarbazoles in crude oils: comment on previous paper. *Analytical chemistry*, **69**, 3128-3129.

Brassell, S.C., Sheng, G., Fu, J. and Eglinton, G., 1988. Biological markers in lacustrine Chinese oil shales. In: Fleet, A.J. et al. (Eds), *Lacustrine Petroleum Source Rocks*, Blackwell, 299-308.

Brincat, D. and Larter, S.R., 1997. Influence of thermal maturity and secondary migration processes on the composition of a suite of source-related oils: a case study from the Central Graben, North Sea, UK. Abstracts, *18th International Meeting on Organic Geochemistry, Maastricht*, 237-238.

Brincat, D., 1996. The petroleum reservoir geochemistry of Kittiwake field: Implications for regional oil migration on the Kittiwake Platform. PhD. thesis. University of Newcastle Upon Tyne, UK.

Burely, S.D, Mullis, J., and Matter, A.., 1989. Timing diagenesis in the Tartan reservoir, North Sea-UK: Constraints from combined cathodoluminiscence microscopy and fluid inclusion studies. *Marine Petroleum Geology*, **6**, 98.

Burollet, P.F., Mugniot, J.M., and Sweeney, P., 1978. The geology of the Pelagian block; The margins and basins off southern Tunisia and Tripolitania, *in* Nairn, A.E.M., Kanes, W.H., and Stehli, F. G., eds., *The ocean basins and margins*: New York, Plenum Press, **4B**, 331–359.

Burruss C.R., 1981. Hydrocarbon fluid inclusions in studies of sedimentary diagenesis. Short course in fluid inclusions: Application to petrology. In Hollister l. S. and Cranford M. L. (Eds), *Mineralogical association of Canada*, **6**, 138-156.

Burruss, R.C., 1987. Diagenetic palaeotemperatures from aqueous fluid inclusions: re-equilibration of inclusions in carbonate cements by burial heating. *Mineralogical Magazine*, **51**, 477-481.

Burruss, R.C., 1992. Phase behaviour in petroleum-water (brine) systems applied to fluid inclusion studies, (abstract) Pacrofi IV, *Pan American Conference Research on fluid inclusions*, Program and abstracts, Lake Arrowhead, CA, **4**, 116-118.

Burruss, R.C., Cerone, K.R., and Harris, P.M., 1985. Timing of hydrocarbon migration: Evidence from fluid inclusions in calcite cements, tectonic and burial history. In: Carbonate Cements, Scheidermann, N. and Harris, P.M. (Eds), *SEPM Spec. Publ.*, **26**, 277-289.

Burruss, R.C., 1991. Practical aspects of fluorescence microscopy of petroleum fluid inclusions. Luminescence Microscopy: Quantitative and Qualitative Aspects, SEPM short course 25 Dallas, Texas. In Barker C. E. and Kopp O. C. (Eds), *Society of Sedimentary Geology*, 1-7.

Cassani, F., Gallango, O., Talukdar, S., Vallejos, C., Ehrmann, U., 1988. Methylphenanthrene maturity index of marine source rock extracts from the Maracaibo basin. *Organic Geochemistry* **13**, 73-80.

Chakhmakhchev, A. and Suzuki, M., 1995. Saturate biomarkers and aromatic sulfur compounds in oils and condensates from different source rock lithologies of Kazakhstan, Japan and Russia. *Organic Geochemistry* **23**, 289-299.

Chakhmakhchev, A., Suzuki, M., Takayama, K., 1997. Distribution of alkylated dibenzothiophenes in petroleum as a tool for maturity assessments. *Organic Geochemistry*, **26**, 483-490.

Chen, M., 1995. Response of pyrrolic and phenolic compounds to petroleum migration and in-reservoir processes. PhD. Thesis. University of Newcastle Upon Tyne, UK.

Clark, J.P. and Philp, R.P., 1989. Geochemical characterisation of evaporite and carbonate depositional environments and correlation of associated crud oils in the Black Creek Basin, Alberta. *Canadian Petroleum Geologists Bulletin*, **37**, 401-416.

Clegg, H., Horsfield, B., Wilkes, H., Sinninghe Damste, J., Koopmans, M.P., 1998b. Effect of artificial maturation on carbazole distributions, as revealed by the hydrous pyrolysis of an organic-sulphur-rich source rock (Ghareb Formation, Jordan). *Organic Geochemistry* **29**, 1953-1960.

Clegg, H., Wilkes, H. and Horsfield, B., 1997. Carbazole distributions in carbonate and clastic source rocks. *Geochimica et Cosmochimica Acta* 61, 5335-5345.

Clegg, H., Wilkes, H., Oldenburg, T. Santamaria-Orozco, D. and Horsfield, B., 1998a. Influence of maturity on carbazole and benzocarbazole distributions in crude oils and source rocks from the Sonda de Campeche, Gulf of Mexico. *Organic Geochemistry* **29**, 183-194.

Connan, J. and Cassou, A.M., 1980. Properties of gases and petroleum liquids derived from terrestrial kerogen at various maturation levels. *Geochimica et Cosmochimica Acta* 44, 1-23.

Connan, J. and Dessort, D., 1987. Novel family of hexcyclic hopanoid alkanes (C_{32}-C_{35}) occurring in sediments and oil from anoxic paleoenvironments. *Organic Geochemistry* **11**, 103-113.

Connan, J., 1984. Biodegradation of crude oils in reservoirs. In: Brooks, J. and Welte, D. Editors, 1984. *Advances in Petroleum Geochemistry 1984* 1 Academic Press, London, 299-335.

Connan, J., Bouroullec, J., Dessort, D., and Albrecht, P., 1986. The microbial input in carbonate-anhydrite facies of an Abkhaz palaeoenvironment from Guatemala: a molecular approach. In: Leythaeuser, D. and Rullkötter, J. (Eds) *Advances in Organic Geochemistry 1985*, *Organic Geochemistry* **10**, 29-50.

Cornford, C., Christie, O., Endresen, U., Jensen, P., and Myhr, M.B., 1988. Source rock and seep oil maturity in Dorset, Southern England. In: Mattavelli, L. and Novelli, L. (Eds) *Advances in Organic Geochemistry 1985*, *Organic Geochemistry* **13**, 399-409.

Cornford, C., Needham, C.E.J. and Walque, De L., 1986. Geochemical habitat of North Sea oils and gases. *Habitat of Hydrocarbons on the Norwegian Continental Shelf.* Graham & Trotman, London, 39-54.

Creany, S. and Allen, J., 1990. Hydrocarbon generation and migration in the Western Canada Sedimentary basin. In: Brooks, J. (Eds), Clastic Petroleum Provinces. London. *Geological Society Special Publication*, **50**, 189-202.

Cumbers, K.M., Alexander, R., Kagi, R.I., 1986. Analysis of methylbiphenyls and dimethylbiphenyls in crude oils. *Journal of Chromatography* **361**, 385-390.

Cumbers, K.M., Alexander, R., Kagi, R.I., 1987. Methylbiphenyl, ethylbiphenyl and dimethylbiphenyl isomer distributions in some sediments and crude oils. *Geochimica et Cosmochimica Acta* **51**, 3105-3111.

Curiale, J.A., 1992. Molecular maturity parameters within a single oil family: a case study from the Sverdrup Basin, Arctic Canada. In: Moldowan, J.M., Albrecht, P. and Philp, R.P. (Eds) *Biological Markers in Sediments and Petroleum*, Prentice-Hall, Englewood Cliffs, New Jersey, 275-300.

Dahl, B. and Spears, G. C., 1986. Geochemical significance of tar mat in the Oseberg field, Norwegian sector, North Sea. In: Leythaeuser, D., Rullkötter, J. (Eds.), Advances in Organic Geochemistry 1985. *Organic Geochemistry* **10**, 547-558.

Dahl, J., Hallberg, R., Kaplan, I.R., 1988. The effects of radioactive decay of uranium on elemental and isotopic ratios of Alum Shale kerogen. *Applied Geochemistry*, **3**, 583-589.

Daniels, R.P., and Emme, J.J., 1995, Petroleum system model, eastern Algeria, from source rock to accumulation; when, where, and how: *Proceedings of the Seminar on Source Rocks and Hydrocarbon Habitat in Tunisia*; Entreprise Tunisienne d'Activités Pétrolières Mémoir **9**, 101–124.

Dastillung, M. and Corbet, B., 1978. La Géochimie des sédiments marins profonds- I-hydrocarbures saturés et insaturés des sédiments. In*: Géochimie Organiques des sédiments marins profonds*, Organ II, Atlantique N .E., Brésil (Eds. A Canbaz and R. Pelet), 293-323. CNRS.

De Lapparent, C., 1961. Hassi Messaoud, giant of the Sahara is tribute to scientific oil search: *Oil and Gas International*, **1**, 43-46.

Debyser, Y., Pelet, R. and Dastillung, M., 1977. Géochimie Organique des sédiments marins récents: Mer Noire, Baltique, Atlantique (Mauritanie). In: *Advances in Organic Geochemistry*, 1975 (Eds. R Campos J Goni), 289-320. Enadimsa, Madrid.

Didyk, B.M., Simoneit, B.R.T., Brassell, S.C., Eglinton, G., 1978. Organic geochemical indicators of palaeoenvironmental conditions of sedimentation. Nature, **272**, 216-222.

Djarnia, M.R. and Fekirine, B., 1998. Sedimentological and diagenetic controls on Cambro-Ordovician reservoir quality in the southern Hassi Messaoud area, Saharan Platform, Algeria. In: Macgregor, D.S et al. (Eds) Petroleum Geology of North Africa 1998. Geological Society, London, Special Publication, **132**, 167-174.

Dorbon, M., Garrigues, P., Ignatiadis, I., Edward, M., Arpino, P. and Guiochon, G., 1984. Distribution of carbazole derivatives in petroleum. *Organic Geochemistry* 7, 111-120.

Earnshaw, J.P., Hogg, A.J.C., Oxtoby, N.H., Cawley, S.J., 1993. Petrographic and fluid inclusion evidence for the timing of diagenesis and petroleum entrapment in the Papuan Basin. Petroleum Exploration and development in Papuan New Guinea. *Proceeding of the second PNG Petroleum convention.* Port Moreshy. Carman, G. J. and Z., (Eds).

Emery, D., Robinson. A, 1993. Inorganic Geochemistry Applications to Petroleum Geology. Oxford, Blackwell Scientific Publications.

Emery, D., Smalley, P.C. and Oxtoby, N.H., 1993. Synchronous oil migration and cementation in sandstone reservoirs demonstrated by quantitative description of diagenesis. *Philosophical Transactions of the Royal Society*, **A344**, 115-125.

England, W.A., 1990. The organic geochemistry of petroleum reservoirs. *Organic Geochemistry*, **16**, 415-425.

England W. A., 1994. Secondary Migration and Accumulation of Hydrocarbons. In Magoon, L. B. and Dow W. G. (Eds). The petroleum system-from source to trap: *American Association of Petroleum Geologists*, Memoir **60**, 211-217.

England, W.A. and Mackenzie, A.S., 1989. Some aspects of the organic geochemistry of petroleum fluids. *Geologische Rundschau* 78, 291-303.

England, W.A., Mackenzie, A.S., Mann, D.M. and Quigley, T.M., 1987. The movement and entrapment of petroleum fluids in the subsurface. *Journal of the Geological Society London* 144, 327-347.

England, W.A., Mann, A.L. and Mann, D.M., 1991. Migration from source to trap. In: Merrill, R.K. (Eds) Source and migration processes and evaluation techniques. Treatrise of petroleum geology, *American Association of Petroleum Geologists Bulletin* Oklahoma, 23-46.

Ensminger, A., Joly, G. and Albrecht, P., 1978. Rearranged steranes in sediments and crude oils, Tetrahedron Letters, **18**, 1575-1578.

Etminah, H. and Hoffmann, C.F., 1989. Biomarkers in fluid inclusions: A new tool in constraining source regimes and its implications for genesis of Mississippi Valley-type deposits. Geology, **17**, 19-22.

Fan Pu, Philp R. P., Zhenxi L. and Guangguo Y. (1990) Geochemical characteristics of aromatic hydrocarbons of crude oils and source rocks from different sedimentary environments. *Organic Geochemistry.* **16**, 427-435.

Fennouh, A., 1996. Pétrologie des réservoirs gréseux, Exemple de l'évolution diagénétique du gisement pétrolier d'Hassi Messaoud, Algérie (Application aux potentialités de production). Thèse présentée à l'université Louis Pasteur de Strasbourg pour l'obtention du diplôme de docteur en science de la terre.

Fisher, S.J., Alexander, R., Kagi, R.I., 1996. Biodegradation of alkylnaphthalenes in sediment adjacent to an offshore petroleum production platform. *Polycyclic Aromatic Compounds* **11**, 35-42.

Fisher, S.J., Alexander, R., Kagi, R.I., Oliver, G.A., 1998. Aromatic hydrocarbons as indicators of petroleum biodegradation in North Western Australian reservoirs. In: Purcell, R.R. (Eds.), The Sedimentary Basins of Western Australia 2,

Proceedings of Petroleum Exploration Society Symposium, Perth, 1998, 185-194.

Fisher, S.J., Alexander, R., Kagi, R.I., 1995. Biodegradation of aromatic hydrocarbons in sediments adjacent to an off-shore petroleum development and production platform. *Polycyclic Aromatic Compounds* **9**, 257-264.

Forster, P. G., Alexander, R., Kagi, R. I., 1989. Identification and analysis of tetramethylnaphthalenes in petroleum. *Journal of Chromatography* **483**, 384-389.

Fowler, M.G. and Douglas, A.G., 1984. Distribution and structure of hydrocarbons in four organic-rich Ordovician rocks. *Organic Geochemistry*, **6**, 105-114.

Fowler, M.G., Abolins, P. and Douglas, A.G., 1986. Monocyclic alkanes in Ordovician organic matter. In: *Advances in Organic Geochemistry1985,* Leythaeuser, D. and Rullkötter, J. (Eds), 815-823, Pergamon Press Oxford.

Frolov, Y.B., 1997. Liquid chromatography of petroleum carbazoles. *Organic Geochemistry* **26**, 43-47.

Frolov, Y.B., Smirnov, M.B., Vanyukova, N.A. and Sanin, P.I., 1989. Carbazoles of crude oil. *Petroleum Chemistry, USSR*, **29**, 87-102.

Fu, J., Sheng, G. and Liu, D., 1988. Organic geochemical characteristics of major types of terrestrial source rocks in China: In: Fleet, A.J. et al. (Eds), *Lacustrine Petroleum Source Rocks*, Blackwell, 279-289.

Fu, J., Sheng, G., Pang, P., Brassell, S, C., Eglinton, G. and Jiang, J., 1986. Peculiarities of salt lake sediments as potential source rocks in China. *Organic Geochemistry* **10**, 119-126.

Garrigues, P., De Vazelhes-De Surry, R., Angelin, M.L., Ewald, M., Oudin, J.L., Connan, J., 1984. Analysis of series of aromatic isomers by high resolution spectrofluorometry and capillary gas chromatography in HPLC fractions of crude petroleums and sedimentary rock extracts. In: Schenck, P.A., de leeuw, J.W., Lijmbach, G.W.M., (Eds.), *Advances in Organic Geochemistry* 1983. Pergamon Press, Oxford, 829-837.

George, S.C., Rubble, T.E., Dutkiewicz, A., Eadington, P.J., 2001. Assessing the maturity of oil trapped in fluid inclusions using molecular geochemistry data and visually-determined fluorescence colours. *Applied Geochemistry* **16**, 451-473.

George, C.S., Lisk, M., Eadington, P.J, Krieger, F.W., Quezada, R.A., Greenwood, P.F., and Wilson, M.A., 1997c. Fluid Inclusion Record of Early Oil Preserved at Jabiru Field, Vulcan Sub-basin. *Exploration Geophysics* **28**, 66-71.

George, S.C., Greenwood, P.F., Logan, G.A., Quezada, R.A., Pang, L.S.K., Lisk, M., Krieger, F.W. and Eadington, P. J., 1997b. Comparison of Palaeo oil charges with currently reservoired hydrocarbons using molecular and isotopic analyses of oil-bearing fluid inclusions: Jabiru Oil Field, Timor Sea. *Australian Petroleum Production and Exploration Association Journal* **37** (1), 490-504.

George, S.C., Krieger, F.W., Eadington, P.J., Quezada, R.A., Greenwood, P.F., Eisenberg, L. I., Hamilton, P. J. and Wilson, M. A., 1997a. Geochemical

comparison of oil-bearing fluid inclusions and produced oil from the Toro sandstone, Papua New Guinea. *Organic Geochemistry* **26**, 155-173.

George, S.C., Lisk, M., Eadington, R.A, Quezada, F.W, Krieger, P.F., 1996. Comparison of palaeo oil charges with currently reservoired hydrocarbons using the geochemistry of oil-bearing fluid inclusions. *Society of Petroleum Engineers*, SPE 36980, Asia Pacific Oil and Gas Conference, 28-31 October, Adelaide, Australia, 159-171.

George, S.C., Lisk, M., Summons, R.E. and Quezada, R.A., 1998. Constraining the oil charge history of the South Pepper oil field from the analysis of oil-bearing fluid inclusions. *Organic Geochemistry* **29**, 631-648.

Goldstein, R.H. and Reynolds, T.J., 1994. Systematics of fluid inclusions in diagenetic minerals. SEPM, *Society for Sedimentary Geology*, Short Course, **51**, 199 p.

Golovko, A. and Ivanov, V., 1999. Changes in triarene composition on the oil filtration through various minerals. In: Abstracts of *19th International Meeting on Organic Geochemistry*, Istanbul, 1999.

Gong, C., Otten, G.A., Richardson, M., Tseng, H.Y, Noke, K., Bennett, B., and Larter, S.R., 2001. Simulating hydrocarbon migration: studying the effects of geochromatography on crude oil compositions. 20th *International meeting on Organic Geochemistry*, Nancy, France, 2001.

Grantham, P.J. and Wakefield, L.L., 1988. Variations in the sterane carbon number distributions of marine source rock derived crude oils through geological time. *Organic Geochemistry*, 12, 61-73.

van Graas, G.W., 1990. Biomarker maturity parameters for high maturities: Calibration of the working range up to the oil/condensate threshold. In: Durand, B. and Behar, F. (Eds) *Advances in Organic Geochemistry 1989, Organic Geochemistry* **16**: 1025-1032.

Greibrokk, T. Lundanes, E., Norli, H.R., Dyrstad, K. and Olsen, S.D., 1994. Experimental simulation of oil migration – Distribution effects on organic compound groups and on metal/metal ratios. *Chemical Geology*, **116**, 281-299.

Guilhaumou, N., Szydlowskii, N. and Pradier, B., 1990. Characterisation of hydrocarbon fluid inclusions by infra-red and fluorescence microspectrometry. Mineralogical Magazine, **54**, 311-324.

Hall, P.B. Schou, L., and Bjorøy, M., 1985. Aromatic hydrocarbon variations in North Sea wells. In: Thomas, B.M. et al. (Eds) *Petroleum Geochemistry in Exploration of the Norwegian Shelf*, Graham and Trotman, London, 293-301.

Hammouda, A., 1980. Petroleum potential – Ouargla region, Triassic basin, Algeria. *American Association of Petroleum Geologists Memoir,* **30,** 539-541.

Hazeldine, R.S., Samson, I.M., and Cornford, C., 1984. Dating diagenesis in petroleum basin, a new fluid inclusion method, *Nature*, **307**, 354-357.

Hillebrand, T. and Leythaeuser, D., 1992. Reservoir geochemistry of Stockstadt oilfield: compositional heterogeneities reflecting accumulation history and

multiple source input. *Advances in Organic Geochemistry 1991, Organic Geochemistry,* **19**, 119-131.

Hills, I.R., Whitehead, E.V., Anders, D.E., Cummins, J.J. and Robinson, W.E., 1966. An optically active triterpane, gammacerane in Green River, Colorado, oil shale bitumen. *Journal of the Chemical Society, Chemical Communications*, **20**, 752-754.

Hobson, G.D, and Tiratsoo, E.N., 1975. *Introduction to Petroleum Geology*, Scientific Press Ltd., Beaconsfield, 300 pp.

Hoffmann, C.F., Foster, C.B., Powell, T.G., and Summons, R.E., 1987. Hydrocarbon biomarkers from Ordovician sediments and the fossil alga *Gloeocapsomorpha prisca* Zalesky 1917. *Geochimica et Cosmochimica Acta,* **51**, 2681-2697.

Holba, A. G., Dzou, L. I. P., Hickey, J. J., Franks, S. G., May, S. J. and Lenney, T. 1996. Reservoir geochemistry of South Pass 61 Field, Gulf of Mexico: compositional heterogeneities reflecting filling history and biodegradation. *Organic Geochemistry*. **24**, 1179-1198.

Holba, A.G., Ellis, L., Dzou, I.L. Hallam, A., Masterson, W.D. Francu, J. and Fincannon, A.L., 2001. Extended tricyclic terpanes as age discriminators between Triassic, Early Jurassic and Middle-Late Jurassic oils. *20th International Meeting on Organic Geochemistry*, Nancy-France, 2001.

Horsfield, B. and McLimans, R.K., 1984. Geothermometry and geochemistry of aqueous and oil-bearing fluid inclusions from Fateh Field, Dubai, *Organic Geochemistry* **6**, 733-740.

Horsfield, B., Bharati, S., Larter, S.R., Leistner, F., Littke, R., Schenk, H.J., Dypvik, H., 1992. On the typical petroleum-generating characteristics of Alginite in the Cambrian Alum Shale. In: Schidlowski, M. et al. (Eds), *Early Organic Evolution: Implications for Mineral and Energy Resources*. Springer-Verlag Berlin Heidelberg 1992.

Horsfield, B., Clegg, H., Wilkes, H. and Santamaria-Orozco, D. 1998. Maturity control of carbazole distributions in petroleum systems. *Naturwissenschaften* **85**, 233-237.

Horstad, I. and Larter, S.R., 1997. Petroleum migration, alteration, and remigration within Troll Field, Norwegian North Sea. *American Association of Petroleum Geologists Bulletin* **81,** 222-248.

Horstad, I., Larter, S.R., and Mills, N., 1995. Migration of hydrocarbons in the Tampen Spur area, Norwegian North Sea: a reservoir geochemical evaluation. In *The Geochemistry of Reservoirs*, ed. J. M. Cubitt and W. A. England, *Geological Society* Special Publication **86,** 159-183.

Horstad, I., Larter, S.R., Dypvic, H., Aagaard, P., Bjørnvik, A.M., Johansen, P. E. and Eriksen, S. 1990. Degradation and maturity controls on oil field petroleum column heterogeneity in the Gullfaks field, Norwegian North Sea. Advances in Organic Geochemistry. *Organic Geochemistry* **16**, 497-510.

Huang, H. and Pearson, M.J., 1999. Source rock paleoenvironments and controls on the distribution of dibenzothiophenes in lacustrine crude oils, Bohai Bay Basin, eastern China. *Organic Geochemistry*, **30**, 1455-1470.

Huang, W-Y. and Meinschein, W.G., 1979. Sterols as ecological indicators. *Geochimica et Cosmochimica Acta,* **43**, 739-745.

Hughes, W.B., 1984 Use of thiophenic organosulfur compounds in characterizing crude oils derived from carbonate versus siliciclastic sources. In petroleum Geochemistry and Source rock Potential of Carbonate Rocks (edited by Palacas J. G.), *AAPG Studies in Geology* **18**, 181-196.

Hughes, W.B., Holba, A.G., Miller, D.E., and Richardson, J.S., 1985. Geochemistry of greater Ekofisk crude oils. In: *Geochemistry in Exploration of the Norwegian Shelf* (B.M Thomas. Ed.), Graham and Trotman, 75-92.

Hwang, R.J., Sundararaman, P. Teerman, S.C. and Schoell, M., 1989. Effect of preservation on geochemical properties of organic matter in immature lacustrine sediments. *14th International Meeting on Organic Geochemistry 1989*, Paris, 18-22

Isaksen, G.H., Pottorf, R.J. and Jensen, A.I., 1998. Correlation of fluid inclusions and reservoired oils to infer trap and fill history in the South Viking Graben, North Sea. *Petroleum Geoscience* **4**: 41-55.

Jacobson, S.R, Hatch, J.R., Teerman, S.C. and Askin, R.A., 1988. Middle Ordovician organic matter assemblages and their effect on Ordovician-derived oils. *American Association of Petroleum Geologists Bulletin* **72,** 1090-1100.

Jasper, J.P. and Gagossian, R.B., 1993. The relationship between organic carbon isotopic composition and organic biomarker compound concentration. *Geochimica Cosmochimica Acta* **57**, 177-186.

Jiang, Z.S. and Fowler, M.G., 1986. Carotenoid-derived alkanes in oils from northwestern China. *Organic Geochemistry* **10**, 831-839.

Jixi, S., Benchao, L., Fu Jiamo, Dehan, L. And Pingan, P. 1987. Organic inclusions and their relations to oil and gas occurrences. Advances in Organic Geochemistry. *Organic Geochemistry* **13**, 1101-1107.

Jones, D.M., Macleod G., 2000. Molecular analysis of petroleum in fluid inclusions: a practical methodology. *Organic Geochemistry* **31**, 1163-1173.

Jones, D.M., Macleod, G., Larter, S.R., Hall, D.L., Aplin, A.C. and Chen, M., 1996. Characterisation of the molecular composition of included petroleum. In: Brown, P.E. and Hagemann, S.G. (Eds*), Biennal Pan-American Conference on Research on Fluid Inclusions (PAC ROFI VI)*, Wisconsin, USA, 64-65.

Jourdan, A., Thomas, M., Brevart, O., Robson, P., Sommer, F. and Sullivan, M., 1987. Diagenesis as the control of the Brent sandstone reservoir properties in the Greater Alwyn area, East Shetland Basin. In: Glennie and Brookes, J. (Eds), *Petroleum Geology of North West Europe*, 951-961.

Jovancicevic, B., Vuèelic, D., Šaban, M., Wehner, H., 1992. Evaluation pf the effects of native minerals on the organic matter of Aleksinac oil shale based on the composition of free and bound bitumens. *Organic Geochemistry* **18**, 511-519.

Jovancicevic, B., Vuèelic, D., Šaban, M., Wehner, H., Victorovic, D., 1993. Investigation of the catalytic effects of indigenous minerals in the pyrolysis in Aleksinac oil shale substrates: steranes, triterpanes and triaromatic steroids in the pyrolysates. *Organic Geochemistry* **20**, 69-76.

Karlsen, D. A., Larter, S.R., 1991. Analysis of petroleum fractions by TLC-FID: applications to petroleum reservoir description, *Organic Geochemistry* **17**, 603-617.

Karlsen, D. A., Nedkvitne, T., Larter, S. R. And Bjørlikke, K. 1993. Hydrocarbon composition of authigenic inclusions: Application to elucidation of petroleum reservoir filling history. *Geochimica et Cosmochimica Acta.* **57**, 3641-3659.

Karlsen, D.A. and Larter, S.R., 1989. A rapid correlation method for petroleum population mapping within individual petroleum reservoirs: Application to petroleum reservoir description. In: Correlation in Hydrocarbon Exploration, *Norwegian Petroleum Society*, Graham and Trotman, 77-85.

Kihle, J., 1996. Adaptation of florescence excitation-emission micro-spectroscopy for characterisation of single hydrocarbon fluid inclusions. *Organic Geochemistry* **23**, 1029-1042.

Klett, T. R., 2000. Total Petroleum Systems of the Trias/Ghadames Province, Algeria, Tunisia, and Libya. The Tannezuft-Oued Mya, Tanezzuft-Melrhir, and Tannezuft-Ghadames. *U.S. Geological Survey Bulletin* 2202-C, 1-22.

Kline, 1994. An easy Guide to Factor Analysis. Routeledge, London and New York.

Kolaczkowska, E., Slougui, N-E., Watt, D.S., Maruca, R.E., and Moldowan, J.M., 1990. Thermodynamic stability of various alkylated dealkylated and rearranged 17α- and 17β-hopane isomers using molecular mechanics calculations. In Durand, B. and Behar F., (Eds) *Advances in Organic Geochemistry 1989, Organic Geochemistry*, **16**, 1033-1038.

Krooss, B.M., Brothers, L., Engel, M.H., 1991. Geochromatography in petroleum migration: a review. In: England, W.A and Fleet, A.J. (Eds) Petroleum migration, *Geological Society of London Special Publication*, **59**, 149-163.

Kvalheim, O.M., 1987.Oil-source correlation by the combined use of principal component modelling, analysis of variance and coefficient of congruence. *Chemometrics and Intelligent laboratory Systems*, **2**, 127-136.

L'Homer, A., 1967. Précisions sur la lithologie et la sédimentologie des grès du Cambrien (Zones Ri et Ra) a Hassi Messaoud sud : Publication du service Géologique de l'Algérie, **35**, 105-125.

Laresse, R.E. and Hall, D.L., 1996. Studying petroleum migration with fluid inclusions: Results from hydrothermal burial simulation experiments. In: Brown, P.E. and Hagmann, S.G. (Eds), *Biennal Pan American Conference on Research on Fluid Inclusions (PACROFI VI)*, 319-330. Wisconsin, USA: Madison.

Larter, S.R. And Mills, N., 1990. Phase-controlled molecular fractionations in migrating petroleum charges. Petroleum migration, *Geological Society*, London *Special Publication* **59**, 137-147.

Larter, S.R., Bjørlykke, K.O., Karlsen, D.A., Nedkvitne, T., Eglinton, T., Johansen, P.E., Leythaeuser, D., Mason, P.C., Mitchell, A.W. and Newcomb, G.A., 1990. Determination of petroleum accumulation histories: examples from the Ula field, Central Graben, Norwegian North Sea. In: Buller et al. (Eds) *North Sea Oil and Gas Reservoir – II*, Graham and Trotman, London, 319-330.

Larter, S.R. And Horstad, I., 1992. Migration of petroleum into Brent Group reservoirs: some observations from the Gullfaks field, Tampen Spur area North Sea. Geology of the Brent Group. *Geological society*, Special Publication No. **61**, 111-452.

Larter, S. R. and A. C. Aplin, 1995. Reservoir geochemistry: methods, applications and opportunities. The Geochemistry of Reservoirs. J. M. Cubitt and W. A. England. London, *Geological Society* **86**, 5-32.

Larter, S. R., Li, M., Bowler, B.F.J., Taylor, P., Chen, M., Noke, K. and Allan, J., 1995. Petroleum Secondary Migration—Geochemical Constraints on Migration Efficiency and Effects on Aromatic Hydrocarbon Distributions. In: *Organic Geochemistry: Developments and Applications to Energy, Climate, Environment and Human History*, Grimalt, J. O. and Dorronsoro, C. (Eds), 286-287. European Association of Organic Geochemists, Donostia-San Sebastian

Larter, S.R., Bowler, B.F.J., Li, M., Chen, M., Brincat, D., Bennett, B., Noke, K., Donohoe, P., Simmons, D., Kohnen,. M, Allan, J., Telnaes, N., and Horstad, I., 1996a. Molecular indicators of secondary oil migration distances. *Nature* **383**, 593-597.

Larter, S.R., Taylor, P.N., Mei, C., Bowler, B.F.J., Ringrose, P., and Horstad, I., 1996b. Secondary migration - visualizing the invisible - what can geochemistry potentially do? *In:* Glennie K. and Hurst A. (Eds) N.W. Europe's Hydrocarbon Industry, *Geological Society of London Special Publication*, 137-143.

Larter, S.R., Bowler, B.F.J., Clarke, E., Wilson, C., Moffat, B. Bennett, B., Yardley, G. and Carruthers, D., 2000. An experimental investigation of geochromatography during secondary migration of petroleum performed under subsurface conditions with a real rock. *Geochemical Transactions* **9**.

Lasater, J.A., 1958. Bubble point pressure correlation. *Petroleum Transactions, AIME*, **213**, 379-381.

Leischner, K. Welte, D. H. And Littke, R. 1993. Fluid inclusions and organic maturity parameters as calibration tools in basin modelling. *Basin modelling: Advances and Applications* edited by Doré, A. G. et al. *NPF Special publication* **3**, 161-172, Elsevier, Amsterdam.

Lewan, M. and Buchardt, B., 1989. Irradiation of organic matter by uranium decay in the Alum shale, Sweden, *Geochimica et Cosmochimica Acta* **53**, 1307-1322.

Leythaeuser, D. And Rückheim, J. 1989. Heterogeneity of oil composition within a reservoir as a reflection of accumulation history. *Geochimica et Cosmochimica Acta* **53**, 2119-2123.

Leythaeuser, D. and Schaefer, R.G., 1984. Effects of hydrocarbon expulsion from shale source rocks of high maturity in Upper Carboniferous strata of the Ruhr area, Federal Republic of Germany. *Organic Geochemistry*, **6**, 671-681.

Leythaeuser, D., Schwark, L., Keuser, Ch. 2000. Geological conditions and geochemical effects of secondary petroleum migration and accumulation. *Marine and Petroleum Geology* **17**, 857-859.

Li, M., Larter, S.R., Stoddart, D. and Bjoroy, M., 1992. Practical liquid chromatographic separation schemes for pyrrolic and pyridinic nitrogen aromatic heterocycle fractions from crude oils suitable for rapid characterisation of geochemical samples. *Analytical Chemistry* 64, 1337-1344

Li, M. and Larter, S.R., 1993. Interactions of organic nitrogen species in crude oils with minerals, water and organic networks: implications for petroleum geochemistry, American Chemical Society Abstracts.

Li, M., Larter, S.R. and Frolov, Y.B., 1994. Adsorptive interactions between petroleum nitrogen compounds and organic/mineral phases in subsurface rocks as models for compositional fractionation of pyrrolic nitrogen compounds in petroleum during petroleum migration. *Journal of High Resolution Chromatography*, **17**, 230-236.

Li, M., Larter, S.R., Mei, B. and Wu, T., 1995a. Maturity assessment of "immature oils" produced from the Shahejie Formation of the Liaohe Basin, N. E. China.

Li, M., Larter, S.R., Stoddart, D. and Bjorøy, M., 1995b. Fractionation of pyrrolic nitrogen compounds in petroleum during migration: derivation of migration-related geochemical parameters. In *The Geochemistry of Reservoirs*, ed. J. M. Cubitt and W. A. England. *Geological Society, London, Special Publication,* **86**, 103-123

Li, M., Huanxin, Y., Stasiuk, L.D., Fowler, M.G. and Larter, S.R., 1997. Effect of maturity and petroleum expulsion on pyrrolic nitrogen compound yields and distributions in Duvernay Formation petroleum source rocks in Central Alberta, Canada. *Organic Geochemistry* 26, 731-744

Li, M., Osadetz, K.G., Yao, H., Obermajer, M., Fowler, M.G., Snowdon, L.R. and Christensen, R., 1998. Unusual crude oils in the Canadian Williston Basin, south-eastern Saskatchewan. *Organic Geochemistry* **28**, 477-488.

Lisk, M., George, S.C., Summons, R.E., Quezada, R.A., O'Brien, G.W., 1996. Mapping hydrocarbon charge histories: Detailed characterisation of the South Pepper oil field, Carnarvon Basin. *Aust. Petrol. Prod. Explor. Assoc. J.* **36**, 445-464.

Lüning, S., Craig, J., Loydell, D.K., Štorch P., and Fitches B., 2000. Lower Silurian "hot shales" in North Africa and Arabia: regional distribution and depositional model. *Earth-Science Reviews*, vol. **49**, 121-200.

Macgregor, D.S., 1996. The hydrocarbon systems of North Africa. *Marine and Petroleum Geology*, **13**, 329-340.

Macgregor, D.S., 1998. Giant fields, petroleum systems and exploration maturity of Algeria, *in* Macgregor, D. S., Moody, R. T. J., and Clark-Lowes, D. D., eds.,

Petroleum geology of North Africa: *Geological Society*, London, Special Publication **132**, 79–96.

Mackenzie, A. S., Patience, R. L., Maxwell, J. R., Vandenbroucke, M., Durand, B., 1980. Molecular parameters of maturation in the Toarcian shales, Paris Basin, France-I. Changes in the configuration of acyclic isoprenoid alkanes, steranes and triterpanes. *Geochimica et Cosmochimica Acta* **44**, 1709-1721.

Mackenzie, A.S. and Quigley, T.M., 1988. Principles of geochemical prospect appraisal. *American Association of Petroleum Geologists Bulletin*, **72**, 399-415.

Mackenzie, A.S. Rullkötter, J., Welte, D.H. and Mankiewicz, P., 1985. Reconstruction of oil formation and accumulation in North Slope, Alaska, using gas chromatography-mass spectrometry. In: Magoon, L.B. and Claypool, G.E. (Eds), Alaska North Slope Oil/Source Rock Correlation Study. *American Association of Petroleum Geologists Studies in Geology*, **20**, 319-377.

Mackenzie, A.S., Hofmann, C.F. and Maxwell, J.R., 1981. Molecular parameters of maturation in the Toarcian shales, Paris Basin, France. III. Changes in the aromatic steroid hydrocarbons. *Geochimica et Cosmochimica Acta* **45**, 1345-1355.

Mackenzie, A.S., Ren-Wei, L., Maxwell, J.R., Moldowan, J.M. and Seifert, W.K., 1983. Molecular parameters of maturation in the Cretaceous shales. From the Overthrust Bel, Wyoming, USA. In: Bjorøy, M. et al. (Eds), Advances in *Organic Geochemistry 1981*, J. Wiley and Sons, Chichester, 496-503.

Macleod, G., Larter, S.R., and Aplin, A.C. and Bigge, A.M., 1995. The application of petroleum bearing fluid inclusions to tracking petroleum evolution in the subsurface. *EAPG 57th Conference and Technical Exhibition*, Glasgow, Scotland. Extended abstracts, **2**, F033.

Macleod, G., Larter, S.R., and Aplin, A.C. and Petch, G.S., 1994. Improved analysis of petroleum fluid inclusions-Application to reservoir studies. *Abstracts of the American Chemical Society*, **207**, 132.

Macleod, G., Petch, G.S., Larter, S.R., and Aplin, A.C., 1993. Investigations of the composition of hydrocarbon fluid inclusions. In: *Abstracts of the American Chemical Society*, **205**, 86.

Magoon, L. B., and Dow, W. G., 1994, The petroleum system, *in* Magoon, L. B., and Dow, W. G., eds., The petroleum system—From source to trap: *American Association of Petroleum Geologists* Memoir **60**, 3–24.

Makhous, M., Galushkin, Y., and Lopatin, N., 1997a, Burial history and kinetic modelling for hydrocarbon generation, part I: The GALO model: *American Association of Petroleum Geologists Bulletin*, **81**, 1661–1678.

Makhous, M., Galushkin, Y., and Lopatin, N., 1997b, Burial history and kinetic modelling for hydrocarbon generation, part II, Applying the GALO model to Saharan basins: *American Association of Petroleum Geologists Bulletin*, **81**, 1679–1699.

Malenfer, J. and Tillous, A., 1963. Etude du champ d'Hassi Messaoud. Stratigraphie, aspect structural, étude de détail du réservoir. *Revue de l'Institut Français du Pétrole*, 18, hors série.

Mann, A.L., Goodwin, N.S. and Lowe S., 1987. Geochemical characteristics of lacustrine source rocks: A combined palynological/molecular study of a Tertiary sequence from offshore China. In: Proceedings of the Indonesian Petroleum Association, 16th Annual Convention. Jakarta, *Indonesian Petroleum Association*, **1**, 241-258.

Marynowski L., Czechowski, F., Simoneit, B. R. T., 2001. Phenylnaphthalenes and polyphenyls in Palaeozoic source rocks of the Holy Cross Mountains, Poland. *Organic Geochemistry* **32**, 69-85.

Mason, P.C., Burwood, R. and Mycke, B., 1995. The reservoir geochemistry and petroleum charging histories of Palaeogene-reservoired fields in the Outer Witch Ground Graben. In *The Geochemistry of Reservoirs*, ed. J. M. Cubitt and W. A. England. *Geological Society* Special Publication **86,** 203-256.

Massa, D., Ruhland, M. and Thouvenin, J., 1972. Structure de fracturation du champ d'Hassi Messaoud, Algérie. *Revue de l'Institut Français du Pétrole*, **4** et **5**, 489-713.

McKirdy, D.M., Aldridge, A.K. and Ypma, P.J.M., 1983. A geochemical comparison of some crude oils from Pre-Ordovician carbonate rocks. In: *Advances in Organic Geochemistry 1981*, Bjoroy, M. et al. (Eds), Wiley, J. and Sons, New York, 99-107.

McKirdy, D.M., Kantsler, A.J., Emmett, J.K. and Aldridge, A.K., 1984. Hydrocarbon genesis and organic facies in Cambrian carbonates of the eastern Officer Basin, South Australia. In: Petroleum Geochemistry and Source Rock Potential of carbonate Rocks, Palacas, J. (Eds). *American Association of Petroleum Geologists,* Studies in Geology No **18**, 13-31.

McLimans, R.K., 1987. The application of fluid inclusions to migration of oil and diagenesis in petroleum reservoirs. *Applied Geochemistry*, **2**, 585-604.

Meglen, R.R., 1992. Examining large databases, a chemometric approach using principal component analysis. Marine Chemistry, **39**, 217-237.

Mello, M.R., Gaglianone, P.C., Brassell, S.C. and Maxwell, J.R., 1988a. Organic geochemical and biological marker assessment of depositional environments using Brazilian offshore oils. Marine and Petroleum Geology, **5**, 205-223.

Mello, M.R. Telnaes, N., Gaglianone, P.C., Chicarelli, M.I., Brassell, S.C. and Maxwell, J.R., 1988b. Organic geochemical characterisation of depositional palaeoenvironments of source rocks and oils in Brazilian marginal basins. In: Mattavelli, L. and Novelli, L. (Eds). *Advances in Organic Geochemistry 1987, Organic Geochemistry*, **13**, 31-46.

Miles, J.A. 1990. Secondary Migration Routes in the Brent Sandstones of the Viking Graben and East Shetland Basin: Evidence from Oil Residues and Subsurface Pressure Data. *The American Association of petroleum Geologists Bulletin,* **74,** 1718-1735.

Moldowan, J.M., Fago, F.J., Carlson, R.M.K., Yong, D.C., Duyne, Van G., Clardy, J., Schoell, M. Pillinger, C.T. and Watt, D.S., 1991.Rearranged hopanes in sediments and petroleum. *Geochimica et Cosmochimica Acta* **55**: 3333-3353.

Moldowan, J.M., Lee, C.Y., Sundararaman, P., Salvatori, T., Alajbeg, A., Gjukic, B., Demaison, G.J., Slougui, N-E. and Warr, D.S., 1992. Source correlation and maturity assessment of selected oils and rocks from Central Adriatic Basin (Italy and Yugoslavia). In: Moldowan, J.M., Albrecht, P. and Philp, R.P. (eds) *Biological Marker In Sediments and Petroleum*, Prentice-Hall, Englewood Cliffs, New Jersey, 370-401.

Moldowan, J.M., Seifert, W.K., and Gallegos, E.J., 1983. Identification of an extended series of tricyclics terpanes in petroleum. *Geochimica et Cosmochimica Acta* **47**, 1531-1534.

Moldowan, J.M., Seifert, W.K., Gallegos, E.J., 1985. Relationship between petroleum composition and depositional environment of petroleum source rocks. *American Association of Petroleum Geologists Bulletin,* **69**, 1255-1268.

Moldowan, J.M., Sundararaman, P., Schoell, M., 1986. Sensitivity of biomarker properties to depositional environment and/or source input in the Lower Toarcian of SW. Germany. *Organic Geochemistry* **10**, 915-926.

Montadert, L., 1963. La sédimentologie et l'étude détaillée des hétérogénéités d'un réservoir. Application au gisement d'Hassi Messaoud. *Revue de l'Institut Français du Pétrole*, **18**, hors série.

Moors, M., Massart, D.L. and McDowall, R.D., 1994. Analyte isolation by solid phase extraction (SPE) on silica-bonded phases. *Pure and Applied Chemistry*, **66**, 277-304.

Munz, I. A., Johansen, H., Holm, K., & Lacharpagne, J. C., 1999. The petroleum characteristics and filling history of the Frøy field and the Rind discovery, Norwegian North Sea. *Marine and Petroleum Geology* **16**, 633 – 651.

Munz, I.A., 2001. Petroleum inclusions in sedimentary basins: systematics, analytical methods and applications. *Lithos* **55**, 195-212.

Murray, R.C., 1957. Hydrocarbon fluid inclusions in quartz. *American Association of Petroleum Geologists Bulletin*, **41**, 950-956.

Nagy, B., 1960. Review of the chromatographic "plate" theory with reference to fluid flow in rocks and sediments, *Geochimica et Cosmochimica Acta*, **19**, 289-296.

Narr, W.M. and Burrus, R.C., 1984. Origin of reservoir fractures in Little Knife Field, North Dakota. *American Association of Petroleum Geologists,* **68**, 1087-1100.

Nedkvitne, T., Karlsen, D. A., Bjørlykke, K. and Larter, S. R. 1993. Relationship between reservoir diagenetic evolution and petroleum emplacement in the Ula Field, North Sea. *Marine and petroleum Geology*, **10**, 255-270.

Noble, R., Alexander, R. and Kagi, R.I., 1985. The occurrence of bisnorhopane, trisnorhopane and 25-norhopanes as free hydrocarbons in some Australian shales. *Organic Geochemistry*, **8**, 171-176.

Odeh, A., 1975. El Agreb-El Gassi oil fields, Central Algerian Sahara. *American Association of Petroleum Geologists,* **59**, 1676-1684.

Oxtoby, N.H, Mitchell, A.W. and Gluyas, J.G., 1995. The filling and empting of the Ula Oilfield: fluid inclusion constraints. The Geochemistry of Reservoirs. In: Cubitt, J.M. and England, W.A. (Eds), *Geological Society Special Publication,* **86**, 257-279.

Palacas, J.G., Anders, D.E., and King, J.D., 1984. South Florida Basin – A prime example of carbonate source rocks of petroleum. In: Palacas, J.G. (Eds) Petroleum Geochemistry and Source Rock Potential of Carbonate Rocks, AAPG studies in Geology, No 18. *The American Association of Petroleum Geochemists*, Tulsa, Oklahoma, 71-96.

Palmer, S., 1984. Effect of water washing on C_{15}+ hydrocarbon fraction of crude oils from northwest Palawan, Philippines. *AAPG Bulletin* **268**, 137-149.

Parfitt, M. and Farrimond, P., 1998. The Mupe Bay Oil Seep: a detailed organic geochemical study of a controversial outcrop. In: Underhill, J.R. (Eds) Development, Evolution and Petroleum Geology of the Wessex Basin. *Geological Society of London, Special Publication,* **133**, 387-397.

Parnell, J., Carey, P.F., Monson, B., 1996. Fluid inclusions constraints on temperatures of petroleum migration from authigenic quartz in bitumen veins. *Chemical Geology,* **129**, 217-226.

Parnell, J., Carey, P. and Duncan, W., 1998. History of hydrocarbon charge on the Atlantic margin: Evidence from fluid-inclusion studies, West of Shetland. *Geology.* **26,** 807-810.

Pedersen, K.S., Fredenslund, A. and Thomassen, P., 1989. Properties of Oils and Natural Gases, 252 pp. *Gulf Publishing*, Houston.

Peters, K.E. and Moldowan, J.M., 1993. The Biomarker Guide. Interpreting molecular fossils in petroleum and ancient sediments. Prentice Hall, New York.

Peters, K.E., Moldowan, J.M. and Sundararaman, P., 1990. Effects of hydrous pyrolysis on biomarker thermal maturity parameters: Monterey Phosphatic and Siliceous members. *Organic Geochemistry*, **15**, 249-265.

Peters, K.E., Moldowan, J.M., Driscole, A.R. and Demaison, G.J., 1989. Origin of Beatrice oil by co-sourcing from Devonian and Middle Jurassic source rocks, Inner Moray Firth, UK. *The American Association of Petroleum Geochemists*, **73**, 454-471.

Peterson, J.A., 1985, Geology and petroleum resources of north-central and north-eastern Africa: *U. S. Geological Survey,* Open-File Report, **54,** 85-709,

Philp, R.P. and Gilbert, T.D., 1986. Biomarker distributions in oils predominantly derived from terrigenous source material. In: Leythaeuser, D. and Rullkötter, J. (Eds). *Advances in Organic Geochemistry 1985*. Pergamon Press, 73-84.

Piggot, N. and Lines, M.D., 1991. A case study of migration from the West Canada Basin. In: England, W.A. and Fleet, A.J. (Eds) Petroleum migration. *Geological Society of London, Special Publication*, **59**, 207-225.

Pironon, J. and Barrés, O., 1990. Semi quantitative FT-IR microanalysis limits: Evidence from synthetic hydrocarbon fluid inclusions in sylvite. *Geochimica et Cosmochimica* Acta **54**, 509-518.

Pironon, J. and Barrés, O., 1992. Influence of brine-hydrocarbon interactions on FT-IR microscopic analyses of intracrystalline liquid inclusions. *Geochimica et Cosmochimica* Acta **56**, 169-174.

di Primio R., Dieckmann V. and Mills N., 1998. PVT and phase behaviour analysis in petroleum exploration. *Organic Geochemistry* **29**, 207-222.

Püttmann, W. and Villar, H., 1987. Occurrence and geochemical significance of 1,2,5,6-tetramethylnaphthalene. *Geochimica et Cosmochimica* Acta **51**, 3023-3029.

Radke, M. and Willsch, H., 1994. Extractable alkyldibenzothiophenes in Posidonia Shale (Toarcian) source rocks: relationship of yields to petroleum formation and expulsion. *Geochimica et Cosmochimica Acta* **58**, 5223-5244.

Radke, M., 1987. Organic Geochemistry of aromatic hydrocarbons. In: Brooks, J., Welte, D. (Eds.), *Advances in Organic Geochemistry*. Academic Press, London, **2**, 141-207.

Radke, M., 1988. Application of aromatic compounds as maturity indicators in source rocks and crude oils. *Marine and Petroleum Geology* **5**, 224-236.

Radke, M., and Welte, D.H., 1983. The Methylphenanthrene Index (MPI): a maturity parameter based on aromatic hydrocarbons. *In advances in Organic Geochemistry* 1981. Edited by Bjorøy M. Et al., 504-512.

Radke, M., Garrigues, P., Willsh, H., 1990. Methylated dicyclic and tricyclic aromatic hydrocarbons in crude oils from the Handil field, Indonesia. *Organic Geochemistry* **15**, 17-34.

Radke, M., Leythaeuser, D. and Teichmuller, M., 1984. Relationship between rank and composition of aromatic hydrocarbons for coals of different origins. *Organic Geochemistry,* **6**, 423-430.

Radke, M., Rullkötter, J., Vriend, S. P., 1994. Distribution of naphthalenes in crude oils from the Java Sea: source and maturation effects. *Geochimica et Cosmochimica Acta* **58**, 3675-3689.

Radke, M., Welte, D. and Willsch, H. 1982a. Geochemical study on a well in the Western Canada Basin: Relation of the distribution pattern to maturity of organic matter. *Geochimica et Cosmochimica Acta* 46, 1-10.

Radke, M., Welte, D.H. and Willsh, H., 1986. Maturity parameters based on aromatic hydrocarbons: influence of the organic matter type. In: Leythaeuser, D. and Rullkötter J. (Eds), *Advances in Organic Geochemistry 1985*, *Organic Geochemistry,* **10**, 51-63.

Radke, M., Willsh, H., Leythaeuser, D., Teichmüller, M., 1982b. Aromatic components of coal: relation of distribution pattern to rank. *Geochimica et Cosmochimica Acta* **46**, 1831-1848.

Reed, J.D., Illich, H.A. and Horsfield, B., 1986. Biochemical evolutionary significance of Ordovician oils and their sources. *Organic Geochemistry* **10**, 347-358.

Requejo, A. G., Allan J., Creaney S., Gray, N. R. and Cole, K. S. 1992. Aryl isoprenoids and diaromatic carotenoids in Palaeozoic source rocks and oils from the Western Canada and Williston Basins. *Organic Geochem*istry **19**, 245-264.

Requejo, A. G., 1994, Maturation of petroleum source rocks II; Quantitative changes in extractable hydrocarbon content and composition associated with hydrocarbon generation. *Organic Geochemistry* **21**, 91-105.

Richter, F.P., Caesar, P.D., Meisel, S.L., and Offenhauer, R.D., 1952. Distribution of nitrogen in petroleum according to basicity. Industrial and Engineering Chemistry, **44**, 2601-2605.

Riediger, C. L., Fowler, M. G., Brooks, P. W., and Snowdon, L. R., 1990. Triassic oils and potential Mesozoic source rocks, Peace River Arch area, Western Canada Basin. *Organic Geochemistry* **16**, 295-305.

Roedder, E and Bodnar, R.J., 1980. Geologic pressure determinations from fluid inclusion studies. *Ann. Rev. Earth. Planet. Sci.*, **8**, 263-301.

Roedder, E., 1984. Fluid inclusions: Mineralogical Society of America, Reviews in Mineralogy, 12, 644.

Roedder, E., 1990. Fluid inclusions – Prologue and epilogue. *Geochimica et Cosmochimica Acta*, **54**, 495-507.

Rohrback, B.G., 1983. Crude oil geochemistry of the Gulf of Suez. In: Bjorøy, M. et al. (Eds), *Advances in Organic Geochemistry 1981*. Wiley, J. and Sons, New York, 39-48.

Rubeistein, I., Sieskind, O. and Albrecht, P., 1975. Rearranged sterenes in shale: occurrence and simulated formation. *Journal of the Chemical Society*, Perkin Transactions I, 1833-1836.

Rullkötter, J. and Marzi, R., 1988. Natural and artificial maturation of biological markers in Toarcian shale from northern Germany. *Organic Geochemistry* **13**, 639-645.

Saigal, G.C., Bjolykke, K. and Larter, S.R., 1992. The effects of oil emplacement on diagenetic processes – examples from the Fulmar reservoir sandstones, central North Sea. *American Association of Petroleum Geologists* 76, 1024-1033.

Sakata, S., Suzuki, N. and Kaneko, N., 1988. A biomarker study of petroleum from the Neogene Tertiary sedimentary basins in Northeast Japan. *Geochemical Journal*, **22**, 89-105.

Santamaria-Orozco, D., Horsfield, B., di Primio, R. and Welte, T.H., 1998. Influence of maturity on distributions of benzo and dibenzothiophenes in Tithonian source rocks and crude oils, Sonda de Campeche, Mexico. *Organic Geochemistry* **28**, 423-439.

Schlepp, L., Landaus, P., Ely, M. and Fare, P., 2001. Influence of paleoenvironment and radiolytic alteration on the geochemistry of organic matter from Attuning

shales of the Lodève uranium deposit, France. *Bulletin Sociéty Géologique de France*, **1**, 99-109.

Schowalter, T. T., 1979. Mechanics of secondary migration and entrapment. *Bulletin of the American Association of Petroleum Geologists* 63, 723-760.

Seifert, W. K. and Moldowan, J. M., 1978. Applications of steranes, terpanes and monoaromatics to the maturation, migration and source of crude oils. *Geochimica et Cosmochimica Acta* **42**, 77-95.

Seifert, W.K. and Moldowan, J.M., 1986. Use of biological markers in petroleum exploration. In: *Methods in Geochemistry and Geophysics*, Jons, RB. (Eds) **24**, 261-290.

Shanmugam, G., 1985. Significance of coniferous rain forests and related organic matter in generating commercial quantities of oil, Gippsland Basin, Australia. *American Association of Petroleum Geologists* 69, 1241-1254.

Shepherd, T.J., Rankin, A.H, Alderton, D.H.M, 1985. A practical Guide to Fluid Inclusion Studies pp 63 Blackie and Son Ltd, Bishobriggs Glasgow.

Sheppard, C.J.R. and Shotton, D.M., 1997. Confocal Laser Scanning Microscopy. BIOS Scientific Publishers, Oxford, UK.

Shou, L., and Myhr, M.B., 1988. Sulphur aromatic compounds as maturity parameters. In: Mattavelli, L., Novelli, L. (Eds.), Advances in Organic Geochemistry 1987, *Organic Geochemistry* **13**, 61-66.

Sieskind, O., Joly, G. and Albrecht, P., 1979. Simulation of the geochemical transformation of sterols: superacid effect of clay minerals. *Geochimica et Cosmochimica Acta* **43**, 1675-1679.

Silliman, J.E., Li, M., Yao, H. and Hwang, R., 2002. Molecular distributions and geochemical implications of pyrrolic nitrogen compounds in the Permian Phosphoria Formation derived oils of Wyoming. *Organic Geochemistry*, **33**, 527-544.

Sofer, Z. 1988 Biomarkers and carbon isotopes of oils in the Jurassic Smackover Trend of the Gulf Coast states, U.S.A. *Organic Geochemistry* **12**, 421-432.

Sofer, Z., Zumberge, J.E., and Lay, V., 1986. Stable carbon isotopes and biomarkers as tools in understanding genetic relationship, maturation, biodegradation, and migration in crude oils in the Northern Peruvian Oriente (Maranon) Basin. *Organic Geochemistry* **10**, 377-389.

Stoddart, D.P., Hall, P.B., Larter, S R., Brasher, J., Li, M. And Bjorøy, M. 1995. The reservoir geochemistry of the Eldfisk Field, Norwegian North Sea. The Geochemistry of Reservoirs. *Geological Society Special Publication*, **86**, 257-279.

Stoddart, D.P., 1993. Petroleum and Nitrogen Compound Reservoir Geochemistry of the Eldfisk chalk reservoir. PhD. Thesis. Fossil Fuels and Environmental Geochemistry, University of Newcastle.

Stojanovic, K., Jovancicevic, B., Golovko, A., Pfendt, P., Cvetkovic, O. and Vitorovic, D., 2001. Phenanthrene and Methylphenanthrene isomers in maturity

estimation of biodegraded crude oils, Sakhalin Russia. Abstract, *in 20th International Meeting on Organic Geochemistry*, 10-14th September, 2001. Nancy-France.

Strachan, M.G., Alexander, R., Kagi, R.I., 1988. Trimethylnaphthalenes in crude oils and sediments: effects of source and maturity. *Geochimica et Cosmochimica Acta* **52**, 1255-1264.

Subroto, E.A., Alexander, R. and Kagi, R.I., 1991. 30-Norhopanes: their Occurrence in sediments and crude oils. *Chemical Geology*, **93**, 179-192.

Swarbrick, R.E., 1994. Reservoir diagenesis and hydrocarbon migration under hydrostatic palaeopressure conditions. *Clay Minerals*, **29**, 463-474.

Talukdar, S.C., De Toni, B. Marcano, F., Sweeney, J. and Rangel, A., 1993. Upper Cretaceous source rocks of northern South America. Abstract, *American Association of Petroleum Geologists,* 77, 351.

Taylor, P.N, Larter, S.R., Jones, M., Dale, J. and Horstad, I, 1997. The effect of oil-water-rock partitioning on the occurrence of alkylphenols in petroleum systems. *Geochimica et Cosmochimica Acta* **61**, 1899-1910.

Taylor, P.N., 1994. The petroleum geochemistry of phenols. PhD. Thesis. University of Newcastle upon Tyne, UK.

Terken, J.M.J., and Frewin, N.L., 2000. The Dhahaban petroleum system of Oman. *American Association of Petroleum Geologists Bulletin*, **84**, 523-544.

Thomas, M.M., Clouse, J.A., and Longo, J.M., 1993. Adsorption of organic compounds on carbonate minerals: 1. Model compounds and their influence on mineral wettability. *Chemical Geology*, **109**, 201-213.

Tissot, B. P. and Welte, D. H., 1984. Petroleum Formation and Occurrence, 2nd Eds. Springer-verlag, New York.

Turgarinov, A.I. and Vernadsky, V.I., 1970. Dependence of the decrepilation temperature of minerals on their gas-liquid inclusions and hardness: *Akademya Nauk SSSR*, Doklady, **195**, 112-114.

Vatan, A., 1962. Les grès et leurs milieux. C.R. *Acad. Sci.*, **254**, 2026-2028.

Verweij, J.M., 1993. Hydrocarbon migration systems analysis. *Developments in Petroleum Science*, **35**, Elsevier, Amsterdam, 276 pp.

Volk, H., Killops, S. C., Ahmed, M., Quezada, R. A., 2001. Charge Histories of Petroleum Reservoirs in the Gippsland and Taranaki Basins-Evidence from the Analysis of Oil Inclusions and Crude Oils. *PESA Eastern Australasian Basins Symposium*. Melbourne, Vic., 413-422.

Volkman, J.K., 1986. A review of sterol markers for marine and terrigenous organic matter. *Organic Geochemistry* **9**: 83-99.

Volkman, J.K., Gillan, F.T., Johns, R.B. and Eglinton, G., 1981. Sources of neutral lipids in a temperate intertidal sediment. *Geochimica et Cosmochimica Acta*, **45**, 1817-1828.

Walderhaug, O. and Fjeldskaar, W. 1993. History of hydrocarbon emplacement in the Oseberg Field determined by fluid inclusion microthermometry and temperature modelling. Basin Modelling: *Advances and Applications*, edited by Doré, A. G., et al. NPF Special Publication **3**, 485-497. Elsevier, Amsterdam.

Walderhaug, O., 1990. A fluid inclusion study of quartz cemented sandstones from offshore mid-Norway – possible evidence for continued quartz cementation during oil emplacement. *Journal of Sedimentary Petrology*, **60**, 203-210.

Wignall, P.B. and Meyers, K.J., 1988. Interpreting benthic oxygen levels in mudrocks: a new Approach. *Geology*, **16**, 452-455.

Wilhelms, A. and Larter, S.R., 1994. Origin of tar mats in petroleum reservoirs. Part I: introduction and case studies. *Marine and Petroleum Geology*, **11**, 418-441.

Wilhelms, A. and Larter, S.R., 1994. Origin of tar mats in petroleum reservoirs. Part II: formation mechanisms for tar mats. *Marine and Petroleum Geology*, **11**, 442-457.

Wilhelms, A., Larter, S.R. And Schulten, H.R., 1993. Characterisation of asphaltenes by pyrolysis-field ionization mass spectrometry - some observations. *Organic Geochemistry* **20**, 1049-1062.

Williams, J.A., Bjorøy, M., Dolcater, D.L., Winters, J.C., 1986. Biodegradation in South Texas Eocene oils - effects on aromatics and biomarkers. *Organic Geochemistry* **10**, 451-461.

Worden, R.H., Oxtoby, N.H., and Smalley, P.C., 1998. Can oil emplacement prevent quartz cementation in sandstones? *Petroleum Geoscience*, **4**, 129-137.

Yamamoto, M., 1992. Fractionation of azaarenes during oil migration. *Organic Geochemistry* **19**, 389-402.

Yamamoto, M., Taguchi, K. and Sasaki, K., 1991. Basic nitrogen compounds in bitumens and crude oils. *Chemical Geology*, **93**, 193-206.

Zalessky, M.D., 1917. On marine sapropelite of Silurian age formed by a blue-green algae. *Izv. Imp. Akad. Nauk. IV series*, 3-18.

Zhang, S.C., Hanson, A.D., Moldowan, J.M., Graham, S.A., Liang, D.G., Chang, E., Fago, F., 2000. Palaeozoic oil-source rock correlation on the Tarim basin, NW China. *Organic Geochemistry* **31**, 273-286.

Zumberge, J.E., 1987. Terpenoid biomarker distributions in low maturity crude oils. *Organic Geochemistry* **11**: 479-496.

Appendices

Appendix 4.1 Biomarker ratios of the Silurian and Ordovician source rock samples.

Well	Depth (m)	Age	20S/ 20S+20R	bb/ aa+bb	$C_{29}Ts/(C_{29}Ts+C_{29}hop)$	$C_{30}diahop/(C_{30}hop+C_{30}d)$	C_{29} hop $/C_{30}$ hop	Ts/Ts+Tm	$C_{23}Tr/C_{30}hop$	$(C_{28}T+C_{29}T)/Ts$	$(C_{28}T+C_{29}T)/C_{29}+C_{30}$ hop.	$C_{21}-+C_{22}$ ster/C_{29} ster.	C_{29}diaster. R/C_{29} stere.R	C_{24} teracyc./C_{26} tricyc.	C_{29}ster./ $C_{29}+C_{30}$ hop.
TKT#1	3868.6	Silurian	0.56	0.58	0.42	0.25	0.58	0.75	0.77	5.22	0.65	0.60	0.69	0.15	0.51
TKT#1	3872.5	Silurian	0.55	0.59	0.36	0.24	0.74	0.74	0.83	5.05	0.67	0.66	0.61	0.19	0.55
OA#1bis	4142	Silurian	0.50	0.57	0.48	0.44	0.79	0.86	0.82	5.67	0.71	0.72	0.74	0.10	0.58
OA#1bis	4145	Silurian	0.50	0.58	0.64	0.51	0.68	0.86	0.88	4.46	0.80	0.78	0.73	0.13	0.66
OA#1bis	4151.55	Silurian	0.50	0.63	0.37	0.29	0.82	0.66	0.83	3.62	0.66	0.81	0.71	0.23	0.49
BAT#1	3947	Silurian	0.51	0.56	0.53	0.39	0.65	0.84	0.79	4.89	0.74	0.64	0.76	0.16	0.62
BAT#1	3957	Silurian	0.54	0.56	0.52	0.42	0.72	0.75	0.81	5.20	0.75	0.61	0.77	0.16	0.65
BAT#1	3959.55	Silurian	0.50	0.58	0.52	0.41	0.73	0.82	0.77	5.73	0.74	0.60	0.76	0.12	0.61
RDC#2	3804	Silurian	0.54	0.55	0.41	0.37	0.78	0.82	0.79	3.15	0.65	0.73	0.60	0.18	0.74
RDC#2	3806	Silurian	0.57	0.57	0.42	0.36	0.71	0.69	0.74	4.00	0.55	0.71	0.59	0.17	0.69
RDC#2	3808	Silurian	0.53	0.53	0.40	0.35	0.69	0.90	0.73	2.75	0.61	0.76	0.58	0.16	0.67
RDC#2	3810	Silurian	0.52	0.65	0.40	0.43	0.71	0.83	0.75	4.26	0.59	0.77	0.61	0.21	0.68
GLNE#3	3803.45	Silurian	0.47	0.61	0.56	0.36	0.40	0.80	0.56	2.06	0.49	0.33	0.70	0.21	0.53
GLNE#3	3809.45	Silurian	0.56	0.63	0.48	0.35	0.52	0.76	0.48	1.83	0.45	0.23	0.78	0.26	0.51
GLNE#4bis	3874.8	Silurian	0.48	0.56	0.19	0.07	0.80	0.70	0.73	1.67	0.30	0.78	0.41	0.83	0.39
GLNE#5	3987	Silurian	0.49	0.58	0.20	0.08	1.15	0.56	0.77	2.90	0.45	0.83	0.51	0.86	0.37
GLNE#5	3994	Silurian	0.44	0.58	0.23	0.25	1.19	0.57	0.72	3.07	0.47	0.76	0.47	0.56	0.37
GLNE#5	4001	Silurian	0.48	0.57	0.22	0.12	0.84	0.58	0.72	1.93	0.32	0.80	0.27	1.04	0.40
BKZ#1	4180	Silurian	0.57	0.56	0.63	0.61	0.78	0.79	0.93	7.64	0.91	0.72	0.81	0.10	0.81
BKZ#1	4183	Silurian	0.54	0.53	0.58	0.45	0.57	0.81	0.83	6.21	0.77	0.71	0.77	0.12	0.65
BKZ#1	4187	Silurian	0.55	0.54	0.51	0.41	0.63	0.91	0.87	3.70	0.76	0.76	0.73	0.09	0.68
BKZ#1	4189	Silurian	0.53	0.59	0.58	0.41	0.64	0.89	0.84	5.41	0.74	0.76	0.76	0.11	0.59
GEC#1	3660	Silurian	0.55	0.58	0.50	0.24	0.43	0.68	0.75	-	0.70	0.50	0.72	0.11	0.64
GBC#1	3213	Silurian	0.59	0.70	0.17	0.00	1.13	0.42	0.77	0.00	0.00	0.72	0.51	2.58	0.23
GBC#1	3259	Silurian	0.58	0.68	0.17	0.04	1.00	0.48	0.69	1.67	0.26	0.73	0.37	1.27	0.29
GD#1bis	3850	Silurian	0.48	0.55	0.19	0.06	0.94	0.45	0.40	1.53	0.18	0.65	0.44	1.47	0.23
OEM#1	3910	Ordovician	0.56	0.49	0.36	0.32	0.94	0.38	0.41	0.57	0.10	0.66	0.54	2.74	0.16
OEM#1	3924	Ordovician	0.45	0.54	0.27	0.28	0.97	0.45	0.44	0.80	0.13	0.60	0.53	2.31	0.14
OEM#1	3930	Ordovician	0.47	0.55	0.32	0.33	1.01	0.46	0.40	0.63	0.12	0.58	0.61	2.24	0.14
OA#1bis	4367	Ordovician	0.55	0.53	0.43	0.30	0.93	0.83	0.60	0.29	0.21	0.75	0.52	1.08	0.22
OA#1bis	4462	Ordovician	0.50	0.49	0.17	0.12	1.24	0.59	0.65	1.17	0.31	0.69	0.49	1.22	0.29
OA#1bis	4599	Ordovician	0.44	0.51	0.14	0.07	1.11	0.45	0.65	1.60	0.25	0.77	0.52	1.57	0.24
RDC#2	3911	Ordovician	0.51	0.49	0.18	0.19	1.25	0.65	0.74	1.01	0.28	0.82	0.59	1.53	0.23
GLNE#3	3936.08	Ordovician	0.48	0.52	0.26	0.03	0.93	0.58	0.33	0.61	0.11	0.38	0.16	1.30	0.22
GLNE#5	4024	Ordovician	0.48	0.48	0.23	0.14	1.16	0.67	0.66	0.60	0.22	0.78	0.48	1.47	0.21
GLNE#5	4026	Ordovician	0.41	0.51	0.17	0.13	1.18	0.66	0.67	0.77	0.26	0.72	0.51	1.15	0.29
BKZ#1	4198	Ordovician	0.52	0.55	0.52	0.43	0.89	0.86	0.38	0.15	0.16	0.38	0.66	1.53	0.24
GEC#1	3770	Ordovician	0.51	0.52	0.37	0.41	0.98	0.56	0.22	0.20	0.08	0.34	0.64	2.64	0.19
GBC#1	3272	Ordovician	0.51	0.49	0.17	0.04	0.92	0.51	0.36	1.90	0.25	0.48	0.37	0.74	0.24
GBC#1	3386	Ordovician	0.43	0.45	0.16	0.03	1.19	0.34	0.21	1.81	0.13	0.35	0.38	0.89	0.18
GBC#1	3394	Ordovician	0.49	0.54	0.19	0.03	0.90	0.47	0.61	2.30	0.27	0.79	0.31	1.30	0.22
GBC#1	3398	Ordovician	0.47	0.51	0.14	0.04	1.02	0.48	0.51	2.47	0.28	0.57	0.30	0.85	0.25
GD#1bis	3921.5	Ordovician	0.53	0.51	0.22	0.22	0.80	0.39	0.60	1.06	0.16	0.84	0.36	2.39	0.18
GD#1bis	3939	Ordovician	0.47	0.54	0.33	0.36	0.86	0.40	0.31	0.63	0.10	0.53	0.55	2.41	0.15
GD#1bis	4025.9	Ordovician	0.40	0.53	0.24	0.17	0.87	0.51	0.62	0.59	0.15	0.80	0.54	2.50	0.20
HGA#1	3391	Ordovician	0.46	0.55	0.27	0.12	0.80	0.55	0.61	2.75	0.42	0.62	0.66	0.25	0.32
HGA#1	3412	Ordovician	0.45	0.53	0.24	0.15	0.99	0.51	0.69	2.81	0.44	0.62	0.64	0.38	0.33
HGA#1	3439	Ordovician	0.43	0.52	0.19	0.10	0.90	0.52	0.58	2.36	0.35	0.54	0.61	0.58	0.31

Appendix 4.1 Biomarker concentrations (ug/g extract) of the Silurian and Ordovician source rock samples.

Well	Depth (m)	Age	$C_{21}T$	$C_{22}T$	$C_{23}T$	$C_{24}T$	$C_{25}T$	C_{24} Tetra	$C_{26}T$	$C_{28}T$	$C_{29}T$	$C_{30}T$	$C_{31}T$	Ts	Tm	C_{29} hop.	C_{29}Ts	C_{30} diahop.	C_{30} hop.	C_{31} hop.S	C_{31} hop.R	C_{32} hop.S	C_{32} hop.R	C_{33}(S+R)	C_{34}(S+R)	C_{35}(S+R)	Sum hopanes	Sumtricys
TKT#1	3668.6	Silurian	27.9	7.0	35.6	24.3	19.6	2.9	19.3	17.5	14.5	9.3	10.3	6.1	2.0	6.3	4.6	3.5	10.8	0.0	2.6	3.3	2.4	0.0	0.0	0.0	41.7	185.2
TKT#1	3672.5	Silurian	19.7	5.7	26.2	17.4	13.4	2.7	14.2	10.9	9.0	6.4	5.0	3.9	1.4	4.1	2.3	1.7	5.5	0.0	0.0	0.0	0.0	0.0	0.0	0.0	18.9	127.8
OA#1bis	4142	Silurian	10.8	4.1	14.1	10.8	8.3	0.7	7.4	7.6	6.6	4.4	5.0	2.5	0.4	2.5	2.3	2.5	3.2	0.0	0.6	1.1	0.6	0.0	0.0	0.0	15.8	79.2
OA#1bis	4145	Silurian	9.6	3.2	11.0	7.9	6.5	0.9	6.8	5.9	4.6	3.5	3.3	2.4	0.4	1.1	1.9	1.7	1.6	0.0	0.5	0.0	0.0	0.0	0.0	0.0	9.4	62.3
OA#1bis	4151.55	Silurian	17.5	6.5	23.1	17.1	12.2	6.5	10.3	9.2	8.4	3.6	3.3	4.9	2.5	4.0	2.4	2.0	4.9	0.0	0.5	0.0	0.0	0.0	0.0	0.0	21.2	111.3
BAT#1	3947	Silurian	18.1	5.4	21.4	15.8	16.4	2.1	13.1	13.9	12.8	8.9	9.6	5.5	1.0	3.6	4.1	3.6	5.5	0.0	1.4	1.3	0.7	0.0	0.0	0.0	26.7	135.4
BAT#1	3957	Silurian	18.9	7.0	22.9	18.8	14.5	2.5	15.4	14.1	13.5	10.3	10.7	5.3	1.7	3.8	4.0	3.8	5.2	0.0	1.7	0.0	0.0	0.0	0.0	0.0	25.6	146.1
BAT#1	3959.55	Silurian	15.4	5.2	20.3	16.5	15.2	1.7	14.8	13.4	15.0	11.1	11.4	5.0	1.1	4.3	4.6	4.0	5.9	0.0	1.9	0.0	0.0	0.0	0.0	0.0	25.8	138.4
RDC#2	3804	Silurian	5.0	1.6	5.0	4.6	3.0	0.9	2.6	2.1	2.3	1.9	0.0	1.4	0.3	1.0	0.7	0.8	1.3	0.0	0.0	0.0	0.0	0.0	0.0	0.0	5.5	28.1
RDC#2	3806	Silurian	4.5	1.4	4.2	3.4	2.1	0.3	1.9	1.6	1.5	0.0	0.0	0.8	0.3	1.0	0.7	0.8	1.5	0.0	0.8	0.7	0.0	0.0	0.0	0.0	6.7	20.7
RDC#2	3808	Silurian	3.5	0.0	3.3	2.4	2.0	0.5	1.5	1.8	1.4	0.0	0.0	1.2	0.1	0.8	0.6	0.7	1.2	0.0	0.0	0.0	0.0	0.0	0.0	0.0	4.6	15.9
RDC#2	3810	Silurian	4.2	1.7	3.9	3.6	2.6	0.4	1.8	1.5	1.7	0.0	0.0	0.7	0.2	0.9	0.6	1.0	1.3	0.0	0.0	0.0	0.0	0.0	0.0	0.0	4.7	21.0
GLNE#3	3803.45	Silurian	21.6	7.7	20.1	13.9	9.8	2.9	13.5	10.7	10.5	4.5	8.4	10.3	2.5	6.4	8.1	8.9	16.1	9.3	5.4	7.6	4.4	8.4	0.0	0.0	87.5	120.7
GLNE#3	3809.45	Silurian	19.7	7.0	19.3	13.6	8.3	3.3	12.9	13.2	13.3	6.5	10.1	14.4	4.4	11.0	10.2	11.5	21.0	12.5	7.1	9.2	6.2	11.7	8.0	0.0	127.3	123.8
GLNE#1bis	3874.8	Silurian	9.3	3.2	11.0	5.3	3.5	2.0	2.5	1.6	1.5	0.0	0.0	1.9	0.8	3.3	0.8	0.3	4.1	1.8	1.0	0.0	0.0	0.0	0.0	0.0	13.9	38.0
GLNE#5	3987	Silurian	8.1	4.0	9.2	5.3	4.1	2.8	3.3	2.6	2.0	0.0	0.0	1.6	1.3	3.1	0.7	0.2	2.7	1.3	1.0	0.0	0.0	0.0	0.0	0.0	11.9	38.7
GLNE#5	3994	Silurian	5.6	2.4	7.1	4.9	3.1	1.9	3.5	2.9	2.7	0.0	0.0	1.8	1.4	3.6	1.1	0.9	2.7	1.7	1.1	0.0	0.0	0.0	0.0	0.0	14.3	32.2
GLNE#5	4001	Silurian	4.6	1.7	6.3	3.9	2.8	2.3	2.2	1.4	0.7	0.0	0.0	1.1	0.8	2.1	0.6	0.3	2.5	0.0	0.0	0.0	0.0	0.0	0.0	0.0	7.3	23.7
BKZ#1	4180	Silurian	7.1	2.7	11.3	8.0	8.4	0.8	8.2	7.3	7.0	6.1	4.5	1.9	0.5	0.7	1.1	1.3	0.8	0.0	0.0	0.0	0.0	0.0	0.0	0.0	6.3	70.7
BKZ#1	4183	Silurian	8.5	4.0	12.4	9.3	8.5	1.0	7.9	6.4	6.9	5.1	4.7	2.2	0.5	1.5	2.1	2.1	2.6	0.0	0.0	0.0	0.0	0.0	0.0	0.0	11.0	73.9
BKZ#1	4187	Silurian	8.0	3.1	10.7	8.2	7.0	0.5	5.6	4.7	3.4	3.4	3.1	2.2	0.2	1.0	1.0	1.1	1.6	0.0	0.0	0.0	0.0	0.0	0.0	0.0	7.1	57.2
BKZ#1	4189	Silurian	6.6	2.8	8.6	6.4	5.2	0.5	4.1	4.6	3.1	2.9	2.3	1.4	0.2	1.1	1.5	1.2	1.7	0.0	0.0	0.0	0.0	0.0	0.0	0.0	7.0	46.5
GEC#1	3680	Silurian	15.9	6.0	25.8	21.3	17.9	1.8	16.5	15.8	13.0	9.0	8.6	2.7	1.3	3.7	3.6	2.7	8.6	0.0	3.0	3.3	2.0	0.0	0.0	0.0	30.8	149.8
GEC#1	3213	Silurian	2.3	2.3	8.9	5.1	0.0	0.0	0.0	0.0	0.0	0.0	0.0	0.9	1.3	3.0	0.6	0.0	2.7	1.5	1.1	0.0	0.0	0.0	0.0	0.0	11.2	18.6
GEC#1	3259	Silurian	16.7	7.9	28.0	12.2	8.5	7.0	4.4	3.9	4.7	3.2	3.3	3.8	4.1	12.5	2.6	0.5	12.5	6.5	4.5	3.9	3.1	5.3	4.7	17.5	81.5	92.8
GD#1bis	3650	Silurian	4.3	1.4	6.5	3.4	3.1	3.2	2.2	1.9	2.4	1.4	0.8	2.8	3.3	9.2	2.2	0.6	9.8	4.9	3.4	3.1	1.9	3.8	2.2	0.0	47.1	27.3
OEM#1	3910	Ordovician	39.9	11.0	34.2	15.4	0.0	33.0	7.0	5.5	5.0	0.0	0.0	18.4	30.0	40.4	22.3	22.9	49.7	24.9	17.5	19.9	13.3	17.5	11.6	6.8	295.0	118.0
OEM#1	3924	Ordovician	44.0	14.2	69.3	32.1	26.5	40.7	17.6	14.2	12.4	0.0	0.0	33.2	41.0	85.5	31.1	34.7	88.3	50.7	35.6	39.1	25.9	37.2	26.3	14.9	543.4	230.3
OEM#1	3930	Ordovician	35.1	8.3	35.0	17.5	11.1	29.0	8.9	7.7	5.8	0.0	0.0	21.3	24.8	46.4	22.0	25.3	52.4	33.0	20.7	26.6	17.2	26.7	17.4	9.5	343.4	129.3
OA#1bis	4357	Ordovician	10.4	5.1	11.7	5.4	4.3	4.3	4.0	2.5	1.6	0.0	0.0	14.2	2.9	7.2	5.5	3.3	7.7	4.4	2.9	2.4	1.6	3.7	2.2	1.5	59.6	45.0
OA#1bis	4462	Ordovician	8.6	4.0	19.4	9.6	7.8	7.5	6.1	5.4	5.2	0.0	0.0	9.0	6.2	12.9	2.6	1.5	10.4	5.1	3.2	2.5	1.6	0.0	0.0	0.0	55.1	66.1
OA#1bis	4599	Ordovician	42.6	18.7	94.8	49.4	43.6	33.2	21.1	18.4	16.3	12.0	0.0	21.6	26.3	55.7	9.3	3.8	50.3	21.9	18.7	12.4	10.8	19.7	0.0	0.0	250.5	316.9
RDC#2	3911	Ordovician	19.8	7.9	29.4	12.9	8.5	9.2	6.0	4.7	4.5	0.0	0.0	9.1	5.0	13.0	2.9	2.4	10.5	4.8	3.4	2.2	1.7	0.0	0.0	0.0	54.9	93.6
GLNE#3	3935.08	Ordovician	2.6	1.4	3.6	1.6	0.9	1.9	1.5	0.9	0.8	0.0	0.0	2.9	2.1	6.8	2.4	0.2	7.4	4.2	3.0	2.0	1.5	0.0	0.0	0.0	32.5	13.5
GLNE#5	4024	Ordovician	16.7	8.9	27.5	12.5	10.6	8.5	5.8	4.6	3.9	0.0	0.0	14.1	7.0	16.3	4.9	2.2	14.1	5.1	4.0	0.0	0.0	0.0	0.0	0.0	67.7	90.5
GLNE#5	4026	Ordovician	11.4	7.2	22.7	10.2	8.2	8.0	7.0	4.9	3.8	0.0	0.0	11.3	5.9	13.2	2.7	1.7	11.2	4.6	3.6	2.8	2.2	3.3	0.0	0.0	62.6	75.5
BKZ#1	4198	Ordovician	9.2	4.0	5.8	3.7	0.0	5.4	3.5	2.0	1.4	0.0	0.0	23.2	3.6	8.3	9.1	7.1	9.3	5.4	4.1	3.9	2.3	2.6	1.4	0.0	80.1	29.7
GEC#1	3770	Ordovician	5.8	2.0	3.4	1.6	0.6	5.2	1.4	1.1	0.7	0.0	0.0	9.1	7.0	8.1	4.8	8.3	12.0	6.1	4.2	5.9	3.5	5.7	3.4	2.2	80.2	16.7
GEC#1	3272	Ordovician	26.7	7.4	28.0	12.1	10.8	6.8	9.2	13.7	18.0	17.4	20.3	10.5	10.0	45.3	9.3	2.0	49.1	33.2	20.6	17.6	12.5	25.4	11.5	14.7	261.7	163.6
GEC#1	3366	Ordovician	13.7	5.8	36.2	19.0	21.8	14.9	16.8	23.0	19.8	14.9	40.2	23.7	47.0	162.1	30.7	4.1	136.2	71.5	53.4	40.5	26.5	53.6	35.8	40.5	725.4	211.1
GEC#1	3394	Ordovician	34.0	12.5	44.7	17.2	11.8	7.7	5.9	9.3	11.0	10.3	8.6	6.5	7.3	25.8	6.0	0.8	28.6	19.0	11.1	8.8	5.6	14.1	5.8	7.1	146.7	165.5
GEC#1	3398	Ordovician	27.9	10.9	37.5	17.0	16.4	7.9	9.3	10.7	17.2	13.9	11.3	8.0	8.7	36.4	6.1	1.4	35.7	21.2	12.5	10.5	7.0	14.3	7.9	8.8	178.4	172.2
GD#1bis	3921.5	Ordovician	22.3	6.4	19.3	7.9	3.9	8.7	2.8	2.5	2.0	0.0	0.0	4.3	6.6	10.4	2.9	3.6	12.9	5.7	3.8	4.3	2.5	4.7	0.0	0.0	61.8	67.2
GD#1bis	3939	Ordovician	25.0	5.2	26.4	13.7	10.7	30.4	9.1	6.5	6.0	0.0	0.0	19.9	29.7	50.7	24.5	33.2	59.2	36.0	24.5	29.5	19.8	29.6	19.1	7.9	383.7	102.6
GD#1bis	4025.9	Ordovician	20.1	7.6	27.6	12.3	8.3	12.8	5.1	2.9	2.7	0.0	0.0	9.5	8.9	14.5	4.5	3.5	16.7	6.1	4.7	5.1	3.6	4.6	0.0	0.0	81.6	86.6
HGA#1	3391	Ordovician	23.5	7.8	32.4	25.5	20.9	4.4	17.6	14.4	13.1	9.0	8.4	7.3	6.0	16.7	6.1	2.9	20.9	11.1	7.3	6.6	5.2	10.7	10.1	5.7	116.5	172.6
HGA#1	3412	Ordovician	25.7	9.5	47.4	32.3	27.6	8.2	21.7	17.5	16.1	9.1	10.7	8.8	8.5	20.9	6.5	3.7	21.1	11.1	7.6	7.3	5.8	10.9	8.6	0.0	120.8	217.6
HGA#1	3439	Ordovician	18.7	8.9	41.6	27.3	24.4	9.7	16.9	16.5	14.5	8.6	9.2	9.2	8.4	27.5	6.5	3.2	30.4	13.4	8.5	8.8	6.6	11.0	8.3	0.0	141.8	186.4

Appendix 4.1 Biomarker concentrations (ug/g extract) of the Silurian and Ordovician source rock samples (continued).

Well	Depth (m)	Age	C_{21} ster.	C_{22} ster.	C_{27} diast.S	C_{27} R diast.	C_{27}aa ster.S	C_{29} diast.S	C_{27}bb ster.S	C_{27}aa ster.R	C_{29} diast.R	C_{29}aa ster. S	C_{29}bb ster.(S+R)	C_{29}aa ster.R	Sum steranes
TKT#1	3868.6	Silurian	21.3	5.5	6.7	4.6	5.9	10.0	4.8	7.0	7.2	4.2	10.3	3.3	90.7
TKT#1	3872.5	Silurian	18.6	4.1	4.9	3.2	2.0	5.2	2.2	4.5	3.8	2.5	7.0	2.4	60.6
OA#1bis	4142	Silurian	16.0	4.9	5.6	3.5	3.3	5.9	2.9	3.3	4.0	1.7	4.5	1.7	57.5
OA#1bis	4145	Silurian	14.9	3.5	4.5	2.6	2.3	3.6	1.6	3.7	2.8	1.1	2.9	1.1	44.5
OA#1bis	4151.55	Silurian	28.3	9.4	7.9	4.1	2.3	6.6	1.9	5.0	3.9	1.6	5.4	1.6	78.0
BAT#1	3947	Silurian	20.1	5.7	10.1	6.5	4.0	12.6	4.4	4.8	9.8	3.3	8.3	3.1	92.7
BAT#1	3957	Silurian	20.4	6.1	11.4	6.9	5.0	13.5	4.9	6.0	10.8	4.0	9.4	3.3	101.9
BAT#1	3959.55	Silurian	18.2	5.2	11.6	7.0	4.6	13.6	5.0	5.7	10.5	3.3	9.2	3.3	97.0
RDC#2	3804	Silurian	13.6	4.1	2.4	1.5	2.3	3.0	1.5	2.9	2.1	1.6	3.7	1.4	40.0
RDC#2	3806	Silurian	10.6	3.4	1.8	1.1	2.5	2.7	1.5	3.6	1.5	1.4	3.2	1.0	34.3
RDC#2	3808	Silurian	9.7	3.5	1.3	0.6	2.2	2.1	1.0	3.3	1.3	1.1	2.2	0.9	29.0
RDC#2	3810	Silurian	11.6	3.9	1.9	0.9	1.8	2.0	1.2	2.9	1.5	0.6	3.0	1.0	32.5
GLNE#3	3803.45	Silurian	10.0	2.4	9.0	5.5	1.8	15.6	3.9	2.9	12.5	4.7	15.6	5.3	89.3
GLNE#3	3809.45	Silurian	7.9	2.0	11.2	7.2	0.0	23.3	5.7	4.6	19.3	6.9	21.1	5.5	114.6
GLNE#4bis	3874.8	Silurian	12.9	3.9	2.0	1.0	0.7	1.7	1.1	3.3	0.8	1.0	2.7	1.1	32.2
GLNE#5	3987	Silurian	12.8	3.7	2.2	1.2	1.5	1.6	0.9	1.9	0.9	0.8	1.9	0.6	30.1
GLNE#5	3994	Silurian	8.9	2.8	2.1	1.7	0.8	2.2	1.2	2.6	0.8	0.7	2.2	0.9	26.8
GLNE#5	4001	Silurian	9.5	2.5	1.5	0.6	0.7	0.9	0.7	2.1	0.2	0.6	1.7	0.7	21.7
BKZ#1	4180	Silurian	12.7	3.2	6.9	4.8	2.0	6.6	2.1	2.8	5.2	1.6	3.5	1.2	52.6
BKZ#1	4183	Silurian	15.3	3.8	7.4	5.6	1.3	7.1	2.4	4.1	5.6	1.9	4.1	1.7	60.3
BKZ#1	4187	Silurian	13.9	3.5	5.4	3.7	2.0	4.2	1.5	4.3	3.6	1.3	3.0	1.3	47.7
BKZ#1	4189	Silurian	9.8	3.1	4.1	2.9	1.9	3.2	1.3	3.2	2.7	0.8	2.4	0.9	36.2
GEC#1	3660	Silurian	15.4	5.9	8.7	5.1	5.9	11.3	5.4	6.0	7.7	5.0	12.6	4.1	93.0
GBC#1	3213	Silurian	3.3	1.0	1.1	0.6	0.4	1.2	0.5	0.8	0.3	0.2	1.2	0.3	10.8
GBC#1	3259	Silurian	20.7	6.5	2.9	2.0	2.9	2.7	1.9	4.1	2.0	2.0	4.8	3.4	55.9
GD#1bis	3850	Silurian	8.2	3.6	3.5	1.9	2.8	3.1	1.8	4.7	1.2	1.3	3.4	1.6	37.2
OEM#1	3910	Ordovician	24.5	7.5	5.1	2.8	3.9	6.5	3.3	4.1	4.3	4.7	8.1	3.7	78.4
OEM#1	3924	Ordovician	32.2	10.5	8.2	4.2	10.1	14.0	7.9	9.0	8.3	5.8	15.2	7.3	132.6
OEM#1	3930	Ordovician	16.3	5.2	4.7	3.1	3.4	7.7	4.2	4.3	5.8	3.3	8.5	3.8	70.4
OA#1bis	4367	Ordovician	9.8	2.9	1.5	1.1	1.0	2.0	1.1	1.9	1.0	1.1	2.2	0.9	26.3
OA#1bis	4462	Ordovician	15.7	5.5	3.4	2.3	4.2	3.9	2.6	5.6	2.4	2.5	4.8	2.5	55.4
OA#1bis	4599	Ordovician	86.3	29.1	18.2	10.4	16.7	18.7	14.5	20.5	10.1	7.5	17.4	9.4	258.7
RDC#2	3911	Ordovician	24.5	6.7	3.0	2.0	3.9	4.0	2.4	4.8	2.5	1.8	3.4	1.8	60.7
GLNE#3	3936.08	Ordovician	1.8	0.7	1.1	0.7	1.4	0.9	0.7	3.1	0.2	0.7	2.1	1.2	14.4
GLNE#5	4024	Ordovician	24.2	7.7	4.5	2.4	5.8	4.8	3.5	7.8	2.3	2.3	4.5	2.5	72.1
GLNE#5	4026	Ordovician	19.0	6.7	3.7	2.7	5.6	5.2	3.7	6.3	3.0	2.0	5.0	2.8	65.7
BKZ#1	4198	Ordovician	2.5	1.0	2.2	1.8	2.3	3.2	1.7	3.2	2.3	1.3	3.1	1.2	25.8
GEC#1	3770	Ordovician	1.9	0.6	1.4	0.9	1.5	2.4	1.5	3.3	2.0	1.2	2.5	1.1	20.2
GBC#1	3272	Ordovician	23.2	4.7	3.8	2.2	7.0	7.6	5.6	10.8	4.4	7.9	14.9	7.5	99.6
GBC#1	3386	Ordovician	25.3	10.1	9.4	5.2	14.8	14.4	9.9	18.4	12.7	15.5	30.0	20.8	186.5
GBC#1	3394	Ordovician	49.3	10.4	2.4	1.3	3.9	3.7	2.6	5.7	1.7	3.6	8.4	3.8	96.7
GBC#1	3398	Ordovician	25.4	6.3	4.3	2.9	5.9	7.4	5.0	8.3	2.6	5.4	12.1	6.1	91.5
GD#1bis	3921.5	Ordovician	21.8	5.7	2.4	1.3	1.8	2.6	1.7	2.7	0.7	1.3	2.6	1.2	45.7
GD#1bis	3939	Ordovician	16.7	6.1	5.9	3.5	3.4	8.7	3.7	3.4	6.0	4.3	10.9	4.9	77.5
GD#1bis	4025.9	Ordovician	25.3	7.5	4.9	2.7	3.2	5.3	3.2	5.4	2.7	1.5	4.3	2.3	68.1
HGA#1	3391	Ordovician	21.7	7.3	12.4	8.3	6.6	12.0	5.7	8.6	8.2	3.6	9.6	4.3	108.5
HGA#1	3412	Ordovician	24.4	9.2	15.4	9.4	7.9	13.3	5.4	11.9	9.2	4.4	10.9	5.3	126.7
HGA#1	3439	Ordovician	22.3	8.5	13.6	8.8	9.3	14.2	7.3	18.0	11.0	5.4	13.5	7.1	139.0

Appendix 4.2 Aromatic hydrocarbon ratios and concentrations (ug/g extract) of the Silurian and Ordovician source rock samples.

Well	Depth (m)	Age	2-MN/1-MN	2,6-+2,7-/1,5-	2,3,6-/1,4,6-+1,3,5-	1,3,7-+2,3,6-/1,3,5-+1,3,6-	1,3,6,7-/1,2,5,6-+1,2,3,5-	2,3,6,7-/1,2,3,6-	MPI 1	3-MP/2-MP	DMPr	2-MP/1-MP	Rc(%)	4-MDBT/1-MDBT	2+3-MDBT/DBT	4,6-DMDBT/1,4	2,4-DMDBT/1,4-	$C_{20}TAS/C_{20}TAS+C_{28}TAS$ (S+R)	Total Alkylnaphthalenes (ug/g extract)	Total alkylphenanthrenes (ug/g extract)	Total Alkylthiophenes (ug/g extract)
TKT#1	3868	Silurian	1.2	4.0	0.8	0.8	3.6	1.3	0.7	0.8	0.2	0.8	0.8	10.2	1.0	6.6	3.0	0.8	5547.7	7871.9	1145.6
TKT#1	3872.5	Silurian	1.1	3.1	0.8	0.7	4.1	1.2	0.7	0.8	0.2	0.8	0.8	10.8	1.3	8.8	2.6	0.8	5840.8	7830.7	1672.1
OA#1bis	4142	Silurian	1.1	3.7	0.7	0.7	6.2	1.7	0.6	0.8	0.2	0.8	0.8	9.0	1.2	6.6	2.4	0.8	8140.9	12271.9	3341.2
OA#1bis	4145	Silurian	1.1	3.7	0.7	0.7	5.7	1.5	0.6	0.9	0.2	0.7	0.8	9.2	1.1	6.3	2.4	0.7	10152.5	14092.2	3867.4
OA#1bis	4151.55	Silurian	1.2	4.0	0.8	0.8	6.1	1.7	0.6	0.8	0.2	0.8	0.8	12.4	1.2	5.3	2.4	0.8	15003.0	20885.7	3491.9
BAT#1	3947	Silurian	1.0	4.0	0.7	0.7	8.3	2.1	0.6	0.9	0.1	0.8	0.8	10.0	1.2	6.7	2.1	0.9	8023.2	8086.3	2603.2
BAT#1	3957	Silurian	1.0	4.0	0.6	0.7	7.5	1.8	0.6	0.9	0.1	0.8	0.8	9.8	1.4	1.4	2.1	0.9	6038.7	6924.7	1691.4
BAT#1	3959.55	Silurian	0.9	3.4	0.8	0.8	7.4	1.5	0.6	0.9	0.1	0.8	0.8	9.4	1.2	6.3	2.0	0.9	3358.1	4944.7	1635.7
RDC#2	3804	Silurian	1.5	3.8	0.7	0.7	6.7	1.6	0.7	0.9	0.2	0.9	0.8	10.5	1.0	5.6	1.9	0.8	11344.9	16152.8	6961.4
RDC#2	3806	Silurian	1.1	4.0	0.7	0.7	6.8	1.5	0.7	0.9	0.2	0.9	0.8	9.7	1.1	6.8	2.3	0.8	10639.6	14982.8	6458.1
RDC#2	3808	Silurian	1.1	3.9	0.6	0.7	6.6	1.5	0.7	0.9	0.2	1.0	0.8	8.8	1.0	6.0	2.1	0.7	9188.8	14185.4	6238.8
RDC#2	3810	Silurian	1.1	4.0	0.8	0.8	6.5	1.5	0.7	0.9	0.2	1.0	0.8	8.9	1.0	4.9	1.7	0.8	10593.8	15514.9	7031.6
GLNE#3	3803.45	Silurian	1.4	6.4	1.2	1.0	6.1	1.8	0.7	0.9	0.2	0.8	0.8	9.6	1.3	5.9	2.4	0.8	7164.5	8039.4	512.3
GLNE#3	3809.45	Silurian	1.3	5.9	1.3	1.0	6.5	2.2	0.6	0.9	0.2	0.8	0.7	10.0	1.1	3.1	2.7	0.8	6999.3	7699.6	275.1
GLNE#4bis	3874.8	Silurian	1.2	4.3	0.8	0.8	5.0	1.6	0.8	0.8	0.2	1.0	0.9	11.0	1.2	9.6	3.9	0.9	6325.4	10111.1	1082.2
GLNE#5	3987	Silurian	1.3	4.8	0.7	0.7	9.1	2.3	0.7	0.8	0.2	0.9	0.8	15.8	1.1	11.4	3.5	0.9	15496.5	23425.0	3222.9
GLNE#5	3994	Silurian	1.3	4.3	0.6	0.7	9.3	2.4	0.7	0.8	0.2	0.9	0.8	16.2	1.1	11.8	3.2	0.9	14029.3	22051.7	2938.4
GLNE#5	4001	Silurian	1.3	4.7	0.7	0.7	9.2	2.1	0.8	0.8	0.2	1.0	0.9	15.0	1.3	9.1	2.8	0.9	16125.4	26520.9	4421.1
BKZ#1	4180	Silurian	1.0	3.6	0.5	0.6	5.9	1.3	0.6	0.8	0.1	0.8	0.8	9.6	1.2	6.7	2.5	0.9	7452.4	7716.8	1969.6
BKZ#1	4183.8	Silurian	1.0	3.7	0.6	0.7	5.8	1.4	0.6	0.8	0.1	0.8	0.8	10.1	1.4	6.9	2.5	0.7	6291.6	7176.9	1797.4
BKZ#1	4187	Silurian	1.1	3.9	0.5	0.6	5.6	1.6	0.6	0.8	0.2	0.8	0.8	10.1	1.3	6.6	2.4	0.7	7354.3	9005.2	2364.8
BKZ#1	4189	Silurian	1.1	3.9	0.5	0.6	5.8	1.5	0.6	0.8	0.2	0.8	0.8	10.0	1.4	6.6	2.4	1.0	6209.6	7700.6	2015.5
GEC#1	3660	Silurian	0.8	2.2	0.6	0.7	2.6	0.8	0.7	0.9	0.1	0.8	0.8	5.7	1.1	5.3	2.3	0.9	510.2	1822.8	472.1
GBC#1	3213	Silurian	1.7	5.2	0.9	0.8	4.7	1.3	1.0	0.8	0.3	1.4	1.0	7.2	1.0	0.1	2.3	0.9	5776.9	11463.7	962.4
GBC#1	3259	Silurian	1.9	7.9	0.9	0.8	7.5	2.2	1.1	0.8	0.4	1.6	1.1	8.9	0.9	0.0	2.0	1.0	11860.2	27620.4	2648.8
GD#1bis	3850	Silurian	1.2	3.8	0.8	0.8	5.5	1.4	0.7	0.9	0.2	0.8	0.8	7.0	1.1	1.0	2.2	1.0	10030.5	11965.7	2792.1
OEM#1	3910	Ordovician	1.1	4.3	1.2	0.9	3.9	1.9	0.6	0.8	0.2	0.8	0.8	5.5	0.7	3.8	1.3	0.8	3644.2	11045.9	417.0
OEM#1	3924	Ordovician	1.1	3.8	1.1	0.9	5.4	2.7	0.7	0.8	0.2	0.9	0.8	4.6	1.0	4.1	1.2	0.7	642.3	4336.3	412.3
OEM#1	3930	Ordovician	1.0	4.2	1.2	0.9	10.4	2.9	0.7	0.8	0.2	0.9	0.8	4.8	1.1	4.2	1.3	0.8	907.9	3525.1	236.0
OA#1bis	4367	Ordovician	1.1	6.7	1.1	0.9	15.6	3.7	0.8	0.9	0.2	1.1	0.9	5.1	1.0	2.9	1.0	0.9	1366.3	4042.1	262.7
OA#1bis	4462	Ordovician	1.3	6.0	1.4	1.0	13.8	3.5	1.1	0.8	0.3	1.4	1.1	3.0	0.9	1.1	1.7	0.9	1031.2	2566.9	166.7
OA#1bis	4599	Ordovician	1.3	5.8	1.3	1.0	9.6	2.2	1.0	0.8	0.4	1.7	1.0	3.9	0.8	3.2	1.0	0.9	1151.4	3941.9	772.5
RDC#2	3911	Ordovician	1.3	4.3	1.0	0.9	9.9	2.9	0.8	0.8	0.2	1.0	0.9	6.0	1.0	4.4	1.3	0.8	822.3	3849.6	624.5
GLNE#3	3936.08	Ordovician	1.7	9.7	1.5	1.0	17.1	3.9	0.9	0.9	0.2	1.1	0.9	4.5	1.2	3.4	2.6	0.6	1723.2	4040.4	180.4
GLNE#5	4024	Ordovician	1.1	6.0	1.1	0.9	19.3	3.5	1.0	0.8	0.3	1.4	1.0	2.7	1.0	10.7	2.2	0.8	1616.9	5068.5	259.0
GLNE#5	4026	Ordovician	1.2	6.4	1.2	1.0	15.4	4.1	1.0	0.8	0.3	1.4	1.0	3.0	0.8	9.3	1.6	1.0	1032.2	3722.4	136.3
BKZ#1	4198	Ordovician	1.2	6.8	1.6	1.1	17.3	4.8	0.7	0.9	0.2	1.0	0.8	13.5	1.1	8.2	2.9	1.0	2173.8	6093.2	165.9
GEC#1	3770	Ordovician	1.3	6.7	1.4	1.0	10.1	3.0	0.6	0.9	0.3	0.8	0.8	5.9	0.8	2.5	1.5	0.8	2625.4	5983.8	232.9
GBC#1	3272	Ordovician	1.3	5.1	1.2	0.9	8.7	2.8	1.0	0.8	0.3	1.4	1.0	4.4	1.1	4.8	1.7	0.3	1761.9	3906.2	1096.5
GBC#1	3386	Ordovician	1.6	6.9	1.5	1.0	13.9	4.0	1.1	0.9	0.3	1.4	1.1	4.8	1.0	2.5	0.9	0.9	1594.5	3763.7	648.7
GBC#1	3394	Ordovician	1.5	6.3	1.3	1.0	9.7	3.1	1.0	0.8	0.3	1.3	1.0	4.6	1.0	0.5	1.6	0.9	1764.1	6328.7	1612.4
GBC#1	3398	Ordovician	1.5	5.8	1.6	1.0	18.4	3.2	1.0	0.9	0.4	1.4	1.0	2.8	0.6	0.2	2.9	1.0	5201.2	9326.1	770.5
GD#1bis	3921.5	Ordovician	1.2	4.7	1.1	0.9	6.1	2.4	0.6	0.9	0.2	0.9	0.8	4.6	0.7	0.1	1.2	0.9	4449.1	9515.9	449.1
GD#1bis	3939	Ordovician	1.0	3.3	1.1	0.9	6.6	3.3	0.7	0.8	0.2	0.8	0.8	4.5	1.1	1.1	1.2	0.9	435.4	3259.8	234.7
GD#1bis	4025.9	Ordovician	0.9	3.5	1.2	0.9	12.4	3.5	0.9	0.8	0.2	1.4	0.9	3.8	1.2	0.8	2.7	0.9	9408.1	42223.1	601.1
HGA#1	3391	Ordovician	1.3	5.4	1.2	0.9	10.0	3.1	0.8	0.8	0.2	1.0	0.9	7.9	1.3	3.0	1.0	0.8	1164.5	4493.0	977.7
HGA#1	3412	Ordovician	1.3	4.9	1.5	1.0	10.4	3.5	0.7	0.9	0.3	0.9	0.8	7.8	1.0	3.7	1.3	0.9	655.6	4570.9	968.6
HGA#1	3439	Ordovician	1.6	6.6	1.9	1.1	9.0	2.5	0.7	0.9	0.3	1.0	0.8	10.3	1.3	2.1	2.9	0.8	1260.3	11359.0	408.0

Appendix 4.3 Biomarker ratios of the oils

Sample	Field	C_{21}ster+C_{22}ster/C_{29}ster	20S/20S+20R	ββ/αα+ββ	C_{29}Ts/(C_{29}Ts+C_{29}hop)	C_{30}diahop/(C_{30}hop+C_{30}diah)	C_{29}hop/C_{30}hop	C_{24} tetra/C_{30}hop	Ts/Ts+Tm	C_{23}T/(C_{30}hop$_{+C23T}$)	(C_{28}T+C_{29}T)/C_{29}+C_{30}hop	(C_{28}T+C_{29}T)/Ts	C_{29}DiasterR/C_{29ster}R	sum Ster/sum Hop	C_{24}tetra/C_{26} tricyc	%C_{28} ster.	%C_{27} ster.	%C_{29} ster.
MD59	HMD	0.56	0.59	0.57	0.39	0.34	0.69	0.29	0.73	0.77	0.54	7.26	0.79	0.64	0.19	21.43	41.06	37.52
MD104	HMD	0.55	0.52	0.57	0.54	0.38	0.44	0.29	0.84	0.75	0.61	7.57	0.77	0.69	0.17	22.46	41.27	36.27
MD165	HMD	0.55	0.55	0.60	0.43	0.37	0.62	0.25	0.69	0.74	0.57	5.85	0.81	0.65	0.15	21.80	40.69	37.51
MD185	HMD	0.59	0.59	0.60	0.39	0.41	0.86	0.34	0.79	0.79	0.56	7.85	0.82	0.66	0.19	22.38	40.63	36.99
MD201b	HMD	0.61	0.61	0.60	0.41	0.38	0.70	0.31	0.82	0.78	0.60	8.06	0.85	0.62	0.17	22.48	40.54	36.98
MD204	HMD	0.57	0.57	0.60	0.36	0.37	0.75	0.37	0.73	0.77	0.61	8.25	0.82	0.65	0.22	21.15	41.16	37.69
MD208	HMD	0.54	0.57	0.57	0.43	0.34	0.65	0.22	0.68	0.75	0.56	9.03	0.78	0.64	0.15	22.36	39.61	38.03
MD239	HMD	0.55	0.55	0.60	0.47	0.37	0.54	0.30	0.72	0.74	0.57	7.75	0.80	0.65	0.19	22.22	40.33	37.45
MD255b	HMD	0.57	0.55	0.61	0.44	0.41	0.70	0.26	0.78	0.79	0.65	8.08	0.82	0.68	0.12	21.31	40.25	38.44
MD279	HMD	0.54	0.57	0.59	0.42	0.35	0.74	0.26	0.70	0.74	0.54	7.29	0.79	0.62	0.17	21.60	40.40	38.00
MD297	HMD	0.51	0.58	0.58	0.38	0.28	0.74	0.26	0.70	0.70	0.48	5.65	0.78	0.55	0.21	22.37	40.10	37.53
MD317	HMD	0.58	0.56	0.62	0.43	0.37	0.56	0.25	0.79	0.76	0.61	8.16	0.83	0.64	0.13	21.32	41.88	36.80
MD322	HMD	0.57	0.53	0.56	0.37	0.31	0.52	0.22	0.69	0.63	0.47	7.26	0.77	0.54	0.21	21.35	41.39	37.26
MD332b	HMD	0.50	0.58	0.56	0.36	0.31	0.83	0.29	0.69	0.70	0.49	6.48	0.77	0.57	0.23	20.58	40.03	39.39
MD348	HMD	0.57	0.59	0.59	0.40	0.32	0.66	0.24	0.68	0.71	0.52	8.62	0.81	0.58	0.17	21.92	39.18	38.90
OMK14	HMD	0.53	0.55	0.60	0.36	0.29	0.77	0.29	0.73	0.71	0.55	6.95	0.80	0.59	0.24	21.27	40.33	38.41
OMP263	HMD	0.57	0.52	0.62	0.38	0.34	0.71	0.17	0.77	0.75	0.58	7.03	0.80	0.64	0.09	23.07	39.88	37.05
OMM33	HMD	0.54	0.60	0.59	0.37	0.32	0.77	0.28	0.70	0.69	0.50	5.15	0.80	0.54	0.23	20.62	39.96	39.43
OMM772	HMD	0.50	0.62	0.59	0.34	0.28	0.72	0.26	0.71	0.66	0.46	5.96	0.80	0.53	0.22	21.59	39.15	39.26
OMN352	HMD	0.57	0.60	0.60	0.42	0.38	0.70	0.27	0.73	0.73	0.55	6.81	0.82	0.59	0.19	21.11	40.14	38.75
OMN412	HMD	0.56	0.54	0.59	0.41	0.31	0.61	0.31	0.70	0.74	0.59	6.73	0.78	0.64	0.20	20.54	41.04	38.42
OMO36	HMD	0.53	0.55	0.59	0.42	0.35	0.65	0.31	0.79	0.77	0.61	8.11	0.79	0.68	0.19	21.31	41.29	37.40
OMO712	HMD	0.55	0.55	0.61	0.44	0.36	0.65	0.37	0.78	0.79	0.62	8.10	0.80	0.70	0.20	21.62	40.78	37.59
OMO751	HMD	0.56	0.59	0.58	0.43	0.31	0.61	0.27	0.86	0.75	0.54	7.55	0.80	0.66	0.16	21.05	40.75	38.20
OMJ422	HMD	0.53	0.57	0.60	0.39	0.29	0.74	0.21	0.66	0.70	0.49	6.39	0.79	0.57	0.15	20.98	40.51	38.52
OMJ832	HMD	0.55	0.57	0.59	0.41	0.30	0.65	0.28	0.65	0.72	0.52	6.82	0.79	0.60	0.23	21.18	41.33	37.49
OM7	HMD	0.57	0.54	0.61	0.42	0.33	0.63	0.22	0.81	0.73	0.58	6.37	0.80	0.64	0.12	20.94	41.10	37.96
OML862	HMD	0.52	0.58	0.64	0.37	0.35	0.70	0.25	0.74	0.71	0.50	7.17	0.83	0.57	0.18	21.67	41.34	36.99
ONI412	HMD	0.55	0.61	0.63	0.40	0.31	0.58	0.26	0.70	0.72	0.54	6.81	0.85	0.58	0.19	21.34	40.87	37.79
ONM36	HMD	0.57	0.59	0.61	0.40	0.30	0.69	0.30	0.61	0.73	0.54	8.18	0.82	0.59	0.21	20.79	40.47	38.74
MD6	HMD	0.55	0.55	0.59	0.52	0.30	0.58	0.18	0.77	0.77	0.64	6.62	0.77	0.62	0.11	19.08	40.91	40.01
MD45	HMD	0.55	0.52	0.61	0.49	0.31	0.57	0.21	0.79	0.74	0.61	7.08	0.77	0.59	0.14	19.71	38.93	41.36
MD46	HMD	0.55	0.62	0.62	0.55	0.36	0.50	0.23	0.83	0.76	0.68	6.55	0.83	0.65	0.13	19.65	40.58	39.77
MD64	HMD	0.54	0.57	0.60	0.52	0.31	0.59	0.18	0.79	0.77	0.65	7.35	0.79	0.62	0.10	18.65	41.47	39.88
MD125	HMD	0.54	0.55	0.59	0.55	0.32	0.54	0.17	0.76	0.77	0.64	6.80	0.76	0.63	0.10	18.95	40.24	40.81
MD129	HMD	0.58	0.53	0.62	0.57	0.36	0.53	0.24	0.84	0.79	0.68	7.41	0.80	0.66	0.12	20.23	40.59	39.18

Appendix 4.3 Biomarker ratios of the oils (continued)

MD134	HMD	0.51	0.57	0.59	0.43	0.27	0.66	0.23	0.72	0.69	0.54	5.96	0.75	0.55	0.19	22.28	39.51	38.21
MD139	HMD	0.54	0.53	0.60	0.58	0.34	0.47	0.20	0.80	0.77	0.66	6.74	0.77	0.65	0.11	19.74	39.34	40.92
MD140	HMD	0.58	0.54	0.61	0.53	0.33	0.62	0.23	0.80	0.79	0.67	6.74	0.80	0.63	0.13	19.18	41.08	39.74
MD141	HMD	0.54	0.53	0.60	0.46	0.24	0.61	0.16	0.77	0.70	0.55	6.20	0.75	0.54	0.13	22.05	38.16	39.79
MD177	HMD	0.57	0.57	0.61	0.55	0.31	0.50	0.20	0.83	0.76	0.68	6.73	0.80	0.65	0.11	19.39	39.95	40.66
MD213	HMD	0.52	0.55	0.62	0.40	0.32	0.64	0.14	0.78	0.73	0.61	6.41	0.80	0.57	0.09	19.91	41.17	38.91
MD215	HMD	0.50	0.53	0.62	0.38	0.25	0.56	0.12	0.78	0.65	0.55	6.49	0.79	0.50	0.10	21.47	38.98	39.55
MD221	HMD	0.47	0.55	0.58	0.37	0.25	0.72	0.16	0.68	0.66	0.50	5.73	0.76	0.48	0.16	21.75	40.03	38.22
MD235	HMD	0.53	0.56	0.61	0.60	0.38	0.47	0.19	0.84	0.78	0.68	6.98	0.81	0.65	0.10	18.36	40.71	40.93
MD269	HMD	0.48	0.58	0.60	0.52	0.29	0.58	0.22	0.74	0.70	0.57	5.23	0.77	0.56	0.18	19.26	39.00	41.73
MD272	HMD	0.54	0.53	0.59	0.51	0.34	0.60	0.17	0.76	0.76	0.63	6.73	0.78	0.62	0.09	18.95	41.98	39.06
MD275	HMD	0.57	0.56	0.63	0.51	0.33	0.57	0.23	0.78	0.78	0.66	7.76	0.80	0.62	0.12	20.27	39.47	40.26
MD280	HMD	0.54	0.57	0.58	0.56	0.34	0.55	0.18	0.78	0.79	0.69	7.19	0.76	0.67	0.09	20.59	39.08	40.32
MD287	HMD	0.51	0.54	0.60	0.53	0.37	0.49	0.12	0.75	0.76	0.67	7.79	0.79	0.64	0.06	17.90	41.16	40.94
MD299	HMD	0.50	0.55	0.58	0.53	0.31	0.56	0.23	0.79	0.73	0.60	5.44	0.76	0.58	0.17	19.65	40.07	40.28
MD300	HMD	0.55	0.54	0.60	0.55	0.34	0.58	0.22	0.79	0.78	0.68	7.35	0.77	0.67	0.11	20.47	38.72	40.81
MD304	HMD	0.52	0.57	0.60	0.58	0.37	0.53	0.23	0.85	0.78	0.67	7.06	0.78	0.68	0.12	19.69	39.42	40.89
MD345	HMD	0.52	0.58	0.61	0.50	0.26	0.57	0.22	0.77	0.73	0.61	5.84	0.78	0.58	0.17	19.56	39.35	41.09
MD409	HMD	0.53	0.56	0.62	0.55	0.38	0.52	0.17	0.82	0.74	0.66	6.99	0.79	0.62	0.08	22.33	38.13	39.54
MD412	HMD	0.51	0.55	0.62	0.56	0.35	0.45	0.14	0.79	0.74	0.66	8.41	0.80	0.62	0.07	20.33	38.42	41.26
OMJ41	HMD	0.54	0.58	0.61	0.52	0.28	0.51	0.18	0.78	0.74	0.61	6.33	0.80	0.57	0.13	20.78	38.72	40.50
OMJ721	HMD	0.51	0.56	0.60	0.53	0.33	0.57	0.18	0.76	0.76	0.63	6.84	0.80	0.61	0.12	25.97	35.90	38.13
OML76	HMD	0.53	0.55	0.62	0.55	0.32	0.54	0.19	0.75	0.75	0.63	6.98	0.82	0.58	0.11	17.50	42.62	39.88
OML82	HMD	0.53	0.56	0.62	0.46	0.31	0.62	0.25	0.78	0.75	0.62	6.50	0.82	0.57	0.17	18.72	40.90	40.38
OML712	HMD	0.52	0.55	0.60	0.47	0.34	0.67	0.18	0.80	0.76	0.63	6.88	0.80	0.58	0.11	19.07	41.41	39.52
OMM67	HMD	0.49	0.55	0.59	0.43	0.23	0.67	0.15	0.71	0.68	0.54	6.02	0.77	0.50	0.13	18.88	40.64	40.48
OMM741	HMD	0.51	0.56	0.60	0.51	0.30	0.59	0.22	0.76	0.73	0.58	6.38	0.80	0.56	0.16	19.87	39.78	40.35
OMM80	HMD	0.52	0.56	0.61	0.56	0.31	0.56	0.16	0.81	0.77	0.65	6.42	0.80	0.64	0.09	19.59	39.62	40.79
OMM532	HMD	0.51	0.53	0.58	0.45	0.29	0.63	0.17	0.71	0.70	0.55	5.22	0.77	0.53	0.14	19.24	39.29	41.47
OMM542	HMD	0.51	0.55	0.60	0.45	0.29	0.66	0.16	0.75	0.70	0.54	5.08	0.77	0.52	0.13	20.16	39.51	40.32
OMM632	HMD	0.50	0.58	0.61	0.48	0.30	0.61	0.22	0.74	0.73	0.59	6.12	0.78	0.56	0.18	19.08	39.86	41.07
OMM763	HMD	0.52	0.56	0.60	0.43	0.29	0.71	0.17	0.78	0.74	0.60	6.53	0.78	0.56	0.09	18.38	42.26	39.37
OMM812	HMD	0.53	0.55	0.59	0.54	0.32	0.56	0.22	0.74	0.76	0.63	6.67	0.78	0.61	0.14	21.10	39.37	39.53
OMN33	HMD	0.53	0.54	0.59	0.53	0.30	0.53	0.23	0.77	0.76	0.64	7.06	0.78	0.61	0.14	20.22	39.42	40.36
OMN681	HMD	0.55	0.52	0.61	0.55	0.31	0.52	0.19	0.75	0.76	0.64	6.98	0.80	0.60	0.12	20.66	38.26	41.08
OMO142	HMD	0.56	0.51	0.62	0.56	0.32	0.55	0.23	0.78	0.79	0.68	7.12	0.80	0.65	0.11	20.94	39.22	39.84
OMO343	HMD	0.55	0.55	0.61	0.57	0.32	0.54	0.15	0.82	0.79	0.69	7.26	0.81	0.66	0.08	19.51	40.38	40.11
OMP33	HMD	0.55	0.54	0.61	0.58	0.34	0.47	0.19	0.81	0.77	0.69	7.52	0.79	0.64	0.10	19.26	39.50	41.24
OMP42	HMD	0.55	0.56	0.62	0.58	0.33	0.46	0.18	0.83	0.78	0.69	7.64	0.81	0.65	0.09	21.01	39.47	39.52
OMP67	HMD	0.54	0.51	0.62	0.52	0.30	0.58	0.17	0.77	0.76	0.63	7.18	0.81	0.58	0.10	19.26	39.12	41.62

Appendix 4.3 Biomarker ratios of the oils (continued)

OMP74	HMD	0.56	0.53	0.62	0.48	0.34	0.62	0.19	0.80	0.77	0.67	6.54	0.81	0.61	0.11	19.13	40.25	40.62
OMP802	HMD	0.54	0.54	0.61	0.50	0.35	0.59	0.16	0.87	0.78	0.68	7.46	0.81	0.63	0.07	19.57	40.81	39.62
ONI403	HMD	0.53	0.53	0.62	0.45	0.32	0.57	0.16	0.84	0.75	0.64	6.41	0.81	0.59	0.09	20.93	38.39	40.67
ONM243	HMD	0.54	0.53	0.61	0.48	0.32	0.59	0.15	0.84	0.76	0.65	6.55	0.79	0.61	0.08	17.74	41.76	40.49
ONM461	HMD	0.53	0.56	0.62	0.57	0.33	0.48	0.14	0.76	0.77	0.66	7.68	0.81	0.62	0.07	20.57	41.43	38.01
GS1	El Gassi	0.57	0.57	0.62	0.55	0.33	0.62	0.27	0.79	0.77	0.64	5.29	0.81	0.56	0.16	19.02	39.53	41.45
AR-61	Zotti	0.53	0.58	0.64	0.53	0.31	0.59	0.21	0.75	0.75	0.61	6.74	0.82	0.61	0.14	20.39	38.54	41.07
AR22	El Agreb	0.56	0.62	0.65	0.54	0.32	0.63	0.00	0.74	0.77	0.63	5.63	0.82	0.59	0.13	19.61	39.33	41.06
DRT#1	D.Temra	0.54	0.61	0.65	0.45	0.31	0.74	0.40	0.74	0.66	0.39	2.45	0.71	0.41	0.39	19.63	35.94	44.43
GLNE#5	Guellala NE	0.37	0.57	0.57	0.49	0.36	0.66	0.17	0.75	0.67	0.54	5.83	0.73	0.91	0.25	21.32	33.01	45.68
GLA#16	Guellala	0.40	0.57	0.59	0.45	0.34	0.68	0.14	0.78	0.64	0.50	4.78	0.74	0.59	0.23	18.62	36.59	44.80
MEK#1	M.El kebch	0.53	0.57	0.61	0.49	0.37	0.62	0.15	0.76	0.67	0.49	4.83	0.75	0.55	0.26	21.30	39.95	38.75
NGS#2	N'goussa	0.43	0.60	0.60	0.46	0.36	0.65	0.14	0.77	0.68	0.52	4.77	0.74	0.55	0.25	18.63	37.01	44.36
OKJ#31	H.Berkaoui	0.40	0.59	0.59	0.41	0.30	0.72	0.28	0.70	0.62	0.43	2.99	0.71	0.41	0.42	19.21	35.96	44.83
OKJ#202	H.Berkaoui	0.44	0.55	0.60	0.41	0.30	0.74	0.26	0.67	0.63	0.44	3.26	0.70	0.46	0.39	20.52	36.48	43.00
OKM#881	H.Berkaoui	0.41	0.62	0.58	0.40	0.28	0.83	0.28	0.68	0.60	0.43	3.36	0.70	0.46	0.44	19.26	36.81	43.93
OKN#77	H.Berkaoui	0.43	0.59	0.58	0.40	0.28	0.71	0.29	0.70	0.61	0.44	3.45	0.69	0.50	0.44	19.19	35.95	44.86
OKP#61	*Benkahla*	*0.46*	0.59	0.59	0.42	0.29	0.85	0.24	0.71	0.62	0.47	4.14	0.71	0.50	0.37	21.82	37.57	40.61
OKP#88	Benkahla	0.43	0.58	0.60	0.42	0.30	0.70	0.28	0.72	0.61	0.46	3.70	0.72	0.46	0.38	20.15	35.18	44.66
RDC-1b	R.Chegga	0.75	0.60	0.60	0.57	0.46	0.62	0.17	0.77	0.83	0.73	6.88	0.78	0.77	0.06	20.39	38.42	41.19
HGA2	H.Guettar	0.56	0.58	0.62	0.35	0.30	0.81	0.30	0.76	0.72	0.73	6.37	0.81	0.52	0.27	20.92	40.74	38.33
HGA3	H.Guettar	0.57	0.59	0.59	0.35	0.31	0.80	0.32	0.79	0.75	0.43	6.41	0.79	0.57	0.23	22.70	40.03	37.27
MDR-7	Mesdar	0.63	0.54	0.59	0.72	0.35	0.42	0.21	0.87	0.87	0.54	7.36	0.66	0.72	0.06	20.47	37.50	42.04
MDR8	Mesdar	0.61	0.52	0.65	0.70	0.33	0.47	0.00	0.84	0.83	0.70	7.88	0.67	0.73	0.05	19.24	36.13	44.63
RB10	El Baguel	0.60	0.60	0.61	0.58	0.30	0.47	0.19	0.76	0.80	0.66	7.29	0.64	0.76	0.08	19.58	35.97	44.44
RB-18	El Baguel	0.58	0.55	0.60	0.56	0.29	0.45	0.29	0.74	0.77	0.91	7.37	0.64	0.77	0.06	22.88	36.17	40.95
OL2	DST	0.55	0.51	0.56	0.25	0.13	0.71	0.13	0.56	0.72	0.50	6.41	0.75	0.37	0.16	22.92	40.00	37.08

Appendix 4.3 Biomarker concentrations (ug/g oil) of the oils.

Sample	Field	C_{21} T	C_{22} T	C_{23} T	C_{24} T	C_{25} T	C_{24} Tetra	C_{26} T	C_{28} T	C_{29} T	C_{30} T	C_{31} T	Ts	Tm	C_{29} Hop.	C_{29} Ts	C_{30} Diah.	C_{30} Hop.	C_{31} Hop R	C_{32} Hop S	C_{32} Hop R	Sum Tric(mg/g)	Sum Hop(mg/g)
MD6	HMD	7.04	2.52	9.77	6.96	6.77	0.64	6.08	6.16	6.12	4.24	4.50	1.86	0.56	1.68	1.82	1.23	2.91	0.95	0.77	0.62	60.15	8.48
MD45	HMD	6.14	1.84	7.83	6.77	5.65	0.76	5.34	5.31	5.76	4.02	4.05	1.56	0.42	1.60	1.53	1.27	2.79	0.94	1.05	0.70	52.71	7.82
MD46	HMD	6.69	1.83	7.86	7.25	6.37	0.75	5.76	5.65	5.74	4.09	4.74	1.74	0.35	1.22	1.50	1.39	2.44	0.83	0.55	0.39	55.96	7.19
MD64	HMD	8.93	2.42	12.11	8.95	8.29	0.80	7.64	8.01	7.96	5.37	5.89	2.17	0.57	2.12	2.29	1.62	3.58	1.07	1.12	0.79	75.57	10.25
MD125	HMD	8.50	2.32	11.23	8.28	7.67	0.72	7.31	7.35	7.60	5.34	5.55	2.20	0.71	1.85	2.30	1.58	3.42	1.15	1.10	0.84	71.16	10.05
MD129	HMD	6.97	1.91	8.31	7.15	6.39	0.67	5.55	5.74	5.64	4.12	4.19	1.53	0.30	1.14	1.54	1.23	2.16	0.90	0.78	0.46	55.96	6 53
MD134	HMD	7.46	2.15	9.68	5.26	6.95	1.31	6.74	6.60	7.08	5.10	5.48	2.29	0.90	2.89	2.21	1.62	4.40	1.52	1.82	0.94	62.50	12.62
MD139	HMD	8.96	2.22	11.48	8.34	7.72	0.84	7.57	7.68	7.46	5.39	5.61	2.25	0.58	1.61	2.25	1.75	3.43	1.11	1.02	0.78	72.44	9.58
MD140	HMD	8.69	2.36	10.84	8.38	7.63	0.88	6.95	7.02	7.12	5.49	5.12	2.10	0.53	1.79	2.00	1.45	2.90	0.91	0.85	0.65	69.58	8.55
MD141	HMD	7.18	2.09	10.32	7.32	7.18	0.80	6.28	6.65	6.85	4.64	4.93	2.18	0.63	2.64	2.29	1.36	4.35	1.45	1.39	1.01	63.45	12.00
MD177	HMD	6.20	1.85	7.01	5.67	5.54	0.54	4.94	4.95	4.85	3.62	3.50	1.46	0.29	1.09	1.35	0.98	2.21	0.54	0.45	0.40	48.14	6.11
MD213	HMD	7.89	2.00	10.01	7.45	7.08	0.60	6.80	6.57	7.51	5.21	5.65	2.20	0.62	2.31	1.57	1.69	3.63	1.16	0.99	0.83	66.19	10.49
MD215	HMD	8.85	2.56	11.77	9.45	8.67	0.88	8.65	9.31	9.40	7.20	7.32	2.88	0.83	3.51	2.15	2.02	6.21	1.87	2.18	1.32	83.18	15.97
MD221	HMD	10.39	2.78	15.05	10.67	9.69	1.50	9.54	10.13	10.31	9.66	7.35	3.56	1.68	5.59	3.35	2.61	7.76	2.76	2.50	1.84	95.56	22.71
MD235	HMD	8.29	2.31	10.19	8.03	7.53	0.69	7.07	7.13	7.83	5.44	6.25	2.14	0.42	1.38	2.07	1.83	2.94	0.91	1.07	0.67	70.06	8.38
MD269	HMD	9.87	2.97	13.76	9.66	9.08	1.65	9.16	9.59	9.00	6.52	7.43	3.56	1.28	3.45	3.76	2.47	5.91	1.84	1.65	1.29	87.03	17.06
MD272	HMD	6.96	2.13	8.95	6.73	6.69	0.60	6.40	5.96	6.61	4.38	5.07	1.87	0.58	1.72	1.83	1.50	2.85	0.98	0.96	0.77	59.85	8.64
MD275	HMD	6.36	1.79	7.73	5.62	5.56	0.66	5.31	5.34	5.09	3.75	3.93	1.34	0.37	1.25	1.32	1.10	2.21	0.84	0.73	0.46	50.48	6.44
MD280	HMD	8.66	3.03	11.45	8.96	7.84	0.66	7.34	7.81	7.50	5.31	5.67	2.13	0.58	1.66	2.14	1.58	3.01	0.86	0.79	0.61	73.59	8.94
MD287	HMD	8.70	2.59	11.26	9.28	8.30	0.47	7.96	8.74	8.23	6.08	6.02	2.18	0.71	1.70	1.92	2.08	3.50	1.27	1.07	0.80	77.15	10.11
MD299	HMD	8.82	2.63	12.52	9.25	8.17	1.36	8.19	8.61	8.18	5.95	5.99	3.08	0.83	2.60	2.94	2.04	4.61	1.50	1.35	1.00	78.31	13.50
MD300	HMD	8.01	2.13	10.04	7.56	7.22	0.77	7.13	6.74	7.06	5.08	5.01	1.88	0.49	1.59	1.91	1.43	2.76	0.88	0.74	0.60	65.98	8.25
MD304	HMD	9.52	2.95	13.21	9.69	9.88	1.10	9.15	9.13	9.13	6.32	7.25	2.58	0.46	1.94	2.68	2.10	3.65	1.38	1.27	0.82	86.23	10.78
MD345	HMD	6.90	2.00	9.46	7.33	6.22	0.96	5.74	6.49	6.09	4.30	4.67	2.16	0.64	1.99	2.02	1.22	3.47	1.06	0.99	0.65	59.20	9.95
MD409	HMD	7.00	2.01	8.25	7.44	6.87	0.57	6.71	6.11	6.93	4.88	5.23	1.86	0.41	1.48	1.81	1.74	2.83	0.93	0.84	0.56	61.44	8.11
MD412	HMD	6.82	1.85	8.65	7.44	6.82	0.49	6.75	6.39	7.16	5.07	4.87	1.61	0.42	1.37	1.75	1.65	3.03	0.93	1.01	0.57	61.82	7.96
OMJ41	HMD	7.33	1.97	10.09	7.01	6.76	0.80	6.03	6.49	6.47	4.20	4.47	2.05	0.58	1.80	1.99	1.41	3.54	1.09	1.17	0.70	60.82	9.68
OMJ721	HMD	7.35	2.06	10.34	7.49	7.19	0.72	6.11	6.89	6.60	4.48	4.51	1.97	0.63	1.88	2.15	1.60	3.30	1.00	0.91	0.69	63.02	9.41
OML76	HMD	10.51	3.29	15.26	11.96	10.04	1.15	10.17	10.43	10.49	7.02	7.61	2.99	1.02	2.71	3.26	2.33	5.01	1.51	1.73	1.13	96.78	14.04
OML82	HMD	9.60	2.93	12.99	10.32	9.67	1.51	8.80	8.87	8.83	6.21	6.42	2.72	0.79	2.75	2.38	2.02	4.43	1.20	1.54	1.09	84.66	12.70
OML712	HMD	12.27	4.77	16.66	12.41	11.70	1.18	10.58	11.80	11.97	8.31	9.07	3.45	0.85	3.59	3.16	2.76	5.39	1.78	1.84	1.25	109.55	16.31
OMM67	HMD	11.37	3.23	16.04	11.78	10.64	1.29	9.83	11.27	10.75	7.41	7.79	3.66	1.47	4.94	3.69	2.26	7.41	2.60	2.42	1.53	100.10	21.04
OMM74	HMD	8.48	2.46	12.06	8.92	8.09	1.26	7.77	8.00	7.23	5.17	6.04	2.39	0.76	2.68	2.79	2.00	4.57	1.44	1.32	0.95	74.22	12.72
OMM80	HMD	9.37	2.57	12.77	9.02	8.59	0.74	8.07	8.73	8.23	5.58	6.59	2.64	0.62	2.12	2.66	1.67	3.79	1.22	1.17	0.76	79.52	11.12
OMM352	HMD	10.00	2.92	13.72	9.55	8.67	1.22	8.45	8.94	8.36	6.22	6.55	3.31	1.32	3.69	3.06	2.43	5.89	1.72	1.63	1.18	83.40	17.28
OMM542	HMD	9.93	2.86	14.07	10.15	9.53	1.17	9.13	8.88	8.96	6.50	6.89	3.51	1.16	3.99	3.25	2.45	6.02	1.81	2.07	1.34	86.89	17.78
OMM632	HMD	14.59	4.79	20.64	14.34	12.91	2.09	11.92	12.56	13.41	10.11	10.15	4.25	1.48	4.59	4.19	3.18	7.58	1.95	2.10	1.58	125.41	20.66

Appendix 4.3 Biomarker concentrations (ug/g oil) of the oils (continued).

OMM63	HMD	10.42	2.67	14.38	10.59	9.57	0.98	10.54	9.37	9.45	6.12	7.00	2.88	0.83	3.49	2.58	1.97	4.93	1.81	1.53	0.99	90.12	15.03
OMM612	HMD	8.64	2.25	11.53	8.52	7.77	1.06	7.60	7.32	7.27	4.97	5.44	2.19	0.76	2.06	2.44	1.70	3.69	1.06	1.10	0.77	71.32	10.14
OMN83	HMD	5.80	1.57	7.87	5.68	5.17	0.72	5.25	5.09	4.92	3.39	3.73	1.42	0.43	1.31	1.48	1.07	2.49	0.79	0.74	0.42	48.48	6.83
OMN881	HMD	8.97	2.80	12.20	8.72	8.42	0.94	7.72	7.65	8.32	5.25	5.89	2.29	0.75	2.04	2.52	1.76	3.90	1.28	0.99	0.66	75.95	11.03
OMO142	HMD	5.71	1.63	7.55	5.45	4.80	0.57	4.98	4.74	5.17	3.39	3.54	1.39	0.40	1.09	1.36	0.93	1.95	0.63	0.55	0.45	46.95	5.99
OMO843	HMD	6.06	1.78	8.16	5.96	5.74	0.39	5.08	5.68	5.66	3.81	3.73	1.55	0.34	1.17	1.53	1.01	2.16	0.77	0.62	0.48	51.65	6.49
OMP33	HMD	9.03	2.65	10.86	9.11	8.07	0.78	7.93	7.72	8.27	5.62	5.85	2.13	0.49	1.54	2.14	1.70	3.26	0.84	0.99	0.71	75.14	8.94
OMP42	HMD	5.85	1.51	7.41	6.08	5.31	0.45	5.04	5.17	5.42	3.24	3.66	1.39	0.29	0.97	1.33	1.06	2.14	0.52	0.66	0.44	48.71	5.72
OMP67	HMD	7.01	2.06	9.47	7.12	6.63	0.61	6.34	6.38	6.36	4.44	4.46	1.78	0.54	1.77	1.95	1.34	3.07	1.01	0.83	0.72	60.27	8.64
OMP74	HMD	8.98	2.70	11.35	9.27	7.88	0.79	7.55	7.70	8.08	5.67	6.09	2.41	0.59	2.06	1.93	1.75	3.34	0.95	0.82	0.75	75.27	10.04
OMP802	HMD	9.60	2.58	11.71	9.02	8.40	0.63	8.42	8.16	8.60	5.97	6.67	2.25	0.32	1.95	1.91	1.78	3.29	0.91	1.03	0.75	79.14	9.42
OMV03	HMD	6.85	2.24	9.40	7.17	6.84	0.57	6.46	6.53	6.38	4.62	4.85	2.01	0.38	1.77	1.47	1.46	3.10	1.00	0.80	0.62	61.35	8.67
OMV243	HMD	10.55	3.00	14.18	10.89	9.99	0.79	10.10	10.10	10.13	6.86	6.36	3.09	0.57	2.62	2.39	2.10	4.44	1.43	1.32	1.01	92.14	13.01
OMV461	HMD	7.19	2.36	10.29	7.39	6.99	0.49	6.83	6.93	6.84	5.10	5.31	1.79	0.55	1.50	1.96	1.55	3.14	0.88	0.91	0.73	65.26	8.57
GS1	El Gassi	8.68	2.55	11.43	8.00	7.98	1.27	8.00	8.13	7.73	5.54	5.91	3.00	0.59	2.16	2.65	1.74	3.50	1.21	1.27	0.73	73.90	11.20
AR61	Zotti	10.03	2.83	14.49	10.60	9.03	1.31	9.21	9.25	9.16	6.98	6.98	2.73	1.28	2.91	3.28	2.25	4.92	1.37	1.89	0.84	88.56	14.34
AR22	El Agreb	9.29	2.42	12.09	9.49	8.45	0.00	7.85	8.26	8.19	5.89	5.93	2.92	0.58	2.32	2.78	1.74	3.70	1.18	1.39	0.93	77.86	10.71
DRT1	D.Terra	10.89	4.09	14.66	10.98	8.92	6.94	10.11	10.09	9.61	6.99	8.30	8.05	3.18	7.62	7.31	4.55	10.32	4.45	4.87	3.31	94.64	37.88
GLNE5	Gudilda NE	12.09	3.78	17.76	13.27	11.46	1.73	11.50	12.72	9.49	7.83	8.50	3.81	1.24	3.93	3.77	2.98	8.58	2.53	2.18	1.34	108.41	21.55
MEK1	ME Ikebch	10.18	3.33	14.20	10.81	9.05	1.37	8.54	9.22	7.98	5.08	6.77	3.56	1.43	3.91	3.73	2.80	7.91	2.24	2.40	1.53	85.17	20.39
NGS2	Ngoussa	8.05	3.35	11.60	8.41	7.53	1.08	7.35	8.28	7.42	5.62	5.83	3.29	1.17	3.58	2.68	2.25	6.50	1.50	1.61	1.21	73.43	17.31
OKI31	HBerkaoui	11.92	3.81	18.02	12.67	10.68	4.17	9.88	11.75	10.09	7.41	9.67	7.30	3.16	7.92	5.44	4.79	10.99	3.55	3.86	2.40	105.89	36.22
OKI202	HBerkaoui	12.44	3.93	17.91	12.15	10.44	3.81	9.71	11.67	10.36	7.34	9.56	6.75	3.40	7.90	5.62	4.64	10.68	3.26	3.95	2.41	105.51	34.36
OKM881	HBerkaoui	10.84	6.34	14.46	11.23	10.15	3.67	8.24	10.25	9.83	7.34	8.58	5.98	2.82	7.98	5.41	3.72	9.59	3.13	3.48	2.11	97.27	31.86
OKN77	HBerkaoui	9.95	2.84	13.20	10.65	9.34	3.44	7.79	9.14	8.30	6.10	7.11	5.05	2.19	6.05	4.04	3.30	8.49	2.69	2.85	1.75	84.41	26.35
OKP61	Berkehla	13.26	4.11	19.74	13.85	12.98	3.18	11.98	12.66	12.83	8.60	9.73	6.15	2.07	8.77	6.23	4.28	10.29	3.07	3.35	2.78	119.75	31.90
OKP88	Berkehla	11.28	6.38	16.11	11.95	11.41	3.89	10.10	11.61	10.82	8.18	8.81	6.05	2.33	7.04	5.11	4.31	10.12	3.08	3.33	2.33	106.66	31.12
RDC1b	R.Chegga	10.15	3.44	12.62	10.91	9.43	0.55	9.55	8.94	9.47	7.41	6.59	2.68	0.79	1.64	2.22	2.22	2.65	0.87	1.15	0.42	88.52	9.28
MDR7	Mesdar	5.24	1.35	6.83	5.99	4.30	0.28	4.63	3.87	3.68	2.59	3.13	2.24	0.32	0.33	0.86	0.57	1.05	0.00	0.00	0.00	41.60	4.54
MDR8	Mesdar	5.20	1.49	6.11	5.55	4.36	0.00	4.10	3.45	3.59	2.51	2.64	1.60	0.31	0.72	0.90	0.61	1.52	0.18	0.32	0.21	39.02	4.65
RB10	El Bagual	5.72	1.68	6.89	5.68	4.70	0.36	4.46	3.92	3.71	2.64	2.57	1.13	0.36	1.11	0.85	0.66	1.55	0.38	0.48	0.36	41.98	4.87
RB18	El Bagual	6.21	1.92	6.75	6.75	4.84	0.82	5.27	25.33	3.84	3.09	3.18	1.19	0.63	0.90	1.25	0.46	1.97	0.00	0.00	0.00	57.18	4.69
OL2	DST	16.04	4.08	17.80	11.67	9.67	1.10	7.96	6.51	5.70	4.16	3.91	1.94	1.53	5.03	1.69	1.09	7.08	1.70	1.51	1.11	87.49	17.28

Appendix 4.3 Biomarker concentrations (ug/g oil) of the oils (continued).

		C_{21} ster	C_{22} ster	C_{27}diast. S	C_{27}diast. R	C_{27} ααα ster. S	C_{29} diast. S	C_{27} αββ ster.S	C_{27} ααα ster.R	C_{29} diast. R	C_{29} ααα ster.S	C_{29} αββ ster. (S+R)	C_{29} ααα ster.R	Sum Steranes
MD6	HMD	6.94	2.13	4.74	2.85	1.69	6.18	2.27	1.53	4.75	1.72	4.43	1.40	40.63
MD45	HMD	5.86	1.76	4.18	2.62	1.25	5.00	1.94	1.41	3.80	1.26	3.76	1.16	33.99
MD46	HMD	6.20	2.14	4.30	2.84	1.40	5.99	1.94	1.17	4.78	1.65	4.28	1.01	37.68
MD64	HMD	8.62	2.58	5.72	3.64	1.78	7.82	2.97	1.98	6.30	2.16	5.61	1.65	50.83
MD125	HMD	7.80	2.82	5.72	3.53	1.98	7.62	2.98	1.87	5.37	2.04	5.37	1.66	48.76
MD129	HMD	6.71	2.15	4.42	2.68	1.38	5.69	2.43	1.25	4.47	1.31	4.02	1.15	37.66
MD134	HMD	6.99	2.36	4.95	3.16	1.79	6.15	2.50	1.75	4.81	2.07	5.25	1.58	43.38
MD139	HMD	8.19	2.78	5.99	3.39	1.78	7.60	2.84	1.25	5.76	1.95	5.48	1.76	48.77
MD140	HMD	8.54	2.83	5.54	3.45	1.58	7.14	2.71	1.53	5.94	1.72	4.96	1.48	47.42
MD141	HMD	7.37	2.27	4.79	2.71	1.72	6.49	2.92	1.84	4.68	1.73	4.94	1.54	43.00
MD177	HMD	6.15	1.99	3.90	2.50	1.22	5.35	1.97	1.26	3.99	1.38	3.78	1.03	34.51
MD213	HMD	6.60	2.19	5.26	3.41	1.77	7.00	2.82	1.75	5.61	1.68	4.90	1.38	44.36
MD215	HMD	7.42	2.46	5.84	3.89	1.83	7.71	3.07	2.17	6.51	1.97	6.07	1.76	50.69
MD221	HMD	8.31	2.85	6.67	4.28	2.61	8.97	4.01	2.55	7.42	2.85	7.26	2.36	60.15
MD235	HMD	6.99	2.15	5.96	3.77	1.44	7.23	2.35	1.16	5.93	1.77	5.00	1.38	45.13
MD269	HMD	8.17	2.83	6.18	4.37	2.21	8.81	3.42	2.21	6.52	2.77	6.99	1.98	56.46
MD272	HMD	6.57	2.05	4.82	3.19	1.78	6.54	2.64	1.72	5.00	1.62	4.37	1.42	41.72
MD275	HMD	5.79	1.77	3.81	2.34	1.16	5.14	2.13	1.33	3.71	1.20	3.56	0.93	32.90
MD280	HMD	8.28	2.77	6.04	3.61	1.82	7.44	2.81	1.52	5.49	2.25	5.42	1.73	49.17
MD287	HMD	7.57	2.31	6.39	4.05	1.93	8.27	3.17	1.67	6.46	2.03	5.66	1.71	51.21
MD299	HMD	7.48	2.47	5.85	3.41	1.98	7.36	2.92	1.47	5.77	2.27	5.82	1.86	48.65
MD300	HMD	8.27	2.55	5.30	3.98	1.86	7.11	2.55	1.78	5.62	1.91	5.31	1.63	47.87
MD304	HMD	9.59	2.95	7.37	4.16	2.43	9.19	3.76	2.19	7.05	2.66	7.04	2.04	60.43
MD345	HMD	6.23	1.88	4.48	2.67	1.60	5.87	2.19	1.41	4.43	1.76	4.63	1.26	38.41
MD409	HMD	6.10	1.86	5.25	2.90	1.35	6.28	2.35	1.40	4.54	1.48	4.31	1.17	38.99
MD412	HMD	5.67	1.80	5.06	3.13	0.93	5.93	2.11	1.35	4.88	1.50	4.46	1.25	38.08
OMJ41	HMD	6.45	1.93	5.16	3.21	1.45	6.50	2.51	1.45	4.72	1.63	4.36	1.20	40.57
OMJ721	HMD	6.72	1.96	5.13	3.34	0.00	6.73	2.83	1.79	5.65	1.83	4.98	1.43	42.37
OML76	HMD	8.69	3.05	7.98	4.98	2.39	10.78	4.01	2.07	8.00	2.19	6.58	1.78	62.50
OML82	HMD	8.15	2.75	7.53	4.27	1.74	9.06	3.44	1.79	7.24	2.11	5.99	1.62	55.68
OML712	HMD	10.24	3.44	9.28	5.46	2.48	11.58	4.57	2.14	8.76	2.70	7.53	2.24	70.41
OMM67	HMD	8.93	2.77	7.71	4.94	2.82	10.10	3.54	2.23	7.74	2.79	7.20	2.29	63.08
OMM74	HMD	7.31	2.43	5.78	3.58	1.96	6.24	3.27	1.83	6.30	2.02	5.53	1.62	47.86
OMM80	HMD	8.41	2.82	6.42	3.92	2.36	8.38	3.24	1.77	7.28	2.28	6.44	1.77	55.07
OMM352	HMD	8.76	2.56	6.54	4.11	2.28	8.47	3.47	1.75	6.87	2.39	6.27	2.10	55.58
OMM542	HMD	8.60	2.69	6.57	4.44	2.27	8.66	3.56	1.85	6.52	2.36	6.40	1.90	55.82
OMM632	HMD	11.70	3.70	10.01	5.76	3.32	11.59	5.11	1.87	9.22	3.54	9.57	2.59	77.99
OMM763	HMD	8.91	2.86	6.93	4.44	2.09	9.05	3.48	1.83	6.61	2.45	6.43	1.90	57.00

Appendix 4.3 Biomarker concentrations (ug/g oil) of the oils (continued).

OMM812	HMD	7.47	2.79	5.57	3.57	1.74	7.20	2.83	1.69	5.96	2.01	5.29	1.66	47.77
OMN33	HMD	5.12	1.63	3.98	2.49	1.34	5.21	1.86	2.48	4.03	1.32	3.59	1.13	34.19
OMN681	HMD	8.48	2.54	6.06	3.71	2.03	8.14	3.17	1.84	6.62	1.83	5.44	1.68	51.53
OMO142	HMD	5.29	1.74	3.95	2.47	1.21	4.98	2.01	1.26	4.03	1.09	3.46	1.03	32.50
OMO343	HMD	5.95	1.95	4.46	3.07	1.46	5.73	2.29	1.45	4.70	1.35	3.88	1.11	37.41
OMP33	HMD	7.94	2.53	6.24	4.38	1.43	6.18	2.89	1.63	6.02	1.80	5.35	1.56	47.95
OMP42	HMD	5.22	1.60	4.19	2.79	1.19	5.34	1.68	1.19	4.10	1.20	3.51	0.94	32.95
OMP67	HMD	6.23	1.82	5.10	3.43	1.63	7.00	2.94	1.53	5.39	1.30	4.19	1.27	41.85
OMP74	HMD	8.07	2.48	6.49	4.18	1.99	8.28	3.20	1.60	6.45	1.71	5.21	1.50	51.16
OMP802	HMD	8.01	2.51	6.73	4.16	1.94	9.01	3.22	1.74	6.77	1.90	5.44	1.60	53.05
ONI403	HMD	6.20	1.71	5.24	3.30	1.64	6.56	2.83	1.38	5.09	1.40	4.34	1.23	40.92
ONM243	HMD	10.16	2.87	7.76	5.14	2.36	9.89	3.69	1.95	7.74	2.27	6.67	2.00	62.50
ONM461	HMD	6.44	2.02	5.49	3.44	1.46	7.00	2.69	1.47	5.48	1.59	4.65	1.24	42.96
GS1	El Gassi	7.20	2.14	5.01	2.94	1.37	6.38	2.27	0.97	4.83	1.53	4.39	1.14	40.16
AR-61	Zotti	8.82	2.49	5.56	3.84	1.45	7.24	2.55	1.85	5.67	1.94	5.88	1.21	48.50
AR22	El Agreb	6.49	1.98	4.50	3.08	1.41	6.34	1.76	1.22	4.60	1.44	4.37	0.90	38.10
DRT1	D.Temra	11.38	3.09	5.18	3.73	1.63	8.38	3.59	2.16	5.84	2.98	7.04	2.26	57.25
GLNE5	Guellala NE	9.67	3.14	6.00	3.73	2.60	9.19	3.68	3.02	7.08	3.91	10.66	2.92	65.61
MEK1	M.El kebch	11.15	4.31	8.53	4.91	3.64	10.59	4.68	2.81	8.30	3.30	8.26	2.34	72.81
NGS2	N'goussa	6.82	2.16	5.32	3.02	2.15	7.80	3.23	1.94	6.10	2.67	7.15	2.19	50.54
OKJ31	H.Berkaoui	7.95	2.68	6.31	4.05	2.64	9.01	3.63	2.64	7.21	4.14	9.11	2.53	61.88
OKJ202	H.Berkaoui	8.79	2.70	5.83	3.97	2.82	9.05	3.88	2.08	6.82	3.70	8.49	2.53	60.67
OKM881	H.Berkaoui	7.26	2.73	5.90	3.56	2.31	8.37	3.24	1.98	6.19	3.46	8.30	2.36	55.68
OKN77	H.Berkaoui	7.02	2.28	5.23	3.01	1.72	7.60	3.24	1.87	5.74	2.78	7.31	2.05	49.87
OKP-61	Benkahla	10.73	3.31	6.82	4.53	2.63	10.65	4.06	2.33	7.80	3.25	10.85	3.51	70.48
OKP88	Benkahla	8.05	3.09	6.12	3.73	2.91	9.59	4.11	2.72	8.00	3.59	8.71	2.50	63.12
RDC-1b	R.Chegga	9.74	2.80	6.82	4.27	1.56	8.26	2.11	1.43	6.73	1.70	6.18	1.58	53.19
MDR-7	Mesdar	9.33	3.08	2.55	1.46	0.00	3.04	1.89	2.11	3.00	2.12	4.89	1.68	35.15
MDR8	Mesdar	9.27	3.03	2.36	1.46	1.20	3.58	1.85	1.34	2.98	1.79	4.65	1.47	34.98
RB10	El Baguel	9.62	3.12	2.58	1.44	1.45	3.74	2.14	1.38	2.82	1.70	5.19	1.58	36.78
RB-18	El Baguel	10.83	3.92	2.92	1.31	1.36	4.30	2.27	2.36	2.52	2.15	6.19	1.56	41.66
OL2	DST	14.62	3.30	5.37	3.16	1.33	5.75	2.28	2.12	4.37	1.65	3.90	1.44	49.28

Appendix 4.4 Aromatic hydrocarbon ratios and concentrations (ug/g oil) in the oils.

		Alkylnaphthalenes								Alkylphenanthrenes					Alkyldibenzothiophenes				Methylbiphenyls		c steroids	Concentrations		
Sample	Field	MNR 2-MN/ 1-MN	DNR-1 (2,6-+2,7-) /1,5-	2,3,6-/ (1,4,6- +1,3,5-)	TMNR-1 1,3,7- /1,2,5-	(1,3,7- +2,3,6-) /1,3,6-	TMNR-2 (1,3,7-+2,3,6-) /(1,3,5-+1,3,6- +1,4,6-)	1,3,6,7-/ 1,2,5,6- +1,2,3,5-	2,3,6,7- /1,2,3,6-	MPI-1	3-/2-MP	DMPr	2-MP/ MP	1-Rc(%)	4- MDBT/ 1-MDBT	2+3- MDBT/ DBT	4,6- DMDBT /1,4-	2,4- DMDBT /1,4-	3MBp/ 2MBp	4MBp/ 2MBp	C_{29} TAS/ [C_{29} TAS + C_{29}(S+R) TAS]	Total alkylnaphthalenes	Total alkylphenanthrenes	Total alkylthiophenes
MD59	HMD	1.40	9.92	0.55	11.01	1.40	0.72	19.69	3.24	0.85	1.04	0.23	1.31	0.91	9.04	0.89	2.67	1.06	6.95	2.70	0.85	46674.9	3088.7	880.2
MD104	HMD	1.45	8.67	0.70	11.41	1.41	0.77	22.41	3.72	0.84	1.08	0.23	1.13	0.91	8.78	1.15	3.16	1.79	7.77	3.01	0.91	50033.7	3315.8	789.9
MD165	HMD	1.47	8.69	0.67	11.92	1.49	0.79	16.58	3.30	0.82	1.09	0.23	1.09	0.89	9.36	1.13	3.20	1.90	7.37	2.86	0.88	52466.3	3343.0	803.9
MD185	HMD	1.53	10.67	0.58	13.61	1.48	0.77	22.64	4.25	0.86	1.04	0.24	1.36	0.92	9.03	0.96	2.74	1.20	7.26	2.79	0.94	58396.5	3952.1	1212.8
MD201	HMD	1.47	9.31	0.52	9.40	1.40	0.70	12.99	2.87	0.77	1.07	0.20	1.22	0.86	10.11	1.19	3.39	1.89	8.14	3.14	0.84	51079.6	2990.5	583.6
MD204	HMD	1.41	7.81	0.42	9.39	1.43	0.67	13.13	2.84	0.77	1.08	0.20	1.19	0.86	9.34	1.08	2.79	1.38	8.57	3.39	0.94	43555.9	2790.6	764.2
MD208	HMD	1.42	10.41	0.53	11.80	1.41	0.72	18.34	3.38	0.86	1.06	0.24	1.36	0.92	8.32	1.14	3.31	1.84	6.82	2.56	0.86	50189.0	3236.6	720.2
MD239	HMD	1.37	8.65	0.59	9.80	1.40	0.72	12.40	3.03	0.80	1.12	0.21	1.06	0.88	9.51	1.20	3.19	1.63	8.48	3.34	0.96	51433.9	3316.3	717.6
MD255	HMD	1.43	9.09	0.30	9.83	1.22	0.56	13.40	2.97	0.78	1.06	0.20	1.21	0.87	9.91	1.26	3.26	1.38	8.27	3.20	0.88	48519.8	3509.9	585.2
MD279	HMD	1.45	9.01	0.39	12.01	1.51	0.71	15.50	3.20	0.84	1.24	0.23	1.13	0.90	9.24	0.89	3.04	1.30	6.02	2.27	0.82	53540.3	3537.5	776.8
MD297	HMD	1.39	7.95	0.64	7.91	1.40	0.75	10.48	2.74	0.78	1.12	0.21	1.02	0.87	8.27	1.08	2.09	0.81	5.81	2.21	0.72	44286.9	2794.9	621.7
MD317	HMD	1.44	9.90	0.46	9.95	1.40	0.68	13.68	2.78	0.77	1.10	0.21	1.22	0.86	10.19	0.96	2.82	1.34	8.12	3.11	0.80	49039.6	2968.3	761.4
MD322	HMD	1.40	8.37	0.63	9.87	1.40	0.74	13.88	3.17	0.78	1.06	0.21	1.04	0.87	9.64	0.95	3.47	1.44	7.54	2.93	0.97	47414.9	2911.3	850.9
MD332	HMD	1.43	8.06	0.65	8.24	1.43	0.76	10.82	2.84	0.81	1.10	0.22	1.05	0.88	9.26	2.61	2.75	1.44	5.91	2.26	0.78	55915.5	3601.4	548.7
MD348	HMD	1.43	8.35	0.70	10.83	1.42	0.77	15.73	3.19	0.84	1.07	0.23	1.09	0.90	8.90	1.19	2.94	1.68	6.62	2.61	0.86	46633.6	3063.8	615.8
OMK14	HMD	1.39	8.17	0.50	9.86	1.37	0.70	15.66	2.99	0.85	1.06	0.23	1.13	0.91	8.58	1.13	2.70	1.58	5.94	2.20	0.81	44471.5	2814.4	551.7
OMP263	HMD	1.38	9.54	0.56	10.46	1.42	0.73	13.50	2.98	0.83	1.06	0.22	1.27	0.90	8.77	1.23	3.32	2.05	6.82	2.69	0.80	47958.8	3147.2	647.8
OMM33	HMD	1.44	7.78	0.66	7.80	1.42	0.76	11.16	2.30	0.79	1.07	0.21	1.03	0.87	9.26	1.32	3.30	1.48	5.57	2.11	0.72	44966.9	2771.7	418.6
OMM772	HMD	1.27	7.96	0.40	7.52	1.42	0.67	9.49	2.29	0.76	1.15	0.20	0.98	0.86	8.39	1.03	2.74	1.37	5.37	1.99	0.62	45791.5	2694.5	330.0
OMN352	HMD	1.40	8.06	0.50	9.99	1.41	0.71	15.05	3.05	0.84	1.10	0.23	1.31	0.91	8.38	1.13	2.79	1.70	5.85	2.21	0.80	46676.3	2972.1	575.7
OMN412	HMD	1.52	10.18	0.52	11.45	1.39	0.71	16.42	3.32	0.84	1.06	0.23	1.13	0.91	8.59	1.16	3.00	1.85	6.29	2.37	0.90	46314.0	3090.1	689.9
OMO36	HMD	1.57	10.73	0.60	12.68	1.41	0.74	18.40	3.48	0.88	1.05	0.24	1.32	0.93	8.27	1.18	3.21	2.12	6.27	2.40	0.87	47564.7	3237.5	691.5
OMO712	HMD	1.42	10.46	0.54	11.01	1.38	0.71	16.93	3.33	0.84	1.06	0.23	1.33	0.90	9.61	1.15	3.51	2.06	7.49	2.85	0.95	45696.1	2958.6	643.7
OMO751	HMD	1.53	8.01	0.57	12.15	1.40	0.73	17.86	3.33	0.86	1.03	0.23	1.14	0.92	8.31	1.16	2.98	1.27	7.10	2.74	0.93	52259.1	3477.9	604.8
OMJ422	HMD	1.32	7.38	0.50	7.50	1.41	0.71	10.07	2.39	0.79	1.08	0.22	1.02	0.87	8.08	1.09	2.56	1.50	5.22	1.98	0.62	44089.7	2681.9	467.0
OMJ832	HMD	1.18	8.43	0.47	9.08	1.42	0.70	10.98	2.60	0.82	1.09	0.23	1.04	0.89	8.28	1.14	2.95	1.84	5.44	2.04	0.75	48172.7	3009.2	530.1
OM7	HMD	1.50	9.17	0.35	12.24	1.51	0.68	15.48	3.18	0.82	1.28	0.22	1.11	0.89	9.31	1.17	2.96	1.39	7.29	2.77	0.79	46594.2	2912.2	551.6
OML862	HMD	1.37	8.55	0.49	7.13	1.40	0.70	10.84	2.24	0.74	1.10	0.19	0.95	0.85	7.42	1.16	2.47	0.84	5.66	2.19	0.72	48443.9	2671.4	434.3
ONI412	HMD	1.39	7.74	0.45	8.87	1.40	0.69	12.34	2.71	0.79	1.12	0.21	1.04	0.87	8.98	1.28	3.11	1.82	6.67	2.57	0.74	47347.7	2759.0	502.3
ONM36	HMD	1.33	8.37	0.37	9.88	1.23	0.60	15.48	3.04	0.79	1.12	0.21	1.05	0.88	9.09	1.24	3.09	1.82	7.66	2.94	0.80	45791.6	2872.1	547.8
MD6	HMD	1.47	6.62	1.06	11.97	1.46	0.88	23.11	3.28	0.86	0.88	0.23	1.04	0.92	8.23	1.02	2.45	0.94	5.68	2.08	0.86	90687.9	5766.8	1368.6
MD45	HMD	1.42	6.50	0.87	11.48	1.46	0.83	18.81	2.85	0.81	0.84	0.20	1.02	0.88	9.19	1.10	2.78	1.00	7.07	2.67	0.89	60786.6	3501.0	926.4
MD46	HMD	1.31	6.24	0.90	10.42	1.46	0.83	19.51	2.60	0.82	0.86	0.20	1.04	0.89	8.92	1.13	0.98	1.76	8.20	3.22	0.90	44992.7	2926.0	665.4
MD64	HMD	1.45	6.48	1.06	11.05	1.50	0.89	17.63	3.08	0.86	0.82	0.23	1.07	0.91	8.11	1.02	2.35	0.91	5.73	2.10	0.80	145056.9	9253.2	2104.3
MD125	HMD	1.27	6.08	1.02	10.87	1.47	0.87	20.97	3.08	0.87	0.86	0.22	1.07	0.92	8.35	1.05	2.48	0.94	8.05	3.05	0.88	39558.1	2748.5	653.8
MD129	HMD	1.49	6.74	1.06	12.52	1.49	0.89	33.14	3.26	0.87	0.88	0.23	1.07	0.92	8.90	1.07	2.64	0.98	6.85	2.55	0.94	101175.2	6549.9	1710.7
MD134	HMD	1.46	6.72	0.98	12.79	1.45	0.86	17.65	3.30	0.87	0.83	0.22	1.08	0.92	8.84	1.07	2.51	0.96	7.35	2.77	0.92	42972.6	2785.6	745.0
MD139	HMD	1.41	6.72	1.04	12.31	1.49	0.89	19.36	3.17	0.87	0.82	0.22	1.10	0.92	8.66	1.06	2.55	0.97	6.79	2.53	0.90	49016.4	3244.0	815.1
MD140	HMD	1.52	7.89	1.13	13.88	1.53	0.93	26.66	3.58	0.88	0.85	0.23	1.08	0.93	8.86	1.07	2.64	1.09	6.58	2.53	0.96	47302.5	3086.3	831.5

Appendix 4.4 Aromatic hydrocarbon ratios and concentrations (ug/g oil) in the oils (continued).

MD141	HMD	1.47	6.74	0.98	12.04	1.47	0.86	19.28	3.15	0.86	0.82	0.22	1.07	0.92	8.43	1.05	2.53	0.93	6.02	2.28	0.86	82308.0	5325.5	1292.7
MD177	HMD	1.50	6.82	1.04	12.48	1.47	0.88	20.50	3.39	0.86	0.88	0.23	1.05	0.92	8.89	1.09	2.55	0.96	6.90	2.64	0.87	64964.3	4335.3	1114.2
MD213	HMD	1.39	6.26	0.88	10.28	1.45	0.83	17.29	2.72	0.79	0.85	0.20	1.00	0.87	9.30	1.12	2.77	1.00	8.01	3.06	0.82	57967.4	3620.9	864.3
MD215	HMD	1.39	6.20	0.86	9.65	1.45	0.81	16.03	2.67	0.78	0.85	0.17	0.97	0.87	9.26	1.12	2.74	0.96	7.59	2.93	0.86	42412.7	2719.8	656.5
MD221	HMD	1.36	6.14	0.98	8.99	1.47	0.86	15.24	2.42	0.82	0.83	0.21	1.01	0.89	7.91	1.01	1.59	0.91	5.63	2.04	0.81	42619.3	2670.5	506.8
MD235	HMD	1.28	5.87	0.79	9.35	1.45	0.79	15.30	2.60	0.78	0.86	0.19	0.99	0.87	9.49	1.13	2.88	1.04	9.50	3.65	0.86	40420.4	2683.3	636.6
MD269	HMD	1.47	5.97	0.89	8.31	1.43	0.83	13.15	2.45	0.82	0.83	0.20	1.01	0.89	8.10	1.02	2.42	0.95	5.71	2.80	0.80	72510.9	4539.4	850.6
MD272	HMD	1.46	6.90	0.96	12.32	1.47	0.86	17.89	3.08	0.86	0.84	0.21	1.09	0.91	8.95	1.09	2.70	1.01	6.91	2.53	0.89	41431.5	2751.5	712.5
MD275	HMD	1.44	6.57	0.90	11.99	1.46	0.84	18.98	3.32	0.83	0.84	0.21	1.03	0.90	9.05	1.09	2.62	0.38	6.99	2.61	0.91	120313.6	7467.1	1878.7
MD280	HMD	1.44	6.80	1.04	12.38	1.48	0.88	20.54	3.40	0.88	0.82	0.23	1.10	0.93	8.23	1.06	2.56	0.99	6.18	2.23	0.89	46369.2	3186.6	767.2
MD287	HMD	1.42	6.52	0.86	10.25	1.45	0.82	17.14	2.76	0.82	0.87	0.20	1.03	0.89	9.15	1.15	2.78	1.04	7.10	2.71	0.87	43910.1	2830.6	641.3
MD299	HMD	1.38	6.35	0.92	9.68	1.44	0.84	16.16	2.70	0.83	0.83	0.22	1.02	0.90	8.05	1.05	2.48	0.94	5.84	2.07	0.83	41162.4	2678.9	557.8
MD300	HMD	1.50	6.85	1.06	13.97	1.48	0.89	32.06	3.56	0.90	0.82	0.24	1.12	0.94	8.62	1.06	2.66	1.02	6.32	2.35	0.89	43971.9	3076.4	791.8
MD304	HMD	1.43	7.48	1.14	11.75	1.51	0.91	27.21	3.40	0.88	0.85	0.23	1.06	0.93	8.18	1.05	2.44	0.93	6.06	2.23	0.86	76072.7	5188.9	1252.4
MD345	HMD	1.43	6.50	0.89	10.13	1.46	0.83	17.06	2.77	0.84	0.83	0.21	1.04	0.91	8.00	1.06	2.54	0.98	5.83	2.13	0.85	87140.7	5793.4	1253.5
MD409	HMD	1.43	6.54	0.85	10.36	1.46	0.82	16.21	2.65	0.78	0.84	0.19	0.98	0.87	9.69	1.14	2.80	1.02	8.57	3.30	0.77	49485.6	3127.9	701.6
MD412	HMD	1.45	6.51	0.87	10.44	1.47	0.83	16.69	2.72	0.79	0.85	0.19	1.00	0.88	9.53	1.15	2.84	1.03	7.61	2.82	0.82	60777.1	3724.6	839.4
OMJ41	HMD	1.41	6.19	0.95	8.99	1.49	0.86	14.02	2.46	0.81	0.83	0.21	0.98	0.89	7.92	1.05	2.25	0.87	5.22	1.92	0.82	41359.4	2655.2	551.8
OMJ721	HMD	1.43	6.57	0.91	9.94	1.47	0.85	15.53	2.64	0.84	0.85	0.21	1.02	0.90	8.28	1.09	2.46	0.94	5.53	2.07	0.84	42525.3	2857.5	618.0
OML76	HMD	1.30	5.66	0.88	7.34	1.46	0.83	11.91	1.98	0.77	0.86	0.12	0.93	0.86	8.38	1.12	0.61	0.92	5.82	2.15	0.77	44948.6	2566.0	415.1
OML82	HMD	1.38	5.89	0.94	7.98	1.49	0.86	13.01	2.32	0.79	0.86	0.19	0.97	0.88	8.30	1.11	2.41	0.93	-	-	0.78	40881.5	2400.8	484.6
OML712	HMD	1.41	5.91	0.99	8.16	1.51	0.88	13.07	2.50	0.80	0.90	0.20	0.95	0.88	8.42	1.12	2.38	0.89	5.87	2.18	0.76	38745.6	2436.4	504.9
OMM67	HMD	1.29	5.67	0.95	6.95	1.47	0.85	11.07	2.17	0.79	0.86	0.20	0.96	0.87	8.03	1.05	2.39	0.90	5.61	2.02	0.78	46762.6	3006.6	525.6
OMM74	HMD	0.81	4.16	0.96	7.59	1.47	0.84	14.02	2.53	0.84	0.84	0.20	1.00	0.90	7.80	1.13	2.42	0.92	-	-	0.82	28191.2	2668.4	533.3
OMM80	HMD	1.39	6.48	0.96	10.45	1.47	0.86	18.59	2.88	0.86	0.82	0.21	1.06	0.91	8.22	1.08	2.42	0.95	5.98	2.22	0.86	47519.1	3277.7	723.2
OMM532	HMD	1.38	6.01	0.93	8.44	1.50	0.86	12.96	2.41	0.82	0.87	0.20	0.99	0.89	7.88	1.07	2.36	0.92	5.60	2.01	0.79	44471.6	2987.6	557.0
OMM542	HMD	1.38	5.82	0.88	7.86	1.46	0.83	12.17	2.27	0.81	0.83	0.19	0.99	0.89	7.98	1.06	2.39	0.90	-	-	0.79	42581.2	2734.3	506.1
OMM632	HMD	0.87	4.49	0.96	6.91	1.47	0.85	13.22	2.35	0.85	0.88	0.21	0.99	0.91	7.50	1.17	2.31	0.91	-	-	0.83	40453.7	3792.2	735.8
OMM763	HMD	1.39	6.98	1.17	8.53	1.52	0.93	15.28	3.03	0.81	0.87	0.21	0.98	0.89	7.90	1.02	2.26	0.97	5.41	1.99	0.67	40456.3	2700.8	545.9
OMM812	HMD	0.83	4.08	1.00	8.56	1.51	0.86	17.76	2.86	0.86	0.83	0.22	1.04	0.92	8.02	1.12	2.39	0.91	-	-	0.86	26790.7	2592.8	560.1
OMN33	HMD	1.33	6.02	0.94	10.51	1.49	0.85	18.26	2.90	0.86	0.81	0.23	1.05	0.92	8.24	1.11	2.43	0.92	6.64	2.61	0.86	37447.5	2702.2	617.0
OMN681	HMD	1.44	6.53	1.03	9.97	1.50	0.88	17.75	2.79	0.86	0.83	0.21	1.04	0.91	8.11	1.06	2.50	0.94	5.48	2.04	0.80	52414.9	3517.1	778.8
OMO142	HMD	1.51	7.01	0.93	11.15	1.46	0.85	19.16	3.20	0.88	0.84	0.23	1.09	0.93	8.49	1.07	2.49	0.97	5.92	2.22	0.95	44217.6	3018.7	716.8
OMO343	HMD	1.25	6.31	0.93	12.17	1.44	0.84	19.83	3.19	0.89	0.81	0.22	1.10	0.93	8.56	1.12	2.60	1.02	-	-	0.92	56386.2	4323.0	1025.6
OMP33	HMD	1.41	6.34	0.94	10.24	1.48	0.85	18.45	2.80	0.83	0.83	0.20	1.04	0.90	8.62	1.13	1.04	0.99	6.53	2.37	0.86	40546.3	2639.3	539.6
OMP42	HMD	1.44	6.49	0.87	9.40	1.44	0.82	18.64	2.83	0.83	0.84	0.21	1.04	0.90	8.84	1.18	2.65	1.02	6.68	2.51	0.92	40013.9	2643.7	610.8
OMP67	HMD	1.39	5.97	0.83	8.27	1.42	0.80	14.87	2.51	0.81	0.85	0.20	1.00	0.89	8.47	1.14	2.55	0.98	6.16	2.40	0.81	40801.7	2654.6	572.9
OMP74	HMD	1.38	6.39	0.88	10.12	1.48	0.84	17.18	2.71	0.83	0.86	0.20	1.02	0.90	8.99	1.16	2.30	1.01	6.96	2.60	0.84	40302.4	2611.6	585.0
OMP802	HMD	1.41	6.31	0.89	10.27	1.50	0.85	17.36	2.77	0.81	0.84	0.20	1.01	0.89	9.11	1.13	2.72	1.01	7.18	2.78	0.88	38711.3	2569.1	590.7
ONI403	HMD	1.45	6.10	0.89	8.68	1.48	0.83	15.38	2.65	0.80	0.86	0.19	0.97	0.88	8.97	1.17	2.73	1.03	7.20	2.78	0.82	35718.6	2316.5	472.3
ONM243	HMD	1.39	6.30	0.91	9.73	1.49	0.84	17.12	2.67	0.74	0.65	0.20	1.02	0.84	8.96	1.16	2.72	1.00	7.07	2.67	0.86	43727.6	2871.7	666.5
ONM461	HMD	1.46	6.23	0.89	10.32	1.45	0.83	17.11	2.71	0.80	0.83	0.19	1.01	0.88	9.40	1.18	2.78	1.02	7.18	2.67	0.84	39330.4	2563.6	556.8
GS1	El Gassi	1.30	5.43	0.81	7.95	1.46	0.81	9.86	2.02	0.75	0.83	0.18	0.92	0.85	8.09	1.00	2.49	0.91	5.40	2.05	0.86	38397.1	1988.2	516.7
AR-61	Zotti	1.25	5.44	0.92	6.98	1.46	0.84	7.84	1.87	0.71	0.80	0.18	0.90	0.83	7.98	0.96	2.34	0.82	5.42	2.12	0.79	33436.0	1695.9	409.1
AR22	El Agreb	1.18	4.36	0.71	6.35	1.45	0.76	8.09	1.96	0.63	0.79	0.15	0.83	0.78	7.68	0.93	2.38	0.81	5.18	1.91	0.79	28967.7	1417.1	409.1
DRT1	D.Temra	0.98	3.81	0.68	3.94	1.41	0.73	5.04	1.20	0.65	0.88	0.16	0.82	0.79	6.84	0.95	1.97	0.79	5.82	2.07	0.67	39084.1	2595.2	395.9

Appendix 4.4 Aromatic hydrocarbon ratios and concentrations (ug/g oil) in the oils (continued).

GLNE-5	Guellala NE	1.17	4.85	0.89	5.33	1.46	0.83	7.22	1.95	0.74	0.87	0.18	0.90	0.84	9.33	1.05	2.36	0.89	7.53	2.92	0.65	78972.4	5194.3	541.7
GLA16	Guellala	1.12	4.31	0.69	4.56	1.42	0.74	5.95	1.40	0.68	0.90	0.16	0.85	0.81	8.33	0.91	2.09	0.79	6.09	2.22	0.63	31117.7	2342.0	256.3
MEK1	M.Kebch	1.17	4.40	0.62	3.52	1.46	0.72	4.12	0.93	0.68	0.92	0.15	0.79	0.81	5.87	0.93	1.72	0.74	5.42	2.08	0.63	53366.9	2823.1	377.4
NGS2	N'goussa	1.12	4.27	0.74	4.85	1.41	0.76	6.60	1.47	0.69	0.86	0.16	0.85	0.82	9.20	1.03	2.38	0.91	6.12	2.18	0.66	41931.9	2871.6	348.4
OKJ31	H.Berkaoui	1.08	3.83	0.65	3.85	1.44	0.73	4.54	1.18	0.62	0.88	0.15	0.79	0.77	6.50	0.83	1.84	0.68	4.51	1.54	0.64	33801.3	2003.8	342.6
OKJ202	H.Berkaoui	1.04	3.68	0.67	3.46	1.42	0.72	4.18	1.18	0.61	0.87	0.14	0.77	0.76	5.99	0.79	1.90	0.70	4.71	1.71	0.64	38145.9	2222.5	418.0
OKM881	H.Berkaoui	1.07	3.58	0.61	3.56	1.42	0.71	4.20	1.07	0.60	0.87	0.14	0.75	0.76	6.38	0.78	1.95	0.73	4.11	1.39	0.66	33239.0	1800.5	355.8
OKN77	H.Berkaoui	1.05	3.51	0.62	3.44	1.39	0.70	4.33	1.04	0.59	0.86	0.14	0.74	0.76	6.38	0.82	1.92	0.71	4.52	1.57	0.65	39382.6	2152.4	437.5
OKP-61	Benkahla	1.06	3.98	0.79	4.24	1.45	0.79	5.21	1.30	0.64	0.89	0.16	0.78	0.78	6.69	0.70	1.99	0.76	5.40	2.00	0.66	90729.7	4535.3	747.5
OKP88	Benkahla	1.14	4.02	0.68	4.03	1.46	0.75	4.95	1.19	0.63	0.89	0.15	0.79	0.78	6.67	0.84	1.94	0.75	5.14	1.76	0.65	17194.7	973.4	161.4
RDC-1b	R.Chegga	1.23	5.66	0.94	9.16	1.45	0.84	12.25	2.48	0.76	0.88	0.19	0.92	0.85	8.78	1.03	2.86	0.97	8.85	3.42	0.83	113702.1	6099.2	1353.5
HGA2	H.Guettar	1.39	7.97	0.46	10.05	1.40	0.69	12.81	2.84	0.81	1.10	0.22	1.08	0.89	8.28	1.11	2.77	1.55	6.36	2.40	0.83	45730.3	2885.0	545.0
HGA3	H.Guettar	1.53	8.30	0.50	11.96	1.42	0.71	16.00	3.24	0.85	1.10	0.23	1.15	0.91	8.46	1.16	3.35	2.12	6.19	2.33	0.88	49730.6	3189.8	623.1
MDR-7	Mesdar	1.55	6.90	1.01	12.72	1.44	0.86	23.46	5.91	0.96	0.84	0.24	1.22	0.98	7.89	1.29	2.81	1.30	8.10	3.17	0.94	102251.0	7228.9	1576.1
MDR8	Mesdar	1.55	6.29	0.89	13.35	1.40	0.81	20.73	3.58	0.96	0.85	0.24	1.22	0.97	8.01	1.26	2.45	1.11	7.78	2.85	0.93	93967.5	3078.2	784.4
RB10	R.Baguel	1.35	5.57	0.72	8.47	1.33	0.73	15.08	2.26	0.85	0.86	0.21	1.13	0.91	6.87	1.14	2.26	1.00	6.14	2.28	0.92	83305.6	2314.8	753.1
RB-18	R.Baguel	1.34	5.35	0.84	7.72	1.31	0.75	12.95	2.40	0.81	0.81	0.22	1.05	0.89	6.98	1.01	2.02	0.82	5.64	2.33	0.89	75265.3	5944.8	2071.8
OL2	DST	1.41	6.82	0.99	10.49	1.50	0.88	16.03	2.62	0.88	0.86	0.23	1.16	0.93	2.07	0.28	3.05	1.13	-	-	0.90	16620.2	-	-

Appendix 5.1 Alkylcarbazole concentrations (ug/g extract) of the source rocks

			Carbazole	Methylcarbazoles				Dimethyl- and ethyl-carbazoles										
Well	Depth (m)	Age	c	1-mc	3-mc	2-mc	4-mc	1,8-dmc	1-ethyl	1,3-dmc	1,6-dmc	1,7-dmc	1,4-dmc+4-ec+1,5-dmc+3-ec	2,6-dmc	2,7-dmc+1,2-dmc	2,4-dmc	2,5-dmc	2,3-dmc	3,4-dmc
TKT#1	3868	Silurian	16.96	63.49	11.48	18.58	22.46	42.07	3.99	41.98	30.48	47.35	102.94	7.64	24.90	17.53	12.56	3.51	5.30
TKT#1	3872.5	Silurian	10.39	58.93	10.59	21.95	21.00	34.47	2.58	34.44	26.77	39.74	93.18	6.66	25.53	18.12	12.51	4.73	4.61
OA#1bis	4142	Silurian	22.86	71.09	11.37	24.93	28.41	44.83	3.36	39.59	33.41	54.75	117.30	5.62	25.88	16.91	15.94	3.07	4.61
OA#1bis	4145	Silurian	40.10	114.99	20.77	46.73	51.28	64.32	6.15	46.93	45.94	81.54	166.27	9.39	40.08	24.20	27.54	4.56	7.71
OA#1bis	4151.55	Silurian	42.89	13.88	2.06	5.52	3.68	10.60	1.04	8.80	3.22	3.75	3.00	1.24	1.53	0.27	0.27	0.65	1.13
BAT#1	3947	Silurian	18.24	70.20	8.88	19.68	22.81	40.86	3.17	41.11	30.40	46.47	104.41	3.71	21.47	14.57	12.73	2.93	3.57
BAT#1	3957	Silurian	19.66	62.77	14.48	24.55	29.49	36.31	2.86	46.31	30.54	43.20	111.84	10.26	27.52	23.06	16.54	3.20	4.31
BAT#1	3959.55	Silurian	14.08	44.51	11.79	17.69	20.92	25.47	1.45	36.90	16.07	38.31	80.62	6.28	20.83	15.34	15.29	3.10	3.79
RDC#2	3804	Silurian	28.66	90.17	21.17	42.22	48.18	63.42	5.91	54.18	51.42	86.82	189.73	15.17	56.47	35.51	38.67	8.15	10.54
RDC#2	3806	Silurian	25.57	77.30	15.67	35.28	40.13	54.59	5.24	43.19	44.46	79.49	163.55	13.81	46.41	30.26	37.82	6.29	8.16
RDC#2	3808	Silurian	36.91	96.11	28.98	46.23	54.74	60.70	6.09	51.23	51.64	96.93	191.64	26.72	64.57	41.82	54.66	7.40	10.42
RDC#2	3810	Silurian	34.49	92.70	23.95	52.08	55.00	55.58	5.79	47.43	65.76	77.48	183.79	25.74	63.04	51.52	41.16	7.19	9.89
GLNE#3	3803.45	Silurian	2.23	9.31	2.09	3.04	3.37	8.66	0.59	7.40	4.73	6.69	13.79	1.06	3.93	2.35	1.77	0.87	0.80
GLNE#3	3809.45	Silurian	2.39	2.46	0.60	0.94	1.05	3.63	0.81	2.50	0.97	2.08	2.96	0.44	1.17	0.46	0.49	0.86	0.40
GLNE#4bis	3874.85	Silurian	15.03	77.47	18.11	32.82	30.62	39.83	3.59	47.06	23.44	52.46	117.99	10.18	32.35	23.57	20.39	4.48	6.25
GLNE#5	3987.55	Silurian	20.67	74.54	8.40	18.63	20.19	34.39	6.25	24.01	19.68	33.58	66.27	3.15	14.32	10.03	6.70	1.04	3.78
GLNE#5	3994	Silurian	30.02	76.48	11.62	24.16	25.09	35.12	5.19	25.11	21.72	37.52	80.79	3.03	18.96	13.15	11.86	3.69	4.71
GLNE#5	4001	Silurian	31.18	79.42	12.98	24.46	26.96	37.15	5.40	37.02	26.02	40.79	94.70	5.21	24.68	18.60	12.14	3.49	5.71
BKZ#1	4180	Silurian	9.45	37.16	5.87	11.60	13.33	23.03	1.86	19.71	15.34	27.02	54.76	2.61	11.62	7.47	6.71	2.13	2.54
BKZ#1	4183.8	Silurian	10.12	47.30	7.44	14.38	16.59	27.17	2.38	26.31	20.38	33.82	71.52	3.52	15.73	10.84	9.52	2.37	3.18
BKZ#1	4187	Silurian	21.32	72.17	13.61	25.75	31.13	40.72	4.02	41.17	34.33	55.73	119.75	7.47	30.98	21.52	19.71	4.45	6.25
BKZ#1	4189	Silurian	19.20	54.78	12.30	22.98	23.90	37.75	4.15	30.57	27.56	45.03	92.71	7.04	25.50	15.84	15.13	3.96	4.84
GEC#1	3660	Silurian	0.71	5.34	0.07	0.50	0.39	4.84	0.45	4.02	2.67	3.75	5.65	0.27	0.64	0.10	0.09	0.16	0.34
GD#1bis	3850	Silurian	10.00	11.27	4.92	5.74	3.84	19.32	1.30	19.72	13.35	17.83	31.31	4.82	11.15	5.38	5.38	2.30	2.47
GBC#1	3213	Silurian	4.51	18.43	10.93	8.95	6.01	5.14	1.76	8.59	7.22	10.74	18.91	1.19	5.38	3.28	2.79	0.42	1.24
GBC#1	3259	Silurian	4.50	6.16	5.15	4.66	1.99	2.10	1.10	2.03	4.57	2.07	2.92	0.89	2.14	0.68	0.80	0.62	0.55
OA#1bis	4462	Ordovician	1.30	0.80	0.56	0.89	0.36	2.57	1.07	1.94	1.47	0.35	1.46	0.56	0.39	0.17	0.31	0.26	0.00
RDC#2	3911	Ordovician	1.44	2.21	1.01	1.27	0.86	3.10	1.07	3.42	2.42	0.00	5.25	0.56	0.34	0.57	0.29	0.56	0.84
GLNE#5	4026	Ordovician	1.25	0.95	0.30	0.66	0.26	1.64	0.64	1.26	0.89	0.25	1.31	0.25	0.18	0.28	0.39	0.20	0.01
OEM#1	3910	Ordovician	0.98	3.60	1.00	1.41	0.73	5.81	1.27	5.43	3.47	4.66	11.77	0.92	2.90	0.72	1.31	0.85	0.28
GEC#1	3770	Ordovician	0.57	2.04	0.20	0.64	0.63	0.00	0.00	0.00	0.00	0.00	0.00	0.00	0.00	0.00	0.00	0.00	0.01
GBC#1	3386	Ordovician	0.38	0.33	0.10	0.17	0.08	0.67	0.15	0.28	0.20	0.38	0.60	0.16	0.16	0.07	0.11	0.03	0.03

Appendix 5.1 Alkylcarbazole concentrations (ug/g extract) of the source rocks (continued).

			Trimethylcarbazoles												Total carbazoles				Benzocarbazoles			
Well	Depth (m)	Age	1	2	3	4	5	6	7	8	9	10	11	12	13	Total MCs	Total DMCs	Total TMCs	Total alkylcarbazoles	benzo [a]	benzo [b]	benzo [c]	Tot Benz-carbazoles
TKT#1	3868	Silurian	0	37.13	58.98	1.44	31.46	14.84	37.59	72.66	7.65	12.91	10.88	22.67	116.01	340.24	308.20	781.41	66.00	3.25	39.92	109.16
TKT#1	3872.5	Silurian	0	31.83	58.93	0.00	43.72	0.00	37.10	67.91	6.29	11.37	8.73	21.21	112.45	303.34	287.08	713.27	44.78	3.06	24.78	72.61
OA#1bis	4142	Silurian	0	42.42	67.96	0.00	35.51	0.00	43.64	83.76	5.56	11.43	10.27	23.69	135.80	365.29	324.24	848.19	93.72	4.10	57.64	155.45
OA#1bis	4145	Silurian	0	57.13	89.97	0.00	43.27	24.14	62.23	116.50	10.00	14.04	12.70	37.02	233.77	524.62	466.98	1265.48	100.92	4.79	58.43	164.14
OA#1bis	4151.6	Silurian	0	8.91	6.08	0.00	6.41	1.44	0.00	3.23	0.80	0.82	1.73	1.90	25.14	35.48	31.32	134.84	0.77	2.06	21.58	24.41
BAT#1	3947	Silurian	0	34.49	57.49	0.00	29.39	14.10	34.84	74.73	4.07	9.36	7.71	16.11	121.57	325.42	282.28	747.50	64.16	2.65	40.46	107.27
BAT#1	3957	Silurian	0	30.08	54.68	0.00	26.32	11.77	31.08	70.19	8.19	8.19	19.61	10.85	131.28	355.94	270.97	777.84	50.51	2.27	33.11	85.89
BAT#1	3959.6	Silurian	0	25.32	40.51	0.00	17.46	10.42	30.70	54.32	6.05	6.97	7.19	18.22	94.92	263.46	217.17	589.62	34.10	2.02	21.90	58.02
RDC#2	3804	Silurian	0	72.22	119.34	7.55	70.76	51.29	93.10	177.71	24.08	28.25	23.16	67.22	201.73	616.00	734.69	1581.09	92.72	3.37	71.83	167.92
RDC#2	3806	Silurian	0	51.71	93.77	7.93	50.32	42.49	75.63	142.19	22.63	23.16	20.51	46.95	168.37	533.26	577.31	1304.50	80.91	2.92	63.14	146.97
RDC#2	3808	Silurian	0	57.45	105.87	11.00	60.55	49.38	84.81	157.79	34.32	27.80	25.82	59.29	226.06	663.83	674.07	1600.87	98.15	4.40	64.15	166.70
RDC#2	3810	Silurian	0	56.78	97.92	7.58	65.25	31.98	80.50	148.51	26.19	24.50	22.96	56.28	223.73	634.38	618.46	1511.06	96.36	4.13	71.26	171.75
GLNE#3	3803.5	Silurian	0	5.66	9.80	0.00	8.21	6.11	0.00	12.27	1.65	1.88	1.64	4.19	17.81	52.65	51.41	124.11	8.01	0.68	4.58	13.27
GLNE#3	3809.5	Silurian	0	1.60	2.63	0.00	2.12	1.63	0.00	2.98	0.61	0.89	0.00	1.13	5.05	16.77	13.57	37.78	2.37	0.41	2.38	5.15
GLNE#4	3874.9	Silurian	0	34.19	63.89	0.00	35.91	17.15	39.29	78.32	8.29	11.44	10.17	25.64	159.03	381.59	324.29	879.94	61.87	4.30	37.22	103.39
GLNE#5	3987.6	Silurian	0	18.51	30.96	0.00	18.29	13.97	14.37	29.25	1.53	3.87	2.49	4.25	121.77	223.21	137.46	503.11	78.26	2.44	46.93	127.63
GLNE#5	3994	Silurian	0	26.60	44.86	0.00	19.48	11.07	27.32	50.08	4.51	5.64	5.32	14.24	137.35	260.84	209.12	637.33	84.77	3.96	51.00	139.73
GLNE#5	4001	Silurian	0	27.05	47.10	0.00	22.83	9.30	26.24	52.05	4.17	7.66	4.53	16.90	143.82	310.92	217.82	703.73	92.80	3.01	51.86	147.67
BKZ#1	4180	Silurian	0	16.50	29.31	0.00	12.72	6.83	17.44	36.16	3.13	4.65	3.99	9.47	67.97	174.78	140.20	392.40	28.51	2.38	17.34	48.23
BKZ#1	4183.8	Silurian	0	22.24	38.02	0.00	16.83	8.74	21.77	49.04	3.88	4.83	5.16	12.46	85.72	226.75	182.98	505.56	39.62	3.18	26.79	69.59
BKZ#1	4187	Silurian	0	39.10	68.30	0.00	31.71	17.51	50.39	89.91	7.51	9.64	9.77	26.07	142.66	386.11	349.91	900.00	62.52	2.88	41.53	106.93
BKZ#1	4189	Silurian	0	30.03	58.76	0.00	25.48	17.46	38.55	75.37	7.41	9.03	6.61	24.95	113.95	310.08	293.65	736.89	43.09	1.62	32.87	77.58
GEC#1	3660	Silurian	0	3.61	4.46	0.00	4.08	0.00	2.39	3.36	0.10	0.63	0.13	0.29	6.31	22.98	19.06	49.06	2.15	0.54	2.25	4.94
GD#1bis	3850	Silurian	0	37.83	54.67	0.00	37.22	21.74	38.98	68.85	7.31	12.32	10.13	22.88	25.77	134.33	311.93	482.03	8.53	0.78	5.80	15.10
GBC#1	3213	Silurian	0	8.77	8.59	3.63	2.30	12.17	6.93	11.32	0.52	1.71	0.98	1.82	44.32	66.66	58.74	174.23	6.84	0.28	5.66	12.78
GBC#1	3259	Silurian	0	1.05	0.91	0.00	0.59	3.33	0.94	0.00	0.00	0.57	0.00	0.61	17.96	20.47	7.98	50.91	1.46	0.17	1.77	3.40
OA#1bis	*4462*	*Ordovici*	*0*	*0.27*	*0.67*	*0.00*	*1.12*	*0.21*	*0.25*	*0.11*	*0.00*	*0.00*	*0.00*	*0.00*	*2.61*	*10.55*	*2.64*	*17.10*	*0.57*	*0.14*	*0.52*	*1.23*
RDC#2	3911	Ordovici	0	0.42	1.15	0.00	0.90	0.38	1.80	0.21	0.66	0.17	0.00	0.00	5.35	18.41	5.69	30.89	0.86	0.82	0.76	2.44
GLNE#5	4026	Ordovici	0	0.18	0.13	0.00	0.30	0.15	0.79	0.39	0.04	0.22	0.14	0.00	2.19	7.31	2.33	13.07	0.29	0.06	0.28	0.63
OEM#1	3910	Ordovici	0	4.22	7.71	0.00	8.53	0.00	6.49	12.02	1.03	2.28	1.30	3.15	6.74	39.38	46.74	93.84	3.99	1.57	2.42	7.98
GEC#1	3770	Ordovici	0	-	0.00	0.00	0.00	0.00	0.00	0.00	0.00	0.00	0.00	0.00	3.52	0.01		4.10	1.64	0.51	1.32	3.47
GBC#1	3386	Ordovici	0	0.32	0.81	0.06	0.50	0.20	0.63	0.62	0.14	0.10	0.08	0.20	0.68	2.86	3.65	7.57	0.14	0.01	0.09	0.24

Appendix 5.1 Alkylcarbazole ratios of the source rocks (continued).

Well	Depth (m)	Age	C3/ (C1+C3)	1,8-DMC/(1,8-+1-MC)	1,8-DMC/(1,8-+4-MC)	1,8-DMC/(1,8-+1-EC)	1,8-DMC/(1,8-+1,6-DMC)	1,8-DMC/(1,8-+2,6-DMC)	1,8-DMC/(1,8-+3,4-DMC)	[a]/[a]+[c]
TKT#1	3868.6	Silurian	0.62	0.66	0.65	0.91	0.58	0.85	0.89	0.62
TKT#1	3872.5	Silurian	0.63	0.59	0.60	0.93	0.56	0.84	0.88	0.64
OA#1bis	4142.25	Silurian	0.61	0.63	0.61	0.93	0.57	0.89	0.91	0.62
OA#1bis	4145.35	Silurian	0.61	0.56	0.56	0.91	0.58	0.87	0.89	0.61
BAT#1	3947	Silurian	0.60	0.58	0.64	0.93	0.57	0.92	0.92	0.61
BAT#1	3957	Silurian	0.58	0.58	0.55	0.93	0.54	0.78	0.89	0.60
BAT#1	3959.55	Silurian	0.61	0.57	0.55	0.90	0.61	0.80	0.87	0.61
RDC#2	3804.7	Silurian	0.68	0.70	0.57	0.91	0.55	0.81	0.86	0.56
RDC#2	3806.4	Silurian	0.66	0.71	0.58	0.91	0.55	0.80	0.87	0.59
RDC#2	3808.35	Silurian	0.65	0.60	0.53	0.94	0.54	0.69	0.85	0.60
RDC#2	3810.8	Silurian	0.64	0.60	0.50	0.91	0.56	0.68	0.85	0.60
GLNE#3	3803.45	Silurian	0.66	0.93	0.72	0.84	0.65	0.89	0.94	0.53
GLNE#3	3809.45	Silurian	0.68	0.87	0.77	0.82	0.69	0.89	0.93	0.50
GLNE#4bis	3874.85	Silurian	0.61	0.51	0.57	0.92	0.63	0.80	0.86	0.62
GLNE#5	3987.55	Silurian	0.53	0.62	0.63	0.90	0.64	0.92	0.90	0.61
GLNE#5	3994.45	Silurian	0.59	0.56	0.58	0.87	0.62	0.92	0.88	0.61
GLNE#5	4001.45	Silurian	0.57	0.57	0.58	0.87	0.59	0.88	0.87	0.60
BKZ#1	4180.6	Silurian	0.58	0.62	0.63	0.93	0.60	0.90	0.90	0.62
BKZ#1	4183.8	Silurian	0.59	0.57	0.62	0.92	0.57	0.89	0.90	0.60
BKZ#1	4187.86	Silurian	0.62	0.56	0.57	0.91	0.54	0.84	0.87	0.60
BKZ#1	4189.5	Silurian	0.63	0.67	0.61	0.90	0.58	0.84	0.89	0.62
GEC#1	3660.6	Silurian	0.61	0.91	0.93	0.82	0.64	0.95	0.93	0.49
GD#1bis	3850	Silurian	0.82	0.68	0.69	0.89	0.59	0.80	0.90	0.60
GBC#1	3213	Silurian	0.61	0.34	0.46	0.74	0.42	0.81	0.81	0.57
GBC#1	3259	Silurian	0.43	0.28	0.51	0.66	0.31	0.70	0.79	0.56
OEM#1	3910.45	Ordovician	0.87	1.61	0.89	0.82	0.64	0.86	1.00	0.62
GEC#1	3770.9	Ordovician	-	-	-	-	0.56	0.81	0.79	0.55
GBC#1	3386.6	Ordovician	0.84	1.82	0.89	0.81	0.65	0.80	0.99	0.60
GLNE#5	4026.3	Ordovician	0.52	1.72	0.86	0.72	0.63	0.87	0.95	0.51
RDC#2	3911.38	Ordovician	0.52	1.40	0.78	0.74	0.64	0.85	1.00	0.53

Appendix 5.2 Alkylcarbazole concentrations (ug/g oil) of the oils.

		Carbazol	'Methylcarbazoles				'Dimethyl- and ethyl-carbazoles											
Sample	Field	c	1-mc	3-mc	2-mc	4-mc	1,8-dmc	1-ethdmc	1,3-dmc	1,6-dmc	1,7-dmc	1,4-dmc+4-ec+1,5-dmc+3-ec	2,6-dmc	2,7-+1,2-dmc	2,4-dmc	2,5-dmc	2,3-dmc	3,4-dmc
MD59	HMD	0.03	0.08	0.03	0.04	0.03	0.22	0.05	0.21	0.17	0.16	0.28	0.07	0.10	0.05	0.05	0.06	0.09
MD104	HMD	0.03	0.10	0.03	0.05	0.02	0.31	0.04	0.22	0.23	0.24	0.42	0.07	0.13	0.08	0.06	0.02	0.11
MD185	HMD	0.04	0.08	0.04	0.05	0.03	0.24	0.03	0.20	0.18	0.18	0.34	0.06	0.08	0.05	0.05	0.08	0.09
MD201b	HMD	0.05	0.25	0.08	0.09	0.07	0.61	0.05	0.47	0.49	0.48	0.82	0.17	0.33	0.14	0.16	0.05	0.13
MD204	HMD	0.03	0.17	0.06	0.06	0.05	0.44	0.04	0.30	0.33	0.37	0.62	0.12	0.25	0.11	0.13	0.04	0.09
MD208	HMD	0.08	0.05	0.02	0.02	0.01	0.19	0.03	0.16	0.14	0.16	0.29	0.06	0.05	0.03	0.04	0.07	0.07
MD239	HMD	0.03	0.17	0.05	0.07	0.03	0.54	0.04	0.45	0.33	0.44	0.60	0.12	0.18	0.08	0.07	0.05	0.16
MD255b	HMD	0.05	0.28	0.08	0.11	0.08	0.61	0.05	0.47	0.48	0.48	0.87	0.16	0.31	0.15	0.15	0.09	0.15
MD279	HMD	0.05	0.29	0.08	0.10	0.10	0.80	0.14	0.54	0.59	0.69	1.34	0.16	0.42	0.23	0.25	0.10	0.30
MD297	HMD	0.02	0.08	0.02	0.03	0.03	0.23	0.03	0.12	0.14	0.17	0.22	0.05	0.10	0.07	0.06	0.01	0.05
MD317	HMD	0.05	0.27	0.08	0.09	0.07	0.61	0.05	0.44	0.47	0.48	0.86	0.14	0.30	0.14	0.14	0.04	0.12
MD322	HMD	0.03	0.15	0.04	0.04	0.04	0.41	0.04	0.29	0.24	0.32	0.56	0.07	0.16	0.09	0.07	0.03	0.09
MD332	HMD	0.05	0.35	0.09	0.16	0.13	0.69	0.04	0.56	0.54	0.68	1.26	0.20	0.38	0.22	0.24	0.08	0.21
MD348	HMD	0.03	0.15	0.04	0.06	0.04	0.42	0.05	0.32	0.31	0.31	0.59	0.09	0.19	0.10	0.09	0.04	0.15
OM7	HMD	0.03	0.16	0.04	0.05	0.04	0.47	0.05	0.36	0.28	0.40	0.62	0.11	0.20	0.11	0.10	0.05	0.14
OMJ422	HMD	0.04	0.27	0.07	0.08	0.08	0.61	0.06	0.49	0.39	0.52	0.97	0.17	0.31	0.21	0.17	0.06	0.17
OMJ832	HMD	0.03	0.14	0.04	0.06	0.04	0.38	0.04	0.32	0.23	0.35	0.56	0.10	0.17	0.10	0.08	0.04	0.12
OMK14	HMD	0.02	0.11	0.03	0.03	0.03	0.30	0.04	0.23	0.23	0.25	0.41	0.06	0.12	0.06	0.06	0.04	0.11
OML862	HMD	0.05	0.16	0.06	0.06	0.05	0.47	0.04	0.29	0.29	0.35	0.62	0.10	0.20	0.11	0.10	0.04	0.12
OMM33	HMD	0.05	0.31	0.08	0.11	0.12	0.63	0.06	0.49	0.39	0.58	1.09	0.17	0.36	0.25	0.21	0.07	0.16
OMM772	HMD	0.08	0.17	0.06	0.06	0.06	0.53	0.06	0.31	0.31	0.34	0.76	0.11	0.25	0.15	0.12	0.04	0.14
OMN352	HMD	0.02	0.13	0.03	0.04	0.03	0.36	0.03	0.26	0.27	0.29	0.53	0.07	0.15	0.08	0.08	0.05	0.11
OMN412	HMD	0.03	0.15	0.03	0.05	0.04	0.44	0.05	0.35	0.26	0.41	0.62	0.10	0.18	0.11	0.08	0.04	0.15
OMO36	HMD	0.05	0.11	0.04	0.04	0.03	0.47	0.09	0.25	0.26	0.30	0.55	0.10	0.17	0.09	0.08	0.03	0.14
OMO712	HMD	0.02	0.07	0.02	0.03	0.02	0.25	0.04	0.16	0.17	0.19	0.30	0.04	0.08	0.05	0.04	0.04	0.08
OMO751	HMD	0.02	0.08	0.02	0.03	0.02	0.26	0.03	0.18	0.18	0.20	0.35	0.05	0.10	0.05	0.05	0.03	0.09
OMP263	HMD	0.02	0.07	0.02	0.02	0.02	0.25	0.02	0.18	0.19	0.19	0.27	0.05	0.08	0.03	0.03	0.03	0.09
ONI412	HMD	0.08	0.48	0.14	0.19	0.16	0.98	0.10	0.73	0.73	0.73	1.42	0.30	0.58	0.34	0.29	0.10	0.27
ONM36	HMD	0.06	0.24	0.08	0.09	0.06	0.78	0.08	0.47	0.51	0.54	0.85	0.18	0.33	0.15	0.13	0.05	0.14
MD6	HMD	0.00	0.01	0.00	0.00	0.00	0.33	0.09	0.26	0.25	0.31	0.53	0.08	0.12	0.10	0.05	0.00	0.12
MD45	HMD	0.00	0.01	0.00	0.00	0.00	0.41	0.06	0.38	0.29	0.28	0.59	0.10	0.16	0.10	0.05	0.02	0.12
MD46	HMD	0.00	0.01	0.00	0.00	0.00	0.32	0.06	0.27	0.24	0.28	0.45	0.06	0.09	0.06	0.02	0.01	0.10
MD64	HMD	0.00	0.01	0.00	0.00	0.00	0.36	0.07	0.30	0.27	0.38	0.60	0.06	0.13	0.07	0.06	0.04	0.12
MD125	HMD	0.00	0.01	0.00	0.00	0.00	0.44	0.08	0.35	0.32	0.45	0.69	0.11	0.18	0.10	0.07	0.06	0.15
MD129	HMD	0.00	0.01	0.00	0.00	0.00	0.29	0.09	0.26	0.24	0.35	0.53	0.07	0.11	0.08	0.04	0.05	0.14
MD134	HMD	0.00	0.01	0.00	0.00	0.00	0.33	0.10	0.27	0.24	0.34	0.58	0.08	0.15	0.09	0.06	0.02	0.13
MD139	HMD	0.00	0.01	0.00	0.00	0.00	0.28	0.10	0.26	0.20	0.28	0.47	0.05	0.08	0.05	0.03	0.02	0.11
MD140	HMD	0.00	0.01	0.00	0.00	0.00	0.41	0.09	0.30	0.25	0.39	0.60	0.10	0.10	0.05	0.04	0.02	0.14
MD141	HMD	0.00	0.01	0.00	0.00	0.00	0.37	0.07	0.28	0.27	0.40	0.73	0.12	0.21	0.13	0.12	0.02	0.18
MD177	HMD	0.00	0.01	0.00	0.00	0.00	0.59	0.05	0.45	0.29	0.51	0.73	0.19	0.11	0.02	0.03	0.03	0.10
MD213	HMD	0.00	0.01	0.00	0.00	0.00	0.47	0.08	0.36	0.36	0.48	0.62	0.09	0.20	0.06	0.04	0.02	0.14
MD215	HMD	0.00	0.01	0.00	0.00	0.00	0.72	0.08	0.49	0.51	0.70	1.08	0.14	3.41	0.14	0.13	0.03	0.16
MD221	HMD	0.00	0.01	0.00	0.00	0.00	0.64	0.10	0.40	0.48	0.81	1.26	0.13	0.41	0.18	0.18	0.03	0.17
MD235	HMD	0.05	0.23	0.05	0.07	0.06	0.76	0.05	0.65	0.55	0.68	1.11	0.13	0.33	0.18	0.13	0.04	0.16

Appendix 5.2 Alkylcarbazole concentrations (ug/g oil) of the oils (continued).

MD269	HMD	0.04	0.17	0.04	0.06	0.07	0.45	0.04	0.36	0.33	0.47	0.88	0.09	0.24	0.15	0.14	0.02	0.10
MD272	HMD	0.00	0.10	0.02	0.03	0.02	0.29	0.06	0.22	0.20	0.27	0.59	0.05	0.12	0.09	0.06	0.01	0.07
MD275	HMD	0.00	0.01	0.00	0.00	0.00	0.17	0.03	0.13	0.12	0.16	0.23	0.02	0.04	0.02	0.01	0.01	0.04
MD280	HMD	0.00	0.01	0.00	0.00	0.00	0.25	0.05	0.22	0.17	0.23	0.35	0.05	0.06	0.03	0.02	0.02	0.06
MD287	HMD	0.00	0.12	0.03	0.04	0.02	0.44	0.05	0.36	0.32	0.40	0.59	0.08	0.16	0.06	0.05	0.03	0.10
MD299	HMD	0.00	0.01	0.00	0.00	0.00	0.33	0.04	0.25	0.22	0.32	0.54	0.05	0.12	0.07	0.05	0.03	0.06
MD300	HMD	0.00	0.01	0.00	0.00	0.00	0.19	0.06	0.15	0.13	0.19	0.28	0.02	0.04	0.02	0.01	0.01	0.05
MD304	HMD	0.00	0.01	0.00	0.00	0.00	0.38	0.05	0.31	0.26	0.32	0.43	0.06	0.07	0.03	0.02	0.02	0.09
MD345	HMD	0.00	0.01	0.00	0.00	0.00	0.29	0.04	0.23	0.19	0.26	0.43	0.04	0.08	0.05	0.03	0.02	0.07
MD409	HMD	0.04	0.26	0.07	0.08	0.08	0.74	0.06	0.50	0.55	0.71	1.12	0.13	0.35	0.14	0.14	0.04	0.12
MD412	HMD	0.01	0.20	0.05	0.06	0.05	0.61	0.05	0.39	0.44	0.60	0.92	0.11	0.29	0.12	0.15	0.03	0.11
OMJ41	HMD	0.02	0.11	0.02	0.03	0.02	0.37	0.06	0.24	0.36	0.37	0.66	0.06	0.19	0.08	0.08	0.03	0.08
OMJ721	HMD	0.02	0.08	0.02	0.03	0.02	0.24	0.03	0.18	0.27	0.28	0.46	0.06	0.12	0.05	0.05	0.01	0.06
OML76	HMD	0.02	0.10	0.03	0.04	0.03	0.36	0.03	0.22	0.35	0.36	0.61	0.07	0.17	0.10	0.07	0.02	0.08
OML82	HMD	0.01	0.12	0.03	0.04	0.03	0.44	0.04	0.27	0.43	0.42	0.67	0.11	0.21	0.11	0.08	0.02	0.11
OML712	HMD	0.02	0.08	0.02	0.02	0.02	0.30	0.03	0.26	0.23	0.31	0.46	0.06	0.12	0.06	0.05	0.01	0.10
OMM67	HMD	0.02	0.14	0.03	0.06	0.04	0.42	0.03	0.28	0.43	0.43	0.81	0.08	0.23	0.14	0.11	0.02	0.09
OMM74	HMD	0.01	0.11	0.02	0.03	0.04	0.34	0.03	0.25	0.26	0.38	0.68	0.07	0.19	0.12	0.10	0.03	0.09
OMM80	HMD	0.00	0.07	0.02	0.02	0.02	0.26	0.04	0.21	0.19	0.27	0.43	0.04	0.11	0.06	0.05	0.02	0.09
OMM532	HMD	0.02	0.18	0.27	0.09	0.05	0.50	0.03	0.41	0.36	0.51	0.95	0.11	0.22	0.11	0.11	0.03	0.10
OMM542	HMD	0.02	0.14	0.03	0.04	0.05	0.42	0.04	0.33	0.33	0.47	0.86	0.09	0.25	0.12	0.13	0.04	0.07
OMM632	HMD	0.03	0.19	0.03	0.06	0.04	0.56	0.07	0.46	0.42	0.51	1.02	0.12	0.24	0.13	0.13	0.05	0.14
OMM763	HMD	0.00	0.04	0.03	0.04	0.05	0.35	0.04	0.26	0.28	0.43	0.67	0.08	0.22	0.10	0.11	0.02	0.09
OMM812	HMD	0.00	0.06	0.01	0.03	0.02	0.26	0.04	0.17	0.18	0.32	0.47	0.05	0.11	0.05	0.06	0.02	0.08
OMN33	HMD	0.00	0.01	0.00	0.00	0.00	0.17	0.02	0.12	0.14	0.24	0.31	0.03	0.04	0.02	0.01	0.03	0.05
OMN681	HMD	0.00	0.06	0.02	0.02	0.03	0.25	0.04	0.20	0.20	0.32	0.49	0.05	0.13	0.05	0.06	0.05	0.07
OMO142	HMD	0.00	0.01	0.00	0.00	0.00	0.25	0.04	0.18	0.19	0.30	0.49	0.05	0.09	0.05	0.05	0.05	0.07
OMO343	HMD	0.00	0.01	0.00	0.00	0.00	0.17	0.04	0.12	0.13	0.19	0.27	0.03	0.05	0.02	0.01	0.03	0.05
OMP33	HMD	0.00	0.01	0.00	0.00	0.00	0.21	0.04	0.16	0.22	0.22	0.33	0.05	0.07	0.03	0.03	0.03	0.06
OMP42	HMD	0.01	0.01	0.00	0.01	0.00	0.30	0.03	0.22	0.22	0.31	0.45	0.05	0.09	0.04	0.04	0.06	0.07
OMP67	HMD	0.00	0.01	0.00	0.00	0.00	0.24	0.05	0.19	0.25	0.22	0.33	0.04	0.07	0.02	0.01	0.04	0.08
OMP74	HMD	0.00	0.01	0.00	0.00	0.00	0.26	0.03	0.19	0.20	0.30	0.36	0.06	0.09	0.03	0.03	0.02	0.07
OMP802	HMD	0.00	0.01	0.00	0.00	0.00	0.28	0.02	0.17	0.20	0.27	0.39	0.04	0.10	0.03	0.03	0.04	0.07
ONI403	HMD	0.00	0.23	0.05	0.06	0.06	0.63	0.03	0.45	0.49	0.72	1.15	0.09	0.36	0.15	0.15	0.09	0.11
ONM243	HMD	0.01	0.01	0.00	0.01	0.00	0.12	0.01	0.06	0.07	0.13	0.15	0.01	0.04	0.01	0.01	0.01	0.02
ONM461	HMD	0.01	0.01	0.00	0.01	0.00	0.66	0.05	0.38	0.46	0.77	0.92	0.16	0.32	0.12	0.13	0.09	0.12
GS#1	El Gassi	0.00	0.00	0.00	0.00	0.00	0.15	0.01	0.13	0.10	0.14	0.29	0.07	0.09	0.08	0.04	0.07	0.03
AR#61	Zotti	0.00	0.01	0.00	0.00	0.00	0.08	0.01	0.04	0.07	0.07	0.14	0.01	0.01	0.00	0.01	0.00	0.01
AR#22	El Agreb	0.00	0.00	0.00	0.00	0.00	0.00	0.00	0.00	0.00	0.01	0.02	0.00	0.00	0.00	0.00	0.00	0.00
DRT#1	D.Temra	0.04	0.30	0.08	0.12	0.12	0.93	0.07	0.73	0.71	1.02	1.87	0.24	0.61	0.36	0.35	0.07	0.17
GLNE#5	Guellala NE	0.30	1.26	0.46	0.54	0.61	2.38	0.28	1.64	1.37	1.79	4.04	0.72	1.47	0.90	0.76	0.22	0.59

Appendix 5.2 Alkylcarbazole concentrations (ug/g oil) of the oils (continued).

GLA#16	Guellala	0.03	0.36	0.06	0.14	0.14	0.86	0.05	0.51	0.62	0.98	1.76	0.20	0.59	0.28	0.36	0.03	0.10
MEK#1	M.Kebch	0.06	0.58	0.15	0.19	0.20	1.79	0.11	1.42	1.36	1.93	3.50	0.44	1.16	0.70	0.70	0.11	0.32
NGS#2	N'goussa	0.09	0.45	0.08	0.22	0.14	1.45	0.05	1.26	0.67	1.48	2.41	0.19	0.52	0.27	0.34	0.15	0.19
OKJ#31	H.Berkaoui	0.02	0.12	0.02	0.05	0.04	0.44	0.03	0.25	0.30	0.51	0.84	0.09	0.24	0.15	0.12	0.03	0.07
OKJ#202	H.Berkaoui	0.02	0.09	0.02	0.04	0.04	0.36	0.02	0.21	0.23	0.39	0.65	0.07	0.18	0.09	0.12	0.02	0.06
OKM#88	H.Berkaoui	0.01	0.06	0.01	0.03	0.03	0.29	0.02	0.14	0.24	0.26	0.51	0.05	0.16	0.07	0.09	0.02	0.03
OKN#77	H.Berkaoui	0.01	0.07	0.01	0.04	0.03	0.34	0.01	0.16	0.27	0.31	0.57	0.06	0.18	0.07	0.10	0.02	0.04
OKP#61	Benkahla	0.03	0.13	0.03	0.06	0.07	0.51	0.02	0.34	0.28	0.38	0.95	0.10	0.25	0.16	0.17	0.05	0.11
OKP#88	Benkahla	0.01	0.11	0.01	0.05	0.06	0.39	0.02	0.24	0.26	0.38	0.87	0.06	0.25	0.15	0.13	0.03	0.05
RDC-1b	R.Chegga	0.10	0.62	0.16	0.22	0.25	1.23	0.12	1.01	0.80	1.00	2.28	0.35	0.89	0.54	0.46	0.13	0.27
HGA#2	H.Guettar	0.06	0.19	0.06	0.08	0.08	0.55	0.08	0.29	0.34	0.41	0.84	0.12	0.28	0.15	0.17	0.05	0.14
HGA#3	H.Guettar	0.10	0.38	0.12	0.21	0.18	0.81	0.12	0.49	0.44	0.81	1.60	0.24	0.55	0.35	0.35	0.07	0.18
MDR#7	Mesdar	0.10	0.69	0.24	0.29	0.21	1.96	0.20	1.60	1.16	1.37	2.62	0.58	1.04	0.66	0.45	0.24	0.56
MDR#8	Mesdar	0.05	0.28	0.13	0.19	0.15	1.64	0.08	1.28	1.30	1.81	2.76	0.38	0.98	0.39	0.41	0.23	0.30
RB#10	R.Baguel	0.00	0.00	0.00	0.00	0.00	0.04	0.01	0.03	0.03	0.05	0.06	0.01	0.01	0.01	0.00	0.02	0.00
RB#18	R.Baguel	0.00	0.00	0.00	0.00	0.00	0.00	0.00	0.00	0.00	0.00	0.00	0.00	0.00	0.00	0.00	0.00	0.00
OL2	DST	0.43	1.00	0.46	0.74	0.48	2.54	0.27	1.71	1.18	1.59	2.67	0.93	1.11	0.70	0.59	0.34	0.23

Appendix 5.2 Alkylcarbazole concentrations (ug/g oil) of the oils (continued).

		Trimethylcarbazoles													Total carbazoles				Benzocarbazoles			
Sample	Field	1	2	3	4	5	6	7	8	9	10	11	12	13	Total MCs	Total DMCs	Total TMCs	Total alkylcar bzoles	benzo [a]	benzo [b]	benzo [c]	Tot Benz-carbazole s
MD59	HMD														0.18	1.50	0.00	1.68	0.01	0.00	0.01	0.02
MD104	HMD	0.14	0.00	1.10	1.01	0.10	0.62	0.42	0.49	0.96	0.09	0.38	0.08	0.19	0.20	1.94	5.58	7.72	0.04	0.00	0.03	0.07
MD185	HMD	0.11	0.00	0.86	0.79	0.07	0.61	0.36	0.39	0.73	0.11	0.32	0.06	0.17	0.20	1.57	4.58	6.35	0.03	0.00	0.02	0.04
MD201b	HMD	0.18	0.02	1.87	1.66	0.10	1.22	0.61	0.95	1.46	0.17	0.51	0.14	0.44	0.48	3.90	9.32	13.70	0.05	0.00	0.03	0.08
MD204	HMD	0.10	0.01	1.29	1.12	0.07	0.84	0.42	0.70	1.08	0.13	0.30	0.10	0.27	0.34	2.84	6.45	9.64	0.04	0.00	0.02	0.06
MD208	HMD	0.08	0.01	0.63	0.60	0.03	0.42	0.21	0.34	0.58	0.07	0.21	0.05	0.09	0.10	1.30	3.32	4.72	0.01	0.00	0.00	0.02
MD239	HMD	0.00	0.00	2.23	1.75	0.18	1.30	0.85	0.81	1.31	0.14	0.62	0.15	0.25	0.32	3.07	9.58	12.97	0.04	0.00	0.03	0.07
MD255b	HMD	0.00	0.00	2.07	1.91	0.11	1.36	0.67	1.09	1.59	0.21	0.51	0.22	0.40	0.54	3.99	10.13	14.66	0.05	0.00	0.03	0.08
MD279	HMD	0.39	0.01	2.57	2.90	0.17	1.75	0.97	1.60	2.73	0.49	0.93	0.19	0.70	0.58	5.55	15.40	21.53	0.09	0.00	0.05	0.14
MD297	HMD	0.00	0.00	0.53	0.57	0.00	0.36	0.21	0.39	0.61	0.08	0.14	0.07	0.18	0.16	1.25	3.14	4.56	0.02	0.00	0.01	0.03
MD317	HMD	0.00	0.00	1.98	1.84	0.10	1.32	0.69	1.07	1.59	0.22	0.51	0.23	0.51	0.51	3.79	10.07	14.36	0.05	0.00	0.02	0.07
MD322	HMD	0.00	0.00	1.28	1.21	0.05	0.69	0.44	0.69	1.00	0.12	0.32	0.07	0.22	0.27	2.38	6.09	8.74	0.03	0.00	0.01	0.04
MD332	HMD	0.00	0.00	2.21	2.63	0.12	1.39	0.82	1.46	2.57	0.27	0.54	0.23	0.49	0.72	5.11	12.74	18.58	0.08	0.00	0.04	0.11
MD348	HMD	0.00	0.00	1.43	1.42	0.08	0.83	0.59	0.70	1.27	0.15	0.41	0.13	0.29	0.29	2.64	7.30	10.23	0.03	0.00	0.02	0.06
OM7	HMD	0.17	0.00	1.64	1.42	0.14	0.95	0.61	0.76	1.27	0.15	0.47	0.12	0.28	0.29	2.90	7.98	11.17	0.03	0.00	0.02	0.05
OMJ422	HMD	0.00	0.00	1.95	2.11	0.15	1.20	0.78	1.14	2.04	0.27	0.43	0.19	0.34	0.50	4.13	10.59	15.23	0.07	0.00	0.05	0.12
OMJ832	HMD	0.00	0.00	1.28	1.26	0.10	0.75	0.50	0.72	1.23	0.15	0.36	0.12	0.30	0.28	2.49	6.77	9.54	0.04	0.00	0.02	0.06
OMK14	HMD	0.00	0.00	1.15	1.05	0.08	0.80	0.40	0.58	1.01	0.16	0.37	0.11	0.24	0.20	1.90	5.95	8.06	0.04	0.00	0.03	0.06
OML862	HMD	0.12	0.06	1.48	1.60	0.10	1.02	0.61	0.96	1.56	0.25	0.41	0.20	0.34	0.32	2.74	8.71	11.78	0.03	0.00	0.03	0.06
OMM33	HMD	0.00	0.00	1.68	2.06	0.12	1.03	0.69	1.25	2.03	0.31	0.52	0.24	0.52	0.63	4.49	10.46	15.57	0.05	0.00	0.04	0.09
OMM772	HMD	0.21	0.08	1.42	1.60	0.11	1.13	0.52	0.97	1.56	0.26	0.41	0.18	0.33	0.35	3.13	8.79	12.28	0.04	0.00	0.02	0.07
OMN352	HMD	0.18	0.00	1.25	1.30	0.11	0.77	0.54	0.77	1.25	0.13	0.39	0.11	0.29	0.24	2.27	7.10	9.61	0.03	0.00	0.02	0.05
OMN412	HMD	0.23	0.00	1.59	1.53	0.13	0.99	0.62	0.89	1.43	0.16	0.47	0.13	0.30	0.27	2.79	8.47	11.53	0.05	0.00	0.03	0.08
OMO36	HMD	0.23	0.15	1.46	1.39	0.12	1.08	0.57	0.81	1.45	0.23	0.62	0.12	0.31	0.22	2.54	8.53	11.29	0.05	0.00	0.02	0.06
OMO712	HMD	0.12	0.00	1.01	0.83	0.07	0.60	0.47	0.48	0.71	0.07	0.36	0.06	0.14	0.13	1.42	4.93	6.48	0.02	0.00	0.02	0.04
OMO751	HMD	0.14	0.00	1.04	0.95	0.09	0.63	0.47	0.54	0.88	0.13	0.40	0.09	0.20	0.16	1.58	5.55	7.28	0.03	0.00	0.02	0.05
OMP263	HMD	0.13	0.00	1.11	0.87	0.07	0.69	0.52	0.46	0.72	0.11	0.42	0.10	0.12	0.13	1.42	5.32	6.87	0.03	0.00	0.02	0.05
ONI412	HMD	0.33	0.03	2.87	3.12	0.23	1.82	1.32	1.80	2.95	0.38	0.67	0.33	0.71	0.97	6.56	16.56	24.09	0.08	0.00	0.06	0.14
ONM36	HMD	0.18	0.11	2.13	0.00	0.13	1.41	1.12	1.30	1.84	0.20	0.57	0.17	0.35	0.47	4.20	9.53	14.19	0.05	0.00	0.03	0.08
MD6	HMD	0.56	0.00	3.28	2.94	0.23	1.80	1.23	1.41	2.83	0.45	0.93	0.13	0.44	0.02	2.23	16.22	18.46	0.00	0.00	0.00	0.00
MD45	HMD	0.29	0.00	2.13	1.85	0.10	1.25	0.64	0.98	1.52	0.20	0.65	0.16	0.31	0.02	2.56	10.09	12.67	0.00	0.00	0.00	0.00
MD46	HMD	0.27	0.00	1.92	1.58	0.12	1.11	0.48	0.81	1.41	0.18	0.49	0.06	0.20	0.02	1.95	8.63	10.60	0.00	0.00	0.00	0.00
MD64	HMD	0.32	0.00	1.91	1.91	0.14	0.99	0.77	0.96	1.77	0.31	0.74	0.15	0.42	0.02	2.44	10.39	12.84	0.00	0.00	0.00	0.00
MD125	HMD	0.00	0.00	2.25	2.05	0.16	1.40	1.08	1.28	1.91	0.33	0.51	0.15	0.30	0.02	3.01	11.43	14.45	0.00	0.00	0.00	0.00
MD129	HMD	0.37	0.00	1.90	1.75	0.12	1.05	0.77	1.02	1.61	0.35	0.29	0.76	0.31	0.02	2.26	10.29	12.57	0.00	0.00	0.00	0.00
MD134	HMD	0.33	0.00	1.81	1.56	0.06	0.94	0.69	0.88	1.48	0.27	0.37	0.10	0.21	0.02	2.39	8.71	11.12	0.00	0.00	0.00	0.00
MD139	HMD	0.32	0.00	1.64	1.50	0.06	0.88	0.62	0.75	1.40	0.35	0.22	0.58	0.29	0.02	1.94	8.60	10.55	0.00	0.00	0.00	0.00
MD140	HMD	0.29	0.03	1.69	1.72	0.10	0.85	0.71	0.87	1.53	0.09	0.22	0.50	0.17	0.02	2.49	8.77	11.28	0.00	0.00	0.00	0.00
MD141	HMD	0.35	0.00	1.91	1.90	0.00	0.95	0.75	1.07	1.78	0.28	0.58	0.19	0.41	0.02	2.91	10.17	13.09	0.00	0.00	0.00	0.00
MD177	HMD	0.31	0.00	1.87	1.61	0.11	0.97	0.36	0.52	1.25	0.38	0.10	0.45	0.05	0.02	3.10	7.98	11.10	0.00	0.00	0.00	0.00
MD213	HMD	0.00	0.00	2.66	2.01	0.00	1.53	1.13	1.03	1.59	0.22	0.54	0.18	0.26	0.02	2.93	11.16	14.11	0.00	0.00	0.00	0.00
MD215	HMD	0.00	0.00	3.19	2.77	0.00	1.76	1.28	1.80	2.27	0.33	0.55	0.15	0.51	0.02	7.57	14.61	22.21	0.00	0.00	0.00	0.00
MD221	HMD	0.00	0.00	2.65	2.94	0.00	1.43	1.28	1.91	2.96	0.39	0.85	0.25	0.94	0.02	4.80	15.61	20.43	0.00	0.00	0.00	0.00
MD235	HMD	0.33	0.00	3.00	2.76	0.18	1.98	0.94	1.57	2.44	0.19	0.68	0.17	0.49	0.42	4.75	14.72	19.89	0.00	0.00	0.00	0.00

Appendix 5.2 Alkylcarbazole concentrations (ug/g oil) of the oils (continued).

MD269	HMD	0.24	0.00	1.59	1.85	0.10	1.04	0.54	1.09	1.88	0.18	0.34	0.11	0.44	0.34	3.27	9.39	13.00	0.00	0.00	0.00	0.00
MD272	HMD	0.16	0.00	1.05	1.16	0.06	0.51	0.46	0.74	1.19	0.00	0.26	0.06	0.23	0.18	2.03	5.89	8.09	0.00	0.00	0.00	0.00
MD275	HMD	0.12	0.00	0.89	0.71	0.03	0.54	0.26	0.44	0.59	0.09	0.24	0.03	0.10	0.02	0.98	4.04	5.04	0.00	0.00	0.00	0.00
MD280	HMD	0.18	0.00	1.19	1.07	0.07	0.57	0.34	0.51	0.92	0.12	0.32	0.04	0.13	0.02	1.51	5.45	6.97	0.00	0.00	0.00	0.00
MD287	HMD	0.21	0.00	2.05	1.75	0.00	1.15	0.64	0.96	1.53	0.20	0.52	0.15	0.26	0.22	2.65	9.40	12.26	0.00	0.00	0.00	0.00
MD299	HMD	0.17	0.00	1.26	1.36	0.07	0.61	0.39	0.71	1.29	0.15	0.25	0.05	0.24	0.02	2.08	6.56	8.66	0.00	0.00	0.00	0.00
MD300	HMD	0.00	0.00	0.95	0.88	0.00	0.48	0.42	0.49	0.79	0.19	1.33	0.34	0.14	0.02	1.15	6.00	7.17	0.00	0.00	0.00	0.00
MD304	HMD	0.00	0.00	1.67	1.57	0.00	1.03	0.52	0.83	1.31	0.09	0.46	0.05	0.15	0.01	2.03	7.68	9.72	0.00	0.00	0.00	0.00
MD345	HMD	0.17	0.00	1.20	1.24	0.10	0.60	0.49	0.61	1.12	0.13	0.27	0.06	0.18	0.02	1.73	6.19	7.93	0.00	0.00	0.00	0.00
MD409	HMD	0.00	0.00	2.65	2.49	0.00	1.75	9.27	1.52	2.14	0.24	0.76	0.25	0.67	0.50	4.60	21.74	26.84	0.00	0.00	0.00	0.00
MD412	HMD	0.00	0.00	2.25	2.11	0.00	1.46	0.79	1.29	1.96	0.20	0.55	0.14	0.46	0.37	3.82	11.21	15.40	0.00	0.00	0.00	0.00
OMJ41	HMD	0.19	0.00	1.55	1.55	0.06	0.86	0.53	0.96	1.53	0.15	0.28	0.06	0.34	0.18	2.57	8.05	10.80	0.00	0.00	0.00	0.00
OMJ721	HMD	0.18	0.00	1.34	1.26	0.05	0.74	0.49	0.69	1.23	0.13	0.27	0.05	0.16	0.14	1.83	6.61	8.58	0.00	0.00	0.00	0.00
OML76	HMD	0.18	0.00	1.53	1.48	0.08	0.91	0.60	0.83	1.47	0.12	0.35	0.09	0.31	0.20	2.44	7.94	10.58	0.00	0.00	0.00	0.00
OML82	HMD	0.21	0.00	1.94	1.78	0.10	1.15	0.90	0.98	1.67	0.17	0.49	0.13	0.36	0.23	2.91	9.89	13.02	0.00	0.00	0.00	0.00
OML712	HMD	0.19	0.00	1.55	1.36	0.06	0.89	0.71	0.70	1.23	0.10	0.31	0.06	0.14	0.14	1.98	7.32	9.44	0.00	0.00	0.00	0.00
OMM67	HMD	0.16	0.00	1.68	1.76	0.06	0.98	0.61	1.01	1.79	0.12	0.28	0.05	0.35	0.28	3.08	8.85	12.21	0.00	0.00	0.00	0.00
OMM74	HMD	0.18	0.00	1.29	1.45	0.05	0.72	0.67	0.91	1.47	0.11	0.24	0.07	0.29	0.20	2.53	7.46	10.20	0.00	0.00	0.00	0.00
OMM80	HMD	0.18	0.00	1.31	1.20	0.07	0.69	0.60	0.72	1.13	0.07	0.28	0.02	0.16	0.13	1.78	6.44	8.34	0.00	0.00	0.00	0.00
OMM532	HMD	0.20	0.00	1.74	2.01	0.10	0.92	0.84	1.16	2.06	0.14	0.24	0.04	0.35	0.60	3.43	9.81	13.84	0.00	0.00	0.00	0.00
OMM542	HMD	0.21	0.00	1.53	1.77	0.06	0.89	0.79	1.14	1.78	0.16	0.36	0.16	0.46	0.26	3.14	9.32	12.71	0.00	0.00	0.00	0.00
OMM632	HMD	0.25	0.00	2.08	2.31	0.08	1.21	1.03	1.45	2.35	0.20	0.44	0.10	0.45	0.33	3.83	11.95	16.11	0.00	0.00	0.00	0.00
OMM763	HMD	0.19	0.00	1.44	1.63	0.05	0.80	0.78	1.11	1.53	0.11	0.21	0.05	0.34	0.16	2.64	8.24	11.04	0.00	0.00	0.00	0.00
OMM812	HMD	0.17	0.00	1.18	1.21	0.07	0.56	0.59	0.77	1.14	0.15	0.23	0.03	0.22	0.12	1.80	6.33	8.25	0.00	0.00	0.00	0.00
OMN33	HMD	0.16	0.00	1.03	0.96	0.05	0.49	0.40	0.66	0.98	0.04	0.18	0.05	0.15	0.02	1.20	5.15	6.36	0.00	0.00	0.00	0.00
OMN681	HMD	0.17	0.00	1.19	1.23	0.05	0.65	0.62	0.70	1.16	0.07	0.18	0.04	0.13	0.13	1.92	6.18	8.23	0.00	0.00	0.00	0.00
OMO142	HMD	0.19	0.00	1.17	1.08	0.06	0.60	0.61	0.74	1.08	0.09	0.26	0.03	0.22	0.02	1.79	6.13	7.94	0.00	0.00	0.00	0.00
OMO343	HMD	0.14	0.00	0.96	0.81	0.05	0.47	0.33	0.53	0.74	0.04	0.19	0.03	0.11	0.02	1.11	4.38	5.51	0.00	0.00	0.00	0.00
OMP33	HMD	0.17	0.00	1.25	1.09	0.06	0.74	0.44	0.65	0.84	0.04	0.26	0.02	0.12	0.02	1.46	5.68	7.17	0.00	0.00	0.00	0.00
OMP42	HMD	0.18	0.00	1.53	1.31	0.08	0.70	0.74	0.78	1.10	0.07	0.38	0.06	0.18	0.02	1.87	7.11	9.00	0.00	0.00	0.00	0.00
OMP67	HMD	0.20	0.00	1.49	1.22	0.07	0.75	0.52	0.73	0.97	0.08	0.36	0.05	0.13	0.02	1.55	6.57	8.14	0.00	0.00	0.00	0.00
OMP74	HMD	0.16	0.00	1.61	1.22	0.07	0.81	0.74	0.75	0.95	0.08	0.32	0.05	0.09	0.02	1.64	6.84	8.50	0.00	0.00	0.00	0.00
OMP802	HMD	0.17	0.00	1.48	1.26	0.07	0.92	0.54	0.82	0.95	0.05	0.28	0.06	0.11	0.02	1.65	6.71	8.38	0.00	0.00	0.00	0.00
ONI403	HMD	0.24	0.00	2.45	2.41	0.09	1.29	1.20	1.52	2.16	0.21	0.39	0.11	0.55	0.40	4.43	12.60	17.43	0.00	0.00	0.00	0.00
ONM243**	HMD	0.05	0.00	0.46	0.44	0.00	0.24	0.24	0.25	0.26	0.10	0.03	0.05	0.07	0.02	0.63	2.19	2.85	0.00	0.00	0.00	0.00
ONM461	HMD	0.27	0.00	2.52	2.39	0.13	1.32	1.28	1.53	1.89	0.12	0.45	0.10	0.35	0.02	4.18	12.34	16.54	0.00	0.00	0.00	0.00
GS#1	El Gassi	0.08	0.00	0.66	0.70	0.01	0.28	0.18	0.34	0.53	0.07	0.09	0.04	0.09	0.02	1.19	3.05	4.27	0.00	0.00	0.00	0.00
AR#61	Zotti	0.03	0.00	0.31	0.35	0.01	0.20	0.13	0.28	0.30	0.02	0.04	0.01	0.07	0.00	0.44	1.75	2.19	0.00	0.00	0.00	0.00
AR#22	El Agreb	0.01	0.00	0.04	0.04	0.00	0.02	0.01	0.03	0.04	0.00	0.00	0.00	0.00	0.00	0.04	0.21	0.25	0.00	0.00	0.00	0.00
DRT#1	D.Temra	0.00	0.00	2.68	3.51	0.00	1.82	1.05	2.10	3.16	0.33	0.49	0.33	0.95	0.63	7.13	16.40	24.15	0.00	0.00	0.09	0.09
GLNE#5	Guellala NE	0.62	0.15	3.88	5.18	0.28	2.48	1.53	3.02	4.68	0.58	0.73	0.40	1.34	2.87	16.16	24.87	43.90	0.25	0.00	0.22	0.46

Appendix 5.2 Alkylcarbazole concentrations (ug/g oil) of the oils (continued).

GLA#16	Guellala	0.31	0.00	2.16	2.79	0.06	1.49	0.92	2.05	2.62	0.36	0.47	0.22	0.93	0.70	6.34	14.37	21.40	0.10	0.00	0.09	0.19
MEK#1	M.Kebch	0.42	0.00	6.04	7.08	0.00	4.21	2.35	3.89	7.06	0.63	1.39	0.58	1.81	1.12	13.54	35.45	50.12	0.18	0.00	0.13	0.31
NGS#2	N'goussa	0.33	0.00	3.35	4.21	0.11	1.89	1.54	2.30	3.86	0.29	0.56	0.25	0.74	0.90	8.98	19.43	29.31	0.14	0.00	0.10	0.24
OKJ#31	H.Berkaoui	0.00	0.00	1.51	1.78	0.00	0.93	0.61	1.09	1.54	0.16	0.28	0.12	0.54	0.24	3.06	8.56	11.86	0.02	0.00	0.03	0.05
OKJ#202	H.Berkaoui	0.00	0.00	1.31	1.59	0.00	0.84	0.51	1.09	1.39	0.12	0.23	0.00	0.41	0.19	2.39	7.48	10.05	0.02	0.00	0.03	0.05
OKM#88	H.Berkaoui	0.00	0.00	1.16	1.27	0.00	0.69	0.43	0.92	1.13	0.10	0.20	0.09	0.38	0.12	1.88	6.37	8.37	0.02	0.00	0.01	0.03
OKN#77	H.Berkaoui	0.00	0.00	1.32	1.55	0.00	0.79	0.51	1.03	1.29	0.10	0.22	0.10	0.44	0.15	2.14	7.34	9.63	0.02	0.00	0.03	0.05
OKP#61	Benkahla	0.16	0.03	1.54	1.92	0.11	0.94	0.68	1.19	1.74	0.24	0.24	0.11	0.49	0.28	3.33	9.40	13.00	0.02	0.00	0.02	0.04
OKP#88	Benkahla	0.00	0.00	1.31	1.67	0.00	0.72	0.52	1.24	1.61	0.14	0.18	0.00	0.65	0.23	2.82	8.04	11.09	0.03	0.00	0.02	0.05
RDC-1b	R.Chegga	0.38	0.05	2.81	3.61	0.16	1.77	1.04	2.09	3.33	0.32	0.54	0.32	0.82	1.24	9.10	17.25	27.59	0.12	0.00	0.08	0.20
HGA#2	H.Guettar	0.21	0.06	1.32	1.40	0.06	0.91	0.52	0.99	1.45	0.26	0.34	0.10	0.45	0.41	3.42	8.06	11.88	0.03	0.00	0.02	0.05
HGA#3	H.Guettar	0.34	0.07	1.79	2.47	0.10	1.35	0.67	1.44	2.42	0.47	0.48	0.17	0.82	0.88	6.01	12.58	19.47	0.07	0.00	0.04	0.11
MDR#7	Mesdar	0.68	0.09	6.39	6.58	0.36	4.02	1.86	3.13	5.59	0.53	1.19	0.32	1.16	1.42	12.43	31.90	45.75	0.07	0.00	0.10	0.17
MDR#8	Mesdar	0.69	0.00	6.53	6.56	0.30	4.57	2.44	4.15	6.06	0.59	1.12	0.27	1.14	0.75	11.56	34.42	46.73	0.07	0.00	0.08	0.15
RB#10	R.Baguel	0.02	0.00	0.47	0.20	0.00	0.24	0.19	0.15	0.14	0.01	0.09	0.01	0.08	0.00	0.26	1.59	1.86	0.00	0.00	0.00	0.00
RB#18	R.Baguel	0.03	0.00	0.30	0.10	0.00	0.15	0.10	0.07	0.10	0.02	0.06	0.02	0.08	0.00	0.00	1.03	1.03	0.00	0.00	0.00	0.00
OL2	DST	0.00	0.00	4.34	4.23	4.62	2.03	4.06	1.45	1.50	0.75	1.02	0.00	0.00	2.69	13.85	24.00	40.54	0.05	0.00	0.10	0.15

Appendix 5.3 Gross composition of the oils.

sample	Field	Aliphatics (mg/g oil)	Aromatics (mg/g oil)	NSO's (mg/g oil) (Resins+ Asphaltenes)	Resins (mg/g oil)	Asphaltenes (mg/g oil)	Aliphatics (%)	Aromatics (%)	NSO's (%) (Resins+ Asphaltenes)
MD104	HMD	426.67	240.88	24.93	17.71	7.22	61.61	34.79	3.60
MD129	HMD	443.69	250.88	30.70	21.55	9.15	61.18	34.59	4.23
MD139	HMD	464.97	271.26	27.75	19.43	8.32	60.86	35.51	3.63
MD165	HMD	472.35	237.05	26.17	19.74	6.43	64.22	32.23	3.56
MD177	HMD	434.40	206.99	40.39	32.44	7.95	63.72	30.36	5.92
MD185	HMD	379.54	226.82	30.15	23.01	7.14	59.63	35.64	4.74
MD201b	HMD	428.90	198.48	14.62	8.96	5.66	66.81	30.92	2.28
MD204	HMD	483.39	226.17	16.14	10.26	5.88	66.61	31.17	2.22
MD208	HMD	409.85	224.33	28.45	21.72	6.73	61.85	33.85	4.29
MD239	HMD	485.22	236.98	25.38	18.09	7.29	64.91	31.70	3.40
MD255b	HMD	456.09	204.82	20.92	16.46	4.46	66.89	30.04	3.07
MD269	HMD	482.35	239.92	29.20	20.02	9.18	64.19	31.93	3.89
MD272	HMD	435.84	241.91	24.88	17.96	6.92	62.03	34.43	3.54
MD279	HMD	413.72	227.24	30.36	20.69	9.67	61.63	33.85	4.52
MD287	HMD	507.10	237.15	22.57	17.08	5.48	66.13	30.93	2.94
MD297	HMD	496.12	258.29	24.42	15.47	8.95	63.70	33.16	3.14
MD300	HMD	431.58	255.38	25.09	17.44	7.65	60.61	35.87	3.52
MD317	HMD	452.70	214.74	23.43	16.13	7.30	65.53	31.08	3.39
MD322	HMD	400.51	198.13	23.97	16.15	7.82	64.33	31.82	3.85
MD332b	HMD	510.81	253.08	38.25	31.34	6.91	63.68	31.55	4.77
MD348	HMD	406.69	214.38	16.30	12.69	3.61	63.81	33.64	2.56
MD45	HMD	449.52	227.01	22.55	15.40	7.16	64.30	32.47	3.23
MD46	HMD	464.76	237.66	24.27	17.58	6.69	63.95	32.70	3.34
MD59	HMD	361.10	193.52	22.12	18.94	3.18	62.61	33.55	3.84
MD6	HMD	420.71	245.91	21.70	13.87	7.83	61.12	35.73	3.15
OM7	HMD	381.88	202.52	28.70	19.56	9.14	62.29	33.03	4.68
OMJ422	HMD	439.33	237.30	26.46	17.65	8.81	62.49	33.75	3.76
OMJ832	HMD	464.86	255.65	30.94	22.06	8.88	61.86	34.02	4.12
OMK14	HMD	417.60	230.25	22.88	16.09	6.79	62.26	34.33	3.41
OML712	HMD	465.78	237.83	21.88	14.76	7.12	64.20	32.78	3.02
OML862	HMD	485.43	238.30	18.95	12.12	6.83	65.36	32.09	2.55
OMM33	HMD	443.87	221.85	35.78	23.06	12.72	63.27	31.62	5.10
OMM532	HMD	323.39	138.74	36.26	24.85	11.41	64.89	27.84	7.28
OMM542	HMD	456.41	239.69	25.12	15.95	9.17	63.28	33.23	3.48
OMM632	HMD	595.69	311.33	43.45	33.53	9.92	62.67	32.76	4.57
OMM67	HMD	497.09	254.16	34.75	25.85	8.89	63.24	32.34	4.42
OMM741	HMD	378.46	208.90	28.41	17.00	11.41	61.46	33.92	4.61

Appendix 5.3 Gross composition of the oils (continued).

sample	Field	Aliphatics (mg/g oil)	Aromatics (mg/g oil)	NSO's (mg/g oil) (Resins+ Asphaltenes)	Resins (mg/g oil)	Asphaltenes (mg/g oil)	Aliphatics (%)	Aromatics (%)	NSO's (%) (Resins+ Asphaltenes)
OMM763	HMD	421.42	238.40	30.88	19.80	11.08	61.01	34.52	4.47
OMM772	HMD	460.66	241.59	28.48	18.11	10.38	63.04	33.06	3.90
OMM80	HMD	406.61	223.55	21.98	15.21	6.78	62.35	34.28	3.37
OMM812	HMD	381.34	202.09	23.50	13.75	9.75	62.83	33.30	3.87
OMN352	HMD	343.54	188.45	27.82	18.08	9.74	61.37	33.66	4.97
OMN412	HMD	356.09	202.66	23.65	14.99	8.67	61.14	34.80	4.06
OMO36	HMD	416.09	241.63	18.90	13.46	5.44	61.50	35.71	2.79
OMO712	HMD	413.67	212.42	21.30	16.40	4.90	63.90	32.81	3.29
OMO751	HMD	459.87	251.01	21.82	17.63	4.18	62.76	34.26	2.98
OMP263	HMD	439.33	242.58	22.56	15.62	6.93	62.36	34.43	3.20
OMP33	HMD	431.43	235.42	23.18	13.39	9.79	62.52	34.12	3.36
OMP67	HMD	473.98	261.20	26.11	18.46	7.65	62.26	34.31	3.43
OMP74	HMD	473.02	224.05	32.52	24.18	8.34	64.83	30.71	4.46
ONI412	HMD	447.64	216.59	26.83	19.49	7.34	64.78	31.34	3.88
ONM243	HMD	522.97	258.40	25.38	20.14	5.24	64.82	32.03	3.15
ONM36	HMD	446.55	226.33	20.40	13.85	6.55	64.41	32.65	2.94
GS1	El Gassi	399.22	212.97	22.37	13.62	8.75	62.91	33.56	3.52
AR61	Zotti	475.58	235.20	27.01	18.19	8.82	64.46	31.88	3.66
AR22	EL Agreb	384.57	213.65	25.47	14.39	11.08	61.66	34.26	4.08
DRT1	D.Temra	662.44	300.70	39.92	30.01	9.91	66.04	29.98	3.98
GLNE-5	Guellala NE	594.61	276.88	25.37	18.77	6.61	66.30	30.87	2.83
GLA16	Guellala	594.72	285.57	26.26	17.71	8.56	65.60	31.50	2.90
MEK1	M.Kebch	514.92	328.97	39.12	30.47	8.65	58.31	37.26	4.43
NGS2	Ngoussa	629.33	296.00	36.23	27.39	8.85	65.45	30.78	3.77
OKJ31	H.Berkaoui	708.88	303.20	40.30	30.66	9.64	67.36	28.81	3.83
OKJ202	H.Berkaoui	673.39	306.02	36.60	28.16	8.44	66.28	30.12	3.60
OKM881	H.Berkaoui	533.13	243.13	32.96	23.64	9.32	65.88	30.05	4.07
OKN77	H.Berkaoui	558.63	256.16	36.29	26.47	9.82	65.64	30.10	4.26
OKP-61	Benkahla	585.75	271.76	28.19	20.55	7.64	66.13	30.68	3.18
OKP88	Benkahla	536.14	241.19	27.31	17.83	9.48	66.63	29.97	3.39
RDC-1b	R.Chegga	518.72	227.04	18.44	11.78	6.66	67.88	29.71	2.41
HGA2	H.Guettar	485.81	266.56	18.49	11.30	7.19	63.02	34.58	2.40
HGA3	H.Guettar	429.88	242.23	22.06	14.15	7.92	61.93	34.90	3.18
MDR-7	Mesdar	461.08	308.71	28.89	21.36	7.53	57.73	38.65	3.62
MDR8	Mesdar	438.41	295.50	28.61	18.48	10.13	57.49	38.75	3.75
RB10	El Baguel	385.31	288.43	32.33	25.99	6.34	54.57	40.85	4.58
RB-18	El Baguel	444.89	332.02	22.66	18.33	4.33	55.64	41.52	2.83
OL2	DST	456.07	169.13	24.72	17.52	7.20	70.17	26.02	3.80

Appendix 5.3 Gross composition of the reservoir core samples, Hassi Messaoud.

OMO#712					MD#177					MD#213				
Depth (m)	Saturates (mg/g R)	Aromatics (mg/g R)	Polars (mg/g R)	Total extract (mg/g R)	Depth (m)	Saturates (mg/g R)	Aromatics (mg/g R)	Polars (mg/g R)	Total extract (mg/g R)	Depth (m)	Saturates (mg/g R)	Aromatics (mg/g R)	Polars (mg/g R)	Total extract (mg/g R)
3297.50	5.94	2.92	0.65	9.51	3275.40	5.95	1.69	0.65	8.29	3416.90	0.13	0.02	0.36	0.51
3300.95	0.14	0.08	0.85	1.07	3278.40	10.37	2.57	1.44	14.38	3419.45	0.07	0.00	0.27	0.34
3303.65	0.63	0.10	0.91	1.64	3281.45	7.04	1.61	1.19	9.84	3451.60	1.30	0.23	0.32	1.85
3306.30	0.30	0.21	0.48	1.00	3284.50	2.76	1.22	0.62	4.60	3452.80	2.17	0.36	0.51	3.04
3309.65	0.22	0.05	0.19	0.46	3287.50	2.01	0.55	0.61	3.18	3454.90	1.49	0.29	0.37	2.16
3311.70	1.34	0.37	0.36	2.07	3291.35	3.18	0.36	0.59	4.13	3456.40	1.86	0.51	0.85	3.22
3314.40	7.76	2.76	0.73	11.25	3294.60	2.21	0.47	0.49	3.17	3458.85	2.21	0.54	0.92	3.67
3315.85	1.05	0.31	0.39	1.75	3297.15	2.95	0.55	0.69	4.19	3460.55	2.26	0.62	1.00	3.88
3317.80	4.47	1.44	0.46	6.38	3300.40	7.24	1.49	1.19	9.92	3462.80	1.43	0.31	0.90	2.64
3319.80	1.32	0.32	0.40	2.04	3303.40	1.84	0.23	0.59	2.66	3464.80	1.77	0.42	0.44	2.63
3322.20	4.52	1.62	0.49	6.64	3306.45	3.48	0.47	0.96	4.91	3468.15	4.65	1.39	0.57	6.61
3324.90	3.69	1.50	0.42	5.62	3309.35	1.26	0.29	0.71	2.27	3470.90	1.89	0.33	0.39	2.41
3326.65	5.00	1.82	0.52	7.34	3312.40	6.82	1.15	1.62	9.59	3472.80	2.09	0.45	0.47	3.00
3328.50	5.32	1.99	0.78	8.10	3315.45	6.00	0.99	1.46	8.45	3474.90	1.70	0.32	0.44	2.45
3330.50	2.82	0.87	0.43	4.12	3318.60	6.23	0.88	2.10	9.21	3475.60	1.89	0.26	0.55	2.69
3332.40	3.92	1.58	0.64	6.13	3321.65	2.93	0.43	0.89	4.26	3477.20	2.72	0.36	0.61	3.69
3334.20	3.12	1.05	0.35	4.53	3324.45	4.13	0.73	1.33	6.19	3479.70	2.64	0.49	0.45	3.57
3336.70	2.45	0.69	0.43	3.58	3327.70	6.07	1.25	1.62	9.14	3481.20	1.83	0.32	0.71	2.86
3338.90	3.75	1.30	0.55	5.60	3330.45	5.03	1.01	1.49	7.53	3483.45	2.96	0.39	2.25	5.59
3340.40	3.05	0.98	0.42	4.44	3333.45	4.83	0.76	0.92	6.52	3485.75	2.70	0.49	1.15	4.33
3341.50	9.12	3.87	0.85	13.84	3336.45	10.28	2.81	1.83	14.73	3487.85	1.53	0.15	1.02	2.69
3343.75	5.98	2.30	0.72	8.98	3339.45	11.03	2.05	1.99	15.06	3489.90	5.04	0.97	1.73	7.74
3345.60	14.42	6.35	1.46	22.23	3342.35	5.73	2.43	0.70	8.87	3491.20	3.58	0.57	2.48	6.63
3348.80	10.48	4.73	1.00	16.21	3345.35	10.69	4.37	1.24	16.30	3493.70	4.67	1.08	1.38	7.13
3350.60	11.49	4.27	1.31	17.07	3348.40	7.28	3.59	0.81	11.69	3495.05	4.87	0.79	1.16	6.82
3352.15	15.93	6.29	1.66	23.87	3351.60	12.12	3.70	1.86	17.68	3497.90	4.04	0.60	1.66	6.31
3354.50	14.63	5.94	1.81	22.37	3354.30	5.39	2.73	0.93	9.05	3499.50	5.26	1.02	2.19	8.47
3356.15	15.52	6.34	1.81	23.67	3357.70	10.42	3.94	1.51	15.87					
3358.45	10.16	4.09	0.86	15.11	3359.65	11.77	3.59	2.30	17.67					
3360.25	11.40	4.57	0.93	16.90	3362.45	11.15	3.30	2.21	16.67					
3362.85	5.18	1.72	0.54	7.44	3365.10	6.91	1.85	1.58	10.33					
3364.50	9.55	3.66	0.86	14.07	3367.40	7.76	3.68	1.22	12.66					
3366.45	9.35	3.95	0.74	14.05	3370.45	7.15	3.33	1.27	11.75					
3368.15	5.19	1.87	0.51	7.56	3373.50	3.01	1.47	0.81	5.29					
3370.25	14.35	5.99	1.21	21.56	3376.80	5.09	1.70	0.84	7.63					
3372.40	8.41	3.32	0.68	12.41	3379.90	6.31	3.25	1.16	10.73					
3374.50	18.42	8.02	1.45	27.89	3382.70	5.40	2.03	0.96	8.39					
3376.60	3.08	1.03	0.48	4.59	3384.70	6.31	2.74	0.95	10.00					
3378.45	10.60	4.40	1.27	16.28										
3380.75	0.83	0.13	0.54	1.51										
3382.40	8.68	4.79	0.81	14.25										
3384.20	7.95	3.22	0.83	12.00										
3386.50	4.26	1.47	0.55	6.27										
3387.10	0.44	0.07	0.24	0.75										
3387.65	13.89	6.23	1.65	21.77										
3390.10	10.97	4.79	1.14	16.89										
3392.10	6.66	2.57	0.77	10.00										
3394.50	10.91	4.62	1.33	16.85										
3396.40	10.77	5.22	0.92	16.91										
3398.35	7.29	2.94	0.87	11.11										
3400.65	7.36	3.08	0.81	11.25										
3402.70	12.99	5.94	1.23	20.16										
3404.55	9.31	3.89	0.87	14.07										
3406.50	3.23	1.15	0.67	5.05										
3408.45	8.76	3.81	0.99	13.56										
3410.45	5.08	1.98	0.50	7.56										
3412.05	2.29	0.71	0.35	3.35										

Appendix 5.3 Gross composition of the reservoir core samples, Hassi Messaoud (continued).

OMJ#41					OMM#33					MD#141					OML#712				
Depth (m)	Saturates (mg/g R)	Aromatics (mg/g R)	Polars (mg/g R)	Total extract (mg/g R)	Depth (m)	Saturates (mg/g R)	Aromatics (mg/g R)	Polars (mg/g R)	Total extract (mg/g R)	Depth (m)	Saturates (mg/g R)	Aromatics (mg/g R)	Polars (mg/g R)	Total extract (mg/g R)	Depth (m)	Saturates (mg/g R)	Aromatics (mg/g R)	Polars (mg/g R)	Total extract (mg/g R)
3367.90	1.00	0.30	0.60	1.90	3399.45	1.56	0.15	0.36	2.08	3349.20	0.16	0.01	0.13	0.30	3401.60	3.82	1.08	0.62	5.51
3368.60	0.93	0.22	0.45	1.59	3402.80	0.65	0.02	0.36	1.03	3353.00	0.31	0.04	0.17	0.53	3403.06	5.66	1.09	0.77	7.52
3370.90	0.69	0.12	0.32	1.13	3405.40	0.06	0.01	0.29	0.36	3355.00	0.70	0.07	0.23	1.00	3404.75	6.65	1.79	0.69	9.13
3371.80	1.79	0.50	0.47	2.76	3406.55	1.16	0.22	0.30	1.67	3358.45	0.95	0.15	0.23	1.32	3406.20	9.04	2.55	0.87	12.46
3372.85	4.61	1.59	0.76	6.95	3408.45	0.13	0.00	0.26	0.39	3361.10	0.20	0.02	0.20	0.42	3407.90	6.37	2.32	0.74	9.43
3374.50	4.53	1.45	0.80	6.78	3411.10	0.27	0.01	0.30	0.58	3363.85	0.51	0.11	0.20	0.82	3409.45	7.68	2.16	0.70	10.54
3376.20	0.69	0.12	0.31	1.13	3413.75	1.11	0.28	0.30	1.69	3366.00	0.63	0.12	0.21	0.96	3422.60	13.83	4.01	1.07	18.91
3380.90	1.40	0.37	0.53	2.31	3415.45	0.07	0.01	0.19	0.26	3372.40	0.42	0.03	0.21	0.66	3424.05	10.31	3.34	0.86	14.50
3383.45	1.39	0.23	0.40	2.02	3417.55	0.55	0.05	0.26	0.85	3378.50	0.81	0.13	0.18	1.12	3425.70	9.26	3.53	0.76	13.55
3385.50	2.50	0.48	0.46	3.44	3420.40	0.49	0.03	0.27	0.80	3381.65	0.87	0.12	0.21	1.20	3426.95	16.31	4.92	0.98	22.21
3387.25	6.37	1.65	0.93	8.95	3422.65	0.06	0.00	0.23	0.29	3384.30	0.56	0.06	0.22	0.84	3429.50	11.24	4.02	0.81	16.07
3387.55	0.99	0.19	0.44	1.61	3425.50	0.67	0.08	0.29	1.05	3387.45	0.96	0.19	0.20	1.36	3430.90	11.90	4.54	0.96	17.40
3390.10	10.03	3.03	1.57	14.63	3427.70	0.14	0.08	0.30	0.52	3393.60	0.48	0.07	0.14	0.69	3432.50	14.02	4.46	0.94	19.42
3393.40	7.42	2.22	1.30	10.95	3428.45	0.42	0.05	0.35	0.82	3396.60	0.32	0.04	0.18	0.55	3434.40	10.52	3.82	0.73	15.07
3395.70	3.26	0.84	0.62	4.72	3432.40	2.03	0.41	0.40	2.84	3399.45	0.80	0.10	0.25	1.15	3435.95	7.21	2.48	0.59	10.29
3398.50	3.94	0.72	1.01	5.67	3435.50	0.60	0.01	0.28	0.90	3404.35	2.52	0.39	0.31	3.22	3437.45	16.48	5.77	1.30	23.55
3400.40	2.50	0.63	0.73	3.85	3438.70	0.83	0.07	0.34	1.25	3407.20	1.82	0.53	0.34	2.69	3439.05	8.99	3.35	0.71	13.05
3401.70	1.57	0.20	0.72	2.49	3441.40	0.96	0.10	0.32	1.39	3410.00	0.50	0.05	0.28	0.83	3440.80	11.21	4.19	0.93	16.33
3403.45	2.04	0.44	0.43	2.90	3444.40	1.42	0.32	0.31	2.05	3413.30	0.15	0.01	0.20	0.37	3442.40	5.82	4.31	1.22	11.34
3405.70	1.22	0.22	0.45	1.89	3446.60	2.20	0.24	0.27	2.72	3416.30	0.81	0.11	0.28	1.20	3443.90	7.32	2.55	0.82	10.69
3408.70	3.62	0.88	0.73	5.23	3448.30	1.62	0.30	0.28	2.20	3419.45	1.06	0.10	0.19	1.36	3445.75	6.77	1.88	0.90	9.55
3410.50	0.64	0.10	0.35	1.08	3451.35	1.05	0.14	0.27	1.46	3422.65	1.48	0.18	0.25	1.91	3446.85	8.39	2.11	0.85	11.36
3412.90	4.53	1.11	0.68	6.32	3453.40	1.34	0.21	0.27	1.82	3425.45	1.65	0.16	0.29	2.11					
3415.25	3.68	0.92	0.63	5.23	3456.80	1.02	0.11	0.28	1.42	3428.55	3.35	0.47	0.33	4.14					
3417.80	2.98	0.62	0.65	4.25	3458.45	1.06	0.15	0.32	1.52	3432.45	3.72	0.62	0.39	4.73					
3421.95	2.35	0.56	0.49	3.40	3460.45	1.74	0.25	0.35	2.35	3435.45	4.35	0.77	0.42	5.54					
3423.80	2.18	0.37	0.68	3.24	3461.35	2.24	0.22	0.41	2.87	3438.65	7.77	1.80	0.57	10.14					
3425.50	8.61	2.50	1.59	12.70	3463.65	1.51	0.25	0.33	2.09	3441.95	4.42	0.58	0.47	5.47					
3428.50	7.78	1.81	2.24	11.83	3464.50	13.47	3.23	1.21	17.90	3444.50	3.97	0.65	0.38	5.00					
3430.75	9.80	2.99	2.00	14.79	3466.85	4.37	0.72	0.57	5.67	3447.75	2.50	0.53	0.24	3.28					
3433.45	3.61	0.80	0.50	4.90	3468.70	2.14	0.33	0.41	2.88	3450.40	4.54	0.68	0.42	5.64					
3435.20	3.14	0.44	0.76	4.34	3471.71	2.96	0.47	0.29	3.72	3453.75	3.16	0.78	0.26	4.19					
3437.00	3.63	0.84	0.56	5.04	3472.10	5.33	1.09	0.48	6.90	3456.40	3.88	0.56	0.37	4.80					
3439.10	0.28	0.01	0.32	0.61	3773.90	7.10	1.39	0.58	9.08	3459.45	3.98	0.68	0.35	5.01					
3439.80	8.82	2.64	1.42	12.88	3474.85	1.47	0.16	0.29	1.92	3461.40	2.54	0.74	0.26	3.55					
3443.50	2.71	0.48	0.66	3.85	3476.85	1.50	0.24	0.34	2.07	3462.55	3.11	0.88	0.25	4.25					
3446.45	1.47	0.30	0.62	2.39	3478.85	1.66	0.25	0.37	2.28	3464.45	1.71	0.33	0.23	2.27					
3449.70	2.56	0.50	0.66	3.72	3480.90	3.49	0.62	0.48	4.59										
3451.70	1.15	0.19	0.42	1.76	3482.65	1.21	0.13	0.39	1.73										
3454.65	4.20	1.00	0.71	5.90	3483.75	7.41	1.96	0.58	9.95										
3457.40	3.50	0.55	0.80	4.85	3484.80	1.46	0.19	0.31	1.97										
3458.75	13.16	2.96	2.39	18.50	3485.85	1.06	0.14	0.29	1.49										
3460.80	7.79	1.78	0.80	10.38	3487.75	0.68	0.11	0.25	1.04										
3463.50	11.86	2.60	1.78	16.24															
3466.65	3.25	0.59	0.64	4.49															
3468.80	7.94	1.73	1.20	10.87															
3470.80	5.48	1.06	0.60	7.15															
3471.25	3.31	0.75	0.42	4.48															
3473.40	4.70	0.92	0.66	6.28															
3475.50	6.17	1.24	0.62	8.03															

Appendix 6.1 *n*-alkane and isoprenoid alkane distributions in the petroleum inclusion samples.